The role of hepatocyte growth factor and β1-integrin/cell-matrix interactions in regulating growth and tunneling nanotube formation in non-small cell lung cancer

Griselda Awanis

Submitted for the degree of Doctor of Philosophy

University of East Anglia

School of Pharmacy

November 2022

This copy of the thesis has been supplied on condition that anyone who consults it is understood to recognise that its copyright rests with the author and that use of any information derived therefrom must be in accordance with current UK Copyright Law. In addition, any quotation or extract must include full attribution.

Abstract

Non-small cell lung cancer (NSCLC) accounts for 85% of all lung cancer cases. It is associated with high mortality rates with the majority of patients diagnosed with advanced metastatic cancer. Evading programmed cell death, increasing cellular motility, suppressing immune reactivity and alterations in the interactions between tumour cells and the extracellular matrix (ECM) proteins outline the complex process of tumour invasion. Another vital understudied aspect in achieving metastasis is the cellular communication existing between cells through the formation of tunneling nanotubes (TNTs). TNTs are non-adherent F-actin-based cytoplasmic protrusions that transport organelles to propagate chemoresistance across long distances in the tumour microenvironment (TME). Moreover, different factors within the TME initiate the pro-tumourigenic processes. Hepatocyte growth factor (HGF) and its receptor, c-Met, are mutationally upregulated in NSCLC leading to aberrant signalling in NSCLC which contributes to enhanced proliferation, migration and invasion. Similarly, other pleiotropic cytokines, such as IL-6 and EGF, are also known to induce growth and invasion in NSCLC. Furthermore, remodelling of the ECM proteins such as collagen IV, fibronectin and laminin results in the propagation of growth factor signalling *via* β1-integrin (Yan et al. 2006). Therefore, the aim of this research was to investigate the crosstalk between HGF with other pleiotropic cytokines (e.g. IL-6 and EGF) and the ECM/β1-integrin signalling axis in inducing proliferation and TNT formation in A549 lung adenocarcinoma cells.

The results of this thesis demonstrate a novel role for the combined HGF and IL-6-induced proliferation via a convergence on the MAPK pathway. Moreover, HGF mediated proliferation in A549 cells occurred via interactions with fibronectin and β1-integrin. Our results also presented a novel role for HGF and its signalling axis in TNT formation, whereby HGF/c-Met crosstalk with β1-integrin to activate Arp2/3 complex, MAPK and PI3K pathways via paxillin. C-Met, β1-integrin and paxillin were also identified as novel components of TNTs. HGF/c-Met also crosstalk with EGF/EGFR via a convergence on the MAPK and PI3K pathways to regulate TNT formation. Moreover, we discovered a subpopulation of A549 cells capable of simultaneous migration, TNT formation and cell division which highlights a novel potential mechanism of metastasis in NSCLC. To recapitulate the 3D TME, our 3D A549 tumouroid studies revealed a physical interaction with occurring between A549 tumouroids and eosinophils. Moreover, novel TNT formation was observed between A549 tumouroids upon triptolide treatment. Overall, our findings highlight the complex interactions within the TME and the importance of multi-drug targeting to fully inhibit the spectrum of pro-tumourigenic effects induced by HGF/c-Met and its signalling partners.

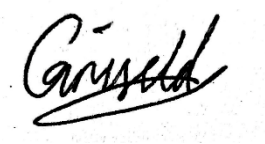
Access Condition and Agreement

Each deposit in UEA Digital Repository is protected by copyright and other intellectual property rights, and duplication or sale of all or part of any of the Data Collections is not permitted, except that material may be duplicated by you for your research use or for educational purposes in electronic or print form. You must obtain permission from the copyright holder, usually the author, for any other use. Exceptions only apply where a deposit may be explicitly provided under a stated licence, such as a Creative Commons licence or Open Government licence.

Electronic or print copies may not be offered, whether for sale or otherwise to anyone, unless explicitly stated under a Creative Commons or Open Government license. Unauthorised reproduction, editing or reformatting for resale purposes is explicitly prohibited (except where approved by the copyright holder themselves) and UEA reserves the right to take immediate ‘take down’ action on behalf of the copyright and/or rights holder if this Access condition of the UEA Digital Repository is breached. Any material in this database has been supplied on the understanding that it is copyright material and that no quotation from the material may be published without proper acknowledgement.

Declaration

I declare that this thesis represents my own work, except where due acknowledgement is made, and that it has not been previously included in a thesis, dissertation or report submitted to this University of to any other institution for a degree, diploma or other qualifications.



Griselda Awanis

PhD candidate

Acknowledgements

I would first like to express my sincere gratitude to my supervisor Dr Anastasia Sobolewski for giving me the opportunity to do a PhD in her lab. Thank you for always pushing me to improve and guiding me towards my own success. I truly owe so much to you, not only professionally but personally too. Thank you for everything you've done for me. My gratitude also extends to my secondary supervisor, Dr Jelena Gavrilovic, for providing me great advice, feedback and encouragement throughout my PhD.

I would next like to thank the Warren and O'Connell lab for all their support and collaboration throughout my PhD. I am especially thankful to Dr Derek Warren for all the advice and help with my project, not only with providing siRNA reagents, the ROCK inhibitor and phalloidin for my TNT work but also for providing expert advice for the migration and paxillin aspect of the TNT project. I would like to thank Dr Robert Johnson for conducting the western blots, teaching me the siRNA protocol and for all his patience with my relentless questions. I would like to extend my gratitude to Reesha Solanki and Finn Worstear for helping me with the western blots. I would also like to thank Dr Teclino Afewerki for teaching me how to do the migration analysis and for being a cheerful and supportive friend in the office. I'd like to extend my thanks as well to Professor Maria O'Connell for giving me the opportunity to collaborate and Emily Hobson for providing the triptolide and other reagents for our collaborative work and for being a supportive friend throughout my PhD. I'd also like to thank Professor Mette Mogensen for kindly providing us with the paxillin and α-tubulin primary antibodies.

Next, I'd like to thank the past and present members of the Sobolewski lab. Especially Dr Sathuwarman Raveenthiraraj, thank you for all the great laughs, music recommendations and most importantly, patience in training me! Also, Salonee Banerjee for giving me moral support in the lab and office. I'd also like to thank the project students Amy Judge, Frances Perrett and Imogen Clarke for their contributions and effort in setting up and analysing the EGF TNT and 'go and grow' experiments. I'd also like to thank Dr Sultan Ahmed and Dr Carla Arnau Del Valle for all their help and encouragement throughout my PhD.

I would like to thank my family, Pa, Ma, San, Jay, Bang and Man for their constant care and support throughout my studies. Especially my dad for funding my PhD, thank you for looking out for the youngest one! I'd also like to thank my extended family, Paul, Jude, Sarah, Toby, Nana, Joe, Hugh, Viola, Cath, Phil, Sam, George, Olek and Kasia! Thank you, Paul and Jude, for always providing a loving home for me in Norwich. To the little girls, Sonja, Maya and Rosa for giving me so much joy

and laughter throughout my PhD journey. Last but not least, thank you Harry, you've always been there to comfort me through the hard times but also celebrated all the joys and successes with me. Thank you for being the most amazing best friend and husband, I am truly grateful to have your loving company throughout this journey.

Table of Contents

Abstract I
Declaration II
Acknowledgements III
Table of Contents V
List of Figures X
List of Tables XIV
Glossary XV
1. Chapter 1. General Introduction 1
1.1 The lung 1
1.2 Lung Cancer 2
1.2.1 Non-small cell lung cancer 2
1.2.2 The tumour microenvironment 3
1.2.3 Treatment of non-small cell lung cancer 8
1.3 Hepatocyte Growth Factor and c-Met 9
1.3.1 Intracellular signalling 11
1.3.2 Biological role of hepatocyte growth factor 14
1.3.3 HGF/c-Met mutations in non-small cell lung cancer 16
1.4 Interleukin-6 17
1.4.1 Intracellular signalling 18
1.4.2 Biological role of IL-6 20
1.4.3 IL-6 in non-small cell lung cancer 21
1.5 The relationship between HGF and IL-6 23
1.6 Epidermal growth factor and epidermal growth factor receptor 24
1.6.1 Intracellular signalling 26
1.6.2 Biological role of EGF 27
1.6.3 EGF/EGFR in non-small cell lung cancer 28
1.7 The relationship between HGF and EGF 28
1.8 Extracellular Matrix: fibronectin, collagen IV and laminin 29
1.8.1 Integrins 31
1.9 Paxillin 34
1.9.1 Interaction between HGF/c-Met, β1-integrin and paxillin in NSCLC 35
1.10 The 'Go or grow' mechanism in cancer 38
1.10.1 The cell cycle 38
1.10.2 The process of migration 40
1.10.3 The evidence surrounding the 'go or grow' hypothesis in cancer 42
1.11 Cellular communication through tunneling nanotubes 42
1.11.1 Characteristics of TNTs 43
1.11.2 Mechanisms regulating TNT formation 48
1.11.3 Biological function of TNTs 51
1.11.4 TNTs in cancer 52
1.12 The clinical landscape and multidrug targeting 54
1.13 Rationale 55
1.14 Experimental approach 58
1.15 Hypothesis 59
1.16 Aims 59

2. Chapter 2. Materials and Methods 61

2.1 Laboratory consumables 61
2.1.1 Reagents 61
2.1.2 Primary and secondary antibodies 62
2.1.3 Laboratory apparatus 63
2.2 Cell culture 64
2.3 Cell counts 64
2.3.1 HGF and IL-6 treatment 64
2.3.2 Collagen IV, laminin and fibronectin coating 65
2.3.3 PD98059 inhibitor 66
2.4 Tunneling nanotube experiments 66
2.4.1 HGF, EGF and FGF dose response 66
2.4.2 Immunofluorescence labelling of TNTs 67
2.4.3 Live-cell imaging of mitochondria and vesicles TNT trafficking 68
2.4.4 TNT inhibitor experiments 69
2.4.5 siRNA paxillin knockdown 70
2.4.6 Western blot 71
2.4.7 Polyacrylamide hydrogels 71
2.4.8 Time-lapse video microscopy 72
2.5 A549 tumouroid growth experiments 72
2.5.1 3D A549 tumouroid culture in Matrigel 72
2.5.2 HGF and IL-6 treatment of A549 tumouroids 73
2.5.3 Immunofluorescence labelling and EdU incorporation of A549 tumouroids 73
2.6 Triptolide treatment of A549 tumouroids 73
2.7 HL-60/eos and A549 tumouroid co-culture model 74
2.7.1 Differentiation of HL-60 cells to eosinophils 74
2.7.2 Characterisation of eosinophils 74
2.7.3 Trypan blue staining assay 74
2.7.4 HL-60/eos survival in DMEM and RPMI media 75
2.7.5 HL-60/eos co-culture with A549 tumouroids 75
2.8 Image analysis 74
2.8.1 TNT identification and quantification 76
2.8.2 Identification and quantification of ‘go and grow’ TNTs 77
2.8.3 Speed and directionality tracking of ‘go and grow’ TNTs 78
2.8.4 Quantification of EdU positive A549 tumouroid nuclei 79
2.8.5 Quantification of the differentiated HL-60/eos 80
2.8.6 Quantification of apoptotic HL-60/eos 80
2.8.7 Quantification of EdU-positive and caspase-3-positive A549 cells in co-culture with HL-60/eos 80
2.9 Statistical analysis 81

3. Chapter 3: The role of HGF, IL-6 and the ECM in A549 cell proliferation 82

3.1 Introduction 82
3.2 Results 85
3.2.1 IL-6 and HGF induces proliferation in A549 cells 85
3.2.2 HGF and IL-6 demonstrate no synergistic or additive effect on A549 cell proliferation 85
3.2.3 HGF and IL-6 induces A549 proliferation *via* convergence on the MAPK pathway 90

3.2.4 Collagen IV, fibronectin and laminin induce proliferation in A549 cells 91
3.2.5 HGF and IL-6 has no effect on A549 cell growth on collagen IV 92
3.3 Discussion 93
3.3.1 Future work 96

4. Chapter 4: HGF induces tunneling nanotube formation in A549 cells 98

4.1 Introduction 98
4.2 Results 100
4.2.1 Effect of *in vitro* culture conditions on TNT formation of A549 cells 100
4.2.2 HGF induces TNT formation in A549 cells in a time and concentration-dependent manner 103
4.2.3 HGF-induced TNTs express characteristic markers of TNTs 113
4.2.4 β1-integrin, c-Met and paxillin are novel components of TNTs in A549 cells ... 120
4.2.5 HGF-induced TNTs transport mitochondria and vesicles 126
4.3 Discussion 128
4.3.1 HGF induces TNT formation in A549 cells 128
4.3.2 HGF-induced TNTs express characteristic marker 130
4.3.3 TNTs express novel components c-Met, β1-integrin and paxillin 132
4.3.4 HGF-induced TNTs transfer mitochondria and vesicles 133
4.3.5 Future work 134
4.4 Conclusions 136

5. Chapter 5: HGF/c-Met/β1-integrin signalling-axis induces TNT formation *via* the MAPK, PI3K and Arp2/3 complex pathways 137

5.1 Introduction 137
5.2 Results 139
5.2.1 C-Met receptor regulates TNT formation in A549 cells 139
5.2.2 C-Met inhibition reduces the expression of F-actin, α-tubulin and M-sec positive TNTs 142
5.2.3 C-Met inhibition reduces the localisation of c-Met and β1-integrin positive TNTs 144
5.2.4 β1-integrin crosstalk with HGF/c-Met to induces TNTs in A549 cells 146
5.2.5 Paxillin is involved in HGF-induced TNT formation 149
5.2.6 CDC42, Rac1 and ROCK pathway inhibition had no effect on HGF-induced TNT formation 151
5.2.7 MAPK, PI3K and Arp2/3 complex pathways mediate HGF-induced TNT formation 169
5.3 Discussion 188
5.3.1 HGF induces TNT formation through activation of its c-Met receptor 188
5.3.2 HGF/c-Met crosstalk with β1-integrin to induce TNT formation in A549 cells .. 190
5.3.3 Paxillin regulates the HGF/c-Met/β1-integrin-induced TNT formation 191
5.3.4 HGF/c-Met/β1-integrin does not induce TNT formation *via* the CDC42, Rac1 and ROCK pathways 191
5.3.5 HGF/c-Met/β1-integrin recruits paxillin to induce TNT formation *via* the MAPK, PI3K and Arp2/3 complex pathways 193
5.3.6 Future work 194
5.4 Conclusion 195

6. Chapter 6: Crosstalk between HGF and EGF in TNT formation of A549 cells 196

6.1 Introduction 196

6.2 Results 199
6.2.1 IL-6 has no discernible effect on TNT formation in A549 cells 199
6.2.2 FGF2 has no discernible effect on TNT formation in A549 cells 200
6.2.3 EGF induces TNT formation in A549 cells in a dose-dependent manner 201
6.2.4 EGF induces F-actin-positive TNTs 202
6.2.5 Co-treatment with HGF and EGF showed no additive or synergistic increase on TNT formation compared to HGF or EGF treatment alone 203
6.2.6 Inhibition of EGFR and c-Met alone had no effect on the combined HGF and EGF-induced TNT formation 204
6.2.7 Both MAPK and PI3K pathway inhibition was required to inhibit the HGF and EGF co-stimulated TNTs 206
6.3 Discussion 209
6.3.1 IL-6 and FGF2 has no effect on TNT formation in A549 cells 209
6.3.2 EGF induces TNT formation in A549 cells 210
6.3.3 Combined HGF and EGF treatment did not induce an additive or synergistic effect on TNT formation 211
6.3.4 Sole EGFR and c-Met inhibition had no effect on the combined HGF and EGF-induced TNT formation 211
6.3.5 Combined PI3K and MAPK pathway inhibition reduced the co-stimulated EGF and HGF TNT effect 212
6.3.6 Future work 213
6.4 Conclusions 214

7. Chapter 7: HGF induces a novel 'go and grow' phenotype in A549 cells 216

7.1 Introduction 216
7.2 Results 218
7.2.1 A549 cells form 'go and grow' cells 218
7.2.2 'Go and grow' TNTs express novel and characteristic markers c-Met, β1-integrin, paxillin and F-actin 219
7.2.3 HGF increased the formation of 'go and grow' cells 221
7.2.4 C-Met inhibitor reduced the HGF-induced 'go and grow' cells 223
7.2.5 Characterisation of the speed and directionality of 'go and grow' TNTs 224
7.2.6 Go and grow' cells are more proliferative than non-'go and grow' cells 225
7.2.7 HGF induced the formation of 'go and grow' cells on collagen IV-coated 12kPa hydrogels 225
7.3 Discussion 227
7.3.1 Characterising the 'go and grow' A549 cells 227
7.3.2 HGF increases the frequency of 'go and grow' cells 228
7.3.3 Characterising the speed and directionality of 'go and grow' cells 229
7.3.4 'Go and grow' cells are proliferate more than non-'go and grow' cells 230
7.3.5 HGF-induced 'go and grow' cells form on hydrogels mimicking lung tumour matrix stiffness 230
7.3.6 The potential role for 'go and grow' cells in NSCLC 231
7.3.7 Future work 232

8. Chapter 8: The 3D tumour microenvironment in influencing A549 cell growth, TNT formation and immune response 234

8.1 Introduction 234
8.2 Results 236
8.2.1 A549 cells cultured in Matrigel grow into tumouroids over a 9-day period 236

8.2.2 72-hour HGF and IL-6 treatment at day 0 had no effect on EdU incorporation of A549 tumouroids 236
8.2.3 72-hour HGF and IL-6 treatment at day 3 had no effect on EdU incorporation of A549 tumouroids 240
8.2.4 Development of a HL-60/eos and A549 tumouroid co-culture model 243
8.2.5 HL-60/eos had no effect on caspase-3 positive A549 cells and EdU-incorporated A549 nuclei 245
8.2.6 Triptolide induced the formation of TNT-like structures between A549 tumouroids 248
8.3 Discussion 250
8.3.1 HGF and IL-6 have no effect on A549 tumouroid development and growth 250
8.3.2 HL-60/eos has no effect on A549 tumouroid growth or death 252
8.3.3 Triptolide induces TNT formation between A549 tumouroids 254
8.3.4 Future work 255
9. Chapter 9. General discussion and future work 257
9.1 Key findings and concepts 257
9.2 Elucidating the integrated biology of HGF using an organ-on-a-chip model 259
9.3 Therapeutic strategies to target the crosstalk HGF signalling in NSCLC 260
9.4 Concluding remarks 262
10. Reference 264

List of Figures

Figure 1: The anatomy of the lung and its heterogenous microenvironment 1
Figure 2: Classification of lung cancer and their cellular origin 3
Figure 3: The cellular characteristics of eosinophils 6
Figure 4: The tumour microenvironment 7
Figure 5: Structure of HGF 9
Figure 6: Structure of c-Met 10
Figure 7: The HGF/c-Met signalling pathway components 12
Figure 8: Diagram depicting the main HGF/c-Met downstream signalling pathways 14
Figure 9: Structure of IL-6 18
Figure 10: The three types of IL-6 signalling: *classic signalling, trans-signalling* and *trans*-presentation 19
Figure 11: The structure of EGF 24
Figure 12: The structure of EGFR 26
Figure 13: A schematic showing the main signalling pathways associated with EGFR 27
Figure 14: Schematic diagram of the integrin outside-in signalling of FAK activation 33
Figure 15: The structure of paxillin and its associated binding partners 35
Figure 16: Schematic diagram of the crosstalk between HGF/c-Met and integrin signalling 36
Figure 17: Schematic diagram of metastasis via 'inside-in signalling' of β1-integrin and c-Met .. 37
Figure 18: The different stages of the cell cycle 39
Figure 19: A schematic depicting cellular migration 41
Figure 20: Diagram of the different types of distinguished thin membrane protrusions 45
Figure 21: Diagram depicting tubulogenesis and tunneling nanotubes 46
Figure 22: The signalling mechanisms involved in TNT formation 50
Figure 23: The formation, stabilisation and roles of TNTs 53
Figure 24: The potential convergence of the pathways induced by HGF, IL-6 and the ECM with their respective receptors in NSCLC 56
Figure 25: The potential HGF/c-Met/β1-integrin signalling involved in mediating TNT formation in A549 cells 57
Figure 26: Diagram depicting the difference between widefield epifluorescence and confocal microscopy 59
Figure 2.1. Negative controls of immunofluorescent labelling specificity 67
Figure 2.2. Negative control of immunofluorescent labelling for caspase-3 76
Figure 2.3: White light TNT quantification 76
Figure 2.4: White light TNT length measurement 77
Figure 2.5. Two examples of 'go and grow' TNTs 78
Figure 2.6. Quantification of DAPI stained and EdU incorporated A549 nuclei 79

Figure 2.7. Characterisation of apoptotic nuclei of HL-60/eos 80
Figure 2.8. Quantification of DAPI stained and caspase-3 positive A549 cells 81
Figure 3.1: IL-6 and HGF induce A549 proliferation in a concentration dependant manner 85
Figure 3.2: No synergistic effect with the EC_{50} concentration of IL-6 and HGF on A549 proliferation 86
Figure 3.3: No additive effect with the maximal concentration of IL-6 and HGF on A549 proliferation 87
Figure 3.4: No synergistic effect with the EC_{50} concentration of IL-6 and HGF on A549 proliferation with a lower seeding density 88
Figure 3.5: No additive effect with the maximal concentration of IL-6 and HGF on A549 proliferation 88
Figure 3.6: IL-6 and HGF induce A549 proliferation in a concentration dependant manner in low serum 89
Figure 3.7: No synergistic or additive effect with the EC_{50} and maximal concentration of IL-6 and HGF on A549 proliferation in low serum 90
Figure 3.8: HGF and IL-6 converge on the MAPK pathway in A549 proliferation 90
Figure 3.9: ECM components induce proliferation in A549 in a concentration dependant manner 91
Figure 3.10: Collagen IV does not induce an additive effect on HGF/IL-6-induced proliferation.. 92
Figure 4.1 Optimal seeding density on plastic to observe HGF-induced TNT-like structures 101
Figure 4.2: HGF induces an increase in TNT formation in 10% and 2% FBS supplemented media 102
Figure 4.3: HGF induces TNT-like structures in A549 lung adenocarcinoma cells in a time dependent manner 108
Figure 4.4: HGF induces TNT-like structures in A549 lung adenocarcinoma cells in a concentration dependent manner at the 24^{th} hour timepoint 105
Figure 4.5: A: Representative white light images of the different morphologies (straight, curved, angled and branched) observed in HGF-treated A549 cells 107
Figure 4.6: The HGF (100ng/ml)-induced TNT length distribution over the 72-hour time course experiment 110
Figure 4.7: HGF induces type 1 and 2 TNTs in A549 cells 109
Figure 4.8: HGF induces an increase in TNT formation on glass and plastic culture surface 112
Figure 4.9: Optimal seeding density on glass coverslips to observe HGF-induced TNTs 116
Figure 4.10: A: Representative images of the white light and the immunofluorescence labelling of F-actin (red) of HGF-treated TNTs 117
Figure 4.11: Characterisation of TNT-like structures using immunofluorescent labelling and confocal microscopy 119
Figure 4.12: β1-integrin is a novel component in TNTs 121
Figure 4.13: C-Met, β1-integrin localise at the protrusion site and along the length of TNTs 123
Figure 4.14: Paxillin localises at the protrusion sites of TNTs 125

Figure 4.15: TNTs in A549 cells functionally transmit mitochondria and vesicles..... 127
Figure 4.16 Diagram depicting the potential signalling mechanisms involved in the HGF-induced TNT formation in A549 cells 136
Figure 5.1: C-Met receptor mediates TNT formation in A549 cells..... 141
Figure 5.2: C-Met inhibition reduced the expression of F-actin, M-sec and α-tubulin positive TNTs 143
Figure 5.3: C-Met inhibition reduced the expression of c-Met and β1-integrin positive TNTs ... 145
Figure 5.4: β1-integrin cross talk with HGF/c-Met induces TNTs in A549 cells 148
Figure 5.5: Paxillin regulates HGF-induced TNT formation 150
Figure 5.6: CDC42 inhibition showed no effect on HGF-induced TNT formation..... 154
Figure 5.7: CDC42 inhibition had no effect on the expression of F-actin, M-sec and α-tubulin positive TNTs 155
Figure 5.8: CDC42 inhibition had no effect on the expression of c-Met and β1-integrin positive 156
Figure 5.9: Rac1 inhibition showed no effect on HGF-induced TNT formation..... 159
Figure 5.10: Rac1 inhibition had no effect on the expression of F-actin, M-sec and α-tubulin positive TNTs 161
Figure 5.11: Rac1 inhibition had no effect on the expression of c-Met and β1-integrin positive TNTs..... 162
Figure 5.12: ROCK pathway inhibition induced an increase in the HGF-TNT formation 166
Figure 5.13: ROCK inhibition had no effect on the expression of F-actin, M-sec and α-tubulin positive TNTs 168
Figure 5.14: ROCK inhibition had no effect on the expression of c-Met and β1-integrin positive TNTs..... 169
HGF induces TNTs *via* the Arp2/3 complex in A549 cells. 172
Figure 5.16: Arp2/3 complex inhibition reduced the expression of F-actin, M-sec and α-tubulin positive TNTs 174
Figure 5.17: Arp2/3 complex inhibition reduced the expression of c-Met and β1-integrin positive TNTs..... 175
Figure 5.18: HGF induces TNTs *via* the MAPK pathway in A549 cells 178
Figure 5.19: MAPK pathway inhibition reduced the expression of F-actin, M-sec and α-tubulin positive TNTs 180
Figure 5.20: MAPK pathway inhibition reduced the expression of c-Met and β1-integrin positive TNTs..... 181
Figure 5.21: HGF induces TNTs *via* the PI3K pathway in A549 cells 184
Figure 5.22: PI3K pathway inhibition reduced the expression of F-actin, M-sec and α-tubulin positive TNTs 186
Figure 5.23: PI3K pathway inhibition reduced the expression of c-Met and β1-integrin positive TNTs..... 187
Figure 5.24: HGF/c-Met and β1-integrin signalling axis drives TNT formation in A549 cells 195

Figure 6.1: IL-6 does not induce TNT formation in A549 cells 200
Figure 6.2: FGF2 has no effect on TNT formation in A549 cells 201
Figure 6.3: EGF induces A549 cell TNT formation in a dose-dependent manner 202
Figure 6.4: EGF induces F-actin positive TNTs 203
Figure 6.5: HGF and EGF do not induce a synergistic or additive effect on TNT formation 204
Figure 6.6: HGF and EGF pathways converge in response to erlotinib and c-Met inhibition 206
Figure 6.7: Both MAPK and PI3K pathway inhibition is required to suppress HGF and EGF-induced TNTs 208
Figure 6.8: HGF/c-Met and EGF/EGFR signalling pathways converge on the MAPK and PI3K pathways to induce TNT formation in A549 cells 214
Figure 7.1: A549 cells undergo a novel 'go and grow' phenomenon 218
Figure 7.2: The starting timepoints of the control and HGF-induced 'go and grow' cells occurring throughout the 24-hour period 219
Figure 7.3: The TNTs formed during the 'go and grow' process positively express F-actin 220
Figure 7.4: C-Met, β1-integrin, paxillin and F-actin are expressed in 'go and grow' TNTs 221
Figure 7.5: HGF significantly increases the percentage of 'go and grow' cells 222
Figure 7.6: HGF significantly increases the percentage of 'go and grow' cells when taken as a percentage over all the TNT-forming cells 223
Figure 7.7: The c-Met receptor inhibitor, PHA-665752 (0.25μM), decreases the percentage of 'go and grow' cells compared to cells treated with only HGF over a 24h period. 223
Figure 7.8: Control and HGF-induced 'go and grow' cells migrate and retract in a similar fashion 224
Figure 7.9: 'Go and grow' cells are more proliferative 225
Figure 7.10: 'Go and grow' cells form when seeded on collagen IV-coated 12kPa hydrogels 226
Figure 7.8 Future aims involved in further characterising the 'go and grow' cells 233
Figure 8.1: A549 tumouroid growth in Matrigel over a 9-day period 236
Figure 8.2: IL-6 and HGF has no effect on A549 tumouroid development 239
Figure 8.3: IL-6 and HGF has no effect on A549 tumouroid growth 242
Figure 8.4: HL-60 cells differentiate towards an eosinophil-likel phenotype 244
Figure 8.5: The 'IN' and 'ON' co-cultures of A549 tumouroids with HL-60/eos 245
Figure 8.6: DMEM and RPMI had no effect on the survival of HL-60/eos 246
Figure 8.7: The 'IN' co-culture of A549 tumouroids with HL-60/eos 247
Figure 8.8: The 'ON' co-culture of A549 tumouroids with HL-60/eos 248
Figure 8.9: Triptolide induced the formation of TNT-like structures between A549 tumouroids 249
Figure 9.1. The implications of the HGF-mediated growth and TNT outcomes in NSCLC 258
Figure 9.2. A schematic showing of the tumour microenvironment of NSCLC in comparison to the microfluidic system 260

Figure 9.3: Schematic representing photodynamic therapy with nanoparticles conjugated with EGFR, c-Met and β1-integrin targeting antibodies 262

List of Tables

Table 1: Summary of the integrin extracellular matrix ligands binding interactions 32

Table 2.1: List of reagents, sources and catalogue numbers 62

Table 2.2: List of primary antibodies used for immunofluorescence labelling and western blot and their sources 62

Table 2.3: List of secondary antibodies used for immunofluorescence labelling and western blot and their sources 63

Table 2.4: List of fluorescent dyes and sources 63

Table 2.5: List of laboratory equipment and sources 63

Table 2.6. List of inhibitors, concentrations used and sources 70

Table 8.1: HL-60/eos trypan blue viability test 243

Table 9.1: Summary of the tarrgeted therapies approved for NSCLC treatment 261

Glossary

ALK - Anaplastic Lymphoma Kinase

AP-1 – Activator Protein 1

ARE – Autophagy-related Endomembrane

Arp2/3 – Actin Related Protein 2/3

AT2 – Alveolar Type II

BAD - BCL-2 Antagonist of Death

Bcl-1 – B-cell Lymphoma 2

BRAF - v-Raf murine sarcoma viral oncogene

BSA – Bovine Serum Albumin

C/EPBβ - CAAT/enhancer-binding Protein β

CCR – CC-chemokine Receptor

CDK – Cyclin-dependent Kinases

COPD – Chronic Obstructive Pulmonary Disease

CTL - Cytotoxic T Lymphocytes

DAPI – Diamindino-2-Pheylindoledihycrochloride

DC – Dendritic Cells

MSO – Dimethyl Sulfoxide

EAR - Eosinophil-Associated RNases

ECP - Eosinophil Cationic Protein

ECM – Extracellular Matrix

EDN – Eosinophil-Derived Neurotoxin

EEP – Eosinophil Extracellular Trap

EGF – Epidermal Growth Factor

EGFR – Epidermal Growth Factor Receptor

EML4 - Echinoderm Microtubule-Associated Protein-Like 4

EMT – Epithelial-Mesenchymal Transition

EPO – Eosinophil Peroxidase

ERK – Extracellular Signal-regulated Kinase

ERBB2 - Epidermal Growth Factor Receptor 2

F-actin – Filamentous actin

FA – Focal adhesion

FAK – Focal Adhesion Kinase

FBS – Fetal Bovine Serum

FERM - Four-point-one, Ezrin, Radixin, Moesin

FGF - Fibroblast Growth Factor

G-actin – Globular actin

GAB1 – GRB2-associated-binding Protein 1

GAP – GTPase-activating protein

GEF – Guanine Nucleotide Exchange Factor

GFP – Green Fluorescent protein

GM-CSF – Granulocyte Macrophage Colony Stimulating Factor

GP130 - Glycoprotein 130

GPCR – G-Protein Coupled Receptor

Grb2 – Growth Factor Receptor-bound Protein 2

GSKβ - Glycogen Synthase Kinase 3β

GTP - Guanosine 5'-Triphosphate

H&E - Hematoxylin & Eosin

HGF - Hepatocyte Growth Factor

HGFA – Hepatocyte Growth Factor Activator

IBD – Inflammatory Bowel Disease

IFN-γ – Interferon-γ

IGF – Insulin Growth Factor

IKK - IκB kinase

IL-1 – Interleukin-1

IL-6 - Interleukin-6

IL-6R – Interleukin-6 Receptor

JAK - Janus Kinase

JNK – c-Jun N-terminal Kinases

LPS – Lipopolysaccharide

KO – Knockout

KRAS - Kirsten rat sarcoma virus

MAPK - Mitogen-Activated Protein Kinase

MBP – Major Basic Protein

MET - Mesenchymal-epidermal transition

MICA - MHC Class I-related chain A

MLC – Myosin Light Chain

MMP – Metalloproteases

mRNA – Messenger RNA

miRNA – MicroRNA

MSC – Mesenchymal Stem Cell

mTOR – Mammalian Target of Rapamycin

NFkB – Nuclear Factor k-light-chain-enchancer of Activated B cells

NGS- Next-generation sequencing

NGS – Next-generation sequencing

NK - Natural Killer

NSCLC – Non-small Cell Lung Cancer

PAX - Paxillin

PDK1 – Phosphoinositide-dependent Kinase-1

PI3K - Phosphatidylinositol-4,5-bisphosphate 3-Kinase

PKA - Protein Kinase A

PKC - Protein Kinase C

PLC - Phospholipase C

PRGF – Plasminogen-related Growth Factors

Rac1 - Ras-related C3 Botulinum Toxin Substrate 1

Rb – Retinoblastoma Protein

ROCK - Rho-associated Protein Kinase

SCC – Squamous Cell Carcinoma

SCLC – Small Cell Lung Cancer

sIL-6R - Soluble Interleukin-6 Receptor

SH2 – Src homology-2 domain

SOS – Son of Sevenless

STAT - Signal Transducer and Activator of Transcription

TABE – Tumour-associated Blood Eosinophilia

TATE – Tumour-associated Tissue Eosinophilia

TGF-β - Transforming Growth Factor β

TKI – Tyrosine Kinase Inhibitor

TLR – Toll-like Receptor

TME – Tumour Microenvironment

TNF-α – Tumour Necrosis Factor α

TNT - Tunneling Nanotube

TP53 – Tumour suppressor gene 53

VEGF - Vascular Endothelial Growth Factor

WL - Wingless

WNT - Wingless-related integration site

WT - Wild type

YAP – Yes-associated protein

1. Chapter 1. General Introduction

1.1 The lung

The anatomy of the lung consists of the proximal, which includes the ciliated cells, secretory club cells, undifferentiated basal cells, goblet cells and neuroendocrine cells whilst the distal airways consist of the alveolar type I and type II cells (Hogan et al. 2014). Moreover, within the airway epithelium, smooth muscle cells, fibroblasts, endothelial cells and immune cells (such as the resident alveolar macrophages and dendritic cells) reside within the lung microenvironment. The alveolar walls are also lined with vascular capillaries to allow for gaseous exchange and for immune cell infiltration (Stevens et al. 2008). Under homeostatic conditions, controlled angiocrine signalling from the endothelium supports the regeneration of the lung alveolus (Lee et al. 2014). The resident macrophages and tissue-resident memory T cells are vital in facilitating the immunological processes within the lung to protect against the development of secondary infections (Takamura 2018).

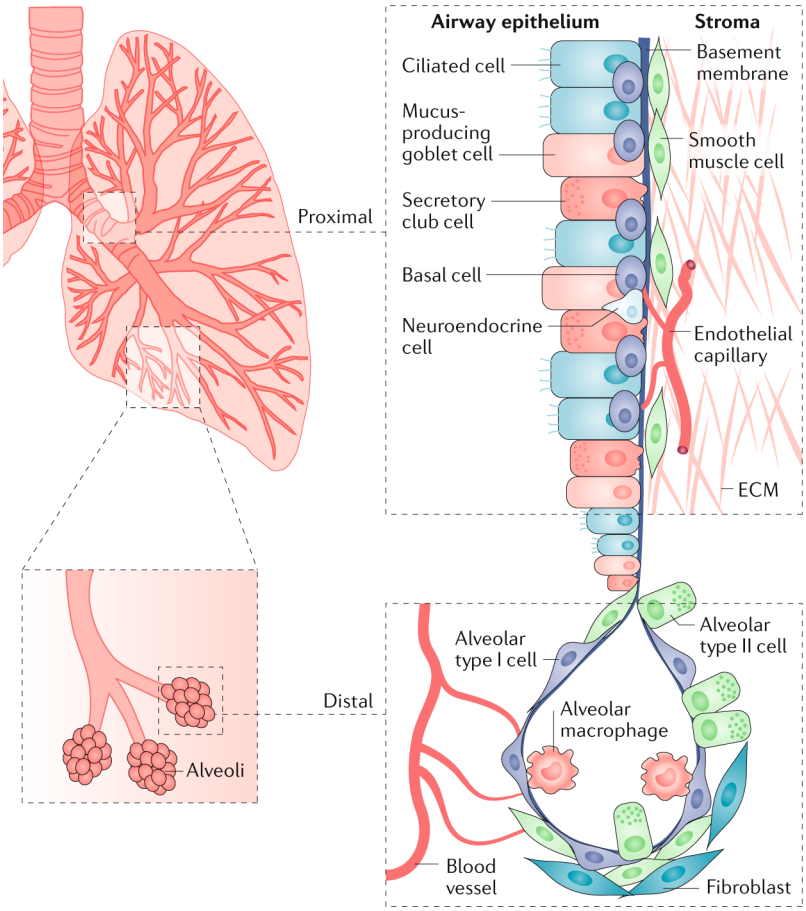


Figure 1: The anatomy of the lung and its heterogenous microenvironment (Altorki et al. 2019).

The lung consists of the proximal and distal airways. Various cell types are found in the proximal airway epithelium which include: ciliated cells, goblet cells, secretory club cells, basal cells and neuroendocrine cells. The stroma of the lining the airway epithelium consists of smooth muscle cells, the endothelial capillary and the extracellular matrix (ECM). The distal airway comprises of alveolar type I and type II cells. The alveolus is also lined with endothelial capillaries to allow for gas exchange and immune cell infiltration.

Although the physiological function of the lung acts as a defensive barrier against airway pathogens, in cancer the cellular features within the lung microenvironment are altered by mutational drivers to support carcinogenesis (Altorki et al. 2019). This gives rise to the different subtypes of lung cancer which are based on its anatomical location and cellular features.

1.2 Lung cancer

Lung cancer accounts for the majority of cancer-related deaths globally (Jemal et al. 2011). Moreover, approximately 70% of patients are diagnosed at a late metastatic stage of the disease (stage III and stage IV)(Travis, Brambilla, and Riely 2013). Lung cancer is also associated with a high mortality rate and has a predicted 5-year survival rate of 15.9% (Jemal et al. 2011; Seigel, Naishadham, and Jemal 2012). Tobacco smoking is the main risk factor for developing lung cancer, with 90% of lung cancer patients being current or former smokers (Alberg et al. 2013). However other environmental risk factors, including exposure to asbestos or ionising radiation, can lead to lung cancer development (Alberg et al. 2013). Lung cancer has been histologically categorised into two groups: 15% are classified as small-cell lung cancer (SCLC) whilst the majority 85% are classified as non-small-cell lung cancer (NSCLC)(Ettinger et al. 2013). The pathophysiology and disease progression between SCLC and NSCLC also vary; SCLC tumours arise from neuroendocrine cells lacking retinoblastoma protein (RB) and TP53 whilst NSCLC tumour development arises from genetic mutations in the lung epithelium (Cruz, Tanoue, and Matthay 2011).

1.2.1 Non-small cell lung cancer

Lung adenocarcinomas (LUAD), squamous cell carcinoma (LUSC) and large cell carcinoma (LCC) are subtypes of NSCLC (Cruz, Tanoue, and Matthay 2011). Each of the subtypes differ in their cellular origin: LUAD originate from alveolar type II (AT2) epithelial cells or cells located in the bronchoalveolar duct junctions, LUSC originate mainly in the bronchi from basal epithelial cells which differentiate into a stratified squamous epithelium and LCC arises from the lung epithelial cells however the lack the cytological features of LUAD and LUSC (Hynds et al. 2021). LUAD represents the majority of NSCLC incidents, especially in Asian women where LUAD accounts for 70% of the Japanese female population (Sanchez-Salcedo et al. 2015). Physiologically, AT2 progenitor cells secrete pulmonary surfactant in the alveoli to reduce the surface tension and prevent alveolar collapse (Sainz de Aja, Dost, and Kim 2021). The malignant transformation of AT2 cells into LUAD is driven by various genetic mutations and the subsequent molecular pathways involved. The diversity in the mutations present in LUAD shapes the heterogeneous molecular pathophysiology of the disease and response to treatment (Best et al. 2019).

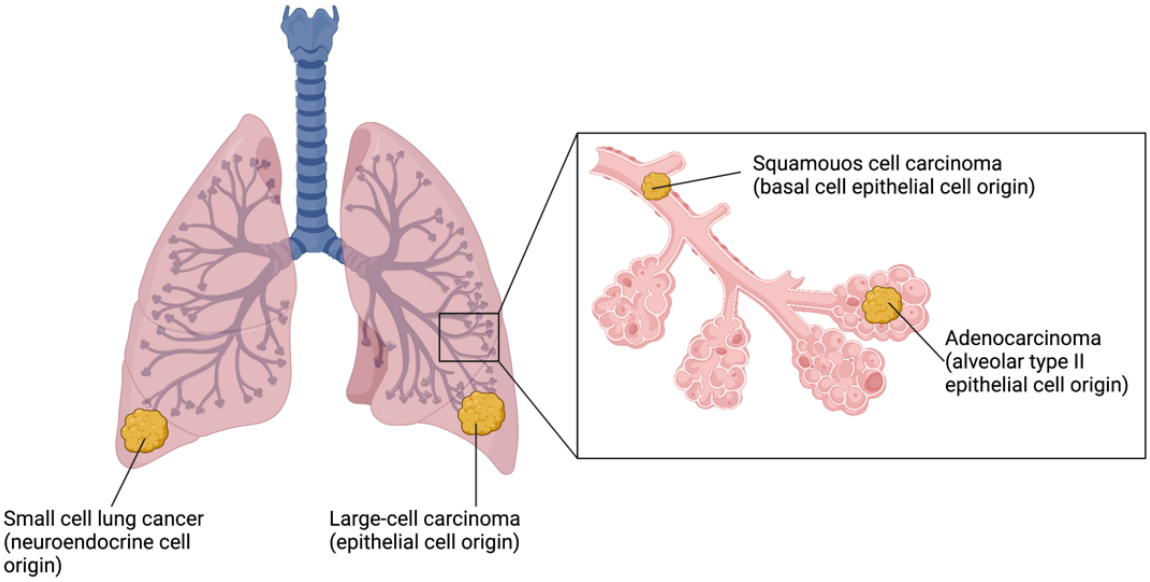


Figure 2: Classification of lung cancer and their cellular origin adapted from (Petrek and Yu 2019)

Lung cancer is classified into either small-cell lung cancer (SCLC, which comprises 15% of lung cancer cases and originates from neuroendocrine cells) or non-small cell lung cancer (NSCLC, which comprises 85% of lung cancer cases and originates from epithelial cells). NSCLC is further classified into three subtypes: adenocarcinoma (LUAD), squamous cell carcinoma (LUSC) and large-cell carcinoma (LCC). The NSCLC subtypes originate from different epithelial cells: LUAD originate from alveolar type II epithelial cells, LUSC originate from basal epithelial cells and LCC derives from various epithelial cells.

Although the tumour epithelial cells possess a range of mutated genes, the mutational heterogeneity also extends to other cell types present within the TME (Junttila and De Sauvage 2013)

1.2.2 The tumour microenvironment

The tumour microenvironment consists of cancer cells and stromal cells surrounded by the ECM. The stromal cells, which include the vascular cells, a diverse range of immune cells and cancer-associated fiborblasts (CAFs) undergo reprogramming by the cancer cells to support tumour growth and metastasis (Hanahan and Weinberg 2011).

Cancer-associated Fibroblasts

CAFs are the most commonly found mesenchymal-derived cells in the TME (Junttila and De Sauvage 2013). Under homeostatic conditions, fibroblasts are involved in wound healing and can inhibit the formation of tumours (Dotto, Weinberg, and Ariza 1988). However, CAFs are able to support cancer progression through enhanced proliferation *via* secretion of a variety of growth factors (including VEGF, PDGF and HGF) (Polanska and Orimo 2013). CAFs also contribute towards the remodeling of the ECM *via* an increase in matrix metalloprotease (MMP) production and enhanced ECM deposition whilst facilitating angiogenesis through the release of pro-angiogenic factors harboured within the matrix (Bergers et al. 2000). The remodeling of the ECM and its pro-tumourigenic integrin-mediated

signalling axis will be discussed in more detail in the latter half of this introduction (see **Introduction, section 1.7**), whilst the individual upregulated growth factor/cytokine signalling in the TME will be explored in **Section 1.2-1.6** of the introduction.

Vasculature

The tumour vasculature is a limiting factor in the growth of the tumour (Ferrara and Kerbel 2005). Cancer cells, natural killer (NK) cells and tumour-associated macrophages (TAMs) produce vascular endothelial growth factor (VEGF) to induce the formation of new vasculature networks (angiogenesis), *via* endothelial cell migration and proliferation, to support the metabolic deficient tumour (Altorki et al. 2019; Hanahan and Weinberg 2011). The process of angiogenesis within the TME also requires degradation and reconstruction of the existing vascular basement membranes and recruitment of endothelial precursors derived from the bone marrow (Kalluri 2003). Vascularisation can vary within the TME with hypoxic microenvironments arising from poorly organised vasculatures and prolonged distance from the vascular bed (Trédan et al. 2007). This leads to inter- and intra-tumour heterogeneity in vascularisation which can influence the prognostic outcomes in NSCLC (Meert et al. 2002).

Immune cells

Within the TME of NSCLC, the innate and adaptive immune cells are able to exert both pro-tumourigenic and anti-tumourigenic effects (Gajewski, Schreiber, and Fu 2013). Myeloid-derived dendritic cells (DC) are known to exert its anti-tumoural effects by cross-presenting tumour antigens thus priming T lymphocytes in the lymph nodes (Kastenmüller et al. 2014). T lymphocytes, specifically $CD4^+$ and $CD8^+$ T cells, infiltrate tumours to exert its cytotoxic effect and facilitate the response to immune checkpoint inhibition (ICI) (Kastenmüller et al. 2014). TAMs and neutrophils also infiltrate the TME however they play a more complex role within the TME. TAMs exist in a range of phenotypes including M1 macrophages, which are associated with pro-inflammatory and anti-tumourigenic effects, whilst M2 macrophages are associated with pro-angiogenic and pro-tumourigenic effects through supressing the immune response (Almatroodi et al. 2016). Likewise with TAMs, neutrophils have been shown to exert either pro-tumourigenic, by enhancing angiogenesis, metastasis, or anti-tumourigenic effects, through an increase in expression of cytotoxic mediators (Sionov, Fridlender, and Granot 2015). Neutrophils are also the most commonly abundant immune cell within the TME of NSCLC and its presence has been associated with poor patient prognosis (Engblom et al. 2017). Eosinophils are also able to infiltrate many tumours and interact within the TME (Davis and Rothenberg 2014), however eosinophils are an understudied immune cell in cancer and limited studies have investigated their role in NSCLC. Moreover, eosinophil-derived MBP were found present in the

tissue of lung metastases (Mattes et al. 2003).Therefore, the function of eosinophils and their role in NSCLC will be further explored in more detail in this thesis.

Eosinophils

Eosinophils are end-stage granulocytes involved in the host defence against parasitic infections and in the inflammatory mechanisms of allergies. They are derived from the pluripotent progenitors in the bone marrow and circulate in the bloodstream before being recruited to the appropriate tissue in response to cytokine interleukin-5 (IL-5)(which induces a sustained survival in the tissue) and eotaxin chemokines (which are the main chemokines for eosinophils) (Blanchard and Rothenberg 2009). Eosinophils consists of a bilobed nucleus surrounded by the cytoplasm which contain an accumulation of specific granules (Weller et al. 1994). Each granule contains a trilaminar matrix enclosing a densely packed crystalline core which is covered in a less dense matrix (Figure 3). When degranulated, cytotoxic granules are released which can damage tissue. The granules mainly consist of four major proteins: major basic protein 1 and 2 (MBP1, MBP-2) which are located in the crystalloid core and the matrix consisting of eosinophil peroxidase (EPO), the ribonucleases eosinophil cationic protein (ECP) and eosinophil-derived neurotoxin (EDN) (as reviewed in (Rosenberg, Dyer, and Foster 2013)). Degranulation of the specific granules occurs as part of a controlled response to an external stimulus and the contents of the granules are released through membrane-bound vesicles (also known as eosinophil sombrero vesicles) whilst the eosinophil itself remains intact. This process is termed 'piecemeal degranulation' and is the main form of eosinophil degranulation (Dvorak, Estrella, and Ishizaka 1994). Additionally, the granules also consist of other cytokines (including IL-6), enzymes and growth factors (including HGF) (Hamid et al. 1992; Cui et al. 2003).

Eosinophils can also express a wide range of surface molecules to facilitate adhesion, growth, chemotaxis, degranulation and cellular interaction (Fig.2). These receptors include adhesion molecules, chemokine receptors, cytokine receptors, immunoglobulin receptors, TLR and Siglec-lectin receptors (as reviewed in (Rosenberg, Dyer, and Foster 2013)). Most notably, the interleukin-5 receptor subunit-α (IL-5Rα) and CC-chemokine receptor 3 (CCR3) are the characteristic receptors associated with eosinophils. CCR3 induces eosinophil chemotaxis when bound to eotaxin-1 (CCL111), eotaxin-2 (CCL24) and eotaxin-3 (CCL26) whilst IL-5 binds to IL-5Rα and mediates the development, activation, and survival of eosinophils. CCR3/eotaxin interactions can also cooperate with IL-5 to induce eosinophilia. Eosinophils also express pattern-recognition receptors (PRRs) which are vital in launching the immune response (Rosenberg, Dyer, and Foster 2013).

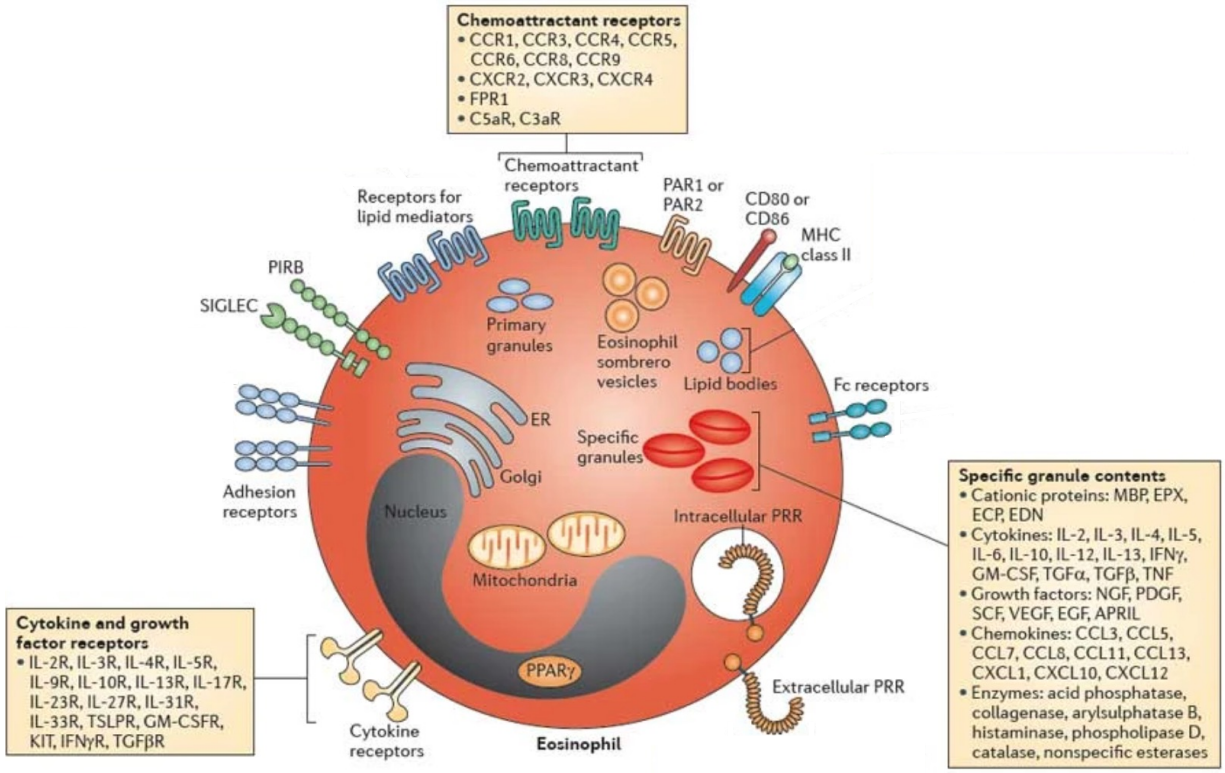


Figure 3: The cellular characteristics of eosinophils adapted from (Rosenberg, Dyer, and Foster 2013)

The schematic diagram of the eosinophil details and lists the various receptor expression which includes adhesion molecules, chemokine receptors, cytokine receptors, immunoglobulin receptors, Toll-like recognition receptors (TLR) and siglec-lectin receptors. Eosinophils also release the contents of their granules when activated. The contents of the granule are also listed and include various cationic proteins, cytokines (including IL-6), growth factors, chemokines and enzymes.

Eosinophils play a multifaceted role in cancer, either inducing improved prognosis or contributing to the deteriorating progression (Sakkal et al. 2016). The prognostic outcome relating to eosinophilia varies in the different types of cancers. A favourable prognosis was observed in colorectal (Cheadle et al. 2007), oral squamous (Dorta et al. 2002b) and prostate cancer (Furbert-Harris et al. 2003). Whilst a poor prognosis was observed in cervical cancer and Hodgkin's lymphoma (Glimelius et al. 2011). However, the mechanism underlying the varied prognostic outcomes remains unclear and there has been limited studies investigating the role of eosinophils in NSCLC. Pandit et al and Verstraeten et al reported two case studies whereby two patients with elevated serum levels of IL-5 with inflammatory lung disease (COPD) were later diagnosed with NSCLC and presented with significant levels of tumour-associated eosinophilia (Pandit et al. 2007; Verstraeten et al. 2011). When the tumour was surgically removed, the levels of intracellular IL-5 and eosinophil normalised which suggests the tumour-associated eosinophilia was mediated by tumour cells secreting IL-5 (Verstraeten et al. 2011; Pandit et al. 2007). Although this observation has only been reported in two

patients with NSCLC, this provides molecular insight to eosinophilia as a potential consequence of tumourigenic processes including tumour necrosis. Eosinophil-derived MBP was also found in the tissue of lung metastases (Mattes et al. 2003).. ECP induces cancer cell death in human oral squamous cell lines through osmotic lysis whereby it binds to the membrane of the tumour cells to form pores thus destabilising the membrane (Dorta et al. 2002b). Despite the evidence of eosinophils exerting a tumouricidal effect in cancer, conversely eosinophils can increase proliferation and induce anti-apoptotic signals through its expression of CD30 and CD40 ligands which can bind to their receptors found in Hodgkin's lymphomas. Eosinophils also produce VEGF, IL-8, TGF, granulocyte macrophage colony stimulating factor (GM-CSF) and fibroblast growth factor-2 which can potentially contribute to tumour growth, extracellular matrix formation and angiogenesis (Davis and Rothenberg 2014) although this has not yet been demonstrated in the tumour microenvironment.

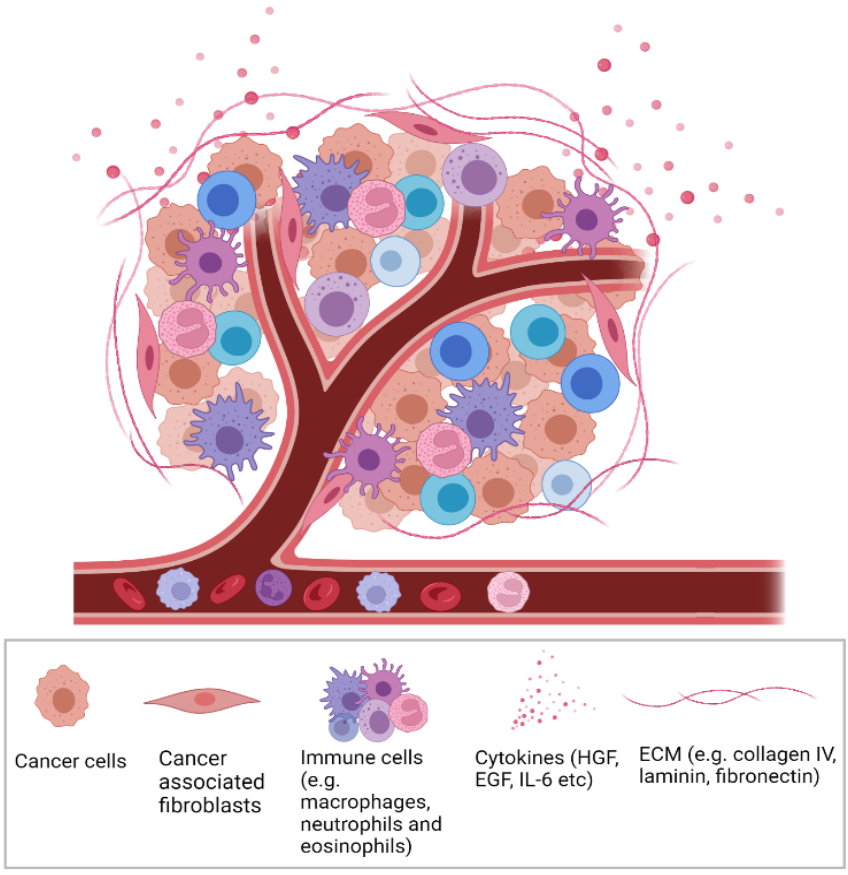


Figure 4: The tumour microenvironment.

The heterogenous tumour microenvironment consists of a diverse range of cells including cancer cells, CAFs and immune cells (e.g. DC, T lymphocytes, TAMs, neutrophils and eosinophils) which infiltrate the tumour via the vasculature of the TME. The cells are also adhered to the ECM which undergoes remodeling in NSCLC. The various cell types within the TME release a variety of pro-tumourigenic cytokines/growth factors, including HGF, IL-6, EGF and FGF2.

Overall, the malignant cancer cells continuously coordinate with various cells within the TME, either through direct cell contact with stromal components or growth factor/cytokine signalling, to drive NSCLC progression (Altorki et al. 2019). Moreover, the heterogenous niche of the TME can alter the response to drug treatment and promote resistance to therapies (Altorki et al. 2019).). Personalised multi-drug targeting is therefore key to fully ameliorating the pro-tumourigenic effects induced by the TME.

1.2.3 Treatment of non-small cell lung cancer

Patients are initially assessed for surgical removal of the tumour regardless of the stage of lung cancer diagnosis however patients ineligible for surgery can undergo radiotherapy to reduce or eliminate the tumour (Zappa and Mousa 2016). Roughly 40% of patients that are diagnosed with stage IV lung cancer are subjected to a combination of a platinum-based drug (either cisplatin or carboplatin) alongside paclitaxel, gemcitabine, docetaxel, vinorelbine, irinotecan or pemetrexel (Masters et al. 2015). The combination of chemotherapeutics administered are based on the individual tolerance and frequency of toxic side effects (Zappa and Mousa 2016). However, the median survival of patients receiving platinum-based doublet therapy was approximately 8-10 months (Scagliotti et al. 2015; Kelly et al. 2001; Schiller et al. 2002). More recently, through novel bioinformatics and next-generation sequencing analyses of patient data, several recurrent gene mutations and amplifications have been identified in NSCLC with the potential as actionable drug targets (Lemjabbar-Alaoui et al. 2015). Genomic analysis of 230 LUADs by the Cancer Genome Atlas Research Network (TCGA) revealed the prevalence of various oncogenic driver alterations: 46% of patients harbouring mutations for TP53 (tumour suppressor gene 53) alongside mutations in KRAS (Kirsten rat sarcoma virus oncogene)(33%), EGFR (epidermal growth factor receptor 1)(14%), BRAF (v-Raf murine sarcoma viral oncogene)(10%), MET (mesenchymal-epidermal transition oncogene)(7%), ERBB2 (epidermal growth factor receptor 2 oncogene)(1.7%), ALK (anaplastic lymphoma kinase)(1.3%), ROS1 (which encodes for the tyrosine kinase ROS)(1.3%) and RET (rearranged during transfection)(0.9%) oncogenes (Network 2014). This has led to the development of targeted therapies in LUAD, mainly EGFR tyrosine kinase inhibitors (TKIs), ALK inhibitors and ROS1 inhibitors, which has improved outcomes in patient response and survival (Zappa and Mousa 2016). However, prolonged treatment with the targeted kinase inhibitors has also resulted in the development of resistance within 9-12 months (Katayama et al. 2012; Kobayashi et al. 2005). Most notably, secondary mutations in the addition of kinase domains in echinoderm microtubule-associated protein-like 4 (EML4)-ALK was identified (Katayama et al. 2012) whilst EGFR-T790M mutations resulted in a higher binding affinity to ATP thus outcompeting EGFR TKI binding (Kobayashi et al. 2005). Moreover, the mutationally upregulated MET kinase signalling has been

implicated in EGFR TKIs resistance (Engelman, Zejnullahu, Mitsudomi, et al. 2007). The hepatocyte growth factor (HGF) ligand-dependent activation of the MET receptor, c-Met, also mediates EGFR resistance in the absence of MET gene amplification (Yano et al. 2008; Yamada et al. 2010). Therefore, to effectively curb resistance, growth and metastasis in NSCLC, a personalised multi-drug strategy must be implemented. Despite the potential therapeutic benefits of c-MET inhibitors for patients harbouring MET gene mutations or upregulating HGF/c-Met signalling, the advancement of therapies targeting MET and its tyrosine kinase activity has had limited success (Liang and Wang 2020). This emphasises the need to extensively study the complex molecular mechanisms regulating HGF/c-Met signalling in NSCLC and the microenvironmental factors regulating the pro-tumourigenic outcomes.

1.3 Hepatocyte Growth Factor and c-Met

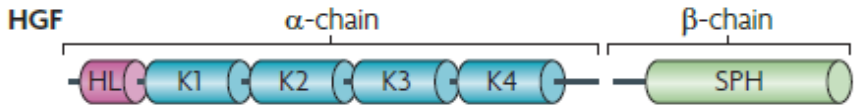


Figure 5: Structure of HGF (Trusolino, Bertotti, and Comoglio 2010)

HGF is secreted as a single-stranded inactive protein form containing 728 amino acids (Mason 2002) which is then converted by extracellular serine proteases (HGF activator) to form a mature heterodimer consisting of a 62 kDa α chain (heavy chain) and a 34 kDa β chain (light chain), linked by a signalling bond (Trusolino, Bertotti, and Comoglio 2010). The α chain includes an N-terminal hairpin loop (HL) and four kringle domains (K1-4). Each kringle is held structurally by three signalling bonds. K1 is essential in providing the high-affinity binding site to c-Met (Maulik, Shrikhande, et al. 2002). The β chain contains a serine protease homology (SPH) however it does not exert any proteolytic activities due to substitution mutations causing glutamate and tyrosine residues in place of the active site instead of histidine and serine residues (Maulik, Shrikhande, et al. 2002).

HGF is part of the plasminogen-related growth factors (PRGF) and was initially discovered as a mitogen for hepatocytes whilst scatter factor was separately identified for its disassociation of MDCK cells having derived from fibroblasts. Both were found to be identical giving rise to its current term HFG/SF. Secretion of HGF occurs through stromal, epithelial or tumour cells which gives rise to paracrine or autocrine signalling loops (Finocchiaro et al. 2015). Mesenchymal cells, specifically endothelial cells and alveolar macrophages in rat lung (Yanagita et al. 1992), are the main source of HGF expression along with fibroblasts (Papaccio et al. 2018). It exists as a single-chain precursor when released and is transformed by extracellular proteases into a mature two-chain heterodimer. It is located inactively bound to the extracellular matrix in the majority of tissues by heparin-like proteoglycans (Trusolino, Bertotti, and Comoglio 2010).

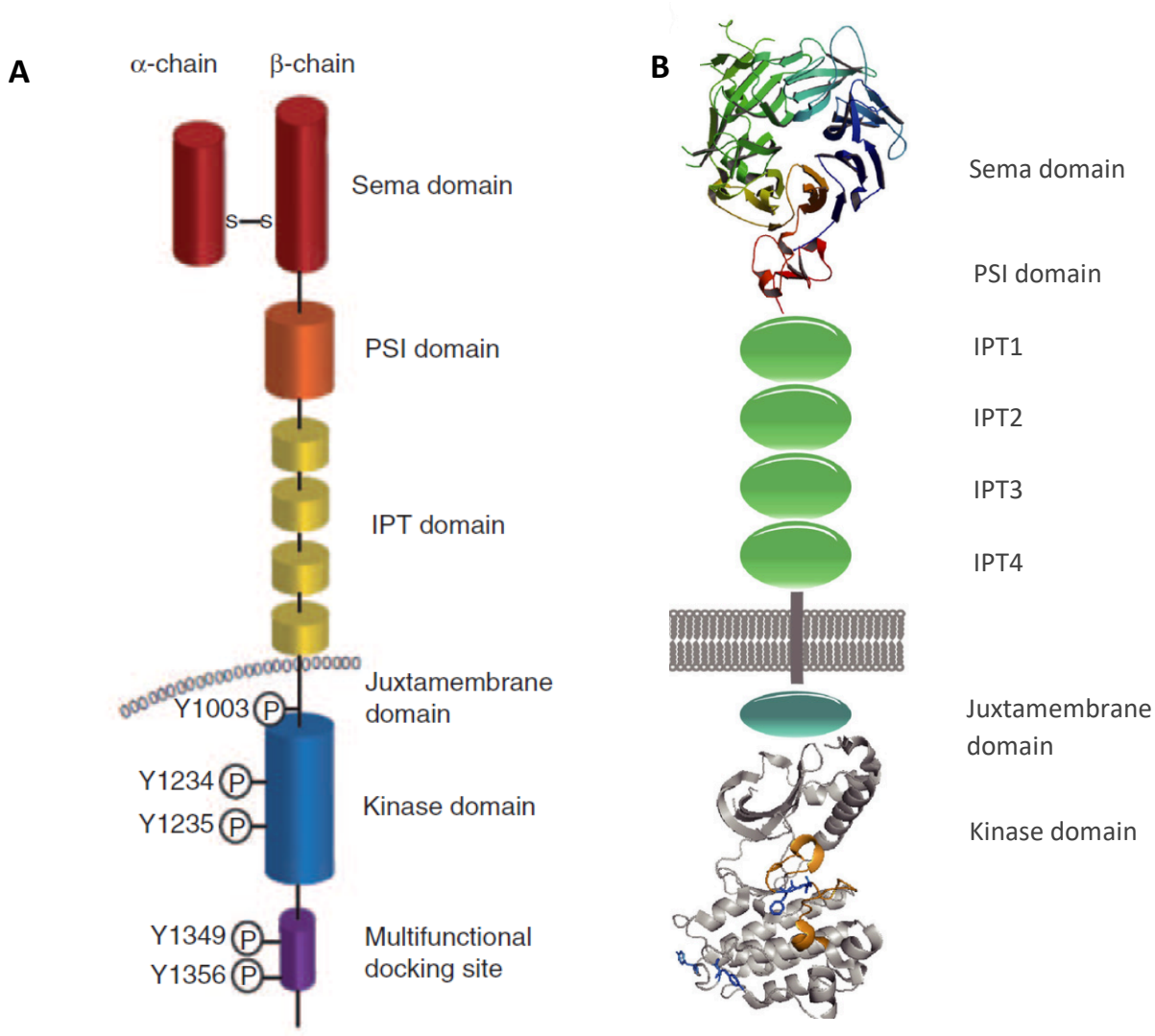


Figure 6: Structure of c-Met adapted from (Organ, Tsao, and de Bono 2011; Matsumoto et al. 2017)

A. The mature MET receptor is a heterodimer consisting of an α-subunit and a β-subunit, which spans from the extracellular region to the membrane and possesses catalytic activity, joined together by a signalling bond. There are three domains in the extracellular space: Sema (500 residues folded at the N-terminus) which entirely includes the α-subunit and a part of the β-subunit; the PSI domain located at plexins, semaphorins and integrins and includes around 50 residues held by four signalling bonds; four IPT domains (1-4) with 400 residues in total and structurally similar to immunoglobulin folds. The intracellular region includes a juxtamembrane sequence, a catalytic region (including tyrosine kinases Y1234 and Y1235, as part of the activation loop) and a carboxy-terminal docking site, Y1349 and Y1356 attracting a variety signalling molecules. Phosphorylation of Y1003 results in negative regulation of the kinase activity whilst trans-phosphorylation of the tyrosine residues in the catalytic region regulates activity (Trusolino, Bertotti, and Comoglio 2010).

B. A 3D representation of c-Met showing the corresponding structures highlighted above.

C-Met was initially identified as an activated oncogene in human osteogenic sarcoma cell line (Park et al. 1986). The Met gene is a proto-oncogene and is located on chromosome 7 at q21-31 and is translated to a 1408 amino acid polyprotein (Park et al. 1987). It is then cleaved to its mature

heterodimer form on the cell surface (Zhang and Vande Woude 2003). It is expressed in the epithelium where it is sequestered mainly at the intercellular junctions along with E-cadherin (Conway et al. 2006). Receptor expression is stimulated by the presence of HGF, epidermal growth factor, phorbol myristate, concanavalin A, IL-1 and IL-6, tumour necrosis factor-α (TNF-α) and hormones such as oestrogen, progesterone, tamoxifen and dexamethasone (Boccaccio et al. 1994; Moghul et al. 1994).

The α-chain of HGF binds with high affinity to c-Met and identifies IPT3 and IPT4 domains regardless of HGF maturation. The low-affinity binding occurs at the β-chain and the site is revealed only following HGF activation and interaction with the Sema domain (Trusolino, Bertotti, and Comoglio 2010).

1.3.1 Intracellular signalling

The receptor kinase activity is activated upon HGF binding, followed by receptor signalling and trans-phosphorylation of Y1234 and Y1235 activating the intrinsic kinase activity consequently leading to the phosphorylation of the tyrosine residues in the carboxy-terminal (Trusolino, Bertotti, and Comoglio 2010). The carboxy-terminal provides a multisubstrate docking site which binds to various adaptor proteins: PI3K, growth factor receptor-bound protein 2 (GRB2), Src, SHC adaptors, SHP2, phospholipase Cγ1 (PLCγ1) and transcription factor signal transducer STAT3. Further recruitment of downstream molecules (SHC, PI3K, SHP2, CRK, PLCγ1 and p120 Ras-GTPase-activating protein) is facilitated via GRB2-associated-binding protein 1 (GAB1). The intricate signalling causes altered gene expression in the nucleus. The main signalling pathways relating to proliferation, differentiation and growth will be covered below (Trusolino, Bertotti, and Comoglio 2010).

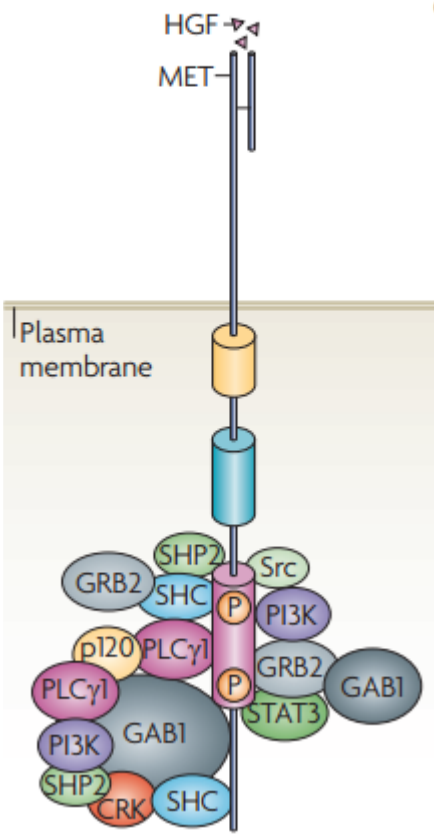


Figure 7: The HGF/c-Met signalling pathway components (Trusolino, Bertotti, and Comoglio 2010)

The c-terminal of the c-Met receptor allows for multiple substrates to bind, this includes molecules with Src homology-2 domain (SH2 domain) such as PI3K, Src, Grb2, SHC, SHP2, PLCγ1 and STAT3 transcription factor. C-Met binds directly to GAB1 (a multi-adaptor protein) *via* its 13 amino-acid binding site (MBS) and indirectly *via* GRB2 bounded to c-Met. GAB1 further recruits SHC, PI3K, SHP2, CrK, PLCγ1 and p120-rasGAP. The numerous components involved in the signalling are involved through various interactions with c-Met, GAB1 or both [3].

MAPK cascades

The mitogen-activated protein kinase (MAPK) cascades feature signalling pathways leading to the final effectors: extracellular signal-regulated kinase 1 and 2(ERK1/ERK2), Jun amino-terminal kinases (JNKs) and p38. Activation of ERKs are led by activation of Ras, a small GTPase, via Grb2-SOS (son of sevenless) complex bound to either the docking site in the C-terminal or through SHC adaptor protein (Ponzetto et al. 1994). SHP2 is also able to activate the Ras-ERK pathway by inhibiting a deactivator of Ras, p120-Ras-GAP, *via* dephosphorylation of its binding site on GAB1 (Maroun et al. 2000). Subsequently Ras activation causes RAF kinases to activate the MEPK subfamilies through to the final effector ERK1 and ERK2 via phosphorylation. Translocation of active ERKs to the nucleus occurs whereby activation of transcription factors regulating G1-S of the cell cycle thus stimulating cell cycle progression, proliferation and scattering (Organ, Tsao, and de Bono 2011). JNKs and p38 are activated by Rac via Ras-PI3K signalling route. This leads to phosphorylation and activation of MEK4 and MEK7, activating JNK1, JNK2 and JNK3 whilst MEK3 and MEK6 activates p38α, p38β, p38γ and p38δ. These mediate effects including differentiation, apoptosis, proliferation and transformation (Trusolino, Bertotti, and Comoglio 2010).

PI3K-Akt axis

Activation of PI3K occurs either through MET or via Ras and this leads to the association of Ser/Thr kinase Akt in the cell membrane. Akt inhibits apoptosis and promotes cell survival by suppressing

apoptotic favouring proteins p53 by activating MDM2 protein ligase and BCL-2 antagonist of death (BAD). Additionally, Akt inhibits cell cycle progression by inhibiting expression of Myc and cyclin D1 via inactivation of glycogen synthase kinase 3β (GSKβ) and inhibits cell growth and protein synthesis via stimulating mammalian target of rapamycin (mTOR) (Trusolino, Bertotti, and Comoglio 2010). The PI3K-Akt pathway is the key driver in promoting cell survival (Xiao et al. 2001). Sustained activation of PI3K in small cell lung cancer (SCLC) promotes invasion via proliferation and anchorage-independent survival (Maulik, Madhiwala, et al. 2002).

STAT pathway

STAT3 binds to the SH2 domain of the c-terminal of the receptor stimulating MET-dependant phosphorylation and leading to eventual detachment and signalling (Trusolino, Bertotti, and Comoglio 2010). The dimers translocate to the nucleus and alters gene expression causing epithelial tubulogenesis (Boccaccio, Ando, et al. 1998) and anchorage-independent cell growth (Fixman et al. 1996).

IκBα–NF-κB complex

NF-κB, a transcription factor located in the cytoplasm mainly kept in its inactive form by inhibitory nuclear factor-κB inhibitor-α (IκB) proteins, activates transcription of genes leading to formation of regulators of mitosis and anti-apoptosis (Müller, Morotti, and Ponzetto 2002). The Iκbs phosphorylation degradation event is stimulated by IκB kinase (IKK) via the PI3K-Akt signal and Src relay pathway however the main stimulatory driver for this event is unknown (Fan et al. 2005).

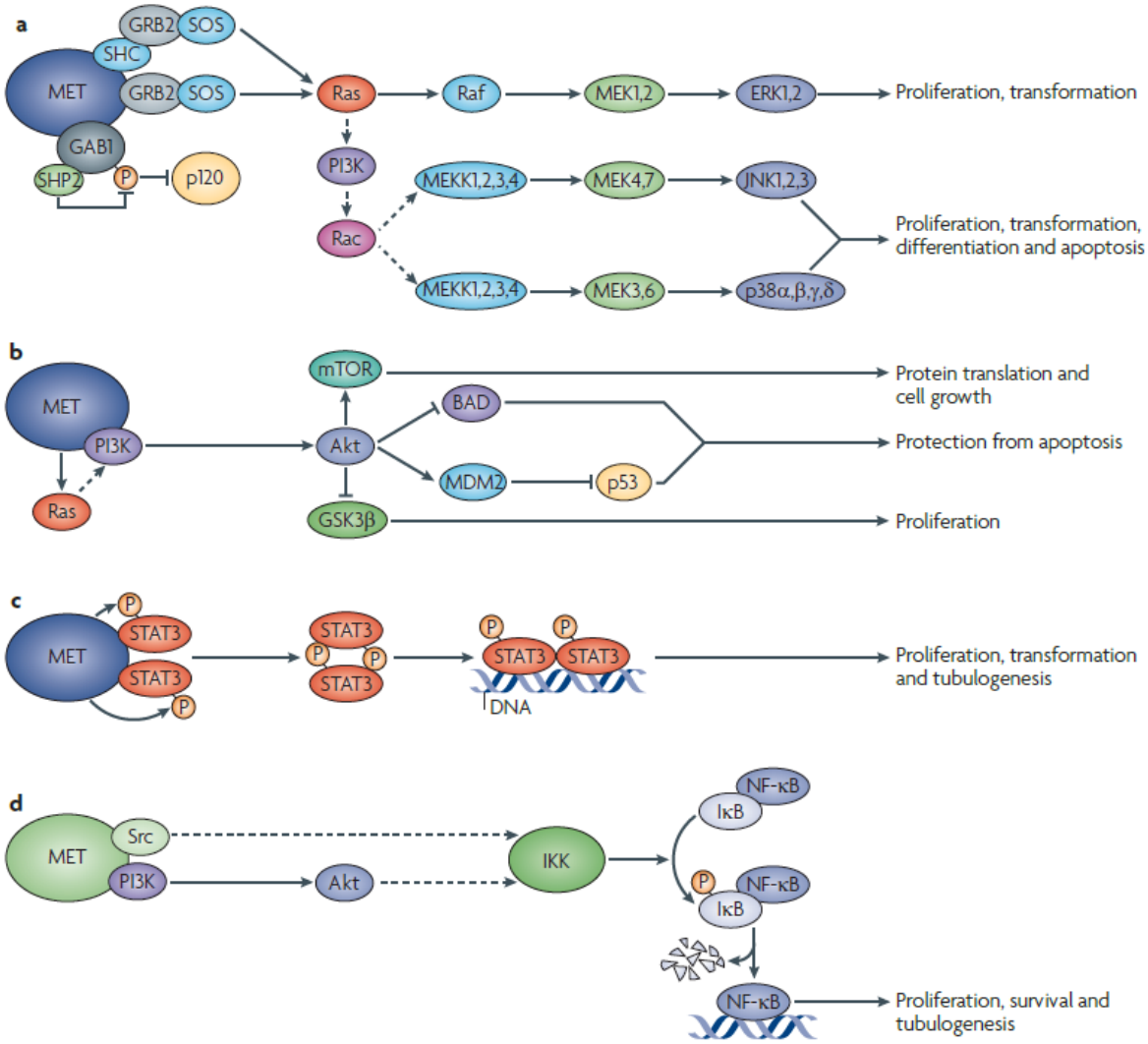


Figure 8: Diagram depicting the main HGF/c-Met downstream signalling pathways (Trusolino, Bertotti, and Comoglio 2010)

The diagrams represent the main signalling pathways of c-Met, each pathway is summarised below:

- **a.** MAPK cascades activate three protein kinase subfamily one after the other and occur via Ras, which is activated by son of sevenless (SOS). P120 Ras-GAP(p120) can prevent activation of Ras. The final effector: ERK, JNK and p38, are able to alter gene expression relating to proliferation, apoptosis and differentiation.
- **b.** PI3K binds to the multifunctional docking site of c-Met leading to the recruitment and activation of Akt. Phosphorylation of the signalling components leads to cell survival, growth and proliferation.
- **c.** STAT3 undergoes trans-phosphorylation after binding to c-Met leading to the signalling of the transcription factor. The dimers migrate to the nucleus and alter gene expression relating to tubulogenesis and proliferation.
- **d.** Nuclear factor-κB inhibitor-α kinase (IKK) is activated via the PI3K and Src signalling and phosphorylates NF-κB associated with nuclear factor-κB inhibitor-α (IκB) proteins. This leads to the ubiquitin-dependant degradation of IκB and transcription of regulatory genes for proliferation, survival and tubulogenesis.

1.3.2 Biological role of hepatocyte growth factor

HGF is essential for embryogenesis and development of the lung (Yamamoto et al. 2007) and other organs (Birchmeier and Gherardi 1998) in physiological conditions. It exhibits tissue reparative properties involving organ regeneration and wound healing. C-Met operates its biological effects in a regulated manner to sustain tissue homeostasis and normal organ functioning.

Lung regeneration

During organ regeneration, HGF/c-Met signalling contributes to the structural changes required to achieve normal tissue patterning. Epithelial cells, attached to the collagen matrix, are able to undergo cellular transformation from spheroids to tubular structures induced by HGF. Epithelial-mesenchymal transition (EMT) is the initial step in the transformation and is mediated by the Raf-MEK-ERK signalling. The STAT3 and NF-κB signalling pathways plays a role in the tubular transformation. Metalloproteases (MMPs) are required for the formation of hollow tubules and HGF activates the mature forms of MMPs and upregulates their transcription (Trusolino, Bertotti, and Comoglio 2010).

HGF undertakes an important role in tissue repair of organs including the lung whereby expression is mediated in response to injury (Yanagita et al. 1993). It also acts in an endocrine manner, whereby elevation of HGF was observed in the lung in response to hepatic injury, therefore, aiding in organogenesis (Yanagita et al. 1992). Studies also indicate HGF in inducing the proliferation of alveolar epithelial cells and the surrounding endothelial vasculature (Sakamaki et al. 2002; Ishizawa et al. 2004). Furthermore, HGF inhibits apoptosis and has demonstrated its ability in overriding TGF-β1 growth arrest (Taipale and Keski-Oja 1996), promoting respiratory endothelial and epithelial growth and survival (Panganiban and Day 2011). Unpublished results have shown HGF increases proliferation in the presence of ECM components such as collagen I, IV and to a lesser extent with laminin in healthy alveolar epithelial cells *via* β1-integrin.

Wound healing

HGF is heavily implicated in wound healing processes. *In vivo*, c-Met plays a role in epithelial hyperproliferation which allows the migration of the epithelium supply from the wound edge to the surrounding matrix of the wound; HGF is also required in the alignment of keratinocytes. The GAB1, Akt, ERK 1/2 signalling are essential to mediate these effects. (Trusolino, Bertotti, and Comoglio 2010)

HGF induces angiogenesis stimulating endothelial cell proliferation and migration to form capillary tubules. HGF activity is increased following injury via upregulation of HGF mRNA and recruitment of HGF activator (HGFA) bound to the ECM allowing localized HGF activation (Conway et al. 2006). The

precursor of HGFA is also converted to its mature form as a response to the clotting cascades (Naldini et al. 1995). HGF, as a morphogen and an inducer of epithelial-mesenchymal transition, contributes to tissue remodelling process of epithelial to mesenchymal transition to facilitate migration (Conway et al. 2006). There are several features of HGF which may contribute to wound healing however the links and the activation mechanisms have not been established. Neutrophils, involved in the immune response, contain a store of HGF and HGF is a priming factor for neutrophils therefore neutrophil migration may be associated with HGF transfer to the wound site. HGF also induces the production of MMPs and uPA which may participate in the matrix degradation (Conway et al. 2006).

The pathological development of organ regeneration and wound healing coincide with tumour metastasis. Cancer cells exploit the regulated biological processes of HGF/c-Met and contribute to the invasion of tumour cells. Successful invasion requires enhanced motility, suppression of apoptosis and stimulation of proliferation, these are achieved through upregulation of activity and the mutations arising in HGF and c-Met.

1.3.3 HGF/c-Met mutations in non-small cell lung cancer

Poor prognosis with significant mortality is associated with overexpression of HGF and c-Met in NSCLC (Ichimura et al. 1996). The Met gene is overexpressed in NSCLC cell lines and promotes proliferation and growth (Lutterbach et al. 2007). Amplification of c-Met mRNA expression in 35% of lung adenocarcinomas was positively associated with tumour differentiation (Tsao et al. 1998). The amplification and overexpression subsequently cause persistent activation of the downstream signalling cascades leading to increased proliferation and invasion. The deletion of exon 14, which encodes for the juxtamembrane region regulating the inhibitory kinase activation, has been reported in NSCLC, thus serving as a vital oncogenic target (Frampton et al. 2015; Awad et al. 2016). Missense mutations on the juxtamembrane domain of c-Met was identified in SCLC which led to motility, migration and enhanced signalling *via* the focal adhesion protein paxillin (Ma, Kijima, et al. 2003). Mutations in the Sema domains were identified in SCLC and adenocarcinomas of lung (Ma et al. 2005). Lung adenocarcinoma cell lines with mutated c-Met had an absence of Y1003 (Onozato et al. 2009), required for recruitment of CBL, thus decreased ubiquitination was observed and oncogenic activation led to sustained Ras-MAPK signalling (Lai, Abella, and Park 2009). Furthermore, an increase In transcriptional expression of the wild-type receptor is triggered by the hypoxic environment, inflammatory cytokines, angiogenic factors and HGF itself, all of which originate from the surrounding tumour stroma (Boccaccio et al. 1994; Pennacchietti et al. 2003).

Conversely, although increased levels of HGF or MET mutations have been observed, this is not always correlated with receptor activation and activity. One study reported a significant difference between HGF protein expression, at 57%, and Tyr1234/1235 phospho-MET activity, which is indicative of receptor activation, at 7% (Onitsuka et al. 2010). Additionally, a study analysing 906 NSCLC patient specimens found 22.2% of c-Met expression compared to only 5.6% of activated Tyr 1234/1235 phospho-MET (Tsuta et al. 2012). Furthermore, transcriptional c-Met overexpression and activation is heavily influenced through crosstalk with other molecules to induce synergistic activation of its downstream cascades (Finocchiaro et al. 2015). Therefore, the crosstalk between HGF/c-Met and its signalling partners such as IL-6 highlight the importance of overcoming cancer progression.

1.4 Interleukin 6

IL-6 is a pleiotropic cytokine and was initially discovered as a T-cell-secreted mediator of B cell differentiation. It is a glycoprotein with 184 amino acids in a 4 helical bundle structure with a molecular weight of 26kDa. It is established in a variety of biological roles involving the immune system, haematopoiesis and cancer progression (Guo et al. 2012). *In vivo*, monocytes and macrophages mainly produce IL-6 at inflammatory sites although various other cell types are also able to produce IL-6. During homeostasis, the serum levels of IL-6 remain low but are elevated in stress conditions. NF-κB, C/EPBβ (CAAT/enhancer-binding protein beta) and AP-1 (activator protein 1) induce IL-6 production. Inflammatory stimuli such as TNF-α, IL-1, lipopolysaccharide (LPS), viral infections, bacterial products and necrotic products stimulate the activation of these transcription factors. Toll-like receptors (TLRs), which are involved in recognising pathogens for the innate immune system, can also stimulate the production of IL-6 when TNF-α and IL-1 are not involved in IL-6 production (Naugler and Karin 2008). Following secretion of IL-6, it can signal and exert its effects to local cells or to other cells systemically.

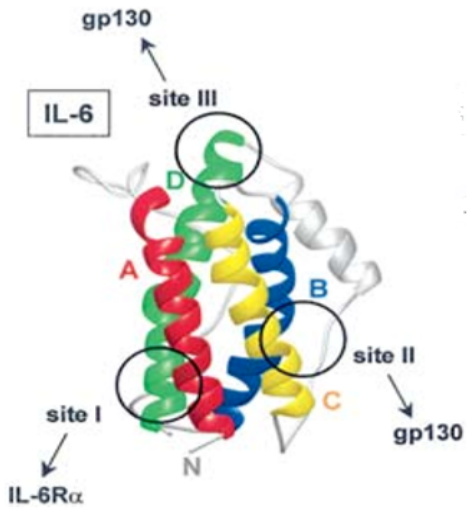


Figure 9: Structure of IL-6 (Heinrich et al. 2003)

The IL-6 tertiary structure consists of a four helical structure (labelled A, B, C and D) joined by connecting grey loops. There are three available binding sites (site I, II and III) for IL-6Rα and gp-130.

1.4.1 Intracellular signalling

There are three signalling pathways for IL-6: *classic, trans-signalling* and more recently discovered *trans*-presentation. In *classic signalling*, IL-6 binds with the non-signalling transmembrane IL-6α receptor (also termed mbIL-6R or CD126) on target cells, this complex then binds with the homodimer of the type I transmembrane transducer protein gp130 (also termed CD130). The complex causes the signalling of both gp130 molecules. Gp130 is expressed in many cell types whereas IL-6R is only found in certain cells such as macrophages, neutrophils, a few T-cells and hepatocytes, therefore, limiting IL-6 classical signalling response on cell types. The consequent attachment and activation of Janus kinase (JAK1) occur at the intracellular section of gp130. STAT3 is then phosphorylated, dimerizes, and translocated to the nucleus inducing gene expression and promoting proliferation, differentiation and inhibition of apoptosis through binding of p53. The genes encoded for Bcl2, Bcl-xL, JunB, cFos, C/EPB, IRF-1 (interferon response factor 1), LPS-binding protein, TIMP (tissue inhibitor of metalloprotease 1) and SOCS3 (suppressor of cytokine signalling 3) are also activated through the IL-6-STAT3 signalling. SOCS3 feedback inhibitors and the PIAS (protein inhibitor of activated STAT) negatively regulate the IL-6-STAT3 signalling (Naugler and Karin 2008). The IL-6 signalling can also induce the MAPK pathway, as JAK can trigger SHP2 which in turn activates the RAS-ERK pathway. The *classic signalling* is anti-inflammatory and often occurs during homeostasis (Scheller et al. 2011).

Trans-signalling involves soluble IL-6Rα (sIL-6Rα), circulating in serum, binding to IL-6 which then binds to gp130. The sIL-6R is formed when the membrane-bound precursor is cleaved by the ADAM family metalloproteases also located in the membrane. *Trans-signalling* is associated with pro-inflammatory outcomes and cancer. The soluble IL-6/sIL-6 receptor complex can signal to a large variety of cells as gp130 is ubiquitously expressed. The regulation of this signalling is still unknown

although soluble gp130 (sgp130) is hypothesised to be a negative regulator by binding to the circulating IL-6-IL-6Rα complex (Naugler and Karin 2008). IL-6 can also induce YES and Src proteins through gp130 signalling. This can lead to the phosphorylation and activation of YES-associated protein (YAP) which is translocated to the nucleus to induce the transcriptional activation of genes causing proliferation and growth (Garbers et al. 2018).

The newly discovered IL-6 *trans*-presentation signalling occurs through dendritic cells whereby IL-6 associates with the IL-6R intracellularly. The IL-6-IL-6R complex is then expressed on the plasma membrane of the dendritic cells and comes into contact with and interacts with the gp130 expressed on T cells. The consequent phosphorylation of STAT3 in the T cell induces proliferation and growth. This novel signalling mode was initially detected in mice and is yet to be determined in human (Heink et al. 2017; Garbers et al. 2018).

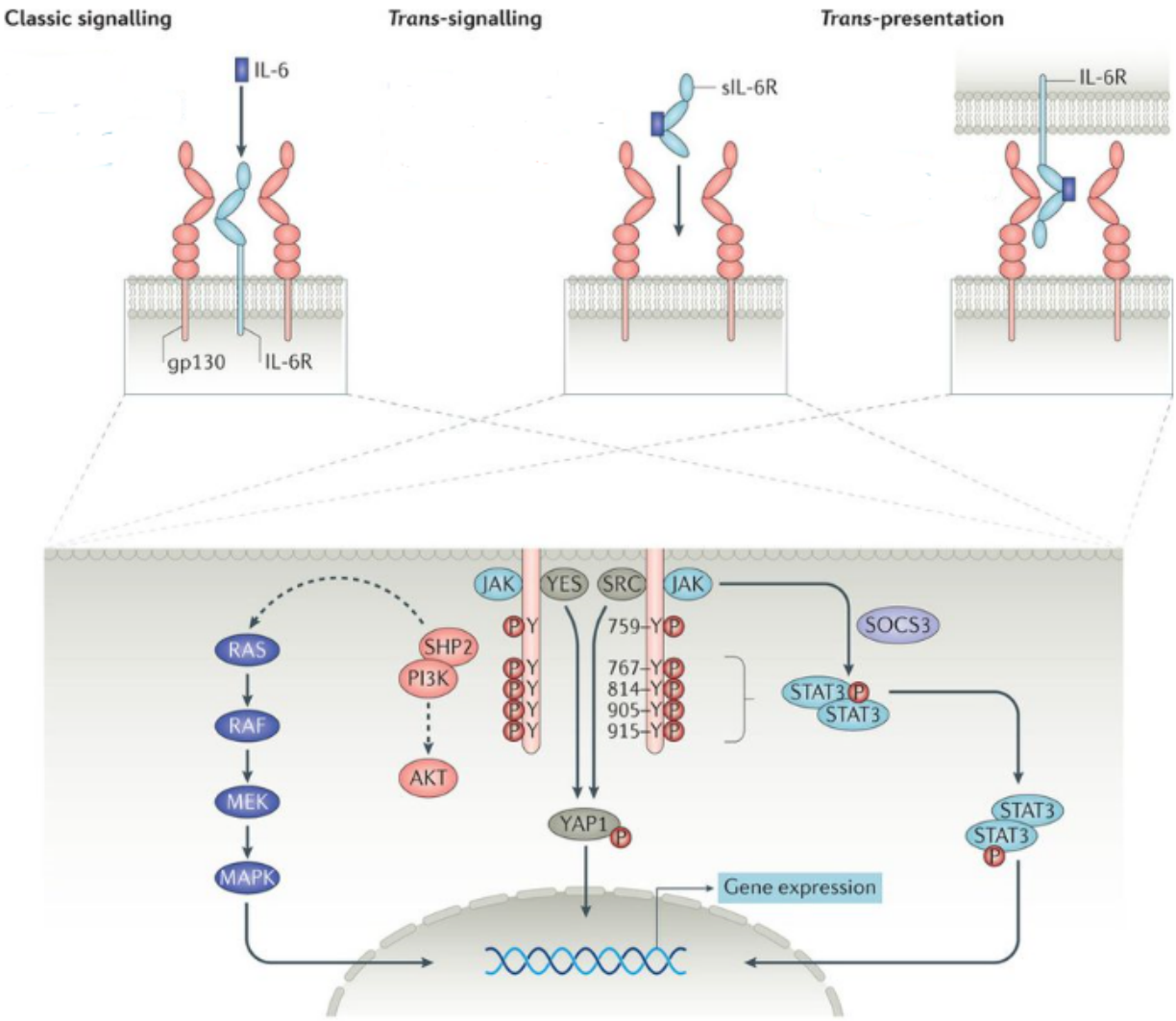


Figure 10: The three types of IL-6 signalling: *classic signalling, trans-signalling* and *trans*-presentation adapted from (Garbers et al. 2018)

The homodimerization of gp130 induces the signalling pathways: JAK, STAT3, MAPK, PI3K and YAP. The phosphorylation of JAK1 occurs on the tyrosine residues of the intracellular gp130. The four carboxy-terminal tyrosing residues allows the STAT proteins to bind to gp130. After the phosphorylation of STAT3, they form homodimers which translocate to the nucleus and alters gene expression. SHP2 binds to the docking site of Tyr-759 on gp130 which activates the PI3K-Akt and MAPK pathways. Tyr-759 also serves as a docking site for the negative receptor regulation through SOCS3. Src and YES, as part of the SRC kinase family, phosphorylates YAP1 and induces the transcriptional activation of genes in the nucleus to induce proliferation and growth.

1.4.2 Biological role of IL-6

Inflammation and Immunity

IL-6 is involved in the switch from innate to acquired immunity. The acute phase of inflammation involves an influx of neutrophils secreting proteases and reactive oxygen species to the site, this is then followed by the arrival of monocytes and T-cells after 24-48 hours to ensure that the neutrophils will not cause tissue damage. Subsequent proteolysis of IL-6R by the neutrophils initiates IL-6 *trans-signalling.* This signalling induces monocytes to the tissues during the acute phase by inhibiting neutrophil chemokines (e.g. CXCL1, CXCL8 and CXCL1) and increasing chemokines for monocytes (e.g. CCL2, CCL8, CXCL5 and CXCL6). IL-6 also increases leukocyte migration through augmenting endothelial adhesion molecules (e.g ICAM-1, VCAM and CD62E) and L-selectin on lymphocytes *via trans-signalling.* IL-6 *trans-signalling* also enhances M-CSF expression and thus shifts monocyte differentiation to macrophages (Scheller et al. 2011).

IL-6 also plays a vital role in the adaptive immune response. It is able to stimulate T-cell recruitment *via* upregulation of chemokines CCL4, CCL, CCL17 and CXCL10 through its *trans-signalling.* IL-6 inhibits the apoptosis of T-cells by enhancing Bcl-2 and Bcl-x_L through STAT3 activation which deregulates the expression of Fas (Jones 2005). IL-6 plays a vital part in influencing B and T cell differentiation. After the antigen-presenting cells are stimulated, naïve T-helper precursors differentiate to effector T-cell subsets: T_H1 (cells which secrete IFNγ against intracellular bacteria), T_H2 (cells which secrete IL-4, IL-5 and IL-13 against parasites), T_H17 (cells which produce IL-17, IL-21 and IL-22 involved in autoimmune disease) and the suppressor T_{reg} cells. IL-6 favours the differentiation towards T_H2 and T_H17 subsets (Scheller et al. 2011). The *trans-signalling* IL-6/sIL-6R complex works to block the differentiation of T_{reg} which is regulated by TGFβ. Furthermore, IL-6 and TGFβ work together to induce the differentiation of T_H17 and subsequently IL-17 which overall leads to autoimmunity. *Classic-signalling* is involved in the differentiation towards T_H17 cells however it is sustained through *trans-signalling* (Naugler and Karin 2008).

IL-6 is also involved in metabolic and bone homeostasis in humans. With inflammation being linked to diabetes and obesity, the implications of IL-6 in regulating metabolism have been reported in

several studies. IL-6 is secreted by adipocytes in obese patients and its levels increase with the volume of adipocyte (Skurk et al. 2007). Glucose intolerance and insulin resistance have been observed in IL-6 deficient mice (Matthews et al. 2010). Moreover, when patients were treated with an IL-6R neutralizing antibody, the body weight of patients rose by 7% with reports of hypertriglyceridemia and hypercholesterolemia (Nishimoto et al. 2005). IL-6 also controls the regulatory balance between osteoblasts and osteoclasts. IL-6 is pivotal in the formation of osteoclasts through increasing the expression of RANK ligand (RANKL) which binds to its receptor RANK and activates the differentiation of osteoclasts from its myeloid precursor cell. This occurs through the *trans-signalling* pathway with IL-6/sIL-6R complex activating the JAK/STAT pathway (Scheller et al. 2011).

Overall IL-6 is involved in a diverse range of homeostatic biological roles however it serves as an important link between inflammation and various diseases including diabetes and cancer. As tumours are akin to a non-healing wound, manipulation of the homeostatic processes to a pro-inflammatory environment occurs to exacerbate tumour progression.

1.4.3 IL-6 in non-small cell lung cancer

With its established biological role in inflammation, its initial association with cancer arises due to the contribution of chronic inflammation in cancer progression. Dysregulation in the expression of IL-6 occurs in chronic inflammatory states and is linked to cancer progression and therapeutic resistance. The levels of IL-6 are often overexpressed in various types of cancers including ovary, prostate, breast, lung, multiple myelomas and leukaemia (Guo et al. 2012).

Likewise, with HGF, IL-6 has established a dual facet: instigating the innate response whilst also being involved in cancer progression. High levels of IL-6 are linked with poor survival rates (Pine et al. 2011) and its circulating levels are an indicator of the prognosis of patients undergoing chemotherapy (Yanagawa et al. 1995). IL-6 is also associated with inducing NSCLC fatigue, anaemia, thromboembolism and cachexia (Yao et al. 2014). A549 cell lines have been shown to express IL-6 mRNA and protein (Bihl et al. 1998) additionally high levels of IL-6 and its receptor component gp80/IL-6R and gp130 are expressed in NSCLC (Haura, Livingston, and Coppola 2006). The effects of IL-6 on NSCLC proliferation have provided mixed findings: IL-6 inhibiting A549 cell growth in one study, (Takizawa et al. 1993) whilst another showed no effect on growth (Yamaji et al. 2004) however Bihl et al showed an increase in proliferation correlated with IL-6 secretion (Bihl et al. 1998) and Kim et al has shown NSCLC growth by demonstrating the antiproliferative effect of an IL-6 antibody (Kim et al. 2015). A positive link between IL-6 production and tumour proliferation in NSCLC in vitro and in vivo was previously reported (Yamaji et al. 2004; Gao et al. 2007). Recently Lee

et al demonstrated the dual roles of IL-6 in stimulating the proliferation of CD133+ A549 cells whilst exhibiting inhibitory proliferative effects on CD133- A549 cells (Lee et al. 2016). This recent finding provides conclusive evidence on the various effects of IL-6 in NSCLC proliferation previously reported. Therefore, screening of the A549 cell line is vital in establishing the proliferative effect observed when stimulated with IL-6. IL-6 also plays a role in the pro-tumourigenic growth of NSCLC through chemoresistance. An autocrine IL-6 loop mediates afatinib resistance whereby IL-6 mRNA and IL-6 levels were upregulated with afatinib treatement in EGFR mutated NSCLC H1975 and PC-9GR cells. The stimulation of IL-6 in NSCLC PC-9 cells also reduced the apoptotic effect of gefitinib (Zheng et al. 2019).

The downstream signalling pathway induced in NSCLC is widely reported in various studies. NF-κB, a signalling effector of IL-6, is a key transcription factor in inhibiting apoptosis and propagating inflammatory signals contributing to chronic inflammation. STAT3 is also a main signalling effector of IL-6 and is involved in proliferation (*cyclin D1* and *c-Myc*), angiogenesis through regulation of VEGF and inhibits apoptosis (Bcl-xL) (Naugler and Karin 2008). IL-6 signalling in NSCLC contributes to production of anti-apoptotic molecules (Bcl-2 and Mcl-1) and DNA repair molecules (p53, CHK, ATM, ERCC1 and TP73) (Duan et al. 2015). A reciprocal relationship has been demonstrated between the NOX/Akt and IL-6/STAT3 pathways in inducing the growth of NSCLC cells. IL-6 treatment in NSCLC cells can also induce NOX4 expression and the production of reactive oxidative species (ROS) which propagates cell proliferation and survival (Li et al. 2015). Although various signalling cascades are implicated in IL-6 proliferation in NSCLC, ongoing research continues to define the full spectrum of pathways involved.

IL-6 has also been reported to be involved in inducing EMT in NSCLC (Chen et al. 2015; Zheng et al. 2019). A549 cell scattering and morphological change towards a fibroblastic phenotype was observed by Zhao et al when A549 cells were stimulated with IL-6 (Zhao et al. 2014). The transformation towards a mesenchymal-like morphology also suggests A549 undergoing EMT and thus possessing enhanced invasive properties to facilitate metastasis. Additionally To et al has shown that IL-6 is able to induce the migration of A549 cells in a dose-dependent fashion possibly *via* chemokinesis (To et al. 2002). Additionally, IL-6 treatment resulted in a reduced expression of e-cadherin whilst upregulation of mesenchymal markers such as vimentin and SNAIL. The signalling mechanism underlying IL-6-induced EMT is still poorly defined. However, the phosphorylation of STAT3 has been identified in mediating the IL-6 induced EMT in A549 cells (Zhao et al. 2014) and IL-6 and CCL2 synergistically amplify and sustain STAT3 activation in EMT (Chen et al. 2015). Most recently, IL-6 has been shown to mediate EMT through IGF-1R (insulin-like growth factor-1 receptor). IL-6/IGF-1R autocrine signalling mediated by STAT3 was identified in PC-9 cells, whereby IL-6

resulted in the autocrine secretion of IL-6, IGF-1 and IGF-2 (Zheng et al. 2019). Overall inhibitors of the pathway will be utilised to map the pathways involved in the proliferative and migratory effects of IL-6.

1.5 The relationship between HGF and IL-6

Although extensive research has established the deregulated activity of HGF and IL-6 independently in cancer proliferation and invasion, there are limited studies identifying the cooperation between HGF and IL-6 together in cancer. One study identified that IL-6 and HGF/c-Met pathways work synergistically in aiding metastasis by enhancing the production of MMPs in A549 cells (To et al. 2002). However, the cooperation between HGF and IL-6-induced proliferation has not been investigated in A549 cells. Synergistic interaction on proliferation has also been previously reported in cholangiocarcinoma cells (Yokomuro et al. 2000) and in myeloma cells (Hov et al. 2009). Furthermore, IL-6 stimulates HGF production in cancer (De Jong et al. 2001) and circulating HGF and IL-6 are able to upregulate c-Met receptor expression in cholangiocarcinoma cells (Yokomuro et al. 2000). The influence of IL-6 on HGF levels or c-Met expression and their converging downstream signalling pathways would be of future interest as limited studies have explored this. The proliferative signalling can be enhanced due to molecular components such as adaptor proteins and kinases increasing activation due to converging pathways. Survival of A549 cells was found to be due to sustained activation of STAT3 *via* Src kinase downstream of HGF, IL-6 and EGF signalling activation (Song et al. 2003). One study on myeloma cells has established the amplification of HGF/c-Met activation on IL-6 induced proliferative signalling, demonstrating IL-6 reliance on c-Met signalling to fully activate Ras and p44/42 MAPK pathway *via* a convergence on Shp2. The presence of IL-6 inducing c-Met expression on the cell surface further sensitizes cells to HGF (Hov et al. 2009). The proliferative signalling pathway induced by HGF activation of c-Met also coincides with IL-6 signalling, however, their relationship has only been minimally explored in studies.

Additionally, both factors cooperate in facilitating invasion by increasing their respective receptors to increase the production of MMP-2 and MMP-9 in A549 cells. The same study also showed pre-treatment of IL-6 can induce migration towards HGF through upregulation of c-Met and vice versa with pre-treatment of HGF inducing migration towards IL-6 (To et al. 2002). Another study of myeloma cells identified the same cooperation, with IL-6 essential in maximizing the HGF-dependent migratory effect by enhancing c-Met expression (Hov et al. 2009).

Aside from HGF and IL-6, the epidermal growth factor (EGF)/epidermal growth factor receptor (EGFR) signalling is widely implicated in NSCLC progression, with the majority of NSCLC tumours positively

expressing the EGFR (as reviewed in (Karlsen et al. 2021). Therefore, EGF/EGFR signalling, and its crosstalk with HGF/c-Met, serve as another critical target in NSCLC treatment.

1.6 Epidermal growth factor and the epidermal growth factor receptor

Human EGF consists of a single 53 amino acid polypeptide chain with three internal disulphide bridges containing six cysteine residues and defines the A, B and C loops respectively (Lu et al. 2001). It has an approximate molecular weight of 6400Da (Lu et al. 2001). Human EGF exists as two A and B molecules which can potentially form a dimer within the asymmetric unit of the crystal (Lu et al. 2001). EGF was first identified in the submaxillary gland in adult male mice and found to induce the proliferation of epithelial tissues (Carpenter and Cohen 1979). In the lung, the main source of EGF expression was found in the mesenchymal cells lining the connective tissue of the pleura, bronchi and large vessels (Ruocco et al. 1996). EGF binds to its receptor, EGFR, to induce receptor dimerization and activate a range of downstream signalling pathways (Jorissen et al. 2003).

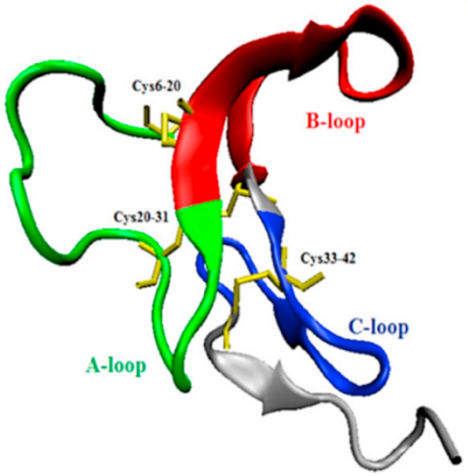


Figure 11: Structure of EGF (Mehrabi et al. 2017)

The 3D structure of human EGF show three loops: A (coloured green), B (coloured red) and C (coloured blue). EGF consists of three cysteine-rich internal disulphide bridges: Cys6-Cys20, Cys14-Cys31 and Cys33-Cys42).

Epidermal growth factor receptor (EGFR) is part of the ErbB family of tyrosine kinase receptors and encompasses four family members: EGFR/HER1/erbB1, HER2/erbB2/neu, HER3/erb3 and HER4/erb4 (Lemmon and Schlessinger 2010). All ErbB receptors consist of two cysteine-rich regions, a transmembrane region, a juxtamembrane cytoplasmic domain and an intracellular kinase which includes numerous C-terminal tyrosine residues involved in phosphorylation and receptor activation (Oda et al. 2005). However, there are structural differences between the receptor members: ErbB3 does not possess an intrinsic kinase activity and ErbB2 does not possess the ability to bind to ligands (Yarden and Sliwkowski 2001). Structurally, the extracellular domain of the EGFR spans 621 amino acids with four subdomains: domain I consist of a large EGF binding domain 1 (L1), domain II which contains the cysteine-rich domain 1 (CR1), domain III which contains the large EGF binding domain 2(L2) and domain IV which contains the cysteine-rich domain 2 (CR2). The region consists of a single

23 amino acid hydrophobic α-helical peptide (Wee and Wang 2017). The tyrosine kinase domain has an ATP-binding site between the N-lobe and C-lobe (Wee and Wang 2017). The C-terminal consists of multiple tyrosine residues which allow for additional docking of intracellular signalling proteins (Wee and Wang 2017). The EGFR gene is located on chromosome 7 short arm q22 and is translated to a 1210 residue-containing precursor before being cleaved to form the mature EGFR with 1186 residues (Jorissen et al. 2003; Wee and Wang 2017).

The ligands that bind to the EbB receptors include EGF (epidermal growth factor), transforming growth factor alpha (TGFα), amphiregulin, betacellulin, heregulin and heparin-binding EGF (Quesnelle, Boehm, and Grandis 2007). Ligand binding at the extracellular region occurs on domain I and domain III, this results in either homodimerisation or heterodimerisation with ErbB2, ErbB3 or ErbB4 receptors (Jorissen et al. 2003). More specifically, for EGF, the B loop binds to site 1 in domain I, the A loop binds with site 2 in domain III whilst the C-terminal region binds with site 3 in domain III (Mehrabi et al. 2017).Domain III facilitates the dimerisation of the receptors through its beta hairpin, also known as the dimerisation loop (Kumar et al. 2008). Following the dimerization of the receptor, autophosphorylation of the tyrosine residues (Y992, Y1045, Y1068 and Y1173) located at the C-terminal occurs which then allows binding of the intracellular signalling proteins *via* their SH2 and phosphotyrosine binding (PTB) domains (Wee and Wang 2017; Normanno et al. 2006).

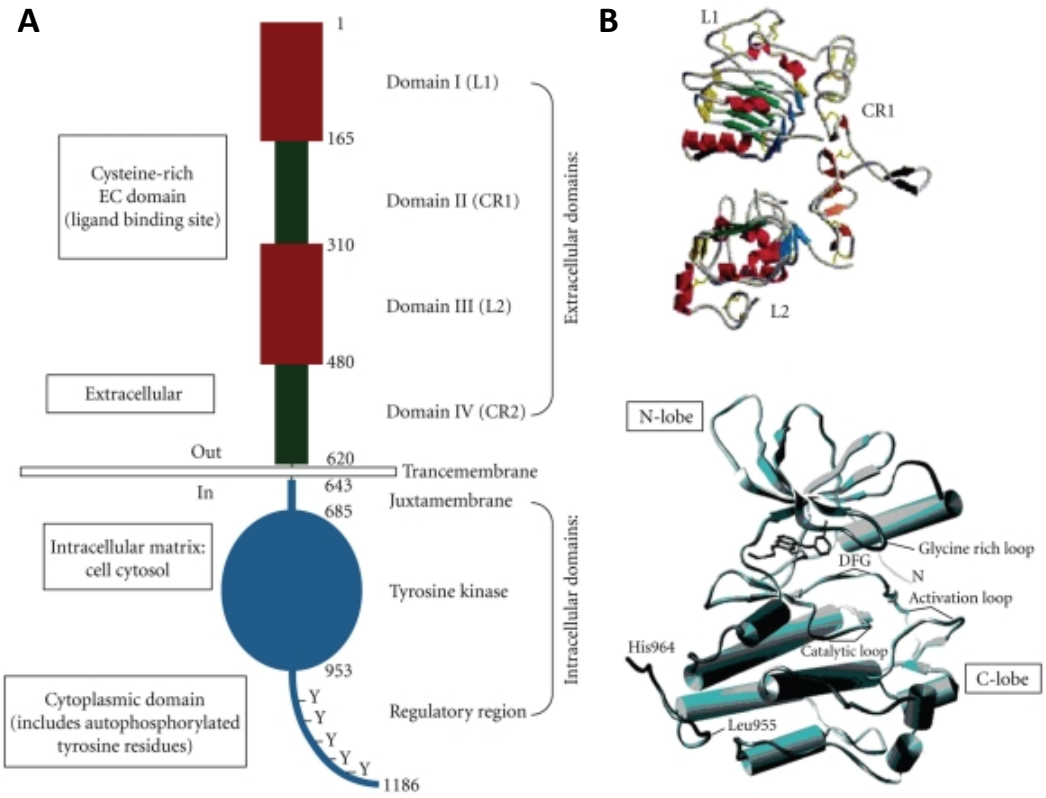


Figure 12: The structure of EGFR (Flynn, Wong, and Wu 2009)

A. The structure of the EGFR consists of the extracellular domain, which includes 4 domains: domain I (L1), domain II (CR1), domain III (L2) and domain IV (CR2). The extracellular domain binds to the EGF ligand via domains I and III whilst domain II dimerises the receptor. The intracellular domain consists of the juxtamembrane domain, the tyrosine kinase domain and the numerous C-terminal tyrosine residues which regulate the activity of the receptor through phosphorylation of the tyrosine kinase domains.

B. A 3D representation of EGFR showing the corresponding structures highlighted above.

1.6.1 Intracellular signalling

The EGFR activates three main pathways: the MAPK, PI3K and STAT pathways to induce proliferation, migration and cellular metabolism. The SH2 containing Grb2 adaptor protein binds with Ras which activates Raf leading to activation of ERK-1 and ERK-2 which translocate to the nucleus to activate transcription factors involved in cell cycle progression and migration (Jorissen et al. 2003). The PI3K is activated *via* GAB1 which directly associates with the receptor, this results in the activation of Akt which promotes cell proliferation by inhibiting apoptosis (Jorissen et al. 2003). Akt can also activate mTOR which regulates cell metabolism and growth (Wee and Wang 2017). STAT is activated through phosphorylation at the SH2 domain of the EGFR causing receptor dimerisation (Quesnelle, Boehm, and Grandis 2007). The activated STAT complex can then

translocate to the nucleus to induce transcription of genes required for proliferation and cell cycle progression (Quesnelle, Boehm, and Grandis 2007).

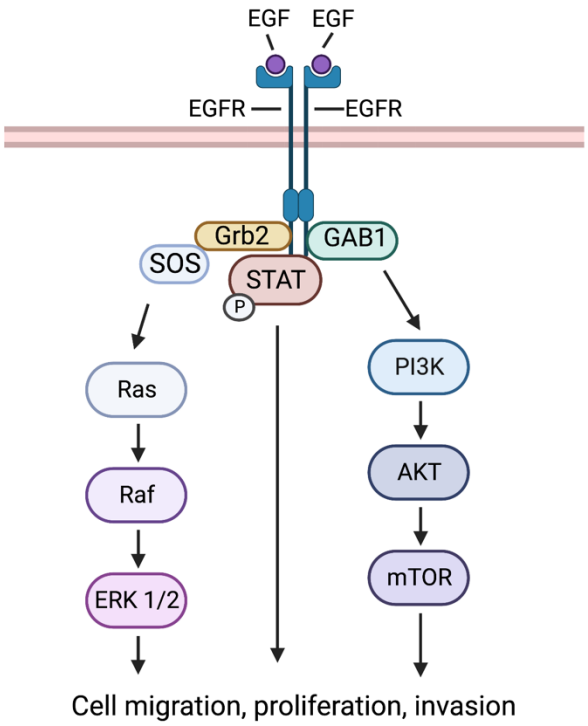


Figure 13: A schematic showing the main signalling pathways associated with EGFR

Upon EGF ligand binding to the EGFR, the receptor dimerises and leads to the autophosphorylation of the tyrosine kinase domain. This allows the adaptor proteins, Grb-2 and GAB1 to associate with the receptor activating Ras and PI3K respectively. Ras can then activate Raf and ERK1/2 to promote cell proliferation and migration. Whereas PI3K can activate Akt and mTOR which also promotes cell proliferation. STAT can bind directly to the EGFR on the SH2 domain leading to activated STAT complexes to activate transcription factors involved in cell proliferation.

1.6.2 Biological role for EGF

Physiologically, EGF is implicated in embryogenesis and fetal development (Whitman and Melton 1989; Snead et al. 1989). EGF was identified as a known mitogen for epithelial cells and fibroblasts in the lung where it is activated in undifferentiated epithelial cells (Jetten 1991; Sundell et al. 1980). Moreover, EGF is known as a crucial growth factor in lung alveolar formation (Warburton et al. 1992). In rat and mouse embryonic lung explants, EGF induced proliferation of both mesenchymal and epithelial cells causing expansion of the lung and the development of branched morphogenesis *via* MMP production (Warburton et al. 1992; Ganser, Stricklin, and Matrisian 2004). EGF was also implicated in lung maturation and has been shown to induce alveolar type II differentiation (Gross et al. 1986) and stimulate surfactant production (Whitsett et al. 1987). However, likewise with HGF, an imbalance towards higher levels of EGF in the lung is implicated in the chronic fibrotic diseases of the lung (Desai and Cardoso 2001). EGF overexpression was found in both asthmatic lung and in the damaged airways of normal lung (Warburton et al. 2000). Moreover, the upregulation of EGF signalling is not unique to only inflammatory states of lung disease but also in cancer whereby

mutations in the EGFR and overexpressed EGF levels contribute towards NSCLC progression (Bethune et al. 2010).

1.6.3 EGF/EGFR in non-small cell lung cancer

The mutationally deregulated EGF/EGFR signalling in NSCLC has been widely reported in the literature (as reviewed in (Wang 2017; Bethune et al. 2010; Karlsen et al. 2021; Pao and Chmielecki 2010). One study showed 43-89% of NSCLC cases had mutations at the intracellular or extracellular regions of the EGFR (Gupta et al. 2009). Another study reported 25% of all NSCLC cases had mutations at the EGFR tyrosine kinase domain which led to an overexpression of EGFR in 75% of the cases (Shigematsu and Gazdar 2006). Most commonly, a deletion in exon 19 or point mutations in exon 21, *via* substitution of leucine with arginine at codon 858 (L858R), were observed in 90% of NSCLC cases (Ladanyi and Pao 2008). These oncogenic mutations lead to constitutive activation of EGF in a ligand-independent manner which promotes the pro-tumourigenic signalling outcomes (Ladanyi and Pao 2008). EGFR mutations were also more commonly observed in non-smokers in NSCLC whilst mutations in the tumour suppressor gene, TP53, were linked to patients with advanced stage of NSCLC (Pao and Chmielecki 2010). This has led to the development and approval of EGFR tyrosine kinase inhibitors (TKI), including gefitinib and erlotinib (Fukuoka et al. 2003; Shepherd et al. 2005). However, 25% of patients with EGFR-mutant tumours do not respond to EGFR TKI and resistance to erlotinib was reported to occur as early as 8-12 months of treatment (Pao and Chmielecki 2010). Crosstalk between EGFR and other growth factor receptors, including c-Met, has been proposed to mediate disease persistence in NSCLC (Bean et al. 2007; Engelman, Zejnullahu, Mitsudomi, et al. 2007). 20% of gefitinib or erlotinib resistance was driven by amplification of HGF/c-Met activating the PI3K pathway *via* ErbB3 (Bean et al. 2007; Engelman, Zejnullahu, Mitsudomi, et al. 2007). Therefore, it is important to uncover the crosstalk signalling between EGF/EGFR and HGF/c-Met to uncover the molecular mechanisms underlying resistance to improve the therapeutic outcomes for patients.

1.7 The relationship between HGF and EGF

The crosstalk between c-Met and EGFR signalling has been widely reported in various cancers, including breast cancer (Harrison et al. 2013; Accornero et al. 2010; Bonine-Summers et al. 2007), colon cancer (Pai et al. 2003), epidermoid carcinoma (Jo et al. 2000), glioblastoma (Reznik et al. 2008), thyroid carcinoma (Bergström, Westermark, and Heldin 2000), pancreatic cancer (Fischer et al. 2004) and lung cancer (Puri and Salgia 2008). Both c-Met and EGFR activate paralleled signalling pathways and their crosstalk has been implicated in tumour growth, migration, invasion and resistance (Bergström, Westermark, and Heldin 2000; Fischer et al. 2004; Puri and Salgia 2008;

Yamada et al. 2012). Both HGF-independent and -dependent manner of c-Met activation were required for crosstalk with EGFR signalling (Bergström, Westermark, and Heldin 2000; Fischer et al. 2004; Puri and Salgia 2008; Bonine-Summers et al. 2007). In thyroid carcinoma crosstalk between EGFR and ligand-independent c-Met activation occurred via a convergence on the MAPK pathway (Bergström, Westermark, and Heldin 2000). Similarly, in epidermoid carcinoma cells, an HGF-independent mechanism of activation was observed via TGF-α /EGFR signalling (Jo et al. 2000).However, in breast cancer cells HGF-dependent ligand activation of c-Met was required to induce EGFR activation (Bonine-Summers et al. 2007). This highlights tumour-specific crosstalk signalling for c-Met and EGFR activation. Moreover, in NSCLC cancer, exogenous EGF and HGF resulted in an additive increase in migration and synergistic increase in proliferation (Puri and Salgia 2008). The same study showed synergistic phosphorylation of the c-Met receptor and activation of both PI3K and MAPK pathways to mediate the cellular effects (Puri and Salgia 2008). The increase in c-Met phosphorylation may be due to an increase in c-Met and EGFR association, as Jo et al reported an increase in co-immunoprecipitates between c-Met and EGFR in A431 epidermoid carcinoma cells (Jo et al. 2000). There may also be transcriptional crosstalk occurring between c-Met and EGFR, as Reznik et al reported c-Met activation induced a transcription-dependent activation of EGFR which upregulated HGF-induced glioma cell proliferation (Reznik et al. 2008).

Although studies have supported the overexpression and crosstalk between HGF and either IL-6 or EGF in NSCLC, components of the microenvironment such as cell surface integrins and the ECM, and their interactions with upregulated growth factors remain poorly defined. The ECM/integrin signalling has also been shown to crosstalk with HGF to propagate the pro-tumourigenic outcomes in NSCLC (Barrow-McGee, Kishi, et al. 2016b; Han et al. 2004; Ju and Zhou 2013).

1.8 Extracellular matrix: fibronectin, collagen IV and laminin

The ECM contains around 300 proteins each with characteristic physical and biochemical functions including acting as barriers, sites for cell anchorage and for migration. It is a three-dimensional structure which comprises of fibrous components such as collagens and elastin and adhesive proteins including fibronectin, laminin and thrombospondin bound within hydrated proteoglycans and glycosaminoglycan (Noriega-Guerra and Freitas 2018). Collagen IV, laminin and fibronectin serve as major components of the ECM. Collagen is made of 3 polypeptide α chains organised together as a three helical structure. Collagen IV is part of the network-forming collagens. Laminins consist of 20 glycoproteins which form a cross-linked network intertwined with collagen IV in the basement membrane. They are heterotrimeric (400-800 kDa) containing an α, β and γ chain each. Laminins organise themselves to networks which are in proximity to the cell surface receptors to facilitate

signalling. Fibronectin is a monomer (250 kDa) consisting of subunits of 3 types of repeats (I, II and III) and play an important role in facilitating the binding and migration of cells. Fibronectin exists as a dimer joined with a disulphide bond when first released (although it can also form multimers) and have binding sites for other fibronectin dimers, collagens, heparins and cell receptors (Yue 2014).

The ECM components are produced by tumour cells and stromal cells which includes the cancer-associated fibroblasts (CAFs). A two-way beneficial relationship occurs between tumour cells and the ECM the cells are able to produce and release ECM components thus undergoing remodelling whilst the ECM can send signals through its receptor governing the cellular outcomes (Yue 2014). The ECM proteins facilitate signalling pathways which lead to tumour growth, cell cycle progression and suppression of apoptosis (Hodkinson et al. 2006). Collagen IV forms the major component of the basement membrane of the lung and in NSCLC collagen IV is found highly expressed (93%) in the stroma as compared to normal lung tissue (39.1%) thus distinguishing remodelling of ECM proteins in cancer (Yan et al. 2006). This was followed by fibronectin with 80.7% expression and 54.4% laminin expression in NSCLC compared to 17.4% fibronectin and 26.1% laminin expression in normal lung tissue. Remodelling of the ECM is implicated in the early stages of lung tumourigenesis rather than in connection with TNM stages with interactions between the ECM and integrins playing a major role in mediating metastasis (Yan et al. 2006). This also coincides with the upregulated transcription and activation of MET as a late stage event as it is triggered during hypoxia and from inflammatory cytokines and pro-angiogenic factors widely circulating in the stroma of fully developed tumours (Pennacchietti et al. 2003).

The role of collagen IV, fibronectin and laminin in cancer varies from facilitating proliferation, angiogenesis, and invasion. In breast cancer cells, the presence of fibronectin through β1-integrin signalling, triggers quiescent cells to proliferate and promote metastatic growth (Barkan et al. 2008). Plasma fibronectin levels were also linked to the early stage of metastasis in Lewis lung carcinoma cells (Malik et al. 2010). Synergistic proliferation between HGF and fibronectin was also reported by Ju et al utilising the NSCLC cell line PC9 (Ju and Zhou 2013). Likewise, with fibronectin, the presence of collagen IV stimulated cell adhesion and migration through β1-integrin in lung squamous carcinoma cell line Calu-1 (Mukhopadhyay et al. 2004). However there have been mixed findings reported in the proliferative effect of collagen IV: in NSCLC Calu-1 cells showed no effect on proliferation (Mukhopadhyay et al. 2004), proliferation was also inhibited in melanoma cells (Han et al. 1997) however proliferation, cell adherence and migration was observed in mammary cells (Kim et al. 1994) and in hepatoma cells (OGATA 1998). In another study collagen IV increased survival and proliferation in a NSCLC cell line, H1299. Collagen IV also reduced cis-platinum-induced apoptosis and increased its IC_{50} thus conferring resistance and impairing NSCLC apoptosis (Yan et al. 2006). This

study also demonstrated that the PI3K-Akt pathway was a major signalling determinant of proliferation as a decrease in proliferation was demonstrated using an inhibitor of the pathway (Yan et al. 2006). Laminin is mainly known for its role in cell adhesion to the matrix, facilitating migration and metastasis in glioma cells and in breast cancer (Koochekpour, Merzak, and Pilkington 1995; Nielsen, Christensen, and Albrechtsen 1983). Although the ECM proteins are implicated in cancer progression in various cell lines, the full spectrum and mechanism of the effects observed remain to be elucidated. Furthermore, the proliferative capacity of the ECM components in NSCLC remains poorly defined and this area serves a wider interest in the role of the ECM as a scaffold to promote pro-tumourigenic signalling outcomes and effects.

1.8.1 Integrins

Integrins are heterodimeric transmembrane glycoprotein receptors, consisting of α and β subunits, found bound to ECM proteins (e.g. laminin, fibronectin and collagens) in intercellular spaces and basement membranes (Miyamoto, Akiyama, and Yamada 1995; Hynes 2002). They also serve as a mediator to the cytoskeleton framework (Hynes 2004). There are 18 α and 18 β subunits and can form 24 distinct integrins. Integrins are categorised accordingly either to their ligand-binding properties or subunit structure (Hynes 2002). Integrins can bind singularly to a specific ECM protein-ligand however some integrins are able to bind to a variety of ECM ligands (Hynes 2004). A table summarising the integrin ligand selectivity is detailed below.

INTEGRIN	ECM LIGAND
α1β1	Collagen type IV, VI and laminins
α2β1	Collagen type I, II, IV and IX; laminins
α3β1	Collagen type IV, laminin-5, -10 and -11 (-1 and -2), thrombospondin, fibronectin, nidogen
α4β1	Fibronectin and thrombospondin
α4β7	Fibronectin, VCAM and MADCAM
α5β1	Fibronectin, fibrinogen and thrombospondin
α6β1	Laminin-5, -3, -1and -4, thrombospondin, merosin, kalinin
α7β1	Laminin-1, -2, -4 and -5
α8β1	Fibronectin, vitronectin, tenascin and osteopontin
α9β1	Thrombin cleaved osteopontin, laminin, tenascin C
α10β1	Collagen type 11, IV, VI and IX
α11β1	Collagen type I, IV and IX
αVβ1	Vitronectin and fibronectin
αVβ3	Tenascin C, thrombospondin, vitronectin, fibronectin, fibrinogen, von Willebrand's factor, laminin and osteopontin
αVβ5	Vitronectin and fibronectin
αVβ6	Fibronectin, tenascin and vitronectin
αVβ8	Vitronectin
α6β4	Laminin

Table 1: Summary of the integrin extracellular matrix ligands binding interactions, adapted from (Jin and Varner 2004; Votteler et al. 2010)

Integrin signalling occurs *via* a bidirectional pathway. Interactions between integrins and components of the ECM facilitates 'outside-in signalling' stimulating clustering (additionally HGF can also initiate clustering) (Trusolino et al. 2000; Hynes 2002) leading to intracellular signalling. Whereas 'inside-in signalling' involves intracellular protein activation which regulates the affinity of integrins towards various components of the matrix; this is influenced by external receptor signals (e.g. receptor tyrosine kinase (RTK))(Desgrosellier and Cheresh 2010). Cells display a specific set of integrins and adapt accordingly to its cellular and external environmental signalling. Various stimuli such as oncogene activation, alterations in components, stiffness of the ECM or growth factors leading to integrin clustering and recruitment of adaptor proteins and thus altering the signalling response (Bianconi, Unseld, and Prager 2016). Integrins do not possess intrinsic kinase activity therefore recruit a range of intracellular proteins to facilitate their signalling response, including focal adhesion kinases (FAK), Src family kinases (SFKs) and scaffolding molecules p1300 CRK-associated substrate (Desgrosellier and Cheresh 2010).

The FAK-associated pathways are one of the main pathways activated following integrin clustering. The four-point-one, ezrin, radixin, moesin (FERM) domain of FAK binds to the cytoplasmic tail of the

β-integrin subunit. This causes the displacement of the FERM domain and provides a docking site for Src tyrosine kinase. The FAK-Src complex stimulates a variety of signalling effectors. Rac1 (Ras-related C3 botulinum toxin substrate 1), which is a part of the Ras superfamily of small GTP-binding protein, triggering cell spreading and initiates migration. Simultaneously Src also inhibits RhoA, a GTPase, through physical interaction with fibronectin and α5β1. This triggers cell spreading whilst inhibiting migration through easing of cytoskeletal tension. Towards the later stages of cell spreading, constitutive RhoA activation induces migration. The FAK-Src complex also triggers the MAPK/ERK pathway which induces the oncogenic transcription factors *c-myc* and *c-jun* which induces proliferation and cell cycle progression. PI3K also binds to the docking site on FAK which subsequently activates AKT *via* PDK1 (phosphoinositide-dependent kinase-1). This leads to inhibition of the pro-apoptotic BAD, activation of the mTOR pathway and transcription factor YAP which promotes survival, proliferation and migration (Bianconi, Unseld, and Prager 2016).

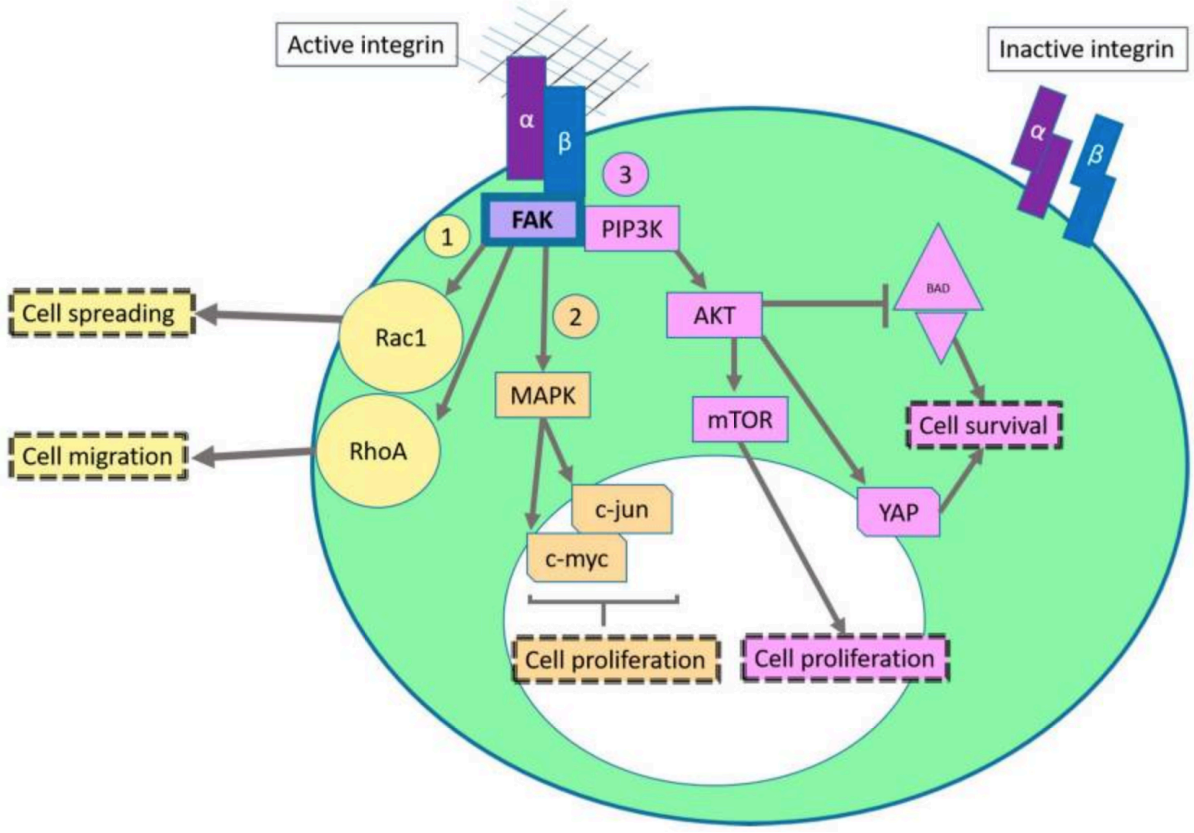


Figure 14: Schematic diagram of the integrin outside-in signalling of FAK activation (Bianconi, Unseld, and Prager 2016)

1. Rac1 facilitates GDP-GTP exchange in the plasma membrane of the cell. This then stimulates actin assembly thus initiating cell spreading. Constitutive RhoA activation leads to activation of the downstream effector ROCK (Rho-associated protein kinase) which causes formation of actin stress fibers and actomyosin contractility.
2. MAPK pathway induces various transcription factors which phosphorylate pro-proliferative genes.

3. The PIP3K/AKT pathway activates the mTOR pathway which causes mRNA translation of genes regulating proliferation and survival which includes VEGF and lipid synthesis. PIP3K/AKT pathway also cross-talks with the Hippo pathway through YAP which induces anti-apoptotic expression of Bcl-xL.

Integrins also serve as an indirect link between the ECM and the actin cytoskeleton. Upon integrin activation, talin can bind to the cytoplasmic region of the β-integrin subunit before recruiting vinculin, paxillin and FAK in a consequential hierarchical chain leading to binding with F-actin (Brown and Turner 2004; Humphries et al. 2007; Hynes 1992; Zhang et al. 2008). Therefore, paxillin plays a major role in linking between integrin/growth factor signalling with the actin cytoskeleton.

1.9 Paxillin

Paxillin is a scaffold focal adhesion (FA) protein which was first discovered as a 68kDa protein substrate which induced tyrosine phosphorylation in Rous sarcoma virus-transformed chick embryonic fibroblasts (Glenney Jr and Zokas 1989). It was later identified to bind to the vinculin tail domain of purified from smooth muscle tissue (Turner, Glenney Jr, and Burridge 1990). The paxillin family also includes other proteins: Hic-5, a 50kDa protein also known as transforming growth factor beta 1 induced transcript 1 (TGFβ1i1), 55kDa androgen receptor coactivator (ARA55) and 45kDa leupaxin. Paxillin is found ubiquitously in the body whilst Hic-5 is found in smooth muscle tissues and leupaxin is mostly found in leukocytes (Alpha, Xu, and Turner 2020). The structure of paxillin consists of a C-terminal and an N-terminal. The C-terminal contains four LIM (Lin11, Isl-1, Mec-3) domains, which are double-zinc-finger motifs, essential for protein binding (Pérez-Alvarado et al. 1994; Schmeichel and Beckerle 1994). The focal adhesions bind and phosphorylate the LIM2 and LIM3 domains of paxillin leading to focal adhesion targeting of paxillin. Tubulin and the tyrosine phosphatase PTP-PEST also bind to the LIM domains (Côté, Turner, and Tremblay 1999; Herreros et al. 2000). The N-terminal domain mainly regulate the signalling activity of paxillin and consists of five leucine- and aspartate-rich LD motifs (LD1-LD5)(Tumbarello, Brown, and Turner 2002). The N-terminal also consists of a proline-rich region targeted for binding to the SH3 domain of the non-receptor tyrosine kinase Src (Weng et al. 1993). Moreover, as a scaffold protein, numerous tyrosine, serine and threonine phosphorylation sites span along paxillin, each site targeted by a variety of kinases, including ERK, PAK, FAK-Src, JNK, p38 MAPK and cyclin-dependent kinase 5 (CDK5)(as reviewed in (Deakin and Turner 2008; Brown and Turner 2004). The activation of paxillin relies on its regulated phosphorylation which is induced by growth factor stimulation, including HGF/c-Met activation, and integrin-mediated adhesion to the ECM (López-Colomé et al. 2017).

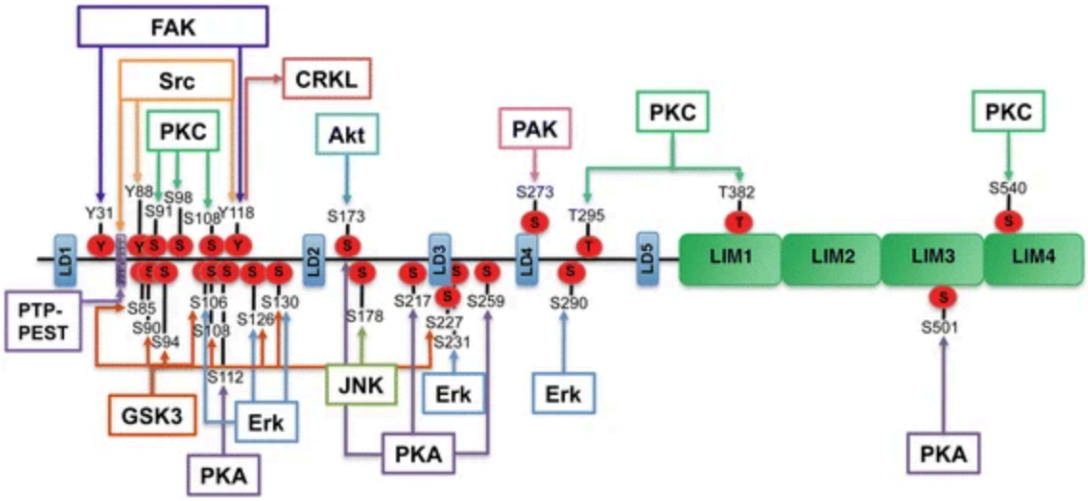


Figure 15: The structure of paxillin and its associated binding partners (López-Colomé et al. 2017)

Paxillin consists of several protein binding motifs: the amino-terminal LD motifs, the carboxy-terminal LIM domains and phosphotyrosine-SH2 domain docking sites. The domains bind to shared and individual partners which alters focal adhesion signalling required for cytoskeletal remodeling and migration. The respective binding partners are identified in the figure.

1.9.1 Interaction between HGF/c-Met, β1-integrin and paxillin in NSCLC

Integrin signalling is implicated in tumour cell proliferation, migration, invasion and survival (Desgrosellier and Cheresh 2010). Integrins 'crosstalk' with receptors, one being the HGF/c-Met pathway, to influence and sustain metastatic behaviour influencing cell migration, proliferation, and differentiation. The integrin α6β4 binds to c-Met creating additional docking for signalling adaptors attracting SHC, PI3K and SHP2 thus stimulating PI3K and Ras pathways contributing to tumour invasion (Trusolino, Bertotti, and Comoglio 2001). αvβ5 integrin also induces the transcription of genes promoting cell migration thus contributing to the c-Met signalling pathway (Crouch, Spidel, and Lindsey 2004). Moreover, paxillin is recruited and phosphorylated at the tyrosine residue pY31 (CRKL-binding site) upon c-Met activation (Parr et al. 2001). Paxillin is also overexpressed in NSCLC due to the upregulation and mutation of the paxillin gene thus amplifying the oncogenic signalling (Jagadeeswaran et al. 2008). Integrin activation also results in the tyrosine phosphorylation of paxillin at the Tyr31, Tyr118, Ser188 and Ser190 regions (López-Colomé et al. 2017).

Tumour cells bind to the ECM via integrins and for metastasis to occur, tumour cells have to overcome the basement membrane and ECM barrier to reach blood circulation. Integrin clustering and HGF/c-Met signalling lead to the formation of focal adhesions recruiting proteins such as paxillin and kinases including FAK and PYK2. P123FAK is a focal adhesion kinase which facilitates cell migration, differentiation and proliferation. Phosphorylation of p125FAK at the PI3K and Src autophosphorylation site activates Src causing migration (Ma, Maulik, et al. 2003). PYK2 is

implicated in the MAKPK signalling via phosphorylation of its Grb2 binding site leading to proliferation and scattering. Paxillin also binds to p125FAK to form a complex. Phosphorylation and activation of paxillin is also mediated by the ECM and β1, β2 cross-linking. Paxillin intercepts with the Rho signalling pathway which mediates migration and cytoskeletal alterations to facilitate invasion (Maulik, Shrikhande, et al. 2002).

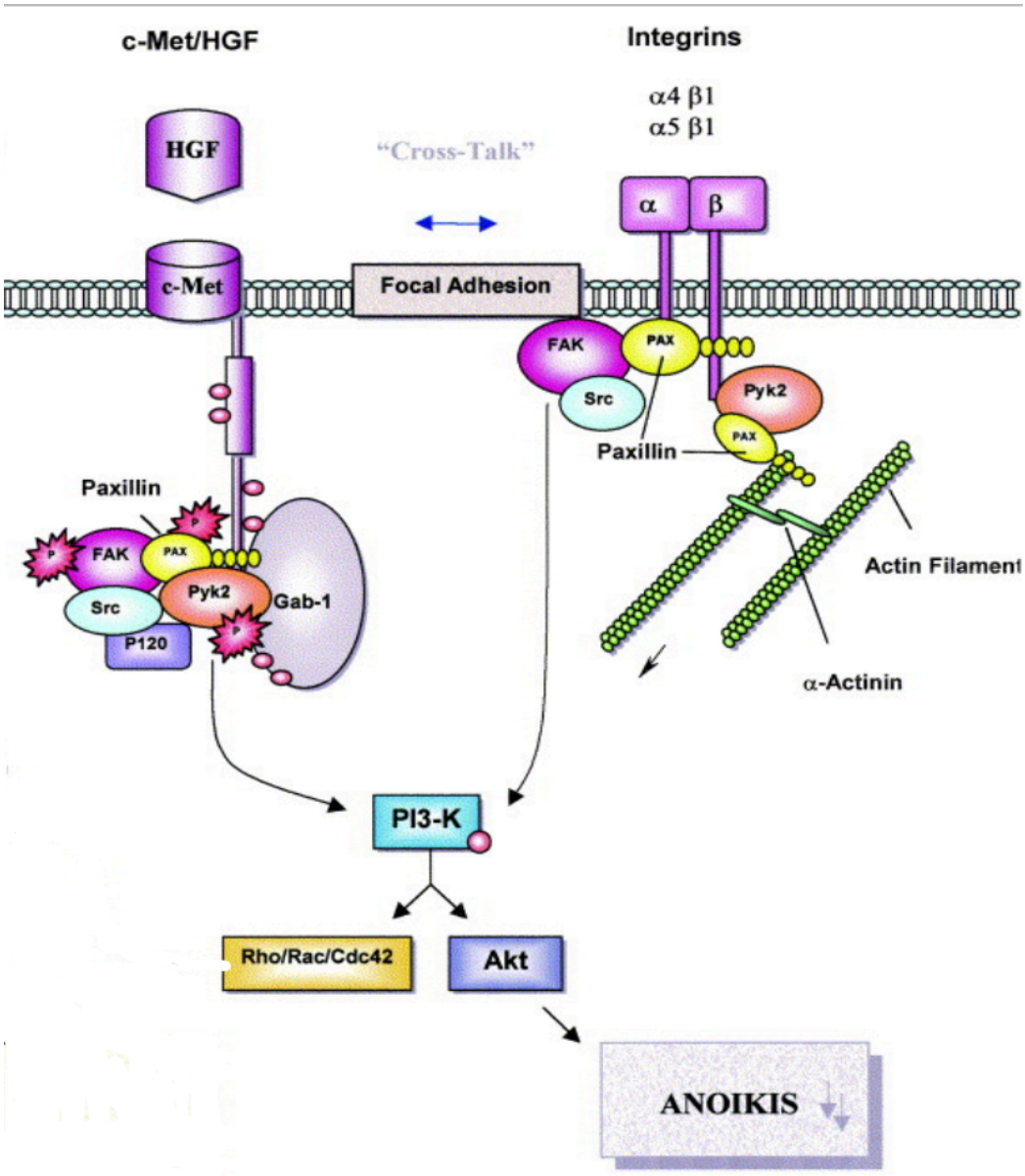


Figure 16: Schematic diagram of the crosstalk between HGF/c-Met and integrin signalling, adapted from (Maulik, Shrikhande, et al. 2002)

Scaffold proteins FAK, PAX, Src and Pyk2 are bound to the cytoplasmic tail of the integrin forming the complex. When HGF binds to c-Met this causes subsequent phosphorylation of FAK, paxillin and Pyk2. The signalling between HGF/c-Met and integrins converge *via* PI3K which in turn suppresses anoikis.

Novel findings have also implicated β1-integrin in playing a critical role involving HGF/c-Met signalling, unpublished results have shown an increase in adhesion of HGF to ECM components such

as fibronectin, collagen I, IV and laminin *via* the β1-integrin in healthy alveolar epithelial cells. A recent study has also shown in detached NSCLC cells that β1-integrin and c-Met undergo a distinct 'inside-in signalling' mechanism which drives anchorage-independent survival thus facilitating metastasis. The signalling components act on the autophagy-related endomembrane (ARE); autophagosomes are positive regulators of intracellular organelle degradation thus contributing to the homeostasis of the environment. Significant findings utilizing lung cancer cell lines have also shown the importance of β1-integrin in controlling the optimal endocytosis and internalisation of activated c-Met requiring co-internalization of both components. Following internalization, β1-integrin and c-Met complex from the cell membrane accumulate on ARE stimulating the ERK1/2 downstream pathway leading to anchorage-independent growth, an essential feature in maintaining survival to form colonies at the secondary distal sites. This discovery further emphasizes the need for targeting integrin signalling in cancer therapy (Barrow-McGee, Kishi, et al. 2016a).

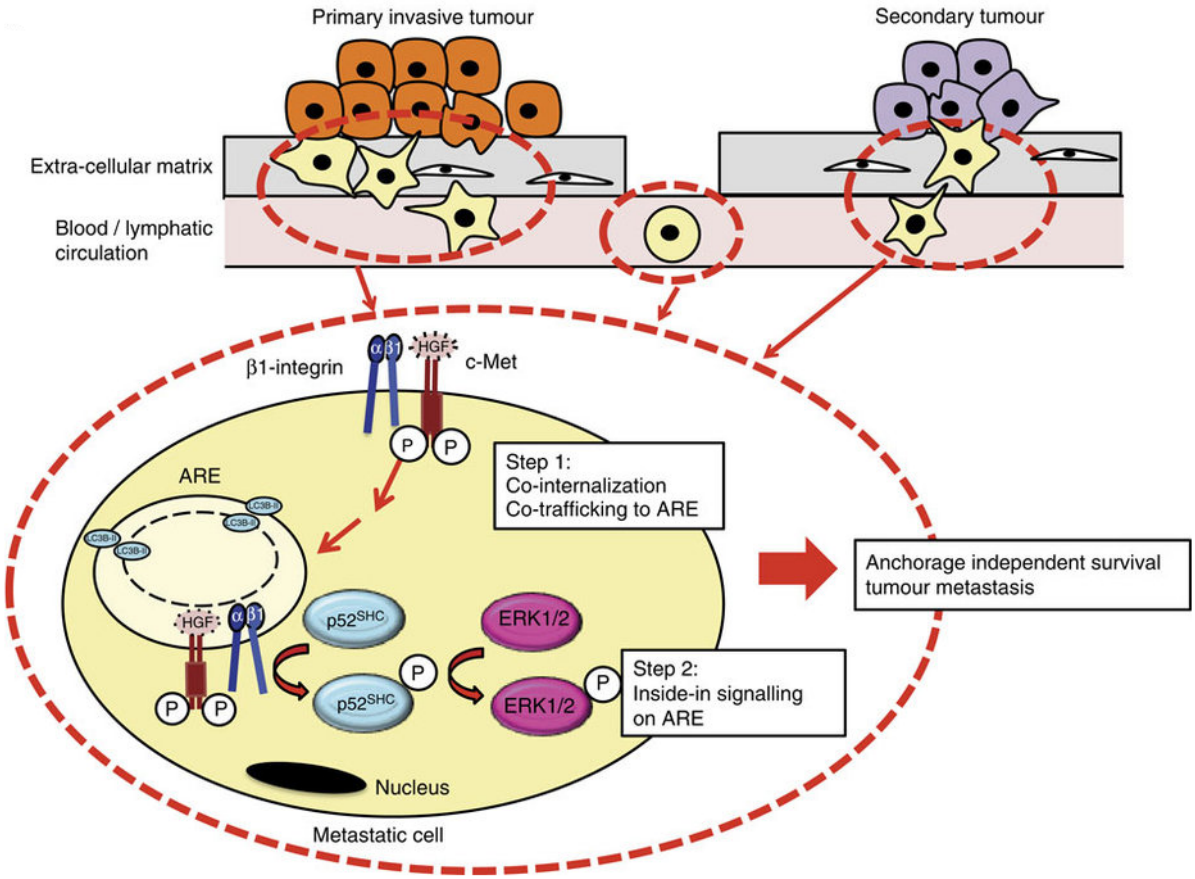


Figure 17: Schematic diagram of metastasis via 'inside-in signalling' of β1-integrin and c-Met (Barrow-McGee, Kishi, et al. 2016a)

β1-integrin and c-Met associate forming a complex at the cell membrane of detached unstimulated lung cancer cell lines. C-Met is activated via a HGF ligand-dependent or independent route leading to activation of β1-integrin precipitating co-internalisation of both activated components; β1-integrin therefore modulates the optimal clathrin-mediated c-Met

endocytosis. Post internalisation, the complex gradually gathers on ARE which acts as a signalling platform. The complex promotes c-Met signalling on this platform activating ERK1/2. B1-integrin functions as an adaptor to this 38signalling acting as a scaffold between c-Met and $p52^{Shc}$ which stimulates ERK1/2 signalling. This 'inside-in signalling' mechanism promotes anchorage-independent survival thus allowing cancer cells to survive after invasion of the primary tumour and metastasizing at secondary tissues.

Other cell lines have also reported signalling cooperation between HGF/c-Met and β1-integrin. In endothelial cells, fibronectin has a specific binding site for HGF to form a complex and this causes the c-Met and α5β1 integrin association to induce endothelial cell migration and proliferation through activation of Ras, ERK 1/2 and PI3K. In the same study, HGF in the presence of collagen I, also induces proliferation and migration through activation of ERK 1/2 and PI3K (Rahman et al. 2005). In glioblastoma and breast cancer, c-Met displaces α5 from the α5β1 integrin and binds with a higher affinity with β1-integrin. This complex forms in hypoxic conditions and induces cellular migration through ligand-independent receptor activation (Jahangiri et al. 2017).

Overall pleiotropic cytokines, such as HGF, are involved in a variety of pro-tumourigenic outcomes however the specific transduction mechanisms involved in preferentially inducing proliferation and migration are still poorly understood. The 'go or grow' hypothesis describes cancer cells engaging in a mutually exclusive phenotypic switch between a proliferative or migratory state (Giese et al. 1996). This hypothesis describes the phenotypic switch from a proliferative to a migratory state underlies the transition from supporting tumour growth to acquiring malignancy (Giese et al. 1996). Therefore, understanding the metabolic and microenvironmental cues in regulating proliferation and migration is critical in optimising drug targeting accordingly to the stage of the disease.

1.10 The 'go or grow' hypothesis in cancer

The 'go or grow' hypothesis was first proposed by Giese and his colleagues in 1996 in astrocytoma cells (Giese et al. 1996). The initial development of the tumour occurs through the sustained proliferation of cancer cells before undergoing transformation to a migratory phenotype for metastasis (Hanahan and Weinberg 2011). The mutational deregulation of the cell cycle underpins limitless proliferation whilst migration requires coordination between the ECM, actin cytoskeleton and adhesion molecules to facilitate cell movement.

1.10.1 The cell cycle

The cell cycle involves the duplication of DNA which occurs during the interphase S-phase followed by consequent chromosomal segregation into two daughter cells during mitosis (M) phase (Vermeulen, Van Bockstaele, and Berneman 2003). Interphase consists of three different phases: Gap 1 (G_1) whereby cells grow and produce proteins, synthesis (S) whereby DNA replication takes

place and Gap 2 (G_2) which allows the cell to prepare for division (Vermeulen, Van Bockstaele, and Berneman 2003). The cell can become quiescent in the G_0-phase from G_1-phase (Matthews, Bertoli, and de Bruin 2022). Under physiological conditions, the cell cycle is tightly regulated by cyclin-dependent kinases (CDKs) and their respective cyclins. There are a total of 9 CDKs known however only 5 are involved in the cell cycle: CDK4, CDK6, CDK2 during G_1, CDK2 for S-phase and CDK1 during G_2-phase and M (Vermeulen, Van Bockstaele, and Berneman 2003). In contrast to the steady levels of CDK, the levels of cyclins fluctuate throughout the progression of the cell cycle. The D type cyclins (cyclin D1, cyclin D2 and cyclin D3) bind to CDK4 and CDK6 to initiate the G_1-phase (Sherr 1994). Growth factor receptor activation is vital in producing sustained levels of cyclin D (Assoian and Zhu 1997). Cyclin E binding to CDK2 initiates progression from G_1 to the S phase (Ohtsubo et al. 1995). The cyclin A and CDK2 complex is essential in the S phase whilst the CDK1/cyclin A complex is involved in progressing into M from the late G_2 phase and early M (Vermeulen, Van Bockstaele, and Berneman 2003).

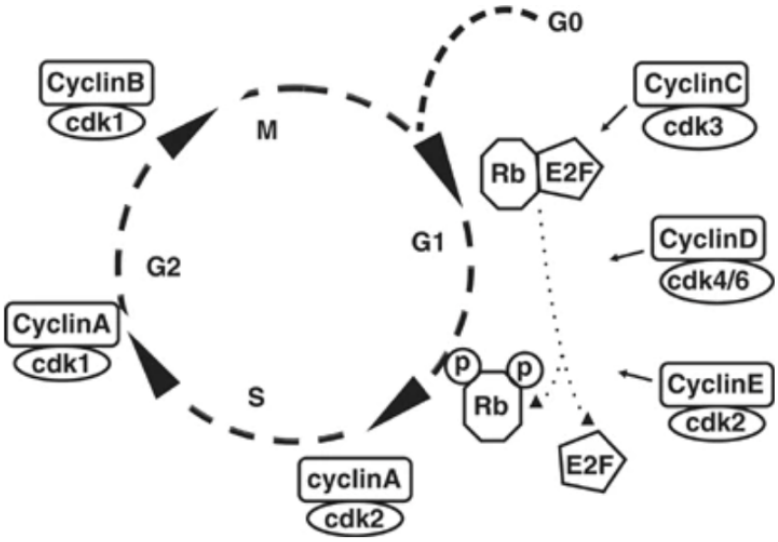


Figure 18: The different stages of the cell cycle (Giacinti and Giordano 2006)

The cell cycle includes the G_1-phase, during which the cell grows and synthesises proteins, the S phase, where DNA replication occurs, the G_2-phase, where the cell continues to grow and prepares for division and the mitosis (M)-phase, where the chromosomes are segregated and the cell divides. Specific cyclins and cyclin-dependent kinases (CDKs) regulate the cell cycle progression as indicated on the schematic. Retinoblastoma protein (Rb) binds to the E2F factors thus inhibiting the transactivation domain during G_0 and early G1-phase. During the late G_1-phase, the phosphorylated Rb releases E2F which leads to the transcription of genes required to progress into the S-phase.

However, in cancer, cells undergo continuous cell divisions due to the accumulation of mutations inhibiting programmed cell death (Matthews, Bertoli, and de Bruin 2022). Growth factor-mediated (e.g. HGF) integrin clustering influences cells to transition from the G_0 to G_1 phase (McNamee, Ingber, and Schwartz 1993). Deregulated RTK signalling, which includes c-Met, activates the MAPK pathway

increasing the levels of MYC which promotes cell cycle progression by activating cyclins and CDKs (Matthews, Bertoli, and de Bruin 2022). Moreover, during the initial tumour development, oxygen and nutrients are abundant in the TME which enables rapid proliferative growth (Gatenby and Gillies 2004). However, as the tumour becomes more densely packed with cells, a metabolic gradient forms from the hypoxic core to the normoxic nutrient-rich tumour periphery (Gatenby and Gillies 2004). The hypoxic environment and accumulation of mutations result in the switch to a migratory phenotype to allow for metastasis (Gatenby and Gillies 2004).

1.10.2 The process of migration

The migratory process relies on the polymerisation and depolymerisation of filamentous actin (F-actin) to alter the cell shape for movement (Pollard and Borisy 2003). The Rho GTPases, which are a part of the subfamily of the Ras superfamily of small G-proteins, are responsible for facilitating the different stages of the migratory process (Tapon and Hall 1997). GTPases are activated when bound to GTP and inactive when bound to GDP (Tapon and Hall 1997). The guanine nucleotide exchange factor (GEF) facilitates the exchange of GDP for GTP whilst the GTPase activating proteins (GAPs) activates the Rho GTPase intrinsically to facilitate the hydrolysis of GTP to GDP (Cook, Rossman, and Der 2014; Lamarche and Hall 1994). Mitogenic stimuli, including HGF/c-Met activation, induces actin polymerisation and activation of the Rho GTPases, CDC42 and Rac, at the leading edge of the cell which leads to the formation of filopodia, which are narrow finger-like protrusions, and lamellipodia, which are broad sheet-like protrusions respectively (Small et al. 1998). CDC42 is also involved in maintaining cell polarity and reorganises the microtubules and Golgi towards the direction of travel (Schliwa et al. 1999). Rac activation also contributes to the generation of contractile forces through phosphorylation of the myosin light chain (MLC) *via* PAK (Bagrodia and Cerione 1999). This leads to small, nascent focal adhesions forming behind the leading edge which bind the cell membrane to the ECM *via* integrins. Meanwhile, at the rear edge of the cell, the small GTPase, RhoA, induces the formation of actin or myosin-based contractile fibres by activating the ROCK thus reorganising the actin filaments and initiating integrin clustering to form mature focal adhesions (Innocenti 2018). Once the focal adhesions mature and stabilise, the cell uses the focal adhesion to pull over the ECM whilst the actin-myosin crosslinking generates contractile force to aid in the propulsion of the cell (Ananthakrishnan and Ehrlicher 2007). Following this, the cytoskeleton then undergoes remodeling to allow the mature focal adhesions to disassemble thus enabling cell deadhesion from the ECM at the rear edge (Ananthakrishnan and Ehrlicher 2007; Raftopoulou and Hall 2004). The cell also releases MMPs to aid in the cell detachment process through the proteolytic degradation of the ECM (Kirfel et al. 2004). The focal adhesions undergo rapid turnover during migration, allowing the

continual reassembly of focal adhesions at the leading edge and the disassembly of mature focal adhesions at the rear edge (Kirfel et al. 2004).

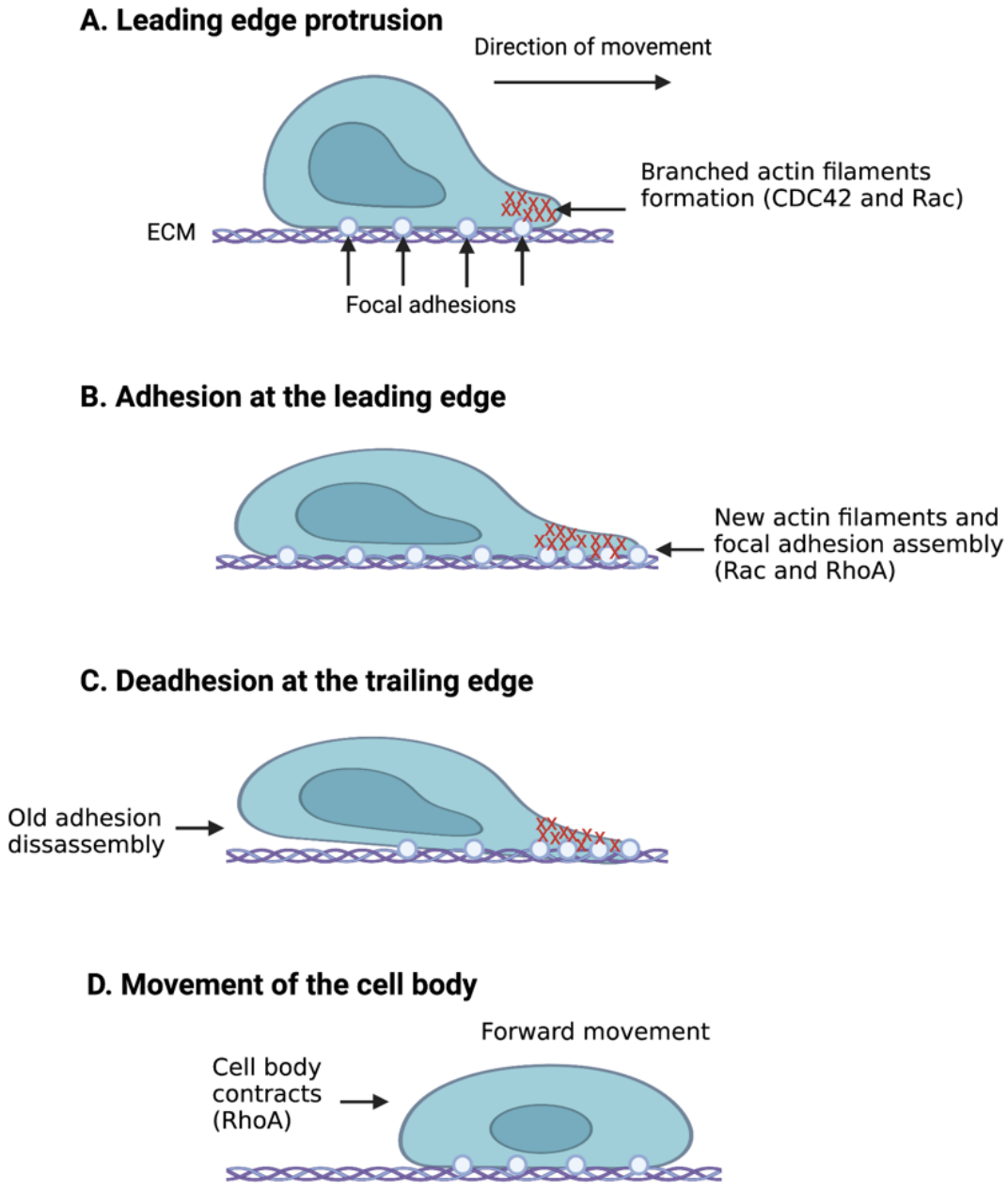


Figure 19: A schematic depicting cellular migration

a. At the leading edge of the cell, actin polymerisation occurs to form lamellipodia and filopodia protrusions via activation of Rac and CDC42 respectively.
b. New focal adhesions form at the leading edge of the cell, adhering the cell to the ECM. This process is driven by Rac and RhoA activation.
c. The focal adhesions at the rear edge disassemble from the ECM *via* MMP being produced by the cell.
d. Actin-myosin crosslinking at the rear edge causes the cell body to contract which propels the cell to move forward. The process is driven by RhoA activation.

Although the molecular mechanism driving both proliferation and migration are distinct, there are mixed findings in proving the mutual exclusivity between proliferation and migration. Therefore, the evidence surrounding the 'go or grow' hypothesis in cancer will be investigated.

1.10.3 The evidence surrounding the 'go or grow' hypothesis in cancer

There are various factors which support the 'go or grow' hypothesis in cancer. Metabolically, the limited availability of ATP in cancer cells would be insufficient to support both proliferation and migration (Czirók et al. 1998). Moreover, during mitosis, actin and microtubules are required to support cell rounding and the mitotic spindle formation thus hindering its availability to facilitate migration (Paluch et al. 2005; Stewart et al. 2011). However, the majority of studies supporting the 'go and grow' hypothesis were conducted on cancers originating from the central nervous system (Corcoran and Del Maestro 2003; Giese et al. 1996; Schultz et al. 2002; Funk and Sage 1991). Proliferation and migration were found to be mutually exclusive in gliomas, meningioma and in primitive neuroectodermal tumours (Giese et al. 1996; Khoshyomn et al. 1999; Roth et al. 2000; Tamaki et al. 1997). However, conversely, a positive correlation between proliferation a migration has also been reported in head and neck carcinoma (Pollack et al. 1999), in medulloblastoma cells (Corcoran and Del Maestro 2003) and in 3D glioma tumouroids (Lund-Johansen et al. 1990). Moreover, in lung cancer cells, concurrent proliferation and migration was also observed (Garay et al. 2013). Moreover, although metastasis is often linked with the late-stage progression of cancer, metastasis has also been reported in the early clinical stages of lung cancer (Kamer et al. 2020; Popper 2016), thus implicating migration occurring during the early tumour development phase. Therefore the 'go or grow' hypothesis may be a simplistic snapshot of cancer cell behaviour and as the TME varies in the different cell types, different extracellular factors can regulate the proliferative and migratory responses. Although recent revelations have highlighted the influence of the ECM/β1-integrin in facilitating the pro-tumourigenic HGF-mediated outcomes, it is unclear how HGF can activate the same downstream molecular effectors and elicit the growth and migratory responses in NSCLC. Furthermore, intercellular communication within the TME remains an understudied aspect in cancer biology despite its role in mediating cancer progression. Emerging studies have implicated a unique and novel F-actin-based protrusion involved in the long-distance cell-to-cell communication (Rustom et al. 2004). These structures are termed tunneling nanotubes (TNT) have been shown to influence the survival and metastatic potential of cancer cells (Rustom et al. 2004).

1.11 Cellular communication through tunnelling nanotubes

TNTs are non-adherent actin-based cytoplasmic protrusions of cells that are either open-ended or connect to cells through connexion-containing protrusions (Lou, Fujisawa, Barlas, et al. 2012). They

were first observed in cultured rat pheochromocytoma PC12 cells, human embryonic kidney (HEK) cells and normal rat kidney cells and are regarded as a novel structure in cell-to-cell communication (Rustom et al. 2004). They were found to form either through extended protrusions from a cell or through the separation of two cells attached to each other during cytokinesis. They are known to transfer a range of cellular components (such as mitochondria, Golgi vesicles and nucleic acids), electric stimuli, viruses and signalling molecules (Ariazi et al. 2017). TNT have been observed highly in a range of diseases such as viral infections, prion-associated disease, synucleinopathies and in cancer. They are ubiquitously found in a range of cells including epithelial cells, endothelial cells, mesenchymal cells, cancer cells, immune cells and stem cells (Ariazi et al. 2017). A549 cells have also been shown to form TNT (Kumar et al. 2017). Having been only recently discovered, the intracellular and extracellular mechanisms in which they are formed and sustained are still unknown and their characteristic traits are still widely debated.

1.11.1 Characteristics of TNTs

The emergence of the appearance of various 'thin filopodia structures' was observed in different tissues of different organisms. Miller et al found that thin filopodia protrusions do not always lead to cell migration but are also associated in intercellular communication (Miller, Fraser, and McClay 1995). This led to the comprehensive categorisation of these structures by researchers and the subsequent discovery of TNTs. In the literature, there is a discrepancy in the way TNTs are characterised. TNTs and TNT-like structures have been interchangeably termed with various similar sounding names including membrane nanotube, cellular bridges, intercellular bridges and tubular bridges (Lou, Fujisawa, Barlas, et al. 2012). Therefore, to establish the characteristics of TNT, a clear distinction from other similar structures needs to be outlined.

Distinguishing TNTs and other types of thin membrane protrusions

Various studies have been conducted to distinguish TNTs from TNT-like structures. TNT-like structures have been commonly termed as cytonemes and microtubule-based nanotubes (MT-nanotubes) in different cell lines (Yamashita, Inaba, and Buszczak 2018). Cytonemes and MT-nanotubes are mainly distinguished from TNT due to their adherence to the substratum whereas TNT do not adhere to the substratum and hover in media of cell cultures (Yamashita, Inaba, and Buszczak 2018). MT-nanotubes also differ from TNTs as they are mainly comprised of microtubules and are formed through mechanisms of cilia formation (Inaba, Buszczak, and Yamashita 2015). Whilst cytonemes are similar to TNTs in regard to their cytoskeletal composition of F-actin and are thus formed through the regulators of actin dynamics, however cytonemes are also close-ended whereas TNTs can be closed or open-ended (Yamashita, Inaba, and Buszczak 2018). There have been

reports of Ca^{2+} signal exchange occurring through TNTs which implies a continuous membrane and cytosolic along the length of the TNTs or that gap junction channels are located at the end of the TNTs (Wang et al. 2010; Osswald et al. 2015; Al Heialy et al. 2015). Inhibition of the gap junctions has been shown to alter the normal functioning of TNT-mediated cellular communication. Thus, indicating that both gap junctions and TNTs cooperate to mutually enhance the cell-to-cell communication (Wang et al. 2010; Ariazi et al. 2017). TNTs can also facilitate long-range transmission *via* an IP_3 gap junction mechanism (Lock, Parker, and Smith 2016). Conversely, TNTs in lymphocytes lack permeability to Ca^{2+} and are unable to transport other membrane proteins which demonstrates a closed-ended TNT (Gerdes and Carvalho 2008). However closed-ended TNTs are also involved in the transmission of cargo, closed-ended TNTs protruding from separate cells (Fig. 11a) are able to transfer viruses to each other (Jansens et al. 2017) and this might be occurring through a synaptic mechanism. However, the mechanisms of TNT formation are still not well defined and the influence of its environment may play a part in whether an open or closed-ended TNT would form.

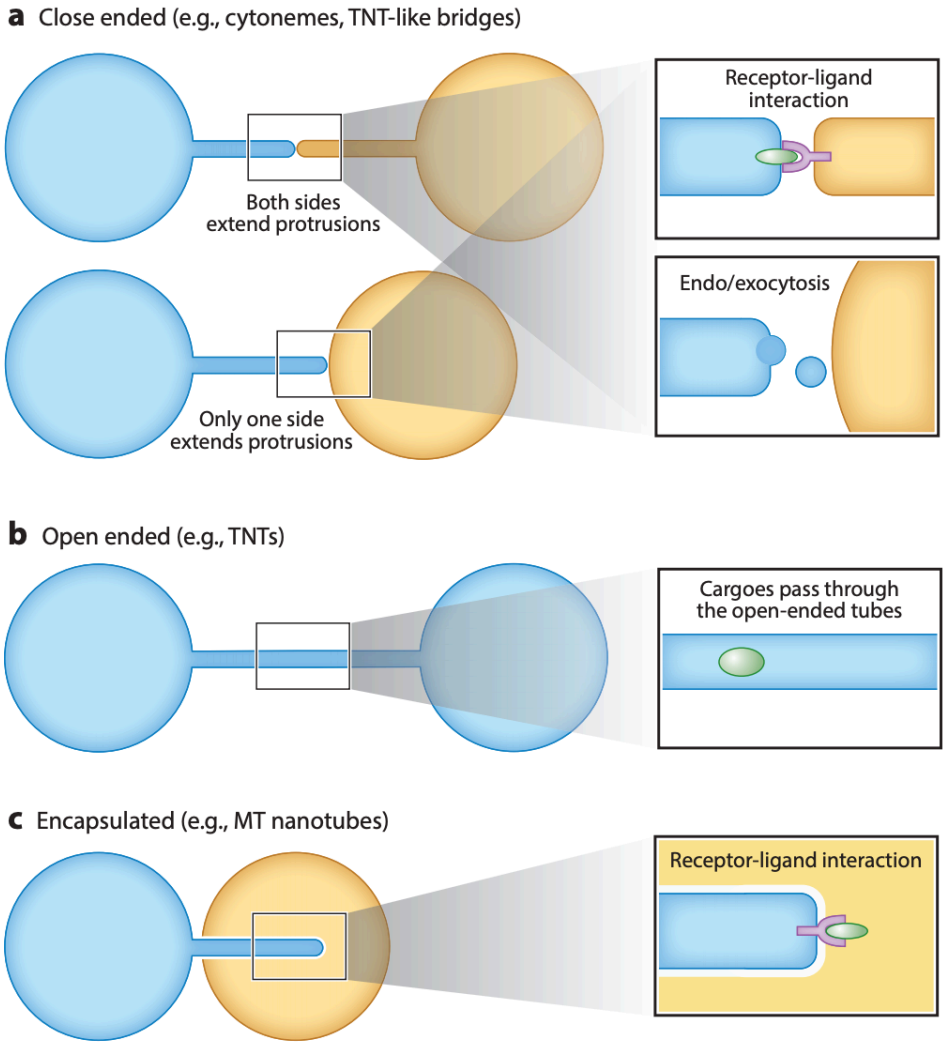


Figure 20: Diagram of the different types of distinguished thin membrane protrusions (Yamashita, Inaba, and Buszczak 2018)

The structures of cytonemes, TNTs and MT-nanotubes are highlighted below:

a. Cytonemes and TNT-like protrusions are close-ended. At the surface end of the protrusions, signalling can either occur through ligand-receptor binding interactions or through endocytosis and exocytosis.
b. TNTs are open-ended which allow for the transfer of cellular components (such as mitochondria, Golgi vesicles etc) to the joined cell.
c. MT-nanotubes protrusions, mainly comprised of microtubules, are found within the neighbouring cell. Receptor-ligand signalling interactions take place at the tip of the protrusion. There is a possibility of endocytosis and exocytosis occurring at the tip of the protrusion although this has not been evidenced yet.

Distinguishing between TNTs and tubular structures

Tubulogenesis is a complex and intricate process whereby epithelial or endothelial cells organise into branched hollow tubular structures (Bowes III et al. 1999). These hollow tubules share a resemblance to TNTs *in vitro* whereby both structures feature elongated morphology and function

as a conduit for nutrient exchange. The molecular mechanisms underlying tubulogenesis have been widely studied in the literature. The intricate process requires cooperation between growth factors, such as HGF (Pollack, Runyan, and Mostov 1998), and various ECM components to facilitate the changes in cell morphology, proliferation, ECM proteolysis and remodelling of the ECM (Zhang and Woude 2003). Epithelial-mesenchymal transition (EMT) is the initial step in the transformation and is mediated by the Raf-MEK-ERK signalling which causes cells to elongate and the cytoplasm to extend to the matrix becoming more fibroblast-like in morphology (Hogan and Kolodziej 2002). The cytoplasmic extensions then become thicker and longer, avoiding anoikis and mediating survival through transcription of the Snail family, and thus transforming into single chains. The STAT3 and NF-κB signalling pathways plays a role in the tubular transformation whereby cells redifferentiate forming mature tubules and thus a continuous lumen (Boccaccio, Andò, et al. 1998). HGF/c-Met signaling pathway also crosstalk with integrin/ECM signaling to facilitate the formation of branching tubules (Chiu et al. 2002). β1-integrin in particular is vital in inducing lung branching morphogenesis *in vivo* (Plosa et al. 2014) and in mammary duct formation (Montesano and Streuli 1999). However, the main defining difference between tubular structures from TNTs are their multicellular reorganisation in lumen formation whereas TNTs are open-ended cytoplasmic protrusions connecting between individual cells. Therefore, TNTs are morphologically distinguished *in vitro* from the multicellular tubular structures.

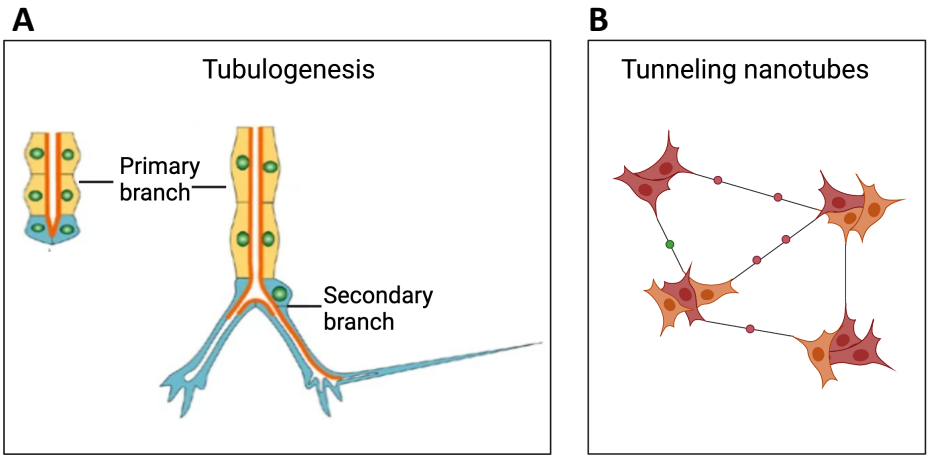


Figure 21: Diagram depicting tubulogenesis and tunneling nanotubes, adapted from (Hogan and Kolodziej 2002)

a. Neighbouring epithelial cells are polarised and extend to form the primary branch which consists of a lumen two cells wide. Growth factors, including HGF and FGF, dictate the cellular reorganisation and ECM remodeling required for tubule formation. The secondary branches form from the elongation of the tip cells.
b. Tunneling nanotubes are open-ended cytoplasmic protrusions connecting between individual cells.

Despite all the findings in distinguishing the various protrusions observed in cell lines and tubular hollow structures *in vitro*, little is still known regarding TNTs, there are no specific biomarkers, and

the morphological description varies across the different cell lines and their growth conditions. This poses a challenge to correctly identify TNT and their functions in studies. Structurally TNTs contain cytoskeletal filaments with F-actin as the main constituent. F-actin is involved in the formation of TNTs as the formation is inhibited when F-actin depolymerization drugs were utilised (Lou, Fujisawa, Barlas, et al. 2012). The presence of connexin-43 (CX43), M-Sec, actin-based motor proteins Myosin-X and Va have been found on various cell types including neuronal, stem cells and astroglial cells (Ariazi et al. 2017). Korenkova et al proposed the main morphological properties of TNTs: a straight structure, containing F-actin, spanning several cell diameter in length and thickness below 1µm (Korenkova, Pepe, and Zurzolo 2020). However, there is variability in length, morphology and diameter of TNTs depending on the experimental procedures, timing, and growth culture conditions of the different cell lines. Various lengths have been reported from 50 to 200µm in PC12 cells and multiple thinner TNTs can join to form a singular TNT (Austefjord, Gerdes, and Wang 2014). The composition of TNT varies between cell lines with some containing microtubules which has given rise to categorising TNTs into 'thin' (<0.7µm) or 'thick' nanotubes (>0.7 µm)(Korenkova, Pepe, and Zurzolo 2020). In A549 cells, TNT has been shown to contain microtubules and F-actin with lengths up to 105µm with a diameter ranging from 400-1500nm (Austefjord, Gerdes, and Wang 2014). Furthermore, TNT in A549 cells exists in multiple forms including curved, straight, multiple and branched (Kumar, Tiwari, and Rajala 2017). This demonstrates the diverse heterogeneity of TNTs between the different cell lines widely established in the literature.

Although TNTs are categorised by their length, thickness and through their cytoskeletal composition of F-actin and microtubules in some cases (Rustom et al. 2004), studies have also shown that stress conditions can alter cytoskeletal composition in TNTs. UV irradiation can induce microtubules in TNTs of the PC12 cell line thus stabilising the TNTs and allowing for mitochondrial transfer to the stressed cells preventing cell death (Wang and Gerdes 2015). Additionally, microtubules are always found in the TNTs of head and neck squamous cell carcinoma culture as part of their stress-survival mechanism in the tumour microenvironment. The same study also demonstrated that the presence of microtubules was vital in transporting vesicles thus suggesting that the cytoskeletal components of the TNTs reflect the types of cellular cargo being transported between the cells (Sáenz-de-Santa-María et al. 2017). Despite the extensive studies highlighting the diversity in cytoskeletal components and dimensions of TNTs, further work is still required to distinguish whether TNTs exist in different forms adapting to environmental stress or whether the differences observed represent the different stages of maturation in the processes of TNTs.

1.11.2 Mechanisms regulating TNT formation

One of the ways TNTs are formed is through the development of F-actin-rich cellular protrusions between one or two cells (Rustom et al. 2004). The mechanisms underlying this process is still unknown although the speculated process may mimic the mechanisms in filopodia formation. Filopodia initiation involves activation of Cdc42, which is part of the Rho GTPase family, which leads to the nucleation of actin filaments. The actin protrusions can further extend directionally through actin polymerisation toward a recipient cell (Faix and Rottner 2006). In TNTs it is still unknown what dictates the direction of its outgrowth however in drosophila wing imaginal disc cell, cytonemes grow accordingly to a chemical gradient of the growth factor Dpp, (Decapentaplegic, a member of the TGF-β) (Hsiung et al. 2005). Recipient cells may exhibit a similar mechanism in TNT extension however this has not been demonstrated. Adhesion molecules, such as cadherins, are also required when the tips of the TNTs connect to the plasma membrane of the recipient cell. For open-ended membrane continuity of TNT to be maintained, fusion molecules such as SNARE proteins and viral fusion proteins mediate membrane fusion at the tips of the TNT by perturbing the lipid bilayer and the membrane curvature (Jena 2011; Abounit and Zurzolo 2012) . The second proposed mechanism of TNT formation is through the migration of two cells in opposing directions with a TNT forming between them (Rustom et al. 2004). Likewise, the mechanisms underlying the process from initial cell adherence then to migration are unknown. Less is known about the involvement of adhesion molecules or membrane fusion molecules. Actin can also induce cell-cell fusion in myoblasts (Chen et al. 2007) thus potentially playing a role in this process.

M-sec, initially discovered as tumour necrosis factor-α induced protein 2 (Sarma et al. 1992), plays a vital role in the plasma membrane protrusion in TNT formation and acts as a marker of TNTs. Knockdown of M-sec in the macrophage cell line, Raw264.7, resulted in a decrease in the number of TNTs and in the transmission of intercellular calcium flux (Hase et al. 2009). M-sec transfected HeLa cells show an increase in the plasma membrane protrusion extending to fuse with the ends of the TNT to the connected cell (Kimura, Hase, and Ohno 2012, 2013). M-sec can facilitate the extension of TNT of HeLa cells through cytoskeletal remodelling. M-sec localises with the active Ras-like small GTPase (Ral GTPase) and further interacts with the exocyst complex (a downstream effector of Ral) to induce TNT formation. These TNT induced by M-sec also only express F-actin and not microtubules (Hase et al. 2009). Therefore M-sec is vital in regulating the cytoskeletal remodeling in TNT formation. Furthermore, in fibroblasts, Ral-A binds to filamin, which are cross-linked actin filament binding proteins, to induce filopida formation (Ohta et al. 1999). Ral-A also induces the activation of Cdc42 to increase filopodia formation and cytoskeleton remodeling (van Dam and

Robinson 2006). The exocyst complex is also involved in the transfer of cytoplasmic vesicles to form new plasma membrane (Moskalenko et al. 2002) and could potentially aid in supplementing plasma membrane to the newly formed TNT. Cdc42 is also involved in the M-sec mediated TNT formation. The presence of the negative form of Cdc42, Cdc4217N, which also selectively binds to GDP, caused a reduction in TNT formation (Hase et al. 2009). Utilising inhibitors of Cdc42 and through siRNA of Cdc42, significantly decreased membrane protrusions and the synaptic HIV-1 transfer. There is also partial localisation of Cdc42 in the M-sec TNTs (Nikolic et al. 2011). The Fas ligand-receptor signalling activates the Rho GTPases leading to TNT formation and transmission of cell death signals in T cells (Arkwright et al. 2010).

TNTs are also formed and sustained under various growth culture conditions. It is widely known that TNT formation increases when cells are exposed to certain stress conditions, ranging from exposure to H_20_2, UV, virus infection, prion aggregation, low serum and high glucose concentration (Thayanithy et al. 2014; Wang et al. 2011; Wang and Gerdes 2012). Studies in astrocytes have also provided more insight into the signalling pathways involved in TNT formation. H_20_2 exposure in astrocytes led to the stress-induced activation of p38 MAPK pathway which caused an increase in TNT formation, reorganisation of the cytoskeleton and decreased the membrane fluidity (Zhu et al. 2005). Furthermore, it has been found that p53 activation, from cellular insults, leads to the upregulation of EGFR receptors which then activates the Akt/PI3KmTOR pathway. This leads to F-actin polymerisation and TNT formation. Although this suggests that the initiating cell is solely responsible for TNT development, there may also be receptor or molecular cues being released from the recipient cell in order to guide the TNT towards a certain direction (Wang et al. 2011). Furthermore, in ovarian cancer cells, the MAPK pathway was activated downstream of the EGF/EGFR receptor signalling to induce TNT formation (Cole, Dahl, and Cowden Dahl 2021).

Most recently, it has been discovered that FAK signalling is involved in TNT formation in head and neck squamous cell carcinoma (SCC) (Sáenz-de-Santa-María et al. 2017). FAK is one of the main pathways activated through integrins and mediates cytoskeletal actin remodeling. In this same study, utilising the inhibitors of the PI3K and MAPK pathways resulted in a 75% decrease in TNTs with the PI3K inhibitor but no significant change was observed with the MAPK inhibitor (Sáenz-de-Santa-María et al. 2017). This suggests that the pathways regulating TNT formation vary between cell types and the other mechanisms driving the actin cytoskeleton remodeling in TNT formation. The use of FRNK, a truncated isoform of FAK which acts as a dominant negative inhibiting FAK activation, reduced the number of TNTs and the length of TNTs in SCC (Sáenz-de-Santa-María et al. 2017). More interestingly, this reduction in TNT was partially reversed by MMP-2 through co-culturing the FRNK-cells with FAK-proficient cells with MMP-2 overexpression (Sáenz-de-Santa-María

et al. 2017). The conditioned culture media from the MMP-2 overexpressed cells were also able to increase TNT formation and this effect was inhibited with an MMP-2 neutralising antibody (Sáenz-de-Santa-María et al. 2017). This suggests that TNT formation in SCC cells occurs through a FAK/MMP-2 signalling axis (Sáenz-de-Santa-María et al. 2017). Furthermore, breast cancer cells grown on collagen type I and fibronectin in 3D cultures displayed long TNTs (Franchi et al. 2020). This evidence demonstrates that the ECM-integrin-FAK signalling axis could potentially be involved in NSCLC TNT formation and stabilisation. Moreover, mature B cells binding to fibronectin *via* its main receptor, the α5β1 integrin, was essential in inducing TNT formation (Osteikoetxea-Molnár et al. 2016). However, the same study showed that inhibition of the α5 and β1 subunit, using the respective functionally blocking antibodies alone, had no effect on TNT formation (Osteikoetxea-Molnár et al. 2016). As β1-integrin has also been widely known to co-operate with the c-Met/HGF signalling pathways in NSCLC (Barrow-McGee, Kishi, et al. 2016b; Mitra et al. 2011), there could be potential signalling cooperation existing to facilitate TNT formation in NSCLC.

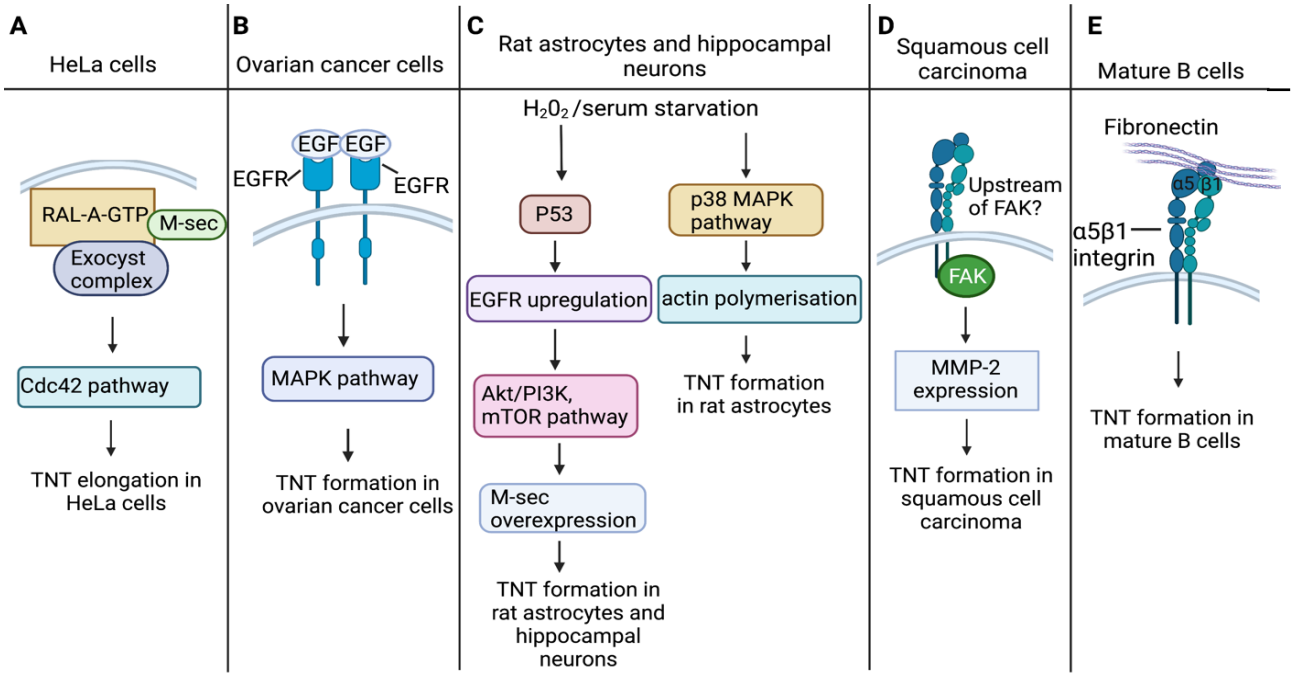


Figure 22: The signalling mechanisms involved in TNT formation

A. In HeLa cells, M-sec associates with the activated Ral-A which subsequently leads to Ral-A binding to its downstream effector, the exocyst complex. The exocyst complex is involved in transferring secretory vesicle to aid in the plasma membrane formation. Ral-A can also bind with Ral binding protein 1 (RalBP1) which then activates Cdc42 leading to TNT formation through actin cytoskeletal remodelling. Ral-A also binds with filamin which induces actin remodeling in filopodia. This may be a potential mechanism in TNT formation (Hase et al. 2009).

B. EGF binding to EGFR activates the downstream MAPK pathway which has been shown to induce TNTs in ovarian cancer cells (Cole, Dahl, and Cowden Dahl 2021).

C. When astrocytes and hippocampal neurons are subjected to stress conditions such as H_20_2 and serum starvation, this activates p53 which subsequently leads to the upregulation of the EGFR and activation of the Akt-PI3K-mTor pathway. P53 also induces M-sec however it is still unclear whether EGFR and the Akt-PI3K-mTor pathway can directly mediate TNT formation. Exposure to H_20_2 in astrocytes can also trigger the p38 MAPK pathway, inducing actin polymerisation to form TNT (Wang et al. 2011).

D. The localisation of FAK to integrins triggers intermediary pathways, still unknown, to upregulate MMP-2 and MMP-2 gene expression. This results in TNT formation *via* actin cytoskeletal remodeling in SCC. However it is not known whether integrins are involved upstream of FAK activation (Sáenz-de-Santa-María et al. 2017).

E. In mature murine B cells, TNT formation relied on interactions with fibronectin and $\alpha5\beta1$ integrin activation (Osteikoetxea-Molnár et al. 2016).

The pathways underlying the development of TNTs is still not clearly elucidated. Gaining a comprehensive understanding underlying TNT formation is important in identifying potential specific markers of TNT. This can then be beneficial for further studies to understand the impact of intercellular communication occurring through TNTs in health and disease.

1.11.3 Biological role of TNTs

TNTs are a relatively novel mode for intercellular communication and are involved in a wide spectrum of roles in disease and health. Likewise, with HGF and IL-6, TNT formation has a dual role as a conduit to either enhance disease transmission or to provide essential organelles and cellular components as part of a stress survival or genetic disease rescue mechanism. Various types of cells utilise TNT to provide essential transport of cellular components in physiological development (including the embryogenesis of the *Drosophila*). TNTs are also known to transfer viruses such as HIV and prions (Ariazi et al. 2017). TNTs are also involved in wound healing, in response to tissue injury TNTs form to exchange mitochondria and energetic components to aid in cell survival (Li et al. 2014; Wang et al. 2011; Thayanithy et al. 2014).

Similarly to HGF, TNT formation is elevated during tissue damage and trauma in the lung (Li et al. 2014). Several studies have shown the therapeutic potential of mesenchymal stem cells (MSCs) *via* the TNT-mediated transport of mitochondria in attenuating lung damage in fibrosis and COPD. MSCs facilitate LPS-injured lung alveolar epithelial repair through the formation of TNTs. MSCs mediate the transfer of mitochondria to the injured cells to initiate repair. The MSCs and the injured alveolar epithelial cell initially form gap junction channels which consist of connexin 43 before developing into TNT (Islam et al. 2012). In another study, MSCs derived from human-induced pluripotent stem cells (iPSC-MSCs) were intravenously administered to cigarette smoke-exposed rats and a reduction in alveolar destruction, due to mitochondrial transfer, was observed in the treated rats compared to control. *In vitro* co-culture revealed that this effect was mediated by the TNT transport of mitochondria from the iPSC-MSCs to the bronchial epithelial cells (Li et al. 2014). This demonstrates

the potential for TNTs in cell-based therapy in inflammatory lung diseases however the specific mechanisms mediating the mitochondrial transfer are still unknown. Furthermore, TNT-mediated transport of mitochondria has also been reported in various cancers (Pasquier et al. 2013; Wang and Gerdes 2015; Lu et al. 2017). Therefore, gaining insight into the regulatory mechanism and functional of TNTs in the pathogenesis of cancer could lead to the development of new therapeutic targets.

1.11.4 TNTs in cancer

Cancer cell communication is vital in coordinating cell reorganisation and synchronisation to facilitate invasion and metastasis however this is still an understudied aspect of tumour progression. Gap junctions and microvesicles are the main known modes of short-range cancer cell communication however TNTs are an emerging novel mode for long-range communication existing between the different cell types that exist in the tumour (Lou, Fujisawa, Barlas, et al. 2012). TNTs spanning over 100µm were commonly observed in various cancer cells such as in lung, breast, ovarian, prostate, pancreatic and colon cancer (Lou, Fujisawa, Barlas, et al. 2012). Moreover evidence has shown that only 10% of a solid tumour consists of cancer cells, the remainder comprises inflammatory and stromal cells (Elenbaas and Weinberg 2001). TNT can therefore serve as a long-range communication mode for cancer cells and stromal cells at a distance from each other. Transfer of miRNA *via* TNT was observed between osteosarcoma cells and stromal murine osteoblast cells, inducing malignant transformation in the recipient cell (Thayanithy et al. 2014). TNTs also transport a range of cellular components to facilitate tumour progression such as transporting Golgi vesicles and mitochondria in malignant mesothelioma cells. In this same study, TNTs were also observed in human lung adenocarcinoma and mesothelioma tumour samples, thus highlighting its evidence in solid tumours outside *in vitro* settings (Lou, Fujisawa, Morozov, et al. 2012). The transfer of mitochondria between endothelial and ovarian cancer cells which aid in chemoresistance has also been observed in a study (Pasquier et al. 2013). Transfer of lysosomal vesicles, mitochondria and autophagosomes also occurred *via* TNT in SCC (Sáenz-de-Santa-María et al. 2017). Therefore, TNTs in cancer mediate the transmission of new materials to transform tumour cells into invasive phenotypes to metastasise and propagate chemoresistance. The hypoxic, acidic and low nutrient state of the tumour environment further supports the ideal conditions for TNT formation. Several studies support this as TNTs have been shown to form as part of the cellular stress response (Lou, Fujisawa, Morozov, et al. 2012). Hypoxic states in ovarian and colon cancer also increase the induction of TNT formation (Desir et al. 2016). Inflammatory states in cancer have also been shown to induce the formation of TNTs as part of a response to metabolic stress (Ariazi et al. 2017).

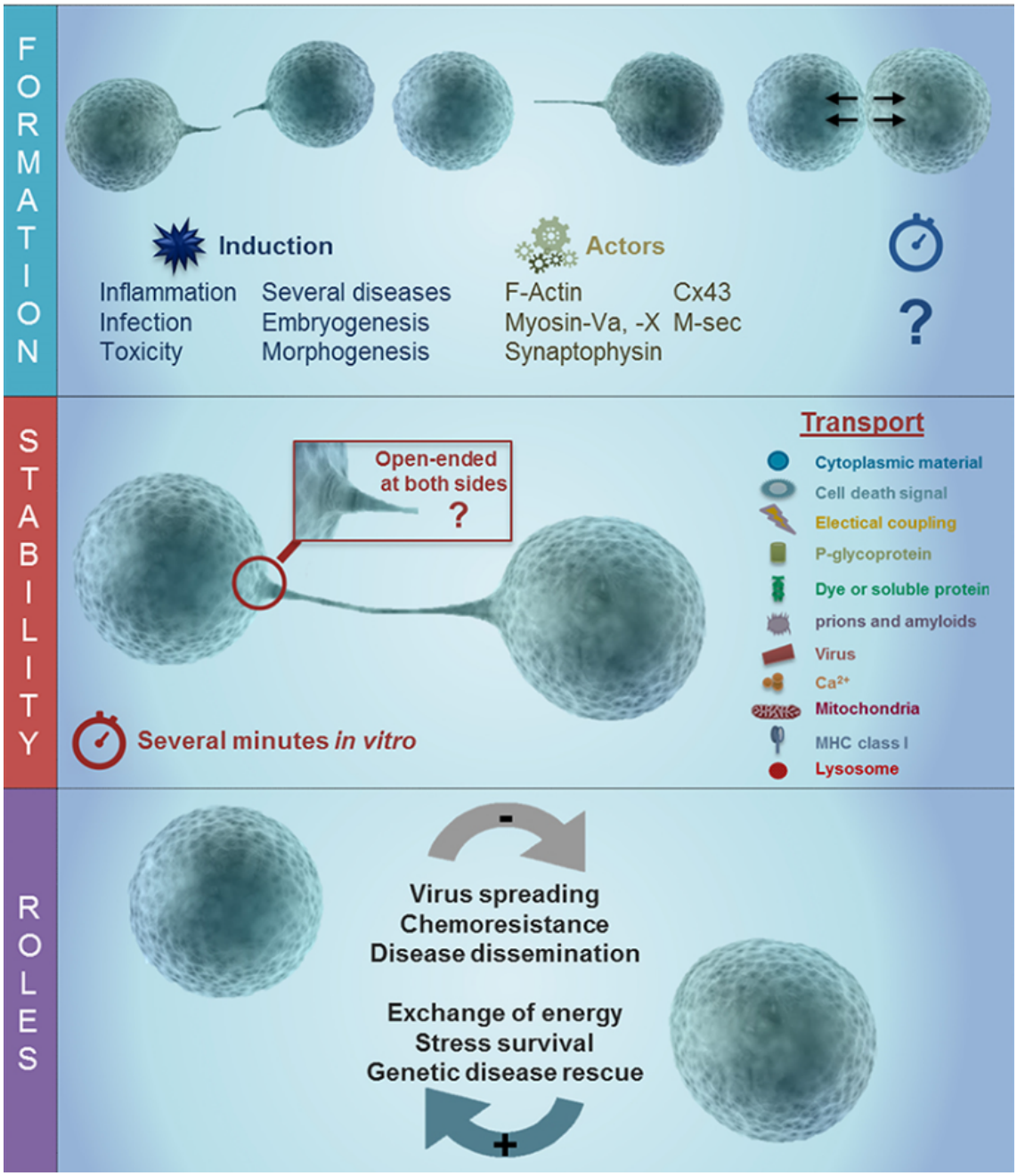


Figure 23: The formation, stabilisation and roles of TNTs (Ariazi et al. 2017).

Various conditions can stimulate the formation of TNTs which include inflammation, infection, toxicity, embryogenesis, morphogenesis and disease. Various cell lines have reported the involvement of proteins such as actin, Myosin VA and X, synaptophysin, CX43 and M-Sec in the formation of TNTs. TNTs transport cytoplasmic material, cell death signals, electric signals, p-glycoprotein, soluble proteins, prions and amyloids, viruses, Ca^{2+}, mitochondria and lysosomes between cells. TNTs are involved in diseases, such as virus transmission, chemoresistance, and disease dissemination. TNTs are also involved in energy survival, stress survival and genetic disease rescue.

Overall TNT research is still in its infancy and there are still many unknown aspects. The mechanisms for TNT to selectively transport certain cellular components over others, regardless of their size, are not yet understood. Furthermore, gaining a full spectrum of the signalling pathways involved in the

formation of TNTs may hold the key to unravelling the intricate long-range communication between cells and the tumour matrix to support cancer progression. The influence of growth factor ligand-receptor signalling in the formation or sustaining of TNTs has not been studied in cancer including NSCLC. The HGF/c-Met signalling pathways may be a potential candidate in inducing TNT formation. Gaining this insight would provide the basis in developing targeted therapies in NSCLC.

1.11 The clinical landscape and multi-drug targeting

Over the last 40 years, the survival rate of lung cancer in the UK has only improved from 3 to 5% highlighting the need for improved targeted therapies (CRUK, 2016). Currently, a combination of cisplatin-based chemotherapies (e.g. cisplatin and another cytotoxic therapy) remains the first-line treatment in NSCLC (Hanna, Johnson, et al. 2017). The issue of unfavourable side effects and resistance to chemotherapeutic agents has led to the development of EGFR tyrosine kinase inhibitors (e.g. erlotinib and gefitinib) and EGFR neutralising antibodies (e.g. cetuximab and bevacizumab) as a second and third-line treatment in NSCLC (Liu, Jin, et al. 2017). However, resistance to EGFR therapies has been reported as early as 8-12 months of treatment (Pao and Chmielecki 2010). However, resistance to EGFR therapies has been reported as early as 8-12 months of treatment (Pao and Chmielecki 2010). Moreover, the HGF/c-Met signalling has been implicated in driving resistance to EGFR therapies (Bean et al. 2007; Engelman, Zejnullahu, Mitsudomi, et al. 2007). This has led to the development of HGF antagonists (e.g. rilotumumab and ficlatuzumab), anti-MET receptor monoclonal antibodies (e.g. onartuzumab) and small molecule MET kinase inhibitors (e.g. crizotinib, foretinib and cabonzantinib). Despite the progress in the development of targeted therapies for MET, clinical trials targeting HGF/c-Met and EGFR have provided mixed results with patients. There have been some studies which have shown good response when patients, with high MET amplification and with the MET exon-14-skipping variants, were given c-Met inhibitor, savolitnib, alongside an EGFR inhibitor, osimertinib (Bahcall et al. 2016; Paik et al. 2015). However, the randomised phase III trials comparing onartuzumab (a monoclonal antibody to c-Met)(Spigel, Edelman, O'Byrne, Paz-Ares, et al. 2017) and tivantinb (a c-Met inhibitor)(Scagliotti et al. 2015) with EGFR inhibitor erlotinib for patients with advanced NSCLC have been unsuccessful. However, this could be explained by ineffective patient recruitment as the patients were not screened for EGFR or MET genetic status and activity. Furthermore, the drug acts to inhibit HGF binding to c-Met and does not affect the intrinsic ligand-independent receptor activity which is the main mode of proliferative signalling. The HGF/c-Met signalling axis may also be implicated in TNT formation and potentially confer a survival phenotype to recipient cells via organelle transfer. Therefore, therapeutically targeting HGF/c-Met may serve a wider effect in inhibiting the pro-tumourigenic intercellular communication in NSCLC. TNTs do not have a specific marker, and their mechanism of formation is

still not well defined. This has led to minimal studies exploring the therapeutic inhibition of TNTs. So far, metformin, everolimus (a mTOR inhibitor) and latrunculin A (an actin depolymerisation drug) were able to individually reduce TNT formation in mesothelioma cells (Lou, Fujisawa, Morozov, et al. 2012). Both drugs were also known to inhibit proliferation in cancer cells and can potentially be repurposed for TNT-targeted therapy. PF-562271, a FAK tyrosine kinase inhibitor undergoing clinical testing in SCC cancer, also decreased TNT formation in SCC cells (Sáenz-de-Santa-María et al. 2017).

Moreover, as HGF/c-Met could potential crosstalk with other pleiotropic cytokines, including IL-6 in NSCLC (Hov et al. 2007; To et al. 2002), IL-6 targeted therapies could also be used in combination with HGF/c-Met therapies in future clinical trials. Currently, the development of monoclonal antibodies against IL-6 are being assessed in clinical trials in NSCLC. The humanised anti-IL-6 antibody, ALD518, has shown promising progress in Phase I and II trials, improving NSCLC-associated anaemia and cachexia (Bayliss et al. 2011). Siltuximab is another monoclonal antibody which has been shown to reduce NSCLC tumour growth by inhibiting STAT3 phosphorylation (Song et al. 2011). The development of natural products are also being made to target integrins in cancer therapy. α-Lipoic acid has been found to reduce levels of β1 and β4 -integrins, sensitising lung cancer cells to chemotherapy and anoikis (Aksorn and Chanvorachote 2019). Lunasin acts as an integrin signalling antagonist by disrupting $\alpha v\beta 1$ and $\alpha v\beta 3$ interactions, which inhibits NSCLC proliferation by blocking phosphorylation of FAK, ERK1/2 and Akt (Inaba, McConnell, and Davis 2014). Furthermore, a phase I clinical trial with volociximab, a chimeric monoclonal functionally blocking antibody for $\alpha 5\beta 1$, showed promising clinical efficacy and tolerance in patients with solid malignancies (including NSCLC) (Ricart et al. 2008).

Despite previous hurdles, there is still potential to exploit the drug mechanism of inhibiting the HGF-dependant signalling in the absence of MET amplification. This is especially applicable within the tumour microenvironment whereby synergistic inhibition of the HGF/c-Met signalling alongside with macrophage targeted depletion through antibodies has shown to inhibit c-MET signalling in macrophages (Comoglio, Trusolino, and Boccaccio 2018). Ultimately establishing the relationship between HGF with other growth factors and the ECM in growth and TNT formation is essential to overcome the clinical challenges present and inform future multi-drug therapies.

1.12 Rationale

Within the tumour microenvironment, pleiotropic cytokines such as HGF, IL-6, EGF and their respective receptors are mutationally overexpressed in NSCLC which leads to aberrant signalling leading to cancer progression (Lee et al. 2016; Naldini et al. 1991; Yarden 2001). Furthermore, the remodeling of the lung ECM leads to the initiation and propagation of pro-tumourigenic signalling

and harbours a reservoir of growth factors (Noriega-Guerra and Freitas 2018). Extensive studies have characterised the individual migrative, proliferative and invasive properties of each of these components in cancer. However, there is mounting evidence that the ECM/β1-integrin crosstalk with HGF and IL-6 to promote EMT and anchorage-independent survival (Barrow-McGee, Kishi, et al. 2016b; Lee et al. 2016). This thesis will explore the potential crosstalk and convergent signalling between HGF and IL-6 on A549 cell proliferation and the role of β1-integrins in mediating the proliferative outcomes.

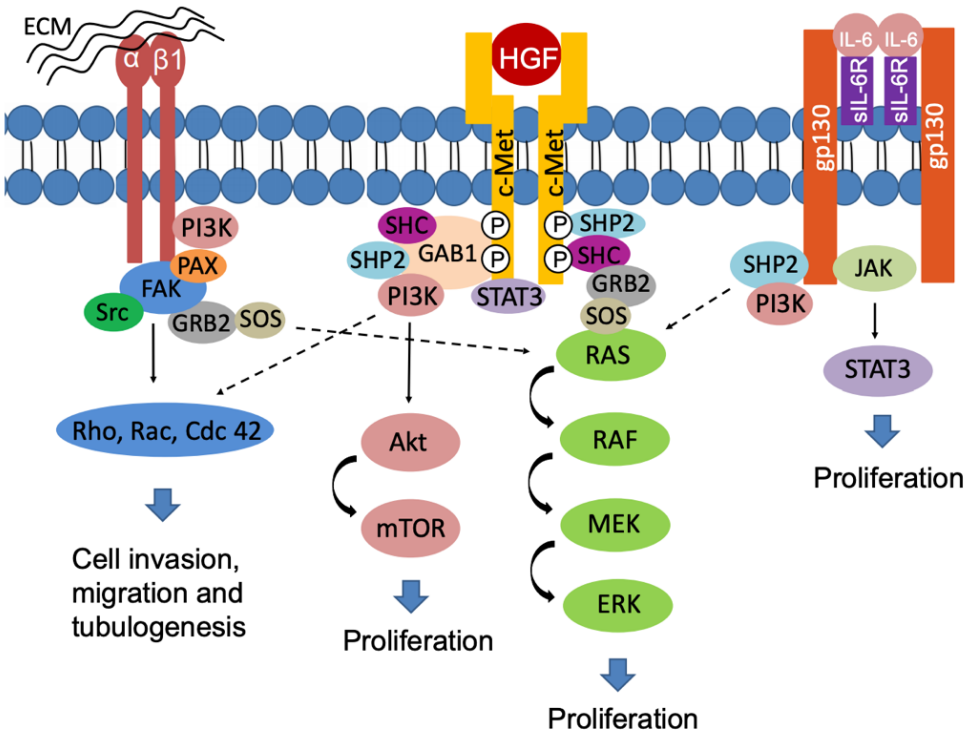


Figure 24: The potential convergence of the pathways induced by HGF, IL-6 and the ECM with their respective receptors in NSCLC

This thesis aims to investigate the potential downstream convergence of the MAPK, PI3K, FAK and STAT3 signalling pathways associated with HGF, IL-6 and the ECM/integrin-induced proliferation in A549 lung adenocarcinoma cells. The dotted arrows represent the potential signalling convergence and the lined arrows indicate the known pathways induced.

Another aspect of focus in this thesis will be investigating the effect of HGF in inducing TNT formation. The complex multi-step development of cancer also involves tumour cells communicating with one another to facilitate cancer progression. TNTs can facilitate this long-range communication and transmit a variety of cellular components to support the invasive phenotypes of the tumour cells (Lou, Fujisawa, Barlas, et al. 2012). Furthermore, the EGF growth factor signalling has been linked to TNT formation in astrocytes (Wang et al. 2011) and evidence of TNT structures are present in human lung adenocarcinoma tissue (Lou, Fujisawa, Morozov, et al. 2012). Moreover, HGF and c-Met are mutationally overexpressed in NSCLC (Onitsuka et al. 2010) and could therefore be a potential

candidate factor in TNT formation. The signalling pathways involved in TNT formation also differ between different cell types and minimal TNT studies have been conducted in NSCLC. Therefore, the potential downstream pathways involved will also be investigated. As an emerging field in cancer communication, the role of HGF would be a novel finding implicated in the development of TNTs.

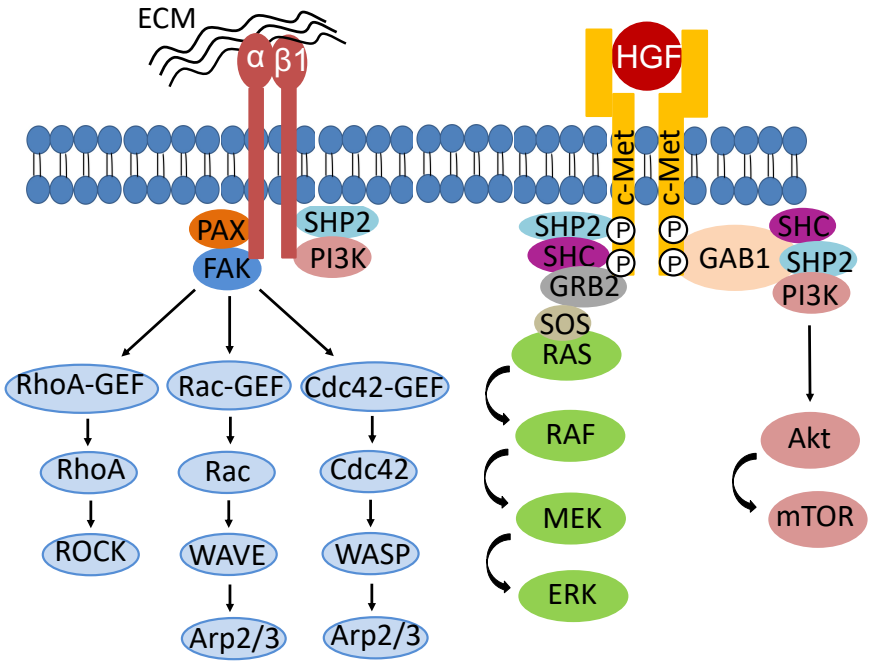


Figure 25: The potential HGF/c-Met/β1-integrin signalling involved in mediating TNT formation in A549 cells

This thesis aims to investigate the potential crosstalk between HGF/c-Met and β1-integrin in A549 cell TNT formation. The downstream MAPK, PI3K, CDC42, Rac and ROCK signalling pathways are associated with HGF/c-Met activation and TNTs may be induced *via* these pathways.

In this thesis, the 'go or grow' hypothesis will also be explored and challenged. The 'go or grow' hypothesis was disputed in lung cancer in a previous study which showed a positive correlation between proliferation and migration (Garay et al. 2013). As HGF can induce both proliferation and migration, we investigated and characterised a subpopulation of A549 cells which can undergo concurrent proliferation and migration.

The last focus of this thesis was to investigate the elusive role of eosinophils in NSCLC. Eosinophils are an understudied immune cell in cancer biology despite being able to infiltrate NSCLC tumours (Davis and Rothenberg 2014). Various studies have shown a favourable prognosis with TATE in solid tumours (Simson et al. 2007; Tepper, Coffman, and Leder 1992). However, the effect of eosinophils in NSCLC is still not known. Therefore, this will be investigated through the development of a novel HL-60/eos-A549 co-culture experimental system which will be described in the latter part of this thesis (see **Method section 2.7**).

1.13 Experimental approach

In this thesis, a variety of experimental approaches was used to assess growth and TNT formation. *In vitro* hemocytometer cell counts were used to identify the potential proliferative capacity of HGF, IL-6, collagen IV, laminin and fibronectin. However, most studies conducted in this thesis required the use of a range of microscopy techniques including white light microscopy, time-lapse microscopy and epifluorescence/confocal immunofluorescence visualisation (fixed and live-cell imaging). To visualise the fluorescent proteins of interest in our growth and TNT studies, a source of light at a specific wavelength illuminates and excites the fluorescent protein to a higher energy state, this involves the electrons to move to an orbital space further from the nucleus. When the fluorescent protein returns to the ground state, this causes a loss of vibrational energy and the emission of light at longer wavelengths. This can then be detected and visualised using either a widefield epifluorescence (Zeiss Axiovert 200M) or a laser scanning confocal microscope (Zeiss LSM 980-Airyscan). An epifluorescence microscope uses a high-intensity light source focused by an objective lens to illuminate the fluorophore. The emitted light passes through a dichroic filter cube which allows specific fluorescence to be focused onto the detector (Fig24.A). Images were then captured using a Zeiss Plan-Neofluar x20 0.5 NA objective in this study. Epifluorescence microscopy was used to rapidly image cells labelled with fluorescently tagged EdU-labelled nuclei of A549 tumouroids or caspase-3 labelled cells. Image analysis, using ImageJ, was then undertaken to quantify the percentage of EdU incorporated nuclei and capase-3 labelled cells in these studies (see **Methods, Section 2.8.4**). The laser scanning confocal microscopy was used to obtain higher-resolution images of the immunofluorescent labelled components of TNTs (which includes F-actin, α-tubulin, M-sec, c-Met, β1-integrin and paxillin) and to visualise live trafficking of mitochondria/vesicles along the TNTs. Confocal microscopy uses light emitted by a laser to excite fluorescent proteins. In addition, a second objective lens directs the emitted light towards a narrow pinhole, which removes out-of-focus light and point illumination of the focal plane (Fig24.B). This further allows for optical sectioning whereby imaging of the 2D focal planes within the sample is undertaken. This allowed for visualisation of the non-adherent nature of TNTs *via* z-stack acquisition of the focal planes to obtain 3D reconstruction and xz/xy orthogonal view. Images on the confocal microscope were captured using a X40 1.3 NA oil immersion objective in this study.

Moreover, the appropriate pharmacological inhibitors were also used to investigate the potential downstream signalling pathways involved in the HGF and IL-6-mediated proliferation, the HGF/c-Met/β1-integrin-induced TNT formation and the HGF/c-Met and EGF/EGFR-mediated TNT formation. Extensive image analysis, using ImageJ, was then undertaken to quantify TNT formation

(see **Methods, section 2.8.1**), EdU positive nuclei (see **Methods, section 2.8.4**) and caspase-3 positive cells (see **Methods, section 2.8.7**).

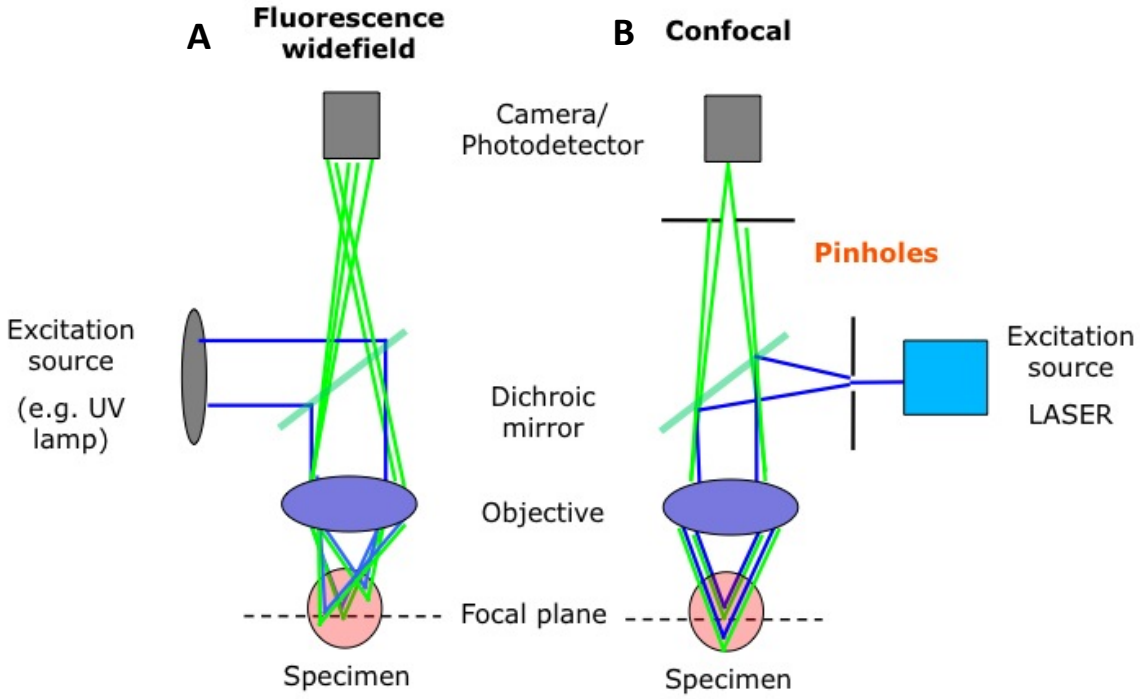


Figure 26: Schematic depicting the difference between widefield epifluorescence and confocal microscope, adapted from (Bretschneider and De Weille 2018).

The schematic shows the widefield epifluorescence (A) and confocal microscope (B) setup. In a widefield epifluorescence microscope, the emitted fluorescence from the sample passes through the dichroic filter cube, which allows for the wavelength specific fluorescence to pass through before being directed to the camera detector *via* the same objective used to excite light. In a laser scanning confocal microscope, the laser scans over the sample and a second objective is used to direct the emitted fluorescence to a narrow pinhole to eliminate background fluorescence. The photomultiplier (PMT) detector will then generate an image using the software to determine the location of the photon from the relative position of the laser during the scan. This ensures for a higher resolution image with less background fluorescence.

1.14 Hypothesis

The HGF/c-Met signalling axis crosstalk with β1-integrin to induce growth and TNT formation in A549 lung adenocarcinoma cells.

1.15 Aims

1. To determine whether HGF, IL-6, lung ECM components (collagen IV, laminin and fibronectin) and the β1-integrin signalling axis cooperate to induce proliferation of A549 cells.

2. To determine the role and signalling pathways involved in the HGF/c-Met/β1-integrin-mediated TNT formation in A549 cells.
3. To determine the potential crosstalk between HGF and other growth factors/cytokines (EGF, IL-6, FGF2) in inducing TNT formation in A549 cells.
4. To characterise a novel 'go and grow' mechanism induced by HGF
5. To investigate the effects of HL-60 differentiated eosinophils in A549 cell death/growth through the development of a novel HL-60/eos-A549 cell co-culture system.

2. Materials and methods

2.1 Laboratory consumables

2.1.1 Reagents

Reagent	Source	Catalogue number
Dulbecco's Modified Eagle's Medium, high glucose	Gibco	11965-092
RPMI 1640 medium	Gibco	21875-091
Phosphate buffered saline	Gibco	10010023
Penicillin Streptomycin	Gibco	15070-063
L-glutamine	Gibco	25030-81
Heat-inactivated fetal bovine serum	Gibco	10500064
Purified recombinant IL-6	Peprotech	200-06
Purified recombinant HGF (insect derived)	Peprotech	100-39
Animal-free recombinant Human EGF	Peprotech	AF-100-15
Recombinant human FGF-basic (154 a.a.)	Peprotech	100-18B
Collagen type IV	Santa Cruz biotechnology Inc.	Sc-29010
Laminin	Santa Cruz biotechnology Inc.	Sc-29012
Fibronectin	Santa Cruz biotechnology Inc.	Sc-29011
Matrigel basement membrane matrix growth factor	Corning	354230
Butyric acid	Merck	B103500
Dimethyl sulfoxide	Merck	D2650
Paraformaldehyde	Merck	P6148
Bovine Serum Albumin	Merck	A1933
Donkey serum	Merck	D9663
Trypsin	Merck	T3924
DPX mountant for histology	Merck	06522
Sodium dodecyl sulfate	Merck	817034100
TruPAGE 4-20% precast gradient gel	Merck	PCG2016
TruPage Transfer buffer, 20X	Merck	PCG3003
Tris Buffered Saline, with Tween 20 (TBST), pH 8.0	Merck	T9039
2-Mercaptoethanol	Merck	M3148
Bromophenol blue sodium salt	Merck	B8026
Glutaraldehyde solution	Merck	G6257
(3-Aminopropyl)triethooxysilane (APES)	Merck	A3648
Triton-X	Roche	11332481001
Vectashield	Vector laboratories	H-1200-10
Ethanol	Honeywell	24194-1L
Cytiva Amersham ECL™ Prime Western Blotting *Detection* Reagent	Fisher Scientific	10308449
Glycerol, 99+%	Fisher Scientific	10795711

Methanol	Fisher Scientific	10284580
Acrylamide solution (40%/Electrophoresis)	Fisher Scientific	BP1402-1
Bis-acrylamide solution (2%w/v/Electrophoresis)	Fisher Scientific	BP1404-250
Quick-Diff staining kit	Reagena	102164
Trypan blue	Thermofisher scientific	15250061
Tetramethylethylenediamine (TEMED)	Thermofisher scientific	17919
EdU Click-iT reaction kit	Thermofisher scientific	C10340
Skim milk powder	Oxoid	LP0031
HiPerFect Transfection reagent	Qiagen	301705
Tritptolide	Selleck Chemicals	PG490
Sulfo-SANPAH, primary amine-niitrophenylazide crosslinker	Abcam	Ab145610

Table 2.1: List of reagents, sources and catalogue numbers

2.1.2 Primary and secondary antibodies

Antibody	**Species Origin**	**Clonality**	**Working concentration**	**Source/Cat. Number**
Anti-β1-integrin	Mouse	Monoclonal	1:100	Abcam/ab24693
Anti-Met	Rabbit	Monoclonal	1:100	Abcam/ab51067
Anti-CD133	Rabbit	Polyclonal	1:100	Abcam/ab16518
Anti-CCR3	Mouse	Monoclonal	1:100	Abcam/ab16231
Anti-paxillin	Mouse	Monoclonal	1:500	Abcam/ab3127
Anti-GAPDH	Rabbitt	Monoclonal	1:500	Cell Signaling Technology/2118S
IgG1 isotype control	Mouse	Monoclonal	1:100	Abcam/ab170190
IgG2a isotype control	Mouse	Monoclonal	1:100	Abcam/ab18415
Anti-cleaved caspase 3	Rabbit	Monoclonal	1:100	Cell signaling technology/9664
Anti-E-cadherin	Goat	Polyclonal	1:100	Thermofisher scientific/13469774
Anti-TNFAIP2/M-sec	Rabbit	Polyclonal	1:100	Thermofisher scientific/ **PA5-104529**
Anti-α-tubulin	Rat	Monoclonal	1:100	Thermofisher scientific/MA1-80017
Anti-paxillin	Mouse	Monoclonal	1:50	BD Biosciences/610620

Table 2.2: List of primary antibodies used for immunofluorescence labelling and western blot and their sources

Conjugate	Reactivity	Species origin	Working concentration	Source/Cat. Number
Alexa Fluor 488	Anti-mouse	Donkey	1:200	Thermofisher scientific/A-21202
Alexa Fluor 488	Anti-rabbit	Donkey	1:200	Thermofisher scientific/PIA32790TR
Alexa Fluor 568	Anti-goat	Donkey	1:200	Thermofisher scientific/A-11057
Alexa Fluor 568	Anti-rabbit	Donkey	1:200	Thermofisher scientific/A10042
Alexa Fluor 647	Anti-rat	Goat	1:200	Thermofisher scientific/A48265
Peroxidase conjugatetd	Anti-rabbit IgG	Goat	1:2000	Merck/A0545
HRP conjugated	Anti-mouse IgG	Rabbit	1:4000	Merck/AP160P
Rhodamine Phalloidin	-	-	1:200	Thermofisher scientific/R415

Table 2.3: List of secondary antibodies used for immunofluorescence labelling and western blot and their sources

Fluorescent dyes	Working concentration	Source	Catalogue Number
DiO'; $DiOC_{18}(3)$ (3,3'-Dioctadecyloxacarbocyanine Perchlorate)	5µM	Thermofisher scientific	D-275
Mitochondrial Staining Kit – Red Fluorescence – Cytopainter	-	Abcam	Ab112145

Table 2.4: List of fluorescent dyes and sources

2.1.3 Laboratory Apparatus

Laboratory equipment	Source
Hemocytometer	Neubauer
Centrifuge	ThermoFisher
Filter cards	ThermoFisher
Epifluorescent microscope	Zeiss Axiovert 200M
Microscope	Zeiss Primovert

Time-lapse microscope	Nikon TE
Cytocentrifuge	Thermo Shandon
Microscope slides	VWR
19mm No. 0 round coverslips	Fisher Scientific
18mm No. 1 round coverslips	VWR
30mm No. 1 round coverslips	VWR
T-75 flask	Starlabs
T-25 flasks	Starlabs
12-well plate	Starlabs
6-well plate	Starlabs
10ml serological pipette	Starlabs
25ml serological pipette	Starlabs
10µl graduated TipOne tips	Starlabs
200µl bevelled TipOne tips	Starlabs
1000µl graduated TipOne tips	Starlabs
Graduated Pasteur pipettes	Starlabs
Cryogenic vial, sterile	Starlabs

Table 2.5: List of laboratory equipment and sources

2.2 Cell culture

The A549 cell line was obtained from the American Type Culture Collection (ATCC). A549 cells are adherent human lung adenocarcinoma epithelial cells. The cells were cultured in Dulbecco's Modified Eagle's Medium (DMEM) and supplementation of the media required 10% Foetal Bovine Serum (FBS), 200mM l-glutamine, 10 000 U/ml penicillin and 10 000µg/ml streptomycin. The cell lines were incubated at 37^{o}C with CO_2 level of 5% in humidified atmosphere to allow growth to confluence. The passage of the A549 cells occurred twice weekly by removal of media, washing with Phosphate Buffered Saline, addition of trypsin EDTA solution for 3-5 minutes in the incubator in humidified atmosphere, as previously described to allow for cell detachment, and DMEM media was added for neutralisation. Cells from passage 3-40 were used for the experiments. ensuring at least 80% confluence and microscopic examination was undertaken before the start of experiments.

Clone 15 HL-60 cell line was obtained from the ATCC and are human promyelocytic leukemic cell line. The cells were grown in RPMI-1640 media supplemented initially with 20% FBS, 2mM l-glutamine, 10 000U/ml penicillin and 10 000µg/ml streptomycin. Once growth of the cells has been established, cells were cultured in 10% FBS with the same supplemented l-glutamine, penicillin and streptomycin as previously. The passage of HL-60 cells occurred twice a week with media change occurring every 2 days. Cells from passage 3-20 were used for experiments. Microscopic examination was undertaken to ensure cells were at least 80% confluent before the start of experiments.

2.3 Cell counts

2.3.1 HGF and IL-6 treatment

A549 cell proliferation at each concentration was measured using a hemocytometer cell count. Initial experiments were conducted to obtain the EC_{50} and maximal values of HGF and IL-6 to use for subsequent experiments. The experiment was repeated three times in triplicates. A549 cells were seeded into two 12-well plates at a seeding density of $1x10^5$ cells/well. They were placed in the incubator for 24 hours in a humidified atmosphere as previously described to allow cells to adhere before stimulation with IL-6. After 24 hours cells were observed in the microscope to ensure they had a low confluence (45%) to allow for further proliferation and prevention of cell-contact inhibition. HGF was used at concentrations of 0.01ng/ml, 0.1ng/ml, 1ng/ml, 3ng/ml, 10ng/ml, 30ng/ml, 100ng/ml and 1000ng/ml in fresh DMEM media. IL-6 was used at concentrations of 0.01ng/ml, 0.1ng/ml, 1ng/ml, 3ng/ml, 10ng/ml, 30ng/ml, 100ng/ml and 300ng/ml. A 1ml volume of each respective concentration was added to its corresponding well and left for 24 hours to allow cells to grow to confluence. Cells were then washed with 500µl of PBS then 500µl of trypsin was added which allowed for cell detachment in the incubator for 5 minutes. Then 10µl of the solution was transferred to the chamber of the moistened glass slide of the hemocytometer and observed under the microscope at x10 magnification. Cells were counted to obtain the total number of cells/ml using the equation: cells/ml = (average count/square) x (dilution factor) x 10^4.

To establish the synergistic or additive effects of HGF and IL-6 on A549 cell proliferation, cell counts were carried out as above utilising the EC_{50} and maximal concentrations of HGF and IL-6. A549 cells were seeded at the same density as above and were then stimulated with HGF (at EC_{50} concentration of 1ng/ml and maximal concentration of 30ng/ml) and IL-6 (at EC_{50} concentration of 0.5ng/ml and maximal concentration of 10ng/ml) as previously described. This experiment was also repeated using a lower seeding density of $5x10^4$ cells/well and with low FBS (2%) supplemented DMEM media. Floater cells were counted whereby the 500µl of DMEM media and 500µl of PBS were collected in an Eppendorf tube and centrifuged for 5 minutes at 500 RCF. The cell pellet was then resuspended in 50µl of DMEM media and counted as previously described.

2.3.2 Collagen IV, laminin and fibronectin coating

To obtain the EC_{50} and maximal value of collagen IV, fibronectin and laminin wells were pre-coated with each component. Collagen IV was diluted in 0.05M of HCL to final concentrations of 0.1µg/ml, 0.3µg/ml, 1µg/ml, 3µg/ml, 10µg/ml and 30µg/ml. Laminin was diluted in cold serum-free DMEM media to final concentrations of 0.03µg/ml, 0.1µg/ml, 0.3µg/ml, 1µg/ml 3µg/ml, 10µg/ml and 30µg/ml. Fibronectin was diluted in PBS to final concentrations of 0.03µg/ml, 0.1µg/ml, 0.3µg/ml, 1µg/ml, 3µg/ml, 10µg/ml and 30µg/ml. The 12-well plates were then coated with 0.9ml of collagen IV, fibronectin and laminin at each respective concentration and allowed to adhere for at least one

hour. The wells were then washed twice with PBS before cells were seeded as previously and cell counts were carried out as previously described. The experiment was repeated three times in triplicates.

To investigate the role of β1-intgerin in the HGF induced A549 cell proliferation, the wells were coated with fibronectin (1µg/ml) for an hour as previously described before A549 cells were seeded at a density of $1x10^5$ cells/well on a 12-well plate. After 24 hours of growth in the incubator, HGF (30ng/ml) was added to the required wells. The IgG or anti-β1 antibody was added to the wells at a concentration of 20µg/ml. Hemocytometer cell counts were undertaken after another 24 hours.

2.3.3 PD98059 inhibitor

To identify whether the signalling convergence of the HGF and IL-6 induced proliferation of A549 cells involved the MAPK pathway, a MEK1 inhibitor PD98059 was used. A549 cells were seeded at a density of $5x10^4$ cells/well on a 12-well plate. After being incubated for 24 hours in a humidified atmosphere as previously described, 400µl of fresh media containing 20µm of PD98059 or DMSO (as a vehicle control) was added to each well for 30 minutes in the humidified atmosphere previously described. The maximal concentrations of HGF (30ng/ml) and IL-6 (10ng/ml) were made up in either DMEM media containing 20µm PD98059 or DMSO and were added at a volume of 100µl to their respective wells. The 12-well plates were then incubated for a further 24 hours before cell counts were undertaken as previously described.

2.4 Tunneling nanotube experiments

2.4.1 HGF, EGF and FGF dose response

The HGF dose response was conducted to observe the tunneling nanotube formation of A549 cells. This was undertaken as a time course over 72 hours to determine the optimal timepoint of TNT formation. The experiment was repeated three times in duplicates. A549 cells were seeded at a seeding density of $5x10^3$ cells/well on a 12-well plate. The cells were left to grow into colonies for 3 days in a humidified atmosphere as previously described. HGF, at concentrations of 10ng/ml, 30ng/ml, 100ng/ml and 300ng/ml, were added in 2% FBS supplemented DMEM media in the 12-well plate on the third day. White light images of the TNT formation of A549 cells were captured on a microscope (Zeiss Primovert) attached to a GXCAM3EY-5 camera with a x10 Zeiss Plan-Achromat 0.45 NA objective. The Gxcapture-T software was used to capture the white light images. At least 20 randomly chosen fields of view for each concentration at 0, 12, 24, 36, 48, 60 and 72 hours.

Once the maximal timepoint of TNT formation was identified, an extensive HGF dose-response curve was undertaken to obtain the maximal concentration required for TNT formation. A549 cells were

seeded and left for 3 days as previously described, before the addition of HGF at increasing concentrations for 24 hours: 0.3ng/ml, 1ng/ml, 3ng/ml, 10ng/ml, 30ng/ml, 100ng/ml, 300ng/ml and 700ng/ml. White light images of the TNT formation of A549 cells were captured as previously described with at least 10 randomly chosen fields of view for each concentration.

An extensive EGF and FGF dose-response curve was also undertaken to determine their role in A549 cell TNT formation. Cells were treated as previously described with the following concentrations of EGF for 24 hours: 0.3ng/ml, 1ng/ml, 3ngml, 10ng/ml, 30ng/ml, 100ng/ml, 300ng/ml and 700ng/ml. Cells were also treated as previously described with FGF for 24 hours: 10ng/ml, 30ng/ml, 100ng/ml and 300ng/ml. White light images were then captured as previously described.

2.4.2 Immunofluorescent labelling of TNTs

A549 cells were seeded on size No. 0 glass coverslips placed within the wells at a seeding density of $7.5x10^3$cells/coverslip. The cells were then left to grow in a humidified atmosphere as previously described for three days before the addition of HGF at its maximal concentration (100ng/ml). The cells were then left to grow for a further 24 hours in a humidified atmosphere before being fixed with 4% paraformaldehyde for 10 minutes at room temperature. Cells were then washed with PBS and permeabilised for 3.5 minutes with 0.5% Triton-X before blocking non-specific binding with 3% BSA. The primary antibodies for M-sec and α-tubulin were added at a concentration of 1:100 and left overnight at 4^{o}C. The donkey anti-rabbit IgG Alexa Fluor 488 conjugated secondary antibody, goat anti-rat IgG Alexa Fluor 647 conjugated secondary antibody and rhodamine phalloidin (1:200) were then added for 2 hours at 4^{o}C in the dark. Negative controls were undertaken using IgG or secondary incubation alone. There was no fluorescent labelling observed in the negative controls, confirming specify of antibodies used in the study. Examples of confocal images displaying negative staining are shown in Figure 2.1. After washing, samples were mounted with Vectashield containing Hoescht for visualisation of nuclei before imaging using an epifluorescent (Zeiss Axiovert 200M) or confocal microscope (Zeiss LSM980-Airyscan).

For immunofluorescent visualisation of c-Met and β1-integrin-labelled TNTs, the cells were fixed with 100% ice-cold methanol for 10 minutes before being washed with PBS and permeabilised for 10 minutes with 0.1% Triton-X before blocking non-specific binding with 3% BSA. The primary antibodies for c-Met and β1-integrin were added at a concentration of 1:100 and left overnight at 4^{o}C. The donkey anti-mouse IgG Alexa Fluor 488 conjugated secondary antibody and donkey anti-rabbit IgG Alexa Fluor 568 conjugated secondary antibody (1:200) were then added for 2 hours at

4°C in the dark. The samples were then mounted with Vectashield containing Hoescht before being imaged on a confocal microscope (Zeiss LSM980-Airyscan).

Immunofluorescence labelling of paxillin and F-actin-labelled TNTs was undertaken as previously described (Sastry et al. 1999). Briefly, the cells were fixed with 3% formaldehyde for 15 minutes at room temperature before being washed with PBS and permeabilised for 15 minutes with 0.4% Triton-X before blocking non-specific binding with 5% donkey serum in PBS for 30 minutes. The primary antibody for paxillin was added at a concentration of 1:100 and incubated at room temperature for an hour. The donkey anti-mouse IgG Alexa Fluor 488 conjugated secondary antibody and rhodamine phalloidin (1:200) were then added for another hour at room temperature in the dark. The samples were then mounted with Vectashield containing Hoescht before undertaking imaging as previously described.

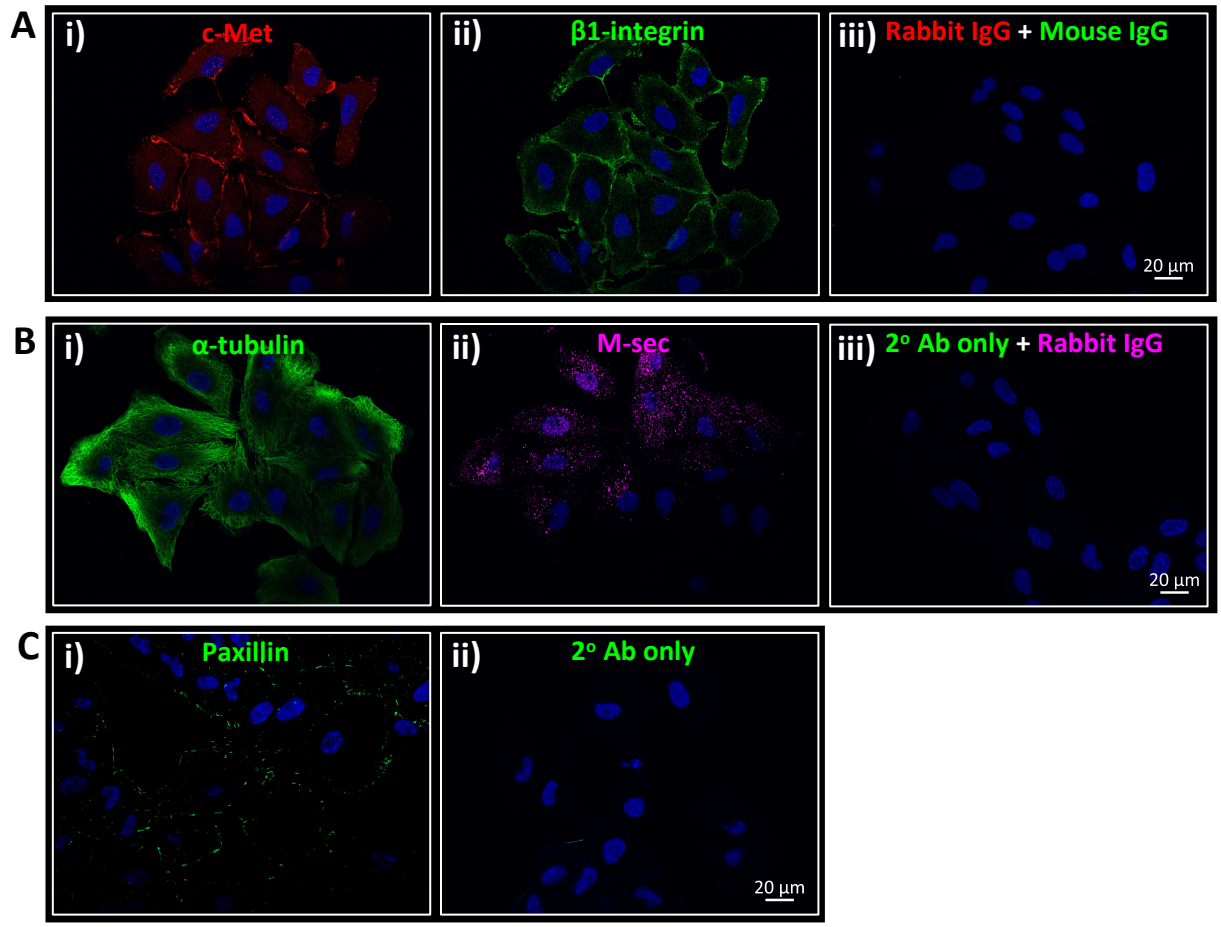


Figure 2.1. Negative controls of immunofluorescent labelling specificity. A: Representative confocal images of (i) c-Met primary antibody (red), (ii) β1-integrin primary antibody (green) and (iii) rabbit IgG control (red) and mouse IgG control (green) combined. B: Representative confocal images of (i) α-tubulin primary antibody (green), (ii) M-sec primary antibody (pink) and (iii) secondary antibody only with no primary antibody to α-tubulin (green) and rabbit IgG control (pink) combined. C: Representative confocal images of (i) paxillin primary antibody (green) and (ii) secondary antibody only with no primary antibody to paxillin (green). Nuclei are stained with DAPI, red. Scale bars 20µm.

2.4.3 Live-cell imaging of mitochondria and vesicles TNT trafficking

To visualise vesicle and mitochondria transfer along the TNTs, A549 cells were seeded on 18mm size 1 glass coverslips (VWR) and treated with HGF for 24 hours as previously described. The red mitochondrial cytopainter was diluted in a live-cell staining buffer accordingly to the working volume required as per the manufacturer's instructions. The cells were then loaded with red mitochondrial cytopainter for 30 minutes in a humidified atmosphere in the dark before being washed three times with PBS. Coverslips were then mounted on a ludin chamber and enclosed in a humidified atmosphere with 5% CO_2. Live cells were imaged with Zeiss LSM980-Airyscan confocal microscope using 40x 1.3 NA oil objective. Real-time acquisition of images was captured at 30 sec-2mins intervals for a duration of 20min-3hrs.

To visualise the directionality of the mitochondria and DiO labelled vesicle transfer in TNTs, A549 cells were seeded at a density of $2x10^4$ cells/well in a 12-well plate and left in a humidified atmosphere previously described for 24 hours. The cells in each well were loaded with DiO (5µM) or red mitochondrial cytopainter for 30 minutes. Both cell populations were then trypsinised and seeded together at a 1:1 ratio on glass coverslips before being treated with HGF for 24 hours. Coverslips were then mounted on a ludin chamber and live cells were then imaged on a confocal microscope in an enclosed humidified atmosphere with 5% CO_2 as previously described.

2.4.4 TNT inhibitor experiments

To investigate the pathways involved in the HGF/EGF-induced TNT formation, pharmacological inhibitors of associated pathways were used (see table 2.6 for more details). An extensive dose-response for each inhibitor and functionally blocking β1-integrin antibody was conducted initially to identify the maximal concentration required to inhibit the HGF-induced TNT formation. To ensure the vehicle controls (DMSO or sterile H_20), did not affect the HGF-induced or basal TNT formation, cells were also pre-treated with the same volume of vehicle controls used for the inhibitor concentrations alongside a plastic control. A549 cells were seeded as previously described and were pre-treated for 30 minutes with either the respective working concentrations of the inhibitors or the vehicle control before treatment with HGF (100ng/ml)/EGF (100ng/ml) for 24 hours. White light images were then captured as previously described.

Name	Function	Concentrations for full dose response	Working concentration	Source/Catalogue number
PHA-6655752	c-Met inhibitor	1nM, 2.5nM, 0.01µM, 0.25µM, 1µM	0.25µM	Cayman Chemicals/ CAY14703
PD98059	MEK 1/2 inhibitor	1µM, 2µM, 10µM, 20µM, 40µM	20µM	Cayman Chemicals/ Cay10006726
LY294002	PI3K inhibitor	1µM, 5µM , 10µM, 50µM, 100µM	50µM	Selleck Chemicals/S1105
CK-666	Arp2/3 complex inhibitor	10µM, 20µM,50 µM, 100µM, 200µM	10µM	Cayman Chemicals/ CAY29038
ML-141	CDC42 inhibitor	0.2µM, 1µM, 2µM, 10µM, 20µM	10µM	Cayman Chemicals/ CAY18496
Y27632	ROCK inhibitor	5µM, 7.5µM	5µM	Merck/688001
6-Thio-GTP	Vac-1-Rac signalling inhibitor	1µM, 2µM, 10µM, 20µM, 50µM	10µM	Jena Bioscience/NU-1106S
Anti-β1-integrin antibody	Functionally blocking antibody to β1-integrin	0.1µg/ml, 0.5µg/ml, 1µg/ml, 5µg/ml, 10µg/ml	10µg/ml	Abcam/Ab24693
Erlotinib	Tyrosine kinase inhibitor of the EGFR	-	100µM	Abcam/Ab141930

Table 2.6. List of inhibitors, concentrations used and sources.

2.4.5 siRNA paxillin knockdown

A549 cells were seeded at a density of $3x10^5$cells/well on a 6-well plate in 1ml volume per well. The non-targeting siRNA (Qiagen) and paxillin siRNA (Qiagen) were transfected with HiPerfect (Qiagen) as per manufacturer's instruction. To produce 20µM of siRNA/6-well 0.5µl of siRNA was added to 108µl of serum-free DMEM media in an Eppendorf before being vortexed to ensure adequate mixing. 14µl of HiPerFect solution was then added and pipetted gently to ensure mixing before incubation at room temperature for 10 minutes. The respective siRNA solution was then added drop-wise over the wells containing the cells. Following 48 hours of transfection in a humidified atmosphere previously described, cells were trypsinised and seeded ($2x10^4$ cells/well) on a 12-well plate for TNT experiments. The remainder of the cells were used for Western blot processing (**Section 2.8**) to confirm paxillin knockdown. The cells seeded for the TNT experiment were allowed to adhere overnight before HGF treatment (100ng/ml) for a further 24 hours before undertaking white light imaging (Zeiss Primovert) as previously described. The following paxillin siRNA target

sequence was used: ATCCAAAGGCAGAGAACCAAA. All reagents required for siRNA transfection were gifted from Dr Derek Warren. SiRNA transfections were also conducted in collaboration with Dr Robert Johnson from Dr. Derek Warren's lab.

2.4.6 Western blot

Protein extraction was performed with 4x Laemmli's Buffer, which comprised of 0.5 M Tris pH 6.8 (12.5%), Glycerol (10%), SDS (2%), Bromophenol Blue (0.08%) and 2-mercaptoethanol (5%) in water. 20µl of the Laemmli's Buffer was added to each well and left on a rocker for 15 minutes to ensure panning around the area of the well. Further physical lysis was performed through scratching of the well surface with the back of a 200µl tip. The protein lysates were then collected in an Eppendorf and stored in -20^{o}C freezer before undertaking the western blot protocol. Protein lysates were boiled at 95°C for 5mins before being loaded into a TruPAGE 4-20% precast gradient gel and undergoing SDS-PAGE at 120 V for 2 hours. Separated proteins were subsequently transferred onto PVDF membrane at 30 V for 3 hours. Membranes were blocked with 5% milk/TBST at room temperature for 1 hr before being incubated overnight at 4°C with paxillin and GAPDH primary antibodies diluted in 5% BSA/TBST (1:500 and 1:4000 respectively). After three washes with TBST, membranes were incubated at room temperature for 2 hours in anti-rabbit (1:2000)(Sigma) and anti-mouse (1:4000)(Sigma) secondary antibodies diluted in 5% milk/TBST (1:2000 and 1:4000 respectively). Following incubation, the signals were detected by ECL (Enhanced Chemi-Luminenscence) detection reagents before imaging on the BioRad Molecular Imager ChemiDoc XRS. Densitometric analysis of the blot intensities were quantified with ImageJ. Western blots were conducted in collaboration with Dr Robert Johnson from Dr. Derek Warren's lab.

2.4.7 Polyacrylamide hydrogels

To determine the effect of matrix stiffness on TNT formation, polyacrylamide hydrogels were used to fabricate the stiffness observed in lung tissue. The preparation of hydrogels was conducted by Dr Robert Johnson in collaboration with Dr Derek Warren's lab.

Hydrogels were prepared as previously described (Minaisah, Cox, and Warren 2016) and hydrogel stiffness was previously confirmed using a JPK Nanowizard-3 atomic force microscope (Porter et al. 2020). Briefly, 30mm coverslips were activated through treatment with (3-Aminopropyl)triethoxysilane for 2 minutes before being washed 3x with dH_20 and fixed in 0.5% glutaraldehyde for 40 minutes. The coverslips were subsequently washed 3x in dH_20 and left to air dry. The required volume of 12 kPa polyacrylamide hydrogel mix (7.5% acrylamide, 0.15% bis-acrylamide in water) was supplemented with 10% APS (1:100) and TEMED (1:1000) before 50µl of the

solution was placed on a standard microscope slide and covered by an activated coverslip. Once set, the fabricated 12 kPa hydrogel was removed, placed into a 6-well plate, washed 3x with dH_20 and crosslinked with sulfo-SANPAH (1:3000) under UV illumination (365nm). Finally, hydrogels were washed with PBS and functionalised and coated with the maximal concentration of collagen IV (3µg/ml) as previously described in **Section 2.3.2**.

A549 cells were seeded at a density of $1.25x10^4$ cells/well. The seeding density was calculated from scaling up the seeding density required for the surface area of an individual well of a 12-well plate to the surface area for the individual well of a 6-well plate. The cells were left in a humidified atmosphere as previously described before treatment with HGF for 24 hours and taken for time-lapse imaging (see **Section 2.4.8**).

2.4.8 Time-lapse video microscopy

A time-lapse system at 37°C and 5% humidified carbon dioxide on a Nikon TE microscope was used. Ten positions were randomly chosen for each well with x-y positions set. Phase contrast images were captured using a motorised stage every 5 minutes for 24 hours using a 10x Plan APO NA 0.45 objective. NIS-Elements imaging software was used to control and generate the time-lapse movies of the respective conditions.

2.5 A549 tumouroids growth experiments

2.5.1 3D A549 tumouroid culture in Matrigel

To better recapitulate the 3D *in vivo* NSCLC tumour and determine the effect of HGF and IL-6 on growth, an A549 tumouroid model was developed. A549 cells formed tumouroids in semi-solid growth factor reduced Matrigel when seeded on coverslips. 12-well plates containing sterilised coverslips were pre-warmed in the incubator. A seeding density of $1x10^4$ cells/coverslips was required. Therefore, cells were trypsinised and counted as previously described to ensure the correct number of cells were collected in an Eppendorf tube. The suspension was centrifuged at 500 RCF for 5 minutes and most of the DMEM media was discarded leaving a volume of 10µl. The cell pellets were gently re-suspended with roughly <10µl of DMEM media and transferred to the appropriate volume of Matrigel in a separate Eppendorf tube. The cell suspension was mixed with the Matrigel and 10µl was seeded on each coverslip and left to gel for 20 minutes in the incubator in a humidified atmosphere as previously described. 100µl of supplemented DMEM media was then added to each gel and the plates were placed in the incubator with humidified atmosphere to grow at a maximum of 9 days with media change occurring every 3 days. The ideal tumouroid size was identified at day 3 for growth experiments.

2.5.2 HGF and IL-6 treatment of A549 tumouroids

To determine the role of HGF and IL-6 on A549 tumouroid development and growth, HGF (0-500ng/ml) and IL-6 (0-500ng/ml) was added in supplemented DMEM media either on day 0 or on day 3 respectively. To assess the effect of HGF and IL-6 on A549 tumouroid development, the treated A549 cells on day 0 were left to grow in humidified atmosphere as previously described for 3 days. To assess the effect of HGF and IL-6 on A549 tumouroid growth, the treated A549 tumouroids on day 3 were left to grow in a humidified atmosphere for a further 3 days in culture. EdU (10μM) was then added to measure cell proliferation before being fixed for immunofluorescent labelling (**Section 2.5.3**).

2.5.3 Immunofluorescence labelling and EdU incorporation of A549 tumouroids

EdU at a concentration of 10μM was added to the DMEM media and left for 4 hours to incubate in the humidified atmosphere previously described. This ensured sufficient time for EdU incorporation to any newly synthesised DNA. The tumouroids were then fixed with 4% paraformaldehyde for 1 hour at room temperature. The tumouroids were then washed with PBS and permeablised through 13 minutes with ammonium chloride followed by 1% sodium dodecyl sulphate (SDS) for 5 minutes and 30 minutes with 1% Triton X-100. The Click-IT reaction was prepared beforehand as per the manufacturer's instructions which consisted of mixing the reaction buffer, copper sulfate, alexafluor azide and the reaction buffer additive. The Click-IT reaction cocktail was added for 30 minutes in the dark at room temperature. Following this, non-specific binding with 10% donkey serum in 1% BSA solution was added for 2 hours at 4^{o}C in the dark. The primary antibodies for e-cadherin and β1-integrin were added and left to incubate in the dark at 4^{o}C overnight (Table 2.2). The respective secondary antibodies (Table 2.3) were then added at a concentration of 1:200 for 2 hours at 4^{o}C in the dark. The coverslips were then mounted with Vectashield containing Hoechst (1:2000) for nuclei staining before fluorescent labelling was visualised and imaged with an epifluorescence microscope (Zeiss Axiovert 200M).

2.6 Triptolide treatment of A549 tumouroids

A549 cells were seeded in Matrigel and allowed to develop into tumouroids after 4 days before being treated with either DMSO (at the equivalent volume required for 0.1μM of the drug) or triptolide (0.1μM). The media was removed and 100μl of each triptolide concentration was added to the respective coverslips before being placed in a humidified atmosphere previously described for 48 hours. Following the incubation, the cells were imaged on white light (Zeiss Primovert) as previously described.

2.7 HL-60/eos and A549 tumouroid co-culture model

2.7.1 Differentiation of HL-60 cells to eosinophils

Clone 15 HL-60 cells are able to differentiate to an eosinophil phenotype through the addition of butyric acid (Fischkoff, Brown, and Pollak 1986). This method has been widely established with similar results being achieved when comparing HL-60 differentiated eosinophils and blood derived eosinophils of healthy donors in a chemotaxis study (Fu et al, 2016). Therefore HL-60 differentiated eosinophils were used to identify the effect of eosinophils on A549 tumouroid death and growth. The differentiation of HL-60 cells to an eosinophil phenotype were followed as per Fischkoff et al which involved resuspending $5x10^5$ cells/ml in the supplemented RPMI media with 0.5mM butyric acid in ethanol and left at 37°C with CO_2 level of 5% in humidified atmosphere for 5 days (Fischkoff, Brown, and Pollak 1986).

2.7.2 Characterisation of eosinophils

To confirm that the HL-60 cells have differentiated to eosinophils, Diff-Quick staining was conducted daily over the 5-day period to observe the development of bi-lobed nucleus and cytoplasmic acidic granule content in the cells (see Chapter 8, Fig8.5A). Cytospins of the HL-60 was firstly undertaken by preparing the cells by resuspending the cells at $1x10^6$ cells/ml. A filter card, microscope slide and cytofunnel were placed onto the cytoclip before 100µl of the cell suspension was transferred to the cytofunnel and centrifuged at 450RPM for 5 minutes. The slides were then air-dried overnight before being fixed with methanol for 2 minutes and stained with the Reastain quick diff red and Reastain quick diff blue for 2 minutes followed by a rinse with water. The slides were left to air dry overnight and mounted with DPX. White light images were then captured as previously described.

Eosinophils also express CCR3 as a specific marker and CCR3 expression of the HL-60/eos was visualised with immunofluorescent labelling (see Chapter 8, Fig8.4D). The HL-60/eos on day 5 underwent cytospins as previously described before being fixed in methanol at -20°C in the dark for 10 minutes. The HL-60/eos were washed with PBS before incubation with the anti-CCR3 primary antibody and its respective mouse IgG2A control. The slides were incubated overnight at 4°C in the dark. The donkey anti-mouse Alexa-fluor 488 secondary antibody was added for 2 hours at 4°C in the dark. The slides were then mounted with Vectashield containing Hoechst for nuclei staining before being imaged with an epifluorescent microscope (Zeiss Axiovert 200M). HL-60 cells which have differentiated to eosinophils are termed HL-60/eos throughout this thesis.

2.7.3 Trypan blue staining assay

Trypan blue staining was undertaken daily to assess the viability of the HL-60/eos cell population. A volume of 50µl of the trypan blue solution and 50µl of the cell suspension was mixed in an Eppendorf. Then 10µl of the solution was transferred to the chamber of the moistened glass slide of the hemocytometer and observed under the microscope at x10 magnification. The total number of cells and the number of trypan blue stained cells were counted to obtain the percentage of viable HL-60/eos cells.

2.7.4 HL-60/eos survival in DMEM and RPMI media

To ensure that the DMEM media affected the survival of the HL-60/eos, HL-60/eos on day 5 were seeded on a 12-well plate at range of seeding densities in either DMEM or RPMI supplemented media: $1x10^5$cells/well, $2x10^5$cells/well and $2x10^5$cells/well. After 48 hours in culture in the humidified atmosphere previously described, cytospins of the cells were undertaken before being stained with Diff-Quick solution as previously described in **Section 2.7.2**. White light images were captured before image analysis of apoptotic nuclei was undertaken.

2.7.5 HL-60/eos co-culture with A549 tumouroids

The day 5 HL-60/eos were cultured with the A549 tumouroids *via* the 'IN' or 'ON' method. For the 'IN' method, $1x10^6$ HL-60/eos or $1x10^5$ HL-60/eos were resuspended together with $1x10^4$ A549 cells in Matrigel and left to grow for 3 days before the addition of EdU (10µM) and fixed for immunofluorescence labelling. For the 'ON' method, $1x10^6$ HL-60/eos or $1x10^5$ HL-60/eos was added in the DMEM media on day 3, i.e. the time-point at which A549 tumouroids had developed in Matrigel. Following two days in culture, EdU (10µM) was added to the DMEM media for 4 hours before fixed with 4% PFA. EdU incorporation and immunofluorescent labelling with e-cadherin and caspase-3 was then undertaken as described in **Section 2.5.3.** The two different co-culture methods were undertaken to determine whether the effect of HL-60/eos on A549 tumouroid death/growth occurred via cell-to-cell contact-mediated or secretory-mediated pathways respectively. EdU incorporation and immunofluorescence labelling with e-cadherin, caspase-3 and their respective negative controls were then undertaken as previously described (see **Section 2.5.3**) followed by image analysis to quantify the EdU-positive nuclei and caspase-3-positive cells in co-culture (see **Section 2.8.7**).

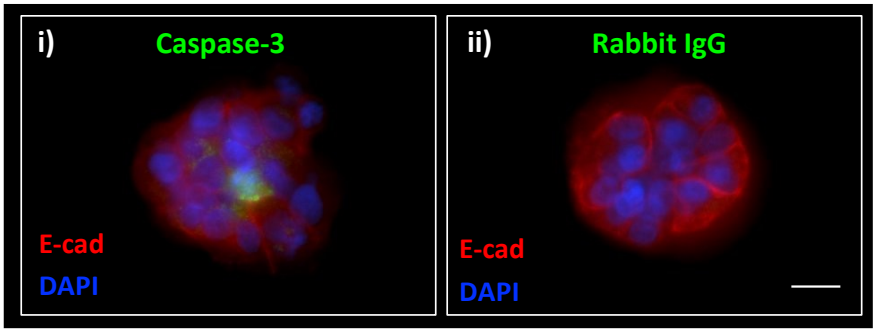


Figure 2.2. Negative control of immunofluorescent labelling for caspase-3. Representative epifluorescence images of (i) caspase-3 primary antibody (green) and (ii) rabbit IgG control (green). Nuclei (blue) are stained with DAPI and immunofluorescent labelling of e-cadherin (red) was also undertaken. Scale bars 10µm.

2.8 Image Analysis

2.8.1 TNT identification and quantification

Identification of TNTs included characteristics previously described by Lou et al. (Lou et al, 2012): (i) lack of adherence to the substratum of the tissue culture surface, which includes TNTs passing over adherent cells; (ii) a narrow base at the cell protrusion site; (iii) TNTs extending alone from a cell or joined with another cell are counted if the width of TNT was appropriately narrow throughout. Cellular protrusions not meeting the criteria above would be excluded from analysis. Three parameters were used to quantify TNT formation: mean percentage of cells with TNTs, mean number of TNTs per cell and length of TNTs. TNTs were quantified using the multi-point tool on the ImageJ software, the total number of cells were counted and the number of cells with TNTs were also counted to obtain the mean percentage of A549 cells with TNT for all growth factor dose responses, time-course experiments, epifluorescence F-actin labelled images and inhibitor experiments. Each cell with a TNT (as previously marked and counted with the multi-point tool) was then quantified for the number of TNT per cell. The remainder of cells with no TNT were also quantified for each field of view. Any cell or TNT cut from the field of view was excluded from analysis and not quantified. An example of TNT quantification is further detailed in figure 2.3.

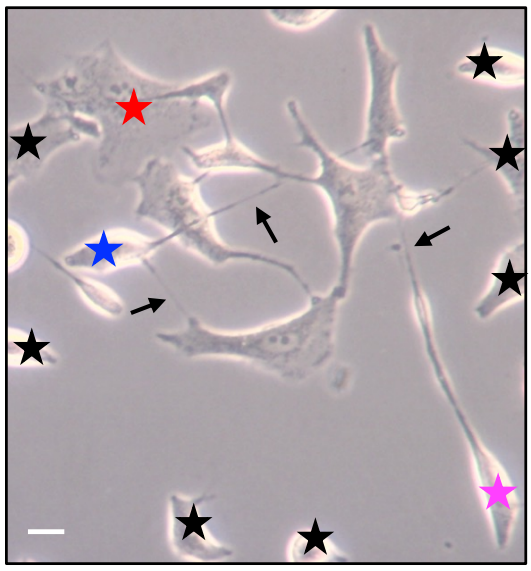


Figure 2.3: White light TNT quantification. ImageJ software was used to perform the image analysis. Each A549 cell within the field of view was quantified for the number of TNTs. The black arrows denote a TNT structure. The cells that are cut off from the field of view are marked with a black star (★) and are excluded from the image analysis. The cell marked with a red star (★) show a cell within the field of view with no TNT. The cell marked with a pink star (★) show a cell within the field of view with one TNT. The cell marked with a blue star (★) indicate a cell within the field of view with two TNTs. Scale bar, 10µm

TNT length was also measured to obtain the length in μm. White light images were captured with 10X magnification, therefore the images were scaled accordingly (*Analyse-Set scale*; *Distance in pixels =6.4516, Known distance = 1).* The length measurements were obtained using the straight- or segmented-line tool on ImageJ by clicking at the start point of the narrow protrusion site of the TNT to the end of the length of the TNT (Fig2.4).

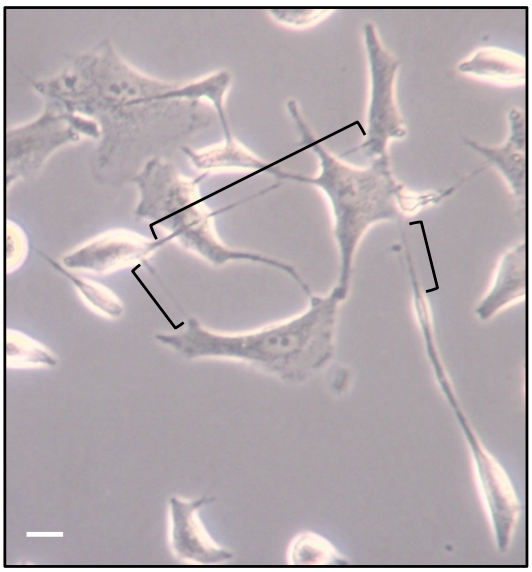


Figure 2.4: White light TNT length measurement. ImageJ software, using the straight- or segmented-line tool, was used to perform the image analysis. The brackets ([) indicate the length of the TNT measured. The length of the TNT was measured from the narrow protrusion site to the end of the TNT length, where the TNT fuses with the cell membrane of the recipient cell. Scale bar, 10μm

The lengths of the TNTs were further categorised accordingly to pre-determined ranges (<5μm, 5-20μm, 20-50μm, 50-100μm, 100-200μm, 200-300μm and >300μm)(see **Chapter 4, Fig4.6**). Furthermore, counts of the different morphologies of A549 TNTs observed, termed straight, angled, curved and branched, were counted for each image at the maximal concentration of 100ng/ml of HGF for all time points (see **Chapter 4, Fig4.5**). This was undertaken to identify the development of the different morphologies over 72 hours.

Non-adherence of TNTs was confirmed through z-stack acquisitions of F-actin, c-Met and β1-integrin labelled TNTs whereby visibility was confirmed only on higher focal planes. Z stack confocal images were acquired at 0.27-1.2μm intervals. The Zenlite software was used to obtain the 3D reconstruction and orthogonal view from the z-stack images (see **Chapter 4, Fig4.11C**).

2.8.2 Identification and quantification of 'go and grow' cells

'Go and grow' TNTs were first observed on time-lapse videos of HGF-treated cells. They are characterised by the unique ability of a subpopulation of A549 cells that migrate while leaving a trailing TNT behind (white arrow) and once the maximum length of TNT is reached, the cell body is released and retracts back along the TNT (white arrow) whilst undergoing cell division (Fig2.5). The daughter cells (red arrow) then migrate apart from one another whilst being connected *via* a TNT (white arrow) (Fig2.5). We termed this novel phenomenon, 'go and grow' TNTs from the characteristic 'go or grow'

phenotype which describes the mutually exclusive nature of proliferation and migration in cancer (Giese et al. 1996). To identify a 'go and grow' TNT, each stage of the process must be evident from the initial formation of TNT to the dividing cell has to retract back along the TNT (Fig2.5). Any observations which do not include the entire sequence of events are not included in the analysis. The percentage of 'go and grow' TNTs were quantified in both control and HGF-treated cells every 5 hours for the 24-hour duration of the time-lapse videos. This ensured that all 'go and grow' TNTs were accounted for throughout the 24-hour duration and to ensure that the entire process would be observed. The total number of cells and cells with TNTs were quantified at the beginning of each 5-hour interval and the number of 'go and grow' TNTs (at any stage of the process) were quantified to obtain the percentage of 'go and grow' TNTs over the whole cell population and over the population of cells with TNTs respectively.

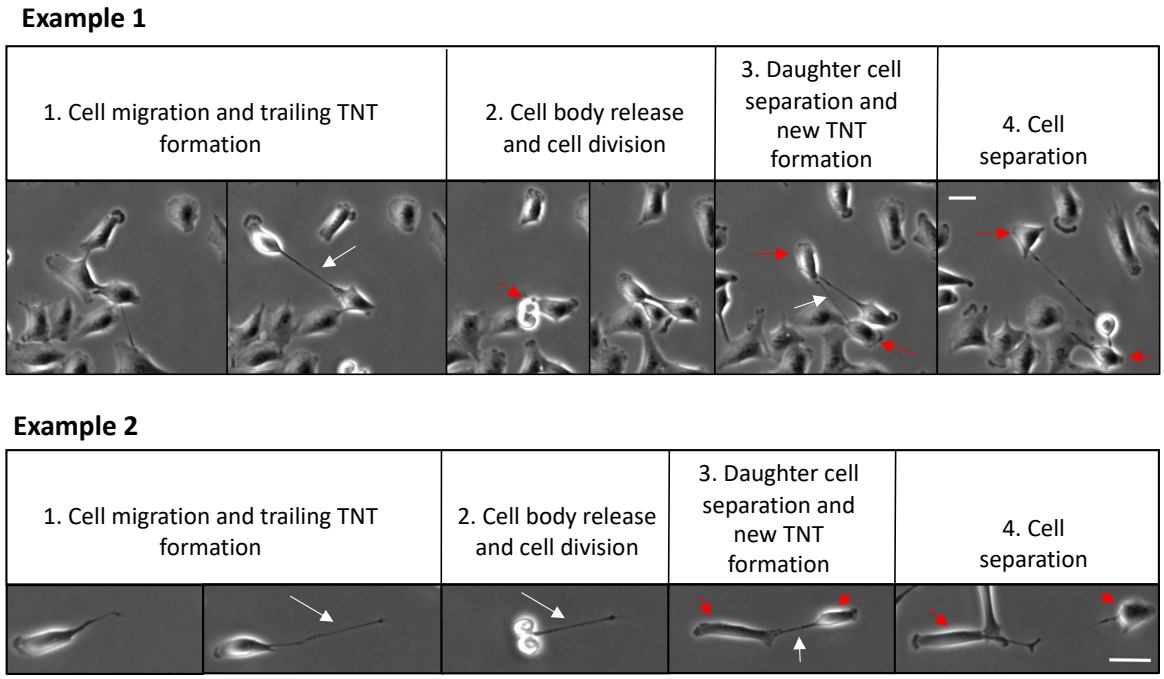


Figure 2.5. Two examples of 'go and grow' TNTs. The white light images show the 4 sequences of events which characterise a 'go and grow' TNT: first the A549 cell undergoes migration whilst leaving a trailing TNT behind, second the cell body is released and the cell divides while retracting back along the TNT, third the daughter cells migrate apart from one another with a TNT forming between and fourthly, the daughter cells separate from one another and the TNT disintegrates. White arrows denote a TNT structure while the red arrows denote the daughter cells. Scale bar, 10µm.

2.8.3 Speed and directionality tracking of 'go and grow' TNTs

Time-lapse movies were exported from NIS elements as TIFF files before undertaking cell tracking with the manual tracking plugin on ImageJ software. 'Go and grow' TNTs were identified as previously described. Cells were manually tracked by clicking the centre of the nuclei throughout consecutive frames. Cells were separately tracked during the TNT formation and retraction stages to compare the speed and directionality of both events. To obtain the tracks for the TNT formation event, cells were

tracked from the timepoint at which cells began to migrate and terminated when the cell reached the maximum TNT length. To obtain the tracks for the TNT retraction event, the cells were tracked from the last point in maximum TNT length to the point at which the cells no longer retracted back along the TNT. Each track was saved as a comma separated value (.CSV) file. The .CSV files were combined for the respective conditions and events before the addition of cumulative numbers as the first column. The .CSV files were then converted to Tab-delimited Text (.txt) files before being imported onto the 'Chemotaxis and Migration Tool' plugin. The X/Y calibration was adjusted from pixel to microns and the time interval was set beforehand. Using the coordinates of the individual tracks, the speed (μm/minute) and directionality (D) was obtained through the statistic feature of the plugin. The directionality was obtained through division of the euclidean distance with the accumulated distance, therefore a value of 1 defines linear motion. The rose plots (circular histogram) displayed the distribution of 'go and grow' TNT trajectories relative to their gradient orientation (0^0) and were also generated using the diagram feature of the plugin.

2.8.4 Quantification of EdU positive A549 tumouroid nuclei

ImageJ software was used to quantify the percentage of EdU-positive A549 nuclei per tumouroid when treated with HGF and IL-6. The individual A549 tumouroids were identified through e-cadherin labelling. The DAPI-stained nuclei (numbered in white) and the EdU-incorporated nuclei were quantified (numbered in pink) using the multi-point tool on ImageJ (Fig2.6). An EdU-positive nucleus was included in the analysis and quantified when weakly fluorescent, as this confirmed EdU incorporation during DNA replication. E-cadherin labelling was used to distinguish epithelial A549 cells from HL-60/eos. Any DAPI-stained or EdU-positive nuclei that were out of focus were excluded from analysis. The percentage of the EdU-positive nuclei was then obtained for each A549 tumouroid in the field of view.

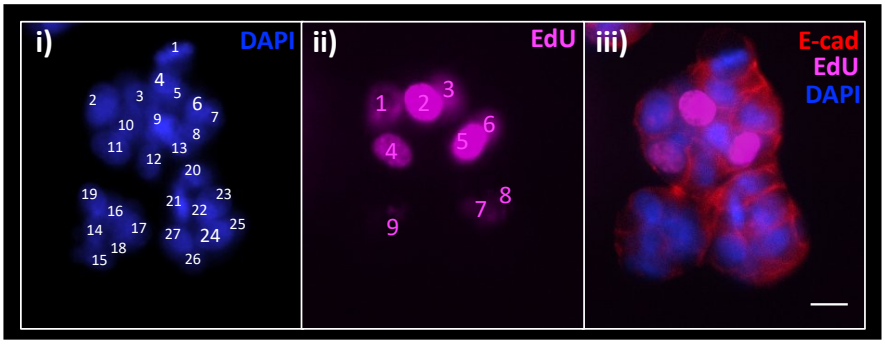


Figure 2.6. Quantification of DAPI stained and EdU incorporated A549 nuclei. Representative epifluorescence images show i) quantification of DAPI-stained nuclei (numbered in white), ii) quantification of the EdU-positive nuclei (numbered in pink) and iii) the merged DAPI, EdU and e-cadherin image show the A549 tumouroid. Weakly fluorescent EdU-positive nuclei were included in the image quantification. The percentage of the EdU-positive nuclei per A549 tumouroid was then obtained. Scale bar, 10μm.

2.8.5 Quantification of the differentiated HL-60/eos

The HL-60/eos cytospin white light images taken over the 5-day differentiation period were analysed on ImageJ software. The number of bi-lobed nucleus and the number of red stained granules were counted over the total number of cells to obtain the percentage of cells with bi-lobed nuclei and red stained granules from day 0 to day 5 (see Chapter 8, Fig8.4A). The images from the immunofluorescent labelling of CCR3 of the HL-60/eos on day 5 were also analysed. The number of cells that were CCR3 positive were also counted over the total number of cells to obtain the percentage of HL-60/eos which were positively expressing CCR3 (see Chapter 8, Fig8.4D). The apoptotic nuclei were also quantified to assess the survival of day 5 differentiated HL-60/eos cultured in DMEM or RPMI media at three seeding densities ($1x10^5$ cells/well, $2x10^5$ cells/well and $3x10^5$ cells/well)(see Chapter 8, Fig8.6).

2.8.6 Quantification of apoptotic HL-60/eos

The Diff-Quick stained HL-60/eos cultured in either DMEM or RPMI were analysed for apoptotic nuclei to assess their survival in the different media. Apoptotic nuclei (black arrow) were characterised by either the presence of nuclear condensation, whereby a deeper concentrated of staining in the nucleus was observed or DNA fragmentation (Fig2.7). The number of apoptotic cells were quantified on ImageJ software (multi-point tool) and the total number of cells were quantified to obtain the percentage of apoptotic cells for each field of view.

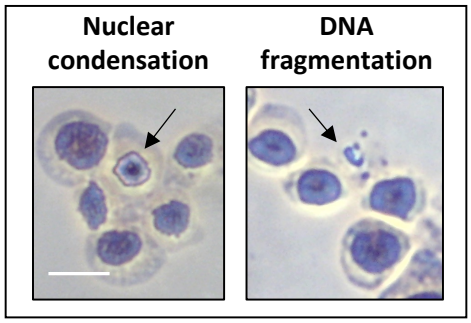


Figure 2.7. Characterisation of apoptotic nuclei of HL-60/eos. The white light images show the morphology of an apoptotic nuclei displayed when undergoing nuclear condensation and DNA fragmentation. Scale bar, 10µm.

2.8.7 Quantification of EdU-positive and caspase-3-positive A549 cells in co-culture with HL-60/eos

After establishing the survival of HL-60/eos cultured was not affected by either DMEM or RMPI media, $1x10^4$ HL-60/eos were co-cultured with the A549 tumouroids with the 'IN' or 'ON' method before undertaking immunofluorescent labelling and imaging, as previously described in **Section 2.7.5**. ImageJ software was then used to quantify the percentage of caspase-3-positive and EdU-positive A549 cells per tumouroid. The EdU quantification was conducted as previously described in **Section 2.8.4**. The individual A549 tumouroids were identified through E-cadherin labelling. The DAPI-stained nuclei (numbered in white) and the caspase-3-positive cells were quantified (numbered in green) using

the multi-point tool (Fig2.8). Any DAPI-stained nuclei that were out of focus were not included in the analysis. E-cadherin labelling was used to distinguish epithelial A549 cells from HL-60/eos. The percentage of the caspase-3-positive cells was then obtained for each A549 tumouroid in the field of view.

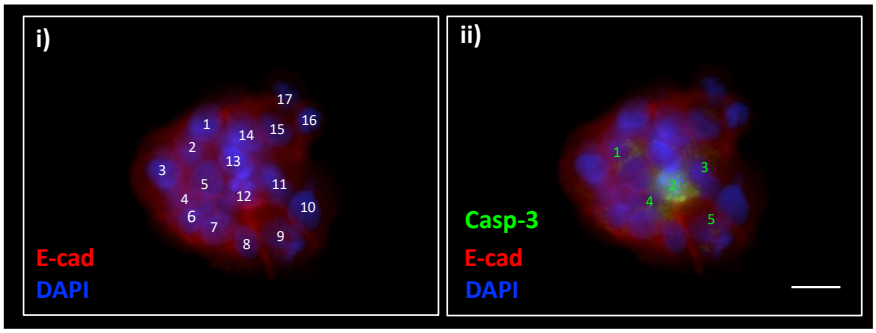


Figure 2.8. Quantification of DAPI stained and caspase-3 positive A549 cells. Representative epifluorescence images show i) quantification of DAPI-stained nuclei (numbered in white) and ii) quantification of the caspase-3-positive cells (numbered in pink). The percentage of the caspase-3-positive nuclei per A549 tumouroid was then calculated. Scale bar, 10µm.

2.9 Statistical Analysis

Experiments were conducted at least three times and data was expressed as the mean ± SEM for log dose-response curves, line graphs, scatter plots and histograms; n= number of experiments conducted, N= number of A549 tumouroids. A sigmoidal curve plotted on Graphpad prism 8 was used to determine the EC_{50} concentrations in proliferation and TNT studies. The IC_{50} concentration was also determined in TNT studies using Graphpad prism 8. Determination of significance of the proliferation and TNT experiments were assessed appropriately with one-way ANOVA and post hoc Tukey's multiple comparisons, two-way ANOVA and post hoc Bonferroni's test or unpaired t-test (for comparison between two groups) using Graphpad Prism 8. All statistical analyses were considered significant when $p<0.05$.

3. Chapter 3: The role of HGF, IL-6 and the ECM in A549 cell proliferation

3.1 Introduction

NSCLC has high mortality rates with the majority of patients diagnosed with advanced metastatic cancer (Ettinger et al. 2010). The development towards malignancy involves initial growth of proliferating cancer cells, which detach from neighbouring cells in the surrounding tissue to migrate through the bloodstream and lymphatic vessels to secondary distal sites. Achieving this involves a complex process with a variety of strategies employed by tumour cells and its microenvironment. Evading programmed cell death and sustained proliferative signalling contributes to the development of the initial malignant tumour growth (Hanahan and Weinberg 2011). Current research has implicated HGF and IL-6 as key players in the tumour microenvironment in influencing cancer growth (Comoglio, Giordano, and Trusolino 2008; Arriola et al. 2011; Lee et al. 2016; Zheng et al. 2019).

HGF is a pleiotropic cytokine and was independently identified as scatter factor (SF) due to its ability to induce disassociation of MDCK cells (Stoker et al. 1987). HGF/SF is largely produced by mesenchymal cells, specifically alveolar macrophages, endothelial cells and stromal fibroblasts (Masuya et al. 2004; Yanagita et al. 1992) as well as in tumour cells (ref). HGF is found mainly inactively bound to the ECM by heparin-like proteoglycans (Lyon et al. 1994). Activation of its tyrosine kinase receptor (RTK) c-Met, a proto-oncogene (Sonnenberg et al. 1993) leads to cellular effects such as morphogenesis, proliferation and migration (Naldini et al. 1991). However HGF/c-Met activity is deregulated in cancer exhibiting angiogenesis (Matsumoto and Nakamura 1997), scattering and an increase in matrix metalloprotease production to facilitate metastasis (Trusolino, Bertotti, and Comoglio 2010). Mutations in the MET gene have shown enhanced NSCLC proliferation and growth (Lutterbach et al. 2007). Activation and overexpression of c-Met was found in the lung tumour periphery front (Ma et al. 2005) and HGF levels are elevated in NSCLC (Harvey et al. 1996). A paracrine route of activation exists in NSCLC between the c-Met expressed tumour cells and the stromal HGF (Masuya et al. 2004) whilst an autocrine activation exists which amplifies the tumourigenicity in lung cancer (Yi and Tsao 2000).

Likewise IL-6, another pleiotropic cytokine, is involved in antigen-specific immune reactions and acts as an inflammatory marker (Naugler and Karin 2008). Its role in NSCLC mirrors HGF, high levels of IL-6 are linked with poor survival rates (Pine et al. 2011) and its levels in serum are an indicator to the prognosis of patients undergoing chemotherapy (Yanagawa et al. 1995). A549 cell lines can also secrete IL-6 (Bihl et al. 1998). The effects of IL-6 on NSCLC proliferation has provided mixed findings:

IL-6 inhibited A549 cell growth in one study, (Takizawa et al. 1993) whilst another showed no effect (Yamaji et al. 2004), or showed an increase in proliferation correlated with IL-6 secretion (Bihl et al. 1998) or that an IL-6 antibody demonstrated anti-proliferative effects (Kim et al. 2015). Like, HGF, IL-6 also induces EMT in NSCLC (Chen et al. 2015), which highlights the role of IL-6 in inducing cell motility in NSCLC.

Although extensive research has established the deregulated activity of HGF and IL-6 independently in cancer proliferation and invasion, there are limited studies identifying the cooperation between HGF and IL-6 together in cancer. One study identified IL-6 and HGF/c-Met pathways which work synergistically in aiding metastasis by enhancing the production of MMPs in A549 cells (To et al. 2002). However, the cooperation between HGF and IL-6 induced proliferation has not been investigated in A549 cells. Moreover, the role of the integrins/ECM signalling and their interaction with HGF and IL-6 remain poorly defined in NSCLC growth.

Tumours remodel the ECM, modifying the integrin-mediated bidirectional communication between tumour cells and the ECM, to support metastasis. Remodelling of the major lung ECM components, collagen IV, fibronectin and laminin (Yan et al. 2006). This alters the biochemical and biophysical properties of the ECM causing changes in cell signalling, enhanced stiffness, migration and overall tumour progression (Winkler et al. 2020). Collagen IV, laminin and fibronectin signal through β1-integrin: α1β1 and α2β1 integrins are the main receptors for collagens (Paulsson 1992; Aumailley and Gayraud 1998), α5β1 integrin is the main receptor for fibronectin (Obara, Kang, and Yamada 1988) whilst laminin also signals through α3β1 and α5β1 in the lung (Kreidberg et al. 1996; Caccavari et al. 2010). The ECM components and their respective integrin partners are implicated in various cancers, increasing adhesion, migration and contributing towards metastasis and resistance (Barkan et al. 2008; Ju and Zhou 2013; Mukhopadhyay et al. 2004; Koochekpour, Merzak, and Pilkington 1995; Yan et al. 2006). Despite its regulatory function in cancer, the effects of the lung ECM components in NSCLC growth are not well defined. There are mixed reports on the effect of collagen IV in various cancer cell lines: with either no effect in Calu-1 cells (Mukhopadhyay et al. 2004), inhibition of proliferation in melanoma cells (Han et al. 1997) or increase in proliferation in mammary cells (Kim et al. 1994), hepatoma cells (OGATA 1998) and in NSCLC cell line, H1299. Laminin has been shown to induce proliferation in pancreatic ductal adenocarcinoma cells (Huang and Chen 2021) however no studies have investigated its proliferative role in NSCLC. Synergistic proliferation was also identified between HGF and fibronectin *via* β1-integrin in PC9 cells (Ju and Zhou 2013). Identifying the proliferative capacity of the ECM serves a wider interest in their role as a scaffold to promote pro-tumourigenic signalling outcomes and effects.

The overall findings have implicated HGF, IL-6 and the ECM in exerting a range of effects ranging from metastasis, cell motility and proliferation of NSCLC. Despite this, no studies have investigated the relationship between HGF, IL-6 and the ECM together in NSCLC growth. Therefore, the aim of this chapter is to investigate the cooperative proliferative effects induced by HGF and IL-6 in the presence of the ECM components in A549 lung adenocarcinoma cells. This work will advance knowledge on the mechanism associated with the factors individually and in combination, thus highlighting the key players in the tumour microenvironment in A549 proliferation.

3.2 Results

3.2.1 IL-6 and HGF induces proliferation in A549 cells

Hemocytometer cell counts were undertaken to initially investigate the proliferative effects of IL-6, HGF on A549 cell proliferation. Both HGF and IL-6 induced proliferation of A549 cells in a concentration-dependent manner. The log concentration response curve was plotted for HGF and IL-6. From the sigmoidal curve, the EC_{50} concentrations of IL-6 and HGF were 0.5ng/ml and 1ng/ml respectively and the maximal concentration was reached at 10ng/ml and 30ng/ml for IL-6 and HGF respectively (Fig 3.1A&B). Both curves plateaued once the maximal concentration was reached. The mean number of cells started to decline at 30ng/ml of IL-6 and continued to do so until 300ng/ml (Fig 3.1A). The mean number of A549 cells returns to baseline levels when stimulated with 1000ng/ml of HGF (Fig 3.1B).

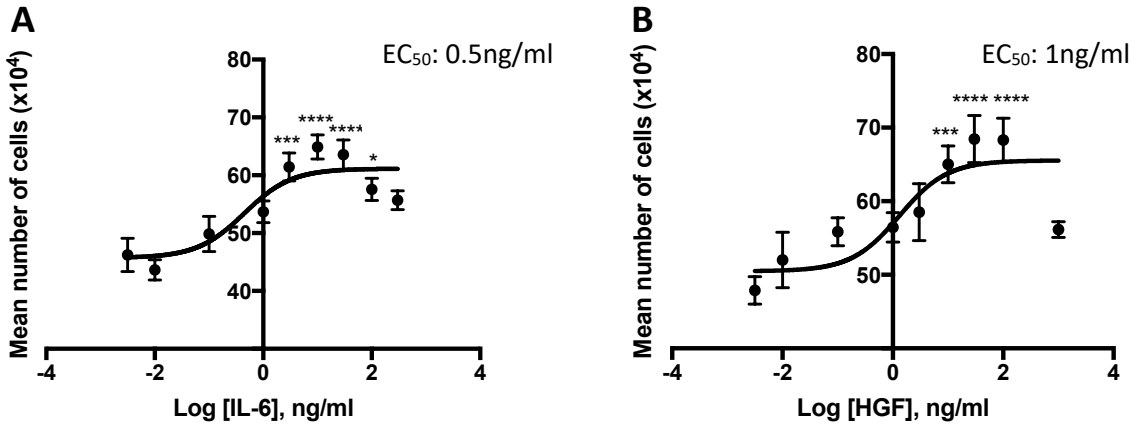


Figure 3.1: IL-6 and HGF induce A549 proliferation in a concentration dependant manner. A549 cells were treated with IL-6 (0.01ng/ml, 0.1ng/ml, 1ng/ml, 3ng/ml, 10ng/ml, 30ng/ml, 100ng/ml and 300ng/ml) and HGF (0.01ng/ml, 0.01ng/ml, 1ng/ml, 3ng/ml, 10ng/ml, 3ng/ml, 100ng/ml and 1000ng/ml) for 24h. A: The IL-6 log concentration-response curve show a dose-dependent increase in mean cell counts. B: The HGF log concentration-response curve show a dose-dependent increase in mean cell counts. Values are expressed as mean number of A549 cells ± SEM, n=*3*. *p< 0.05, ***p< 0.001, ****p< 0.0001 in comparison to control.

3.2.2 HGF and IL-6 demonstrate no synergistic or additive effect of on A549 cell proliferation

Following the determination of the EC_{50} and maximal concentrations of IL-6 and HGF required for cell proliferation. The proliferative effects of HGF or IL-6 on A549 cells were compared separately and in combination. The EC_{50} concentrations of HGF and IL-6 were used to identify whether there was a synergistic effect in proliferation. The results show a significant increase in A549 cell counts when treated with the EC_{50} concentrations of HGF and IL-6 compared to control (Fig 3.2A). However, there was no significant difference in cell counts between cells treated with HGF and IL-6 in combination compared to either IL-6 or HGF alone (Fig 3.2A), thus no synergistic effect was observed. The

percentage of floater cells was obtained from the number of floater cells counted and the total cell counts in the well for each condition. The percentage of floater cells was quantified to account for the non-adherent cells in the media and during PBS wash (Fig 3.2B). There was no significant difference in the mean percentage of floater cell counts between control and the HGF and IL-6 -treated cells alone or in combination (Fig 3.2B).

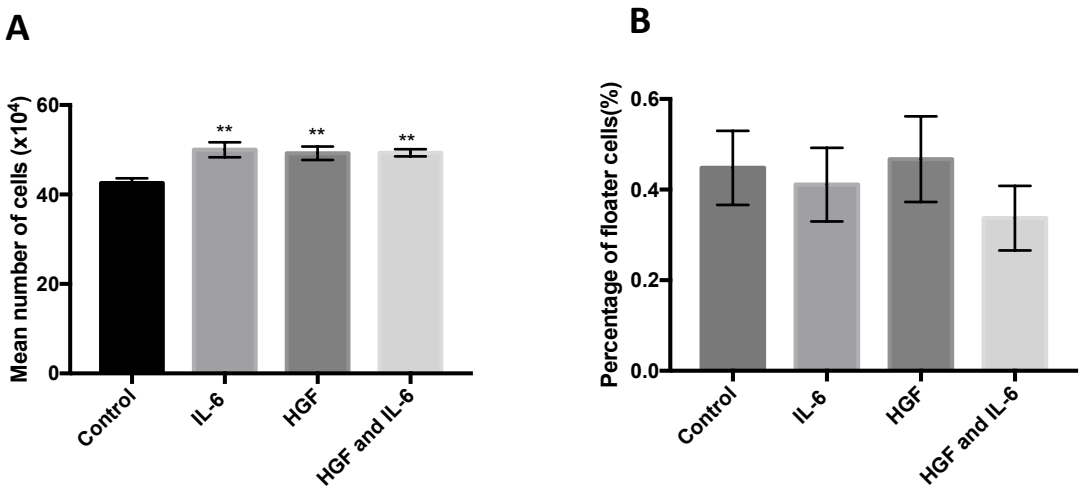


Figure 3.2: No synergistic effect with the EC_{50} concentration of IL-6 and HGF on A549 proliferation. A: A549 cells were stimulated with the EC_{50} concentration of HGF (1ng/ml) and IL-6 (0.5ng/ml) individually and in combination for 24h. B: The histogram represents the mean percentage of floater cells counted for the experiment. There was no significant difference in mean percentage of floater cells between control and cells treated with HGF alone, IL-6 alone and HGF+IL6 in combination. Both histograms represent the mean number of A549 cells ± SEM, *n=3*. *$p<$ 0.05, ***$p<$ 0.001, ****$p<$ 0.0001 in comparison to control by one-way ANOVA and Tukey's multiple comparison test.

The maximal concentrations of HGF and IL-6 were used to identify whether there was an additive effect in proliferation. There was a significant increase in A549 cell counts with the maximal concentrations of HGF and IL-6 compared to control (Fig 3.3A). No additive effect was observed as there was no significant difference in cell counts between cells treated with the maximal concentration of HGF and IL-6 in combination compared to either IL-6 or HGF alone (Fig 3.3A). There was also no significant difference in the mean percentage of floater cell counts between control and the HGF or IL-6-treated cells alone or in combination (Fig 3.3B).

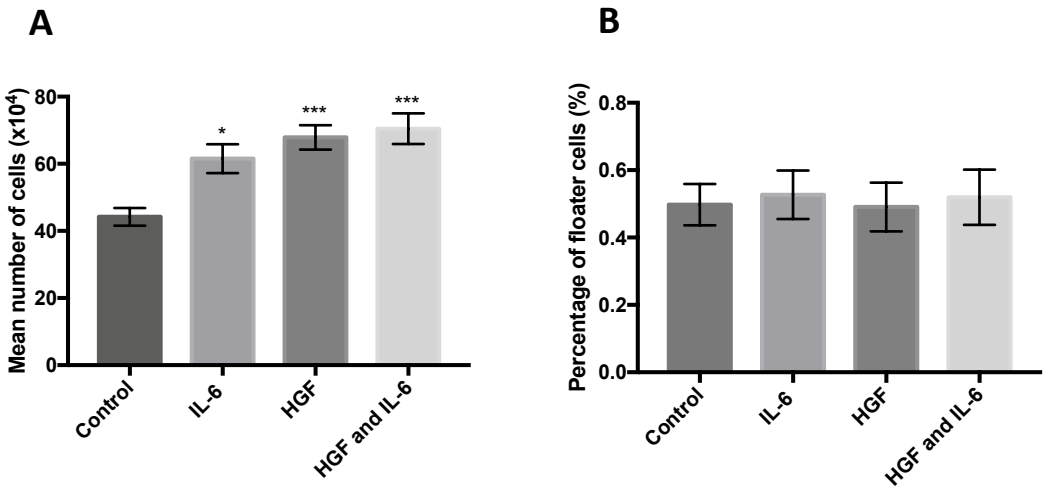


Figure 3.3: No additive effect with the maximal concentration of IL-6 and HGF on A549 proliferation. A: A549 cells were stimulated with the maximal concentration of HGF (30ng/ml) and IL-6 (10ng/ml) individually and in combination for 24h. B: The histogram represents the mean percentage of floater cells counted for the experiment. There was no significant difference in mean percentage of floater cells between control and cells treated with HGF alone, IL-6 alone and HGF+IL6 in combination. Both histograms represent the mean number of A549 cells ± SEM, n=3. *p< 0.05, ***p< 0.001, ****p< 0.0001 in comparison to control by one-way ANOVA and Tukey's multiple comparison test.

To ensure that the lack of additive or synergistic effect was not due to the density of cells in the well, the experiment was repeated with a lower seeding density of $5x10^4$ cells/well. There was no significant increase in the mean cell counts with the EC_{50} concentration of IL-6 alone and HGF alone when compared to control but a significant increase was observed when treated with HGF and IL-6 in combination (Fig 3.4A). There was no significant difference in cell counts between cells treated with HGF and IL-6 in combination compared to either IL-6 or HGF alone (Fig 3.4A), therefore no synergistic proliferation was observed. There was also no significant difference in the mean percentage of floater cell counts between control and the HGF or IL-6-treated cells alone or in combination (Fig 3.4B).

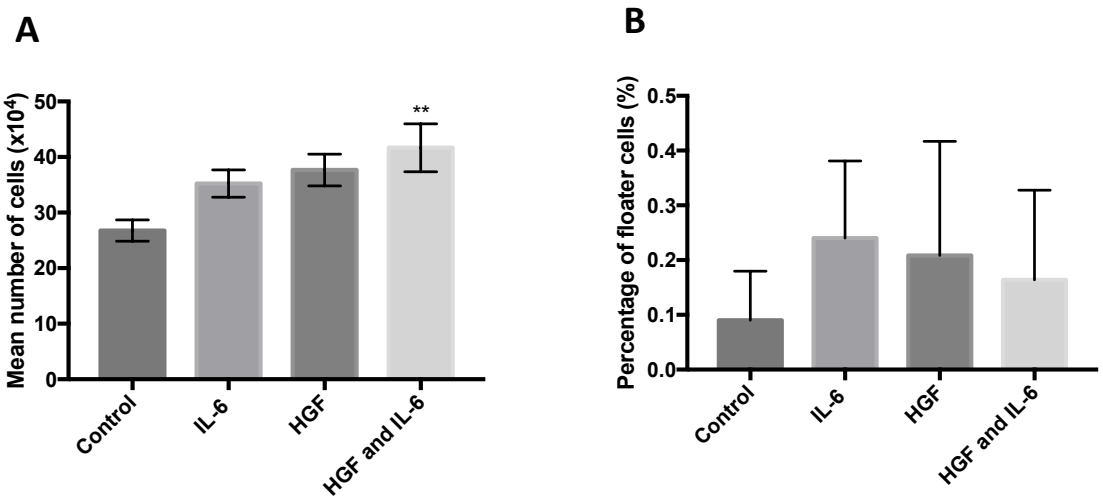


Figure 3.4: No synergistic effect with the EC_{50} concentration of IL-6 and HGF on A549 proliferation with a lower seeding density. A: A549 cells seeded at a lower density of $5x10^4$ cells/well and treated with the EC_{50} concentration of HGF (1ng/ml) and IL-6 (0.5ng/ml) individually and in combination for 24h. B: The histogram represents the mean percentage of floater cells counted for the experiment. There was no significant difference in mean percentage of floater cells between control and cells treated with HGF alone, IL-6 alone and HGF+IL6 in combination. Both histograms represent the mean number of A549 cells ± SEM, n=3. ***p*<0.01 in comparison to control by one-way ANOVA and Tukey's multiple comparison test.

There was a significant increase in the mean cell counts with the maximal concentration of either IL-6, HGF alone and in combination compared to control. However, there was no significant difference in cell counts between the cells treated with HGF and IL-6 in combination compared to either HGF or IL-6 alone (Fig 3.5A), therefore no additive proliferation was observed. There was also no significant difference in the mean percentage of floater cell counts between control and the HGF or IL-6-treated cells alone or in combination (Fig 3.5B). There was no significant difference in the mean percentage of floater cell counts between control and the HGF or IL-6-treated cells alone or in combination (Fig 3.5B).

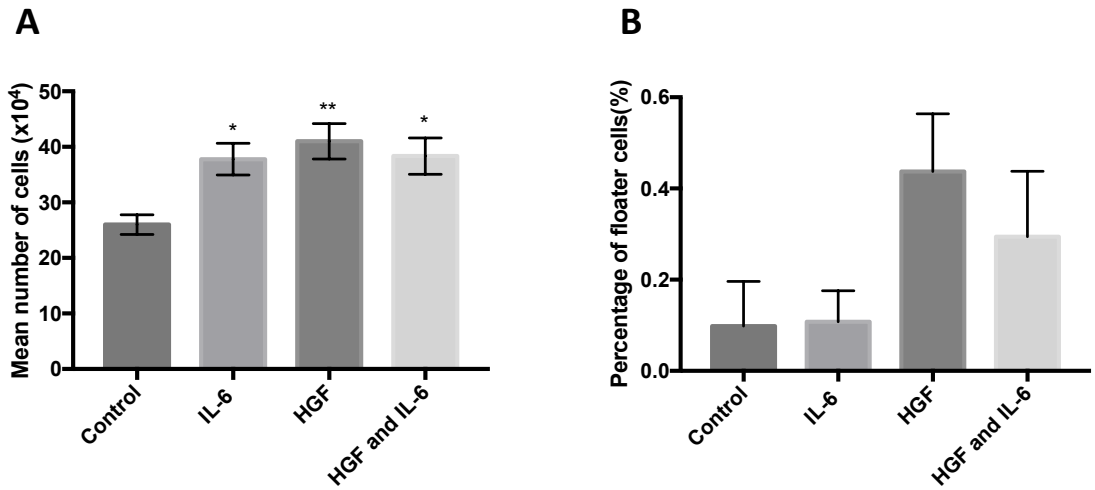


Figure 3.5: No additive effect with the maximal concentration of IL-6 and HGF on A549 proliferation. A: A549 cells seeded at a lower density of $5x10^4$ cells/well and treated with the maximal concentration of HGF (30ng/ml) and IL-6 (10ng/ml) individually and in combination for 24h. B: The histogram represents the mean percentage of floater cells counted for the experiment. There was no significant difference in mean percentage of floater cells between control and cells treated with HGF alone, IL-6 alone and HGF+IL6 in combination. Both histograms represent the mean number of A549 cells ± SEM, n=3.**p*<0.05 when compared to control by one-way ANOVA and Tukey's multiple comparison test.

The experiment was further repeated with low serum (2%) to ensure that growth factors abundantly present in the FBS-supplemented DMEM media would not mask any proliferative effects from HGF and IL-6. The log concentration-response curve was initially plotted to obtain the EC_{50} and maximal concentrations of HGF and IL-6 in low serum. From the sigmoidal curve, the EC_{50} concentrations of HGF and IL-6 was determined to be 2ng/ml and 1ng/ml respectively and the maximal concentration was reached at 30ng/ml and 10ng/ml for HGF and IL-6 respectively (Fig 3.6A&B). The maximal concentrations was reached at 30ng/ml for HGF before plateauing.

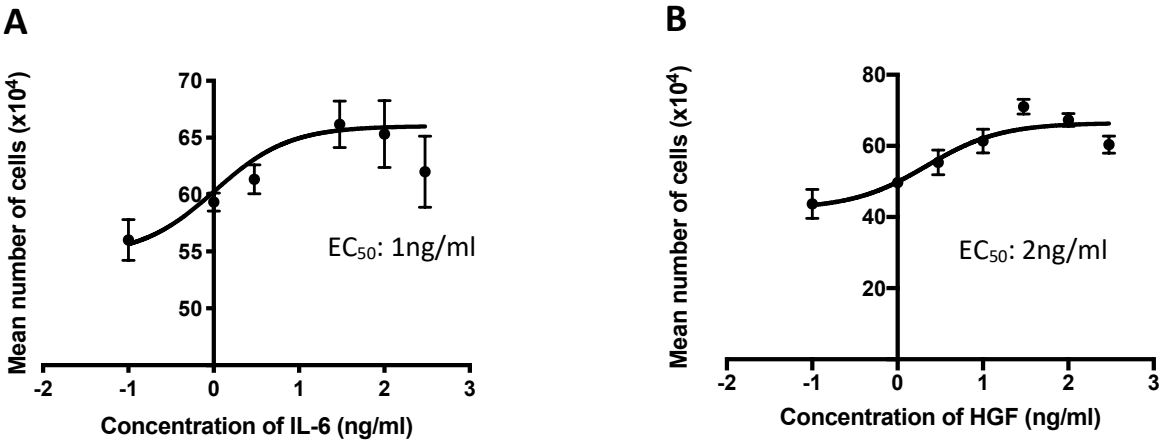


Figure 3.6: IL-6 and HGF induce A549 proliferation in a concentration dependant manner in low serum. A549 cells were treated with HGF (0-300ng/ml) and IL-6 (-300ng/ml) for 24h in 2% FBS-supplemented serum. A: The IL-6 log concentration response curve displays the mean number of A549 cells ± SEM, n=2. B: The HGF log concentration response curve displays the mean number of A549 cells ± SEM, n=*1*.

Following the determination of the EC_{50} and maximal concentrations of IL-6 and HGF in low serum, the experiment was repeated in low serum to determine whether a synergistic or additive effect in proliferation occurred. There was no significant difference in mean cell counts with the EC_{50} concentrations of HGF and IL-6 compared to control (Fig 3.7A). No synergistic effect was observed as there was no significant difference in cell counts between cells treated with the EC_{50} concentrations of HGF and IL-6 in combination compared to either IL-6 or HGF alone (Fig 3.7A). There was a significant increase in A549 cell counts with the maximal concentrations of HGF and IL-6 compared to control (Fig 3.7B). No additive effect was observed as there was no significant difference in cell counts between cells treated with the maximal concentration of HGF and IL-6 in combination compared to either IL-6 or HGF alone (Fig 3.7B).

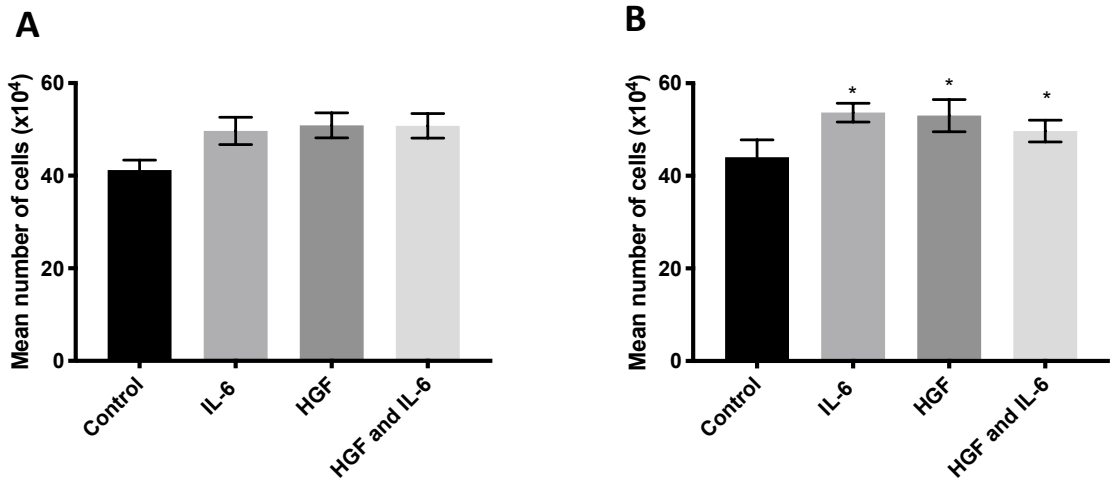


Figure 3.7: No synergistic or additive effect with the EC_{50} and maximal concentration of IL-6 and HGF on A549 proliferation in low serum. A: The histogram shows the mean cell counts when A549 cells were treated with the EC_{50} concentrations of IL-6 (1ng/ml) and HGF (2ng/ml) individually and in combination in low serum for 24h. B: The histogram shows the mean cell counts when A549 cells were treated with the maximal concentration of HGF (30ng/ml) and IL-6 (10ng/ml) individually and in combination in low serum for 24h. Values represent the mean number of A549 cells ± SEM, n=3.*p<0.05 when compared to control by one-way ANOVA and Tukey's multiple comparison test.

As there was a lack of additive or synergistic proliferation induced by HGF and IL-6 in A549 cells, the HGF and IL-6 induced proliferation would occur *via* the convergence of their signalling pathways. Therefore, the next aim was to identify the convergent signalling pathway involved.

3.2.3 HGF and IL-6 induces A549 proliferation *via* convergence on the MAPK pathway

The MEK inhibitor, PD98059, was used to identify the involvement of the MAPK pathway in HGF and/or IL-6-induced A549 proliferation. In the presence of DMSO, there was an increase in mean cell counts for HGF, IL-6 and HGF+IL-6 treated cells compared to control (Fig 3.8). However, the presence of a MAPK inhibitor decreased the mean cell counts for the HGF, IL-6 and HGF+ IL-6 treated cells (Fig 3.8).

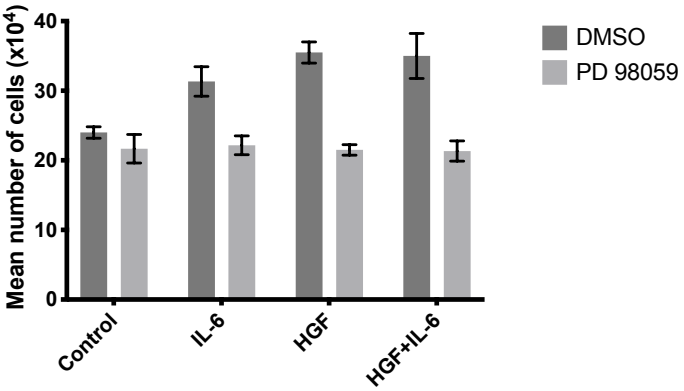


Figure 3.8: HGF and IL-6 converge on the MAPK pathway in A549 proliferation. A549 cells were pre-treated for 30 minutes with 20µM of PD98059 or DMSO. The cells were then treated with the maximal concentration of HGF (30ng/ml) and IL-6 (10ng/ml). After 24 hours cell were counted using a haemocytemeter. The histogram represents the mean number of A549 cells ± SEM, *n=2.*

Following this, the role of the lung ECM components in A549 proliferation was investigated with a view to determining whether the ECM components would cause an additive or synergistic effect with HGF and /or IL-6.

3.2.4 Collagen IV, fibronectin and laminin induce proliferation in A549 cells

Hemocytometer cell counts were undertaken to investigate the proliferative effects of the ECM components (collagen IV, fibronectin and laminin) on A549 cell proliferation. Each component induced a significant concentration-dependent increase in proliferation of A549 cells as previously observed with the growth factors. From the sigmoidal curve of the log concentration response curve, the EC_{50} concentrations of collagen IV, fibronectin and laminin were determined to be 0.33μg/ml (Fig 3.9A), 0.16μg/ml (Fig 3.9B) and 0.44μg/ml respectively (Fig 3.9C). A significant increase in mean cell counts was reached at 3μg/ml for collagen IV before the curve plateaued (Fig3.9A). A significant increase in mean cell counts was reached at 0.3μg/ml for both fibronectin (Fig3.9B) and laminin (Fig3.9C) before the curve plateaued.

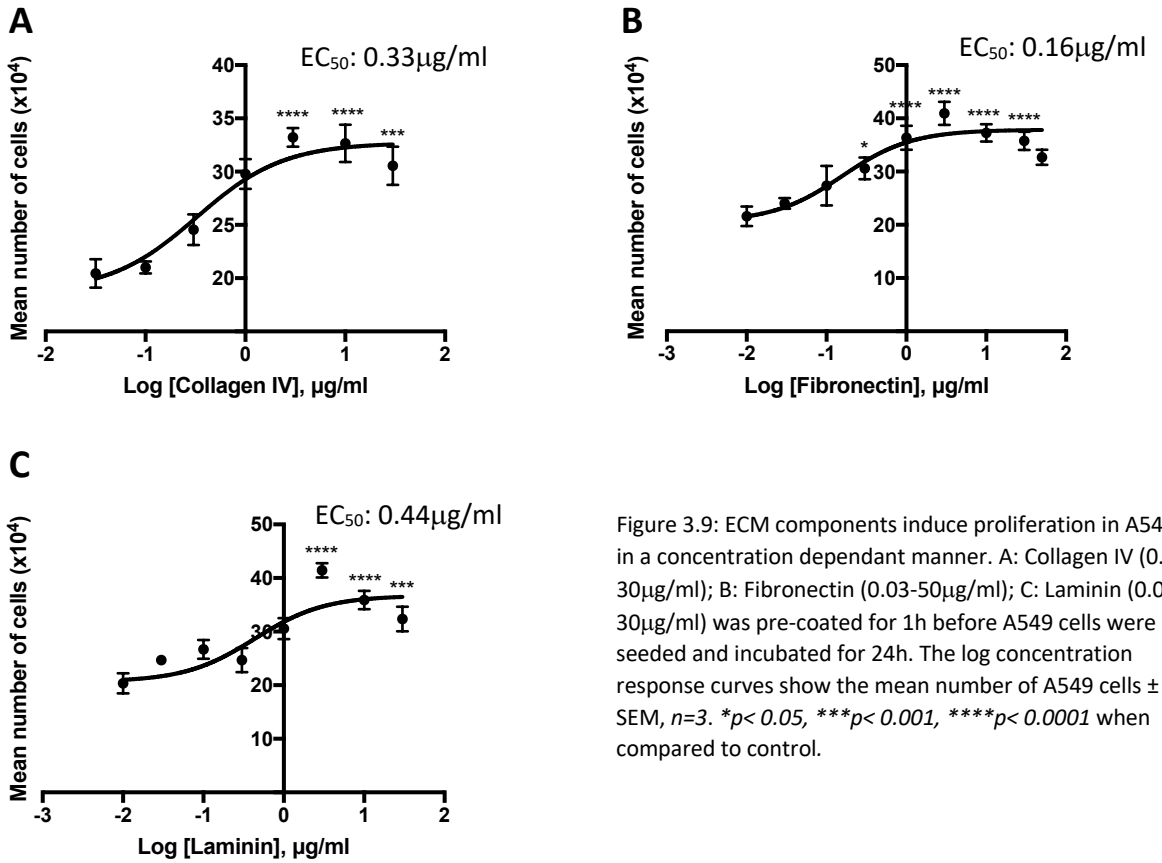


Figure 3.9: ECM components induce proliferation in A549 in a concentration dependant manner. A: Collagen IV (0.1-30μg/ml); B: Fibronectin (0.03-50μg/ml); C: Laminin (0.03-30μg/ml) was pre-coated for 1h before A549 cells were seeded and incubated for 24h. The log concentration response curves show the mean number of A549 cells ± SEM, *n=3*. **p< 0.05, ***p< 0.001, ****p< 0.0001* when compared to control.

3.2.5 HGF and IL-6 have no effect on A549 cell growth on collagen IV

To identify the effect of collagen IV on the HGF and IL-6-induced A549 cell proliferation, cell counts were undertaken with HGF (1ng/ml) and IL-6 (0.5ng/ml) treated cells seeded on collagen IV (3μg/ml) alone or in combination. When cells were cultured on plastic, there was a significant increase in mean cell counts for HGF, IL-6 and HGF+IL-6-treated cells compared to control (Fig 3.10). There was also a significant increase in cell counts between cells seeded on plastic compared to cells seeded on collagen IV (Fig 3.10). However, there was no significant increase in cell counts in the presence of collagen IV in the HGF, IL-6 or HGF + IL-6 treated cells compared to collagen IV alone (Fig3.10.

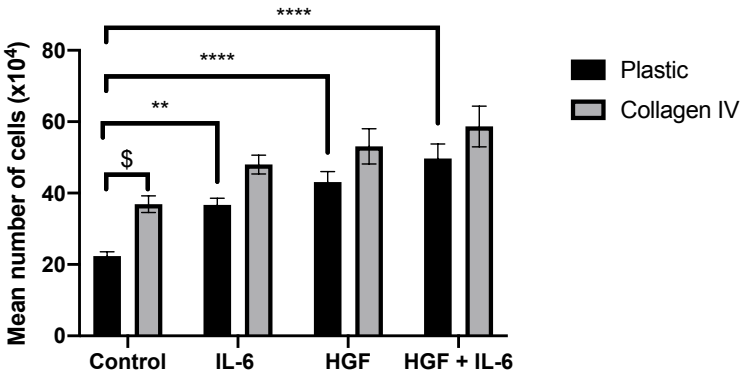


Figure 3.10: Collagen IV does not induce an additive effect on HGF/IL-6-induced proliferation. A549 cells were pre-coated with collagen IV (3ng/ml) for 1h before A549 cells were seeded and treated with HGF (1ng/ml) and IL-6 (0.5ng/ml) After 24 hours cell counts were undertaken. The histogram represents the mean number of A549 cells ± SEM, n=3,** $p<0.05$ and ****$p<0.0001$ when comparing between control and HGF, IL-6 and HGF+IL-6-treated cells on plastic. $ $p<0.05$ when comparing the control cells grown on plastic or collagen IV. Statistical significance was determined by two-way ANOVA and Bonferroni's multiple comparison test.

3.3 Discussion

In this chapter, the effect of HGF, IL-6 and lung ECM components on A549 cell proliferation was investigated. HGF, IL-6, collagen IV, fibronectin and laminin induced a dose-dependent increase in A549 proliferation. HGF and IL-6 treatment in combination had no synergistic or additive effect on A549 cell proliferation compared to IL-6, HGF or Collagen IV alone. The proliferative effects of IL-6 and HGF effects were mediated by the MAPK pathway. These findings demonstrate a previously unrecognised convergence of the MAPK signalling pathway during the combined HGF and IL-6-induced proliferation. Moreover, collagen IV did not induce an additive effect on HGF/IL-6-induced proliferation suggesting their pathways also converge in A549 proliferation.

The pleiotropic effects of HGF and IL-6 mirror one another, in our study a dose-dependent increase in proliferation was observed for HGF and IL-6. HGF is a known mitogen (Nakamura 1994) and the same maximal concentration used in our study was identified for PC-9, HCC827 and H1975 EGFR mutant lung adenocarcinoma cell lines in a separate study (Kang et al. 2013). A similar concentration of 40ng/ml was used in A549 cells (Jiao et al. 2016). Likewise, with IL-6, another study had used the same maximal concentration (10ng/ml) to induce A549 cell growth (Liu et al. 2015). Despite previous mixed findings showing IL-6 either supporting (Kim et al. 2015; Bihl et al. 1998; Gao et al. 2007; Zheng et al. 2019), inhibiting (Takizawa et al. 1993) or having no effect on NSCLC growth (Yamaji et al. 2004), our study demonstrates IL-6 induces proliferation in A549 cells. Lee et al has shown the dual roles of IL-6 in stimulating proliferation in CD133+ A549 cells whilst inhibiting the proliferative effects on CD133- A549 cells (Lee et al. 2016). Experiments to identify the CD133+ population of the A549 cells *via* flow cytometry or western blot analyses would be required to confirm its presence in culture. Further HGF and IL-6 cell proliferation counts can then be undertaken through fluorescence-activated cell sorting (FACS) of the separate CD133+ and CD133- population of A549 cells. Therefore, this will determine whether cancer stem cells are the proliferative phenotype within the cell population.

Although extensive studies have investigated HGF and IL-6 independently in NSCLC proliferation, there are limited studies identifying the cooperation between HGF and IL-6 together in cancer. Our study revealed no additive or synergistic effect on A549 proliferation at a lower seeding density or in low serum culture. Furthermore, at a lower seeding density and low serum culture, the EC_{50} concentrations of HGF and IL-6 alone had no effect on A549 cell proliferation. This highlights the influence of cell culture conditions in mediating the proliferation of cells. Studies have shown a higher seeding density increases proliferation due to an increase in intercellular contacts occurring between neighbouring cells which stimulates paracrine signalling of growth factors (Heng et al. 2011; Dulbecco and Stoker 1970; Stoker and Rubin 1967; Todaro, Lazar, and Green 1965). Therefore, at the lower

seeding density, the EC_{50} concentration of HGF and IL-6 alone may not stimulate sufficient cell contact thus limiting cell proliferation. However, there was an increase in proliferation observed when cells were treated with HGF and IL-6 in combination and this may be due to a combined enhanced migration of cells allowing for more cell contacts to occur. The concentration of serum in culture also plays a vital role in cell proliferation as growth factors including IGF, EGF, TGFβ and FGF-2 are abundantly present, although the concentrations vary accordingly with each batch (Lennon et al. 1996; Lennon et al. 1995). Several studies have shown HGF and IL-6 can additively/synergistically induce proliferation with other growth factors: IGF, IL-6 and HGF synergistically cooperate to induce proliferation in multiple myeloma cells (Hov et al. 2007) and EGF and HGF also induce proliferation in a synergistic manner in A549 cells (Puri and Salgia 2008). Therefore, in low serum, the EC_{50} concentration of HGF and IL-6 did not induce an increase in proliferation possibly due to the lack of additive/synergistic effect with growth factors present in serum. The crosstalk proliferative signalling induced by HGF, IL-6, IGF and EGF can be further explored in future studies.

As there was a lack of additive/synergistic proliferation, this suggests downstream convergent activation of pathways involved in mediating the HGF and IL-6-induced proliferation. The use of a MEK inhibitor revealed for the first time HGF and IL-6 induce proliferation *via* convergence on the MAPK pathway. A study in myeloma cells also showed IL-6 reliant on c-Met signalling to fully activate Ras and p44/42 MAPK pathway *via* a convergence on Shp2 (Hov et al. 2007). Western blot analyses would be required to validate these findings in future work. Other signalling pathway convergence between HGF and IL-6 has also been reported in the survival of A549 cells, whereby sustained activation of STAT3 *via* Src kinase downstream of HGF, IL-6 and EGF simulation was required (Song et al. 2003). IL-6 has also been shown to induce c-Met cell surface expression and sensitise cells to HGF (Hov et al. 2009). Both HGF/c-Met and IL-6 can activate the PI3K and STAT3 downstream signalling pathways. Future studies using inhibitors of the PI3K (e.g. LY294002) and STAT3 (e.g. STATTIC) can determine whether HGF and IL-6 also converge on these pathways during A549 cell proliferation.

Although IL-6 and HGF and their relationship in proliferation has been examined, it is important to understand the context of the tumour microenvironment in sustaining proliferation. Tumour cells bind to the ECM *via* integrins to facilitate signalling pathways involved in NSCLC growth, cell cycle progression and suppression of apoptosis (Hodkinson et al. 2006; Hastings et al. 2019). A dose-dependent increase in A549 cell proliferation for collagen IV, fibronectin and laminin was observed in our study. The lung ECM components play an active role, promoting the survival of SCLC cells through overriding chemotherapy-induced DNA damage (Hodkinson et al. 2006). Furthermore, remodelling of the ECM in NSCLC upregulates collagen IV, laminin and fibronectin expression to 93%, 80.7% and 54.4% from 39.15%, 54.4% and 17.4% respectively (Yan et al. 2006). There are mixed findings on the

proliferative effects of the individual lung ECM components in various cell lines. Collagen IV showed no effect on proliferation in Calu-1 cells, (Mukhopadhyay et al. 2004), and inhibition of proliferation was observed in melanoma cells (Han et al. 1997) but increased proliferation, cell adherence and migration in mammary cells (Kim et al. 1994) and hepatoma cells (OGATA 1998). Laminin facilitates EMT (Liu et al. 2018; Moon et al. 2015) and adhesion (Hastings et al. 2019) in NSCLC but the proliferative effect of laminin in NSCLC has not yet been investigated in the field. Several studies have demonstrated the proliferative role of fibronectin in NSCLC. In PC9 cells, fibronectin induced proliferation with the same maximal concentration used in our study (Ju and Zhou 2013). Another study showed fibronectin induces NSCLC growth and inhibits apoptosis *via* activation of α5β1 and cyclooxygenase-2 (COX-2) whilst reducing gene expression for the cyclin-dependent kinase inhibitor $p21^{Waf1/Cip1}$ (Han et al. 2004). The fibronectin-mediated inhibition of p21 genes relies on downstream activation of ERK and Rho kinase (Han, Sidell, and Roman 2005). Fibronectin also activates the PI3K/mTOR pathway signalling pathway to induce NSCLC proliferation (Han, Khuri, and Roman 2006). Fibronectin binding to α5β1 has also been shown to consequently activate FAK and Src to support proliferation in endothelial cells (Mitra and Schlaepfer 2006).

As the ECM/integrin signalling is known to crosstalk with the HGF/MET pathway to influence and sustain metastatic behaviour including migration, proliferation and differentiation (Desgrosellier and Cheresh 2010; Crouch, Spidel, and Lindsey 2004; Trusolino, Bertotti, and Comoglio 2001), the role of ECM/β1-integrin interactions with HGF and IL-6 was explored. However, despite the individual proliferative capacity of HGF, IL-6 and collagen IV, no additive or synergistic effect on the HGF/IL-6-induced proliferation with collagen IV was observed suggesting a convergence in their pathways. Further repeats would be required in low serum and using the EC_{50} concentration of collagen IV instead of the maximal concentration (3μg/ml) to confirm these findings. HGF in the presence of collagen I, has been shown to induce proliferation and migration *via* activation of ERK 1/2 and P13K (Rahman et al. 2005). Therefore, inhibitors of ERK1/2 (PD98059) and PI3K (LY294002) can be used in future studies to identify other potential convergent signalling pathways downstream of HGF, IL-6 and collagen IV. Furthermore, as HGF, IL-6 and the ECM proteins are known to induce EMT (Shintani et al. 2008; Lee et al. 2006; Chen et al. 2015; Zheng et al. 2019), the crosstalk between the components may be inducing a migratory behaviour associated with EMT rather than proliferation. Further cell tracking migration studies would be needed to measure the speed and distance and confirm whether HGF and IL-6 treated cells are more migratory in the presence of collagen IV. Future studies using a β1-integrin functionally blocking antibody can also be used to characterise this potential effect. Other studies have shown HGF induces proliferation *via* interactions with fibronectin and β1-integrin. Ju et al reported synergistic proliferation between HGF and fibronectin in PC9 cells (Ju and Zhou 2013). The potential

additive or synergistic effect of fibronectin on HGF and IL-6-induced proliferation was not explored in this study however this can be investigated in future studies. HGF-dependent activation of c-Met has been shown to co-internalisation with β1-integrin in NSCLC (Barrow-McGee, Kishi, et al. 2016b). Following internalisation, the β1-integrin and c-Met complex accumulate on the ARE to activate the ERK1/2 pathway leading to anchorage-independent growth (Barrow-McGee, Kishi, et al. 2016b). C-Met can also displace α5 subunit from α5β1 integrin to form a c-Met/β1-integrin complex which binds with a stronger affinity to fibronectin in glioblastoma cells (Jahangiri et al. 2017). Studies have also associated α5β1 levels with an increase in lymph node metastasis and poor prognosis (Han et al. 2003). Both fibronectin and laminin also promoted the amplification and ligand-independent c-Met signalling through the binding with α5β1 and α6β4 in ovarian and breast cancer cells respectively (Mitra et al. 2011; Chung et al. 2004). Therefore, future studies could investigate the role of laminin in the HGF/IL-6-mediated proliferation in A549 cells. Furthermore, the role of integrin-associated crosstalk with IL-6 is less defined in the literature. Lee et al observed significant levels of integrin expressed and IL-6 regulation in the CD133+ subpopulation of A549 cells (Lee et al. 2016), thus integrins may play a role in mediating the proliferative and metastatic effects. Multiple myeloma cells cultured on fibronectin and treated with IL-6 induced a significant increase STAT3 activation leading to an increase in proliferation and survival. The same study also reported β1-integrins were able to amplify the IL-6-mediated STAT3 activation (Shain et al. 2009). Therefore, there may be a potential role in NSCLC for HGF and IL-6 to mediate proliferation through crosstalk with fibronectin, laminin and β1-integrin. Future studies can be conducted to fully map out the signalling crosstalk between HGF, IL-6 and the various ECM components.

3.3.1 Future work

The overall findings highlight the complex nature of the tumour microenvironment and its influence in mediating cancer progression. This study provides novel insight into the signalling convergence in the HGF and IL-6-induced proliferation *via* the MAPK pathway. A novel convergence between HGF, IL-6 and collagen IV-induced proliferation. Further confirmation of the HGF, IL-6, collagen IV, fibronectin and laminin-induced proliferation from cell counts would be needed to be validated through another method. The use of a functionally blocking β1-integrin antibody would also be used alongside to further confirm the role of ECM/β1-integrin crosstalk with HGF and IL-6-induced proliferation. Quantification of EdU-incorporated nuclei is a robust method to measure the proliferation of cells and can be used for future studies. EdU is a modified thymidine analogue which is incorporated during DNA synthesis and fluorescent visualisation can be undertaken through a click reaction with an Alexa Fluor dye. Furthermore, to better recapitulate the 3D tumour microenvironment with similar cell-cell and cell-extracellular interactions, A549 cells can be

cultured in Matrigel to develop A549 tumouroids (Li et al. 2022). Matrigel is a reconstituted basement membrane extracted from the Engelbreth-Holm-Swarm (EHF) mouse sarcoma. Matrigel mostly comprises of laminin (60%), collagen IV (30%) and entactin (8%) and can substitute the combined ECM protein composition and activation required for future 3D growth studies. A growth factor reduced form of Matrigel can be used to investigate the potential additive or synergistic effect of HGF and IL-6 in A549 tumouroid proliferation using the respective EC_{50} and maximal concentrations either alone or in combination. The proliferative effect of the HGF and IL-6 treated tumouroids can then be assessed *via* EdU incorporation. These experiments were further conducted in chapter 8 to explore the role of the 3D TME in influencing A549 tumouroid growth. Further pathway inhibitors for MAPK, PI3K and STAT3 can then be used to identify the potential downstream signalling pathways involved in the HGF and IL-6-mediated proliferation of A549 tumouroids.

During our growth studies with HGF, a novel effect was observed whereby long and thin protrusions that resembled TNTs formed in HGF-treated A549 cells. The thesis then took a change of direction to investigate this observation further, still with a focus on the effects of HGF alone and in combination with other growth factors as well as crosstalk with cell signalling pathways like MAPK and integrin growth factor receptor crosstalk.

4. Chapter 4: HGF induces tunneling nanotube formation in A549 cells

4.1 Introduction

TNTs are a form of long-range intercellular communication. TNTs are non-adherent, open-ended F-actin-based cytoplasmic protrusions and were initially discovered in cultured rat pheochromocytoma PC12 cells (Rustom et al. 2004). TNTs are characteristically long and thin structures, spanning up to 130µm in length and between 0.4-1.5µm in width in lung cancer cells (Wang et al. 2012). They display variability in their cytoskeletal composition, with microtubules present in thicker TNTs (Önfelt et al. 2006). There are two ways TNTs can form: either through one cell extending its actin-driven membrane protrusion towards another cell (type 1) or through cells which migrate apart forming a tubular cytoplasmic connection in between (type 2)(Gerdes, Rustom, and Wang 2013). TNTs exist to transport cellular organelles such as mitochondria, cellular vesicles, lysosomes etc. to non-adjacent cells (as reviewed in (Ariazi et al. 2017)). Although there are no known specific markers for TNTs, their presence is confirmed through morphological analysis of their cytoskeletal composition, non-adherent nature and ability to traffick organelles.

In cancer, TNT-mediated transfer of organelles has been shown to facilitate chemoresistance and confer an aggressive phenotype to recipient cells (Hanna et al. 2019; Pasquier et al. 2013; Lu et al. 2019; Lu et al. 2017; Desir et al. 2018; Thayanithy et al. 2014). TNTs have been observed in various cancer cell lines including HeLa cells (Hase et al. 2009), mesothelioma cell lines (Lou, Fujisawa, Morozov, et al. 2012), breast and ovarian cancer cell lines (Pasquier et al. 2013) and lung adenocarcinoma cells (Austefjord, Gerdes, and Wang 2014; Kumar, Tiwari, and Rajala 2017; Spees et al. 2006; Dubois et al. 2018; Wang et al. 2012). TNTs can also form in heterotypic and homotypic cultures (Kretschmer et al. 2019). *In vivo* TNTs, which have been rarely observed, were found present in human lung adenocarcinoma and mesothelioma tumour samples, thus highlighting its evidence in solid tumours outside *in vitro* settings (Lou, Fujisawa, Morozov, et al. 2012). TNTs have been widely found in stress conditions that mimic the tumour microenvironment, this includes hypoxic, low serum, acidic pH and hyperglycaemic states (Thayanithy et al. 2014; Wang et al. 2011; Wang and Gerdes 2012). Furthermore, cancer treatments including radiotherapy (Matejka and Reindl 2019), chemotherapy (Kretschmer et al. 2019) and radiofrequency treatment (Ware et al. 2015) stimulate the formation of TNTs. Despite its important role in cancer, the molecular mechanisms and signalling pathways involved remain poorly defined, especially in NSCLC.

Stress-induced TNT formation is regulated by small GTPases and actin-driven proteins such as myosin and filamin. A cytosolic protein, M-sec, is a known marker of TNTs. In HeLa cells M-sec, aided by LST1, localises with RalA GTPase and the exocyst complex at the cell membrane to induce actin polymerisation required to form TNTs (Hase et al. 2009). Although studies continue to unravel the mechanisms involved in TNT formation, different cell types regulate TNT formation *via* different mechanisms and pathways. Moreover, the upstream factors involved remain poorly defined. As there are no specific markers for TNTs, identifying their upstream regulators will help to therapeutically inhibit TNT formation in cancer.

More recently, factors that influence EMT have been implicated in TNT formation (Lou, Fujisawa, Morozov, et al. 2012). EMT in NSCLC is associated with poor prognosis and cancer progression (Schliekelman et al. 2015), therefore TNT-mediated cellular communication has the potential to propagate resistance and metastasis in NSCLC. Most studies have mainly shown the role of EGF in TNT formation in rat astrocytes and breast cancer cells (Cole, Dahl, and Cowden Dahl 2021; Carter et al. 2019). Furthermore, within the tumour microenvironment of NSCLC, studies have established HGF and its signalling axis in the metastatic process. Despite this, the role of HGF in TNT formation has not yet been explored.

Crosstalk between β1-integrin with the HGF/c-Met pathways has been implicated in A549 cell growth (as described in more detail in chapter 3) and is widely documented in other NSCLC studies (Ju and Zhou 2013; Mitra et al. 2011; Barrow-McGee, Kishi, et al. 2016a). Furthermore, HGF activation induces integrin clustering recruiting FAK and paxillin which lead to migration and proliferation *via* the MAPK and PI3K pathways (Liu et al. 2002; Lai et al. 2000; Ishibe et al. 2004). The HGF/c-Met/β1-integrin crosstalk activation involves similar actin-driven proteins required in the cytoskeletal remodelling required for TNT formation. However, its role in TNT formation has not been studied.

Therefore, the aim of this study was to determine whether HGF/c-Met and β1-integrin crosstalk to regulate TNT formation in A549 lung adenocarcinoma cells. This work demonstrates a novel role for the co-activation of HGF/c-Met, β1-integrin and paxillin in A549 TNT formation.

4.2 Results

4.2.1 Effect of *in vitro* culture conditions on TNT formation of A549 cells

In vitro culture conditions are vital factors in studying TNT formation. Studies have shown culture conditions which mimick the tumour microenvironment, i.e hypoxic, hyperglycaemic, acidic and serum deprivation, favour TNT formation (Lou, Fujisawa, Morozov, et al. 2012; Kretschmer et al. 2019). Therefore the culture conditions could potentially impact the HGF-induced TNT formation. In order to determine the optimal TNT effect for future experiments, the optimal seeding density and serum concentration were first assessed.

The cell density plays a major role in determining the length of TNTs as confluent cells in close proximity are less likely to form TNTs (Benard et al. 2015; Dubois et al. 2020). To investigate the effect of cell density on TNT formation, A549 cells were seeded at various low seeding densities on plastic for 72hrs before being treated with HGF at a concentration (100ng/ml) and timepoint (24hrs) used in previous proliferation (as described in chapter 3) and migration studies in NSCLC (To et al. 2002; Jagadeeswaran et al. 2007). White light images were then captured on an inverted microscope (Fig4.1A). Across all the seeding densities, HGF induced thin cellular protrusions, narrow at the base and spanning various lengths to connect to distant cells. Therefore, we termed these protrusions TNT-like structures, as they display morphology akin to TNTs (denoted by the white arrows). To quantify the TNT-like structures, three parameters were measured for each field of view: mean percentage of cells with TNT-like structures (Fig4.1B), mean number of TNT structures per cell (Fig4.1C) and the length of TNT-like structures (Fig4.1D) as described in **Section 2.8.1**. An increase in mean percentage, mean number per cell and length was observed across all the seeding densities (Fig4.1B-D). At higher seeding densities the TNT-like structures often pass over confluent cells and were more difficult to identify for analysis. Furthermore, at the lowest seeding density (1000 cell/well), the error bars were larger due to the low number of cells counted therefore a higher seeding density of 5000 cells/well was used for future experiments.

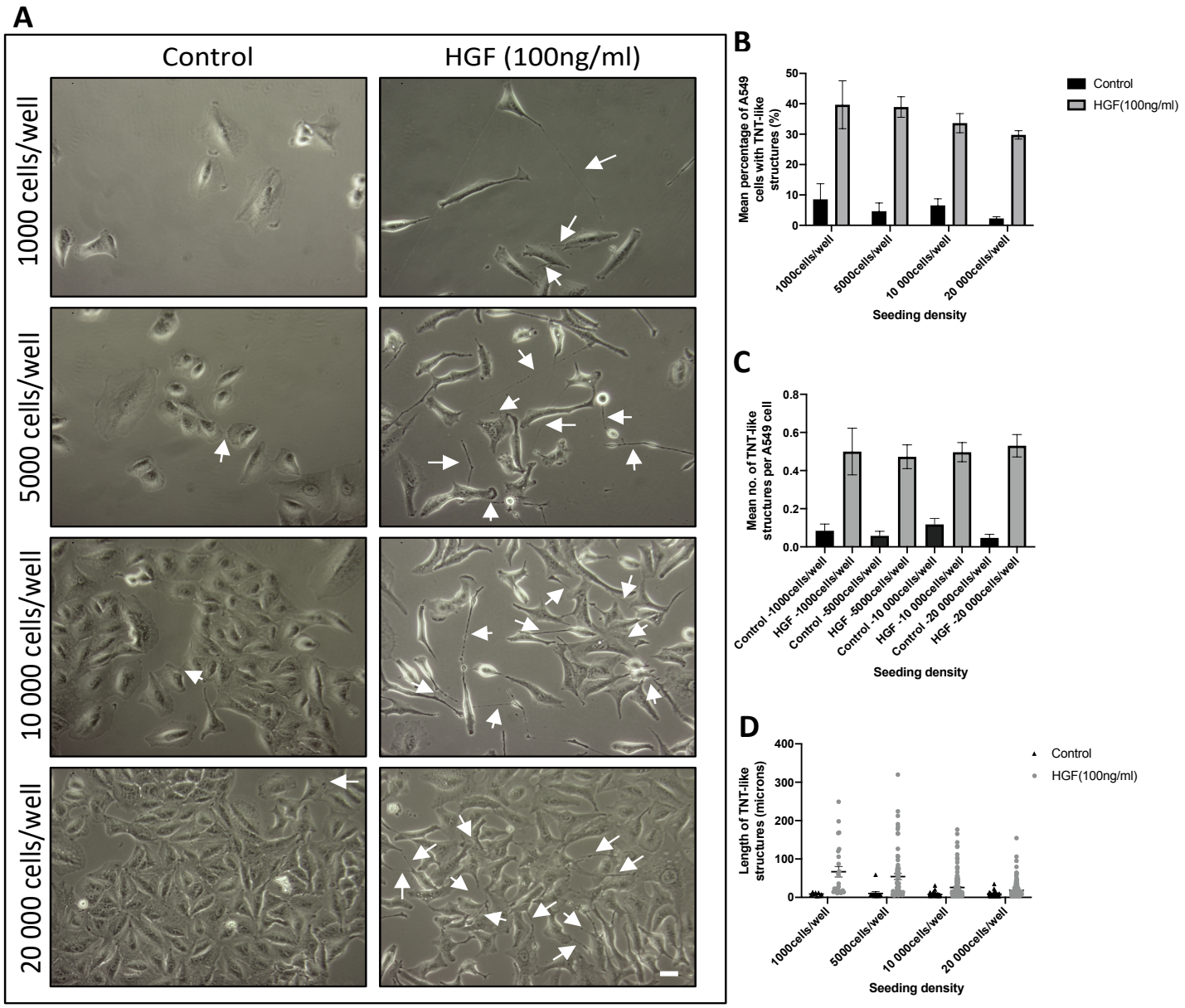


Figure 4.1 Optimal seeding density on plastic to observe HGF-induced TNT-like structures. A: Representative white light images demonstrate an increase in TNT-like structures (white arrow) when treated with HGF (100ng/ml) across the different seeding densities. White light images were captured using 10x objective lens on an inverted microscope. Scale bar: 10µm. B-D: The white light images were quantified for TNT-like structures and the histogram and scatter plot displays the mean percentage (B), number of TNT-like structures per cell (C) and length of TNT-like structures (D). There was an increase in the mean (B), number (C) and length (D) of the HGF-induced TNT-like structures between control and HGF(100ng/ml) treated cells. The optimal effect was observed at a seeding density of 5000 cells/well. Values are expressed as mean ± SEM, n=1 with at least 50 cells analysed per condition.

Next, to investigate the effect of serum on TNT formation, cells were treated with HGF (100ng/ml) in either 10% or 2% FBS supplemented DMEM media for 24hrs (Fig4.2A). The control in both FBS concentrations were similar in mean percentage (Fig4.2B), number (Fig4.2C) and length (Fig4.2D) of TNT-like structures. There was an increase in mean percentage (Fig4.2B) and number (Fig4.2C) in HGF-induced TNT-like structures in the 2% FBS-supplemented media compared to the 10% supplemented media. There was no difference in the mean length of HGF-induced TNT-like structures between 2% and 10% FBS-supplemented media (Fig4.2D). Therefore for the majority of future experiments, A549 cells were treated with HGF in 2% FBS supplemented media to maximise TNT formation.

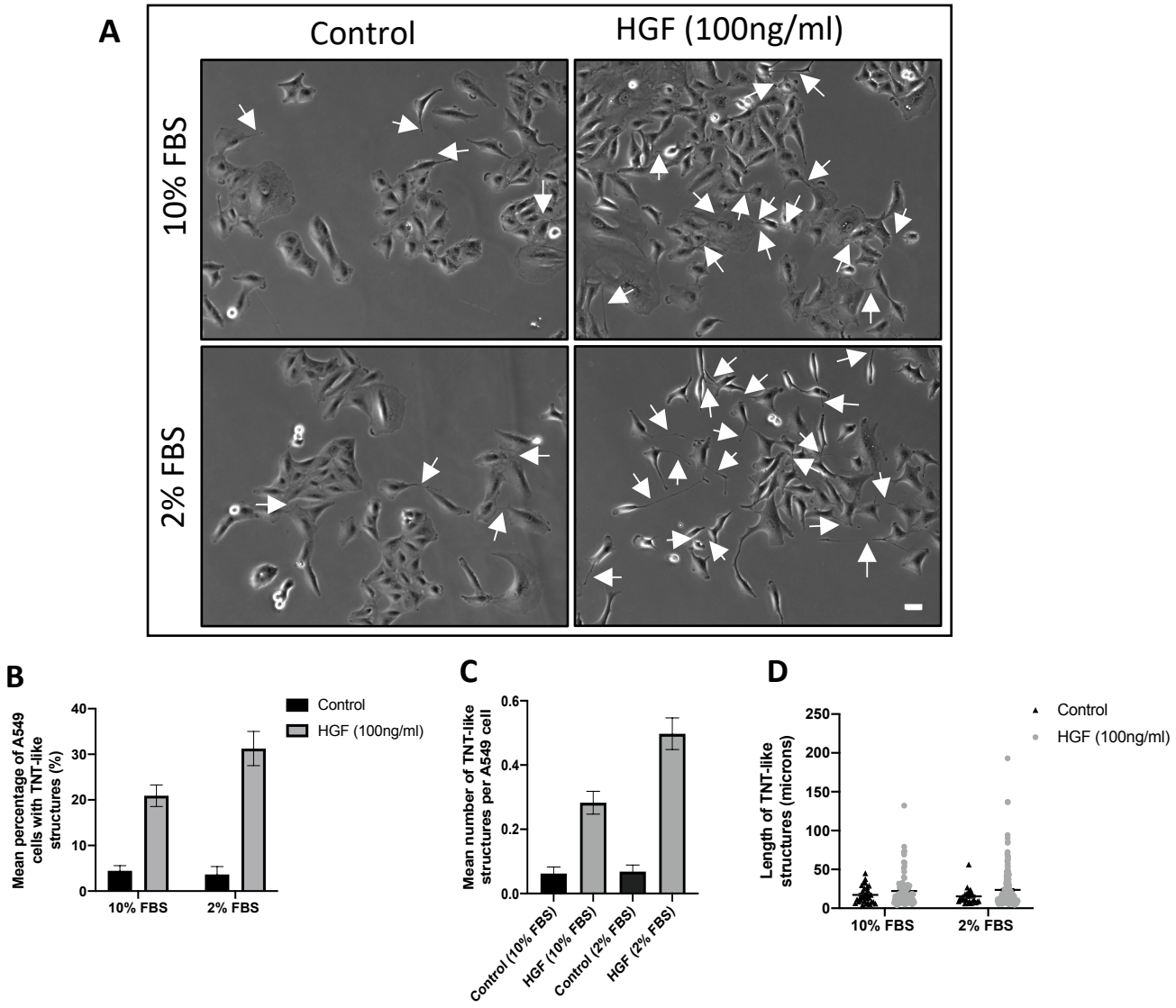
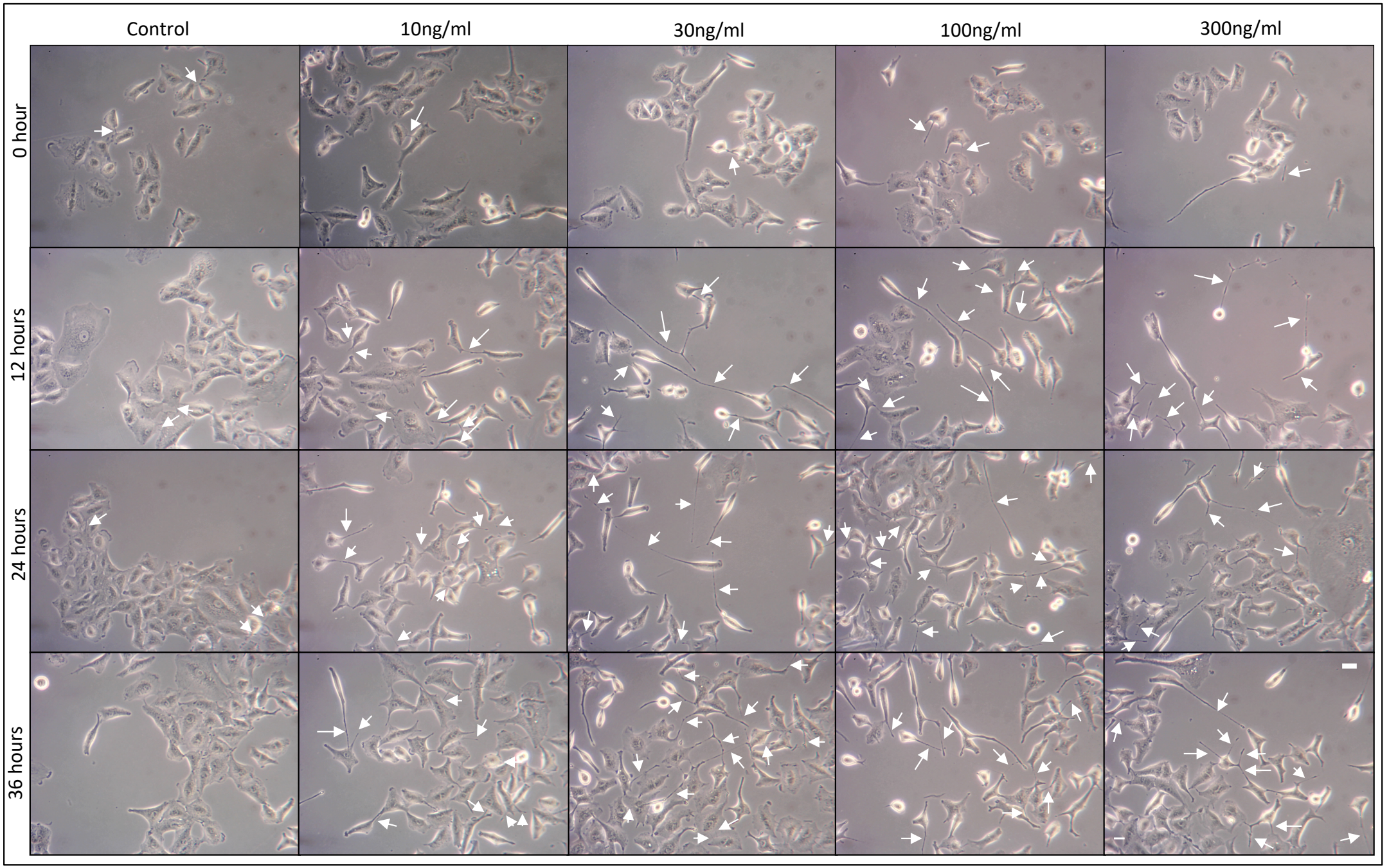


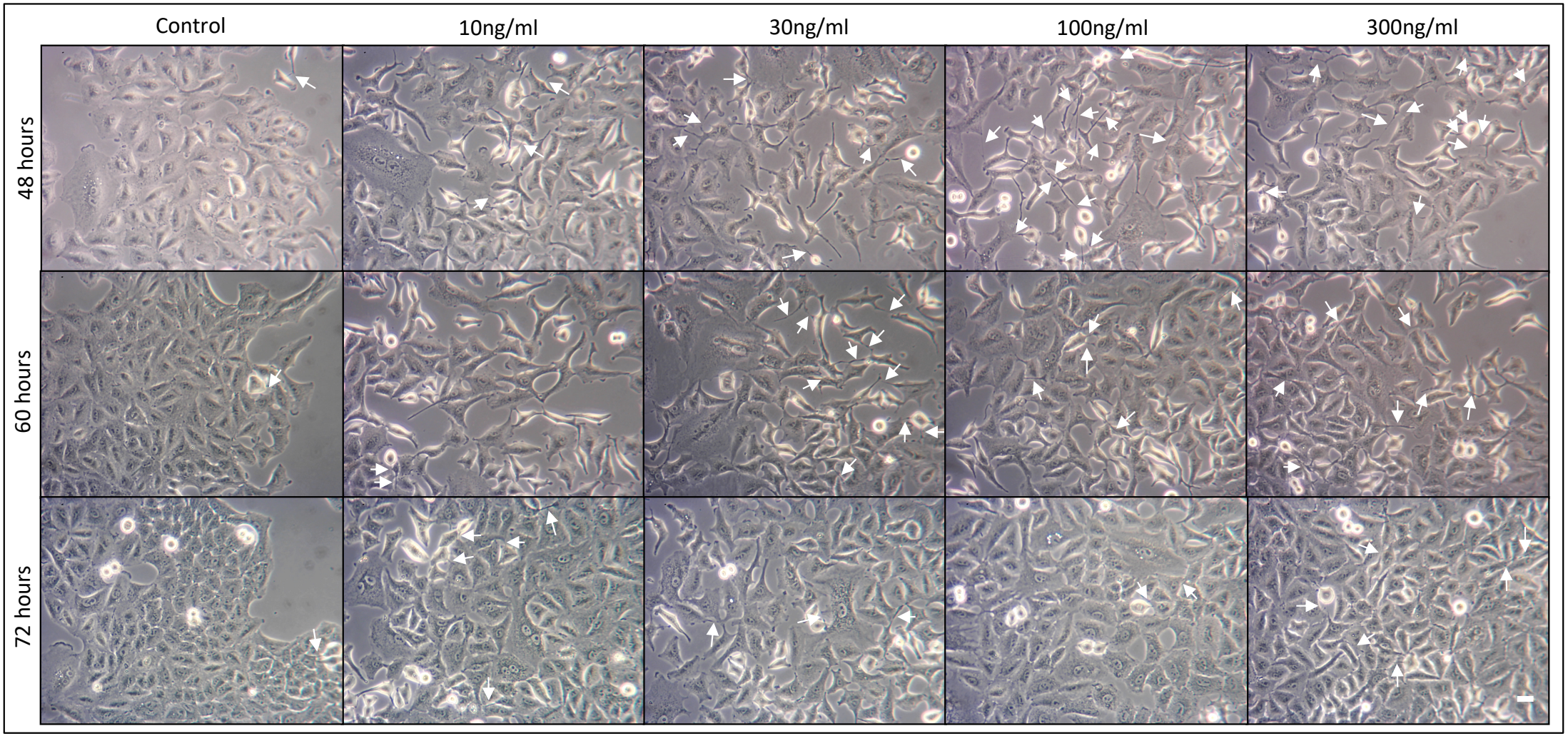
Figure 4.2: HGF induces an increase in TNT formation in 10% and 2% FBS supplemented media. A: Representative white light images show an increase in TNTs (white arrow) in HGF treated cells in both concentrations of FBS supplemented media compared to their respective controls. White light images were captured using 10x objective lens on an inverted microscope. Scale bar: 10µm. B-D: The white light images were quantified for TNT-like structures and the histogram (B,C) and scatter plot (D) displays the mean percentage (B), number of TNT-like structures per cell (C) and length of TNT-like structures (D). Values are expressed as mean ± SEM, n=1, with at least 300 cells analysed per condition.

4.2.2 HGF induces TNT formation in A549 cells in a time and concentration-dependent manner

Once the optimal culture conditions were determined, the effect of HGF in A549 TNT formation was thoroughly investigated. Therefore, a 72-hour time course experiment was conducted for HGF at increasing concentrations (0-300ng/ml). White light images were taken every 12 hourly for 72 hours to observe the TNT-like structures (Fig4.3A). TNT-like structures begin to form between 10-30ng/ml of HGF treatment, as A549 cells scatter due to an increase in migration, transforming from an oval epithelial to spindle-shaped morphology and exhibiting filopodia-like extensions. At higher concentrations between 100-700ng/ml, TNT-like extensions begin to lengthen across the field of view (white arrows)(Fig4.3A). The TNT-like structures were quantified and the line graph (Fig4.3B-D) display a dome-shaped response curve with significant (n=3, p<0.0001) increase in mean percentage, number per cell and length of TNT-like structures over 72 hours across the concentrations of HGF. The maximal concentration was reached at 100ng/ml for two of the parameters: in mean percentage and mean number of TNT-like structures at the 12th hour time point before plateuing over the time course experiment (Fig 4.3B&C). Furthermore, the maximal timepoint was reached at the 24th hour for two of the parameters at 100ng/ml concentration: mean percentage (Fig4.4B) and mean length (Fig4.3D) of TNT-like structures. Moreover, TNTs were more easily identifiable at lower timepoints (0, 12th, 24 and 36th hour) due to the lower confluency (Fig4.3A). Therefore, the maximal concentration (100ng/ml) and time point (24h) induced by HGF was used for subsequent experiments.

A


Control
10ng/ml
30ng/ml
100ng/ml
300ng/ml
0 hour
12 hours
24 hours
36 hours


Control
10ng/ml
30ng/ml
100ng/ml
300ng/ml
48 hours
60 hours
72 hours

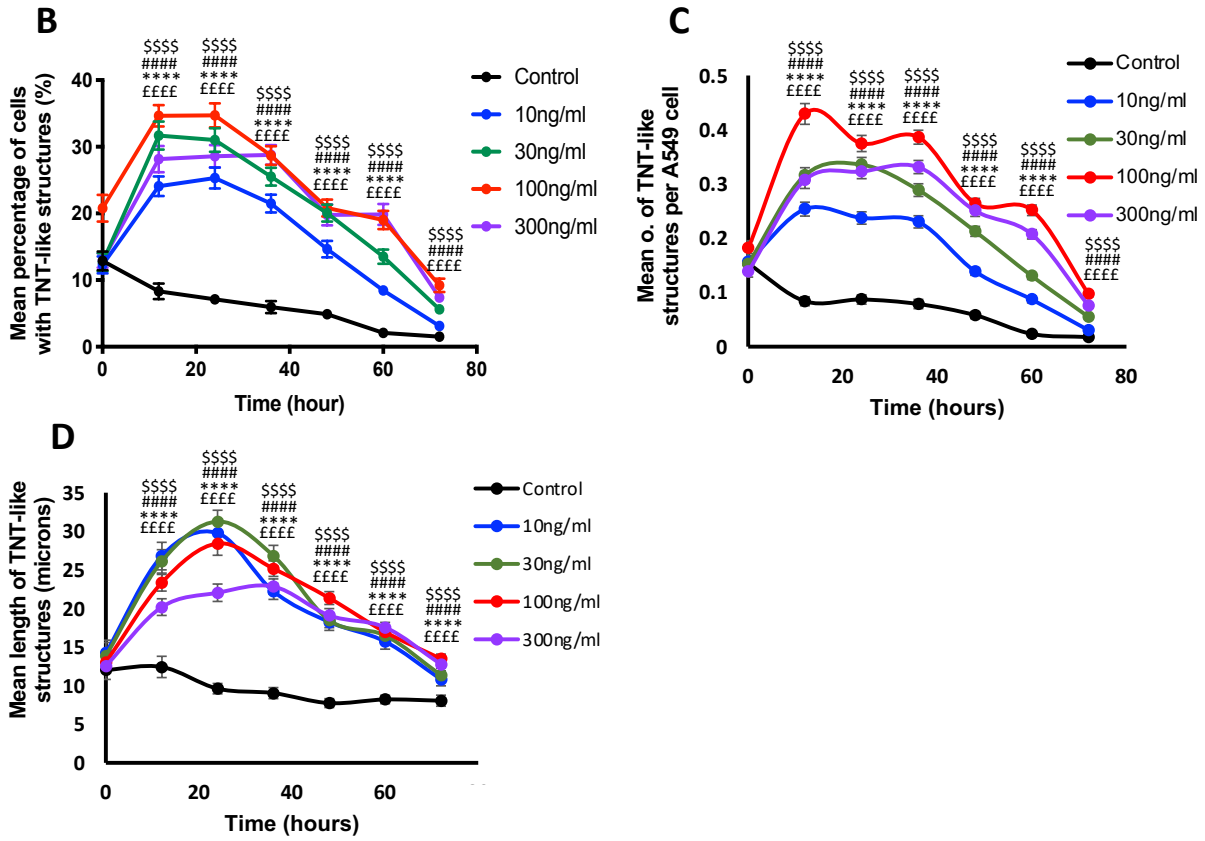


Figure 4.3: HGF induces TNT-like structures in A549 lung adenocarcinoma cells in a time dependent manner. A: Representative white light images demonstrate an increase in TNT-like structures (white arrow) with increasing concentrations of HGF (0-300ng/ml)(10%FBS) over 72 hours. White light images were captured using 10x objective lens on an inverted microscope. Scale bar: 10µm. The white light images were quantified for TNT-like structures and the line graphs show the dose-dependent increase in the mean (B), number (C) and length (D) of the HGF-induced TNT-like structures between control and the different concentrations of HGF-treated cells over a 72-hour time period. The maximal effect was observed at the 24th hour timepoint for mean percentage and length. Values are expressed as mean ± SEM, n=3 with at least 1500 cells analysed per condition. £££p<0.0001 when comparing control to 10ng/ml, ****p<0.0001 when comparing control to 30ng/ml, ####p<0.0001 when comparing control to 100ng/ml, $$$$$p$<0.0001 when comparing control to 300ng/ml by one-way ANOVA and Tukey's multiple comparison test.

To determine the maximal concentration at the 24th-hour time point, A549 cells were treated with HGF (0-700ng/ml) for 24hrs (Fig4.4A). The log concentration-response curve show HGF induces a dose-dependent significant (*n*=3, ****p<0.0001) increase in mean percentage, mean number per cell and length of TNT-like structures, with a maximal concentration reached at 100ng/ml plateauing through 300ng/ml and 700ng/ml (Fig4.4B-D). TNT-like structures were observed at lengths spanning several hundred microns, reaching up to 350µm in this study.

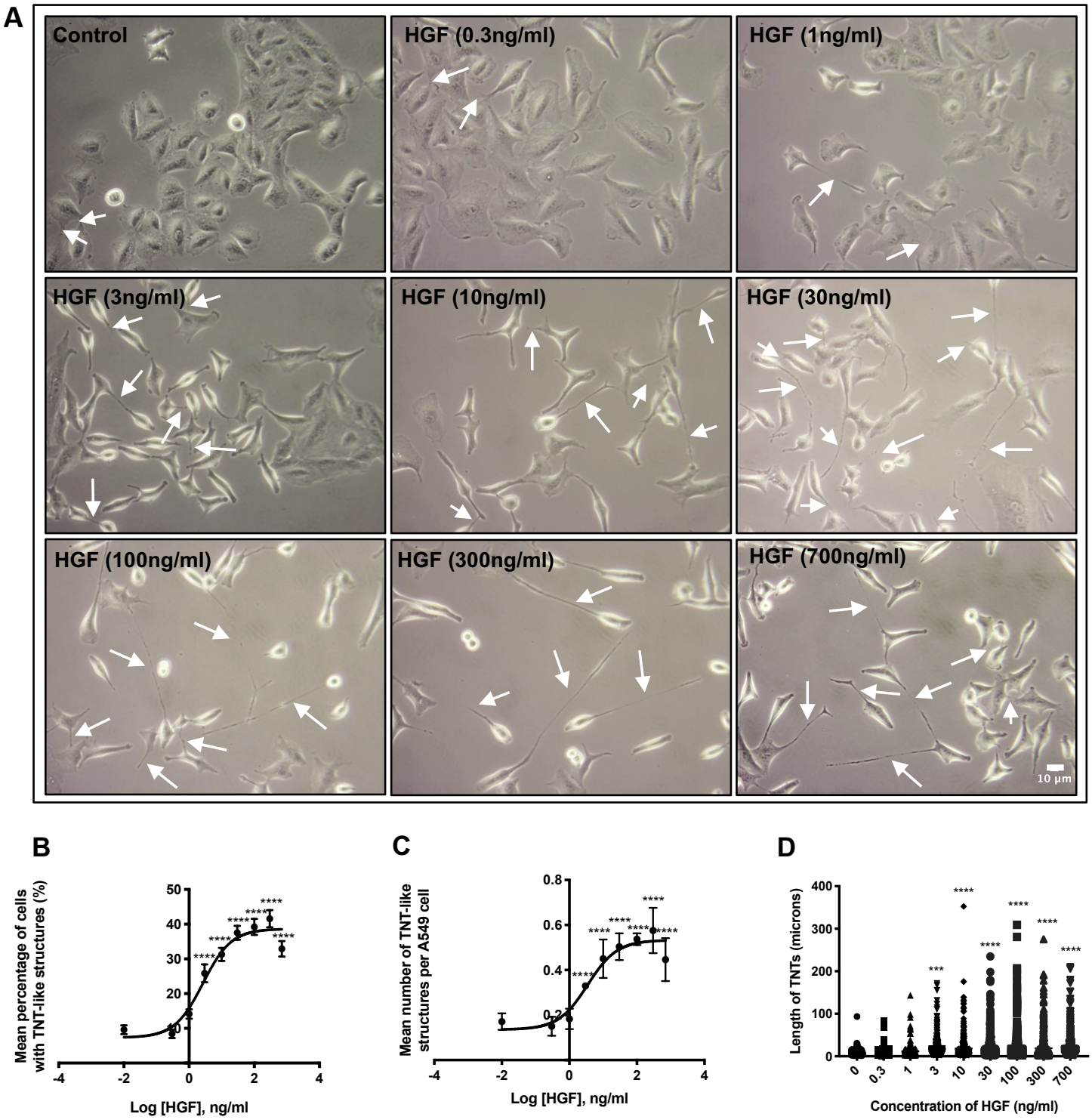


Figure 4.4: HGF induces TNT-like structures in A549 lung adenocarcinoma cells in a concentration dependent manner at the 24th hour timepoint. A: Representative white light images demonstrate an increase in TNT-like structures (white arrow) with increasing concentrations of HGF (0-700ng/ml)(2% FBS). White light images were captured using 10x objective lens on an inverted microscope. Scale bar: 10µm. The white light images were quantified for TNT-like structures and the HGF log concentration response curve displays the mean percentage (B), number of TNT-like structures per cell (C) and length of TNT-like structures (D). Values are expressed as mean ± SEM, n=3, with at least 1000 cells analysed per condition. ****p<0.0001 when compared to control by one-way ANOVA and Tukey's multiple comparison test.

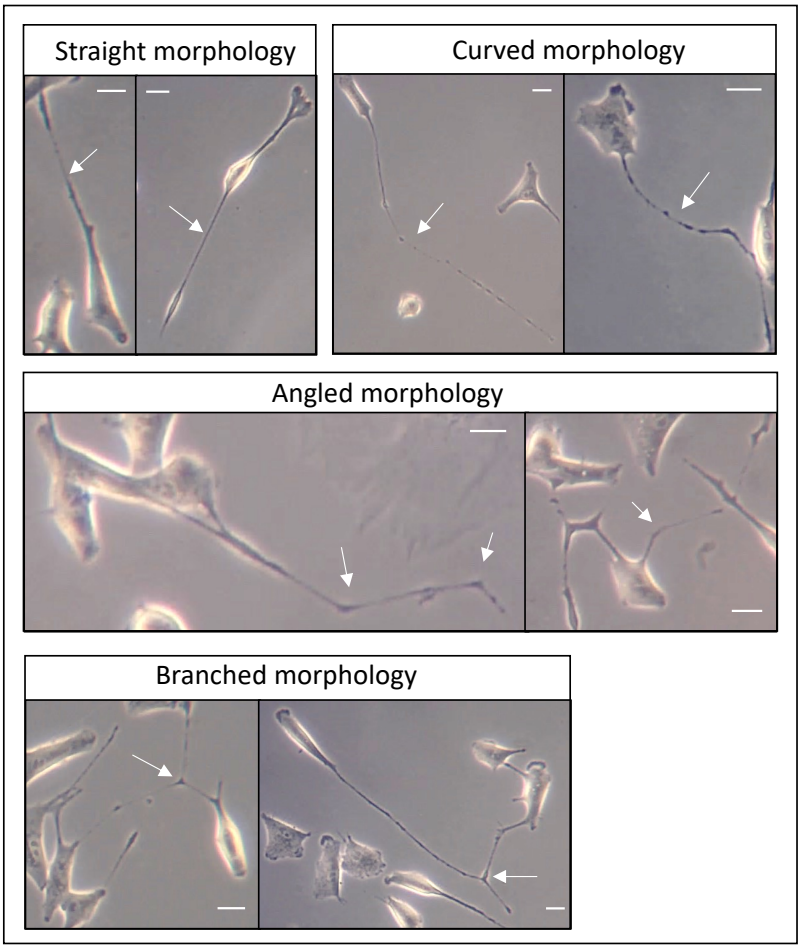
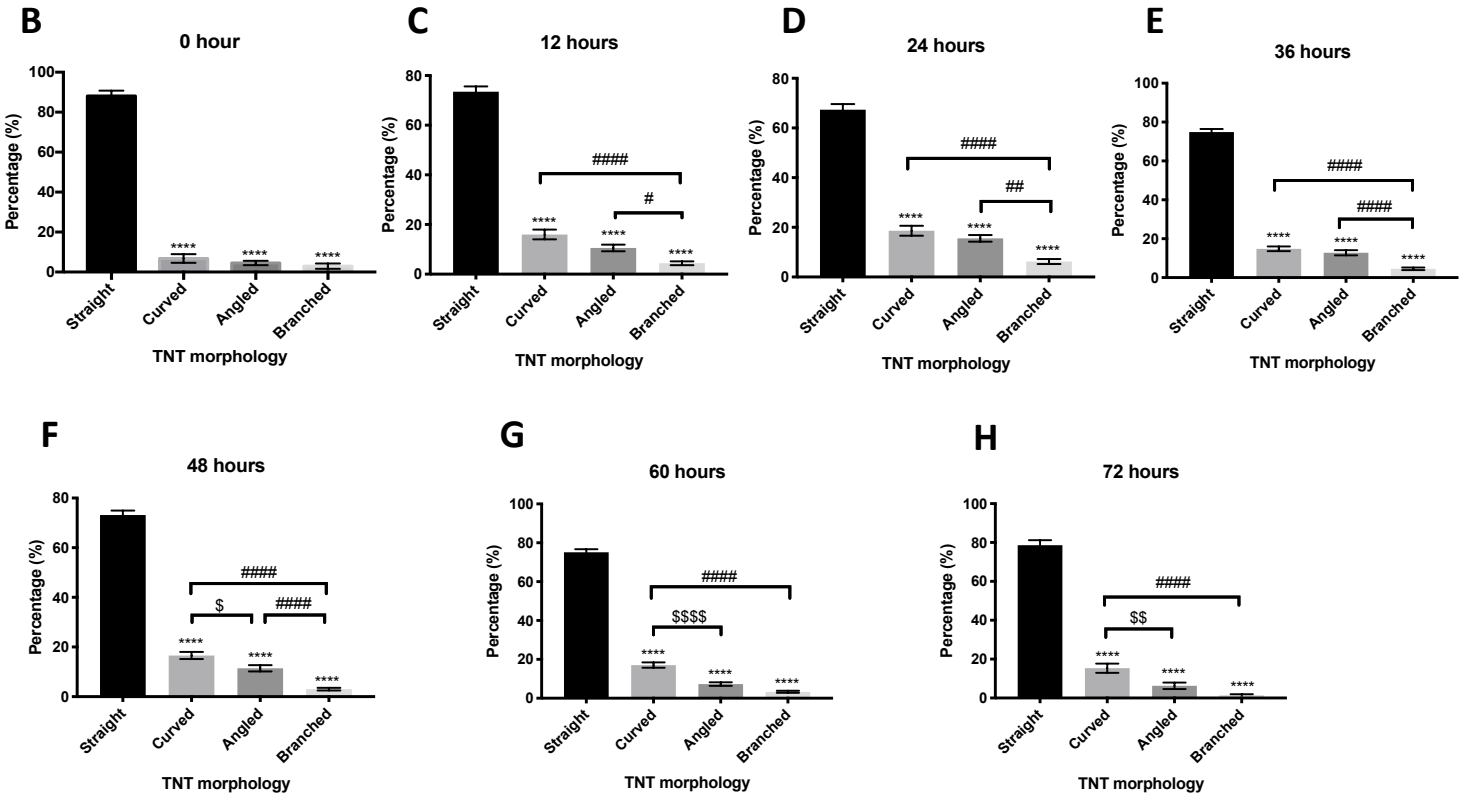


Figure 4.5: A: Representative white light images of the different morphologies (straight, curved, angled and branched) observed in HGF-treated A549 cells. White arrow represents the distinct feature of the respective morphologies. B-H: The histogram represents the mean percentage of each morphology (straight, curved, angled and branched) over the 72- hour time course. TNTs induced by HGF are mainly a straight morphology across all the timiepoints. Data expressed as mean percentage mean ± SEM, n=3. Statistical significance was determined by one-way ANOVA and Tukey's multiple comparison test. ****p<0.0001 when the straight morphology is compared to other morphologies, #p<0.05, *##p<0.01, ####p<0.0001* when the branched morphology is compared to other morphologies and $$p$<0.05, *$$p<0.01, $$$$p<0.0001* when the curved and angled morphology are compared. At least 500 cells were analysed for each condition.



Furthermore, previous studies investigating TNTs in A549 cells have only reported a maximum length of 105µm (Wang et al. 2012), whereas TNT lengths spanning several hundred microns were observed multiple times in the white light images in our study. Therefore, the length distribution of TNTs at the maximal concentration of HGF (100ng/ml) were categorised as a percentage accordingly to several ranges (<5µm, 5-20µm, 20-50µm, 50-100µm, 100-200µm, 200-300µm and >300µm) in order to identify any pattern in length formation over time (Fig4.6A-G). The pie charts (Fig4.6A-G) show the majority of TNT were between 5-20µm in length with the highest percentage found at a concentration at the 72nd hour (Fig4.6G). Between the 24th-48th timepoints (Fig4.6C-E), TNTs spanning >300µm in length constituted 0.1% of all TNTs. Additionally, the length of TNTs higher than 50µm increased in percentage after the 12th hour although by the 48th hour the length of TNTs higher than 100µm would decrease as the cells grew more confluent.

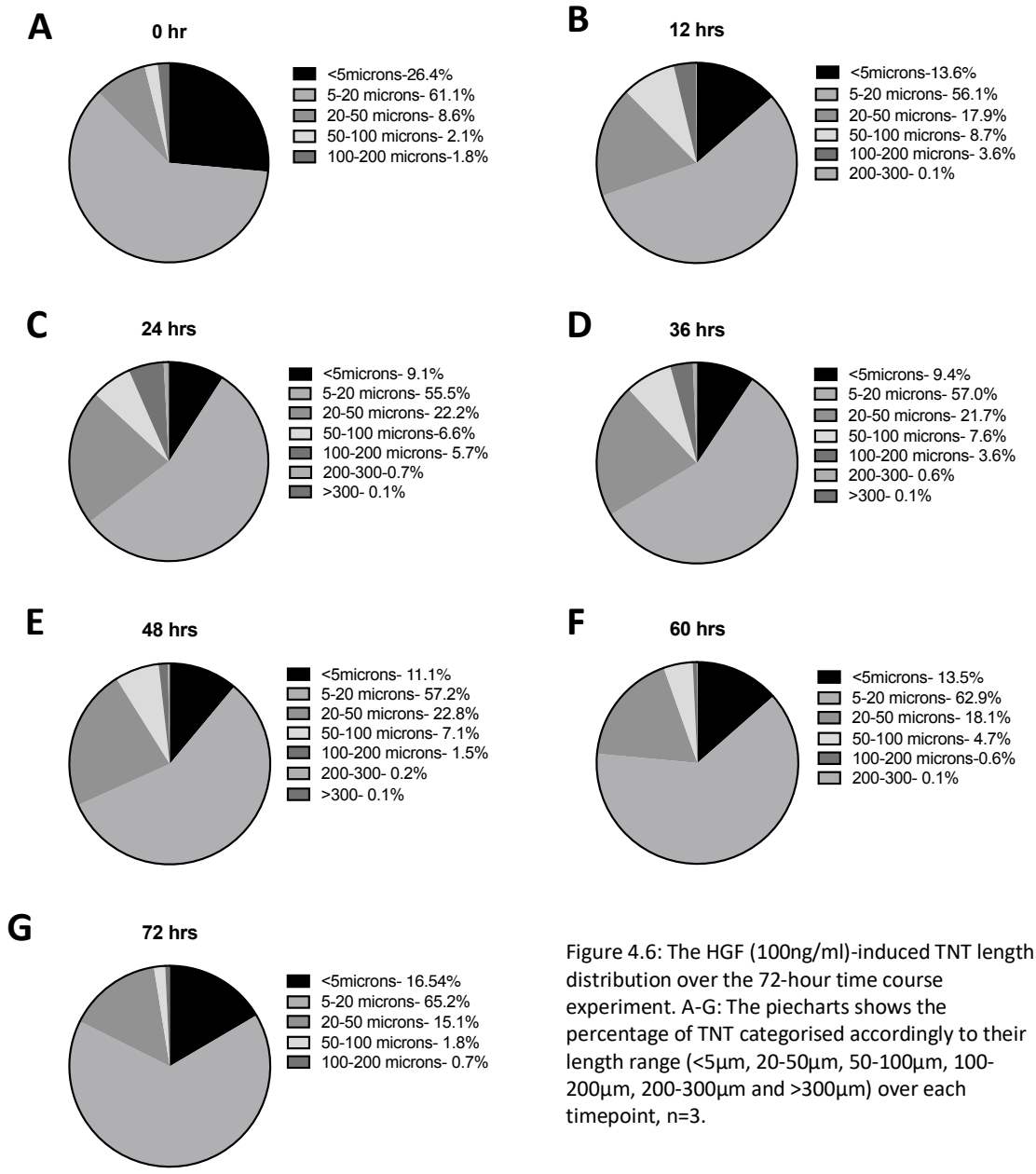


Figure 4.6: The HGF (100ng/ml)-induced TNT length distribution over the 72-hour time course experiment. A-G: The piecharts shows the percentage of TNT categorised accordingly to their length range (<5µm, 20-50µm, 50-100µm, 100-200µm, 200-300µm and >300µm) over each timepoint, n=3.

As TNTs are highly dynamic structures, phase contrast time-lapse microscopy was then used to better visualise the process of TNT formation. There are two main mechanisms by which TNTs can form: type 1 involves the initial actin-driven formation of a filopodia-like protrusion before extending in length to become a TNT and type 2 occurs when adherent neighbouring cells migrate apart forming TNTs in between (Gerdes, Rustom, and Wang 2013). To confirm whether HGF-induced TNT formation occurs *via* both mechanisms, a 24-hour time-lapse video was undertaken. The sequence of phase-contrast time-lapse images show the formation of HGF-induced TNTs occurring either through filopodia formation (Fig4.7A) or through the cell dislodgement mechanism (Fig4.7A,B).

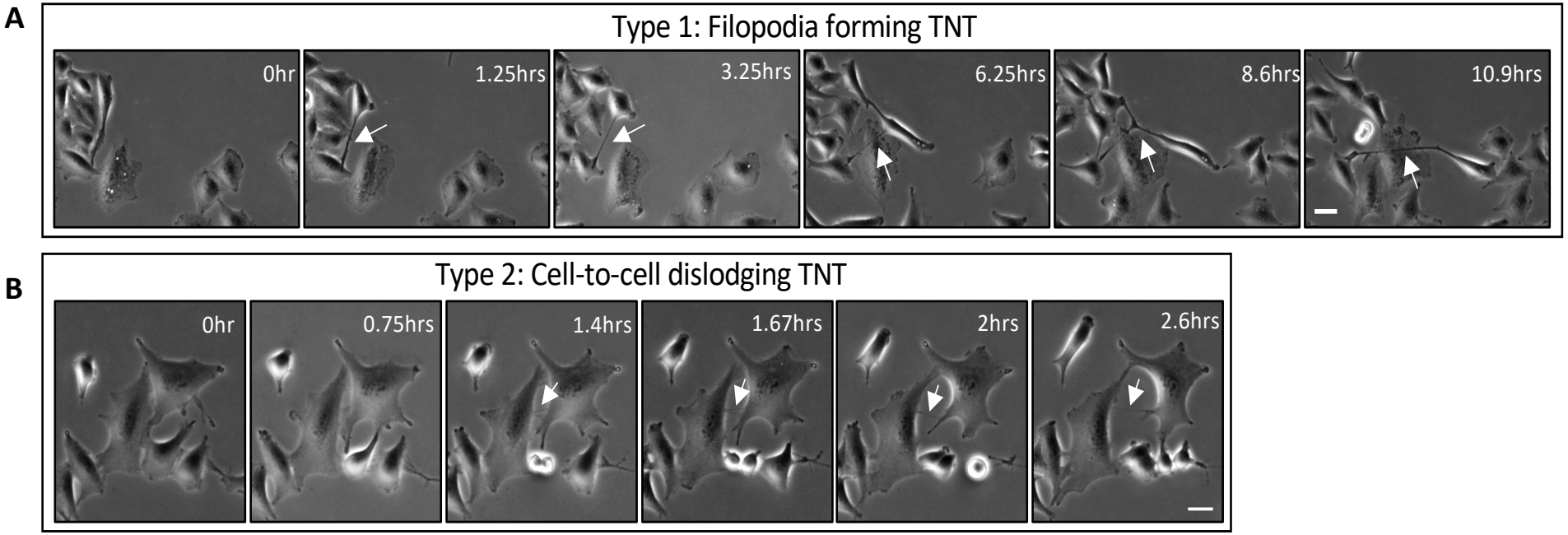


Figure 4.7: HGF induces type 1 and 2 TNTs in A549 cells. A549 cells were treated with HGF (100ng/ml) before being imaged on phase contrast time-lapse microscopy for 24 hrs. A: Representative white light images with the inidicated time points from a time-lapse movie showing the formation of a type 1 TNT (white arrow) through initial formation of a flipodia-like extension. B: Representative white light images with the inidicated time points from a time-lapse movie showing the formation of a type 2 TNT (white arrow) through initial migration of two adjacent cells before being connected with a TNT.

Moreover the thicker type 1 TNTs are known to contain both actin and microtubules whereas thinner TNTs are known to only contain actin. To investigate this further, the cytoskeletal composition of TNTs was determined using epifluorescent and confocal microscopy studies.

4.2.4 HGF-induced TNTs express characteristic markers

Although there are no specific markers for TNTs, assessment of their cytoskeletal composition and non-adherence remains the preferred method in confirming the presence of TNTs. To conduct immunofluorescent labelling of TNTs, A549 cells are seeded on glass coverslips before being fixed for epifluorescent/confocal microscope visualisation. Previous experiments utilised plastic surfaces which are ideal for long time-lapse microscopy or to capture white light images at specific time points. Culture surface has been shown to affect TNT formation due to their differences in adhesion and migratory properties (Dubois et al. 2020). To investigate the effect of culture surface on TNT formation, cells were seeded on either plastic or glass coverslips before being treated with HGF (100ng/ml) for 24hrs before undertaking white light analysis. There was a decrease in mean percentage (Fig4.8B) and number (Fig4.8C) of TNTs on glass compared to plastic in control cells. There was no difference in mean percentage (Fig4.8B), number (Fig4.8C) and length (Fig4.8D) of TNTs on glass compared to plastic in HGF-treated cells. The effect of HGF-induced TNTs are comparable on both plastic and glass therefore future experiments were conducted on glass coverslips for either white immunofluorescent microscopy studies.

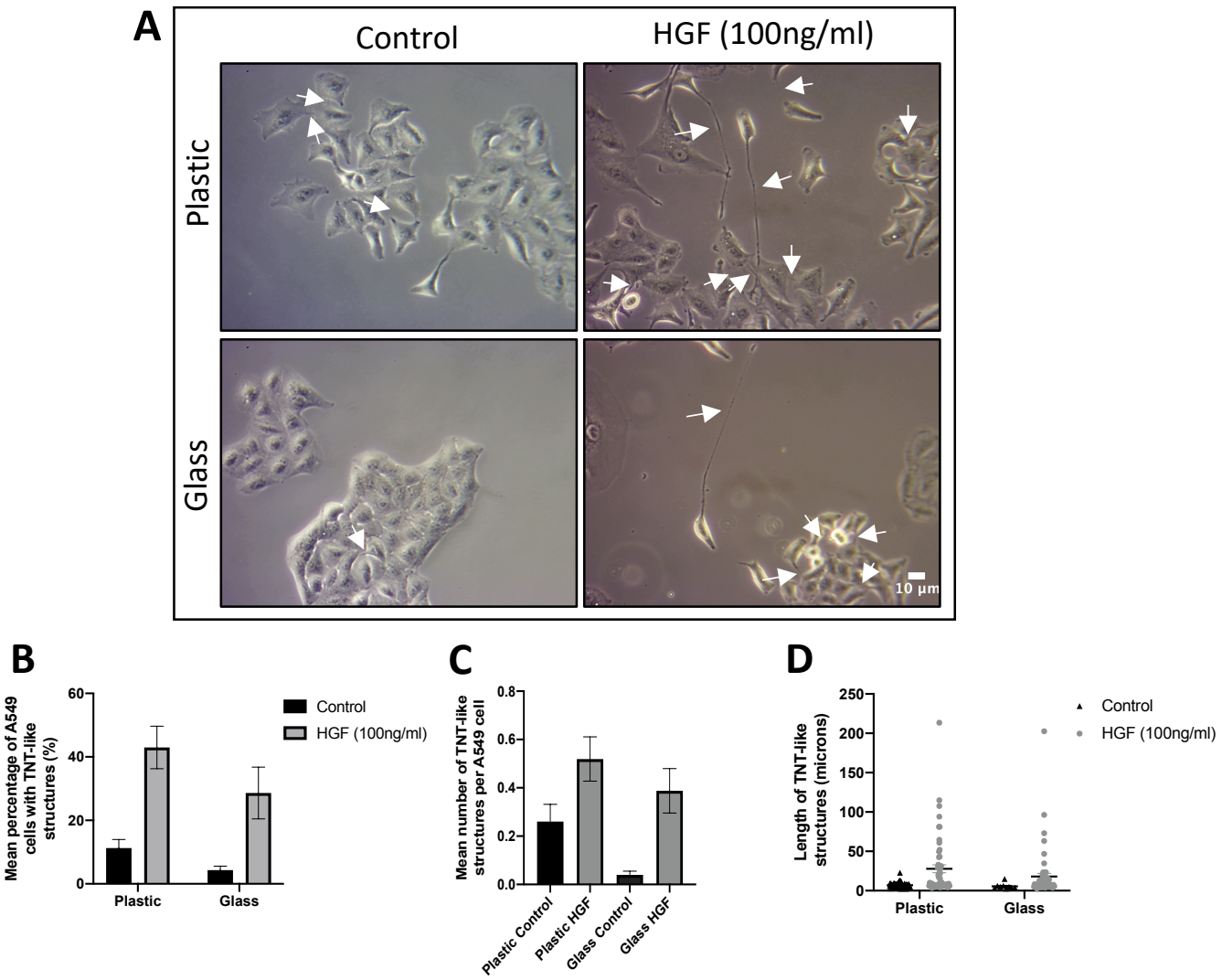
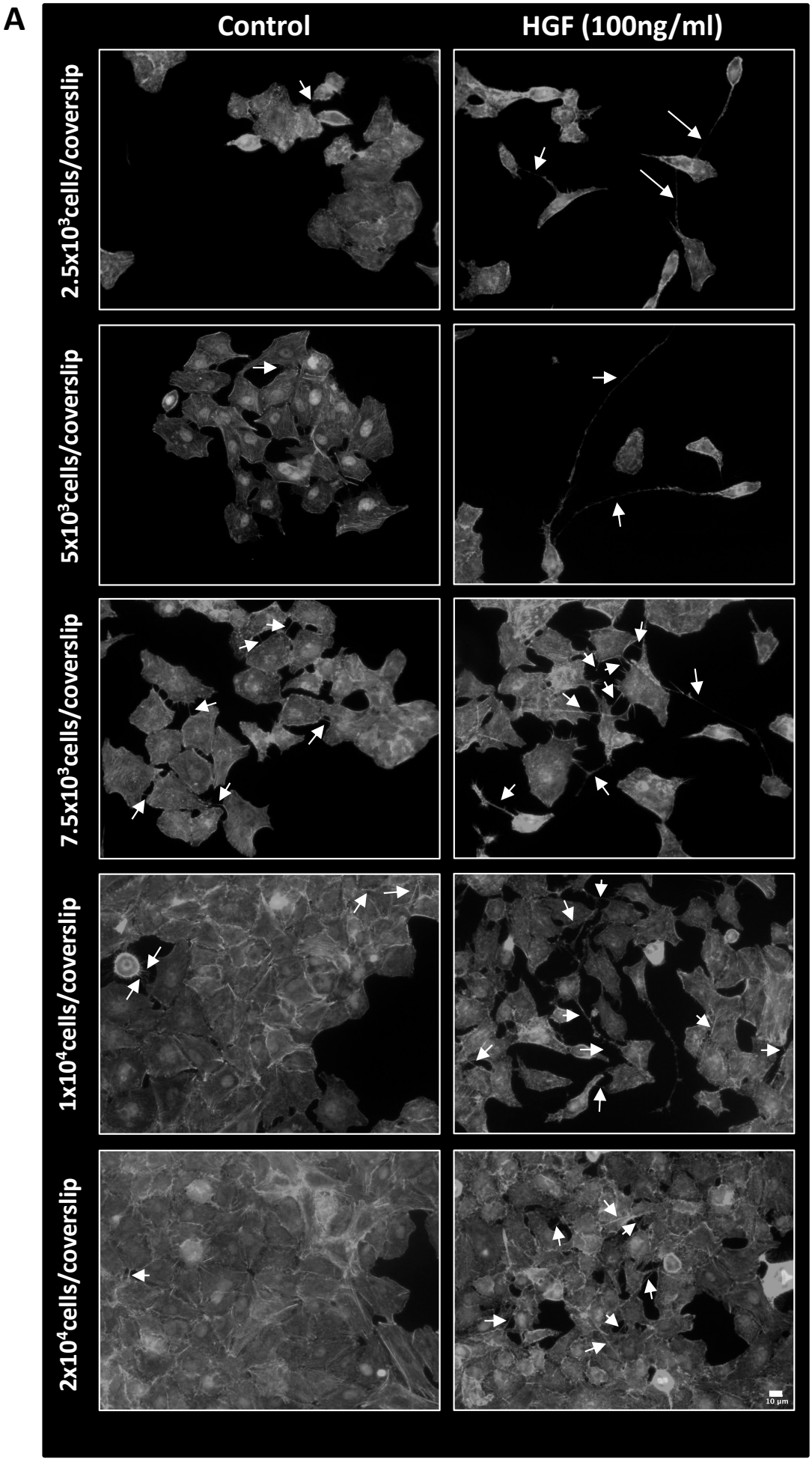


Figure 4.8: HGF induces an increase in TNT formation on glass and plastic culture surface. A: Representative white light images show an increase in TNTs (white arrow) in HGF treated cells in both plastic and glass coverslips compared to their respective controls. White light images were captured using 10x objective lens on an inverted microscope. Scale bar: 10µm. B-D: The white light images were quantified for TNT-like structures and the histogram (B,C) and scatter plot (D) displays the mean percentage (B), number of TNT-like structures per cell (C) and length of TNT-like structures (D). Values are expressed as mean ± SEM, n=1, with at least 100 cells analysed per condition.

TNTs are mainly comprised of F-actin (Rustom et al. 2004). Therefore, to identify the ideal seeding density to visualise F-actin labelled TNTs on glass coverslips, A549 cells were seeded at a range of seeding densities and quantified for image analysis. Immunofluorescent labelling with phalloidin confirmed the TNT-like structures contain F-actin throughout and an increase in F-actin labelled TNTs was observed in the 24hr-HGF-treated (100ng/ml) cells compared to control across the seeding densities (Fig4.9A). There was an increase in the mean percentage, number and length of TNTs for the HGF treated cells when seeded at 5000 cells/coverslip, 7500 cells/coverslip and 10 000 cells/coverslip compared to (Fig 4.9B-D). As the increase in TNT formation was similar across the three seeding densities, a seeding density of 7500 cells/coverslip was used for future experiments on glass coverslips.


A
Control
HGF (100ng/ml)
2.5x10³cells/coverslip
5x10³cells/coverslip
7.5x10³cells/coverslip
1x10⁴cells/coverslip
2x10⁴cells/coverslip
10 µm

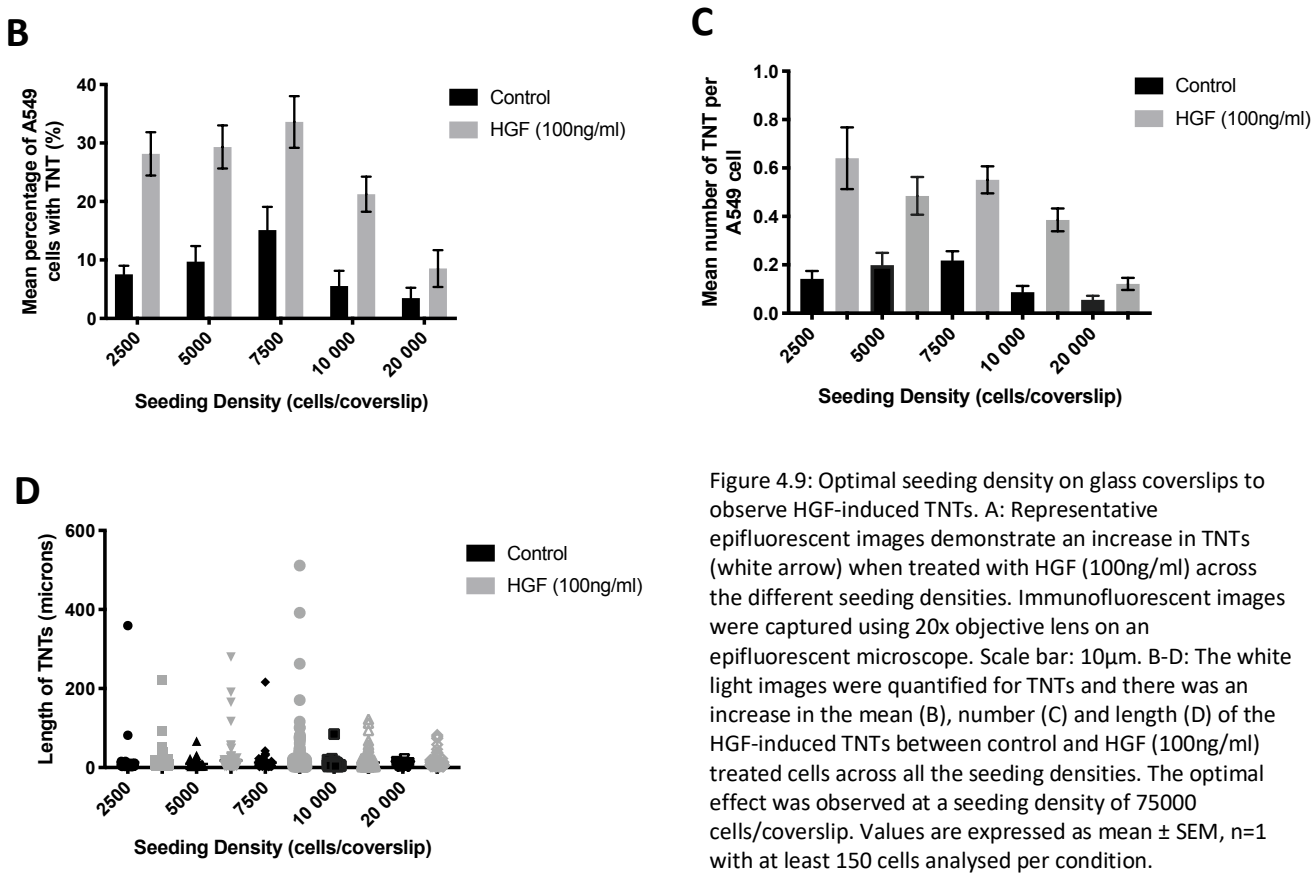


Figure 4.9: Optimal seeding density on glass coverslips to observe HGF-induced TNTs. A: Representative epifluorescent images demonstrate an increase in TNTs (white arrow) when treated with HGF (100ng/ml) across the different seeding densities. Immunofluorescent images were captured using 20x objective lens on an epifluorescent microscope. Scale bar: 10µm. B-D: The white light images were quantified for TNTs and there was an increase in the mean (B), number (C) and length (D) of the HGF-induced TNTs between control and HGF (100ng/ml) treated cells across all the seeding densities. The optimal effect was observed at a seeding density of 75000 cells/coverslip. Values are expressed as mean ± SEM, n=1 with at least 150 cells analysed per condition.

Once the optimal seeding density on glass coverslips was identified, we sought to determine whether the TNT-like structures observed on the white light images corresponded with the F-actin-labelled TNTs. Therefore, a HGF dose response was repeated and white light images were also taken in parallel on an epifluorescent microscope to determine whether the quantification of TNTs would coincide with the F-actin-labelled TNTs. There were more F-actin labelled TNTs (white arrows) present compared to the corresponding white light image (Fig4.10A). This could be attributed to poor visibility of the thinner TNTs due to the lower resolution of white light images taken on the epifluorescent microscope. Quantification of TNTs also showed a significant (n=3,p<0.05, **p<0.01,***p<0.001) increase in the mean percentage of TNTs at HGF concentrations of 10ng/ml, 100ng/ml and 300ng/ml between the F-actin labelled TNTs white light TNT (Fig4.10B). There was a significant (n=3, ****p<0.0001) increase in the mean number of TNTs per cell at HGF concentrations of 10ng/ml, 30ng/ml, 100ng/ml and 300ng/ml between the F-actin labelled TNTs white light TNT (Fig4.10C). There was also a significant (n=3,**p<0.01) increase in the mean length of TNTs at HGF concentrations of 30ng/ml and 100ng/ml between the F-actin labelled TNTs white light TNT (Fig4.10D).

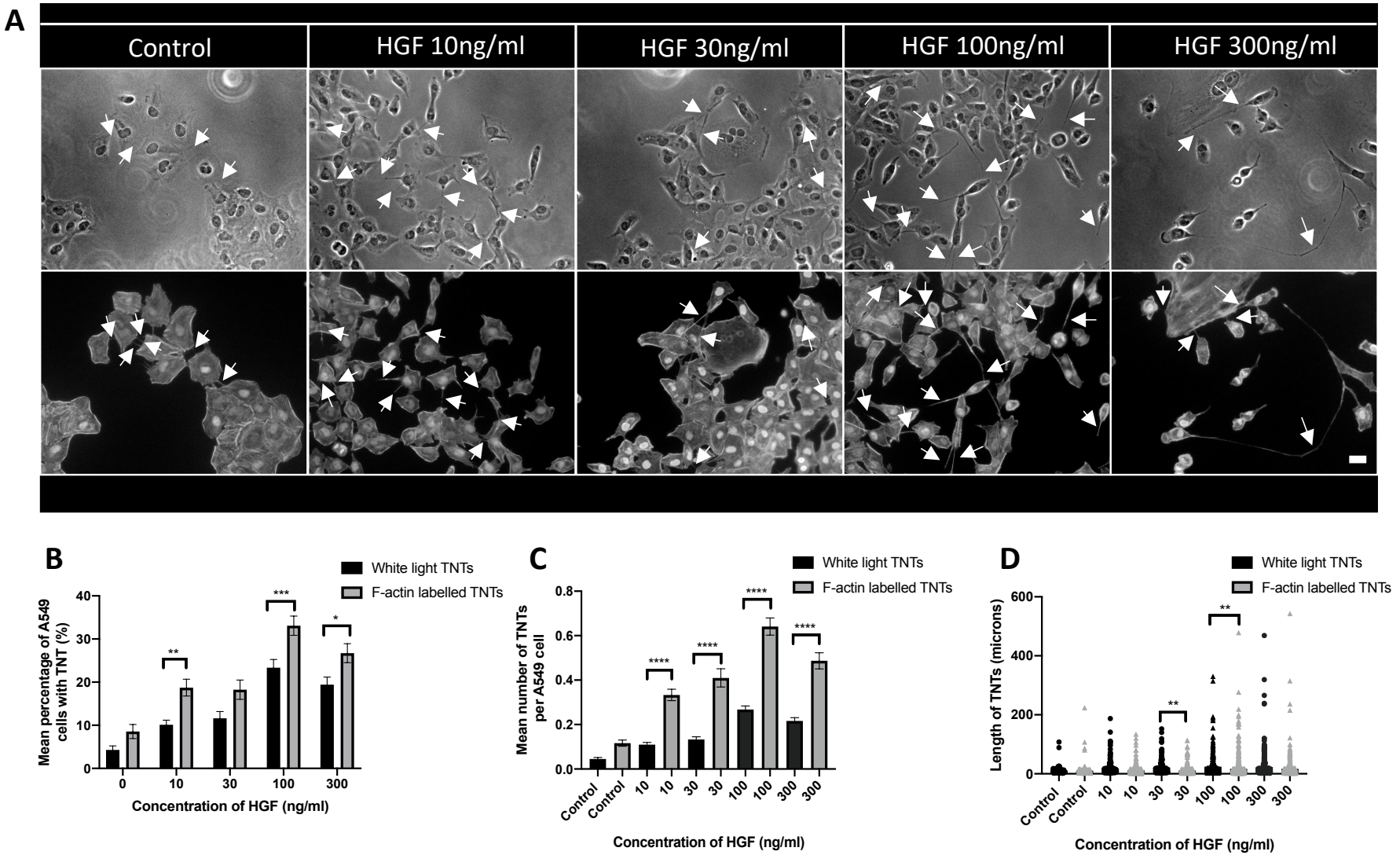


Figure 4.10: A: Representative images of the white light and the immunofluorescence labelling of F-actin (grey) of HGF-treated TNTs. A549 cells were treated with HGF (0-300ng/ml) for 24 hours before immunofluorescent labelling with F-actin. White light and immunofluorescent images were captured using 20x objective lens on an epifluorescent microscope The white arrow represents a TNT. Scale bar 10µm. B-D: The histogram shows the mean percentage (B), number of TNT per A549 cell (C) and a scatter plot of the lengths (D) of TNT image analyses. HGF induced a dose-dependent increase in TNT formation in both white light and F-actin-labelled images. There is a higher dose response across all the parameters in the F-actin labelled TNTs compared to the white light TNTs. Values are expressed as mean ± SEM, n=3 with at least 500 cells analysed per condition. Statistical significance was determined by two-way ANOVA and Bonferroni's multiple comparison test. *p<0.05, **p<0.01, ***p<0.001 and ****p<0.0001 in comparison between white light TNTs and F-actin labelled TNTs.

Aside from F-actin, TNTs in various cell lines, including A549 cells, contain microtubules in the thicker regions of TNTs (Rustom et al. 2004; Önfelt et al. 2006). M-sec, a cytosolic protein has also been implicated in the formation of TNTs in multiple cell lines (Hase et al. 2009; Kimura et al. 2016; Barzilai et al. 2016). Immunofluorescent labelling with phalloidin, α-tubulin and M-sec confirmed the TNT-like structures contain F-actin throughout (white arrow), as previously observed, with α-tubulin (green arrow) expressed at the thicker regions (Fig.4.11A) and M-sec (green arrow) appearing as punctate structures localising at the F-actin-driven protrusion sites of TNTs (Fig.4.11B). An important morphological characteristic of TNTs is a lack of adherence to the substratum of the tissue culture surface, which includes passing over adherent cells. Non-adherence of TNTs was assessed through z-stack acquisition; 3D reconstruction and orthogonal view ensured TNTs were non-adherent through passing over another cell or visible only on higher focal planes (Fig4.11C). The TNT-like structures observed are in accordance with the defined characteristics thus confirming their presence.

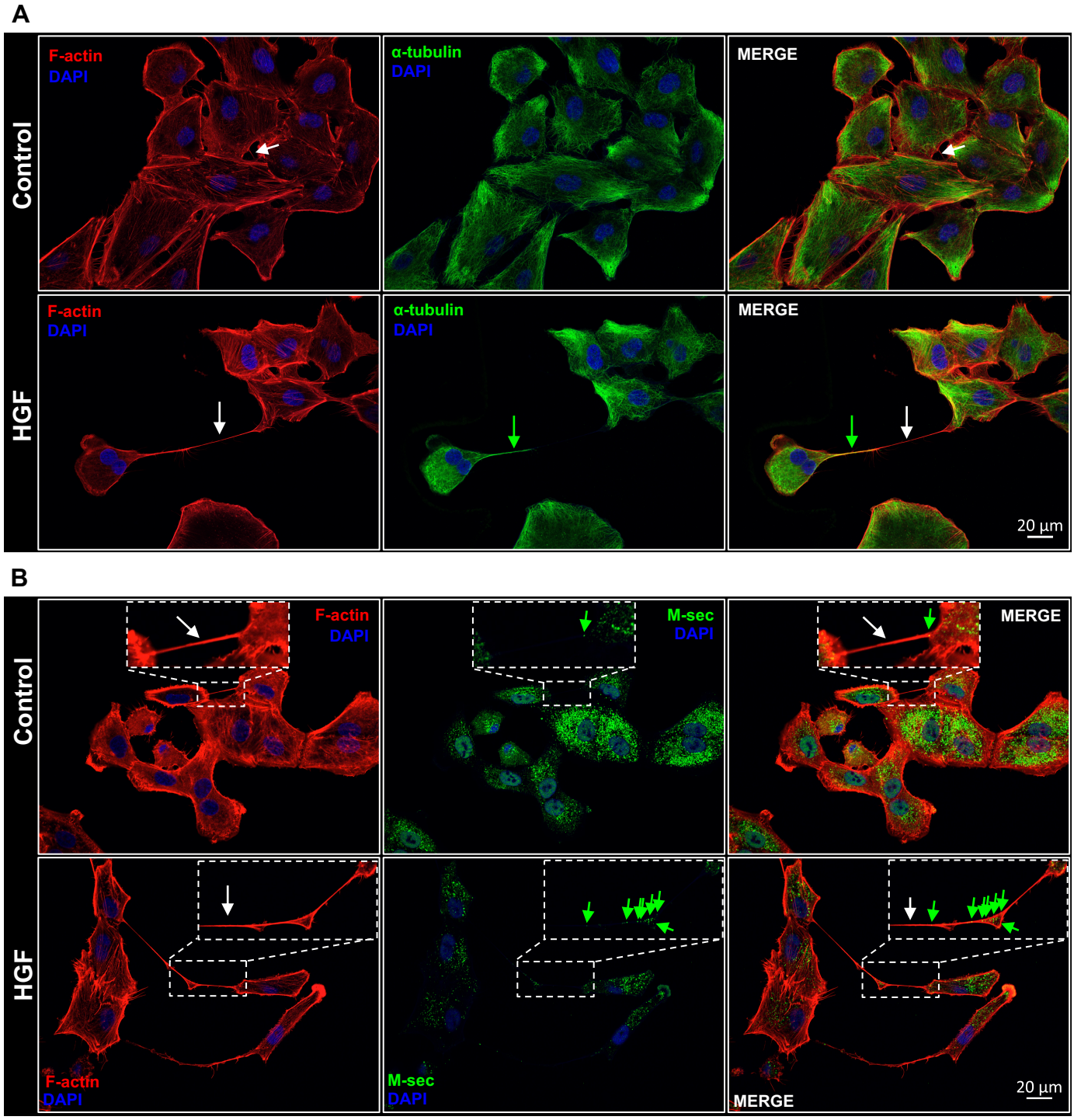


Figure 4.11: Characterisation of TNT-like structures using immunofluorescent labelling and confocal microscopy. Representative confocal images for control and 24h HGF-treated cells (100ng/ml) labelled with (A) F-actin (red) and α-tubulin (green) and (B) F-actin (red) and M-sec (green). M-sec (green arrow) is expressed along F-actin labelled TNTs. White arrows denote TNT structures and the dotted area denotes a zoomed area. (C) Three-dimensional reconstruction F-actin positive non-adherent TNT. The three-dimensional reconstruction was acquired using the ZEN lite software from 49 sections of Z-stacked images (with Z step of 0.27µm). The maximum xz projection images demonstrates two TNTs hovering above the surface of the substratum. Scale bar, 20µm. Confocal images are representative of n=3 independent experiments.

4.2.4 β1-integrin, c-Met and paxillin are novel components of TNTs in A549 cells

HGF signals through its receptor, c-Met, and crosstalk with β1-integrin to facilitate anchorage-independent cell survival, invasion and resistance in NSCLC (Barrow-McGee, Kishi, et al. 2016b). Therefore, to confirm the presence of β1-integrin in TNTs, immunofluorescent labelling of known markers, F-actin (white arrow) and M-sec (pink arrow), was undertaken alongside β1-integrin (green arrow). In both control and HGF-treated cells, β1-integrin localised along the entire length of the F-actin and M-sec positive TNT (Fig4.12A). Furthermore, to assess the non-adherence of the β1-integrin, F-actin and M-sec positive TNTs, z-stack acquisition was obtained to visualise an aerial and XZ orthogonal view of the TNT (Fig4.12B). The xz orthogonal view shows F-actin, M-sec and β1-integrin positive TNT non-adherent to the substratum thus further confirming β1-integrin as a novel component of TNTs.

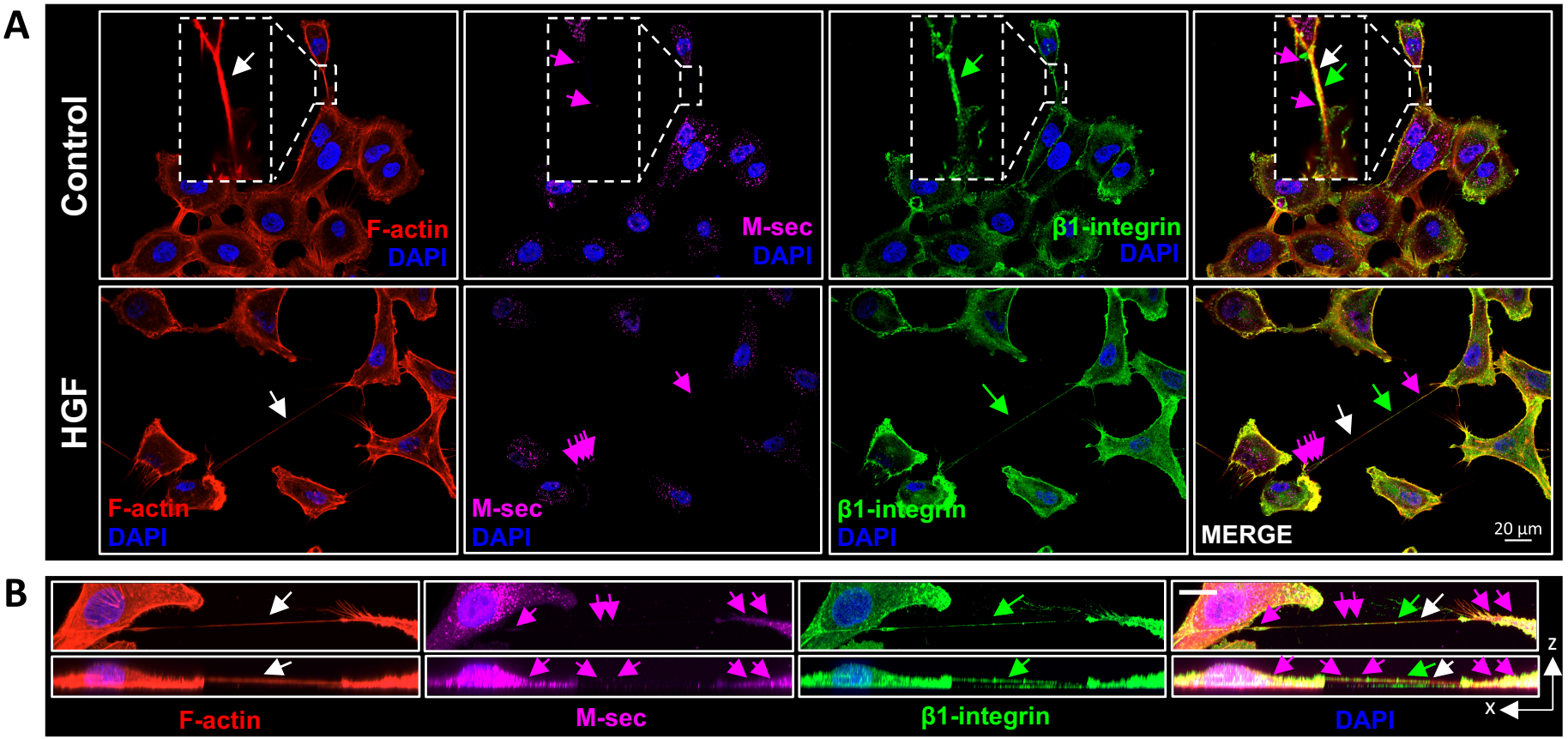


Figure 4.12: β1-integrin is a novel component in TNTs. A: Representative confocal images for immunofluorescent labelled TNTs with F-actin (white arrow), M-sec (pink arrow) and β1-integrin (green arrow) in control and HGF treated A549 cells. β1-integrin localise along the F-actin and M-sec positive TNT (white arrow). B: An example of a non-adherent TNT expressing F-actin (white arrow), M-sec (pink arrow) and β1-integrin (green arrow). The aerial and orthogonal xz projection image was obtained using ZEN lite software from 39 sections of Z-stacked images (with Z step of 0.27µm). The maximum xz projection image below demonstrates a TNT hovering above the surface of the substratum. Scale bar, 20µm. Confocal images are representative of n=3 independent experiments.

Since β1-integrins are an integral component in TNTs, the next step was to determine whether co-localisation would occur between HGF/c-Met and β1-integrin TNTs. To investigate this, immunofluorescence labelling was undertaken with the c-Met receptor and β1-integrin in control and HGF-treated cells. Cytosolic Internalisation of the c-Met receptor was observed in the HGF-treated cells (pink arrow) whilst in control c-Met staining was observed at the cell membrane of adjacent cells (Fig4.13A). C-Met staining (red arrow) largely concentrated at the protrusion site of the HGF-induced TNTs (Fig4.13A). C-Met (red arrow) also co-localised with β1-integrin (green arrow) at these protrusion sites of TNTs in control and HGF-treated cells (yellow arrow). β1-integrin is expressed throughout the entire length of TNTs whilst c-Met is expressed at the thicker portion of the TNT length (Fig4.13A). To assess the non-adherence of the c-Met and β1-integrin labelled TNTs, z-stack acquisition was obtained to visualise an aerial and XZ orthogonal view of the TNT (Fig4.13B). The xz orthogonal view shows a c-Met and β1-integrin positive TNT non-adherent to the substratum, which confirms the presence of a TNT.

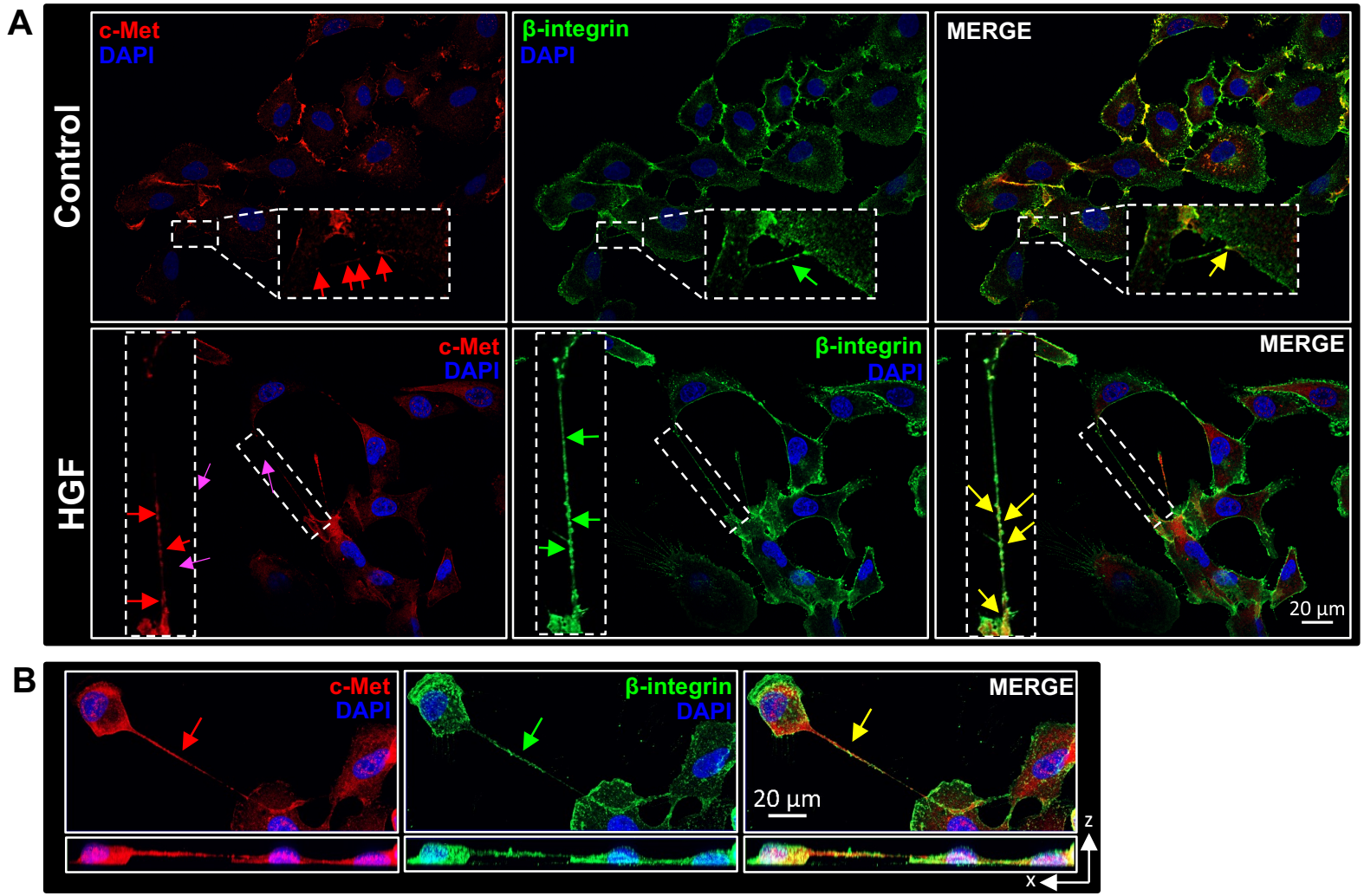


Figure 4.13: C-Met, β1-integrin localise at the protrusion site and along the length of TNTs. A: Representative confocal images for immunofluorescent labelled TNTs with c-Met (red arrow) and β1-integrin (green arrow) in control and HGF treated A549 cells. HGF treatment induced c-Met internalization (pink arrow). C-Met and β1-integrin co-localise along the TNTs (yellow arrow). Boxed region denotes a zoomed area. B: An example of a non-adherent TNT expressing c-Met (red arrow) and β1-integrin (green arrow). The aerial and xz orthogonal view was obtained using the ZEN lite software from 39 sections of Z-stacked images (with Z step of 0.27µm). The maximum xz projection image below demonstrates the TNT hovering above the surface of the substratum. Scale bar, 20µm. Confocal images are representative of n=3 independent experiments.

Furthermore, HGF/c-Met and β1-integrin activation also increases the tyrosine phosphorylation and thus the association of paxillin *via* FAK, acting as a point in downstream convergence between HGF and β1-integrin signalling (Liu et al. 2002; Crowe and Ohannessian 2004; Schaller et al. 1995). Therefore, paxillin expression was assessed through immunofluorescent labelled TNTs. Paxillin (green arrow) staining appeared as punctate structures at the protrusion site of F-actin positive TNTs in control and HGF-treated cells (Fig4.14A). Non-adherence was also demonstrated through xz orthogonal view of paxillin expressing TNTs (Fig4.14B).

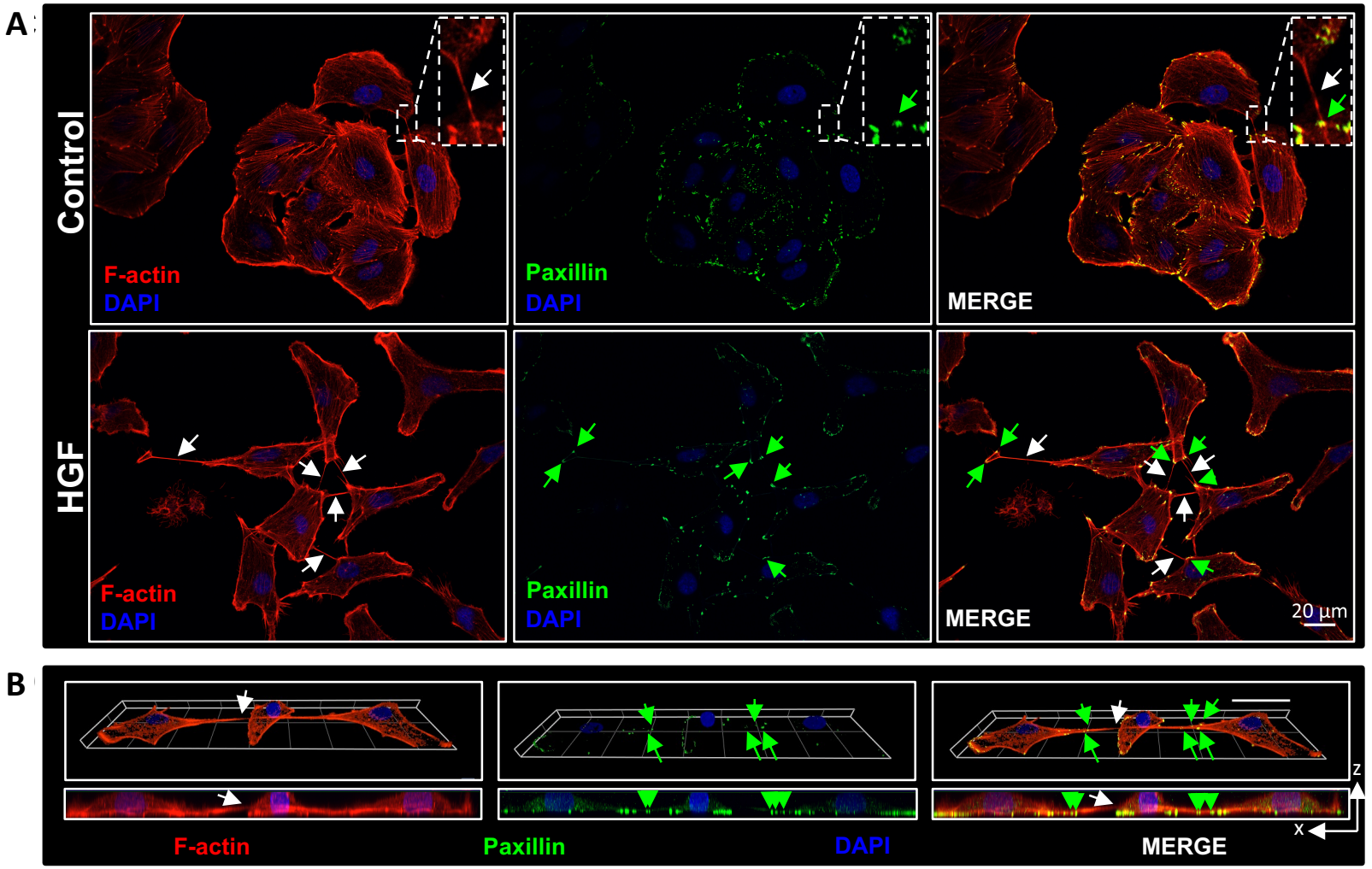


Figure 4.14: Paxillin localises at the protrusion sites of TNTs. A: Representative confocal images for immunofluorescent labelled TNTs with paxillin (green arrow) and F-actin (white arrow) in control and HGF treated A549 cells. Paxillin is expressed at the protrusion site of the TNT (green arrow). White arrow denote a TNT structure and a boxed region denotes a zoomed area. (D) An example of a non-adherent F-actin labelled TNT (white arrow) with paxillin (green arrow) expressed at the protrusion site at both ends of the TNT. The three-dimensional reconstruction was acquired using the ZEN lite software from 39 sections of Z-stacked images (with Z step of 0.27µm). The maximum xz projection image below demonstrates the TNT hovering above the surface of the substratum. Scale bar, 20µm. Confocal images are representative of n=3 independent experiments.

4.2.5 HGF-induced TNTs transport mitochondria and vesicles

TNTs are unique structures known to transport large organelles, such as mitochondria, and vesicles (Rustom et al. 2004; Lou, Fujisawa, Morozov, et al. 2012). Live-cell confocal microscopy was used to investigate whether HGF-induced TNTs were able to transport mitochondria or vesicles between TNT connected cells. The time-lapse white light images showed two vesicles (white arrows) transferred along a TNT, from a donor cell into the acceptor cell (Fig4.15A). To visualise mitochondria transfer, A549 cells were treated with HGF and loaded with a red mitochondrial cytopainter before live-cell confocal imaging was undertaken. The sequence of time-lapse images demonstrates mitochondria (white arrow) transferred along TNT connected cells (Fig4.15B). Furthermore, cells were loaded with either the red mitochondrial cytopainter or DiO lipophilic vesicle dye, before seeding together the two different labelled cell populations and treated with HGF. Fig4.15C shows two DiO labelled vesicles (white arrows) moving along a TNT towards a mitochondria-labelled cell above, furthermore the cell below contains both DiO and mitochondria suggesting prior mitochondria transfer occurred along the TNT. This suggests a bidirectional exchange of cellular components between TNT connected cells.

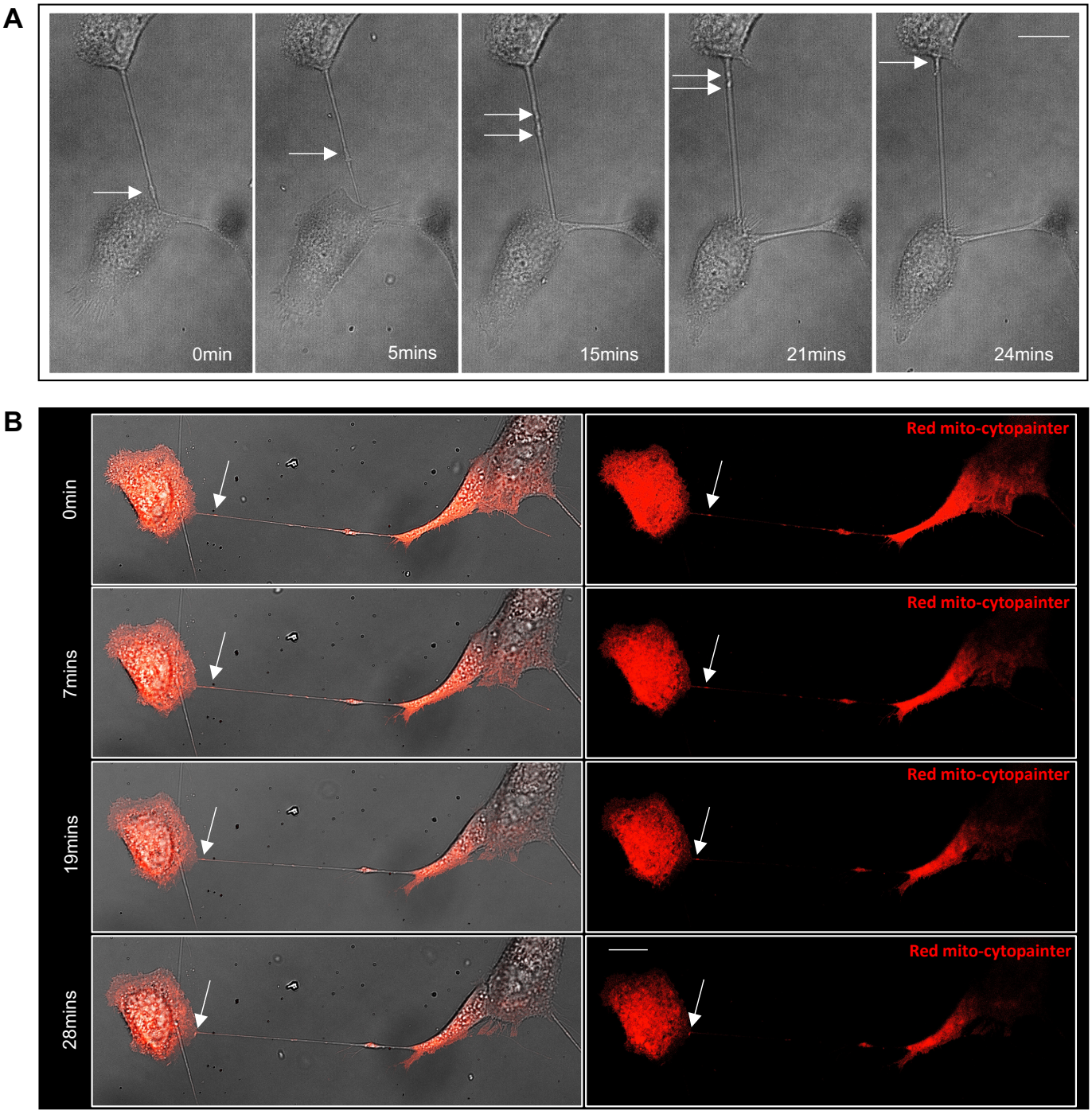


Figure 4.15: TNTs in A549 cells functionally transmit mitochondria and vesicles. (A) Representative white light images with the indicated time points from a time-lapse movie showing two vesicles (indicated by the white arrows) travelling along a TNT to the cell above. (B) Representative overexposed fluorescent images with the indicated time points from a time-lapse movie showing mitochondria transfer along a TNT. A549 cells were loaded with red mitochondrial cytopainter and treated with HGF (100ng/ml) for 24 hours before being imaged on live confocal microscopy. Unidirectional mitochondria transfer along the TNT was observed (indicated by the white arrow). (C) Representative merged light and fluorescence image of two DiO labelled vesicles (indicated by the green arrows) travelling along a TNT towards a red mitochondria-stained cell. Separate populations of A549 cells were loaded with either DiO or red mitochondrial cytopainter and seeded together before HGF treatment and undertaking confocal imaging as above. Bi-directional transfer is suggested through the presence of mitochondria in the DiO labelled cell below. Scale bar, 20µm.

4.3 Discussion

This work highlights a novel role for HGF inducing TNT formation A549 cells. HGF stimulation was shown to increase TNT formation in a time and dose-dependent manner, with a maximal effect observed at the 24th hour timepoint at 100ng/ml HGF concentration. HGF induced non-adherent TNTs which express characteristic F-actin, α-tubulin and M-sec. Furthermore, immunofluorescent studies revealed novel components of TNTs, which include the c-Met receptor, β1-integrin and paxillin. HGF-induced TNTs are also functional and can transmit mitochondria and vesicles in a bidirectional manner. These data suggest the importance of HGF in modulating cellular communication *via* TNTs within the TME of NSCLC.

4.3.4 HGF induces TNT formation in A549 cells

Our study showed HGF induces TNTs in A549 cells in a time and concentration-dependent manner. TNTs have been observed previously in A549 cells (Wang et al. 2021; Dubois et al. 2018; Kumar et al. 2017; Wang et al. 2012). However, A549 TNT formation has not been investigated within the context of overexpressed exdogenous factors in the tumour microenvironment. TNTs have been widely studied within the context of stress with emphasis on the effect of low serum, high glucose, confluency and hypoxia on TNT formation (Lou, Fujisawa, Morozov, et al. 2012; Dubois et al. 2020; Wang et al. 2011). TNTs in A549 cells have also been shown to form spontaneously after initial seeding in culture (Dubois et al. 2018). To eliminate this factor in influencing the TNTs quantified, A549 cells were left to form colonies for 3 days before treatment with HGF. A low seeding density (5000 cells/well) was identified for optimal TNT image analysis however a similar increase in mean percentage, number and length of TNTs was also observed across all the seeding densities. This contrasts with findings which suggest TNT formation decrease with increasing confluency due to the limited range of distance between cells (Benard et al. 2015; Dubois et al. 2020). Despite the higher confluency, numerous HGF-induced TNTs were still observed passing over neighbouring colonies of cells, therefore this suggests TNT formation was not limited by the cell density in our study.

An increase in HGF-induced TNTs was also observed when treated with 2% FBS-supplemented media compared to 10% FBS-supplemented media. Serum deprivation is commonly used to induce stress and consequentially TNT formation in various cell lines including in A549 cells (Lou, Fujisawa, Morozov, et al. 2012; Cole, Dahl, and Cowden Dahl 2021; Dubois et al. 2018). However, there was no difference between the basal levels of TNT formation between 2% and 10% FBS supplemented media which suggests the increase in HGF-induced TNT response was not due to an exacerbation of stress. FBS contains EGF, amongst other growth factors, and matrix components which have been

shown to induce TNTs (Cole, Dahl, and Cowden Dahl 2021; Carter et al. 2019; Franchi et al. 2020). There may be a lower effect of HGF-induced TNTs at the higher concentration of FBS due to an increase in receptor convergence with EGF or the matrix components which would cause internalisation and deregulation of the c-Met receptor. This further supports the role of HGF in inducing TNTs.

To further confirm a dose-dependent relationship between HGF and TNT formation, an extensive time course experiment was undertaken which showed HGF inducing TNTs in a time and concentration-dependent manner exhibiting a dome-shaped curve. The optimal time point was identified at 24 hours, the same time point was also used in another study to characterise the effect of EGF on TNT formation in ovarian cancer cells (Cole, Dahl, and Cowden Dahl 2021). C-Met internalisation *via* clarithrin-mediated endocytosis (Kermorgant and Parker 2005) occurs rapidly post HGF stimulation, occurring within 30 minutes (Barrow-McGee, Kishi, et al. 2016b) followed by sustained activation of ERKs which phosphorylates focal adhesion targets such as paxillin to induce associated pathways (Liu et al. 2002). This could explain the maximal plateau reached between the 12^{th} and 24^{th}-hour time point in HGF-induced TNT formation. Furthermore, a decrease in TNT formation after the 24^{th} hour time as saturation of the receptor occurs and lysosomal degradation of the internalised receptor leads to receptor desensitisation (Sorkin and Von Zastrow 2009). The maximal effect may be sustained through repeated treatments of HGF as the confluency does not limit the HGF-induced TNT formation, being able to pass over neighbouring cells. The log dose-response curve also shows a maximal effect at 100ng/ml for the mean percentage, number and length of TNTs. There was a four-fold increase in mean percentage of HGF-induced TNTs at 100ng/ml compared to control. The basal mean percentage of TNTs in control A549 cells was found similarly between 5-10% in other studies (Kumar et al. 2017; Wang et al. 2021). In comparison, EGF treatment (20nM) similarly for 24 hours only induced <10% increase in TNTs in ovarian cancer cell lines (Cole, Dahl, and Cowden Dahl 2021). Furthermore, HGF induced TNTs of up to several hundred microns in length (200-400µm) whereas the maximum TNT length observed in A549 cells was reported at 131µm (Wang et al. 2021). This demonstrates the extent which TNTs can reach distant cells to transport cellular cargo required for survival and invasion within the deregulated and dense TME.

TNTs in A549 cells have been reported to exist in different morphologies including straight, curved, branched and angled morphology (Kumar et al. 2017). The same types of morphologies identified by Kumar et al were also observed in the HGF-induced TNTs in our study (Kumar et al. 2017). Straight TNTs constituted the majority of HGF-induced TNTs across all the time points. Similarly, straight TNTs were often observed in PC12 cell and HBEC-3 cells (Dubois et al. 2020), although the branched morphology was also observed in culture. Interestingly TNTs in neuronal cells only exhibit a straight

morphology (Sartori-Rupp et al. 2019). This further highlights the spectrum of morphological properties of TNTs between the different cell lines and their unique molecular mechanism of formation. The cytoskeletal architecture of straight TNTs has been uncovered by Sartori-Rupp et al through correlative cryo-electron microscopy (cryo-EM) studies of neuronal cells. TNTs have the potential to comprise of a bundle of intertwined thin individual TNTs (termed iTNTs) in neuronal cells (Sartori-Rupp et al. 2019). A similar structure of TNTs was also observed in stromal cells (Kolba et al. 2019). However, serial sectioning transmission electron microscopy (ssTEM) of Jurkat T cells shows TNTs only existing as single structures (Sowinski et al. 2008). Furthermore, scanning electron microscopy (SEM) analysis of TNTs in HBEC-3 cells shows the existence of single branched TNT structures (Dubois et al. 2020). Interestingly SEM imaging of TNTs in mesothelioma cells also reveal that long TNTs may be formed through continuations of several individual TNTs or through multiple insertion points along the cell membrane (Lou, Fujisawa, Morozov, et al. 2012; Lou et al. 2018). Overall these findings emphasise the heterogeneity in the morphological characteristics of TNTs in different cell lines. To further unravel the cytoskeletal architecture of straight and branched TNTs in A549 cells, electron microscopy (EM)-based approaches would be required. This would allow insight into the organisation of its cytoskeletal makeup.

TNTs are also dynamic structures, which adds another layer of complexity to their rapidly modifying cytoskeletal status over time. The two main types TNTs (type 1: filopodia forming TNT and type 2: cell-to-cell dislodging TNT) were observed in our study (fig4.7). Type 1 TNTs are thicker in width, ranging between 100-650nm, and can span up to 300µm whilst type 2 TNTs are thinner, ranging between 60-200nm, and are shorter in length with a maximum length of 20µm (Dubois et al. 2020). In our study type 1 TNTs were observed connecting to distant isolated cells whilst type 2 TNTs mainly formed between adjacent cells, which has been previously described (Dubois et al. 2018; Dubois et al. 2020). Furthermore, type 1 TNTs are known to contain both actin and microtubules whereas type 2 TNTs only contain actin therefore immunofluorescent studies were undertaken to fully characterise the cytoskeletal composition of TNTs.

4.3.5 HGF-induced TNTs express characteristic marker

Before undertaking immunofluorescent visualisation of the cytoskeletal elements of TNTs, the effect of TNT formation on glass was taken into account due to the differences in adhesive and migratory properties between different culture surfaces. There was a decrease in control levels of TNTs on glass compared to plastic, this has also been previously observed when PC12 cells were cultures on plastic and glass surfaces (Dubois et al. 2020). However, the HGF-induced effect on TNT formation was comparable between plastic and glass, although further experimental repeats would be

required to determine the significance. Another vital aspect of both glass and plastic culture surfaces are their rigid biophysical nature, being approximately 100 000 kPa in stiffness (Caliari and Burdick 2016). Whereas in the normal lung parenchyma, the elastic modulus occurs between 0.5-5kPa whilst in the lung tumour a stiffer environment is observed between 20-30 kPa (Pankova et al. 2016; Booth et al. 2012). This is in contrast to the stiffness of plastic/glass cultures and could therefore alter the mechanical cues in TNT formation. Studies have shown substrate stiffness influences cell growth and migration in lung cancer cells (Miyazawa et al. 2018; Shukla et al. 2016). To better recapitulate the biomechanical cues within the TME, cells could be cultured on hydrogels at the specified stiffness of healthy or cancer lung tissue and thus provide novel insight into the effect of stiffness on TNT formation.

Fluorescent epifluorescent microscopy visualisation of TNTs in A549 cells reveals positive expression of F-actin throughout the entirety of the TNT length. Furthermore, F-actin labelled TNT quantification showed a significantly higher dome-shaped response in TNT formation compared to the TNTs quantified on white light. These results could be due to the lower resolution of the white light images taken on the epifluorescence microscope compared to the white light images taken on a different inverted microscope. Therefore, the thinner TNTs were not visible for analysis which caused a lower percentage and number of TNT counts. However, the F-actin labelled TNTs still corresponded to the TNT structures observed on white light, which confirmed previous white light image analyses of TNT quantification.

Confocal microscopy visualisation also revealed the presence of microtubules on the thicker regions of TNTs. This aligns with the type 1 and 2 TNTs characteristics and in the cytoskeletal composition of TNTs reported other studies with A549 cells (Dubois et al. 2018; Kumar et al. 2017; Panasiuk et al. 2018). Moreover, other macrophages (Önfelt et al. 2006; Dupont et al. 2020), urothelial cells (Resnik et al. 2018; Veranič et al. 2008), B cells (Osteikoetxea-Molnár et al. 2016), PC12 cells (Wang and Gerdes 2015), astrocytes and cardiac myoblasts (Austefjord, Gerdes, and Wang 2014) have TNTs which contain microtubules. TNTs which contain microtubules have been shown to sustain longer in culture due to the resistance of a more rigid cytoskeletal backbone (Dupont et al. 2020). Moreover, the presence of microtubules also indicates a mode for mitochondria transfer. As mitochondria transfer occurs *via* the Rho-GTPase, Miro1, which binds mitochondria with KIF5 motor proteins to facilitate movement along the microtubules (Ahmad et al. 2014). However, several EM studies reveal mitochondria transfer occurring in the absence of microtubules suggesting an actin-mediated mode for mitochondria transfer *via* other actin-driven motor proteins (Wang et al. 2021; Sartori-Rupp et al. 2019).

M-sec expression was also found at the protrusion site and localising along the length of the TNT, which eludes to the involvement of exocyst-mediated TNT formation. M-sec is a cytosolic protein with association to the Sec6 component of the exocyst complex. It is also as a known marker of TNT formation whereby it interacts with the RalA small GTPase which activates the exocyst complex *via* LST1 to initiate exocyst-mediated actin polymerisation and membrane supplementation (Hase et al. 2009; Schiller et al. 2013). LST1 can also localise RalA GTPase thereby recruiting filamin to the plasma membrane to induce actin-crosslinking for TNT formation (Schiller et al. 2013). As M-sec is only involved in actin remodeling, microtubule-containing TNTs may form independently of M-sec or in conjunction with other unknown associated proteins. There may be a cooperation between M-sec mediated TNT formation and HGF signalling, as RalA GTPase is generated from RAS which is downstream of the MAPK pathway (Padavano et al. 2015). This proposed mechanism may be dependent on HGF-induced TNT formation.

Three-dimensional reconstruction of F-actin labelled TNTs also shows non-adherence to the culture surface. This is another distinguishing characteristic of TNTs *in vitro* (Rustom et al. 2004). However, this criteria poses a challenge in 3D models such as tumouroids/organoids (Zhang et al. 2018; Pulze et al. 2020; Whitehead et al. 2020; Sáenz-de-Santa-María et al. 2017), ex vivo explants (Chinnery, Pearlman, and McMenamin 2008) and resected tissues (Lou, Fujisawa, Morozov, et al. 2012). Although 3D cultures are a better representation of cell-to-cell interaction with the matrix, TNTs have only been identified in the periphery of the cultured tumouroid (Sáenz-de-Santa-María et al. 2017; Pulze et al. 2020) whereas possible TNTs in the core are more difficult to identify due to the dense environment. Therefore, only the transfer of organelles can confirm the presence of TNTs in 3D models. Further studies to identify TNTs in 3D A549 tumouroids will be explored in chapter 8.

4.3.6 TNTs express novel components c-Met, β1-integrin and paxillin

Our study presents a previously undiscovered role for c-Met, β1-integrin and paxillin in TNT formation. M-sec was also found present in the F-actin and β1-integrin positive TNTs which further confirms β1-integrin as a novel component of TNTs. Although M-sec and F-actin positive TNTs were not investigated with c-Met labelled TNTs, due to incompatible fixation protocols, c-Met labelled TNTs were positively expressed with the β1-integrin labelled TNTs. The xz orthogonal view also showed c-Met and β1-integrin labelled TNTs to be non-adherent to the substratum, which is characteristic of TNTs. Future live-cell imaging studies of cells transfected with c-Met/β1-integrin conjugated with GFP would provide insight into receptor trafficking during TNT formation. The role of upstream regulators involved in TNT formation is not well defined. The direct role of integrins in TNT formation has only been reported in one study whereby $\alpha 5\beta 1$ integrin was required to induce

TNTs in mature B cells (Osteikoetxea-Molnár et al. 2016). Breast cancer cells cultured on fibronectin and collagen I showed an increase in TNT formation (Franchi et al. 2020). FAK is also recruited to upregulate MMP-2 production for TNT formation in SCC cells. However, the role of integrins was only postulated due to the regulation of actin dynamics involved between integrins and focal adhesion sites (Sáenz-de-Santa-María et al. 2017). Another study showed an increase in acute myeloid leukaemia cell adhesion to fibronectin *via* β1-integrin was also a suggested mechanism in TNT formation (Omsland et al. 2020). Interestingly both studies demonstrated a decrease in migration was associated with TNT formation which highlights the changes in cellular adhesion or ECM remodeling as the driving force behind the cytoskeletal reorganisation required for TNT formation (Sáenz-de-Santa-María et al. 2017; Omsland et al. 2020). It would be of interest for future studies to visualise whether TNTs also express β1-integrin and c-Met *in vivo.* Resected human lung adenocarcinoma tissue can be used to identify whether the presence of TNTs is correlated with c-Met or β1-integrin overexpression. However, obtaining samples of lung tissue whilst identifying TNTs *in vivo* poses its own technical difficulties. Alternatively, HGF-treated A549 cells can be implanted to an immunocompromised mouse and tumour growth can be observed before being surgically resected, fixed and labelled for TNT identification with mitotracker, as previously done by Lou and his colleagues (Lou, Fujisawa, Morozov, et al. 2012). A comparison can then be made with implanted tumours of non-treated A549 cells to observe whether there was an increase in tumour growth and mitochondria labelled TNTs, demonstrating its tumourigenic function *in vivo*.

Moreover, our study also demonstrates the presence of paxillin in TNTs. Paxillin which acts as a scaffold protein, is recruited during the activation of both c-Met and β1-integrin clustering. The presence of paxillin at the protrusion sites of TNTs further links the role of altered adhesion dynamics in mediating TNT formation. Furthermore, paxillin consequentially activates the PI3K, MAPK and Arp2/3 complex pathways through activation of FAK (Crowe and Ohannessian 2004; Ishibe et al. 2003; Lai et al. 2000). Therefore, the signalling pathways associated with HGF/c-Met/ β1-integrin-induced TNT formation will be investigated in the next chapter.

4.3.7 HGF-induced TNTs transfer mitochondria and vesicles

Live cell imaging of HGF-induced TNTs shows a bidirectional exchange of mitochondria and vesicles, which may derive from early endosomes, the endoplasmic reticulum, Golgi apparatus and lysosomes (Wang et al. 2011; Smith, Shuai, and Parker 2011). The ability to transport large organelles is a unique and determining feature of TNTs. Several studies have alluded to TNT-mediated mitochondria transfer as part of a survival mechanism (Wang and Gerdes 2015; Caicedo et al. 2015; Lin et al. 2019). A549 cells are able to transfer healthy mitochondria to other cells suffering drug-

induced mitochondrial loss, therefore, restoring aerobic metabolism and delaying apoptosis (Spees et al. 2006). Similarly, when PC12 cells were exposed to UV radiation, TNT-mediated mitochondria transfer from healthy cells also rescued cells from undergoing apoptosis (Wang and Gerdes 2015). Rustom also proposed mitochondrial transfer correlating with an increase in reactive oxidative species (ROS) levels which allows mitochondria to either rescue cells from apoptosis or to clear the excess ROS (Rustom 2016). Interestingly, within the context of our study, cells are not subjected to stress conditions but live-cell imaging of HGF-treated cells demonstrates widespread mitochondrial exchange occurring in nearby and distant cells. Another possibility proposed by Pinto et al suggests that mitochondria or miRNA exchange in cancer facilitates the transformation towards an aggressive phenotype (Pinto, Brou, and Zurzolo 2020). To support this theory, breast cancer cells have shown a malignant phenotypic transformation after establishing TNT connections with macrophages (Hanna et al. 2019). Although this study does not specifically identify mitochondria transport in mediating the effect or eliminating the possibility of miRNA transfer, breast cancer cells have been shown to increase migration and proliferation after mitochondria uptake from mesenchymal cells (Caicedo et al. 2015). TNT transfer of mitochondria was also linked to an increase in invasion in bladder cancer cells. Furthermore, when implanted in nude mice, the tumours developed a larger vascularisation network and were overall larger in size (Lu et al. 2017). This may be a mechanism by which HGF induces invasion and metastasis within the TME although it is still unclear how mitochondria can facilitate this phenotypic transformation. The phenotypic changes may be attributed to mutations in mtDNA which has been previously shown to alter cell behaviour through retrograde mitochondria-to-nucleus signalling, leading to poor prognosis (Guaragnella, Giannattasio, and Moro 2014). Interestingly, mtDNA can increase ROS levels which consequentially can activate associated MAPK, PI3K and HIF-1α pathways (Pelicano et al. 2006). TNTs are also implicated in chemoresistance therefore HGF-induced TNTs may also play a role in drug redistribution. In pancreatic cancer cells, TNT-mediated doxorubicin transfer from chemo-resistant to chemo-sensitive cells occurs causing the selection towards the resistant cell population (Desir et al. 2018). However, it is also unclear whether this process occurs actively or passively in the co-cultured cells. P-glycoprotein can also be transferred via TNTs in breast cancer cells, further highlighting their role in promoting chemoresistance (Pasquier et al. 2012).

4.3.8 Future work

The identification of TNTs relies on morphological and cytoskeletal characterisation however, only partial aspects of the criteria are checked within the different experiments. The non-adherence criteria is not possible to assess in white light image analysis and when using an epifluorescence microscope. However confocal microscopy studies were used to visualise to confirm the non-

adherence of the TNT-like structures, thus this limited the potential discrepancies in TNT identification in white light and epifluorescent analysis. Furthermore, in immunofluorescent studies, organelle transfer is not simultaneously identified alongside the characteristic/novel markers of TNTs.

Our study has identified M-sec localising in HGF-induced TNTs which demonstrates a potential role in the exocyst-mediated TNT formation. To confirm the HGF/c-Met-RalA GTPase-M-sec activation loop is occurring, a RalA GTPase inhibitor can be used to observe whether there is a decrease in HGF-induced TNTs. Although c-Met and β1-integrin co-localise in TNTs in this study, their crosstalk activation in TNT formation will be explored in the next chapter using inhibitors for c-Met, β1-integrin and associated pathways. The downstream pathways involved in TNT formation are not well defined in NSCLC, therefore the next chapter will investigate the pathways associated in inducing the HGF-mediated TNT formation in A549 cells.

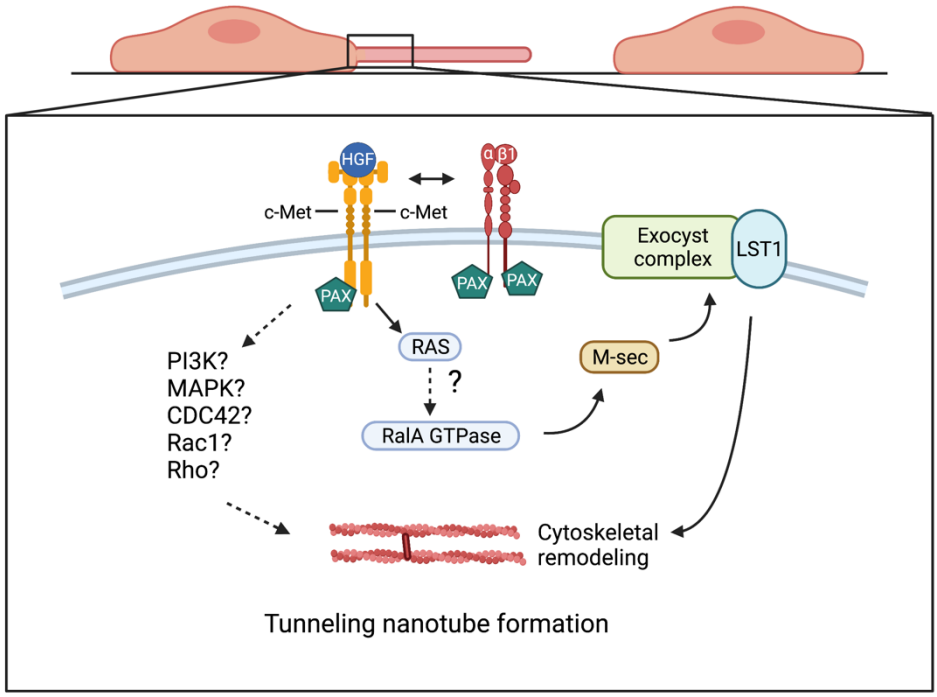


Figure 4.16 Diagram depicting the potential signalling mechanisms involved in the HGF-induced TNT formation in A549 cells. C-Met, β1-integrin and paxillin are expressed during TNT formation upon HGF stimulation. The characteristic TNT marker M-sec is also expressed during HGF-induced TNT formation. This suggests a potential activation of the M-sec/exocyst complex due to the RalA GTPase generated from HGF/c-Met activation. Other pathways associated with HGF/c-Met/β1-integrin signalling axis (i.e. PI3K, MAPK, CDC42, Rac1, Rho pathways) may also play a part in TNT formation.

4.4 Conclusions

This chapter has identified novel expression of c-Met, β1-integrin and paxillin in TNTs. Morphological and cytoskeletal characterisation show HGF-induced TNTs express characteristic markers F-actin, α-tubulin and M-sec. HGF-induced TNTs are also able to undergo vesicle and mitochondria transport.

Although this chapter revealed c-Met, β1-integrin and paxillin are present in TNTs, the next step is to confirm whether there is crosstalk activation between HGF/c-Met and β1-integrin during TNT formation of A549 cells. The next chapter will investigate the potential role of HGF/c-Met/β1-integrin co-activation and downstream pathways involved in TNT formation.

5. Chapter 5: HGF/c-Met/β1-integrin signalling-axis induces TNT formation *via* the MAPK, PI3K and Arp2/3 complex pathways

5.1 Introduction

Since the discovery of TNTs by Gerdes and his colleagues (Rustom et al. 2004), numerous studies emerged highlighting its key role in cancer cell communication, promoting malignant transformation, metabolic adaptation and chemoresistance (as reviewed by (Pinto, Brou, and Zurzolo 2020)). However, despite its important role in cancer, the molecular mechanisms are still not well defined in the literature. Moreover, the molecular mechanisms underlying TNT formation have been widely studied within the context of stress-induced factors (Kretschmer et al. 2019; Wang et al. 2011; Hanna, McCoy-Simandle, et al. 2017; Rustom 2016). Actin-driven proteins including myosin, RalA GTPase, filamin, M-Sec, LST1 and CDC42, have been shown to coordinate with the exocyst complex to form TNTs in stress-induced HeLa cells (Hase et al. 2009; Schiller et al. 2013). Other Rho GTPases have also been implicated in TNT formation, in RAW/LR5 macrophages the Arp2/3 complex is activated during TNT formation (Hanna, McCoy-Simandle, et al. 2017). Arp2/3 complex binds to both WASP and WAVE2, which are downstream to CDC42 and Rac1 activation respectively, to induce actin nucleation of F-actin filaments (Takenawa and Suetsugu 2007). Both CDC42 and Rac1 Rho GTPases have been implicated in TNT formation in RAW/LR5 macrophage cells (Hanna, McCoy-Simandle, et al. 2017).

Lou and his colleagues also reported the role of EMT factors in inducing TNT formation in mesothelioma cells (Lou, Fujisawa, Morozov, et al. 2012). Despite this, minimal studies have focused on the molecular mechanism underlying the formation of TNTs through upregulated factors in the TME. Therefore, our novel findings from the previous chapter implicating HGF/c-Met and β1-integrin co-localisation during TNT formation highlight the crucial role of the deregulated signalling cues within the TME in regulating TNT formation. Amongst the various mutationally upregulated EMT-inducing cytokines present in the TME, only EGF and its receptor signalling have been identified to induce TNTs. In ovarian cancer cells, EGF induces TNTs *via* the MAPK pathway (Cole, Dahl, and Cowden Dahl 2021). Furthermore, in stress-induced rat astrocytes, p53 is activated causing an upregulation of EGFR, this then activates the PI3K/Akt/mTOR pathway and leads to overexpression of M-Sec. The same study also showed the p38 MAPK pathway activated to induce TNTs *via* actin polymerisation (Wang et al. 2011). However, these molecular mechanisms are also cell-line specific, as EGF-induced TNTs in ovarian cancer cells do not form *via* the PI3K pathway (Cole, Dahl, and Cowden Dahl 2021). Moreover, inhibiting the Arp2/3 complex increased the number of TNTs in neuronal (CAD) cells, further supporting the exclusive nature of TNT formation between different

cell types. There are minimal studies looking into the molecular mechanisms involved in NSCLC TNT formation. In one study, the RASSF1 (Ras association domain family member 1) tumour suppressor gene induces TNT formation *via* two proposed mechanisms: either through a Rho and LIM kinase (LIMK)-mediated loss of actomyosin network or an increase in vimentin expression by an EMT marker (Dubois et al. 2018), although it is uncertain how vimentin can regulate TNT formation. Although this study has highlighted a novel gene regulatory mechanisms involved in TNT formation, no studies have investigated the role of upregulated growth factors in TNT formation and the signalling pathways involved in NSCLC have not been defined.

Gaining a comprehensive understanding of TNT formation is important in identifying potential specific markers of TNT. This serves clinical relevance in specific drug targeting of TNTs to inhibit tumour growth and prevent chemoresistance in NSCLC. Therefore, this chapter aims to determine the signalling pathways associated with the HGF-mediated TNT formation in A549 cells through pharmacological inhibition of pathways and siRNA transfection knockdown. This chapter confirms HGF/c-Met and β1-integrin crosstalk to recruit paxillin to activate the PI3K, MAPK and Arp2/3 complex downstream pathways. However, we also report that the HGF-induced TNTs are not mediated downstream of the CDC42, Rac and Rho pathways.

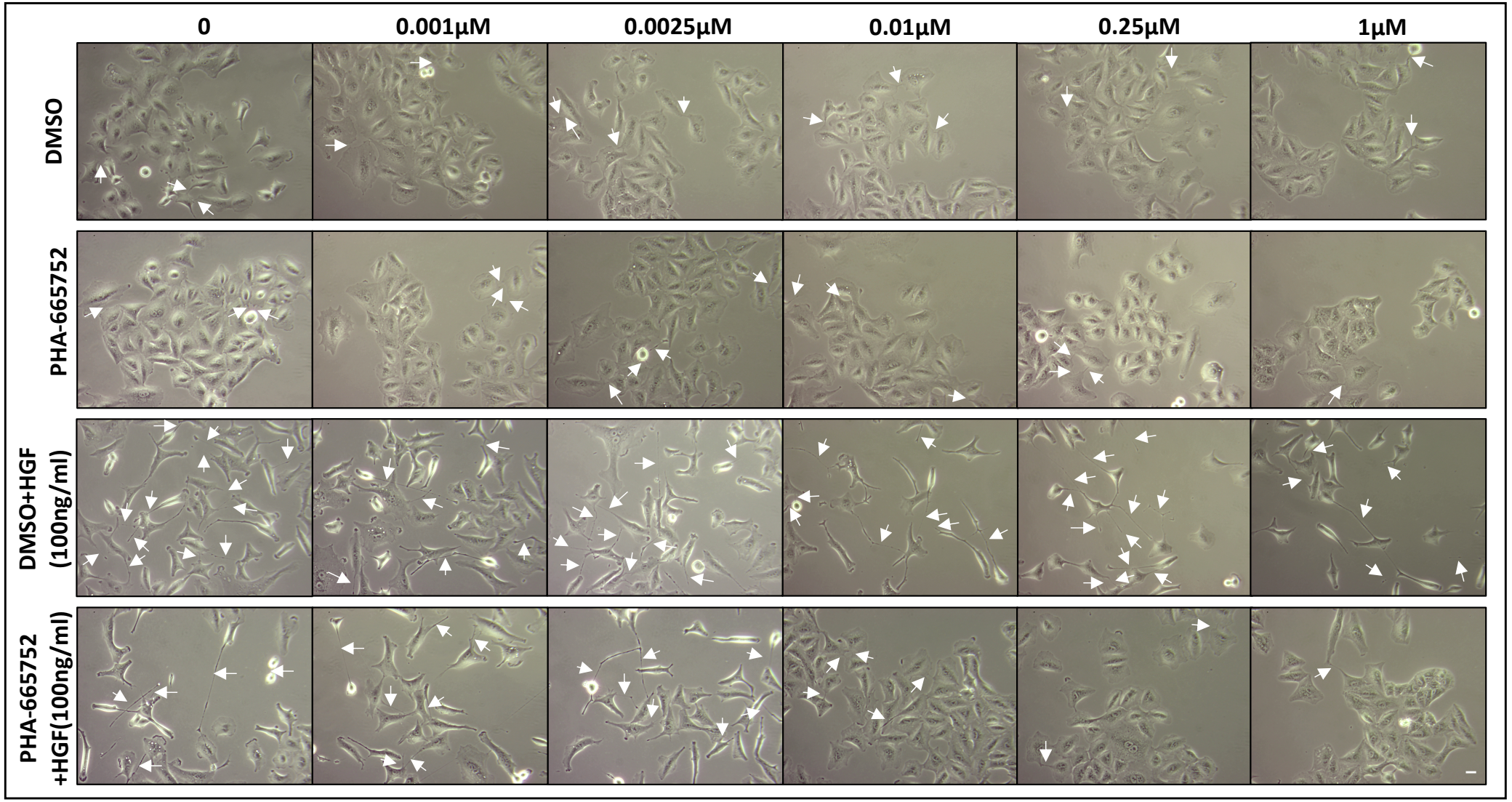
5.2 Results

5.2.1 C-Met receptor regulates TNT formation in A549 cells

To confirm that HGF binding to the c-Met receptor causes TNT formation in A549 cells, a c-Met receptor inhibitor (PHA-665752≤1µM) was used. The cells were pre-treated for 30mins with the c-Met inhibitor (PHA-665752≤1µM) alongside its DMSO vehicle control and either treated further with HGF (100ng/ml) or in the absence of HGF for 24 hours. To ensure that the vehicle control, DMSO, did not affect the HGF-induced or basal TNT formation, cells were also pre-treated with the same volume of DMSO used for the c-Met inhibitor concentrations alongside control. The white light images showed cells with an epithelial cell morphology and minimal TNTs (white arrow) present when treated with increasing concentrations of DMSO (0-1µM) and the c-Met inhibitor (PHA-665752;0-1µM) alone (Fig5.1A). The HGF-treated A549 cells showed an elongated morphology with multiple TNTs (white arrow) observed across all the concentrations of DMSO (0-1µM)(Fig5.1A). There were also multiple TNTs (white arrow)in the HGF-treated A549 cells in the presence of the c-Met inhibitor at lower concentrations (PHA-665752;0-1µM)(Fig5.1A). However, at higher concentrations of the c-Met inhibitor (PHA-665752;0.01µM, 0.25µM and 1µM), the cells reverted to an epithelial cell morphology with minimal presence of TNTs (white arrow), as similarly observed in control DMSO and PHA-665752 conditions (Fig5.1A). Quantification of the white light images showed DMSO treatment alone had no significant effect on TNT formation when compared control. A dose-dependent decrease in HGF-induced TNTs in the presence of the c-Met inhibitor across the three parameters (n=3,****p<0.001)(Fig5.1B-D). The c-Met inhibitor, PHA-665752, significantly decreased the mean percentage (Fig5.1B), mean number (Fig5.1C) and length (Fig5.1D) of the HGF-induced TNTs at 0.01µM before plateauing to basal control levels between 0.25µM and 1µM. The log concentration-response curve for PHA-665752+HGF treated cells showed an IC_{50} of 0.01µM in mean percentage (Fig5.1B) and mean number of TNT per cell (fig5.1C) whereas an IC_{50} of 0.006µM was found for the mean length (Fig5.1D).

Furthermore, c-Met inhibitor treatment alone at lower concentrations (0.001µM-0.25µM) had no significant effect in the mean percentage (Fig5.1B), number (Fig5.1C) and length (Fig5.1D) of TNTs. However, at the highest concentration of PHA-665752 (1µM), there was a significant (n=3. $<$p$0.05) decrease in the mean percentage of TNTs when compared to DMSO-treated cells (1µM)(Fig5.1B). At the highest concentration of PHA-665752 (1µM), there was also a significant (n=3. $$$<p0.001) decrease in the mean number of TNTs when compared to DMSO-treated cells (Fig5.1C). However, PHA-665752 (1µM) induced a significant increase (n=3, £££p<0.001) in TNT length when compared to DMSO-treated cells, although the mean difference in length was roughly only 2µm (Fig5.1D).

A


0
0.001μM
0.0025μM
0.01μM
0.25μM
1μM
DMSO
PHA-665752
DMSO+HGF (100ng/ml)
PHA-665752 +HGF(100ng/ml)

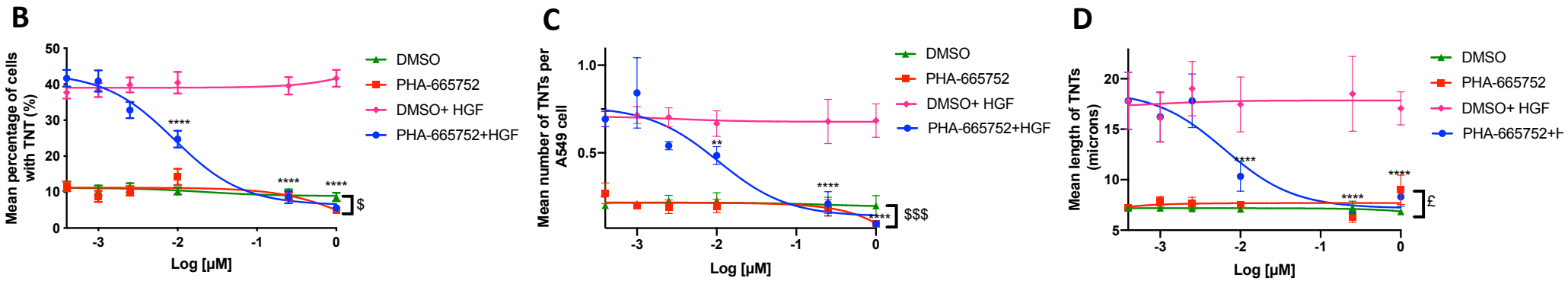


Figure 5.1: C-Met receptor mediates TNT formation in A549 cells. A: Representative white light images of PHA-665752 (≤1µM) or DMSO with or without HGF (100ng/ml) treatment. There were fewer TNTs (white arrows) as the concentration of c-Met inhibitor increased in comparison to the DMSO+HGF treated cells. White light images were captured using x10 objective on an inverted microscope. Scale bar, 10µm. B-D: The log dose curve shows a dose dependent decrease in HGF-induced TNTs in mean (B), number (C) and length (D) of TNTs in the presence of PHA-665752 compared to HGF DMSO. There was also a significant decrease in mean percentage (B) and mean number (C) of control TNTs between DMSO and PHA-665752 (1 µM). A significant increase in TNT length in the PHA-665752 treated control cells compared to DMSO. Values are expressed as mean ± SEM, n=3 with at least 900 cells analysed per condition. $^{**}p<0.01$ and $^{***}p<0.0001$ when comparing between HGF DMSO control and the concentrations of PHA-665752 in the presence of HGF. $\$p<0.05$ and $\$\$\$$ $p<0.001$ when comparing between DMSO and PHA-665752 treated cells.

5.2.2 C-Met inhibition reduces the expression of F-actin, α-tubulin and M-sec positive TNTs

After establishing the inhibitory effect of the c-Met inhibitor on the HGF-induced TNTs, we next sought to determine whether a similar decrease was observed with immunofluorescent labelled TNTs with its characteristic markers (F-actin, α-tubulin and M-sec). A549 cells were pre-treated with either DMSO or PHA-665752 (0.25μM), to inhibit TNT formation to basal control levels, for 30 minutes before further treatment with HGF (100ng/ml) for 24 hours. In the presence of DMSO and PHA-665752 alone, the cells displayed an epithelial cell morphology with minimal F-actin-labelled TNTs observed (red arrow)(Fig5.2). The TNTs observed in the cells treated with DMSO and PHA-665752 alone showed punctate M-sec labelling (pink arrow) at the protrusion site of the individual TNTs (Fig5.2). In the HGF+DMSO-treated cells, the cells displayed a fibroblast-like morphology and there was an increase in F-actin-labelled TNTs (red arrows) when compared to the DMSO-treated cells(Fig5.2). Moreover, punctate M-sec labelling (pink arrow) was also observed at the protrusion site and along the length of the TNTs in the HGF+DMSO-treated cells (Fig5.2). There was a decrease in F-actin-labelled TNTs (red arrow) in the HGF+PHA-665752 treated cells and the cells also displayed an epithelial cell morphology (Fig5.2). Punctate M-sec labelling (pink arrow) was observed at the protrusion site of the TNTs (Fig5.2). Overall, the observations in the white light images (Fig5.1A) and immunofluorescent labelled images (Fig5.2) mirrored one another in the frequency of TNTs observed between the conditions and the immunofluorescent images confirmed the expression of characteristic expression of F-actin, α-tubulin and M-sec.

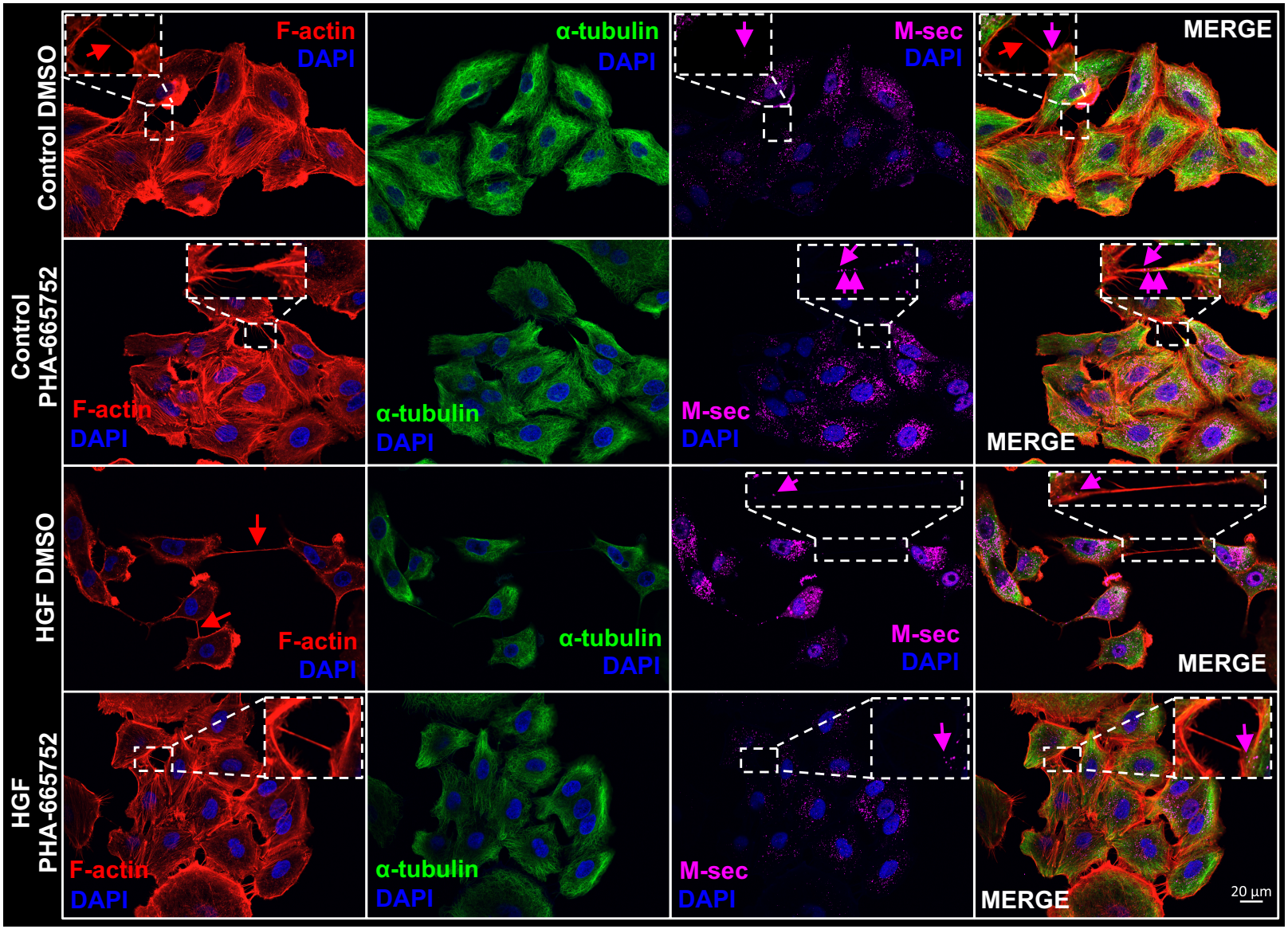


Figure 5.2: C-Met inhibition reduced the expression of F-actin, M-sec and α-tubulin positive TNTs. Representative confocal images for immunofluorescent labelled F-actin (red arrow), α-tubulin (green arrow) and M-sec (pink arrow). There are less F-actin and M-sec positive TNTs observed in the presence of PHA-665752 (0.25µM) compared to DMSO in HGF treated cells. M-sec labelling (pink arrow) at the protrusion site of TNTs confirm the presence of TNTs. Scale bar, 20µm.

5.2.3 C-Met inhibition reduces the localisation of c-Met and β1-integrin positive TNTs

We next sought to determine whether c-Met inhibition also reduced the expression of β1-integrin and c-Met labelled TNTs. In the presence of DMSO and PHA-665752 alone, the cells displayed an epithelial cell morphology and minimal presence of β1-integrin (green arrow) and c-Met (red arrow) labelled TNTs (Fig5.3). In the HGF+DMSO-treated cells, there was an increase in c-Met (red arrow) and β1-integrin (green arrow) labelled TNTs and the cells displayed fibroblast-like morphology (Fig5.3). However, the HGF+PHA-665752-treated cells showed a decrease in c-Met (red arrow) and β1-integrin (green arrow) labelled TNTs and displayed epithelial cell morphology (Fig5.3). For all the TNTs observed, c-Met (red arrow) and β1-integrin (green arrow) localisation was concentrated at the protrusion site of TNTs and along the TNT length (Fig5.3). Co-localisation of c-Met and β1-integrin (yellow arrow) was also observed at the protrusion site of TNTs and along the length of TNTs (Fig5.3). As the observations on white light images (Fig5.1A) reflect the observations in the c-Met and β1-integrin immunofluorescent images (Fig5.3), this confirms the effect of c-Met inhibition in reducing TNT formation in our study.

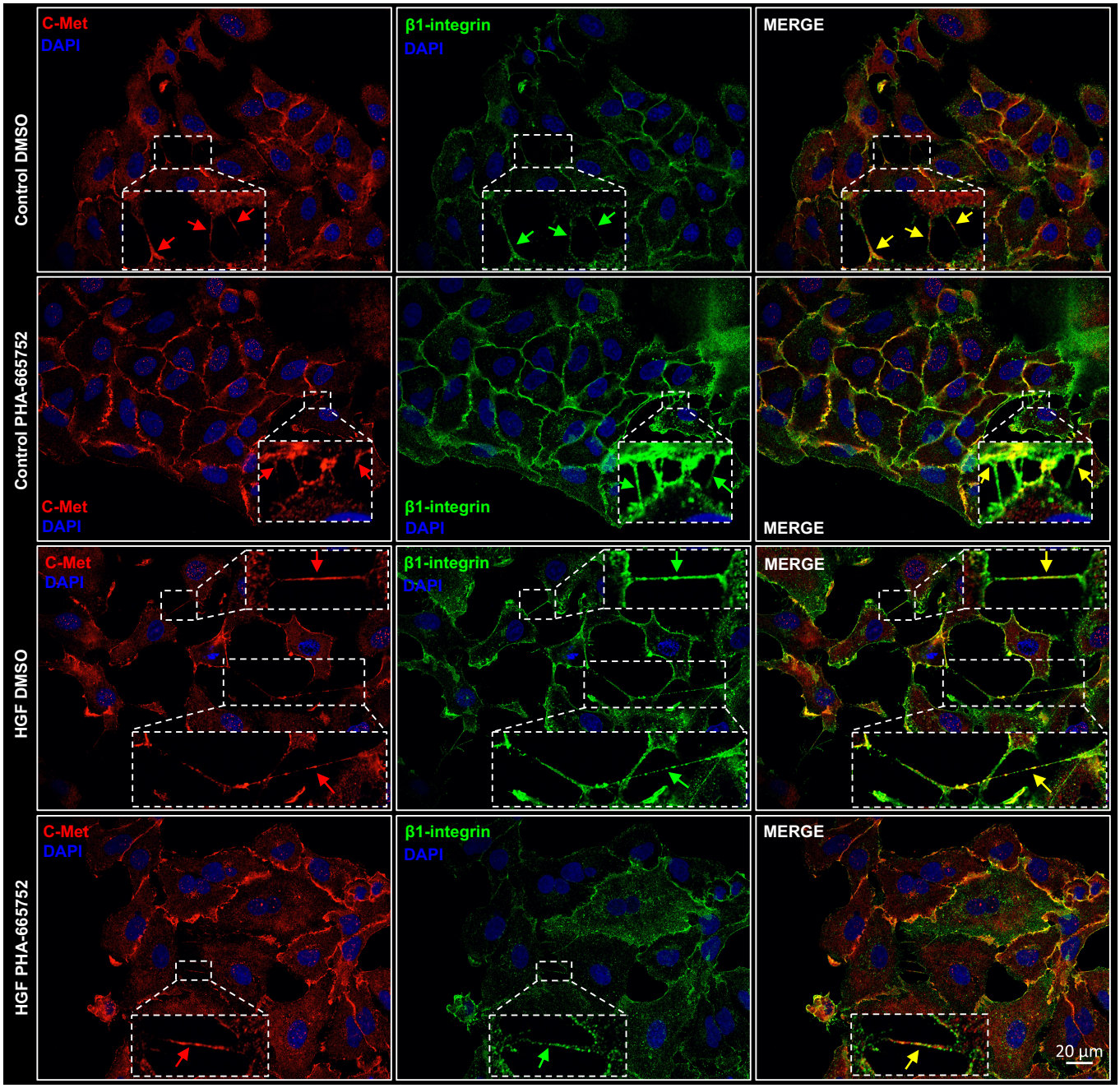
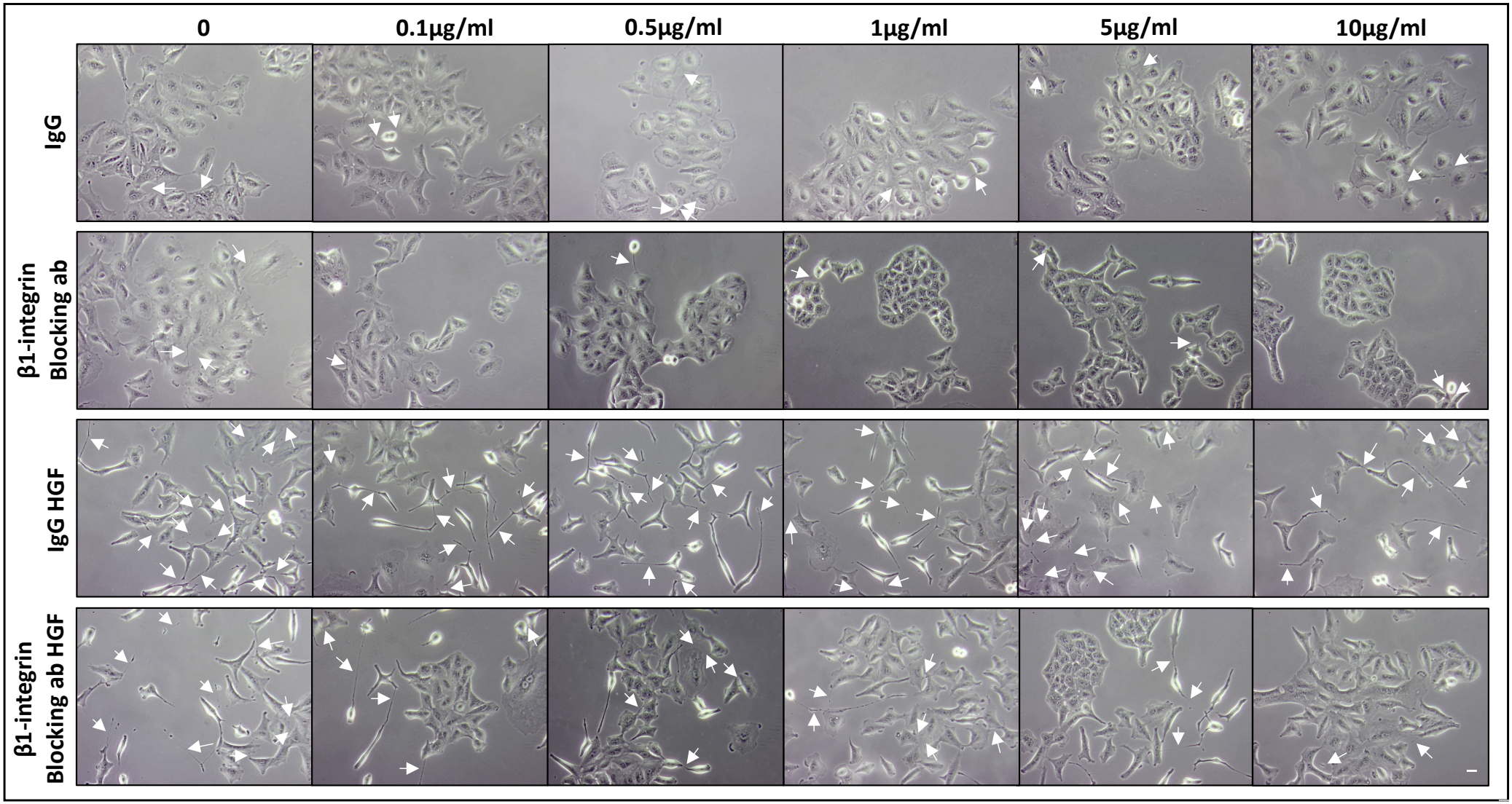


Figure 5.3: C-Met inhibition reduced the localisation of c-Met and β1-integrin positive TNTs. Representative confocal images for immunofluorescent labelled c-Met (red arrow) and β1-integrin (green arrow) TNTs. There are less c-Met and β1-integrin positive TNTs observed in the presence of PHA-665752 (0.25µM) compared to DMSO in HGF treated cells. Co-localisation of c-Met and β1-integrin labelled TNTs (yellow arrow) were observed. Scale bar, 20µm.

5.2.4 β1-integrin crosstalk with HGF/c-Met to induces TNTs in A549 cells

Since β1-integrin has been shown to co-localise with c-Met during TNT formation (Chap 4, Fig4.13), the next step was to determine whether crosstalk between HGF/c-Met and β1-integrin signalling axis modulates TNT formation in A549 cells. The cells were pre-treated for 30mins with a functionally blocking β1-integrin antibody (≤10μg/ml) alongside its respective IgG concentrations and either treated further with HGF (100ng/ml) or in the absence of HGF for 24 hours. To ensure that the IgG control did not affect the HGF-induced or basal TNT formation, cells were also pre-treated with the same volume of IgG as the β1-integrin antibody concentrations alongside control. The white light images showed cells with an epithelial morphology and minimal TNTs (white arrow) present when treated with increasing concentrations of IgG (0-10μg/ml) and the β1-integrin functionally blocking antibody (0-10μg/ml)(Fig5.1A) alone (Fig5.4A) The HGF-treated A549 cells showed an elongated morphology with multiple TNTs (white arrow) across all the concentrations of IgG (0-10μg/ml)(Fig5.4A). The presence of the β1-integrin antibody (0.1-10μg/ml) inhibited the effects of HGF, reverting cells to an epithelial cell morphology observed in cell colonies similarly to untreated IgG control cells (Fig5.4A). There were also fewer HGF-induced TNTs observed in the presence of β1-integrin antibody (0.1-10μg/ml) compared to DMSO (shown by the white arrow)(Fig5.4A). Quantification of the white light images showed that sole treatment with IgG and the β1-integrin antibody alone had no effect on basal control levels of TNTs (Fig5.4B-D). Moreover, the IgG-treated cells did not significantly affect the HGF-induced TNT formation (Fig5.4B-D). However, a dose-dependent decrease in HGF-induced TNTs in the presence of the β1-integrin antibody (n=3,* $p<0.05$, ****$p<0.001$)(Fig5.4B-D). The log concentration-response curve for β1-integrin antibody and HGF-treated cells showed an IC_{50} of 0.03μg/ml, 0.001μg/ml and 1μg/ml in mean percentage (Fig5.4B), mean number of TNT per cell (Fig5.4C) and mean length (Fig5.4D) respectively. Across the three parameters, the curves plateaued to reach basal TNT levels between 1-10μg/ml (Fig5.4B-D). These results demonstrate a novel role between β1-integrin and HGF/c-Met in regulating TNT formation in A549 cells.

A


0
0.1µg/ml
0.5µg/ml
1µg/ml
5µg/ml
10µg/ml
IgG
β1-integrin Blocking ab
IgG HGF
β1-integrin Blocking ab HGF

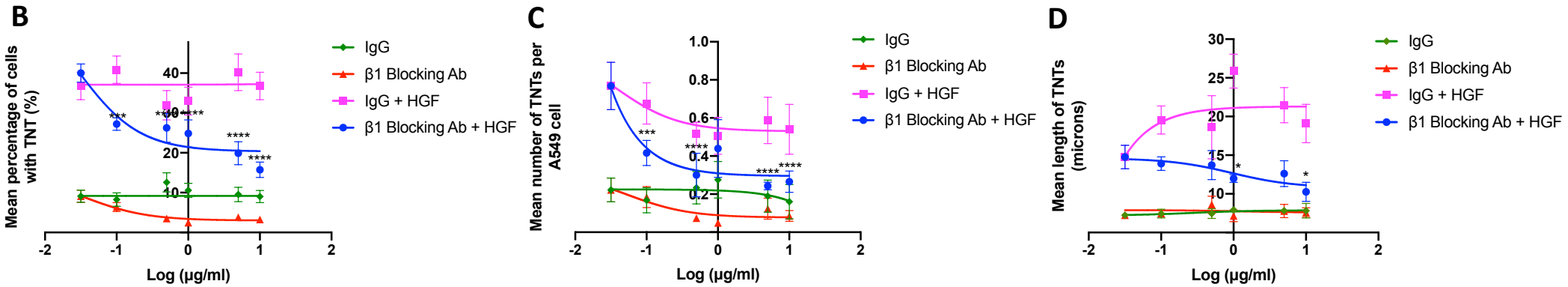


Figure 5.4: β1-integrin cross talk with HGF/c-Met induces TNTs in A549 cells. A: Representative white light images of A549 cells treated with either a functionally blocking β1-integrin antibody (≤10µg/ml) or IgG ± HGF (100ng/ml) for 24 hrs. There was a decrease in HGF-induced TNTs (white arrows) in the presence of the β1-integrin blocking antibody compared to the respective IgG HGF treated concentrations. White light images were captured using x10 objective on an inverted microscope. Scale bar, 10µm. B-D: The log dose curve shows a dose dependent decrease in HGF-induced TNTs in mean (B), number (C) and length (D) of TNTs in the presence of a β1-integrin antibody compared to HGF IgG. Values are expressed as mean ± SEM, n=3 with at least 900 cells analysed per condition. *p<0.05, ***p<0.001 and ****p<0.0001 when comparing between HGF DMSO control and the concentrations of the β1-integrin blocking antibody in the presence of HGF.

5.2.5 Paxillin is involved in HGF-induced TNT formation

Paxillin is a multi-domain scaffold protein, recruiting a range of cytoskeletal and signalling proteins upon β1-integrin and HGF/c-Met-mediated activation (Lai et al. 2000; Crowe and Ohannessian 2004). Therefore, paxillin plays a central role in coordinating between the upstream regulators and downstream effectors. To confirm whether paxillin regulates the formation of TNTs *via* activation of the HGF/c-MET/β1-integrin signalling axis, A549 cells were transfected with a paxillin siRNA to achieve knockdown. Western blot analysis confirmed significant downregulation of paxillin expression, observed at approximately 68kDa, in the A549 cells transfected with the siRNA compared to a non-targeting siRNA (Fig5.5A). GAPDH was used as a loading control and its expression, at approximately 36kDa, confirmed equal protein loading for lysates generated from cells transfected with the non-targeting siRNA and the siRNA for paxillin (Fig5.5A). The white light images showed the minimal presence of TNTs (white arrow) in control for both cells transfected with a non-targeting siRNA and paxillin siRNA (Fig5.5B). There was an increase in TNTs (white arrow) observed in the HGF-treated cells transfected with the non-targeting siRNA (Fig5.5B). However, there was a decrease in HGF-induced TNTs observed when the cells were transfected with the paxillin siRNA (Fig5.5B). Quantification of the white light images showed there was a significant decrease (n=3, *p<0.05, ****p<0.0001) in the mean percentage (Fig5.5C), the mean number of TNTs (Fig5.5D) and mean length (Fig5.5E), of HGF-induced TNTs when transfected with the paxillin siRNA compared to the cells transfected with the non-targeting siRNA.

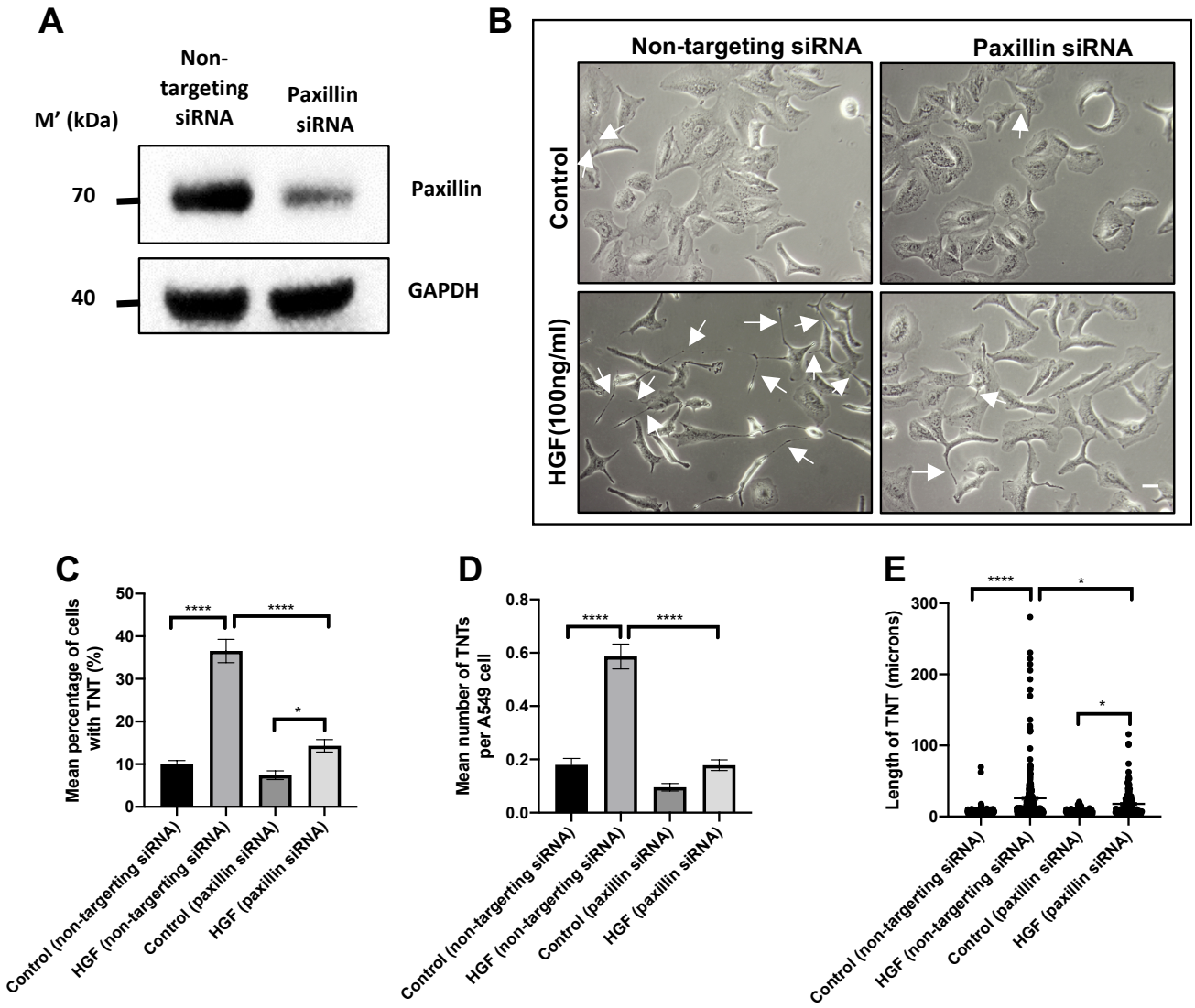


Figure 5.5: Paxillin regulates HGF-induced TNT formation. A: Western blot shows knockdown of paxillin in A549 cells after 48h transfection with paxillin siRNA. GAPDH indicates equal protein loading (approximately 20µl of respective protein lysates was loaded). B: Representative white light images of A549 cells transfected with paxillin siRNA or non-targeting siRNA for 48h before 24h HGF treatment (100ng/ml). (C-E) There was a significant decrease in mean percentage (C), number (D) and length (E) of TNTs between HGF-treated cells transfected with paxillin siRNA compared to cells transfected with non-targeting siRNA. All experiments (western blot and TNT experiments) were conducted in triplicates. Values on the histogram are expressed as mean ± SEM, n=3 with at least 500 cells analysed per condition.*p<0.05 and ****p<0.0001 when comparing between the A549 cells transfected with either a non-targeting siRNA or paxillin siRNA in the HGF treated cells.

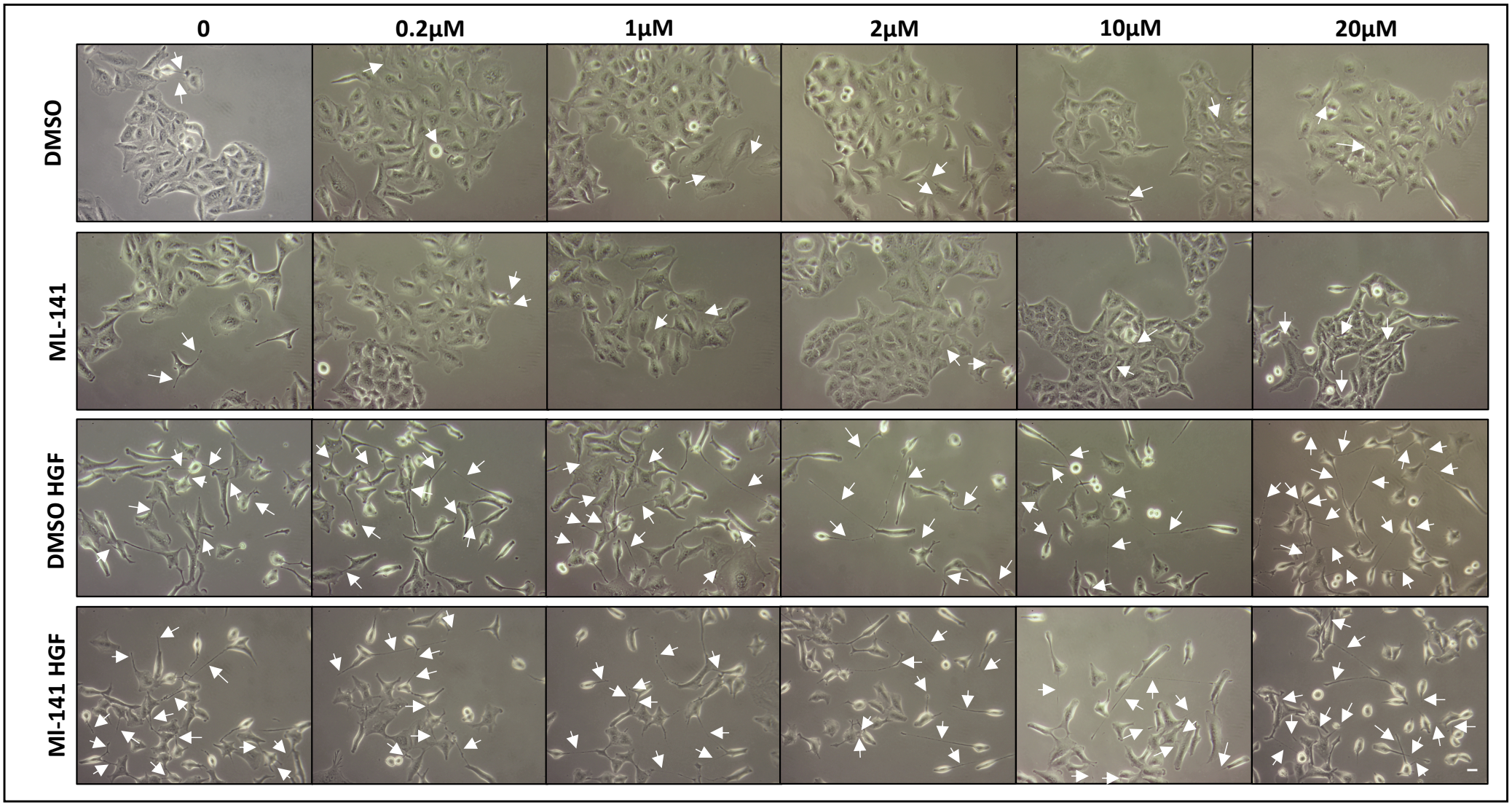
Moreover, paxillin phosphorylation allows consequent binding of other adaptor proteins which activate the MAPK, PI3K and FAK pathways (including CDC42, Rac1 and RhoA)(Ishibe et al. 2004; Brown, Perrotta, and Turner 1996; Ishibe et al. 2003). Therefore, after establishing the role of paxillin in regulating the HGF/c-Met/β1-integrin-induced TNT formation, we next investigated the potential downstream pathways involved.

5.2.6 CDC42, Rac1 and ROCK pathway inhibition had no effect on HGF-induced TNT formation

After establishing HGF/c-Met/β1-integrin co-activation leads to TNT formation of A549 cells, the role of the Rho GTPases (Rho, Rac1 and CDC42) were next investigated to identify the potential downstream pathways involved. The cells were pre-treated with a CDC42 inhibitor (ML-141≤20μM) alongside its DMSO vehicle control and either treated further with HGF (100ng/ml) or in the absence of HGF for 24 hours (Fig5.6A-D). To ensure that the vehicle control, DMSO, did not affect the HGF-induced or basal TNT formation, cells were also pre-treated with the same volume of DMSO used for the CDC42 inhibitor concentrations alongside control. The white light images showed cells with an epithelial morphology and minimal TNTs (white arrow) present when treated with increasing concentrations of DMSO (0-20μM) and the CDC42 inhibitor (ML-141;0-20μM) alone (Fig5.6A). The HGF-treated A549 cells showed an elongated morphology with multiple TNTs (white arrow) present across all the concentrations of DMSO (0-20μM) and across all the treated concentrations of ML-141 (0-20μM)(Fig5.6A). Quantification of the white light images showed DMSO and CDC42 inhibitor treatment alone had no significant effect on TNT formation when compared to control (Fig.6B-D). Moreover, there was no significant decrease in the mean percentage (Fig5.6B), number (Fig5.6C) and length (Fig.6D) of TNTs when comparing the concentrations of HGF+ML-141(0.2-20μM) and HGF+DMSO (0.2-20μM)-treated cells respectfully. Therefore, the white light image analysis revealed the CDC42 inhibitor had no effect on HGF-induced TNT formation.

We next determined whether CDC42 inhibition also showed no effect on the HGF-induced TNTs through immunofluorescent labelling with the characteristic markers for TNTs (F-actin, α-tubulin and M-sec)(Fig5.7). In the presence of DMSO (10μM) and ML-141 (10μM) alone, the cells displayed an epithelial cell morphology with minimal F-actin-labelled TNTs observed (red arrow)(Fig5.7). The TNTs observed in the cells treated with DMSO and ML-141 alone showed punctate M-sec labelling (pink arrow) at the protrusion site of the individual TNTs (Fig5.7). In the HGF+DMSO and HGF+ML-141-treated cells, the cells displayed a fibroblast-like morphology and there was an increase in F-actin-labelled TNTs (red arrows) when compared to the control DMSO-treated cells (Fig5.7). Punctate M-sec labelling (pink arrow) was also observed at the protrusion site and along the length of the TNTs in the HGF+DMSO and HGF+ML-141-treated cells (Fig5.7). α-tubulin (green arrow) was also present at the thicker region of the TNTs observed in the HGF+DMSO and HGF+ML-141-treated cells (Fig5.7). There was no decrease in F-actin (red arrow) and M-sec (pink arrow) expressing TNTs observed in the HGF+ML-141 treated cells compared to the HGF+DMSO treated cells (Fig5.7).

We then undertook immunofluorescent labelling with the novel TNT markers, c-Met and β1-integrin to determine whether CDC42 inhibition also showed no effect on the HGF-induced TNTs. In the presence of DMSO and ML-141 alone, the cells displayed an epithelial cell morphology and minimal presence of β1-integrin (green arrow) and c-Met (red arrow) labelled TNTs (Fig58). In the HGF+DMSO and HGF+ML-141-treated cells, there was an increase in c-Met (red arrow) and β1-integrin (green arrow) labelled TNTs and the cells displayed fibroblast-like morphology (Fig5.8). There was also no decrease in the c-Met (red arrow) and β1-integrin (green arrow) labelled TNTs observed between the HGF+ML-141 and HGF+DMSO-treated cells (Fig5.8). For all the TNTs observed, c-Met (red arrow) and β1-integrin (green arrow) localisation was concentrated at the protrusion site of TNTs and along the TNT length (Fig5.8). Moreover, co-localisation of c-Met and β1-integrin (yellow arrow) was also observed at the protrusion site of TNTs and along the length of TNTs (Fig5.8). Overall, the observations in the white light images (Fig5.6A) and immunofluorescent labelled images (Fig5.7&8) mirrored one another in the frequency of TNTs observed between the conditions and the immunofluorescent images confirmed the expression of characteristic and novel markers of TNTs.


A
0
0.2μM
1μM
2μM
10μM
20μM
DMSO
ML-141
DMSO HGF
MI-141 HGF

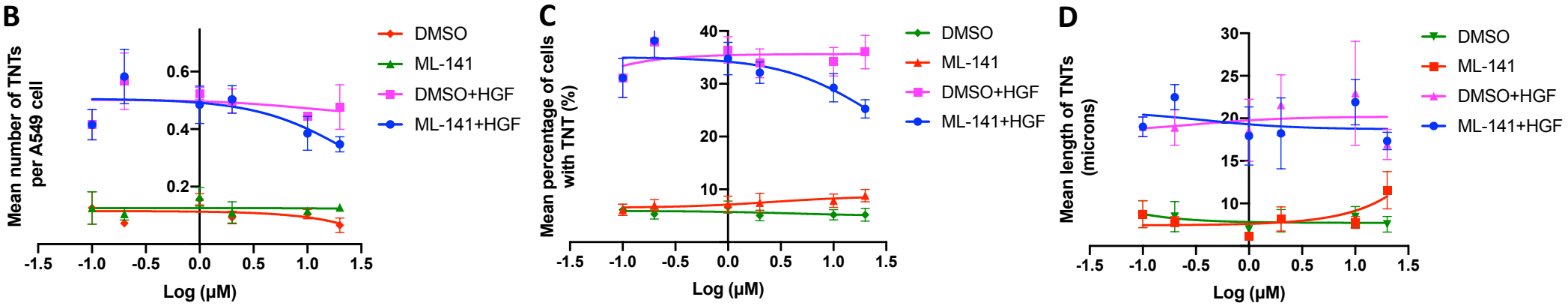


Figure 5.6: CDC42 inhibition showed no effect on HGF-induced TNT formation. A: Representative white light images of ML-141 (≤20μM) or DMSO with or without HGF (100ng/ml) treatment. The presence of ML-141 did not decrease the formation of TNTs (white arrows) in both control and HGF-treated cells. White light images were captured using x10 objective on an inverted microscope. Scale bar, 10μm. B-D: The log dose curve showed no significant decrease in HGF-induced TNTs in mean (B), number (C) and length (D) in the presence of ML-141 compared to HGF DMSO. Values are expressed as mean ± SEM, n=3 with at least 900 cells analysed per condition.

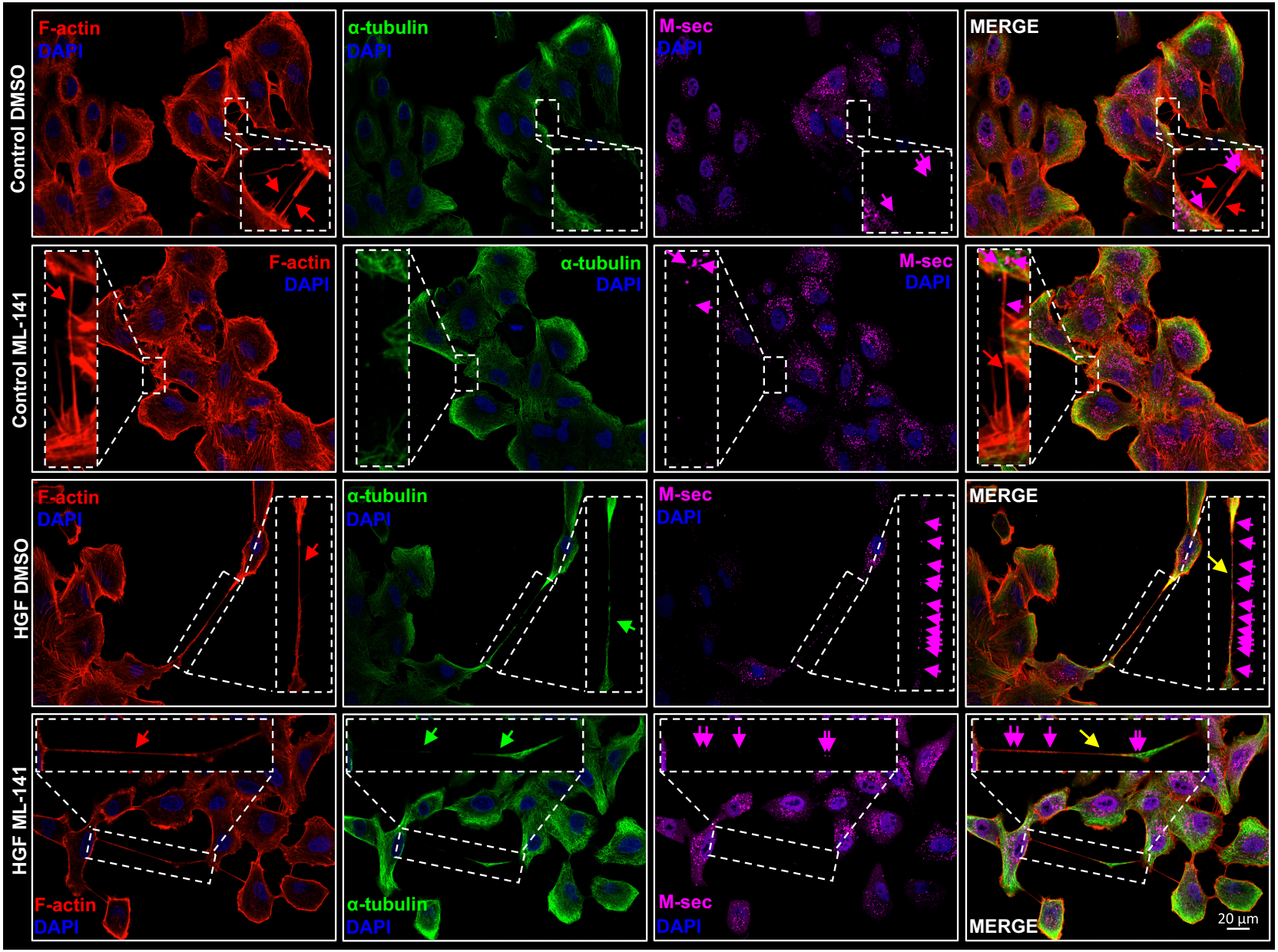


Figure 5.7: CDC42 inhibition had no effect on the experrssion of F-actin, M-sec and α-tubulin positive TNTs. Representative confocal images for immunofluorescent labelled F-actin (red arrow), α-tubulin (green arrow) and M-sec (pink arrow). The dotted region denotes a zoomed area. There is no difference between the F-actin and M-sec positive TNTs observed in the presence of ML-141 (10µM) and DMSO for both control and HGF treated cells. M-sec labelling (pink arrow) at the protrusion site of TNTs confirm the presence of TNTs. Scale bar, 20µm.

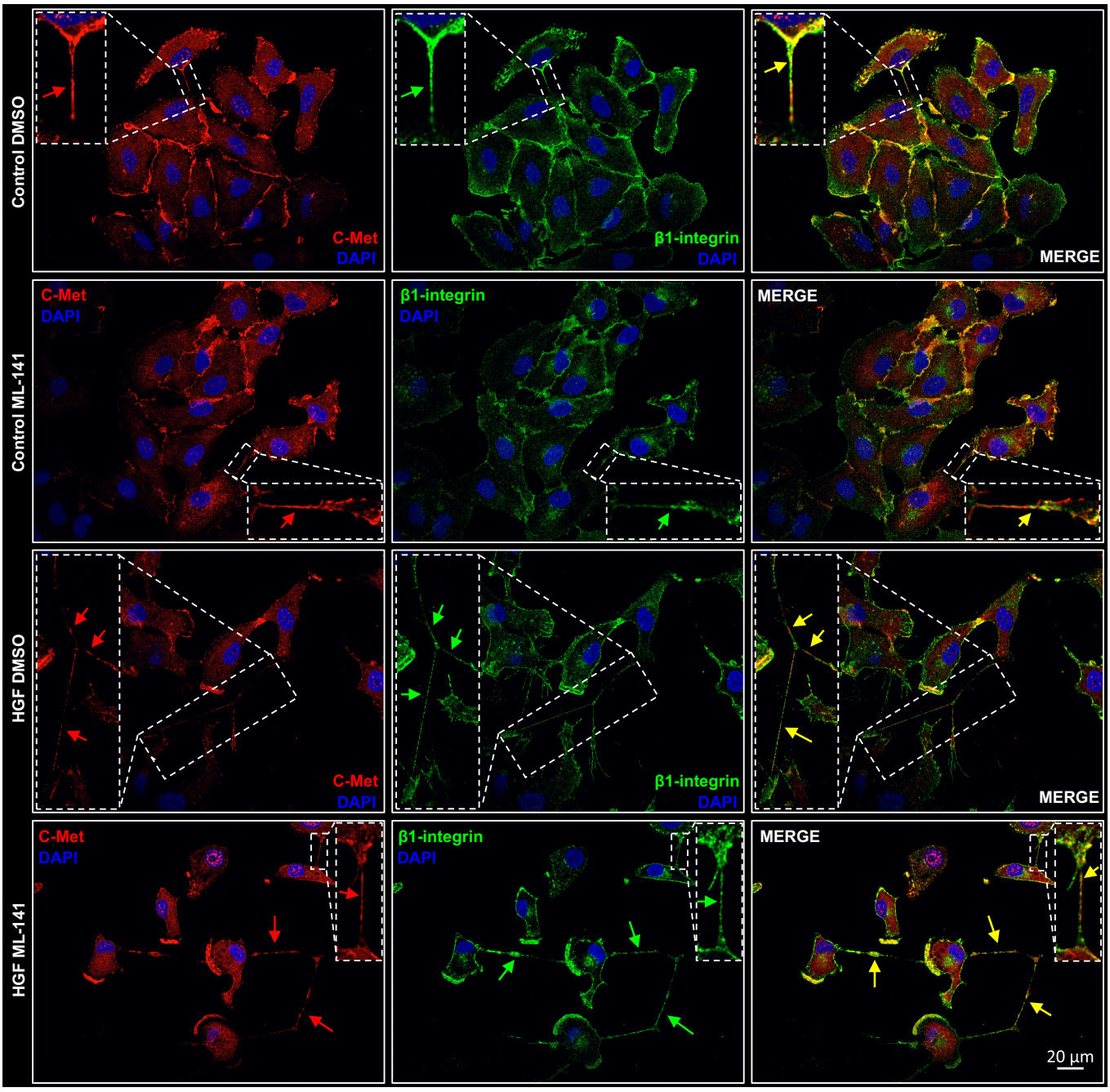
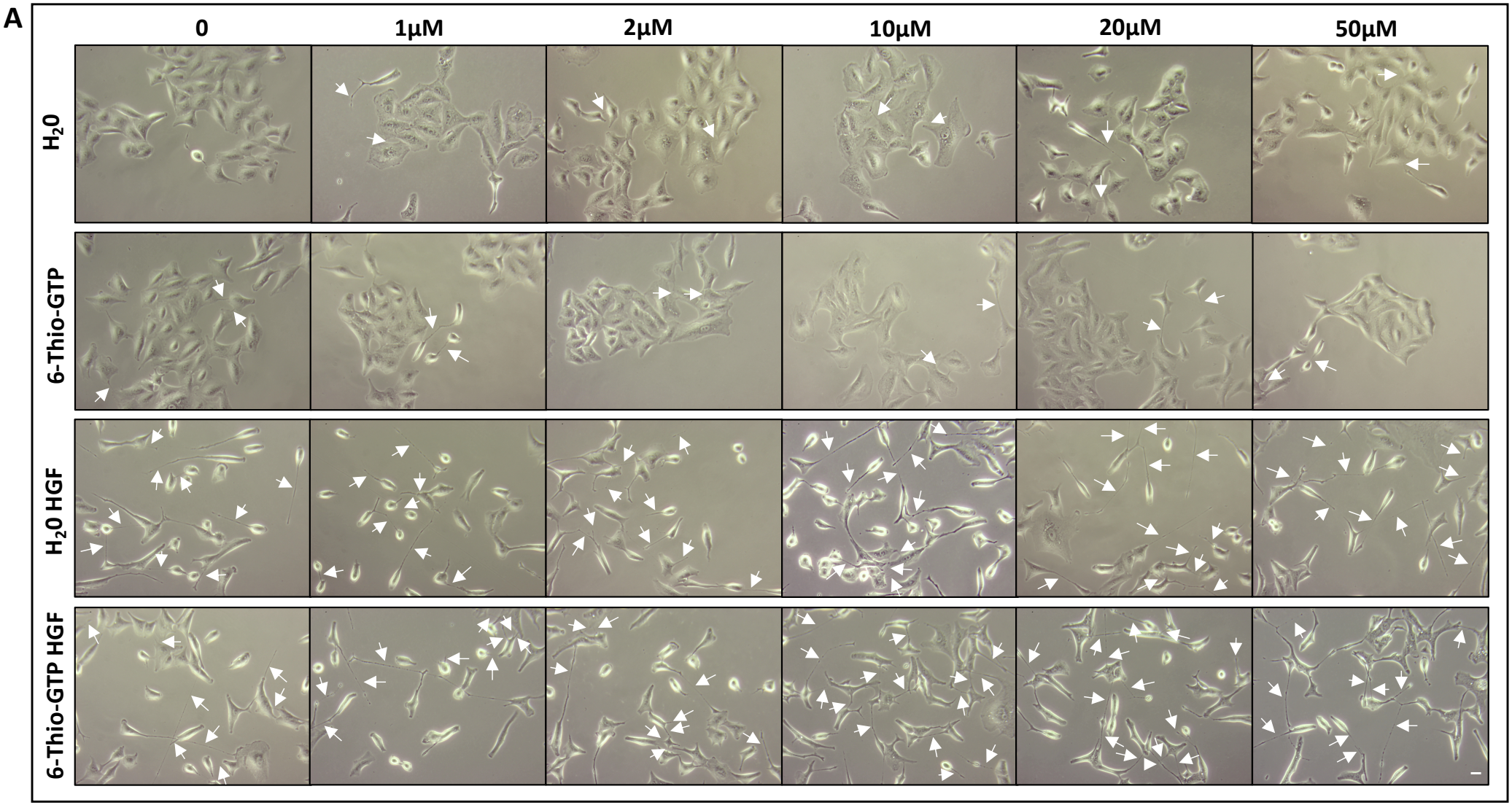


Figure 5.8: CDC42 inhibition had no effect on the localisation of c-Met and β1-integrin positive TNTs. Representative confocal images for immunofluorescent labelled c-Met (red arrow) and β1-integrin (green arrow) TNTs. There is no difference between the c-Met and β1-integrin positive TNTs observed in the presence of ML-141 (10µM) compared to DMSO in control HGF treated cells. Co-localisation of c-Met and β1-integrin labelled TNTs (yellow arrow) was observed at the protrusion site of the TNTs and along the length of the TNTs. Scale bar, 20µm.

After establishing CDC42 inhibition had no effect on HGF-induced TNT formation, we next determined whether the Rac1 pathway was involved in the HGF-induced TNT formation. The cells were pre-treated with a Rac1 inhibitor (6-Thio-GTP≤50μM) alongside its H_20 vehicle control and either treated further with HGF (100ng/ml) or in the absence of HGF for 24 hours. To ensure that the vehicle control, H_20, did not affect the HGF-induced or basal TNT formation, cells were also pre-treated with the same volume of H_20 used for the Rac1 inhibitor concentrations alongside control. The white light images showed cells with an epithelial morphology and minimal TNTs (white arrow) present when treated with increasing concentrations of H_20 (0-50μM) and the Rac1 inhibitor (6-Thioi-GTP;0-50μM) alone (Fig5.9A). The HGF-treated A549 cells showed an elongated morphology with multiple TNTs (white arrow) present across all the concentrations of H_20 (0-50μM) and across all the treated concentrations of 6-Thio-GTP (0-50μM)(Fig5.9A). Quantification of the white light images showed H_20 and Rac1 inhibitor treatment alone had no significant effect on TNT formation when compared to control (Fig.9B-D). Moreover, there was no significant decrease in the mean percentage (Fig5.9B), number (Fig5.9C) and length (Fig.9D) of TNTs when comparing the concentrations of the HGF+6-Thio-GTP (1-50μM) and the HGF+H_20 (1-50μM)-treated cells respectfully. Therefore, the white light image analysis revealed the Rac1 inhibitor also had no effect on the HGF-induced TNT formation.

We next determined whether Rac1 inhibition also showed no effect on the HGF-induced TNTs through immunofluorescent labelling with the characteristic markers for TNTs (F-actin, α-tubulin and M-sec)(Fig5.10). In the presence of H_20 (10μM) and 6-Thio-GTP (10μM) alone, the cells displayed an epithelial cell morphology with minimal F-actin-labelled TNTs observed (red arrow)(Fig5.10). The TNTs observed in the cells treated with H_20 and 6-Thio-GTP alone showed punctate M-sec labelling (pink arrow) at the protrusion site of the individual TNTs and α-tubulin (green arrow) present at the thicker region of the TNTs (Fig5.10). In the HGF+ H_20 and HGF+ 6-Thio-GTP-treated cells, the cells displayed a fibroblast-like morphology and there was an increase in F-actin-labelled TNTs (red arrows) when compared to the control DMSO-treated cells (Fig5.10). Punctate M-sec labelling (pink arrow) was also observed at the protrusion site and along the length of the TNTs in the HGF+DMSO and HGF+ML-141-treated cells (Fig5.10). α-tubulin (green arrow) was also present at the thicker region of the TNTs observed in the HGF+ H_20 and HGF+6-Thio-GTP -treated cells (Fig5.10). There was no decrease in F-actin (red arrow), M-sec (pink arrow) and α-tubulin (green arrow) expressing TNTs observed in the HGF+6-Thio-GTP treated cells compared to the HGF+ H_20 treated cells (Fig5.10).

We then undertook immunofluorescent labelling with the novel TNT markers, c-Met and β1-integrin to determine whether Rac1 inhibition also showed no effect on the HGF-induced TNTs. In the presence of H_20 and 6-Thio-GTP alone, the cells displayed an epithelial cell morphology and minimal presence of β1-integrin (green arrow) and c-Met (red arrow) labelled TNTs (Fig5.11). In the HGF+ H_20 and HGF+6-Thio-GTP treated cells, there was an increase in c-Met (red arrow) and β1-integrin (green arrow) labelled TNTs and the cells displayed fibroblast-like morphology (Fig5.11). There was also no decrease in the c-Met (red arrow) and β1-integrin (green arrow) labelled TNTs observed between the HGF+ML-141 and HGF+DMSO-treated cells (Fig5.11). For all the TNTs observed, c-Met (red arrow) and β1-integrin (green arrow) localisation was concentrated at the protrusion site of TNTs and along the TNT length (Fig5.11). Moreover, co-localisation of c-Met and β1-integrin (yellow arrow) was also observed at the protrusion site of TNTs and along the length of TNTs (Fig5.11). Overall, the observations in the white light images (Fig5.9A) and immunofluorescent labelled images (Fig5.10&11) mirrored one another in the frequency of TNTs observed between the conditions and the immunofluorescent images confirmed the expression of characteristic and novel markers of TNTs.


A
0
1μM
2μM
10μM
20μM
50μM
H20
6-Thio-GTP
H20 HGF
6-Thio-GTP HGF

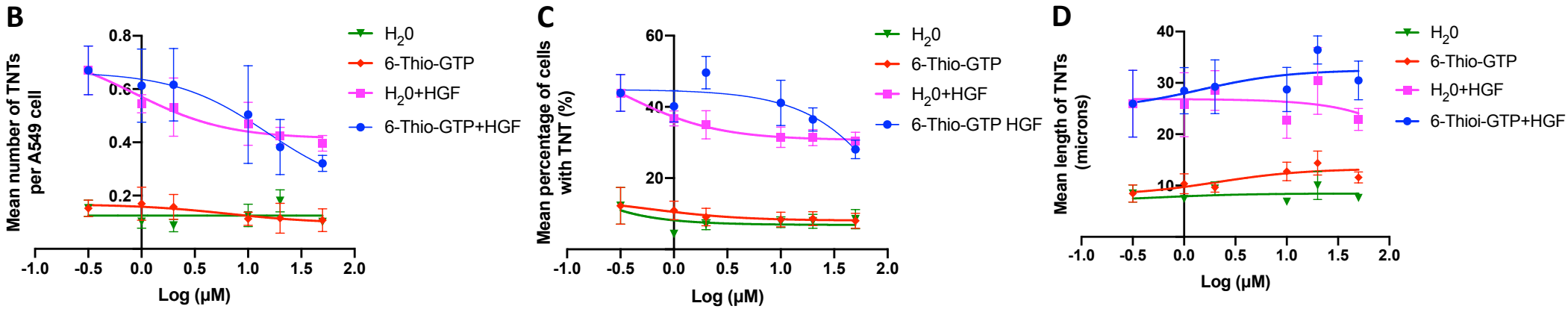


Figure 5.9: Rac1 inhibition showed no effect on HGF-induced TNT formation A: Representative white light images of 6-Thio-GTP (≤50μM) or H_20 with or without HGF (100ng/ml) treatment. The presence of 6-Thio-GTP did not decrease the formation of TNTs (white arrows) in both control and HGF-treated cells. White light images were captured using x10 objective on an inverted microscope. Scale bar, 10μm. B-D: The log dose curve showed no significant decrease in HGF-induced TNTs in mean (B), number (C) and length (D) in the presence of 6-Thio-GTP compared to HGF H_20. Values are expressed as mean ± SEM, n=3 with at least 900 cells analysed per condition.

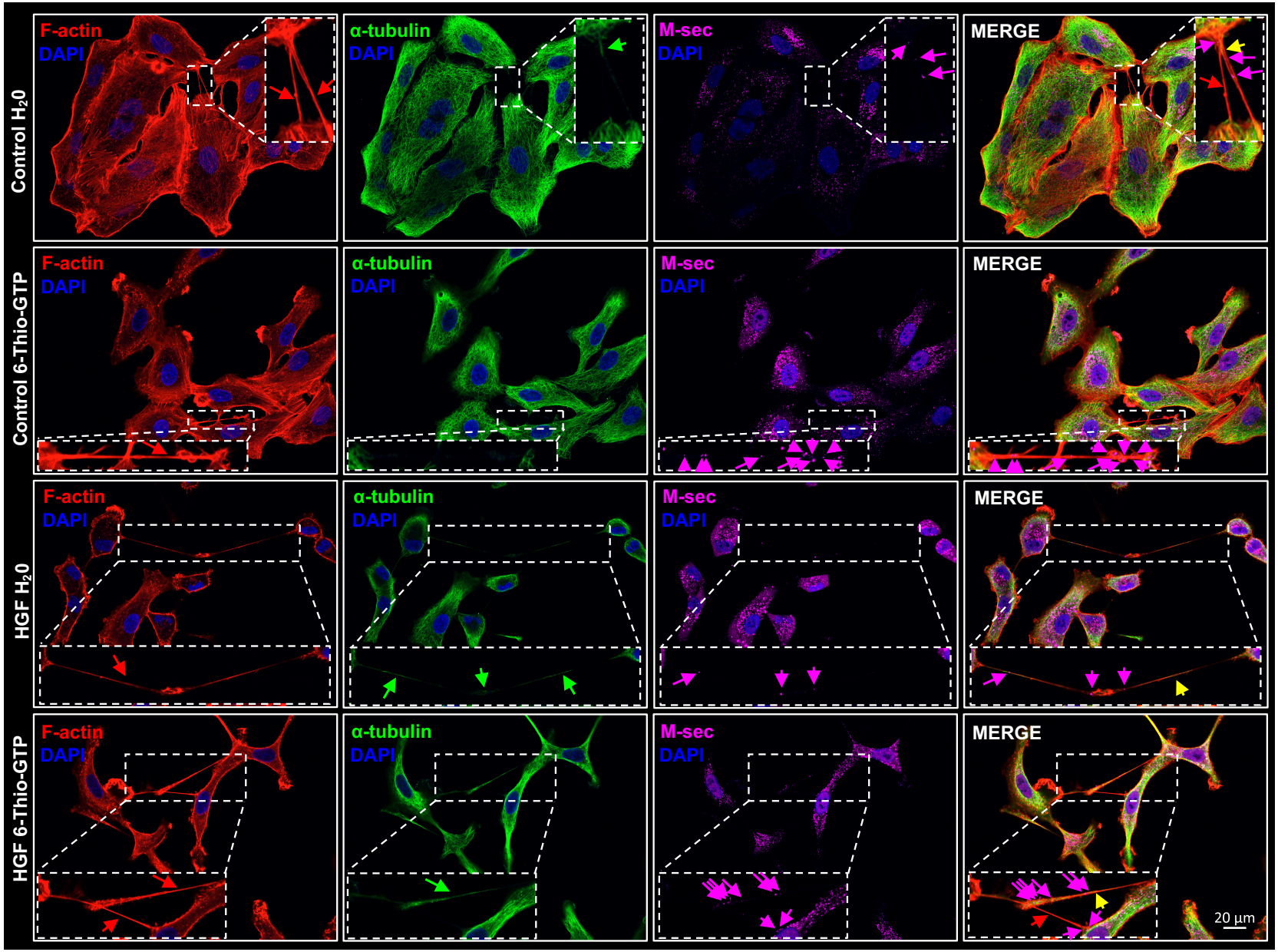


Figure 5.10: Rac1 inhibition had no effect on the expression of F-actin, M-sec and α-tubulin positive TNTs. Representative confocal images for immunofluorescent labelled F-actin (red arrow), α-tubulin (green arrow) and M-sec (pink arrow). The dotted region denotes a zoomed area. There was no difference between the F-actin and M-sec positive TNTs observed in the presence of 6-Thio-GTP (10µM) and DMSO for both control and HGF treated cells. M-sec labelling (pink arrow) at the protrusion site of TNTs confirm the presence of TNTs. Scale bar, 20µm.

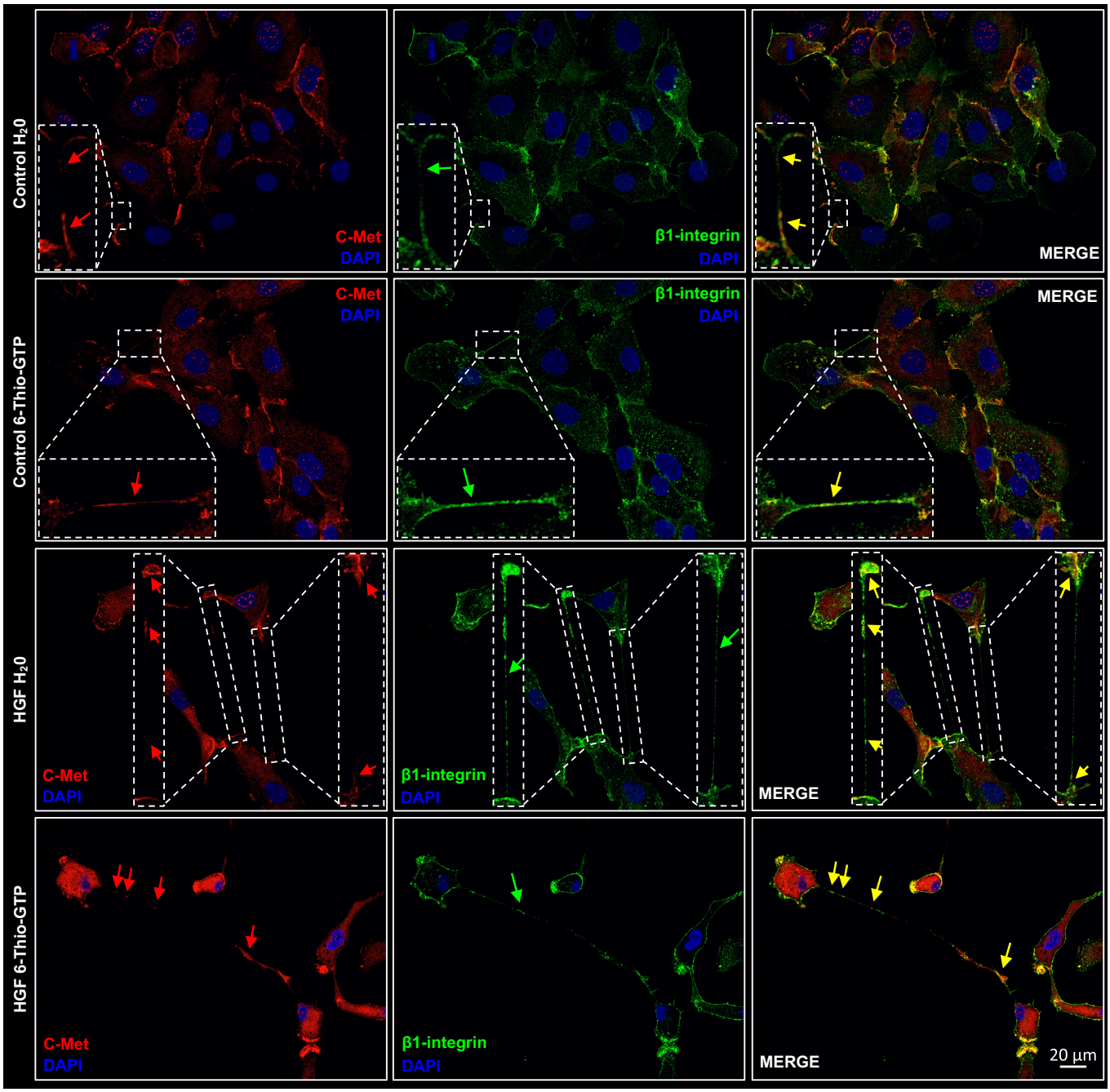


Figure 5.11: Rac1 inhibition had no effect on the localisation of c-Met and β1-integrin positive TNTs. Representative confocal images for immunofluorescent labelled c-Met (red arrow) and β1-integrin (green arrow) TNTs. There is no difference between the c-Met and β1-integrin positive TNTs observed in the presence of 6-Thio-GTP (10µM) compared to DMSO in control HGF treated cells. Co-localisation of c-Met and β1-integrin labelled TNTs (yellow arrow) was observed at the protrusion site of the TNTs and along the length of the TNTs. Scale bar, 20µm.

We lastly aimed to determine whether HGF-induced TNTs formed *via* the ROCK pathway. A549 cells were pre-treated with a ROCK inhibitor (Y27632≤7.5μM) alongside its DMSO vehicle control and either treated further with HGF (100ng/ml) or in the absence of HGF for 24 hours. To ensure that the vehicle control, DMSO, did not affect the HGF-induced or basal TNT formation, cells were also pre-treated with the same volume of DMSO used for the Y27632 concentrations alongside a control. The white light images showed cells with an epithelial morphology and minimal TNTs (white arrow) present when treated with increasing concentrations of DMSO (0-7.5μM) alone (Fig5.12A). Similarly, there were minimal TNTs present (white arrow) when treated with Y27632 alone at concentrations 0.1-5μM (Fig5.12A). However, at the highest concentration of Y27632 (7.5μM), there was an increase in TNTs observed (white arrows)(Fig5.12A). Moreover, the HGF+DMSO-treated cells showed an elongated morphology with multiple TNTs (white arrows) present across all the concentrations of DMSO (0-7.5μM)(Fig5.12A). Numerous HGF-induced TNTs were also observed when treated with the lower concentrations of the ROCK inhibitor (Y27632;0.1-1μM), however an increase in HGF-induced TNTs (white arrow) were observed at the higher concentrations of the ROCK inhibitor (Y27632;5-7.5μM) when compared to its respective HGF+DMSO concentrations (Fig5.12A). Furthermore, there was an increase in the branched morphology of HGF-induced TNTs (blue arrow) with increasing concentrations of the ROCK inhibitor (0-7.5μM)(Fig5.12A).

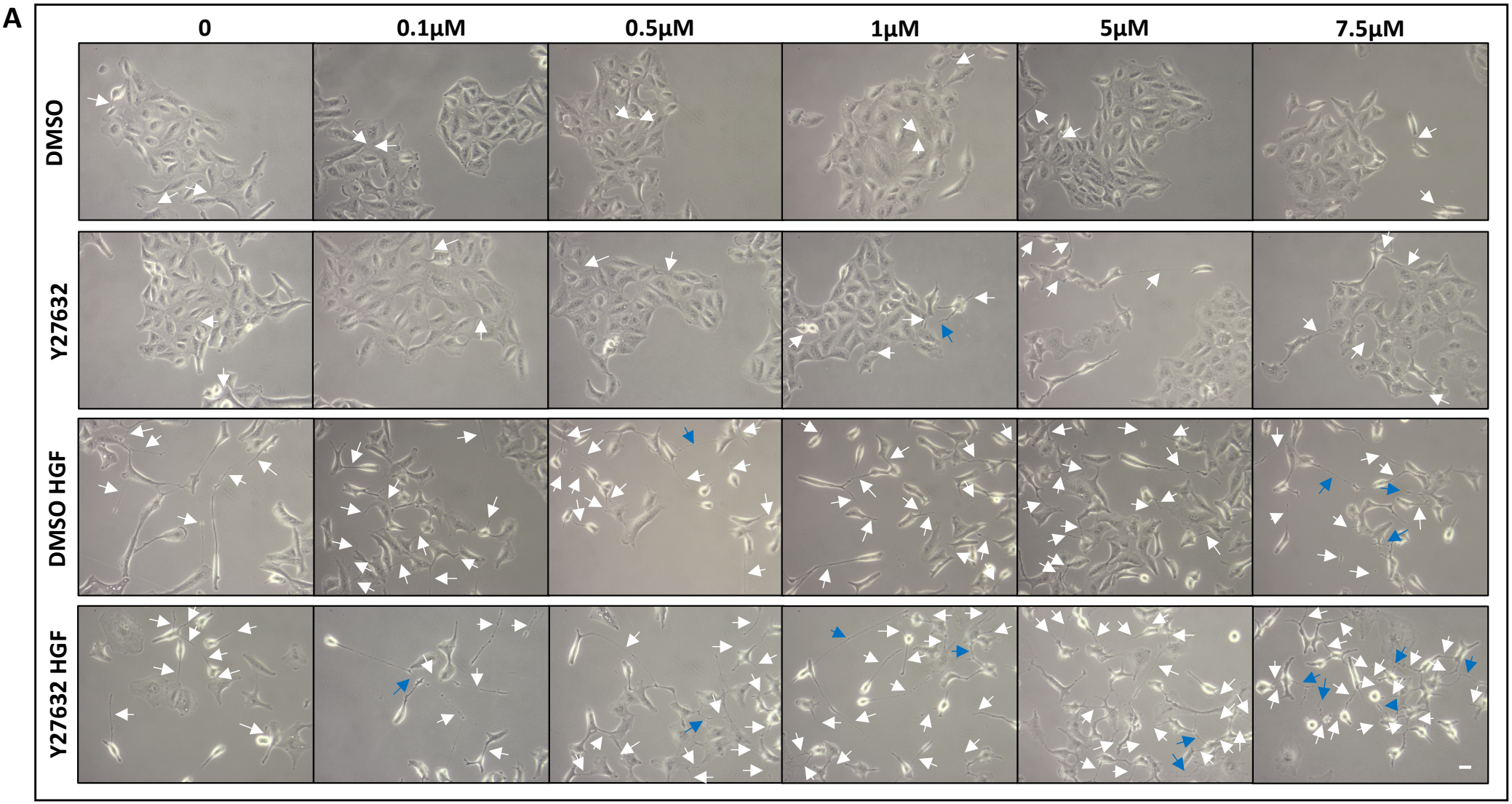
Quantification of the white light images showed DMSO treatment alone had no significant effect on basal TNT formation when compared to control (Fig5.12B-D). There was also no significant effect between the different concentrations of DMSO (0-7.5μM) in the mean (Fig5.12B), number (Fig5.12C) and length (Fig5.12d) of the HGF-induced TNTs. However, in the presence of the ROCK inhibitor, there was a significant (n=3, ****p<0.0001) dose-dependent increase in the HGF-induced TNT formation across the three parameters (Fig5.12B-D). The ROCK inhibitor, Y27632, significantly increased the mean percentage (Fig5.12B) and mean number (Fig5.12C) at 1μM before plateauing to its maximal effect between 5μM and 7.5μM. There was no significant difference between the HGF-induced TNT lengths in the DMSO and Y27632-treated cells across all the concentrations (0-7.5μM)(Fig5.12B-D). The log concentration-response curve for Y27632+HGF treated cells showed an EC_{50} of 0.1μM and 0.7μM for mean percentage (Fig5.12B) and mean number of TNT per cell (Fig5.12C) respectively. Furthermore, the presence of the ROCK inhibitor alone, at higher concentrations (Y27632;1-7.5 μM), induced a dose-dependent significant (n=3, *p<0.05) increase in TNT length (Fig5.8D). The log concentration-response curve for Y27632 treatment alone showed an EC_{50} of 0.3μM for TNT length and the maximal TNT length was also achieved at 5μM before plateauing (Fig5.12D). At the highest concentration of the ROCK inhibitor (7.5μM), there was a

significant increase in the mean percentage (Fig5.12B) and mean number (Fig5.12C) of TNTs compared to its respective DMSO control.

We next determined whether ROCK inhibition also increased the HGF-induced TNTs through immunofluorescent labelling with the characteristic markers for TNTs (F-actin, α-tubulin and M-sec)(Fig5.13). In the presence of DMSO (5μM) and Y27632 (5μM) alone, the cells displayed an epithelial cell morphology with minimal F-actin-labelled TNTs observed (red arrow)(Fig5.13). The TNTs observed in the cells treated with DMSO and Y27632 alone showed punctate M-sec labelling (pink arrow) at the protrusion site of the individual TNTs and α-tubulin (green arrow) present at the thicker region of the TNTs (Fig5.13). In the HGF+ DMSO and HGF+Y27632-treated cells, the cells displayed a fibroblast-like morphology and there was an increase in F-actin-labelled TNTs (red arrows) when compared to the control DMSO-treated cells (Fig5.13). Punctate M-sec labelling (pink arrow) was also observed at the protrusion site and along the length of the TNTs in the HGF+DMSO and HGF+ML-141-treated cells (Fig5.13). α-tubulin (green arrow) was also present at the thicker region of the TNTs observed in the HGF+DMSO and HGF+ML-141-treated cells (Fig5.13). There was an increase in the F-actin (red arrow), M-sec (pink arrow) and α-tubulin (green arrow) expressing TNTs observed in the HGF+6-Thio-GTP treated cells compared to the HGF+ DMSO treated cells (Fig5.13). Overall, the observations in the white light images (Fig5.12A) and immunofluorescent labelled images (Fig5.13) mirrored one another in the frequency of TNTs observed between the conditions and the immunofluorescent images confirmed the expression of characteristic expression of F-actin, α-tubulin and M-sec.

We then undertook immunofluorescent labelling with the novel TNT markers, c-Met and β1-integrin to determine whether ROCK inhibition also increased the HGF-induced TNTs. In the presence of DMSO and Y27632 alone, the cells displayed an epithelial cell morphology and minimal presence of β1-integrin (green arrow) and c-Met (red arrow) labelled TNTs (Fig5.14). In the HGF+ DMSO and HGF+Y27632 treated cells, there was an increase in c-Met (red arrow) and β1-integrin (green arrow) labelled TNTs and the cells displayed fibroblast-like morphology (Fig5.14). There was an increase in the c-Met (red arrow) and β1-integrin (green arrow) labelled TNTs observed in the HGF+ML-141-treated cells compared to the HGF+DMSO-treated cells (Fig5.14). For all the TNTs observed, c-Met (red arrow) and β1-integrin (green arrow) localisation was concentrated at the protrusion site of TNTs and along the TNT length (Fig5.14). Moreover, co-localisation of c-Met and β1-integrin (yellow arrow) was also observed at the protrusion site of TNTs and along the length of TNTs (Fig5.14). Overall, the observations in the white light images (Fig5.12A) and immunofluorescent labelled images (Fig5.13&14) mirrored one another in the frequency of TNTs observed between the

conditions and the immunofluorescent images confirmed the expression of characteristic and novel markers of TNTs.


A
0
0.1μM
0.5μM
1μM
5μM
7.5μM
DMSO
Y27632
DMSO HGF
Y27632 HGF

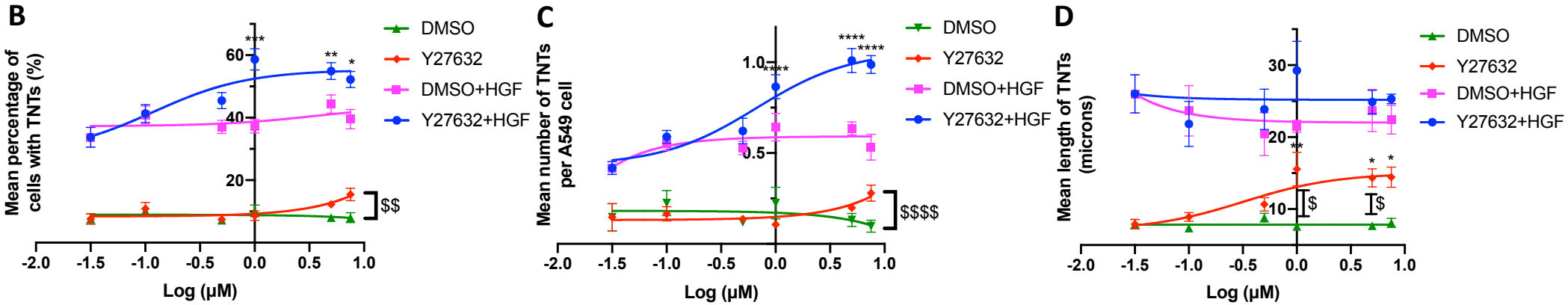


Figure 5.12: ROCK pathway inhibition induced an increase in the HGF-TNT formation A549 cells. A: Representative white light images of Y27632 (≤7.5μM) or DMSO with or without HGF (100ng/ml) treatment. The presence of Y27632 increased the presence of TNTs with a straight morphology (white arrows) and TNTs with a branched morphology (blue arrows) in both control and HGF-treated cells compared to DMSO-treated cells. White light images were captured using x10 objective on an inverted microscope. Scale bar, 10μm. B-D: The log dose curve showed a significant increase in HGF-induced TNTs in mean (B), number (C) and length (D) in the presence of Y27632 compared to HGF DMSO treated cells. Values are expressed as mean ± SEM, n=3 with at least 900 cells analysed per condition. *p<0.05, **p<0.01, ***p<0.001 and ****p<0.0001 when comparing HGF DMSO control with the concentrations of Y27632 in the presence of HGF. $$p$<0.05, $$$p$<0.01 and $$$$$p$<0.0001 when comparing DMSO and Y27632 treated cells at the respective concentrations.

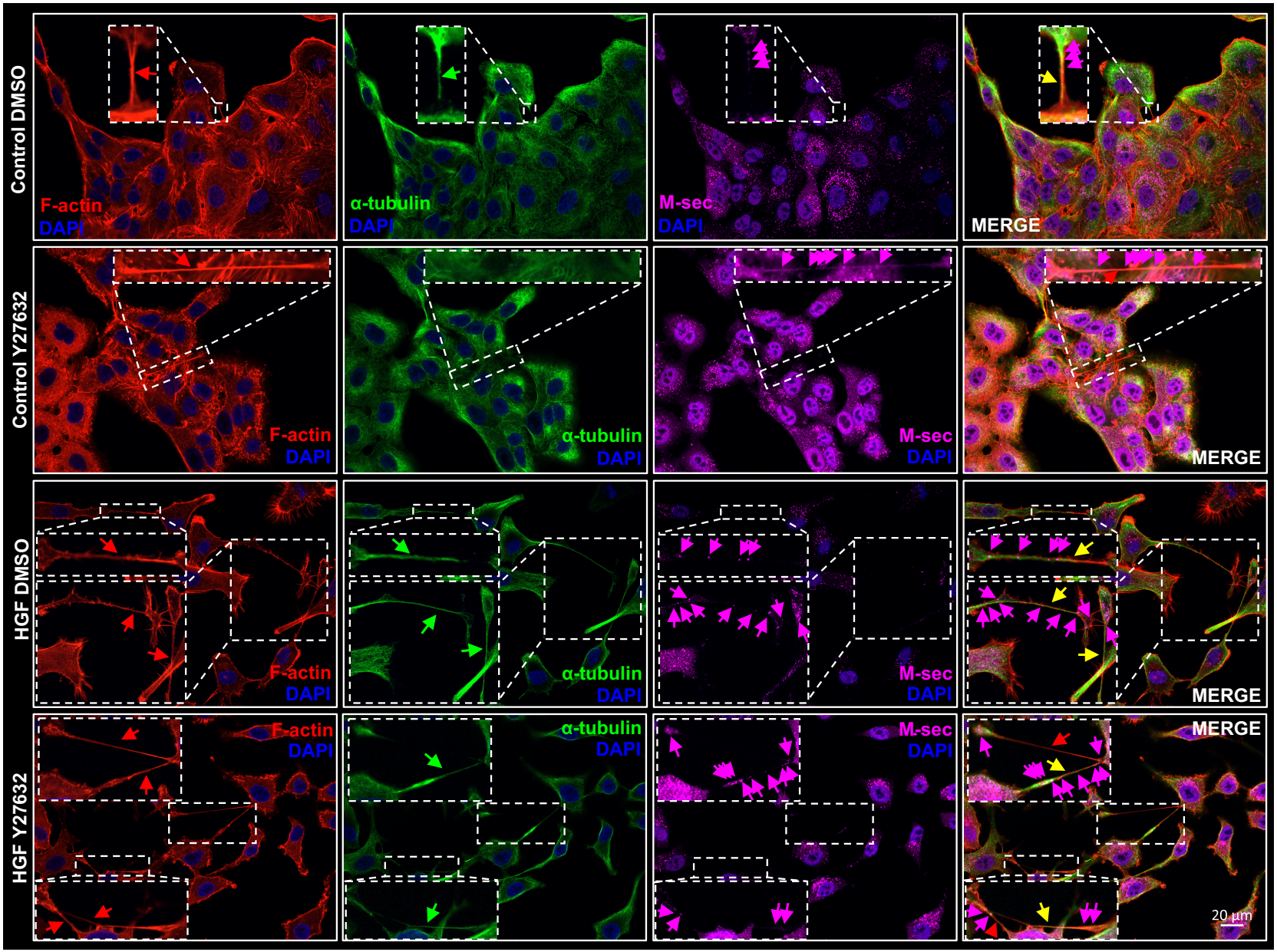


Figure 5.13: ROCK inhibition had no effect on the expression of F-actin, M-sec and α-tubulin positive TNTs. Representative Representative confocal images for immunofluorescent labelled F-actin (red arrow), α-tubulin (green arrow) and M-sec (pink arrow). The dotted region denotes a zoomed area. There is an increase between the F-actin and M-sec positive TNTs observed in the presence of Y27632 (5µM) compared to the HGF DMSO treated cells. M-sec labelling (pink arrow) at the protrusion site of TNTs confirm the presence of TNTs. Scale bar, 20µm.

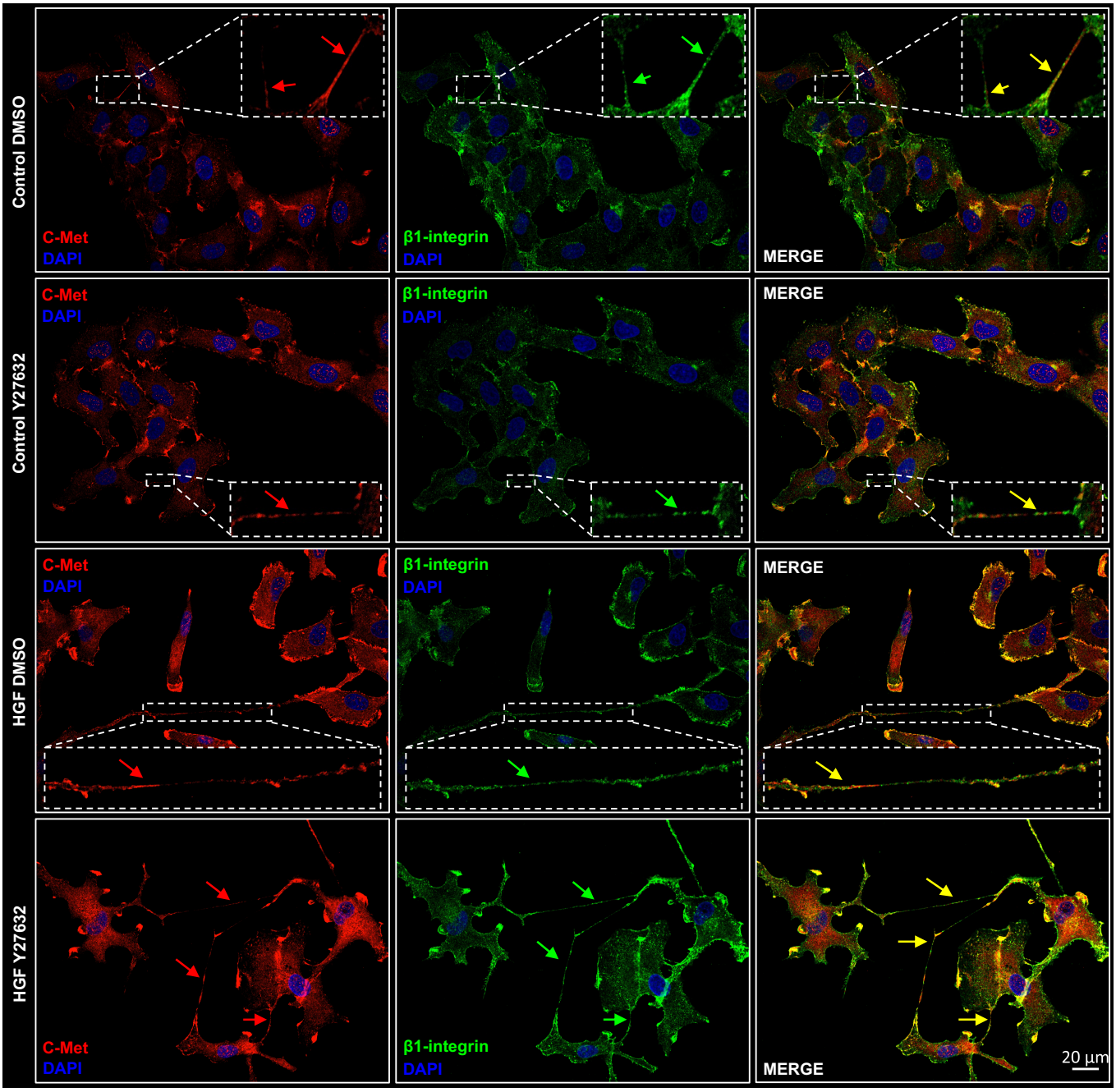


Figure 5.14: ROCK inhibition had no effect on the expression of c-Met and β1-integrin positive TNTs. Representative confocal images for immunofluorescent labelled c-Met (red arrow) and β1-integrin (green arrow) TNTs. There was an increase in the c-Met and β1-integrin positive TNTs observed in the presence of Y27632 (5µM) compared to HGF DMSO treated cells. Co-localisation of c-Met and β1-integrin labelled TNTs (yellow arrow) was observed at the protrusion site of the TNTs and along the length of the TNTs. Scale bar, 20µm.

5.2.7 MAPK, PI3K and Arp2/3 complex pathways mediate HGF-induced TNT formation

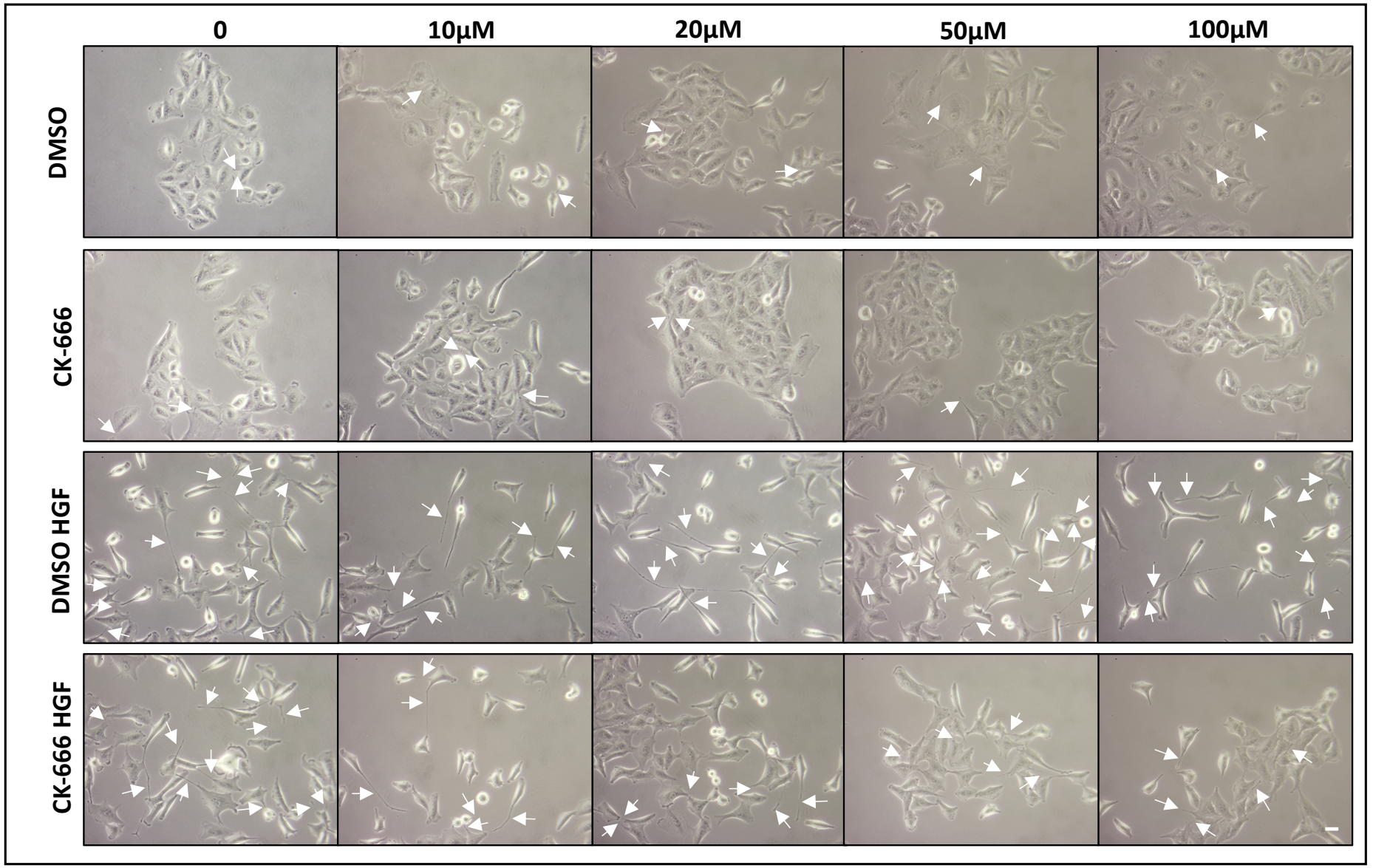
To investigate other pathways involved in regulating the HGF/c-Met/β1-integrin-mediated TNT formation, inhibitors of the MAPK, PI3K pathways and Arp2/3 complex were next used to determine the downstream pathways involved. The A549 cells were pre-treated with an Arp2/3 complex inhibitor (CK-666≤100µM) alongside its DMSO vehicle control and either treated further with HGF (100ng/ml) or in the absence of HGF for 24 hours. To ensure that the vehicle control, DMSO, did not affect the HGF-induced or basal TNT formation, cells were also pre-treated with the same volume of

DMSO used for the c-Met concentrations alongside control. The white light images showed an epithelial cell morphology and minimal TNTs (white arrow) present in cells treated with increasing concentrations of DMSO (10µM -100µM) and the Arp2/3 complex inhibitor (CK-666;10µM - 100µM)(Fig5.15A). There were also multiple TNTs (white arrow) present in the HGF-treated A549 cells in the presence of the Arp2/3 complex inhibitor at lower concentrations (CK-666;10µM and 20µM)(Fig5.15A). However, at higher concentrations of the Arp2/3 complex inhibitor (CK-666;50µM and 100µM), the cells reverted back towards an epithelial cell morphology and fewer TNTs (white arrows) were present (Fig5.15A). Quantification of the white light images showed DMSO and CK-666 treatment alone had no significant effect on TNT formation when compared to control (Fig5.15B-D). A dose-dependent decrease in HGF-induced TNTs in the presence of the Arp2/3 complex inhibitor across the three parameters (n=3,****p<0.001)(Fig5.15B-D). A significant (n=3, ****p<0.0001) decrease in HGF-induced mean (Fig5.15B), number (Fig5.15C) and length (Fig5.15D) of TNT was observed at 10µM CK-666 treatment before the curve plateaued between 20-100µM. Across the three parameters, CK-666 only partially inhibited the HGF-induced TNTs instead of fully inhibiting TNTs to basal levels (Fig5.15B-D).

After establishing the partial inhibitory effect of the Arp2/3 complex inhibitor on the HGF-induced TNTs, we next sought to determine whether a similar decrease was observed with immunofluorescent labelled TNTs with its characteristic markers (F-actin, α-tubulin and M-sec). A549 cells were pre-treated with either DMSO or CK-666 at 10µM, which was the lowest concentration where a significant decrease was observed from the white light studies(Fig5.15A-D). In the presence of DMSO and CK-666 alone, the cells displayed an epithelial cell morphology with minimal F-actin-labelled TNTs observed (red arrow)(Fig5.16). The TNTs observed in the cells treated with DMSO and CK-666 alone showed F-actin expressed throughout the entire TNT length (red arrow) and punctate M-sec labelling (pink arrow) at the protrusion site of the individual TNT (Fig5.16). In the HGF+DMSO-treated cells, there was an increase in F-actin-labelled TNTs (red arrows)(Fig5.16) and the cells displayed a fibroblast-like morphology (Fig5.16). Moreover, punctate M-sec labelling (pink arrow) was also observed at the protrusion site and along the length of the TNTs (Fig5.16). α-tubulin (green arrow) was also expressed at the thicker region of the TNT (Fig5.16) There were fewer F-actin (red arrow), M-sec (pink arrow) and α-tubulin (green arrow) expressing TNTs (red arrow) in the HGF+CK-666 treated cells compared to the HGF+DMSO treated cells (Fig5.16). Overall, the observations in the white light images (Fig5.15A) and immunofluorescent labelled images (Fig5.16) mirrored one another in the frequency of TNTs observed between the conditions and the immunofluorescent images confirmed the expression of characteristic expression of F-actin, α-tubulin and M-sec.

We next wanted to determine whether Arp2/3 complex inhibition also reduced the expression of β1-integrin and c-Met labelled TNTs. In the presence of DMSO and CK-666 alone, the cells displayed an epithelial cell morphology and minimal presence of β1-integrin (green arrow) and c-Met (red arrow) labelled TNTs (Fig5.17). In the HGF+DMSO-treated cells, there was an increase in c-Met (red arrow) and β1-integrin (green arrow) labelled TNTs and the cells displayed fibroblast-like morphology (Fig5.17). However, the HGF+CK-666-treated cells showed a decrease in c-Met (red arrow) and β1-integrin (green arrow) labelled TNTs when compared to the HGF+DMSO treated cells (Fig5.17). For all the TNTs observed, c-Met (red arrow) and β1-integrin (green arrow) expression was concentrated at the protrusion site of TNTs and along the TNT length (Fig5.3). Co-localisation of c-Met and β1-integrin (yellow arrow) was also observed at the protrusion site of TNTs and along the length of TNTs (Fig5.17). As the observations on white light images (Fig5.15A) reflect the observations in the c-Met and β1-integrin immunofluorescent images (Fig5.17), this confirms the presence of TNTs in our study.

A



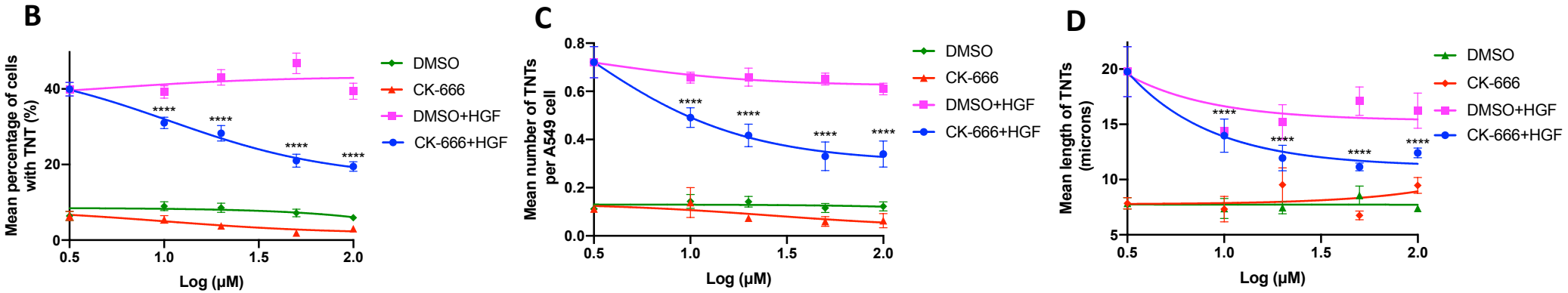


Figure 5.15: HGF induces TNTs *via* the Arp2/3 complex in A549 cells. A: Representative white light images of CK-666 (≤100μM) or DMSO with or without HGF (100ng/ml) treatment. There were fewer TNTs (white arrows) as the concentration of Arp2/3 complex inhibitor increased in comparison to the respective HGF+DMSO treated cells. White light images were captured using x10 objective on an inverted microscope. Scale bar, 10μm. B-D: The log dose curve shows a dose dependent decrease in HGF-induced TNTs in mean (B), number (C) and length (D) in the presence of CK-666 compared to HGF DMSO. Values are expressed as mean ± SEM, n=3 with at least 900 cells analysed per condition. ****p<0.0001 when comparing HGF DMSO control with the CK-666 treated concentrations in the presence of HGF.

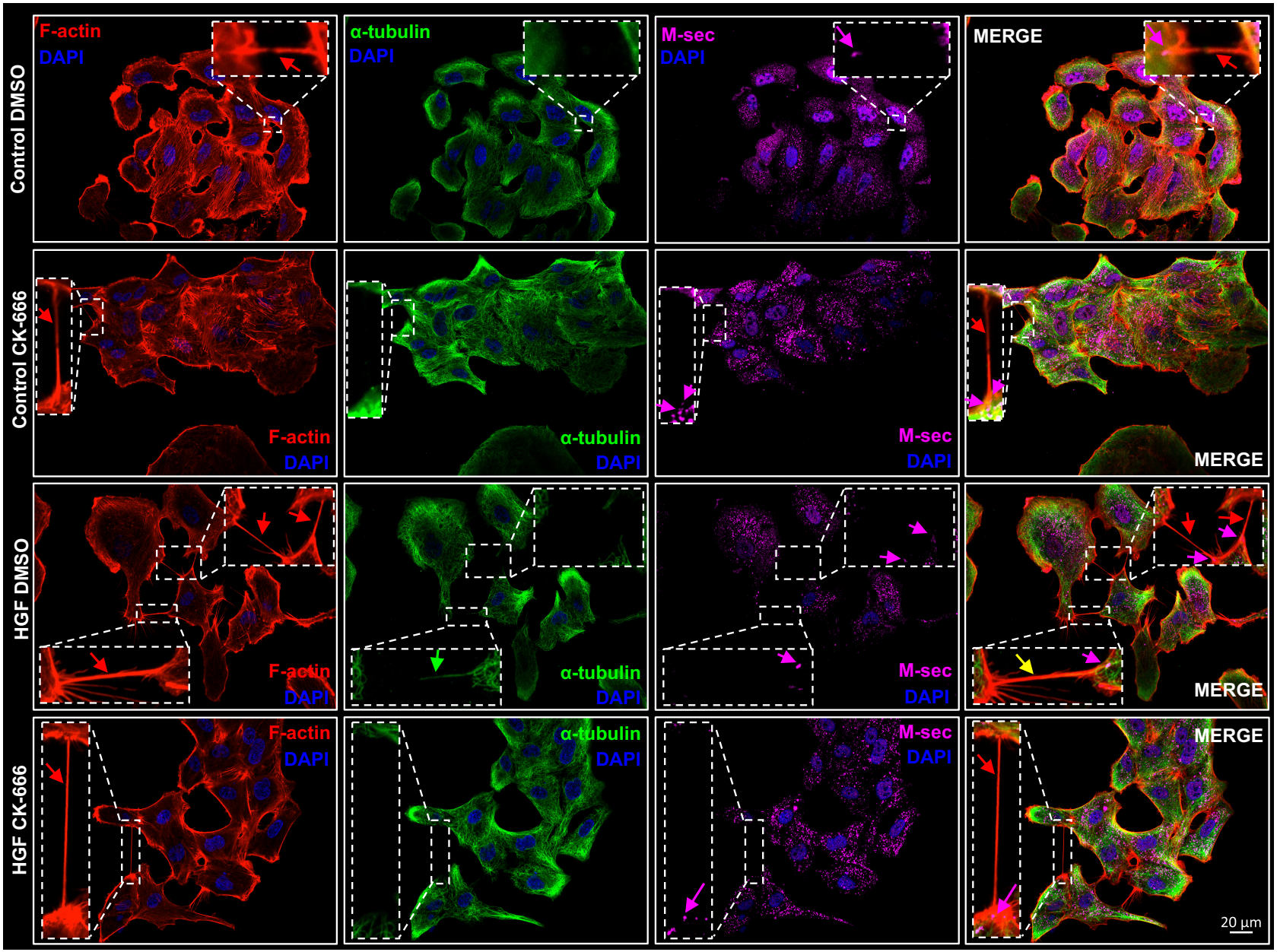


Figure 5.16: Arp2/3 complex inhibition reduced the expression of F-actin, M-sec and α-tubulin positive TNTs. Representative confocal images for immunofluorescent labelled F-actin (red arrow), α-tubulin (green arrow) and M-sec (pink arrow). The dotted region denotes a zoomed area. There are less F-actin and M-sec positive TNTs observed in the presence of CK-666 (10µM) compared to DMSO in HGF treated cells. M-sec labelling (pink arrow) at the protrusion site of TNTs confirm the presence of TNTs. Scale bar, 20µm.

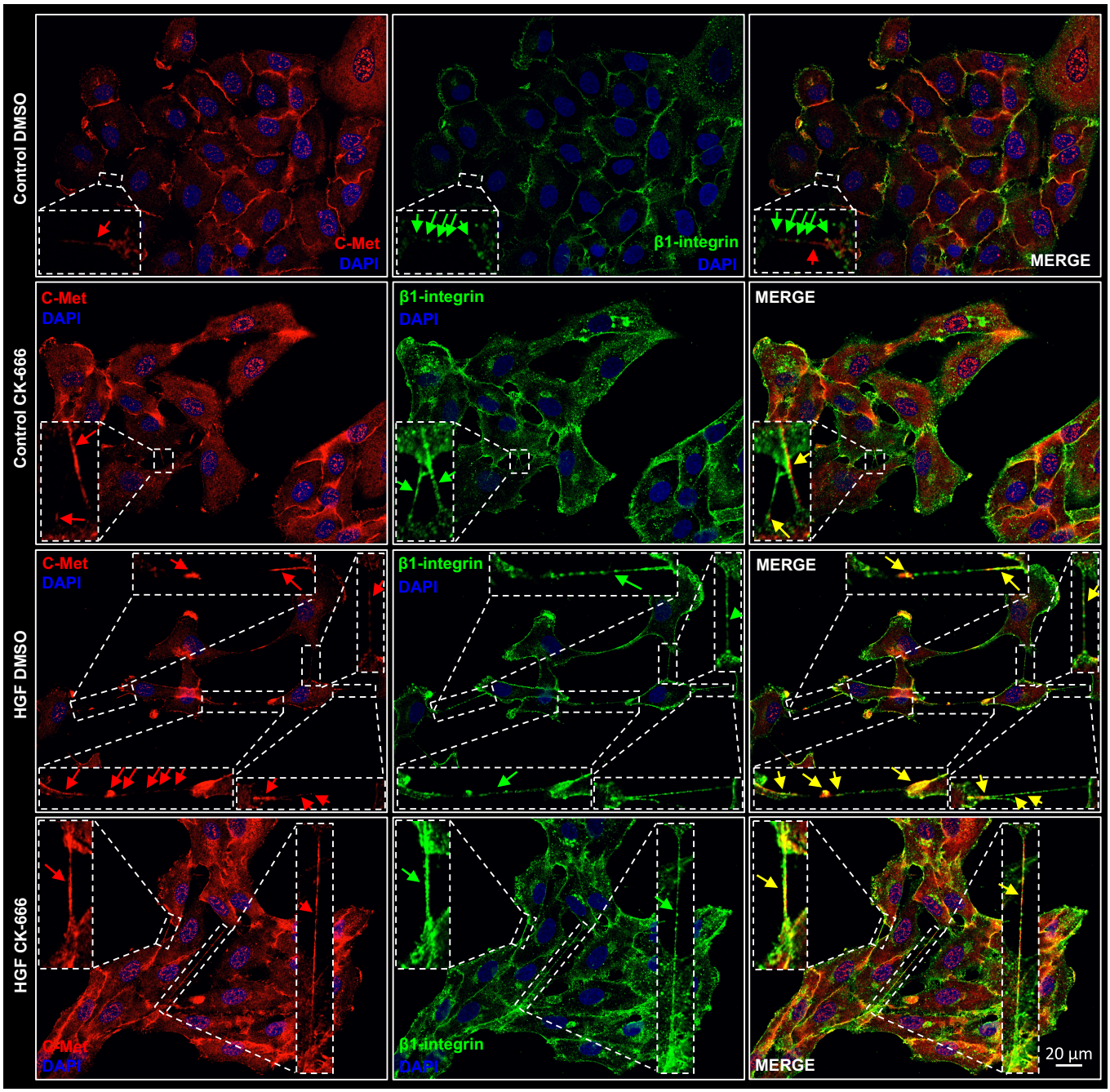


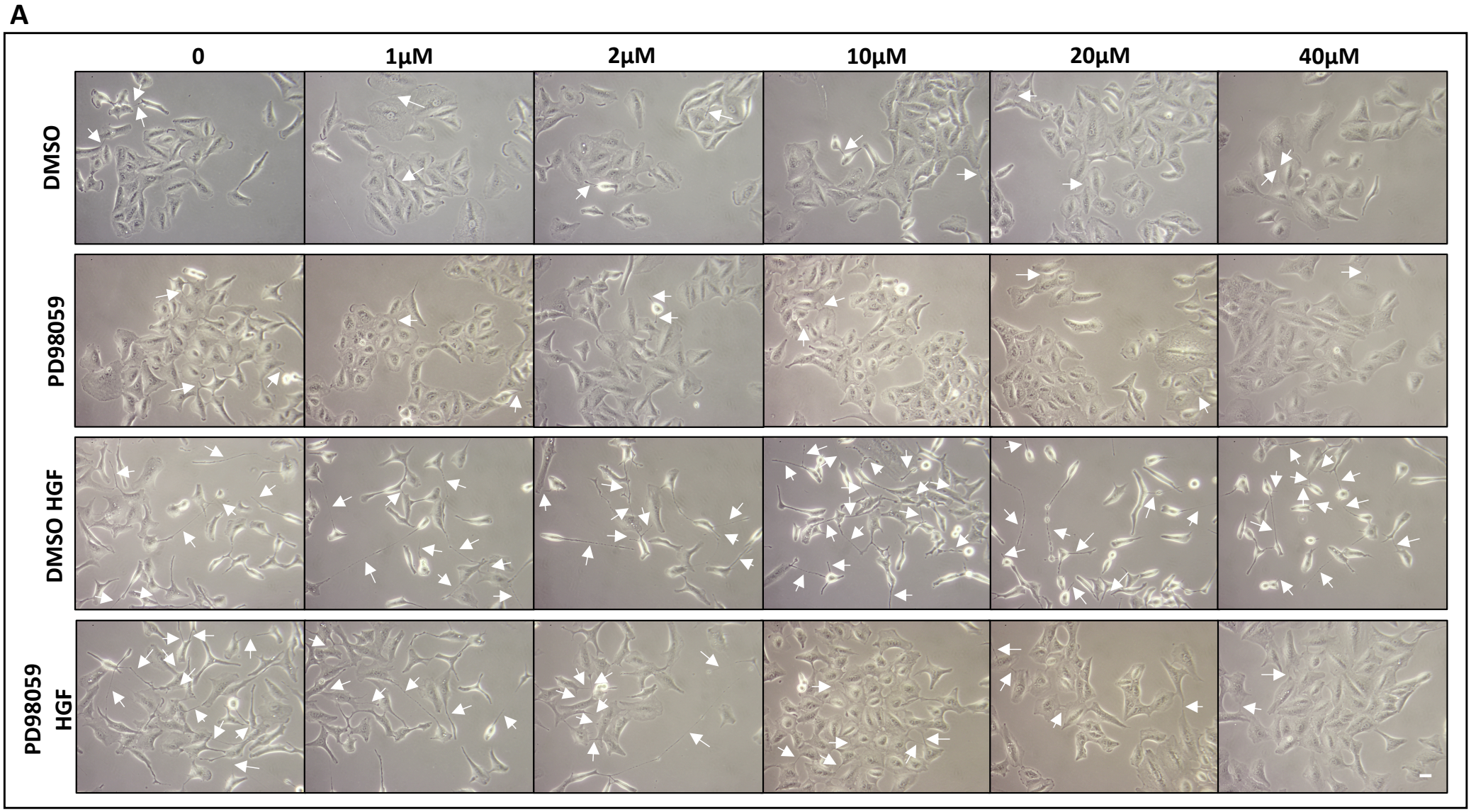
Figure 5.17: Arp2/3 complex inhibition reduced the localisation of c-Met and β1-integrin positive TNTs.. Representative confocal images for immunofluorescent labelled c-Met (red arrow) and β1-integrin (green arrow) TNTs. There are less c-Met and β1-integrin positive TNTs observed in the presence of CK-666 (10µM) compared to DMSO in HGF treated cells. Co-localisation of c-Met and β1-integrin labelled TNTs (yellow arrow) was observed at the protrusion site of the TNTs and along the length of the TNTs. Scale bar, 20µm

The cells were also pre-treated for 30mins with the MAPK pathway inhibitor (PD98059≤40μM) alongside its DMSO vehicle control and either treated further with HGF (100ng/ml) or in the absence of HGF for 24 hours. To ensure that the vehicle control, DMSO, did not affect the HGF-induced or basal TNT formation, cells were also pre-treated with the same volume of DMSO used for the MAPK concentrations alongside control. The white light images showed an epithelial cell morphology and minimal TNTs (white arrow) present in cells treated with increasing concentrations of DMSO (0-40μM) and the MAPK inhibitor (PD98059;0-40μM)(Fig5.18A). There were also multiple TNTs (white arrow) present in the HGF-treated A549 cells in the presence of increasing concentrations of DMSO (0-40μM)(Fig5.18A). The white light images also showed the increasing concentrations of the MAPK inhibitor caused a decrease in HGF-induced TNTs (shown by white arrows) compared to HGF DMSO treated cells (Fig5.18A). At higher concentrations of the MAPK inhibitors (20 μM and 40 μM) the HGF-treated cells reverted to an epithelial cell morphology observed in cell colonies, similar to the morphology of untreated DMSO control cells (Fig5.18A). Quantification of the white light images showed DMSO treatment alone had no significant effect on TNT formation when compared to control (Fig5.18B-D). There was a dose-dependent decrease in HGF-induced TNTs in the presence of the MAPK inhibitor across the three parameters (n=3,****p<0.001)(Fig5.18B-D). The log concentration-response curve for HGF+PD98059 treated cells showed an IC_{50} of 5μM, 3.5μM and 10μM in mean percentage (Fig5.18B), mean number of TNT per cell (Fig5.18C) and mean length (Fig5.16D) respectively. Across the three parameters, the curves plateaued to reach basal TNT levels at 20-40μM (Fig5.18B-D). Furthermore, inhibition of the MAPK pathway at the highest concentration (40μM) in the absence of HGF also resulted in a significant (n=3, $$$p$<0.01) decrease in the mean percentage of TNTs between DMSO and PD98059 (Fig5.18B). A significant decrease (n=3, $$$$$p$<0.0001) in the mean number of TNTs per cell between DMSO and PD98059 treated cells (Fig5.18C) was also observed.

After establishing the inhibitory effect of the MAPK inhibitor on the HGF-induced TNTs, we next determined whether a similar decrease was observed with immunofluorescent labelled TNTs with its characteristic markers (F-actin, α-tubulin and M-sec). A549 cells were pre-treated with either DMSO or PD98059 (20μM), to inhibit TNT formation to basal control levels, for 30 minutes before further treatment with HGF (100ng/ml) for 24 hours. In the presence of DMSO and PD98059 alone, the cells displayed an epithelial cell morphology with minimal F-actin-labelled TNTs observed (red arrow)(Fig5.19). The TNTs observed in the cells treated with DMSO and PD98059 alone showed F-actin expressed throughout the entire TNT length (red arrow), punctate M-sec labelling (pink arrow) at the protrusion site of the individual TNTs and α-tubulin (green arrow) expressed at the thicker region of the TNTs (Fig5.19). In the HGF+DMSO-treated cells, there was an increase in F-actin-

labelled TNTs (red arrows) and the cells displayed a fibroblast-like morphology (Fig5.19). Moreover, punctate M-sec labelling (pink arrow) was also observed at the protrusion site and along the length of the TNTs and α-tubulin (green arrow) was expressed throughout the thicker region of the TNTs (Fig5.19). There was a decrease in F-actin (red arrow), M-sec (pink arrow) and α-tubulin (green arrow) expressing TNTs in the HGF+PD98059 treated cells whilst the cells also displayed an epithelial cell morphology (Fig5.19). Overall, the observations in the white light images (Fig5.18A) and immunofluorescent labelled images (Fig5.19) mirrored one another in the frequency of TNTs observed between the conditions and the immunofluorescent images confirmed the expression of characteristic expression of F-actin, α-tubulin and M-sec.

We next determined whether MAPK inhibition also reduced the expression of β1-integrin and c-Met labelled TNTs. In the presence of DMSO and PD98059 alone, the cells displayed an epithelial cell morphology and minimal presence of β1-integrin (green arrow) and c-Met (red arrow) labelled TNTs (Fig5.20). In the HGF+DMSO-treated cells, there was an increase in c-Met (red arrow) and β1-integrin (green arrow) labelled TNTs and the cells displayed fibroblast-like morphology (Fig5.20). However, the HGF+PD98059-treated cells showed a decrease in c-Met (red arrow) and β1-integrin (green arrow) labelled TNTs and displayed an epithelial cell morphology (Fig5.20). For all the TNTs observed, c-Met (red arrow) and β1-integrin (green arrow) localisation was concentrated at the protrusion site of TNTs and along the TNT length (Fig5.20). Co-localisation of c-Met and β1-integrin (yellow arrow) was also observed at the protrusion site of TNTs and along the length of TNTs (Fig5.20). As the observations on white light images (Fig5.18A) reflect the observations in the c-Met and β1-integrin immunofluorescent images (Fig5.20), this confirms the presence of TNTs in our study.


A
0
1μM
2μM
10μM
20μM
40μM
DMSO
PD98059
DMSO HGF
PD98059 HGF

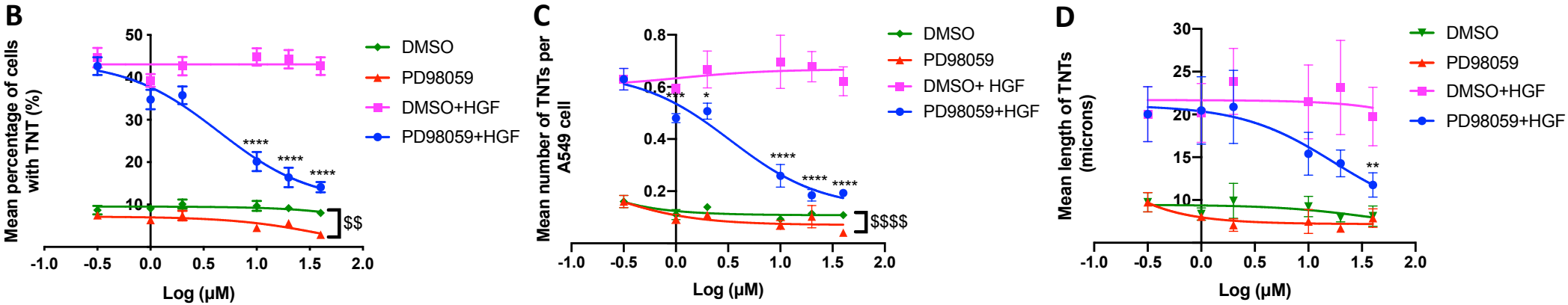


Figure 5.18: HGF induces TNTs *via* the MAPK pathway in A549 cells. A: Representative white light images of PD98059 (≤40μM) or DMSO with or without HGF (100ng/ml) treatment. There were fewer TNTs (white arrows) as the concentration of MAPK inhibitor increased in comparison to the HGF+DMSO treated cells. White light images were captured using x10 objective on an inverted microscope. Scale bar, 10μm. B-D: The log dose curve shows a dose-dependent decrease in HGF-induced TNTs in mean (B), number (C) and length (D) in the presence of PD98059 compared to respective HGF DMSO control. There was also a significant decrease in mean percentage (B) and mean number (C) of control TNTs between DMSO and PD98059 (40 μM). Values are expressed as mean ± SEM, n=3 with at least 900 cells analysed per condition. ***p*<0.01, and *****p*<0.0001 when comparing between HGF DMSO control and PD98059 concentrations in the presence of HGF. $$*P*<0.01 and $$$$*p*<0.0001 when comparing DMSO and PD98059 treated cells.

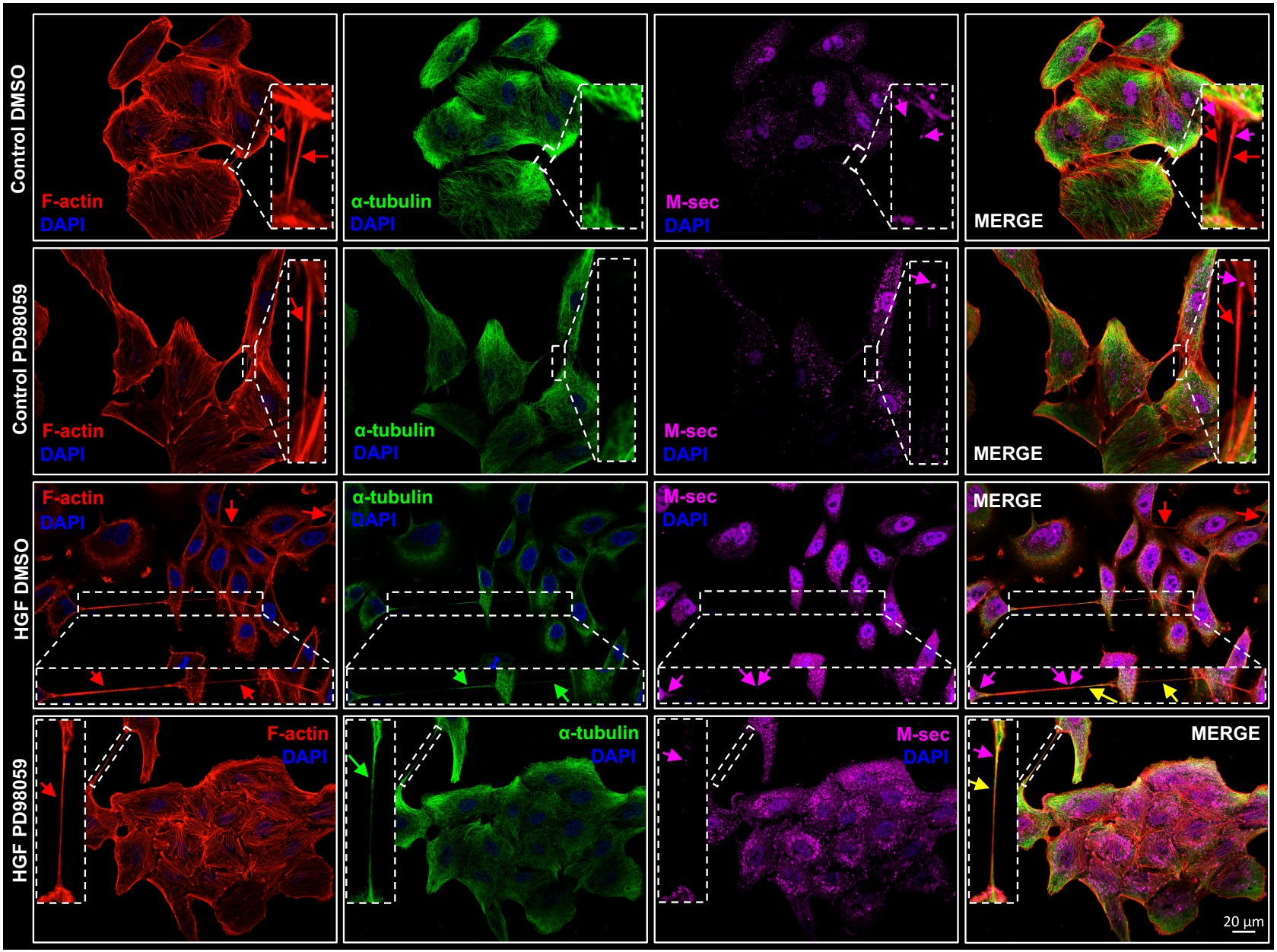


Figure 5.19: MAPK pathway inhibition reduced the expression of F-actin, M-sec and α-tubulin positive TNTs. Representative confocal images for immunofluorescent labelled F-actin (red arrow), α-tubulin (green arrow) and M-sec (pink arrow). The dotted region denotes a zoomed area. There are less F-actin and M-sec positive TNTs observed in the presence of PD98059 (20µM) compared to DMSO in HGF treated cells. M-sec labelling (pink arrow) at the protrusion site of TNTs confirm the presence of TNTs. Scale bar, 20µm.

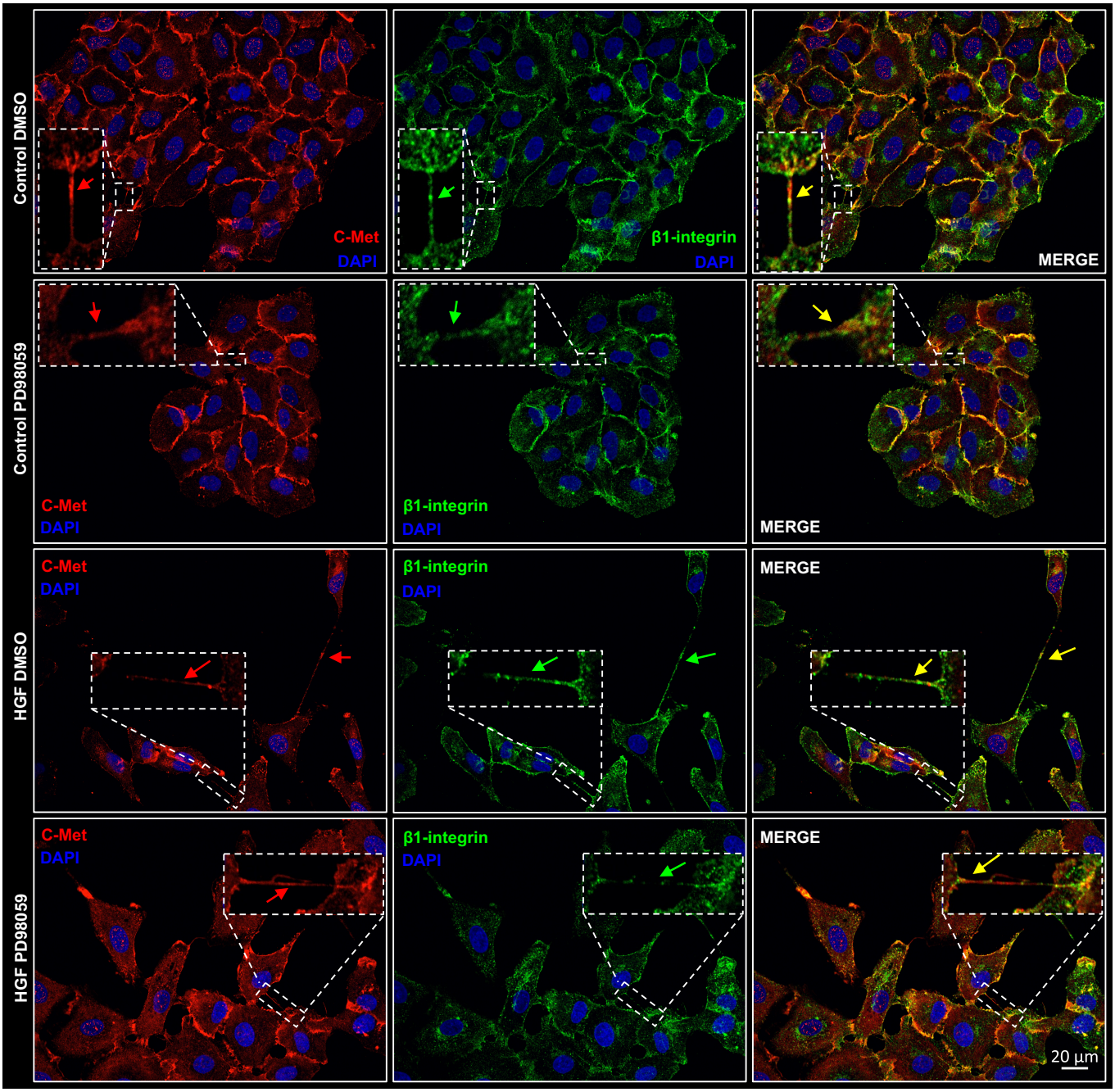


Figure 5.20: MAPK pathway inhibition reduced the localisation of c-Met and β1-integrin positive TNTs. Representative confocal images for immunofluorescent labelled c-Met (red arrow) and β1-integrin (green arrow) TNTs. The dotted region denotes a zoomed area. There are less c-Met and β1-integrin positive TNTs observed in the presence of PD98059 (20µM) compared to DMSO in HGF treated cells. Co-localisation of c-Met and β1-integrin labelled TNTs (yellow arrow) was observed at the protrusion site of the TNTs and along the length of the TNTs. Scale bar, 20µm.

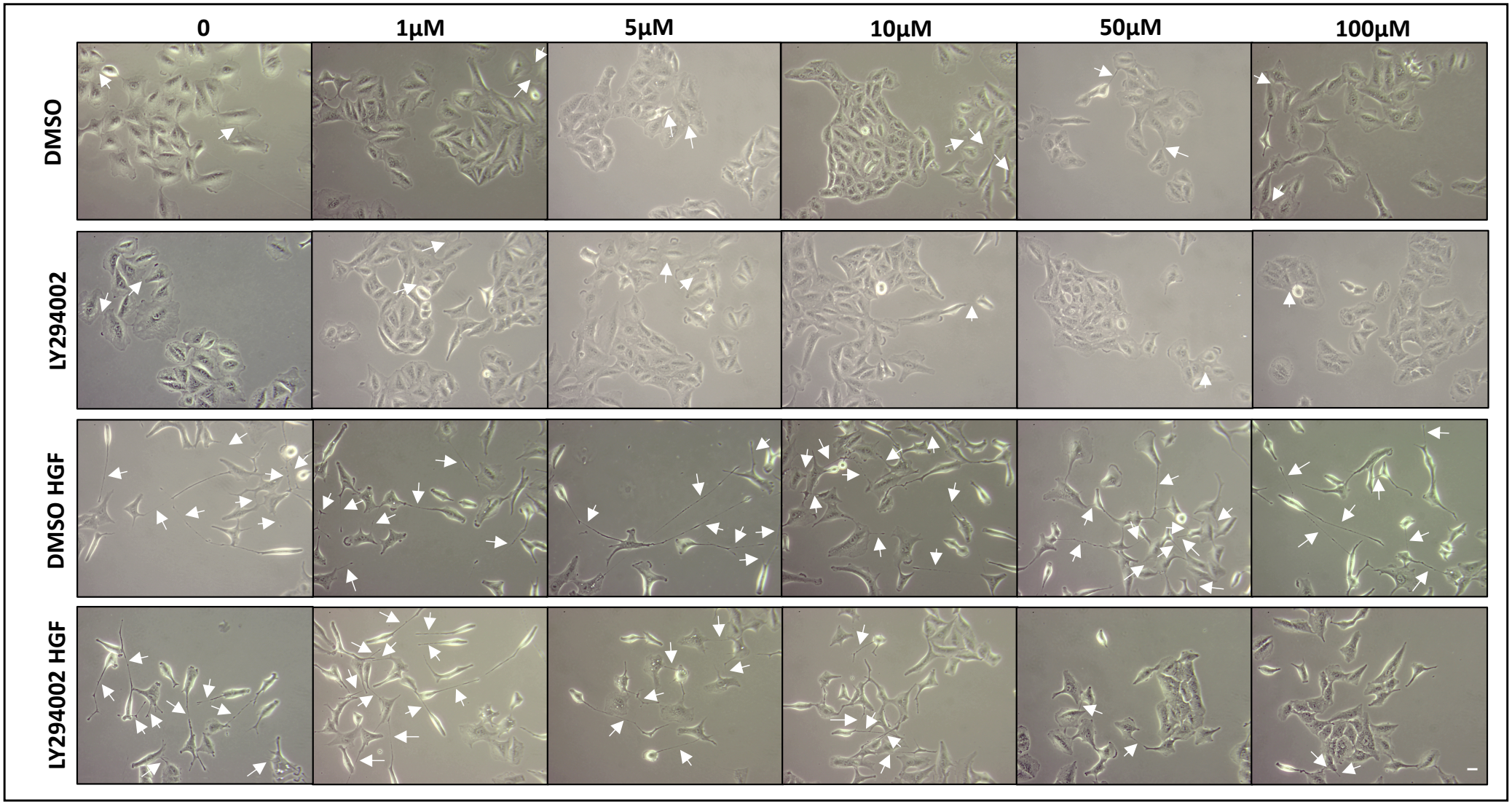
The cells were also pre-treated for 30mins with the PI3K pathway inhibitor (LY294002≤100µM) alongside its DMSO vehicle control and either treated further with HGF (100ng/ml) or in the absence of HGF for 24 hours. To ensure that the vehicle control, DMSO, did not affect the HGF-induced or basal TNT formation, cells were also pre-treated with the same volume of DMSO used for the PI3K inhibitor concentrations alongside control. The white light images showed an epithelial cell morphology and minimal TNTs (white arrow) present in cells treated with increasing concentrations of DMSO (0-100µM) and the PI3K inhibitor (LY294002;0-40µM)(Fig5.21A). There were also multiple TNTs (white arrow) present in the HGF-treated A549 cells in the presence of increasing concentrations of DMSO (0-100µM)(Fig5.21A). The white light images also showed the increasing concentrations of the PI3K inhibitor caused a decrease in HGF-induced TNTs (shown by white arrows) compared to HGF DMSO treated cells (Fig5.21A). At higher concentrations of the PI3K inhibitors (50 µM and 100 µM), the HGF-treated cells reverted to an epithelial cell morphology observed in cell colonies, similar to the morphology of untreated DMSO control cells (Fig5.21A). Quantification of the white light images showed DMSO treatment alone had no significant effect on TNT formation when compared to control across the three parameters (Fig5.21B-D). There was a dose-dependent decrease in HGF-induced TNTs in the presence of the PI3K inhibitor across the three parameters (n=3,****p<0.001)(Fig5.21B-D). The log concentration-response curve for HGF+LY294002 treated cells showed an IC_{50} of 10µM, 9µM and 22µM in mean percentage (Fig5.21B), mean number of TNT per cell (Fig5.21C) and mean length (Fig5.21D) respectively. Across the three parameters, the curves plateaued to reach basal TNT levels at 50-100µM (Fig5.21B-D). Furthermore, inhibition of the PI3K pathway at the highest concentration (10µM) in the absence of HGF also resulted in a significant (n=3, $$$$$p$<0.0001) decrease in the mean percentage of TNTs between DMSO and LY294002 (Fig5.21B).

After establishing the inhibitory effect of the PI3K inhibitor on the HGF-induced TNTs, we next determined whether a similar decrease was observed with immunofluorescent labelled TNTs with its characteristic markers (F-actin, α-tubulin and M-sec). A549 cells were pre-treated with either DMSO or LY294002 (50µM), to inhibit TNT formation to basal control levels, for 30 minutes before further treatment with HGF (100ng/ml) for 24 hours. In the presence of DMSO and LY294002 alone, the cells displayed an epithelial cell morphology with minimal F-actin-labelled TNTs observed (red arrow)(Fig5.22). The TNTs observed in the cells treated with DMSO and LY294002 alone showed F-actin expressed throughout the entire TNT length (red arrow), punctate M-sec labelling (pink arrow) at the protrusion site of the individual TNTs and α-tubulin (green arrow) expressed at the thicker region of the TNTs (Fig5.22). In the HGF+DMSO-treated cells, there was an increase in F-actin-labelled TNTs (red arrows) and the cells displayed a fibroblast-like morphology (Fig5.22). Moreover,

punctate M-sec labelling (pink arrow) was also observed at the protrusion site and along the length of the TNTs with α-tubulin (green arrow) expressed throughout the thicker region of the TNTs (Fig5.22). There was a decrease in F-actin (red arrow), M-sec (pink arrow) and α-tubulin (green arrow) expressing TNTs in the HGF+LY294002 treated cells whilst the cells also displayed an epithelial cell morphology (Fig5.22). Overall, the observations in the white light images (Fig5.21A) and immunofluorescent labelled images (Fig5.22) mirrored one another in the frequency of TNTs observed between the conditions and the immunofluorescent images confirmed the expression of characteristic expression of F-actin, α-tubulin and M-sec.

We next wanted to determine whether MAPK inhibition also reduced the expression of β1-integrin and c-Met labelled TNTs. In the presence of DMSO and LY294002 alone, the cells displayed an epithelial cell morphology and minimal presence of β1-integrin (green arrow) and c-Met (red arrow) labelled TNTs (Fig5.23). In the HGF+DMSO-treated cells, there was an increase in c-Met (red arrow) and β1-integrin (green arrow) labelled TNTs and the cells displayed fibroblast-like morphology (Fig5.23). However, the HGF+LY294002-treated cells showed a decrease in c-Met (red arrow) and β1-integrin (green arrow) labelled TNTs and displayed an epithelial cell morphology (Fig5.20).

For all the TNTs observed, c-Met (red arrow) and β1-integrin (green arrow) localisation was concentrated at the protrusion site of TNTs and along the TNT length (Fig5.23). Co-localisation of c-Met and β1-integrin (yellow arrow) was also observed at the protrusion site of TNTs and along the length of TNTs (Fig5.23). As the observations on white light images (Fig5.21A) reflect the observations in the c-Met and β1-integrin immunofluorescent images (Fig5.23), this confirms the presence of TNTs in our study.


A
0
1μM
5μM
10μM
50μM
100μM
DMSO
LY294002
DMSO HGF
LY294002 HGF

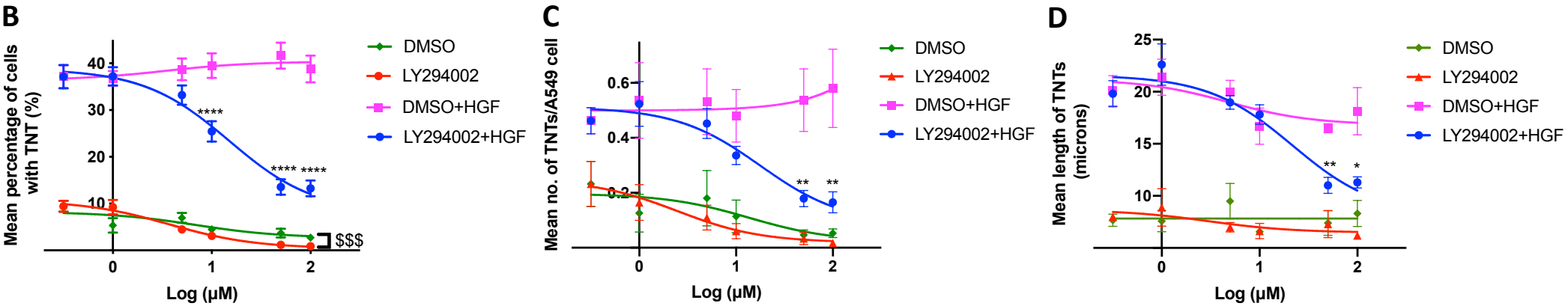


Figure 5.21: HGF induces TNTs *via* the PI3K pathway in A549 cells. A: Representative white light images of LY294002 (≤100μM) or DMSO with or without HGF (100ng/ml) treatment. There were fewer TNTs (white arrows) as the concentration of PI3K inhibitor increased in comparison to the DMSO+HGF treated cells. White light images were captured using x10 objective on an inverted microscope. Scale bar, 10μm. B-D: The log dose curve shows a dose dependent decrease in HGF-induced TNTs in mean (B), number (C) and length (D) in the presence of LY294002 compared to respective HGF DMSO control . There was also a significant decrease in mean percentage (B) TNTs between DMSO and LY294002 (100 μM). Values are expressed as mean ± SEM, n=3 with at least 900 cells analysed per condition. ***p*<0.01 and *****p*<0.0001 when comparing between HGF DMSO control and LY294002 concentrations in the presence of HGF. $$$$*p*<0.0001 when comparing DMSO and LY294002 treated cells.

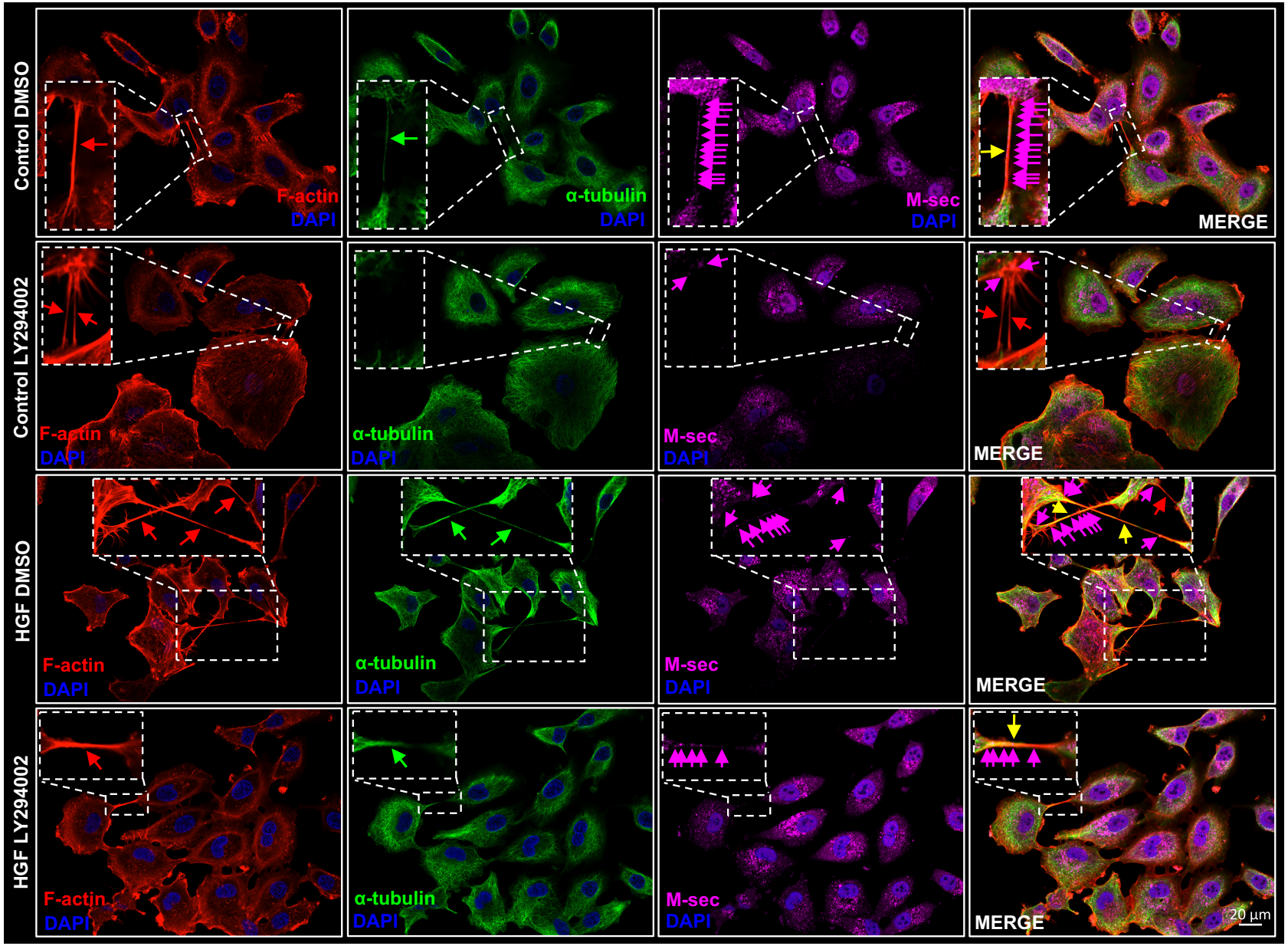


Figure 5.22: PI3K pathway inhibition reduced the expression of F-actin, M-sec and α-tubulin positive TNTs. Representative confocal images for immunofluorescent labelled F-actin (red arrow), α-tubulin (green arrow) and M-sec (pink arrow). The dotted region denotes a zoomed area. There are less F-actin and M-sec positive TNTs observed in the presence of LY294002 (50μM) compared to DMSO in HGF treated cells. M-sec labelling (pink arrow) at the protrusion site of TNTs confirm the presence of TNTs. Scale bar, 20μm.

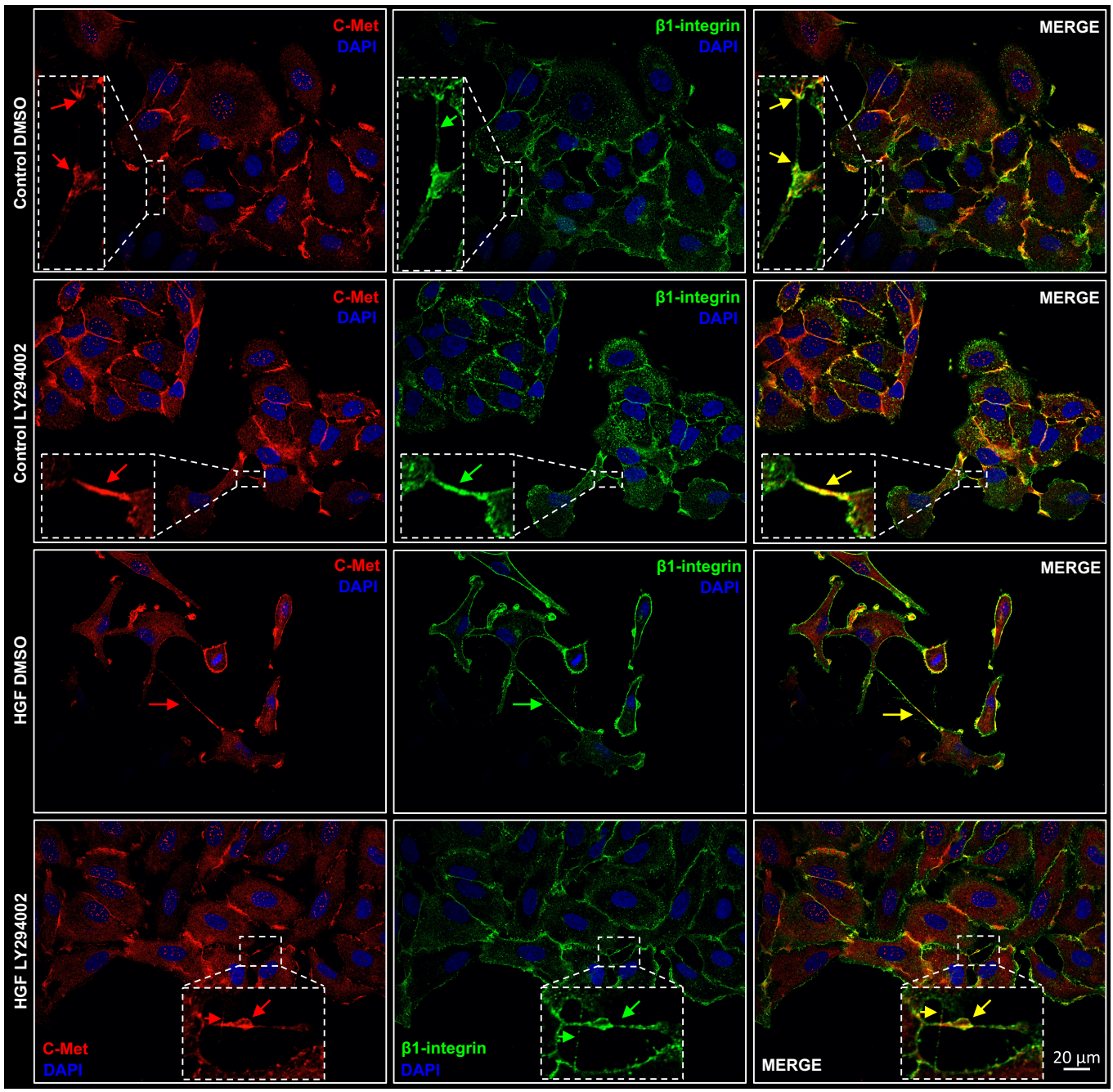


Figure 5.23: PI3K pathway inhibition reduced the localisation of c-Met and β1-integrin positive TNTs. Representative confocal images for immunofluorescent labelled c-Met (red arrow) and β1-integrin (green arrow) TNTs. The dotted region denotes a zoomed area. There are less c-Met and β1-integrin positive TNTs observed in the presence of LY294002 (50µM) compared to DMSO in HGF treated cells. Co-localisation of c-Met and β1-integrin labelled TNTs (yellow arrow) was observed at the protrusion site of the TNTs and along the length of the TNTs. Scale bar, 20µm.

5.3 Discussion

This work demonstrates a novel signalling axis between HGF/c-Met and β1-integrin in TNT formation of A549 cells. A pharmacological inhibitor approach was used to map out the upstream molecules and downstream pathways involved in the HGF-induced TNT formation. Use of a c-Met inhibitor PHA-665752 showed HGF ligand-dependent and autocrine ligand-independent activation of the c-Met receptor activation in TNT formation. The functionally blocking β1-integrin antibody inhibited HGF-induced TNTs demonstrating crosstalk activation with HGF/c-Met in TNT formation. Furthermore, knockdown of paxillin, through siRNA transfection, inhibited HGF-induced TNTs thus identifying paxillin recruitment in the HGF/c-Met/β1-integrin signalling axis. Lastly, the MAPK inhibitor PD98059, PI3K inhibitor LY294002 and Arp2/3 complex inhibitor CK-666 inhibited HGF-induced TNTs demonstrating the downstream pathways involved. This work has expanded the fundamental tumourigenic effects mediated by HGF/c-Met signalling, presenting a novel role in cellular communication *via* TNT formation.

5.3.1 HGF induces TNT formation through activation of its c-Met receptor

These findings demonstrate that HGF binds to the c-Met receptor and mediates TNT formation in A549 cells. The previous chapter revealed the discovery of c-Met as an integral novel component of TNTs in A549 cells (Chap 4, Fig4.13). The inhibition of the c-Met receptor showed a dose-dependent decrease in HGF-induced TNT formation to basal control levels. This confirms the ligand-dependent HGF activation of its receptor, c-Met, occurs to induce TNT formation. No other studies have investigated the HGF/c-Met signalling axis in regulating TNT formation. Immunofluorescent labelling of TNTs with their characteristic (F-actin, M-sec and α-tubulin) and novel components (c-Met and β1-integrin) further confirms the inhibited effect of c-Met-inhibited TNTs observed on white light.

Most studies in cancer have stimulated the formation of TNTs through subjecting the cells to inflammatory and stress conditions (e.g. hypoxia, acidic pH, H_20_2 exposure, serum starvation, UV and chemotherapy/radiotherapy-induced ROS production)(Kretschmer et al. 2019; Desir et al. 2018; Lou, Fujisawa, Morozov, et al. 2012; Hase et al. 2009; Wang et al. 2011; Rustom 2016). Currently, various actin regulators and motor proteins have been implicated in TNT formation however the signalling mechanisms have been found to vary between cell lines (Hase et al. 2009; Schiller et al. 2013). In our experimental system, the cells are seeded at a low density and are not subjected to serum starvation or nutrient deprivation. Therefore, our study provides a new perspective on TNT regulation whereby TNTs form due to the mutational upregulation of growth factor signalling rather than induced as part of a survival mechanism from stress conditions. Furthermore, using a higher concentration of the c-

Met inhibitor caused a significant decrease in basal TNT formation. Moreover, c-Met is overexpressed in A549 cells (Ma et al. 2004), therefore, our study suggests the potential role for c-Met in basal TNT formation *via* a ligand-independent autocrine route of activation (Yi et al. 1998; Yi and Tsao 2000). However, there is a reciprocal link between c-Met signalling and hypoxia and inflammation conditions of the TME. C-Met is transcriptionally activated by inflammatory cytokines and pro-angiogenic factors produced in the stroma of the tumour. The c-Met-driven cancer progression mainly occurs *via* gene amplification and point mutations of the receptor which results in a prolonged steady-state activation (Trusolino, Bertotti, and Comoglio 2010). However, HGF-dependent paracrine and autocrine signalling of c-Met has also been reported in NSCLC (Yi et al. 1998; Yi and Tsao 2000). Within the dynamic TME, the complex microenvironmental cues evolve throughout the development and growth of the tumour. Cancer-associated fibroblasts (CAFs) and immune cells including macrophages and neutrophils, are able to secrete HGF in response to hypoxic and inflammatory cues, therefore playing an active role in mediating the c-Met-mediated tumourigenic outcomes (Trusolino, Bertotti, and Comoglio 2010). Both ligand-dependent and independent activation of c-Met co-exist in the highly dynamic TME, and therefore emphasises the need for effective patient stratification in targeting HGF/c-Met activation in NSCLC.

Another unknown aspect of TNT formation are the factors mediating the direction of the TNT to fuse with its recipient cell. It is likely that the protrusive TNT are following a chemotactic gradient emitted from the target cell. In neurons and astrocytes, microscopic and proteomic studies revealed S100A4, an extracellular calcium-binding protein, and its receptor RAGE (receptor for advanced glycation end products) mediated the direction of TNT (Sun et al. 2012). This study showed that p53-induced caspase-3 activation led to the cleavage of S100A4 and therefore to maintain the concentration, the TNT-forming cell were guided to recipient cells with a higher concentration of S100A4 (Sun et al. 2012). A similar mechanism may be occurring in our study whereby receptor hyperactivation through gene amplification or point mutation, especially in the juxtamembrane domain containing Y1003 region involved in c-Cbl induces polyubiquitination and degradation of the receptor (Lee and Yamada 1995), causes the depletion of HGF-dependent concentration within the TNT-forming cells. Therefore, TNTs are guided towards recipient cells which produce HGF thus providing a chemotactic gradient for TNT direction. This may explain the higher proportion TNTs forming past the 12th-hour post-HGF stimulation, as TNTs only start to form after exhausting exogenous HGF in the media.

HGF/c-Met signalling is not only implicated in carcinogenesis in the lung but also in lung regeneration and wound healing (Crestani et al. 2012; Ohmichi et al. 1998; Ito et al. 2014). In homeostatic conditions, cytonemes have been found to mediate the formation of the imaginal disk of Drosophila flies (Ramírez-Weber and Kornberg 1999) and microtubule-containing TNTs also

contribute toward activating the Dpp signalling in germline stem cells (Inaba, Buszczak, and Yamashita 2015). Future time-lapse microscopy work can reveal whether HGF can induce TNT formation during wound closure of human alveolar epithelial cells.

5.3.2 HGF/c-Met crosstalk with β1-integrin to induce TNT formation in A549 cells

Inhibition of β1-integrin with a functionally blocking antibody also significantly decreased the HGF-induced TNT formation in A549 cells. This result coupled with the co-localisation between c-Met and β1-integrin along the TNT length and at the protrusion site of TNTs (Chap 4, Fig4.13) demonstrates crosstalk between HGF/c-Met and β1-integrin. Previous studies have highlighted the signalling cross-activation between HGF/c-Met and β1-integrin in mediating NSCLC anchorage-independent survival (Barrow-McGee, Kishi, et al. 2016b), chemoresistance (Ju and Zhou 2013), metastasis and invasion (Jahangiri et al. 2017). Moreover, FAK has been shown to regulate TNT formation via upregulating MMP-2 metalloprotease production in SCC cells (Sáenz-de-Santa-María et al. 2017). Focal adhesion sites are in direct contact between the neighbouring cell-cell contacts, the ECM microtubule and actin regulatory networks. Integrins localising at these focal adhesion sites are activated upstream of the signalling pathways regulating changes in the actin cytoskeletal dynamics (Case and Waterman 2015). An increase in TNT formation was also observed in breast cancer cells cultured on collagen I and fibronectin (Franchi et al. 2020). Although the role of integrins has been inferred in the TNT field, no studies have investigated the role of integrins in TNT formation. The HGF/c-Met/β1-integrin signalling axis has been implicated in the metastatic transformation of NSCLC cells. Therefore, inhibition of the HGF/c-Met/β1-integrin signalling axis may decrease TNT formation from impaired cell migration. The likelihood of TNT formation *via* the cell-to-cell dislodging mechanism would reduce with decreased cell migration. This was observed in another study when mesothelioma cells were cultured on bioengineered aligned ECM fibres. There was a positive correlation between the cell migration and the frequency of TNTs forming *via* the cell-to-cell dislodging mechanism (Jana et al. 2022). Although migration was not measured in this study to identify any correlation between TNT frequency in the presence of the functionally blocking β1-integrin antibody, it is likely that the decrease in migration contributes to the perturbation of the HGF/c-Met/β1-integrin-induced TNT formation. Moreover, the functionally blocking β1-integrin antibody can also inhibit the actin cytoskeletal dynamics driving TNT formation. In SCC cells, the FAK-inhibited TNTs did not correlate with reduced cell migration suggesting that TNT formation occurred through actin/ECM-remodeling or *via* a decrease in cell adhesion (Sáenz-de-Santa-María et al. 2017). The changes in actin dynamic and adhesion networks are often associated with the filopodia-forming mechanism of TNTs. Therefore, as both mechanisms of TNT formation exist in A549 cells, the reduction in TNT could be due to a combination of reduced migration and changes in actin/ECM dynamics. The role of β1-

integrin in regulating basal TNT formation was not investigated in this study therefore it would be of interest if a higher concentration of the functionally blocking β1-integrin antibody would cause a significant decrease in TNTs in untreated control cells.

5.3.3 Paxillin regulates the HGF/c-Met/β1-integrin-induced TNT formation

Our study presents a previously undiscovered role for paxillin in HGF/c-Met/β1-integrin-mediated TNT formation. In NSCLC, mutations and amplification of the paxillin gene result in its overexpression (Jagadeeswaran et al. 2008). C-Met activation induces the phosphorylation of the tyrosine residue of paxillin at the pY31 (CRKL-binding site) and thus mediates pro-tumourigenic migration and invasion (Parr et al. 2001). Integrin activation also results in the tyrosine phosphorylation of paxillin at the Tyr31, Tyr118, Ser188 and Ser190 regions (López-Colomé et al. 2017). HGF/c-Met and integrin cross-linking can trigger the formation of focal adhesions (Matsumoto et al. 1995) and has been shown to consequently phosphorylate paxillin which can then alters the cytoskeletal organisation of actin and mediate anchorage-independent survival *via* activation of the PI3K pathway (Maulik, Shrikhande, et al. 2002). Similarly, the crosstalk observed in our study between HGF/c-Met and β1-integrin induces the actin cytoskeletal reorganisation required for TNT formation *via* paxillin. As previous findings in our study showed paxillin (Chap 4, Fig4.14) localised only at the adherent protrusion site of the TNTs, this indicates the spatially restricted role for paxillin within the focal adhesions in initiating the HGF/c-Met/β1-integrin-mediated TNT formation. In SCC cells, paxillin and FAK bind to the cytoplasmic domain of β1-integrin upon binding to collagen IV (Crowe and Ohannessian 2004). However, paxillin can independently be recruited to focal adhesion sites without phosphorylation by FAK (Laukaitis et al. 2001). Paxillin localises at the leading edge of membrane protrusions as part of the early stages of focal adhesion formation (Laukaitis et al. 2001). This further supports the notion of paxillin being involved in the initial stages of TNT formation. Furthermore, paxillin can also bind to various adaptor proteins and multiple downstream signalling effectors through the activation of FAK (Crowe and Ohannessian 2004; Ishibe et al. 2003; Lai et al. 2000). Thus, paxillin acts as the link between the upstream and downstream players involved in the HGF/c-Met/β1-integrin-mediated TNT formation. The downstream signalling pathways associated with paxillin phosphorylation are further detailed in section 5.3.5.

5.3.4 HGF/c-Met/β1-integrin does not induce TNT formation *via* the CDC42, Rac1 and ROCK pathways

The mechanistic formation of TNTs requires the prerequisite protrusive polymerisation of the double-helical F-actin into parallel bundles. The organised geometry of actin filaments defines the type of protrusive structure formed, which ranges from lamellipodia, filopodia or TNT formation.

Various studies have relied on the actin regulatory mechanism involved in filopodia formation to aid in unravelling the mechanistic formation of TNTs as dorsal filopodia form a requisite to TNTs in various cell lines (Ljubojevic, Henderson, and Zurzolo 2021). The Rho GTPases (CDC42, Rac1 and RhoA) have been widely studied in TNT formation (as reviewed (Zhang, Kazanietz, and Cooke 2020). White light image quantification and immunofluorescent labelling in our study showed no significant decrease in the control or HGF-induced TNT formation in the presence of the CDC42 and Rac1 pathway inhibitors. Although the Rho GTPases have been implicated in TNT formation, mixed findings have been reported on their role in TNT formation. In RAW/LR5 macrophage cells, use of the same CDC42 and Rac1 inhibitors decreased the number of TNTs (Hanna, McCoy-Simandle, et al. 2017). The same study showed Rac1 localising along the entire TNT length however CDC42 was only found at the protrusion site and ends of the TNTs. Both WASP and WAVE, effectors of CDC42 and Rac1 respectively, were also activated during TNT formation in the RAW/LR5 macrophage cell line (Hanna, McCoy-Simandle, et al. 2017). Similarly another study looking at Jurkat T cells found CDC42 localising at the protrusion site of TNTs (Lachambre, Chopard, and Beaumelle 2014). TNT formation was also reduced when the dominant negative construct of CDC42 was transfected in HeLa cells (Hase et al. 2009). However, the same study also showed the dominant negative construct of Rac1 had no effect on TNT formation (Hase et al. 2009). Moreover in neuronal CAD cells, CDC42 and Rac1 inhibition caused a significant increase in TNT formation (Delage et al. 2016). These studies highlight the specific nature of the signalling pathways involved with the different cell lines. Furthermore, the molecular mechanisms underlying filopodia and TNT formation are distinct from one another. The filopodia forming CDC42/VASP/IRSp53 signalling network negatively regulates TNT formation and Eps8, a negative regulator of filopodia formation, induces TNT formation (Delage et al. 2016). This opposing mechanism suggests a possible paradigm shift occurring between favouring the formation of filopodia over TNTs or vice versa. However, it is unclear what regulatory processes cause the shift from the formation of one structure to another.

Our study also found a dose-dependent increase in control and HGF-induced TNT formation in the presence of the ROCK inhibitor (fig5.8). The role of the RhoA-ROCK-mediated signalling has been more consistently associated as a positive regulator for TNT formation in various cell lines. In trabecular meshwork cells, the same ROCK inhibitor (Y27632) increased TNT numbers and TNT-mediated vesicle transfer whilst inhibiting stress fibre formation (Keller 2020; Keller et al. 2017). An increase in TNT formation was also observed in the presence of the same ROCK inhibitor in mesothelioma cells cultured on ECM scaffolds (Jana et al. 2022) and in microglia cells alongside an increase in α-synuclein transfer. This is due to the ROCK inhibitor promoting TNT formation *via* Myosin II controlled F-actin regulation (Scheiblich et al. 2021). Therefore after characterising the

redundant role of the Rho-GTPases in TNT formation in A549 cells, we next used other HGF-associated pathway inhibitors to identify the signalling pathways involved.

5.3.5 HGF/c-Met/β1-integrin recruits paxillin to induce TNT formation *via* the MAPK, PI3K and Arp2/3 complex pathways

Our study shows that HGF/c-Met/β1-integrin induces TNTs *via* activation of Arp2/3 complex, MAPK and PI3K pathways. A partial decrease was observed in the presence of the Arp2/3 complex inhibitor. The signalling pathways involved in TNT regulation have been established to be fundamentally unique in different cell types. A partial decrease was observed in the presence of the Arp2/3 complex inhibitor. Similarly in macrophages, partial inhibition of TNT formation was also observed (Hanna, McCoy-Simandle, et al. 2017). Arp2/3 complex is involved in the formation of branched networks of actin, as most TNTs observed in our study have a straight morphology there would only be a partial inhibition. The branched morphology of HGF-induced TNTs only constitutes 6% of TNTs (Chap 4, Fig4.5). TNTs which only display the straight morphology, e.g. in neuronal CAD cells, do not rely on Arp2/3 complex activation during TNT formation (Sartori-Rupp et al. 2019). However, most surprisingly, previous results showed both CDC42 and Rac1 inhibitors had no effect on the control and HGF-induced TNT formation. The Arp2/3 complex is known to induce actin nucleation on existing F-actin filaments at the base of protrusions conventionally by CDC42 stimulated WASP or Rac1 stimulated WAVE activation (Takenawa and Suetsugu 2007). Alternatively, Arp2/3 complex may be activated *via* an ERK-dependent phosphorylation of WAVE (Mendoza et al. 2011). This mechanism of Arp2/3 complex activation has been observed in EGFR activation in the formation of lamellipodial protrusions (Mendoza et al. 2011). Another study promotes this notion, whereby the WAVE-Arp2/3 complex was shown to induce filopodia formation in HeLa cells (Beli et al. 2008) therefore this mechanism may occur as a prerequisite to the formation of TNTs. To confirm the WAVE-mediated phosphorylation of Arp2/3 complex involved in TNT formation, future studies knocking down the expression of WAVE with a siRNA could be undertaken. Therefore, a decrease in HGF-induced TNTs would confirm the role in the ERK-dependent phosphorylation of WAVE in activating the Arp2/3 complex.

MEK and PI3K inhibition also significantly decreased both basal and HGF-induced TNTs in our study, thus highlighting both signalling pathways as the main regulatory mechanism of TNT formation in A549 cells. The MAPK pathway has been implicated in TNT formation in several studies in various cell lines (Cole, Dahl, and Cowden Dahl 2021; Desir et al. 2019; Zhu et al. 2005). Interestingly, in ovarian cancer cells, the PI3K inhibitor did not inhibit TNT formation whereas inhibition of the MAPK pathway decreased the number of TNTs (Cole, Dahl, and Cowden Dahl 2021). This further highlights

the different molecular mechanisms underlying TNT formation in different cell types. Moreover, these studies used stress triggers to induce TNT formation in the various cell lines and there may be a different regulatory mechanism involved in growth factor-mediated TNT formation. Several studies have established the relationship between HGF/c-Met, β1-integrin, paxillin and both MAPK and PI3K pathways in mediating various other cellular effects. HGF/c-Met activation in mouse inner medullary collecting duct (miMCD-3) epithelial cells led to ERK-dependent phosphorylation of paxillin on Ser 83, thus implicating the paxillin-MAPK signalling as a vital point in regulating migration (Ishibe et al. 2004). Inhibition of HGF-induced ERK activation also perturbed the association between FAK and paxillin thus inhibiting the migratory effects (Liu et al. 2002). As the Rho GTPases are not involved in HGF/c-Met/β1-integrin-induced TNT formation, this may be one of the primary mechanisms involved in supporting the migration-dependent TNT formation *via* the paxillin-ERK-mediated focal adhesion turnover. Likewise, the PI3K pathway has been shown to be involved in TNT formation (Kretschmer et al. 2019; Wang et al. 2011). HGF/c-Met and β1-integrin-mediated phosphorylation of paxillin also resulted in the downstream convergent activation of the PI3K pathway (Ma et al. 2007). Akt also phosphorylates paxillin at the Ser173 region thus providing another direct link to the activation of the PI3K pathway (López-Colomé et al. 2017). Although the phosphorylation of paxillin and its signalling partners are well documented, how this process is coordinated to mediate the adhesion dynamics involved in migration, let alone in TNT formation, are not known. However, this study demonstrates the potential importance of ERK in mediating the Arp2/3 complex activation and in sustaining the paxillin-MAPK/PI3K activation. There may also be an exocyst complex-mediated mechanism of TNT formation. The exocyst complex subunit Exoc7 (Exo70) can associate with the Arp2/3 complex (Liu et al. 2012). Furthermore, PIP2 can bind with Exoc1 and Exoc7 subunits recruiting the exocyst complex to the cell membrane (Martin-Urdiroz et al. 2016), thus potentially inducing TNT formation *via* both Arp2/3 complex and PI3K pathway.

5.3.6 Future work

A pharmacological approach was undertaken in this study to determine the signalling pathways involved in the HGF-dependent TNT formation. Whilst we were able to conclude HGF/c-Met/β1-integrin activated the Arp2/3 complex, MAPK and PI3K downstream pathways *via* paxillin to induce TNT formation in A549 cells, the study was limited by the specificity of pharmacological inhibitors commercially available. It would be of interest for future studies to use the monoclonal antibodies or drugs in clinical trials for combined therapeutic targeting of c-Met, β1-integrin, Arp2/3 complex, MAPK and PI3K pathways with nanoparticles. This mode of localised drug delivery for NSCLC is advantageous in limiting toxicity, enhancing efficacy and preventing the development of chemotherapeutic resistance from prolonged treatments in patients (Gurunathan et al. 2018). These

nanoparticle drug systems have been tested in vitro in several cancer cell lines (Buchner et al. 2019) however it would be of interest to see whether in vivo use of combination therapy in nanoparticles would inhibit TNT formation in resected lung tumours screened with high c-Met activation.

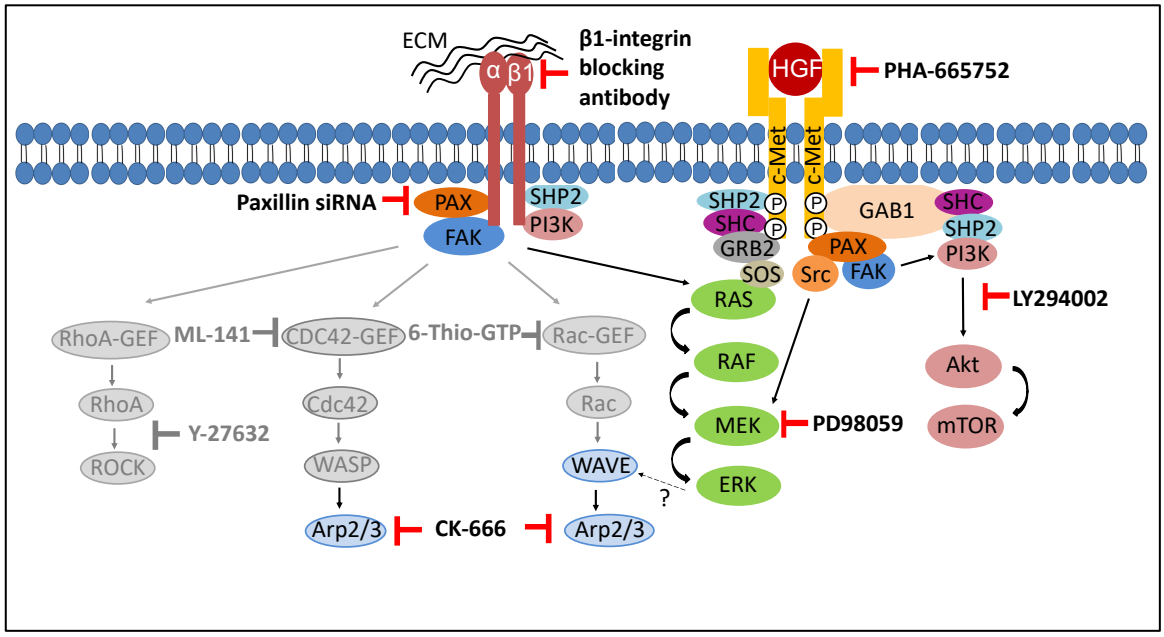


Figure 5.24: HGF/c-Met and β1-integrin signalling axis drives TNT formation in A549 cells.

Paxillin is recruited after HGF/c-Met and β1-integrin activation and acts as a scaffold protein to activate the PI3K and MAPK pathways. The Rho GTPase-associated pathways (Rho, CDC42 and Rac1) are not involved in A549 TNT formation however the Arp2/3 complex mediates the branched morphology of TNTs. This may occur *via* ERK-mediated phosphorylation of WAVE.

5.4 Conclusion

This study shows a novel co-activation between HGF/c-Met and β1-integrin in inducing TNT formation *via* recruitment of paxillin and downstream activation of Arp2/3 complex, MAPK and PI3K pathways. This highlights the need for a more personalised approach in NSCLC treatment.

The next chapter will look at the potential signalling crosstalk between HGF and other upregulated cytokines in the TME of NSCLC in TNT formation of A549 cells. These pleiotropic cytokines, including IL-6, FGF2 and EGF, are mutationally upregulated in NSCLC and contribute towards pro-tumourigenic effects. Investigations to investigate whether these pleiotropic cytokines can induce TNT formation and whether an additive or synergistic effect with HGF was observed in TNT formation.

6. Chapter 6: Crosstalk between HGF and EGF in TNT formation of A549 cells

6.1 Introduction

Tumour development relies on the accumulation of genetic alterations to upregulate a combination of pleiotropic growth factor signalling to create a hyperproliferative, inflammatory and invasive tumour microenvironment. In NSCLC, aside from enhanced mutational overexpression of HGF and c-Met and EGFR genes are most prevalently reported (Ding et al. 2008). Likewise, with HGF, EGF overexpression is associated with a poor prognosis, inducing pro-tumourigenic biological effects including increased proliferation, migration, and invasion (Gately et al. 2014). Moreover, EGF/EGFR signalling is the only growth factor implicated in TNT formation in cancer. Studies in astrocytes have demonstrated p53 activation, from cellular insults, leads to the upregulation of EGFR receptors which then activates the Akt-PI3K-mTOR pathway required for F-actin polymerisation and TNT formation (Wang et al. 2011). Furthermore, in mesothelioma cells (Lou, Fujisawa, Morozov, et al. 2012), breast cancer cells (Carter et al. 2019) and ovarian cancer cells (Cole, Dahl, and Cowden Dahl 2021), EGF was used to stimulate the formation of TNTs. Currently, the poor prognosis of NSCLC has been attributed to the late diagnosis of the disease and a lack of efficacious therapies. Although specific drug targeting of EGFR TKIs has led to the development of licensed gefitinib and erlotinib treatment (Fukuoka et al. 2003; Zhou et al. 2011), clinical trials of other EGFR inhibitors have had limited success (Sridhar, Seymour, and Shepherd 2003). Moreover, clinical trials in conjunction with targeting both EGF/EGFR and HGF/c-Met signalling have also demonstrated poor results. The randomised phase III trials comparing onartuzumab (Spigel, Edelman, O'Byrne, Paz-Ares, et al. 2017) and tivantinb (a MET inhibitor) (Scagliotti et al. 2015) with EGFR inhibitor erlotinib for patients with advanced NSCLC have been unsuccessful. As the pro-tumourigenic profiles of HGF and EGF mirror one another, a cooperative crosstalk signalling may exist between both growth factors to induce TNT formation. Several studies have demonstrated synergistic activation between HGF and EGF in mediating proliferation, migration and invasion in various cancers (Zhou, Pon, and Wong 2007; Puri and Salgia 2008). HGF-dependent c-Met activation has also been shown to rescue colorectal cells from the effects of EGFR inhibition (Liska et al. 2011). Furthermore, TNT formation has been implicated in the survival of cancer cells, propagating resistance and the malignant transformation of recipient cells (as reviewed in (Pinto, Brou, and Zurzolo 2020). This highlights the importance of multi-drug targeting to optimally inhibit the effects induced by EGF or HGF as TNTs may serve as a mechanism for chemoresistance from EGFR and c-Met inhibitors.

Aside from EGF, other pleiotropic cytokines are implicated in NSCLC progression. Cytokines that induce EMT are also implicated in TNT formation (Lou, Fujisawa, Morozov, et al. 2012). However, no other studies have investigated the role of various other upregulated cytokines in inducing TNT formation in NSCLC. Another growth factor and its receptor, FGF/FGFR signalling has been recently shown to facilitate the development and progression of NSCLC. Similarly to HGF and EGF, mutational amplification of FGFR1 and its serum FGF2 levels has been correlated with poor prognosis whilst supporting invasion and growth in NSCLC (Bremnes, Camps, and Sirera 2006; Donnem et al. 2012; Müller-Tidow et al. 2005). FGF was also used to stimulate the formation of mesothelioma cells in one study (Lou, Fujisawa, Morozov, et al. 2012). Therefore, there may be crosstalk between HGF/c-Met and FGF2/FGFR in TNT formation. Several clinical trials targeting FGFR are ongoing in NSCLC, although only a minimal effect was observed in a phase II trial with a non-selective FGFR inhibitor (AZD4547) in patients with FGFR upregulation or mutation (Aggarwal et al. 2017). Although other members of the FGF family can bind to FGFRs (Ornitz and Itoh 2015), initial studies will investigate the role of FGF2 in TNT formation.

Furthermore, IL-6 shares similar biological properties with HGF and EGF, influencing NSCLC growth and EMT (Lee et al. 2016; Zheng et al. 2019). Circulating levels of IL-6 also act as a biomarker for predictive poor prognosis and response to NSCLC therapies(Pine et al. 2011; Silva et al. 2017). A549 cell lines have been shown to express IL-6 mRNA and protein (Bihl et al. 1998) additionally high levels of IL-6 and its receptor component gp80/IL-6R and gp130 are expressed in NSCLC (Haura, Livingston, and Coppola 2006). However, the role of IL-6 has not been explored in the context of TNT formation despite its dual role in inflammation and EMT. Moreover, there has been more progress in targeting IL-6 in NSCLC. The Phase I and II clinical trials with humanised anti-IL-6 antibody, ALD518, has shown improvement in NSCLC-associated anaemia and cachexia (Bayliss et al. 2011). Siltuximab is another monoclonal antibody which showed a reduction in NSCLC tumour growth *via* inhibiting STAT3 phosphorylation (Song et al. 2011). Therefore, with the current promising outlook on the development of IL-6 therapies, there may be a potential novel effect in TNT formation implicated in the reduction of tumour growth or chemoresistance.

Although there are numerous other upregulated cytokines present within the TME that can be targeted, different patients will harbour different amplification of genes. Therefore, the best personalised strategy would involve stratifying patient populations accordingly to the mutation they harbour which will then inform the best combination of drugs required. Potential synergistic, additive or convergent signalling between the different cytokines needs to be investigated to ensure optimal inhibition of pro-tumourigenic effects, including the role between HGF and IL-6 in growth (as

explored in Chapter 3) and potential novel effects of IL-6 or FGF2 in TNT formation. This will further inform the strategies required to prevent the emergence of chemoresistance.

The aim of this chapter was to identify any crosstalk signalling present between HGF and other upregulated cytokines present in the TME of NSCLC in mediating A549 cell TNT formation. The effect of IL-6, FGF2 and EGF on TNT formation were individually assessed in A549 cells. This chapter demonstrates a previously unrecognised convergent signalling between HGF and EGF in A549 cell TNT formation and only a full inhibitory effect in the presence of both MAPK and PI3K pathway inhibitors in HGF+EGF-treated cells. Some of the work in this chapter was conducted by two Msc project students: Amy Judge and Frances Perrett under my supervision. Their individual contributions are highlighted throughout the results section.

6.2 Results

6.2.1 IL-6 has no discernible effect on TNT formation in A549 cells

Lou and his colleagues were the first to discover cytokines that can induce EMT are also implicated in TNT formation (Lou, Fujisawa, Morozov, et al. 2012). IL-6 has been shown to induce EMT in A549 cells (Lee et al. 2016) however, there have been no studies to date exploring its potential role in TNT formation. To establish whether IL-6 could induce TNTs in A549 cells, cells were seeded ($5x10^4$ cells/well) and after 24 hours were treated with IL-6 (100ng/ml) for another 24 hours. White light images were captured on an inverted microscope before image analysis was undertaken to quantify TNT formation. The white light images show an oval epithelial cell morphology in control and in the IL-6-treated cells whereas the HGF and IL-6+HGF-treated cells display an elongated fibroblast-like morphology (Fig6.1A). Moreover, there was no increase in TNTs (white arrow) observed between the control and IL-6-treated A549 cells (Fig6.1A). There was an increase in TNTs (white arrow) observed in the HGF and IL-6+HGF-treated cells (Fig6.1A). White light image quantification showed HGF induced a significant (n=3, **** p<0.0001) increase in the mean percentage (Fig6.1B), mean number of TNT/cell (Fig6.1C) and mean length (Fig6.1D) when compared to control. HGF+IL-6 treatment also induced a significant increase in the mean percentage (Fig6.1B), mean number of TNT/cell (Fig6.1C) and mean length (Fig6.1D) when compared to control. However, there was no significant increase in TNT formation between control and IL-6-treated cells in mean percentage (control 7.2%±1.4; IL-6 11.9%±2.5)(Fig6.1B), mean number of TNT/cell (control 0.09±0.01; IL-6 0.1±0.01)(Fig6.1C) and mean length (control 17.6µm±3.1; IL-6 17.6µm±0.01)(Fig6.1D).

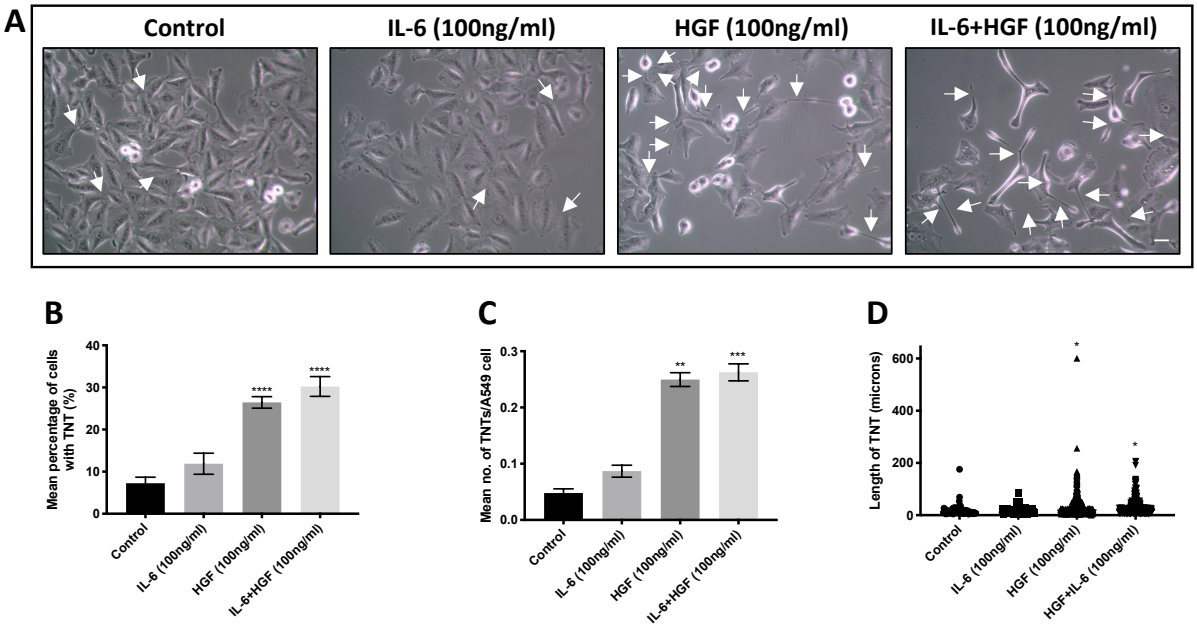


Figure 6.1: IL-6 does not induce TNT formation in A549 cells. A: Representative white light images show no increase in TNTs (white arrow) in IL-6-treated cells compared to control. White light images were captured using x10 objective lens on an inverted microscope. Scale bar:10µm. B-D: The white light images were quantified for TNTs and the histogram (B, C) and scatter plot (D) display the mean percentage (B), mean number of TNT/cell (C) and length of TNTs (D). Values are expressed as mean ± SEM, n=3, with at least 500 cells analysed per condition.

6.2.2 FGF2 has no discernible effect on TNT formation in A549 cells

We next wanted to confirm whether FGF2 could induce TNTs in A549 cells as FGF2 was used previously in mesothelioma cells to induce TNTs (Lou, Fujisawa, Morozov, et al. 2012). To investigate whether FGF2 could induce TNTs in A549 cells, cells were seeded and after 72 hours were treated with increasing concentrations of FGF2 (0-300ng/ml) for another 24 hours. White light images were captured on an inverted microscope before image analysis was undertaken to quantify TNT formation (Fig6.2A-D). There was no increase in TNTs (white arrow) observed between the control and the different concentrations of FGF2-treated cells (Fig6.2A). There was also no dose-dependent increase in TNT formation between control and FGF2-treated cells in mean percentage (Fig6.2B), mean number of TNT/cell (Fig6.2C) and mean length (Fig6.2D).

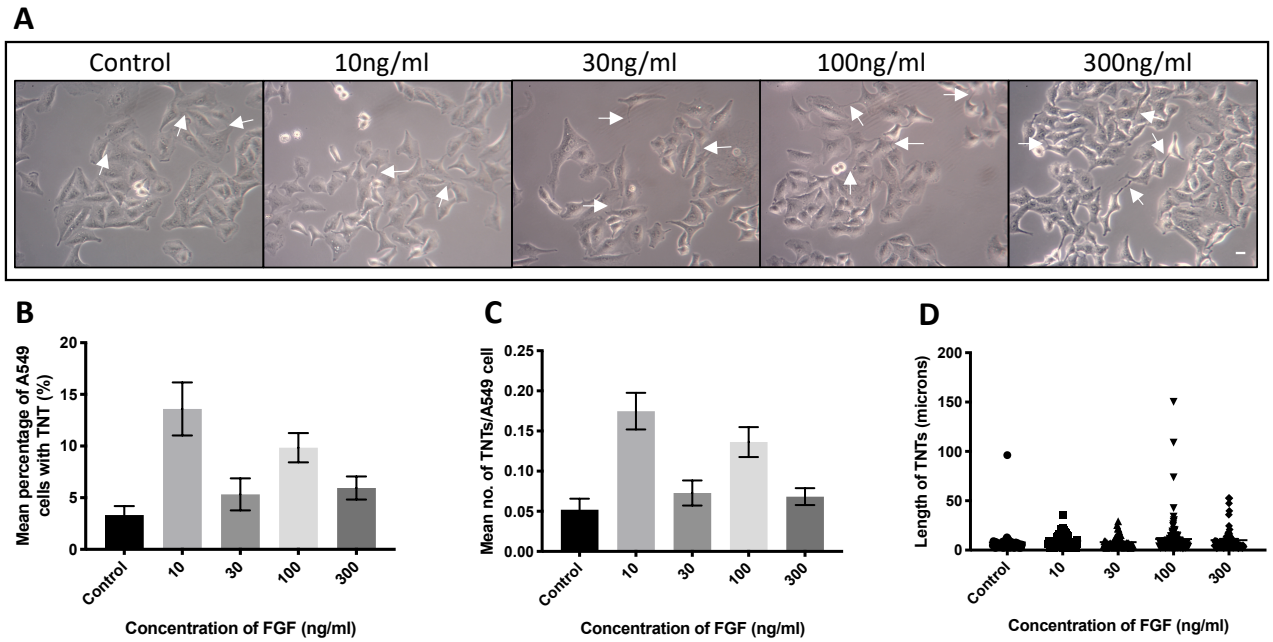


Figure 6.2: FGF2 has no effect on TNT formation in A549 cells. A: Representative white light images show no increase in TNTs (white arrow) when treated with increasing concentrations of FGF (10-300ng/ml) compared to control. White light images were captured using x10 objective lens on an inverted microscope. Scale bar:10µm. B-D: The white light images were quantified for TNTs and the histogram (B, C) and scatter plot (D) display the mean percentage (B), mean number of TNT/cell (C) and length of TNTs (D). Values are expressed as mean ± SEM, n=1, with at least 500 cells analysed per condition.

6.2.3 EGF induces TNT formation in A549 cells in a dose-dependent manner

We next wanted to determine whether EGF was able to induce TNTs in A 549 cells, as previous studies have shown EGF as an inducer of TNTs in ovarian cancer cells (Cole, Dahl, and Cowden Dahl 2021), mesothelioma cells (Lou, Fujisawa, Morozov, et al. 2012)and breast cancer cells (Carter et al. 2019). To determine the effect of EGF on A549 cell TNT formation, white light images were captured on an inverted microscope after 24-hour treatment of EGF (0-700ng/ml)(Fig6.3A-D).EGF induced thin cellular protrusions, narrow at its base and span various lengths to connect to distant cells. TNTs begin to form between 3-30ng/ml, as A549 cells scatter due to increasing cell migration and undergoing EMT, transforming from an oval epithelial to spindle-shaped morphology and exhibiting filopodia-like extensions. At higher concentrations between 100-700ng/ml, TNT-like extensions begin to lengthen across the field of view. The log concentration-response curve show EGF induces a dose-dependent significant (n=3, ****p<0.0001) increase in mean percentage (Fig6.3B), mean number per cell (Fig6.3C) and length of TNT-like structures (Fig6.3D), with a maximal concentration reached at 100ng/ml plateauing through 300ng/ml and 700ng/ml (Fig6.3B-D). The EC_{50} for the log concentration-response curve was obtained at 1ng/ml (Fig6.3B) for both mean percentage and mean number of TNT/cell whilst the EC_{50} for the mean length of TNTs was calculated at 0.2ng/ml

(Fig6.3D). Overall an EC_{50} of 1ng/ml and maximal concentration of 100ng/ml was used for future experiments.

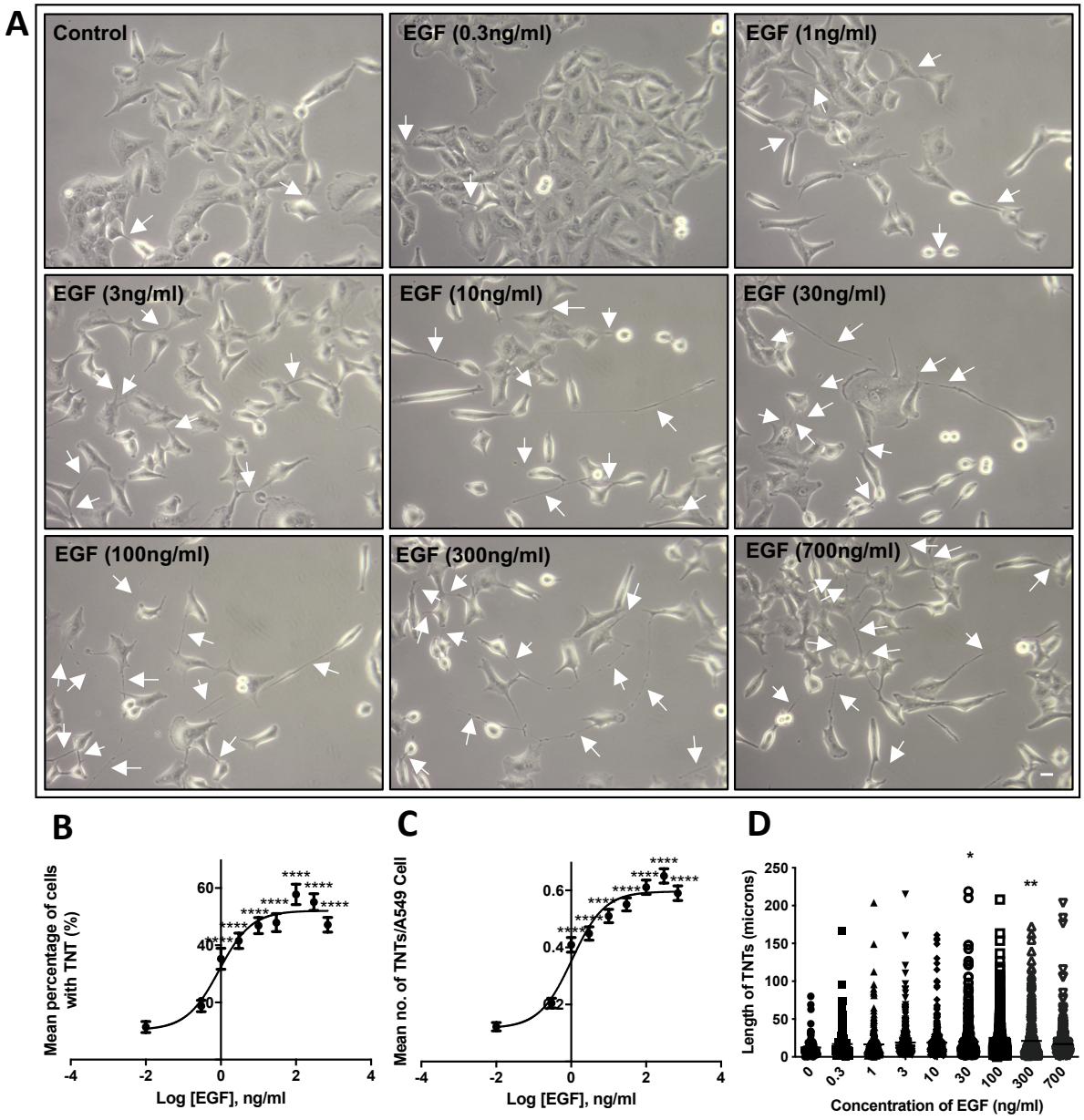


Figure 6.3: EGF induces A549 cell TNT formation in a dose-dependent manner. A: Representative white light images show an increase in TNTs (white arrow) when treated with increasing concentrations of EGF (0-700ng/ml) compared to control. White light images were captured using x10 objective lens on an inverted microscope. Scale bar:10µm. B-D: The white light images were quantified for TNTs and the histogram (B, C) and scatter plot (D) display the mean percentage (B), mean number of TNT/cell (C) and length of TNTs (D). Values are expressed as mean ± SEM, n=3, with at least 600 cells analysed per condition. *p<0.05, **p<0.01 and ****p<0.0001. Experiments conducted by AJ.

6.2.4 EGF induces F-actin-positive TNTs

Characterisation of the EGF-induced TNTs was undertaken using immunofluorescent labelling of F-actin and visualised with confocal microscopy. The immunofluorescent images also showed EGF-treated cells displayed an elongated fibroblast-like morphology with multiple F-actin labelled TNTs (white arrows) present whilst the control cells were cuboidal and epithelial-like in morphology and

displayed minimal presence of F-actin labelled TNTs (white arrow)(Fig6.4). The control and EGF-induced TNTs (white arrows) expressed characteristic F-actin throughout the entire TNT length (Fig6.4), thus confirming the presence of TNTs in our study.

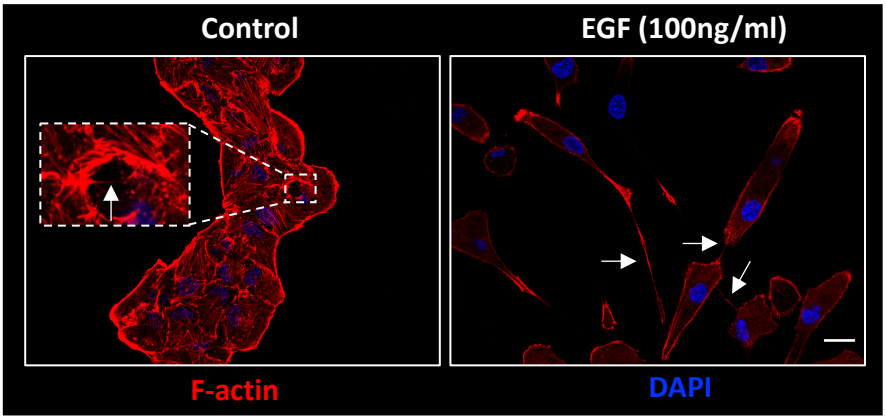


Figure 6.4: EGF induces F-actin positive TNTs. Representative confocal images for control and 24h EGF-treated cells (100ng/ml) were labelled with F-actin. F-actin (white arrow) is expressed throughout the TNT structure. White arrows denote TNT-structures and dotted area denotes a zoomed area. Scale bar, 20 µm

6.2.5 Co-treatment with HGF and EGF showed no additive or synergistic increase on TNT formation compared to HGF or EGF treatment alone

Following the determination of the EC_{50} and maximal concentration of EGF, the HGF and EGF-induced TNT formation were compared individually and in combination to assess whether there was a synergistic or additive effect between HGF and EGF in TNT formation. To determine whether there was a synergistic effect between HGF and EGF, the cells were treated with the EC_{50} concentrations of HGF (4ng/ml) and EGF (3ng/ml). There was no significant increase in mean percentage between EC_{50} HGF+EGF-treated cells compared to EC_{50} HGF-treated cells alone or EC_{50} EGF-treated cells alone (Fig6.5B). The results showed a significant (**p<0.01, n=3) increase in mean number of TNT/cell with the EC_{50} HGF+EGF-treated cells compared to EC_{50} HGF-treated cells alone (Fig6.5C). There was also no significant increase in mean length between EC_{50} HGF+EGF-treated cells compared to EC_{50} HGF-treated cells alone or EC_{50} EGF-treated cells alone (Fig6.5D). As two of the parameters (percentage and length) showed no significant increase between EC_{50} HGF+EGF-treated cells compared to the EC_{50} HGF or EGF-treated cells alone, no synergistic effect was concluded.

To determine whether there was an additive effect between HGF and EGF, the cells were treated with the maximal concentration of HGF (100ng/ml) and EGF (100ng/ml). There was no significant increase in mean percentage between max HGF+EGF-treated cells compared to max HGF-treated cells alone or max EGF-treated cells alone (Fig6.5B). There was also no significant increase in the mean number of TNT/cell between max HGF+EGF-treated cells compared to max HGF-treated cells

alone or max EGF-treated cells alone (Fig6.5C). Lastly, no significant increase in mean length between max HGF+EGF-treated cells compared to max HGF-treated cells alone or max EGF-treated cells alone (Fig6.5D). As no additive effect was observed between the three parameters, therefore HGF and EGF induce TNTs in A549 cells through convergent signalling pathways.

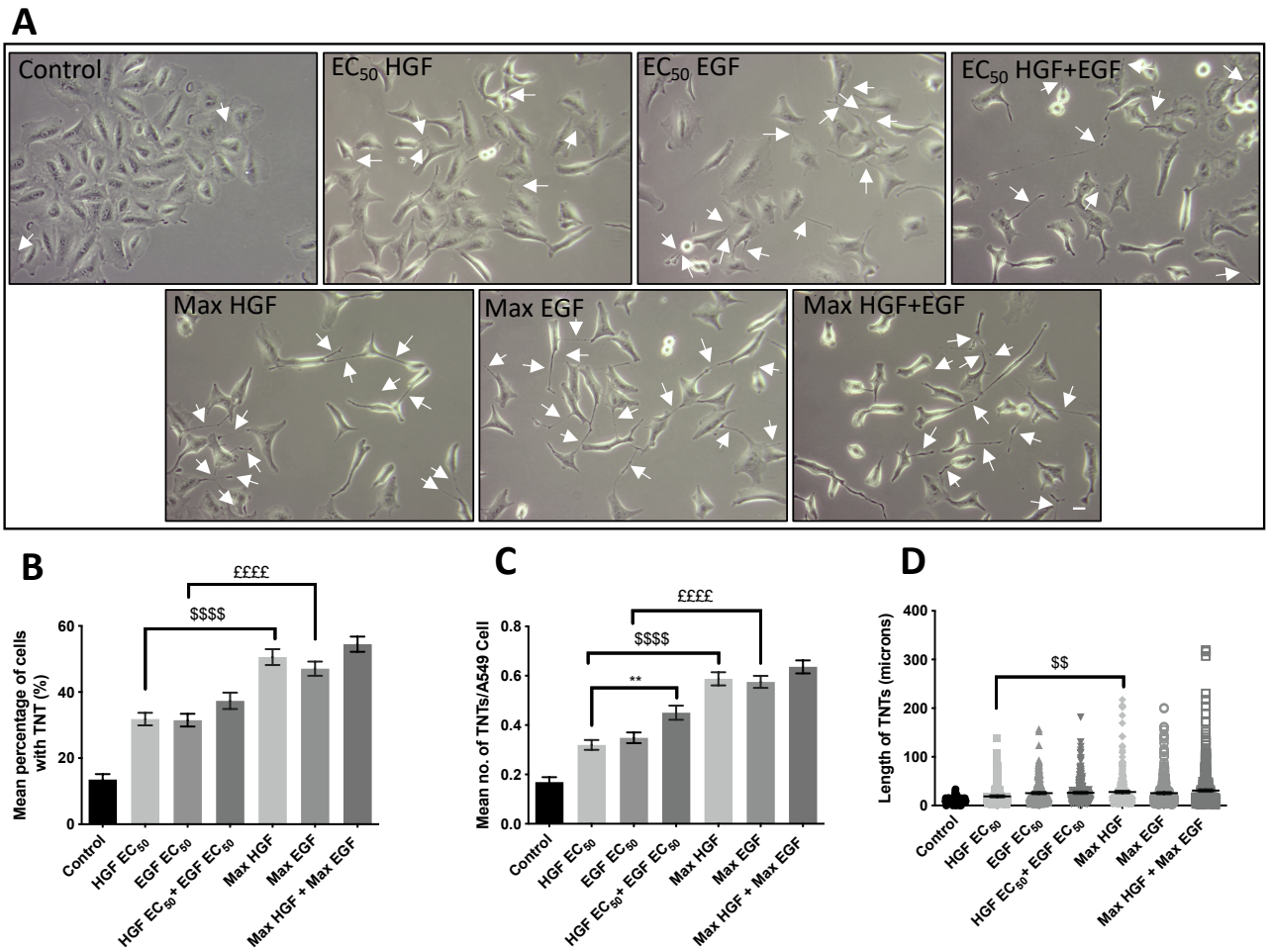


Figure 6.5: HGF and EGF do not induce a synergistic or additive effect on TNT formation. A: Representative white light images show an increase in TNTs (white arrows) when cells were treated with the EC_{50} or maximal concentrations of HGF and EGF alone or in combination compared to control. White light images were captured using x10 objective lens on an inverted microscope. Scale bar:10µm. B-D: The white light images were quantified for TNTs and the histogram (B, C) and scatter plot (D) display the mean percentage (B), mean number of TNT/cell (C) and length of TNTs (D). Values are expressed as mean ± SEM, n=3, with at least 500 cells analysed per condition. *p<0.05, **p<0.01 and ****p<0.0001. Note that EC_{50} for EGF was initially thought to be 3 ng/ml, hence its use in this experiment (after further repeats EGF EC_{50} was found to be 1 ng/ml as stated in figure 6.3). Experiments conducted by AJ.

6.2.6 Inhibition of EGFR and c-Met alone had no effect on the combined HGF and EGF-induced TNT formation

Erlotinib is routinely used in NSCLC treatment and competes with adenosine triphosphate for binding at the tyrosine kinase domain of the EGFR thus preventing the tyrosine kinase activity (Arteaga 2003). Therefore, further investigation into the crosstalk between HGF/c-Met and EGF/EGFR signalling was investigated using Erlotinib (100µM) and the c-Met inhibitor PHA-665752

(0.25µM). The white light images showed an increase in TNTs (white arrow) in the EGF+DMSO, HGF+DMSO and HGF+EGF+DMSO-treated cells when compared to control+DMSO-treated cells (Fig6.6A). Furthermore, the cells in the EGF+DMSO, HGF+DMSO and HGF+EGF+DMSO conditions also displayed elongated fibroblast-like morphology whereas the control+DMSO-treated cells were epithelial-like in morphology (Fig6.7A). There was a decrease in TNTs (white arrows) in the presence of erlotinib in the EGF+DMSO-treated cells alone but not in the HGF+DMSO-treated cells alone and combined HGF+EGF+DMSO treated cells (Fig6.6A). White light images also showed a decrease in TNTs (white arrows) in the presence of PHA-665752 in the HGF+DMSO-treated cells alone (Fig6.6A) but not in the EGF+DMSO-treated cells alone and combined HGF+EGF+DMSO treated cells (Fig6.6A).

White light image quantification showed no significant difference in the mean (Fig6.6B), number (Fig6.6C) and length of TNTs (Fig6.6D) between the combined EGF+HGF+DMSO-treated cells compared to EGF+DMSO alone or HGF+DMSO-treated cells alone. There was a significant (££££p<0.0001) decrease in the mean percentage (Fig6.6B), number (Fig6.6C) and length (Fig6.6D) of TNTs in the EGF+erlotinib-treated cells alone when compared to the EGF+DMSO-treated cells alone. However, there was no significant difference in the mean percentage (Fig6.6B), number (Fig6.6C) and length (Fig6.6D) of TNTs between the HGF+erlotinib-treated cells alone and HGF+DMSO-treated cells. There was no significant difference in the mean percentage (Fig6.6B), number (Fig6.6C) and length (Fig6.6D) of TNTs between the combined HGF+EGF+erlotinib-treated cells when compared to the combined HGF+EGF+DMSO-treated cells.

White light image quantification also showed a significant decrease in the mean percentage (Fig6.6B), number (Fig6.6C) and length (Fig6.6D) of TNTs in the HGF+PHA-665752-treated cells alone when compared to the HGF+DMSO-treated cells alone. However, there was no significant difference in the mean percentage (Fig6.6B), number (Fig6.6C) and length (Fig6.6D) of TNTs between the EGF+PHA-665752-treated cells alone and the EGF+DMSO-treated cells. Moreover, there was no significant difference in the mean percentage (Fig6.6B), number (Fig6.6C) and length (Fig6.6D) of TNTs between the combined HGF+EGF+PHA-665752-treated cells when compared to the combined HGF+EGF+DMSO-treated cells.

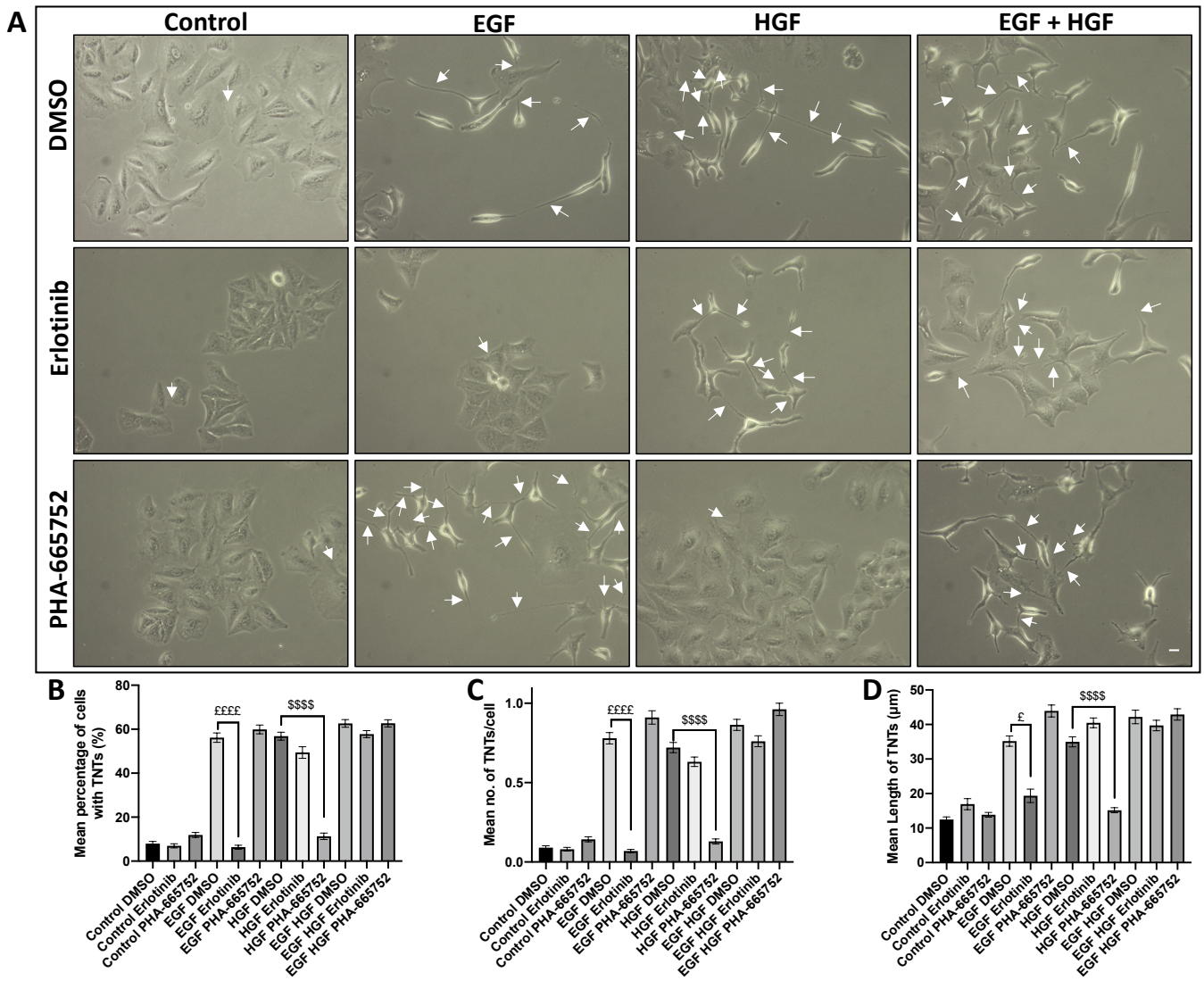


Figure 6.6: HGF and EGF pathways converge in response to erlotinib and c-Met inhibition. A: Representative white light images show a decrease in EGF-induced TNTs (white arrows) in the presence of erlotinib (100µM) and a decrease in HGF-induced TNTs (white arrows) in the presence of PHA-665752. White light images were captured using x10 objective lens on an inverted microscope. Scale bar:10µm. B-D: The white light images were quantified for TNTs and the histogram display the mean percentage (B), mean number of TNT/cell (C) and length of TNTs (D). Values are expressed as mean ± SEM, n=3, with at least 600 cells analysed per condition. £££££ $p<0.0001$ when comparing EGF DMSO with EGF+erlotinib and $$$$$p<0.0001$ when comparing HGF DMSO with HGF+PHA-665752. Experiments conducted by FP.

6.2.7 Both MAPK and PI3K pathway inhibition is required to inhibit the HGF and EGF co-stimulated TNTs

After establishing convergent crosstalk between HGF and EGF in TNT formation, we next wanted to determine the downstream signalling pathways involved. In chapter 5, HGF was shown to induce TNT formation *via* the MAPK and PI3K pathways, therefore the same concentrations of both inhibitors of the MAPK (PD98059;20µM) and PI3K (LY294002;50µM) pathways were used for this study. The white light images showed an increase in TNTs (white arrow) in the EGF+DMSO, HGF+DMSO and HGF+EGF+DMSO-treated cells when compared to control+DMSO-treated cells (Fig6.7A). Furthermore, the cells in the EGF+DMSO, HGF+DMSO and HGF+EGF+DMSO conditions

also displayed elongated fibroblast-like morphology whereas the control+DMSO-treated cells were epithelial-like in morphology (Fig6.7A). In the presence of PD98059, the cells reverted to an epithelial cell morphology with minimal presence of TNTs (white arrow), as similarly observed in control DMSO, in the HGF+PD98059 and EGF+PD98059-treated cells alone (Fig6.7A). However, combined HGF+EGF+PD98059 treatment resulted in an elongated cell morphology with an increase in TNTs present (white arrow)(Fig6.7A). Similarly, in the presence of LY294002, the cells also reverted to an epithelial cell morphology with minimal presence of TNTs (white arrow), as similarly observed in control DMSO, in the HGF+LY294002 and EGF+LY294002-treated cells alone (Fig6.7A). Moreover, combined HGF+EGF+LY294002 treatment resulted in an elongated cell morphology with an increase in TNTs present (white arrow)(Fig6.7A). However, in the presence of both PD98059 and LY294002, the cells reverted to an epithelial cell morphology with a decrease in TNTs (white arrow) observed in the HGF+PD98059+LY294002, EGF+PD98059+LY294002 and HGF+EGF+PD98059+LY294002-treated cells (Fig6.7A).

White light image quantification showed there was a significant (n=3, $$$$ $p<0.0001$) decrease in the mean percentage (Fig6.7B), number (Fig6.C) and length (Fig6.7D) of TNTs in the HGF+PD98059, HGF+LY294002 and HGF+PD98059+LY294002-treated cells when compared HGF+DMSO alone. There was also a significant (n=3, **** $p<0.0001$) decrease in the mean percentage (Fig6.7B), number (Fig6.C) and length (Fig6.7D) of TNTs in the EGF+PD98059, EGF+LY294002 and EGF+PD98059+LY294002-treated cells when compared EGF+DMSO alone. However, there was no significant difference between the combined HGF+EGF+DMSO-treated cells and the combined HGF+EGF+PD98059-treated cells in mean percentage (Fig6.7B), number (Fig6.7C) and length of TNTs (Fig6.7D). There was no significant difference between the combined HGF+EGF+DMSO-treated cells and the combined HGF+EGF+LY294002-treated cells in mean percentage (Fig6.7B), number (Fig6.7C) and length of TNTs (Fig6.7D). However, there was a significant (££££$p<0.0001$) decrease in the mean percentage (Fig6.7B), number (Fig6.C) and length (Fig6.7D) of TNTs in the combined HGF+EGF+PD98059+LY294002-treated cells compared to the combined HGF+EGF+DMSO-treated cells.

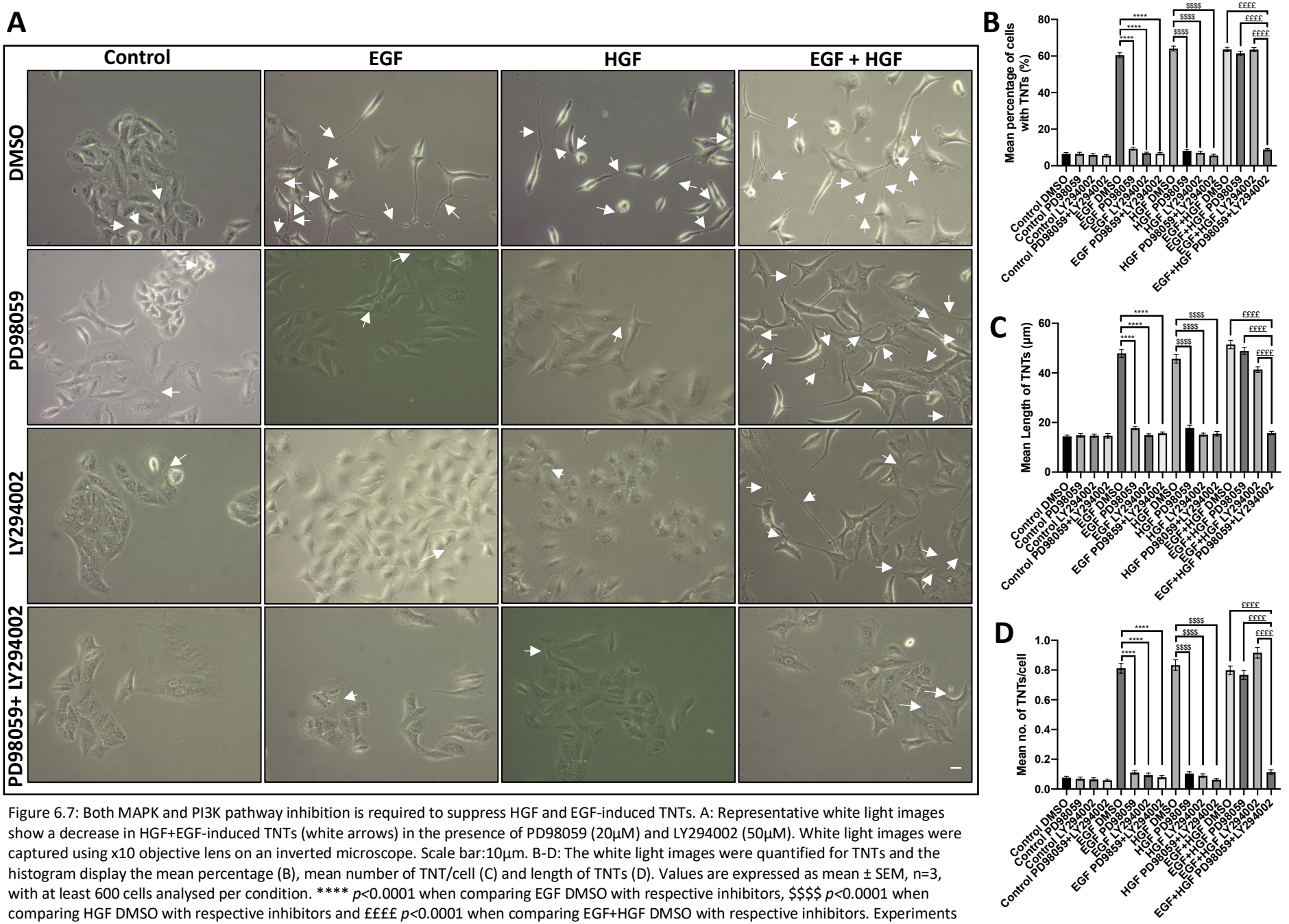


Figure 6.7: Both MAPK and PI3K pathway inhibition is required to suppress HGF and EGF-induced TNTs. A: Representative white light images show a decrease in HGF+EGF-induced TNTs (white arrows) in the presence of PD98059 (20µM) and LY294002 (50µM). White light images were captured using x10 objective lens on an inverted microscope. Scale bar:10µm. B-D: The white light images were quantified for TNTs and the histogram display the mean percentage (B), mean number of TNT/cell (C) and length of TNTs (D). Values are expressed as mean ± SEM, n=3, with at least 600 cells analysed per condition. **** $p<0.0001$ when comparing EGF DMSO with respective inhibitors, $$$$ $p<0.0001$ when comparing HGF DMSO with respective inhibitors and £££££ $p<0.0001$ when comparing EGF+HGF DMSO with respective inhibitors. Experiments conducted by FP.

6.3 Discussion

In this chapter, we showed both IL-6 and FGF2 had no effect on TNT formation whilst EGF induced induce a dose-dependent effect on TNT formation in A549 cells. Furthermore, pharmacological inhibitor studies revealed that sole inhibition of the c-Met receptor (with PHA-665752) and the EGFR (with erlotinib) had no effect on the combined EGF and HGF-stimulated TNTs. A novel convergent signalling, *via* the MAPK and PI3K pathways, was identified in mediating the combined EGF and HGF-induced TNT formation. Moreover, our study showed a novel equilibrium shift occurring between the MAPK and PI3K pathways in mediating the co-stimulated HGF and EGF-induced TNTs. Sole inhibition of the MAPK pathways, during co-treatment with HGF and EGF, shifted TNTs to form *via* the PI3K pathway and vice versa. The combined inhibition of both MAPK and PI3K pathways was required to inhibit the co-stimulated EGF and HGF-induced TNTs. This signalling crosstalk between EGF/EGFR and HGF/c-Met provides novel regulatory insight into the complex regulation underlying TNT formation.

6.3.1 IL-6 and FGF2 has no discernible effect on TNT formation in A549 cells

In our study, treatment with FGF did not induce TNT formation or characteristic elongated EMT morphology. Despite the link between EMT factors inducing TNT formation (Lou, Fujisawa, Morozov, et al. 2012), our study showed both FGF2 and IL-6 did not induce TNTs. This was also similarly observed in FGF-treated NSCLC cells, whereby FGF2 only induced an elongated fibroblast-like morphology when treated in combination with TGF-β (Li et al. 2018). Cole et al also showed FGF2 and FGF9 did not induce TNT formation in ovarian cancer cells (Cole, Dahl, and Cowden Dahl 2021). Conversely, Lou and his colleagues stimulated their cells with 2ng/ml of FGF to induce TNT formation in mesothelioma cells (Lou, Fujisawa, Morozov, et al. 2012). However, this study did not specify the exact FGF ligand family member used (Lou, Fujisawa, Morozov, et al. 2012). Furthermore, the study used a combination of other reagents, which included EGF and TGF-β3 to induce TNT formation (Lou, Fujisawa, Morozov, et al. 2012). Therefore, either another FGF ligand could potentially induce TNT formation, or the combined effects of the growth factor-supplemented media contributed towards TNT development. Moreover, as the molecular mechanism underlying TNT formation differ between cell types, it is also possible that the different combination of cytokines can induce TNT formation in different cell types.

Similarly, IL-6 also did not induce TNT formation or exhibit characteristic EMT-like morphology in our study. This is in contrast with another study which showed IL-6 transforming A549 cells from an epithelial to a fibroblast-like morphology (Zhao et al. 2014). However this could possibly be due to IL-6 only inducing EMT in CD133+ A549 cells (Lee et al. 2016), therefore it may be possible that the

CD133+ population of A549 cells undergoing EMT may also form TNTs upon IL-6 treatment. Future studies through FACS sorting of the CD133+ subpopulation of A549 cells could determine whether IL-6 can induce TNTs in the CD133+ population of A549 cells. In our study, IL-6 also did not cooperate with HGF to additively induce TNT formation. However, a study showed co-stimulation of HGF and IL-6 in A549 cells induced a mutual upregulation of their respective receptors to additively mediate invasion (To et al. 2002). This suggests the crosstalk between HGF and IL-6 exists in mediating other cellular effects but not in TNT formation. Despite the link between EMT factors in inducing TNT formation (Lou, Fujisawa, Morozov, et al. 2012), the role of the different upregulated EMT-inducing factors in the TME has not been explored in any other TNT studies.

6.3.2 EGF induces TNT formation in A549 cells

EGF/EGFR signalling axis is central to the pathogenesis of NSCLC (Ding *et al.,* 2008) and is the only growth factor known to induce TNT formation in various cell lines (Lou, Fujisawa, Morozov, et al. 2012; Carter et al. 2019; Cole, Dahl, and Cowden Dahl 2021; Wang et al. 2011; Hanna et al. 2019). Our study showed a dose-dependent significant increase in TNTs formation with EGF. The EGF-induced TNTs also expressed characteristic F-actin and future immunofluorescent studies can be conducted to confirm the presence of novel components c-Met, β1-integrin and paxillin in the EGF-induced TNTs. The role of EGFR activation in TNT formation was first implicated in stress-induced astrocytes although the same study did not show an increase in TNTs with EGF treatment (Wang et al. 2011). However, Carter et al also reported a similar significant increase (35.4%) in TNT percentage in macrophages post-24hr-treatment with EGF (Carter et al. 2019). Hanna et al also reported an EGFR-dependent response in the formation of heterotypic TNTs between macrophages and breast cancer cells (Hanna et al. 2019). In ovarian cancer cells, 24hr treatment with EGF significantly increased the percentage of TNTs, although the total increase was reported to be <10% in the EGF-treated cells whereas our study observed a 41.6% increase (Cole, Dahl, and Cowden Dahl 2021). This may be due to the difference in the inclusion criteria of TNTs measured in the study as only TNTs >30μm in length were quantified in the study (Cole, Dahl, and Cowden Dahl 2021) and therefore there may be an underestimation of the total TNT counts. Overall, the results of this study confirmed the role of EGF in inducing TNT formation in A549 cells. Further investigation into other commonly overexpressed growth factors in NSCLC, such as those in the ErbB receptor family (e.g. amphiregulin, TGF-α, betacellulin, heparin-binding EGF and epiregulin (Yarden 2001) would be of interest for future studies. TGF-β3 has also been implicated in TNT formation in mesothelioma cells (Lou, Fujisawa, Morozov, et al. 2012) and could be explored as another potential candidate factor in inducing TNT formation in NSCLC.

6.3.3 Combined HGF and EGF treatment did not induce an additive or synergistic effect on TNT formation

Both EGFR and c-Met are overexpressed in NSCLC with both pathways associated with an increase in migration, ROS levels and angiogenesis (Ciardiello et al. 2004). However, our study showed HGF and EGF did not induce a synergistic or additive effect on TNT formation, thus suggesting pathway convergence occurring during TNT formation. HGF and EGF convergent signalling has also been observed in breast carcinoma cells whereby migration was mediated by MLCK downstream of the Rho pathway (Harrison et al. 2013). Conversely, Puri and Salgia identified an additive effect between EGF and HGF in NSCLC cell migration and a synergistic effect on NSCLC proliferation (Puri and Salgia 2008). This was due to EGF and HGF inducing synergistic phosphorylation of the c-Met receptor and of downstream Akt and ERK (Puri and Salgia 2008). Interestingly, this increase in c-Met phosphorylation may occur *via* an increase in physical association between c-Met and EGFR (Jo et al. 2000) or an upregulated transcription of c-Met and EGFR (Reznik et al. 2008). However, both mechanisms may only be exclusively mediating synergistic proliferation induced by both HGF and EGF and not in TNT formation. It would also be of interest to investigate, through immunofluorescent studies, whether EGFR could co-localise with c-Met, β1-integrin and paxillin during TNT formation, thus further establishing the crosstalk between HGF/c-Met/β1-integrin with EGF/EGFR signalling.

6.3.4 Sole EGFR and c-Met inhibition had no effect on the combined HGF and EGF-induced TNT formation

In our study, erlotinib treatment alone had no effect on the combined HGF and EGF-induced TNT formation and c-Met inhibition alone also did not affect the co-stimulated HGF and EGF-mediated TNT formation. This demonstrates the ability for HGF/c-Met signalling to bypass the inhibited EGFR signalling in TNT formation and vice versa. Similarly, amplification of c-Met was reported to activate MAPK and PI3K downstream pathways to bypass the apoptotic effects induced by EGFR-TKIs in lung cancer (Zhang, Yang, and Wang 2019). Therefore, the result of our study emphasises the need to simultaneously target both HGF and EGF in patients harbouring EGFR or c-Met mutations to fully inhibit the potential pro-tumourigenic TNT-mediated effects. Future work to determine whether combined erlotinib and c-Met inhibition (with either PHA-665752 or a c-Met inhibitor used in clinical trials) can inhibit the TNTs induced from the co-treatment of HGF and EGF.

Moreover, although erlotinib has been licensed for treatment of patients with chemotherapy-resistant advanced NSCLC, resistance to erlotinib also occurs within 8-12 months from the start of

treatment (Bareschino et al. 2007). Interestingly, 20% of this drug resistance can be attributed to the amplification of c-Met (Bean et al. 2007). Therefore, TNTs may be a mechanism by which EGF or HGF acquire resistance in NSCLC. Future studies can also focus on the functional consequence of the combined EGF and HGF-induced TNT formation and to determine whether the TNT-mediated transport of mitochondria can propagate chemoresistance in cancer (Pasquier et al. 2013; Kolba et al. 2019). It would be of interest to visualise mitochondria transfer through live cell imaging in combined EGF and HGF-treated cells in comparison with EGFR or c-Met inhibitors to measure the number or rate of TNT-mediated mitochondria transfer. Overall, effective patient stratification is required to ensure the optimal outcome from targeted EGFR and c-Met therapy. Previous phase III clinical trials using a combination of erlotinib with either onartuzumab (a monoclonal antibody to c-Met)(Spigel, Edelman, O'Byrne, Paz Ares, et al. 2017) or tivantinib (a c-Met inhibitor)(Scagliotti et al. 2015) has been unsuccessful due to ineffective patient recruitment as patients were not screened for EGFR or MET genetic status and activity. However, in another patient with NSCLC harbouring the EGFR L858R mutation and MET amplification, a combination of full-dose osimertinib (a third generation EGFR-TKI) and crizotinib (a multi-kinase ALK/ROS1/MET inhibitor) was administered whereby a sustained partial response was observed with good tolerance. Therefore, this demonstrates the potential success in future personalised strategies in targeting EGFR and MET in NSCLC (Zhu et al. 2019).

6.3.5 Combined PI3K and MAPK pathway inhibition reduced the co-stimulated EGF and HGF TNT effect

Our study also showed a novel signalling convergence between the PI3K and MAPK pathways during the co-stimulated HGF and EGF-induced TNTs. In breast cancer cells, EGF induced TNTs *via* the MAPK pathway, similarly to our study (Cole, Dahl, and Cowden Dahl 2021). Although this same study showed EGF-induced TNT formation did not occur *via* the PI3K pathways (Cole, Dahl, and Cowden Dahl 2021), studies in astrocytes have demonstrated p53 activation and upregulation of EGFR receptors activated the Akt-PI3K-mTOR pathway required for F-actin polymerisation and TNT formation (Wang et al. 2011). Other inhibitors of pathways associated with TNT formation (such as the Rho-GTPase associated pathways-CDC42, Rac1, ROCK, Arp2/3 complex pathways) were not investigated in this study. It would be of interest to fully map out the pathways involved in the EGF-mediated TNT formation and compare any differences with the pathways associated with HGF/c-Met signalling-axis.

Most strikingly, combined inhibition of the PI3K and MAPK pathways was required to inhibit the co-stimulated HGF and EGF-induced TNTs whilst sole inhibition of the PI3K or MAPK pathways had no effect on the co-stimulated HGF and EGF-induced TNTs. These results demonstrate an equilibrium shift occurring between the MAPK and PI3K pathways in mediating the HGF and EGF combined TNT effect. There has been recent interest in developing inhibitors to target the PI3K and MAPK pathways with several drugs undergoing various stages of clinical trials in NSCLC (Tan 2020; Jain et al. 2021). However, clinical trials targeting the MAPK and PI3K pathways have provided mixed results with patients. A MEK inhibitor, PD-184352, demonstrated a lack of efficacy in the phase II clinical study (Cheng and Tian 2017). Similarly, a clinical trial with PI3K inhibitor (e.g. pictilisib) combined with standardised chemotherapy in NSCLC has yielded poor results with no improvements in overall survival or progression-free survival (Chen et al. 2019). As TNT-mediated mitochondria transport has been shown to induce chemoresistance and promote cell survival (Pasquier et al. 2013; Kolba et al. 2019), this signalling pathway switch may underly sustained TNT formation and thus the ineffective therapeutic outcomes in the clinical trials. However, a prolonged response has been observed in a patient harbouring PIK3CA mutation when treated with a PI3K inhibitor (PX866) after completing docetaxel treatment (Bowles et al. 2013). This further emphasises the need for effective patient stratification for c-Met, EGFR, PI3K and MAPK-associated mutations to ensure patients receive the appropriate combination of drugs to inhibit NSCLC progression. Moreover, TNTs can be exploited as a mode for drug transport, as daunorubicin was shown to localise with lysosomes in TNTs found in acute myeloid leukaemia (Omsland et al. 2017). Therefore, TNTs may also help to deliver effective drug targeting to the hypoxic core of the tumours which are regions with low efficiency of drug penetration/delivery. However, no studies have shown whether other chemotherapeutic agents can localise with other organelles such as mitochondria. Moreover, TNT-mediated drug delivery could also still lead to the survival and selection of the subpopulation of resistant cells.

6.3.6 Future work

The studies in this chapter relied on the use of pharmacological inhibitors to identify the downstream pathways involved in the EGF/HGF-induced TNT formation. Therefore, the study is limited by the specificity of pharmacological agents commercially available. Resected NSCLC patient tumour can be evaluated to identify whether there is a correlation between EGFR and c-Met overexpression and TNT formation. The result of this study also emphasises the potential for TNTs to mediate resistance through EGF/HGF signalling. Therefore, another future aim of this work would be to investigate whether TNT-mediated mitochondria transport occurs more frequently during co-treatment with EGF and HGF compared to EGF/HGF individually. Live confocal imaging can be used to quantify the rate and number of mitochondria being transferred along the TNTs. Moreover, to

better recapitulate the 3D TME, EGF/HGF-treated A549 cells seeded in Matrigel can be treated with the c-Met, PI3K, MAPK inhibitors and erlotinib. The tumouroid area, EdU incorporation, caspase-3 labelling and image analysis of TNTs between tumouroids could then be used to determine whether HGF/EGF pre-treatment had any effect on decreasing apoptosis in the drug-treated cells and thus the development of resistance in cells.

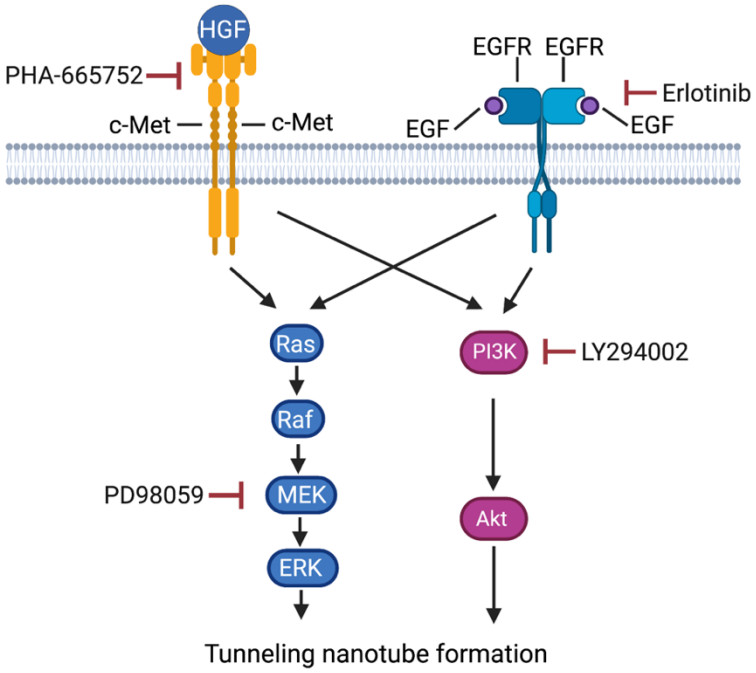


Figure 6.8: HGF/c-Met and EGF/EGFR signalling pathways converge on the MAPK and PI3K pathways to induce TNT formation in A549 cells. Combined inhibition of the PI3K and MAPK pathways was required to inhibit the co-stimulated HGF and EGF-induced TNTs whilst sole inhibition of the PI3K or MAPK pathways had no effect on the co-stimulated HGF and EGF-induced TNTs. These results demonstrate an equilibrium shift occurring between the MAPK and PI3K pathways in mediating the HGF and EGF combined TNT effect.

6.4 Conclusion

This chapter showed IL-6 and FGF2 had no effect on TNT formation in A549 cells. However, EGF induced TNT formation in a dose-dependent manner. A novel convergent signalling, *via* the MAPK and PI3K pathway, was identified in the combined EGF/EGFR and HGF/c-Met-induced TNT formation. Combined PI3K and MAPK inhibition was required to fully inhibit the co-stimulated HGF and EGF-induced TNTs. Furthermore, an equilibrium between both pathways was observed in mediating the co-stimulated HGF and EGF-induced TNT formation whereby sole inhibition of the MAPK pathways resulted in TNT formation *via* the PI3K pathway and vice versa. These findings highlight the importance of personalised multi-drug targeting in cancer.

From our HGF and EGF TNT studies, a novel phenomenon was observed whereby a subpopulation of A549 cells were able to undergo TNT formation whilst proliferating and migrating simultaneously. We termed the subset of cells undergoing this novel phenomenon ‘go and grow’ cells. Whilst previous chapters have extensively characterised the crosstalk between HGF/c-Met with β1-integrin and EGF/EGFR in regulating TNT formation in A549 cells, we also wanted to investigate the role of HGF in inducing this novel phenomenon, as the unique behaviour of these cells may reflect the highly metastatic cells in the TME of NSCLC.

7. Chapter 7: HGF induces a novel 'go and grow' phenotype in A549 cells

7.1 Introduction

Sustained proliferation and enhanced invasiveness are fundamental to the progression of cancer (Hanahan and Weinberg 2011). In cancer, traditionally, uncontrolled proliferation underlies the benign growth of the tumour before a malignant switch induces highly migratory invasive tumour (Hanahan and Weinberg 2011; Giese et al. 2003). Rapid initial growth of cancer cells develop from an abundant supply of oxygen and nutrients however as the tumour becomes dense quickly, this supply quickly diminishes leaving a hypoxic environment. The combined factors from hypoxia and high accumulation of mutation and damaged genetic material lead to the conversion of highly migratory cells capable of anaerobic metabolism and inducing angiogenesis (Gatenby and Gillies 2004). Therefore, proliferation and migration have been widely regarded as mutually exclusive processes in cancer. This proposed rationale arises from the distinct highly migratory phenotype of cells only observed in malignant tumours and not in benign tumours (Giese et al. 2003). Moreover, during cytokinesis, the actin and microtubule apparatus are required to uphold the changes in mitotic cell rounding and should therefore be unavailable for supporting cell migration (Paluch et al. 2005; Stewart et al. 2011). Metabolically, competition for the limited ATP resources would hinder cells from undergoing both proliferation and migration (Czirók et al. 1998). Cell division is also an irreversible process whilst migration is not whilst migration also requires non-symmetrical polarisation of cells whereas proliferation does not (De Donatis, Ranaldi, and Cirri 2010). However, most studies investigating the 'go or grow' hypothesis have been conducted on cells with an origin to the central nervous system (Corcoran and Del Maestro 2003; Giese et al. 1996; Schultz et al. 2002; Funk and Sage 1991). Although several studies have shown an inverse correlation between proliferation and migration in gliomas, meningioma and primitive neuroectodermal tumours (Giese et al. 1996; Khoshyomn et al. 1999; Roth et al. 2000; Tamaki et al. 1997), there are also conflicting studies reporting a positive correlation between proliferation and migration (Corcoran and Del Maestro 2003; Lund-Johansen et al. 1990; De Donatis, Ranaldi, and Cirri 2010; Pollack et al. 1999).

However, in lung cancer cells, a significant positive correlation between proliferation and migration was identified (Garay et al. 2013). Moreover, the extracellular factors in the TME have been implicated in eliciting the different proliferative and/or migratory responses. Growth factor/RTK signalling has been shown to mediate a reciprocal response between proliferation and migration in various responses (De Donatis, Ranaldi, and Cirri 2010). A concentration gradient for PDGF induced during wound healing stimulates fibroblasts to undergo migration to the wound healing site but

once a threshold of cytokine concentration is reached, the fibroblasts switch to a proliferative phenotype (De Donatis et al. 2008). However, EGF stimulation was able to increase concurrent growth and migration of human glioma tumouroids (Lund-Johansen et al. 1990). These studies highlight the complex role of growth factor signalling in mediating its pro-tumourigenic effects. The specificity of the pleiotropic responses induced by HGF/c-Met has been questioned in the literature. The ability for HGF to signal through the same transduction mechanisms and intracellular molecular effectors and yet selectively exhibit specific combinations of cellular effects within the TME is not well understood. However, therapeutic inhibition of the c-Met receptor has demonstrated concurrent inhibition in growth, migration and invasion (Ayoub et al. 2017). In this chapter, use of long-term time-lapse video microscopy of 2D A549 cell cultures revealed a novel subset of A549 cell population undergoing simultaneous TNT formation, migration and proliferation, and are therefore termed as ‘go and grow’ TNTs in our study. We aimed to characterise the novel ‘go and grow’ TNTs induced by HGF as this subset population may be implicated in early metastasis in NSCLC.

7.2 Results

7.2.1 A549 cells form 'go and grow' cells

24-hour time-lapse video microscopy of HGF (100ng/ml)-treated A549 cells revealed a novel observation of a subpopulation of cells undergoing simultaneous migration, TNT formation and proliferation which we termed 'go and grow' cells. The two timelines show examples of a cell undergoing the 'go and grow' process with the duration of each of the sequence events: 1) the initial migration of the cell whilst leaving behind a trail of TNT either unconnected (Fig7.1A) or connected to another cell (Fig7.1B); 2) Once the maximal length of TNT is reached (shown by the white arrow), the cell body will release and retract back along the TNT length whilst simultaneously undergoing cell division; 3) Lastly, the daughter cells (indicated by the red arrows) would then migrate apart from one another, forming a TNT between before the TNTs would progressively thin and break as the cells migrate further apart (Fig7.1A&B). There were There was no significant difference between control and HGF in the duration of each of the sequence of events (Fig7.1C-E).

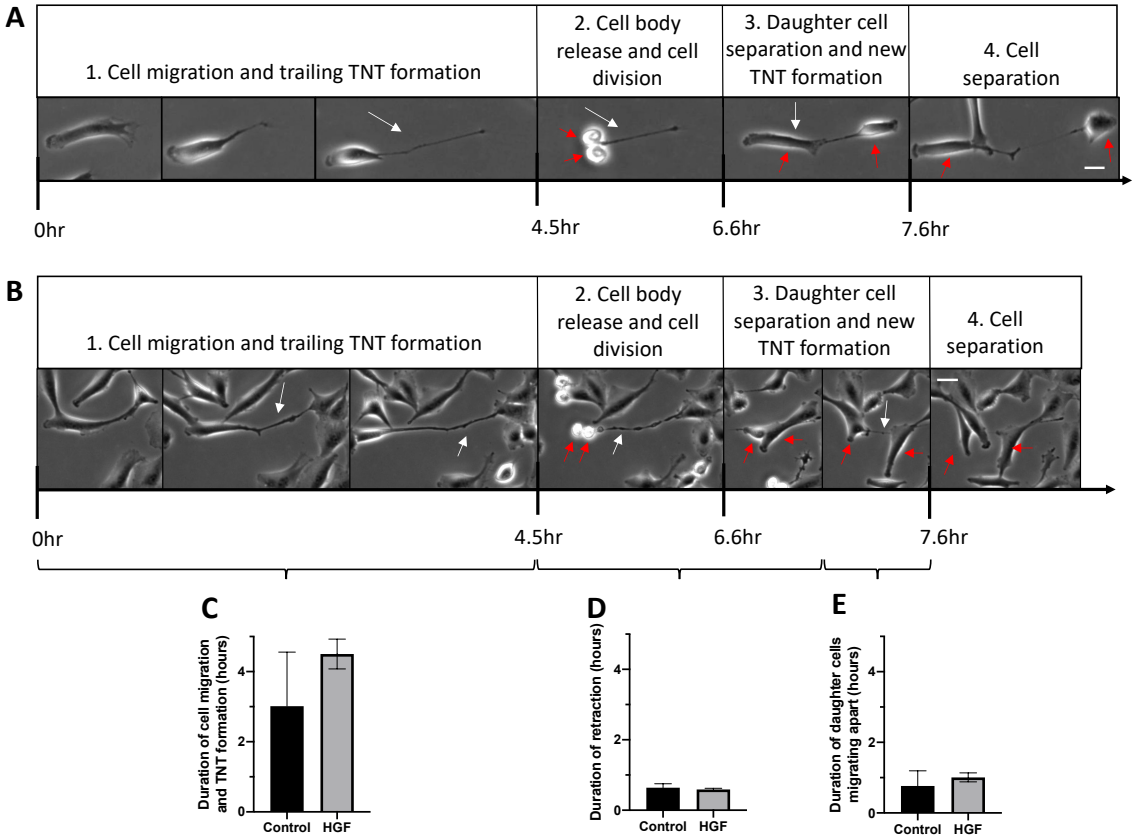


Figure 7.1: A549 cells undergo a novel 'go and grow' phenomenon. A&B: Representative white light images demonstrate the 'go and grow' sequence of events: 1. The cell migrates forming either an unconnected TNT (A) or TNT connected to another cell (B); 2. The simultaneous retraction along the TNT whilst undergoing cell division; 3. The subsequent formation of two daughter cells migrating apart and connected with a TNT; 4. Lastly the TNTs progressively thin as the daughter cells migrate further away from each other. White arrows denote a TNT and red arrows denote the daughter cells. White light images were captured using 10x objective lens on an epifluorescence microscope. Scale bar: 10µm. B-D: The duration of each sequence of events was averaged from the 24-hour time-lapse videos of control and HGF-treated cells and the histogram displays the mean time in hours for each listed event. Values are expressed as mean ± SEM, n=3.

We next wanted to determine the time range at which 'go and grow' cells were most frequently observed over the 24-hour duration. The time points at which cells began to undergo the initial cell migration and TNT formation process were plotted on the scatter plot (Fig7.2). There was no significance between control and HGF-induced 'go and grow' cells in the starting timepoint of the event.

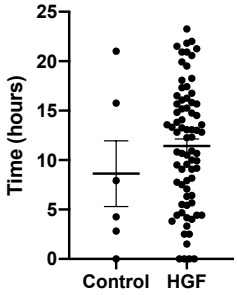


Figure 7.2: The starting timepoints of the control and HGF-induced 'go and grow' cells occurring throughout the 24-hour period. The scatter plot shows no significant difference between the control and HGF 'go and grow' starting timepoint. Values are expressed as mean ± SEM, n=3.

7.2.2 'Go and grow' TNTs express novel and characteristic markers c-Met, β1-integrin, paxillin and F-actin

We next aimed to characterise the 'go and grow' TNTs by undertaking immunofluorescent labelling of their characteristic and novel markers. Immunofluorescent labelling with F-actin was first undertaken to confirm the TNT structures formed during the 'go and grow' process expressed the characteristic marker. The F-actin labelled images show the key stages of the 'go and grow' process (Fig7.3A-F). The trailing TNTs observed in the 'go and grow' cells (white arrow)(Fig7.3B&C) and the TNT connecting the daughter cells (white arrow)(Fig7.3F) expressed F-actin throughout its entire length, thus confirming the presence of TNTs in our study.

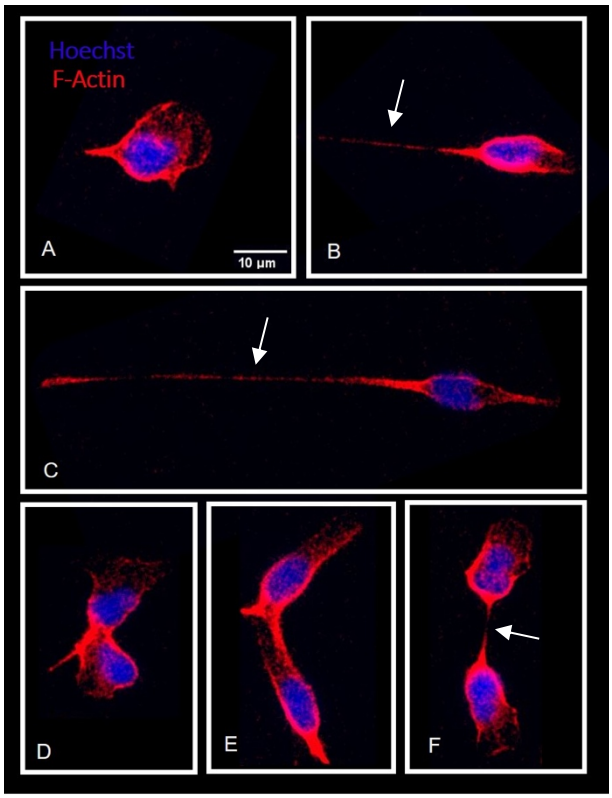


Figure 7.3: The TNTs formed during the 'go and grow' process positively express F-actin. A-F: Representative immunofluorescent images show a F-actin labelled cell undergoing the 'go and grow' process. A: The rounded cell starts to migrate forming a filopodia; B: The cell then elongates and migrates to leave a trailing F-actin positive TNT(white arrow); C: The F-actin positive TNT (white arrow) continues to lengthen as the cell further migrates; D: The cell undergoes mitosis and retracts back along the TNT; E: The daughter cells elongate and migrate apart from one another; F: As the daughter cells migrate apart, a F-actin positive TNT (white arrow) connects between the daughter cells before the TNT disintegrates. Scale bar 10µm.

We next characterised the 'go and grow' cells using immunofluorescent labelling of the novel TNT markers identified in chapter 4: c-Met, β1-integrin and paxillin alongside F-actin. 'Go and grow' cells were identified by cells undergoing mitosis with a TNT attached, this reflects the 2nd stage of the 'go and grow' process. F-actin (white arrow) was expressed throughout the length of the 'go and grow' TNT whilst paxillin (green arrow) was observed at the adherent tail end of the 'go and grow' TNT (Fig7.4A). The cell attached was undergoing metaphase, as the chromosomes align along the metaphase plate. The xy (Fig7.4A) orthogonal view also shows the F-actin and paxillin-positive TNT non-adherent to the substratum. C-Met (red arrow) and β1-integrin (green arrow) were also expressed along the length of the 'go and grow' TNT whilst the cell attached was undergoing cytokinesis (Fig7.4B). To assess the non-adherence of the c-Met and β1-integrin labelled TNTs, z-stack acquisition was obtained to visualise an aerial and xz orthogonal view of the TNT. The xz orthogonal view showed a c-Met and β1-integrin positive TNT non-adherent to the substratum (Fig7.4B).

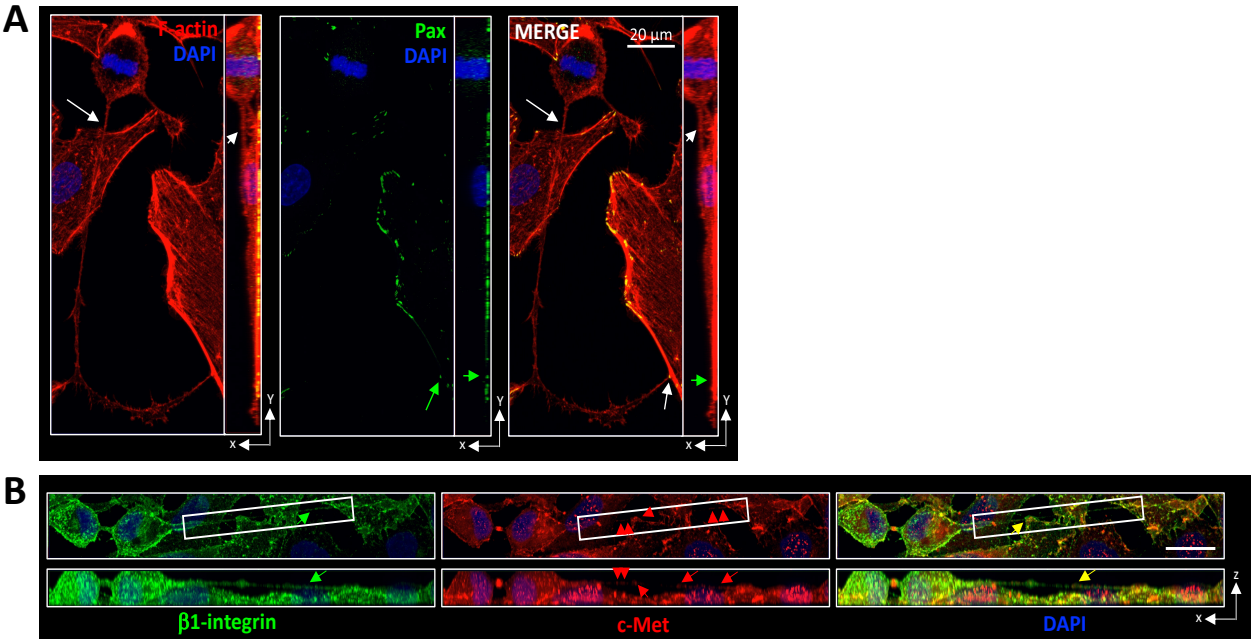


Figure 7.4: C-Met, β1-integrin, paxillin and F-actin are expressed in 'go and grow' TNTs. A: An example of a 'go and grow' cell (white arrow) labelled with F-actin (red) and paxillin (green arrow). Paxillin (green arrow) was expressed at the adherent tail end of the 'go and grow' TNT. The maximum xy projection image demonstrates a region of the TNT hovering above the culture surface. B: Representative confocal images for immunofluorescent labelled HGF-induced 'go and grow' TNTs with β1-integrin (green arrow) and c-Met (red arrow). The white boxed region denotes the length of the TNT. The maximum xz projection image below demonstrates the TNT hovering above the culture surface. Both aerial and orthogonal xz/xy projection images were obtained using ZEN lite software from 28 sections of Z-stacked images (with Z step of 0.4µm). Scale bar, 20µm.

7.2.3 HGF increased the formation of 'go and grow' cells

To further characterise the subpopulation of A549 cells the 'go and grow' cells, the percentage of 'go and grow' cells were quantified every 5 hours over the 24-hour duration over the entire population of A549 cells within each field of view. There was an increase in HGF-induced 'go and grow' cells compared to control at the 5th (Fig7.5B), 10th (Fig7.5C), 15th (Fig7.5D) and 20th-hour (Fig7.5E) timepoint. The highest percentage of 'go and grow' cells was identified at the 15th-hour timepoint at 2.7% ± 0.6 (Fig7.5D).

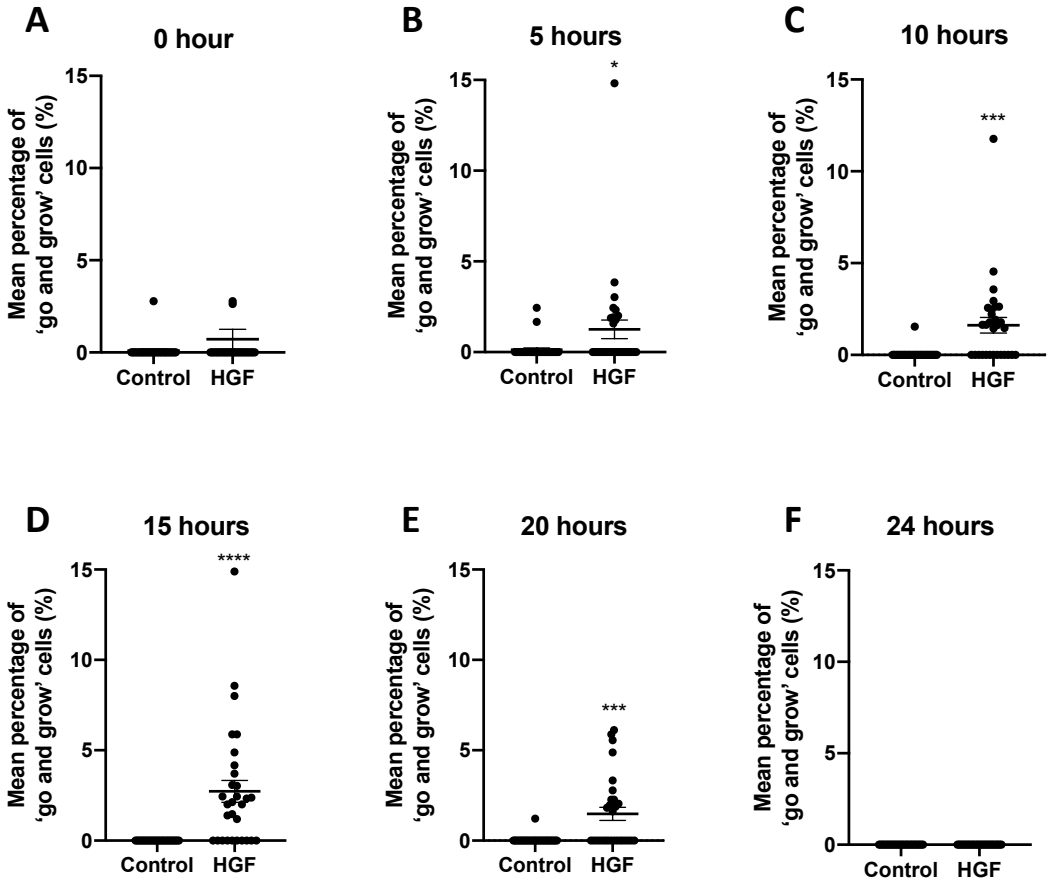


Figure 7.5: HGF significantly increases the percentage of 'go and grow' cells. A-F: The time-lapse videos for control and HGF-treated (100ng/ml) cells were quantified for the percentage of 'go and grow' cells every 5 hours over the 24-hour duration. B-E: The scatter plot displayed a significant increase in the mean percentage of 'go and grow' cells in HGF-treated cells compared to control at the 5th, 10th, 15th and 20th hour. Values are expressed as mean ± SEM, n=3. *p<0.05, ***p<0.001, ****p<0.0001.

After quantifying the percentage of 'go and grow' cells within the entire cell population, we next aimed to quantify the percentage of 'go and grow' cells amongst the TNT-forming cells. There was a significant increase in 'go and grow' cells when quantified over the cells that formed TNTs at the 10th (Fig7.6C), 15th (Fig7.6D) and 20th-hour (Fig7.6E) timepoint. The highest percentage of 'go and grow' cells when quantified over TNT-forming cells was identified at the 15th-hour timepoint at 8.9% ± 2 (Fig7.6D).

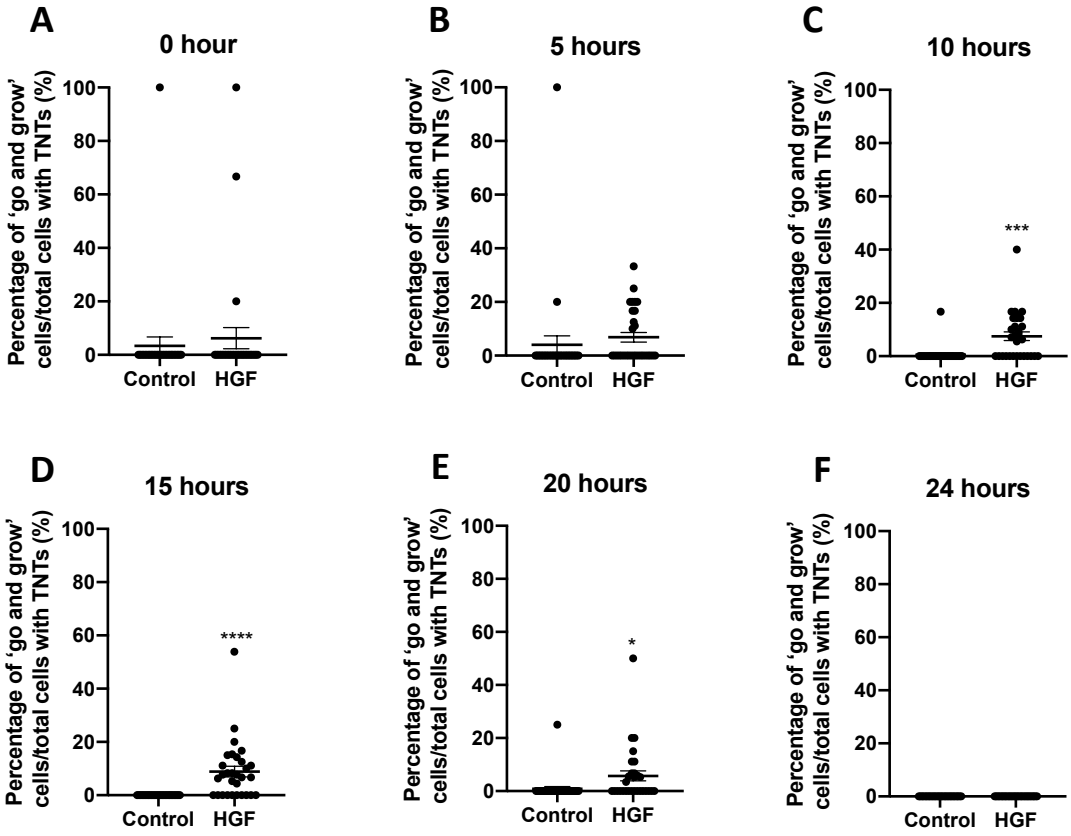


Figure 7.6: HGF significantly increases the percentage of 'go and grow' cells when taken as a percentage over all the TNT-forming cells. A-F: The time-lapse videos for control and HGF-treated (100ng/ml) cells were quantified for the mean percentage of 'go and grow' cells over the total number of cells forming TNTs every 5 hours over the 24-hour duration. B-E: The scatter plot displayed a significant increase in the mean percentage of 'go and grow' TNTs in HGF-treated cells compared to control at the 5th, 10th, 15th and 20th hour. Values are expressed as mean ± SEM, n=3. *p<0.05, ***p<0.001, ****p<0.0001.

7.2.4 C-Met inhibitor reduced the HGF-induced 'go and grow' cells

A c-Met inhibitor, PHA-665752 (0.25µM), was identify whether HGF ligand activation of c-Met was occurring during the formation of 'go and grow' cells. There was a decrease in mean percentage of HGF-induced 'go and grow' cells (0.57% ± 0.3) compared to the HGF DMSO treated cells (5.8% ±1.4). There was also no incidence of 'go and grow' cells in the PHA-665752-treated control cells (Fig7.7).

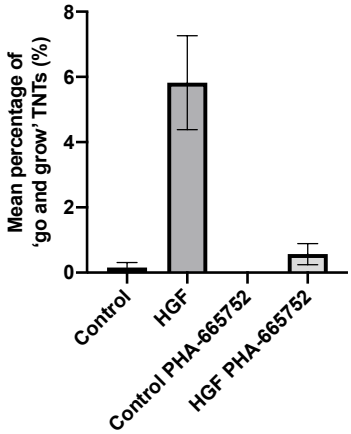


Figure 7.7: The c-Met receptor inhibitor, PHA-665752 (0.25µM), decreases the percentage of 'go and grow' cells compared to cells treated with only HGF over a 24h period. Values are expressed as mean ± SEM, n=1. Data was analysed by Imogen Clarke.

7.2.5 Characterisation of the speed and directionality of 'go and grow' cells

The speed and directionality of the 'go and grow' cells were next characterised to assess whether the migratory nature of the cell was random or occurred directionally upon HGF stimulation. The individual cells that formed 'go and grow' cells were manually tracked separately during the initial cell migration and TNT formation stage and during the cell retraction stage. The 'Chemotaxis and Migration Tool' plugin was used to obtain the speed and directionality of the individual tracking. There was a significant (n=3, ****p<0.0001) increase in the speed of retraction compared to the speed of the migrating TNT-trailing cell in control and HGF-induced 'go and grow' cells (Fig7.8A). However, there was no significant difference when comparing the speed of the initial cell migration/TNT formation and the retraction event between control and HGF 'go and grow' cells. There was also a significant (n=3, ****p<0.0001) increase in the speed of retraction compared to the speed of the migrating TNT-trailing cell in both control and HGF-induced 'go and grow' cells (Fig7.8B). HGF induced a significant increase in directionality, and thus moved in a more linear fashion, when compared to control during the initial cell migration/TNT formation (Fig7.8B). The rose plots (Fig7.8C-F) show the circular distribution of the directional data for the control and HGF-induced 'go and grow' TNTs when forming or retracting.

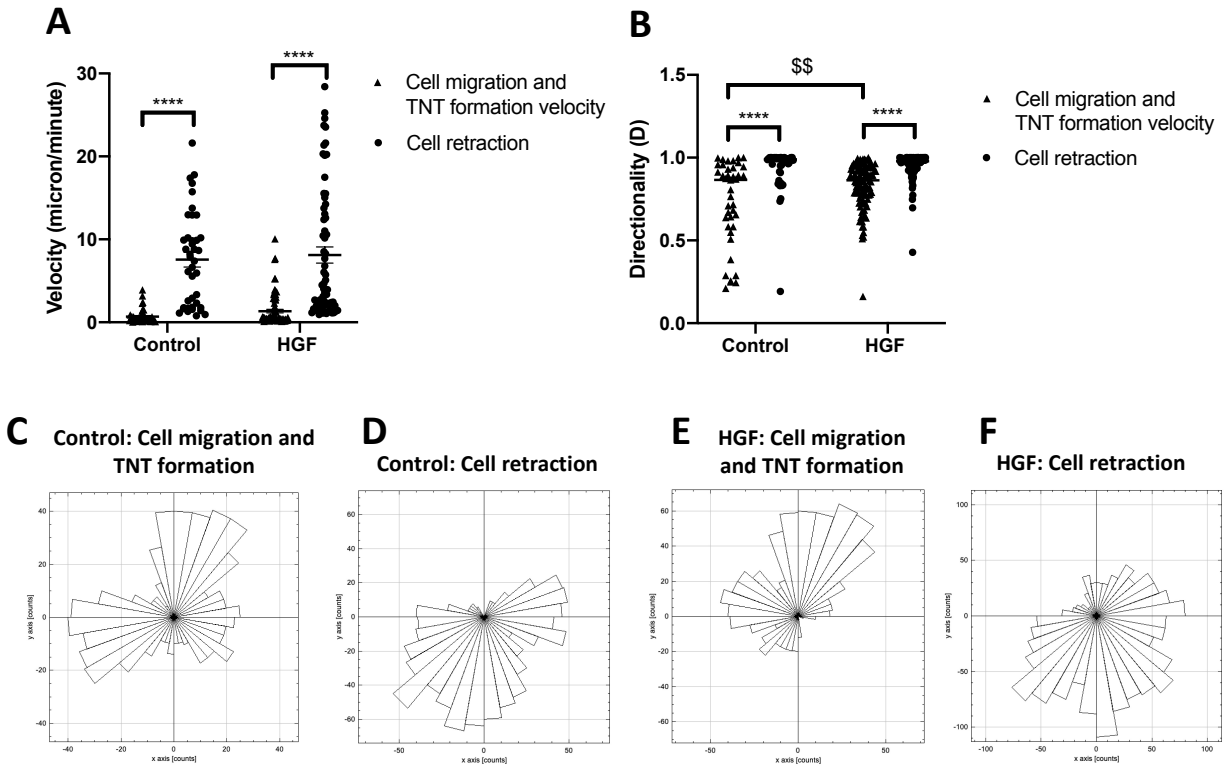


Figure 7.8: Control and HGF-induced 'go and grow' cells migrate and retract in a similar fashion. 'Go and grow' cells were tracked before analysed for the speed and directionality with the 'Chemotaxis and Migration Tool' ImageJ plugin. A-B: The scatter plot shows the speed (A) and directionality (B) of the migrating/TNT forming and the retraction event. C-F: The Rose plots (circular histograms) represent the total number of cells with an average angle of migration falling within a particular interval. Values are expressed as mean ± SEM, n=4, N ≥ 43. $$$p$<0.05 when comparing control with HGF migration/TNT formation directionality. ****p<0.0001 when comparing between the migration/TNT formation and retraction speed and directionality.

7.2.6 'Go and grow' cells are more proliferative than non-'go and grow' cells

To determine whether the cells undergoing 'go and grow' TNTs are more proliferative, the number of cell divisions was quantified for both 'go and grow' cells and non-'go and grow' cells within the 24-hour time period. There was a significant (n=3, p<0.05) increase in the number of cell divisions in 'go and grow' cells compared to the non-'go and grow' cells (Fig7.9).

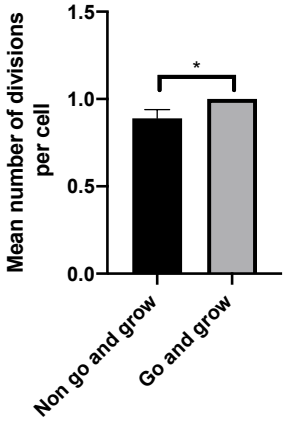


Figure 7.9: 'Go and grow' cells are more proliferative. The histogram shows an increases in the number of cell division in the 'go and grow' population of cells compared to the non-'go and grow' cells over the 24 hrs. Values are expressed as mean ± SEM, n=3, N≥30. *p<0.05. Data was analysed by Imogen Clarke.

7.2.7 HGF induced the formation of 'go and grow' cells on collagen IV-coated 12kPa hydrogels

After characterising the functional proliferative capacity of the 'go and grow' cells, we next wanted to confirm whether 'go and grow' cells would form when the *in vivo* stiffness of the lung tumour was replicated in our 2D culture. Therefore, to assess this, A549 cells were seeded on collagen IV(3μg/ml)-coated hydrogels, at a similar tensile stiffness of the lung tumour (i.e. 12kPa), before being treated with HGF (100ng/ml)(24hrs) and brought for time-lapse imaging. The white light image panel (Fig7.3) demonstrates a cell undergoing the entire 'go and grow' process: from the initial migration and TNT formation (white arrow) on the collagen IV-coated hydrogel to retracting back along the TNT whilst undergoing cell division and forming two daughter cells (red arrows) connected *via* a TNT (white arrow). This demonstrates the novel occurrence of the 'go and grow' process when A549 cells were seeded at a similar matrix stiffness to lung cancer.

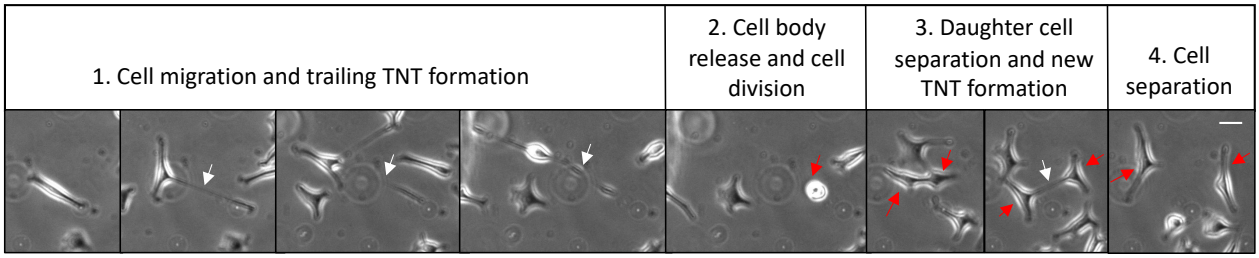


Figure 7.10: 'Go and grow' cells form when seeded on collagen IV-coated 12kPa hydrogels. The white light image panel shows an example of the cell undergoing the 'go and grow' process on collagen IV-coated 12kPa hydrogels. First, the cell undergoes migration while leaving a trailing TNT behind (white arrow). Secondly, the cell body will release once the maximum TNT length is reached and retracts back along the TNT. The cell simultaneously undergoes cell division whilst retracting back. Next, the daughter cells (red arrow) migrate apart from one another whilst connected by a TNT (white arrow). Lastly, the daughter cells migrate further apart and the TNT disintegrates. Scale bar, 10µm.

7.3 Discussion

In this chapter, we reveal a novel mechanism whereby a small subpopulation of A549 cells migrate to leave a trailing TNT behind before undergoing cell division whilst retracting back along the TNT, the daughter cells then migrate apart from one another whilst connected *via* a TNT. The A549 cells undergoing this novel process were termed 'go and grow' cells in our study. The 'go and grow' cells formed more frequently in HGF-treated cells and were observed in collagen IV-coated 12kPa hydrogels, which mimicked the tensile stiffness of the lung tumour. Furthermore, the TNTs formed by the 'go and grow' cells also express characteristic F-actin and novel markers, c-Met, β1-integrin and paxillin, thus confirming the presence of TNTs in our study. Image analysis and cell tracking of time-lapse videos revealed the duration, speed, directionality, and proliferative capacity of these cells. The retraction event occurred at a faster rate compared to their initial migratory/TNT formation stage and the HGF-induced 'go and grow' cells displayed a significant increase in directionality compared to control. Moreover, the 'go and grow' cells are more proliferative than the non-'go and grow' cell population thus implicating its potential role in metastasis of NSCLC.

7.3.1 Characterising the 'go and grow' A549 cells

The 'go and grow' cells observed in this study stands as a novel discovery within the field of cancer research. Traditionally, cancer cells undergo cell division or migration (Hanahan and Weinberg 2011), however, our study demonstrates a small subpopulation of A549 cells with the ability to do both, thus challenging the current dogma of the 'go or grow' hypothesis in cancer. Although the 'go or grow' hypothesis in cancer was first introduced by Giese et al in 1996 (Giese et al. 1996), several studies have contradicted this notion of cellular behaviour demonstrating concurrent proliferation and migration (Corcoran and Del Maestro 2003; Lund-Johansen et al. 1990; De Donatis, Ranaldi, and Cirri 2010; Pollack et al. 1999; Garay et al. 2013). Moreover, a study examining 10 lung cancer cell lines found a positive correlation between proliferation and migration, regardless of the cell density (Garay et al. 2013). This observation was further described in four stages in our study. The initial stage involves the leading cell body migrating forward leaving a very thin and long TNT behind, similarly to the type 1 filopodia-forming TNTs observed in various TNT studies (Dubois et al. 2020; Cordero Cervantes and Zurzolo 2021). Secondly, the cell body is released and undergoes cell division whilst retracting back along the TNT length to the original starting point. Next, the daughter cells migrate away from each other with a TNT connecting between them before the TNT breaks apart. This TNT forms similarly to the type 2 cell-to-cell dislodging mechanism (Dubois et al. 2020; Cordero Cervantes and Zurzolo 2021), however, studies have also shown intercellular bridges formed between daughter cells after incomplete cytokinesis (Korenkova, Pepe, and Zurzolo 2020; Haglund, Nezis, and Stenmark 2011). Therefore, future studies to observe specific organelle transfer, *via* the

appropriate fluorescent dye (i.e. Mitotracker red), can distinguish whether the structures between the daughter cells are intercellular bridges as a by-product of cytokinesis or are functional TNTs. The novel components of TNTs (c-Met, β1-integrin and paxillin) were also observed in the 'go and grow' TNTs. Interestingly, paxillin was expressed adherent at the point between a non-'go and grow' cell and the tail-end of the 'go and grow' TNT. Paxillin thus acts as an adhesive site tethering the TNT to its initial migration point and allowing the dividing cell to retract back along the TNT to its original starting point.

7.3.2 HGF increases the frequency of 'go and grow' cells

In our study, HGF was found to increase the frequency of 'go and grow' cells compared to control and c-Met inhibition reduced the HGF-induced formation of 'go and grow' cells. This confirms the HGF ligand-dependent activation of c-Met in regulating the formation of 'go and grow' cells. Interestingly, an increase in both proliferation and migration was observed in human glioma tumouroids upon EGF stimulation (Lund-Johansen et al. 1990). The concurrent relationship between proliferation and migration has also been observed during growth factor/RTK signalling (De Donatis, Ranaldi, and Cirri 2010). Moreover, it is possible that the HGF concentration gradient may be inducing the phenotypic switch in the 'go and grow' cells. The cells may be migrating towards the HGF gradient whilst undergoing the cell cycle and once the threshold for the HGF concentration is reached, the cell would stop migrating and then completes mitosis. Similarly, a concentration gradient for PDGF induced fibroblast migration to the wound healing site before switching to a proliferative phenotype once the threshold for PDGF concentration was reached (De Donatis et al. 2008). Therefore, it would be of interest to visualise when the HGF-induced 'go and grow' cells are undergoing the stages of the cell cycle. Future studies with a fluorescent ubiquitination-based cell cycle indicator (FUCCI) can be used to observe the fluorescent changes in live cells. FUCCI comprises of a fragment of Cdt1 fused with a fluorescent monomeric Kusabira-Orange 2 (mKO2) which accumulates in the G1 phase whilst the fragment Geminin fused with fluorescent monomeric Azami-Green 1 (mAG1) accumulates in the S, G2 and M phases (Sakaue-Sawano et al. 2008). It is also not known how HGF/c-Met activation can specifically induce the different pleiotropic cellular effects despite signalling through the same transduction mechanism and intracellular molecular effectors. Despite this, therapeutic inhibition of the c-Met receptor has resulted in an inhibition of all the pleiotropic HGF-mediated effects (Ayoub et al. 2017). Likewise, with our study, c-Met inhibition also resulted in a significant decrease in the 'go and grow' cells. Although proliferation and migration of the cells were not analysed in this study, the HGF-treated cells were observed to be less migratory in the presence of PHA-665752. Therefore, this highlights the importance of therapeutic targeting of c-Met to fully inhibit the spectrum of pro-tumourigenic pleiotropic effects.

7.3.3 Characterising the speed and directionality of 'go and grow' cells

We next assessed the migratory nature of the 'go and grow' cell and found the retraction speed was significantly higher than the speed of the migrating cell. However, there was no significant difference between the control and HGF-induced speed of both events. This highlights the similar nature of the 'go and grow' TNTs in both control and HGF-treated cells. During mitosis, the cell body rounds due to a loss of adhesion, as the integrin/ECM complexes are disassembled (Dao et al. 2009). The cell body is only loosely held via retraction fibres containing β1-integrin (Dix et al. 2018). Therefore, the dividing 'go and grow' cell can passively retract back to the adherent paxillin starting point with minimal resistance whereas the initial process requires active migration and TNT formation along the ECM. There was also a significant increase in directionality in the initial migration/TNT formation stage in the HGF-induced 'go and grow' TNTs compared to control. Directional migration relies on a chemotactic gradient (Etienne-Manneville 2008), which may explain the significant increase in the directionality of the HGF-induced 'go and grow' TNTs. Future chemotaxis experiments can be conducted to determine whether the directionality relies on the gradient of HGF. Moreover, the Rho GTPases (RhoA, Rac and CDC42) drive the actin cytoskeleton to induce polarisation of the migrating cells, with CDC42 and Rac localising at the front edge forming protrusions whilst Rho is activated at the rear-edge to induce actomyosin contractility for retraction. However, when a TNT forms, the cell body migrates in the opposite direction from the leading edge and leaves behind a TNT along its path. Furthermore, our studies conversely show that inhibiting the Rho GTPases did not inhibit TNT formation and instead the MAPK and PI3K pathways regulated TNT formation (see chapter 5). Therefore, it is likely that MAPK and PI3K pathways also drive the 'go and grow' TNT formation in its initial migratory/TNT-forming stage. The Par proteins (Par3, Par6), which are involved in mediating the polarisation of migrating cells, may be implicated in the directional formation of the 'go and grow' TNTs. The localisation of Par proteins at the protrusive sites are linked to the cell orientation. A study has shown that HGF/c-Met-mediated production of PIP3 binds to Par3 and activates CDC42 and Rac at the protrusive sites (Etienne-Manneville 2008). This crosstalk between the PI3K/Par3/CDC42 pathways may be a mechanism for dictating the direction of TNT outgrowth. Future studies to visualise the co-localisation of Par3, CDC42 and p85a at the protrusion site can be used to determine whether HGF-mediated PIP3 activation recruits Par3. The molecular mechanism of the disassembly/retraction of the F-actin-containing TNT is still not known. Traditionally TNTs either retract back along the recipient or donor cell or disintegrate during their termination. However, both retraction and disintegration mechanisms are still not well defined in the literature. A high concentration of cytoplasmic calcium ions was shown to induce TNT retraction in A20 murine B cells through treatment with ionomycin (an ionophore which binds to calcium ions)

and thapsigargin (inhibitor of ER calcium ATPase) (Osteikoetxea-Molnár et al. 2016). Conversely, TNTs may retract through actin depolymerisation mechanisms which involve cofilins and actin oxidisers to destabilise F-actin (Frémont et al. 2017) and may be involved in the retraction stage of the 'go and grow' TNTs. Although future studies would be required to unravel the signalling mechanisms regulating the migration/TNT formation and retraction stages, the functional consequence of the 'go and grow' cells were also identified in our study

7.3.4 'Go and grow' cells are proliferate more than non-'go and grow' cells

Our study revealed the 'go and grow' cells are capable of enhanced proliferation compared to the non-'go and grow' population of A549 cells. This highlights the potential for 'go and grow' cells to engage in metastatic behaviour in the TME. Howevre, it is unknown how these cells metabolically support the simultaneous migration, TNT formation and cell proliferation. The initial TNT may potentially be providing metabolic support through the transfer of dysfunctional mitochondria which enables aerobic fermentation to take place in the 'go and grow' cell. Cancer cells often undergo aerobic fermentation, as coined by Warburg, whereby glycolysis occurs to produce lactic acid even in normoxic conditions (Warburg 1956), and is attributed to enhanced proliferation in cancer and non-cancerous cells (Abdel-Haleem et al. 2017). Aerobic fermentation, in the presence of unlimited glucose supply produces 15 times higher glycolytic flux compared to TCA cycle flux, thus leading to a significant surge in ATP production (Shestov et al. 2016). The A549 cell DMEM media contains high glucose, thus mimicking the conditions required for aerobic fermentation to take place. Therefore, the 'go and grow' cells may undergo aerobic fermentation to supply the cell with more ATP required for the 'go and grow' process. The rate of mitochondria transferred along a 'go and grow' TNT compared to non-'go and grow' TNTs can be determined for future studies. A study also demonstrated lung cancer cells undergoing cell division were migrating at higher speeds compared to non-dividing cells (Garay et al. 2013). Although the migration speed was not analysed for this study, it would be of interest to compare the migratory speeds of 'go and grow' cells with the non-'go and grow' cells. Overall, the results of these findings highlight the insidious nature of these cells equipped with a higher proliferative capacity and potential to migrate and metastasise.

7.3.5 HGF-induced 'go and grow' cells formed on hydrogels mimicking lung tumour matrix stiffness

An important aspect of our study was to determine whether the 'go and grow' phenomenon may also occur *in vivo*. Although previous observations were made in 2D *in vitro* plastic cultures, HGF-induced 'go and grow' cells were also observed on collagen IV-coated hydrogels mimicking the stiffness of the lung tumour. This is especially relevant in translating our observations *in vivo*, as

tissue culture plastic is roughly 100 000 kPa stiff (measured in Young's elastic modulus) whereas the stiffness of solid lung tumours range between 16-30 kPa (Booth et al. 2012; Miyazawa et al. 2018) and the healthy lung parenchyma is roughly 1 kPa (Goss et al. 2006). The matrix stiffness plays an active role in altering the biophysical cues and has been shown to regulate lung cancer cell proliferation, migration and invasion (Ishihara and Haga 2022; Navab et al. 2016; Yuan et al. 2015). Although the presence of 'go and grow' cells at a lung tumour stiffness was identified in our study, future image analysis would be required to quantify the incidence of 'go and grow' cells at the lung tumour stiffness in comparison to healthy lung stiffness. Therefore, the biomechanical role of the tumour matrix can be further identified in the formation of 'go and grow' cells. A study showed an increase in A549 cell proliferation and migration at higher stiffness (4.8 kPa) compared to low stiffness (0.15 kPa)(Tilghman et al. 2010). Interestingly, the same study also showed an increase in elongated morphology when cells were cultured at the higher stiffness (Tilghman et al. 2010). An increase in matrix stiffness has also been linked to EMT (Wei et al. 2015; Fattet et al. 2020), as HGF is known to also induce EMT (Liu, Song, et al. 2017), this process may be driving the invasive switch in the 'go and grow' cells. Moreover, an integrin-induced 'outside-in' signalling may be involved in initiating the 'go and grow' process. One study identified $\alpha 11\beta 1$ associating with collagen cross-linking amplified the stiffness in NSCLC leading to an increase in cell invasion and migration (Navab et al. 2016). Therefore, it is important to identify the role of the 'go and grow' cells in NSCLC and to determine whether they are involved in *in vivo* metastasis.

7.3.6 The potential role for 'go and grow' cells in NSCLC

In NSCLC, cells can metastasise in the early stages of the disease to a wide range of organs, most commonly to the brain (Ballard et al. 2016; Kamer et al. 2020; Zhu et al. 2020). NSCLC metastasis is a multistep orchestration driven by enhanced proliferation, migration, metabolic pressures, and immune evasion. The 'go and grow' cells discovered in this study could potentially reflect the early metastatic subpopulation of cancer cells. 'Go and grow' cells may drive the intravasation and extravasation process due to their highly migratory and proliferative abilities. The subpopulation of cells may arise from clonal expansion in the tumour as driver mutations in MET often occur through clonal expansion in NSCLC (Testa, Castelli, and Pelosi 2018). Clonal mutations occur earlier in the disease stage, developing ubiquitously in all the areas of the tumour, also termed 'trunk' mutations (Zhang et al. 2014). Therefore, genetic alterations of the MET gene could drive the HGF/c-Met induced 'go and grow' cells to metastasise. It would be of interest to isolate and characterise the cells that form the 'go and grow' TNTs. These cells could potentially be lung cancer stem cells as their properties mirror one another. Lung cancer stem cells can initiate tumour formation and are highly metastatic. In NSCLC, the percentage of CD133+ cells are roughly <1% (Eramo et al. 2008)

which is similar to the percentage of ‘go and grow’ TNT-forming cells observed in this study (2.7%). Moreover, recent studies have identified a subpopulation of CSCs which can evolve into CTCs in the bloodstream of patients with NSCLC, possessing the characteristic stem cell properties whilst adopting EMT phenotypes. CTCs exist as either single cells or clusters and their presence is correlated with poor prognosis and used for treatment efficacy in NSCLC (Pantazaka et al. 2021; Yang et al. 2019). Moreover, a study showed gemcitabine was able to inhibit the EpCAM-positive CTCs and their metastatic EMT effects through the HGF/c-Met pathway (Liao et al. 2014). This implicates HGF/c-Met signalling in inducing migration and invasion in CTCs, thus potentially mimicking the ‘go and grow’ phenomenon in our study. It would be of interest to isolate and enrich CTCs from NSCLC patients, through a size-based filtration microfluidic device or microchip system (Chemi et al. 2021), and observe whether they are able to undergo the ‘go and grow’ TNT phenomenon. The ‘go and grow’ TNTs serve a wider therapeutic implication in NSCLC. Future studies are required to further characterise the cells and determine whether they are CSCs or CSCs that have evolved to CTCs.

7.3.7 Future work

In this study, the immunofluorescent labelled ‘go and grow’ TNTs were identified from fixed cells and required rapid identification to ensure bleaching would not occur. Furthermore, although it is likely that a TNT connected to a dividing cell is undergoing the second stage of the ‘go and grow’ process, it does not confirm whether the cell retracts back along the TNT. To visualise the complete process, live cell imaging probes for F-actin and tubulin can be used to visualise the changes in cytoskeletal dynamics during migration and cell division, especially in the formation of the microtubule-based mitotic spindle. To better understand when the migrating/TNT-forming cells are undergoing the stages of the cell cycle, FUCCI can be used to observe the fluorescent changes in live cells (Sakaue-Sawano et al. 2008).

The study also did not characterise the signalling pathways involved during the formation of the ‘go and grow’ TNTs. However, it is difficult to isolate cells that form ‘go and grow’ TNTs based on their low incidence and are difficult to distinguish from other cells that form TNTs. A549 cells can be seeded on a transwell insert with HGF-containing media on the lower compartment. The cells that are highly migratory can then be collected at an appropriate timepoint at which ‘go and grow’ TNTs are likely to form. To determine the time at which ‘go and grow’ TNTs are formed, cells could be synchronised to the G0/G1 phase of the cell cycle through serum starvation and imaged for time-lapse after HGF treatment. These cells can then be used for HGF-associated inhibitor experiments to determine which pathways (e.g. PI3K, MAPK or Par3/CDC42) are involved at the different stages of the ‘go and grow’ TNT formation. Furthermore, to better recapitulate the physiological stiffness of

the tumour, cells can be seeded on hydrogels with fluorescent beads at the appropriate stiffness. The tensile stiffness of the plastic culture surface is roughly 100 000kPA whereas the lung tumour is between 20-30kPA (Miyazawa et al. 2018; Skardal et al. 2013). Matrix stiffness can impact the mechanical cues which alter the migration, proliferation and gene expression of the cells (Asano et al. 2017; Lo et al. 2000). Traction force microscopy in conjunction with the different inhibitors at the appropriate timings can be carried out to measure the forces during the TNT formation and retraction.

The daughter cell fate has also not been determined in this study therefore longer (e.g. 48 hours) time-lapse videos are needed to identify whether the daughter cells can form 'go and grow' TNTs and further tracked to determine whether they display higher migratory or proliferative capacity compared to the mother cell. Moreover, CTCs can be isolated from NSCLC patients to observe whether they are able to form 'go and grow' TNTs and detect whether the mutations for MET are present in ctDNA through real-time PCR or next-generation sequencing (NGS).

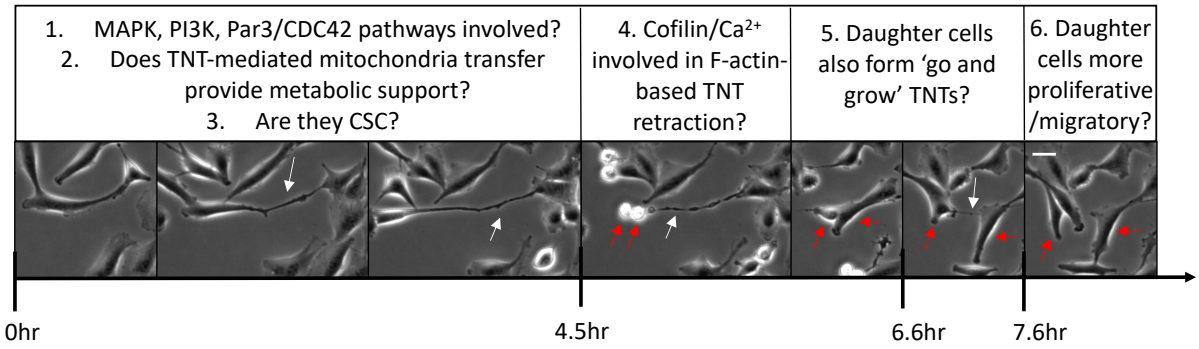


Figure 7.8 Future aims involved in further characterising the 'go and grow' cells. The timeline of the 'go and grow' TNTs show the respective potential molecular mechanisms involved during the formation and retraction stage. Furthermore, the unknown biological outcomes of the daughter cell fate are highlighted for the later stages of the process.

Throughout the studies conducted in this thesis, HGF and its interactions with the different upregulated cytokines in the TME have been shown to regulate A549 cell growth, TNT formation and induce a novel 'go and grow' effect. However, these *in vitro* findings utilised 2D monolayer A549 cell cultures. Therefore, to better recapitulate the 3D TME of NSCLC, an *in vitro* 3D A549 tumouroid culture in Matrigel was developed to explore the role of HGF and IL-6 in A549 tumouroid growth, the role of HL-60/eos in regulating A549 tumouroids growth/death *via* a novel co-culture system and the effect of a chemotherapeutic agent, triptolide, in A549 tumouroid TNT formation.

8. Chapter 8: The 3D tumour microenvironment in influencing A549 cell growth, TNT formation and immune response

8.1 Introduction

The complex 3D tumour microenvironment of NSCLC consists of tumour, stromal and immune cells surrounded by the ECM. A complex set of interactions exist between tumour cells and components of the TME to support the phases involved in cancer progression (as reviewed in (Baghban et al. 2020). The cause of the dynamic cross-signalling outcomes are mediated by growth factors (including HGF), chemokines, cytokines (including IL-6) and proteolytic enzymes which are harboured within the ECM (Baghban et al. 2020). Studies have highlighted the role of IL-6 in NSCLC proliferation (Zheng et al. 2019; Lee et al. 2016) and the crosstalk between HGF and IL-6 in inducing invasion in A549 cells (To et al. 2002). Our previous findings in chapter 3 demonstrate a novel downstream convergent signalling involved in the HGF and IL-6-mediated proliferation of A549 cells. Furthermore, another important aspect influencing cancer progression is the ability of cancer cells to survive in the pro-inflammatory TME (Hanahan and Weinberg 2011). Immune cells, such as eosinophils, often infiltrate tumours releasing cytokines (including IL-6) and chemokines to influence either a pro-tumourigenic or anti-tumourigenic effect (Sakkal et al. 2016; Wang et al. 2022). Cancer cells have been shown to release HGF, IL-3, IL-5, eotaxin-1 and CCL17 to promote differentiation and attract an influx of eosinophils to the tumour site (Ito et al. 2007; Rosenberg, Dyer, and Foster 2013). However, there have been conflicting reports on the effect of eosinophils within the TME. A favourable prognosis was observed through the cytotoxic activity of the degranulation of eosinophils: ECP has been shown to exert its cytotoxic effect on oral squamous cells through osmotic lysis (Dorta et al. 2002a) and eosinophil-derived MBP were also found in the tissue of lung metastases (Mattes et al. 2003). Conversely, studies have also implicated eosinophils in exacerbating cancer progression: tumour-associated blood eosinophilia (TABE) is associated with the metastatic stages of cancers (including of kidney, thyroid, liver, gallbladder, pancreas, breast, cervical and in Hodgkin's lymphoma) which correlated with poor survival rates (Samoszuk 1997; Molin 2004). Limited studies have observed the effect of eosinophils in NSCLC and the evidence suggests eosinophils may either induce NSCLC growth and contribute to unfavourable outcomes or induce cell death *via* degranulation of their cytotoxic granules. Overall, HGF, IL-6 and eosinophils have the potential to induce NSCLC growth however their role has not been explored within the 3D TME of NSCLC. Therefore, o better replicate the function and biology of solid tumours *in vivo,* a 3D A549 tumouroid culture in Matrigel was used in our study to investigate the role of HGF, IL-6 and eosinophils in A549 tumouroid growth. Various studies have used reconstituted Matrigel to study the morphological characteristics of epithelial tumours (Martin et al. 2008; Sempere,

Gunn, and Korc 2011), including the lung (Fessart, Begueret, and Delom 2013). Matrigel is extracted from mouse Englebreth-Holm-Swarmm tumour and mainly consists of laminin, collagen IV, entactin and a range of growth factors (Oridate, Lotan, and Lotan 1996). Expanding the dimensions of the ECM in 3D Matrigel culture alters the cell-to-cell and cell-to-matrix interactions which impacts cell proliferation, cell survival and mechano-transduction signalling (Duval et al. 2017).

Whilst 3D cultures are useful to study the different basic biology involved in tumour formation and metastasis, they have also proven to be a reliable tool for rapid drug screening for personalised therapies. Retaining similar properties of *in vivo* tumours is vital to accurately assess drug responses for future clinical development. However, conventional chemotherapeutic agents and other targeted kinase-inhibitor therapies in NSCLC are often only effective temporarily with the emergence of resistance (as reviewed in (Rotow and Bivona 2017). Furthermore, TNTs have been overlooked as a means for propagating chemoresistance in cancer *via* transport of mitochondria, vesicles and miRNA (Pasquier et al. 2013; Kolba et al. 2019; Kretschmer et al. 2019). TNTs can also transport p-glycoprotein thus promoting drug efflux as a resistance mechanism (Desir et al. 2018). However, most TNT studies have been conducted in 2D monolayer cultures and are rarely studied *in vivo* or observed in tumouroid models due to the technical difficulty in retaining and identifying the thin, fragile structures. There have been recent efforts to visualise TNTs in 3D tumouroid cultures of MCF7 cells (Pulze et al. 2020), mesenchymal stem/stromal cells (MSCs) (Whitehead et al. 2020; Zhang et al. 2018) and in SCC (Sáenz-de-Santa-María et al. 2017). As TNTs have been observed upon drug treatment (Pasquier et al. 2013; Kolba et al. 2019; Kretschmer et al. 2019), we aimed to visualise TNTs through triptolide treatment of A549 tumouroids. Triptolide, a diterpenoid triepoxide isolated from the Chinese plant *Tripterygium wilfordii* Hook F (Kupchan et al. 1972). As a traditional Chinese medicine, triptolide is used as an anti-inflammatory agent in rheumatoid arthritis, systemic lupus erythematosus, nephritis and psoriasis (Liu 2011). However, it is currently an emerging drug in development for cancer therapeutics, displaying apoptotic effects *in vitro* and *in vivo* models of NSCLC (Rousalova et al. 2013; Kumar et al. 2016). Therefore, we aimed to visualise the effects of triptolide on A549 tumouroid TNT formation in this chapter.

Overall, this chapter aims to elucidate the role of various factors within the TME in NSCLC progression using A549 tumouroid 3D culture. The effect of HGF and IL-6 on growth, the role of eosinophils in A549 cell death or growth, through a novel co-culture experimental system, and the effect of triptolide on TNT formation will be explored in this chapter.

8.2 Results

8.2.1 A549 cells cultured in Matrigel grow into tumouroids over a 9-day period

To initiate the growth of A549 cells into tumouroids in Matrigel, A549 cells were grown in Matrigel at a density of $1X10^4$ cells/coverslip (Fig 8.1), to observe the tumouroid growth over a 9-day period. Over the 9-day period, the cells developed into tumouroids on day 3 and increased in size and confluency daily whilst in culture. The ideal tumouroid size was identified at day 3 for future experiments (Fig 8.1). This ensured an appropriate tumouroid size was for visualisation of the differences in tumouroid growth, TNT formation and eosinophil interactions in co-culture

A

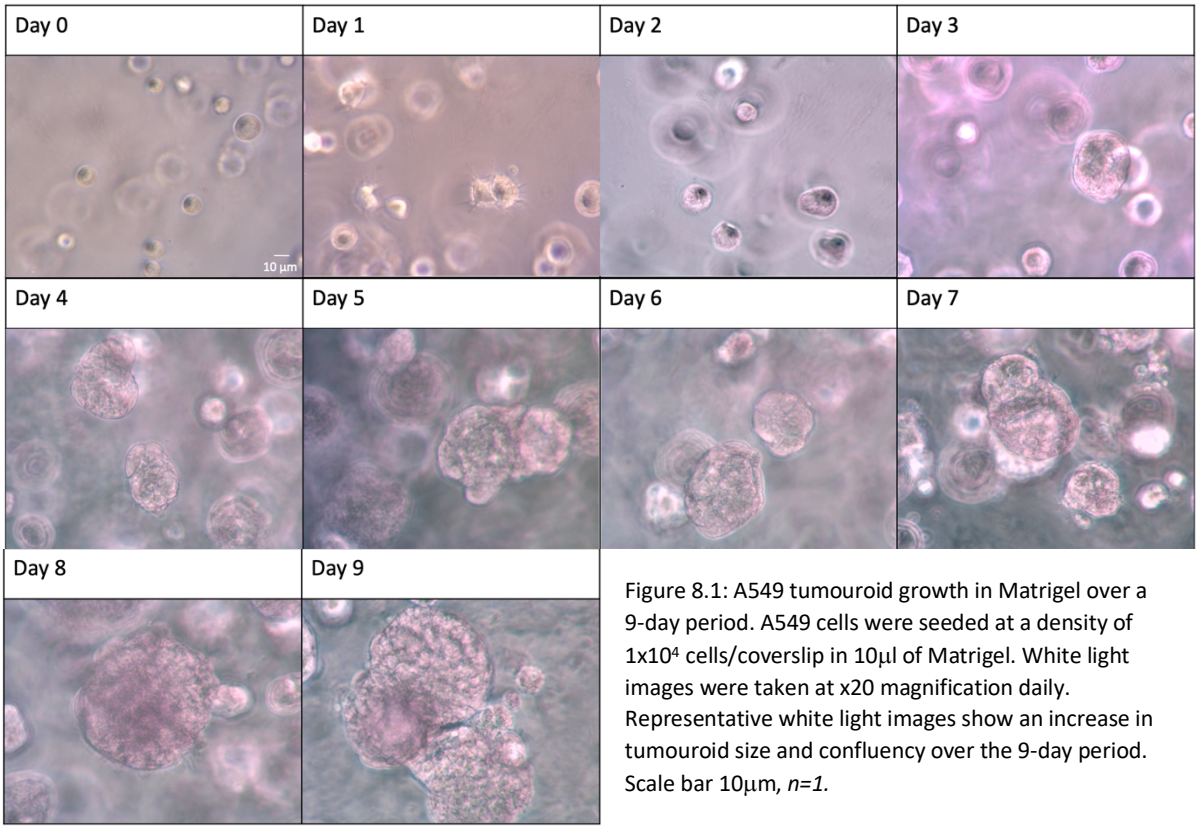
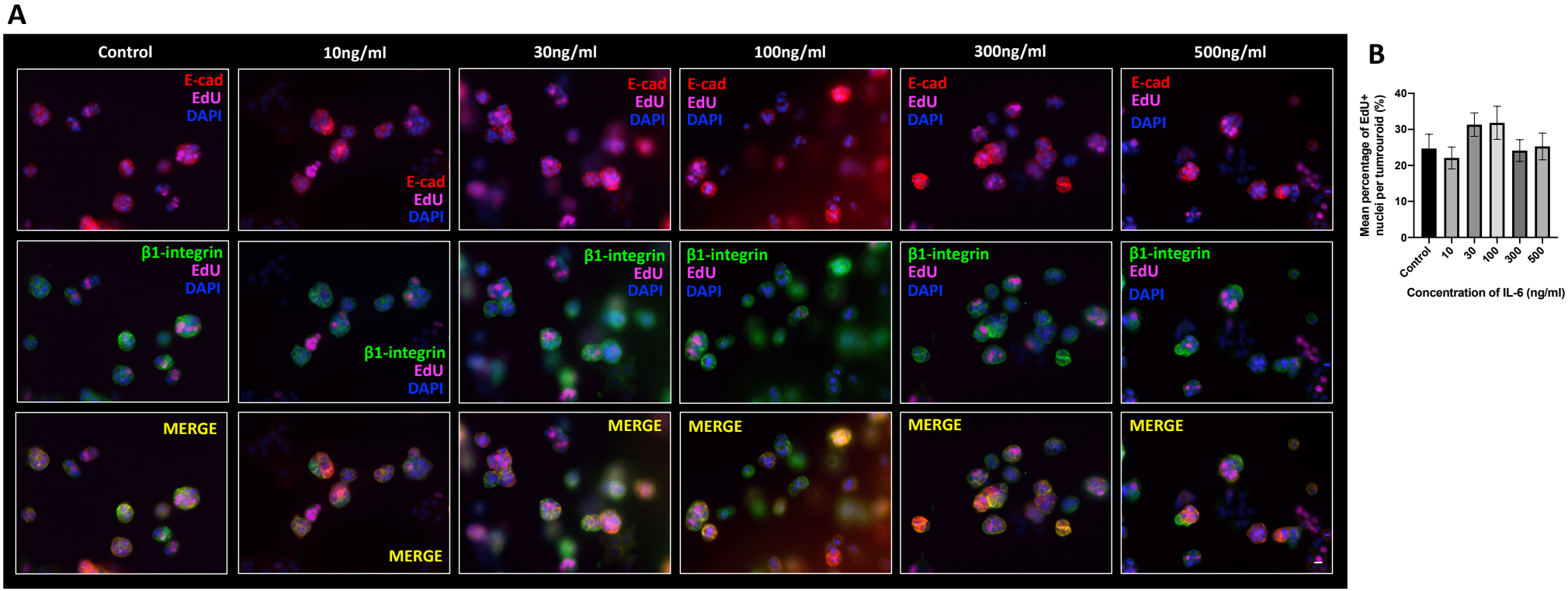


Figure 8.1: A549 tumouroid growth in Matrigel over a 9-day period. A549 cells were seeded at a density of $1x10^4$ cells/coverslip in 10µl of Matrigel. White light images were taken at x20 magnification daily. Representative white light images show an increase in tumouroid size and confluency over the 9-day period. Scale bar 10µm, *n=1.*

8.2.2 72-hour HGF and IL-6 treatment at day 0 had no effect on EdU incorporation of A549 tumouroids

A549 cells seeded in Matrigel were treated with IL-6 (0-500ng/ml) and HGF (0-500ng/ml) in 10% FBS supplemented DMEM media on day 0 and left to grow for 72 hours to determine the effects of IL-6 and HGF on tumouroid development. EdU (pink) incorporation and immunofluorescence labelling of cell surface markers E-cadherin (red) and β1-integrin (green) was undertaken for the A549 tumouroids (Fig8.2A&C). In control, IL-6-(10-500ng/ml) and HGF-treated (10-500ng/ml) cells, there

was no change in E-cadherin (red) and β1-integrin (green) localisation, both E-cadherin (red) and β1-integrin (green) remained localised at the cell membrane of bordering individual A549 cells within the tumouroids across all conditions (Fig8.2A&C). Moreover, In the presence of HGF (10ng/ml-500ng/ml), the A549 cells did not scatter in the Matrigel and the tumouroids remained intact throughout the 72-hour culture period (Fig8.2C). There was no increase in EdU incorporated nuclei of A549 tumouroids across the treated concentrations of IL-6 compared to control (Fig8.2B). There was also no increase in EdU incorporated nuclei of A549 tumouroids across the treated concentrations of HGF compared to control (Fig8.2D).


A
Control
10ng/ml
30ng/ml
100ng/ml
300ng/ml
500ng/ml
E-cad
EdU
DAPI
β1-integrin
MERGE
B
Mean percentage of EdU+ nuclei per tumrouroid (%)
0
10
20
30
40
Control
10
30
100
300
500
Concentration of IL-6 (ng/ml)

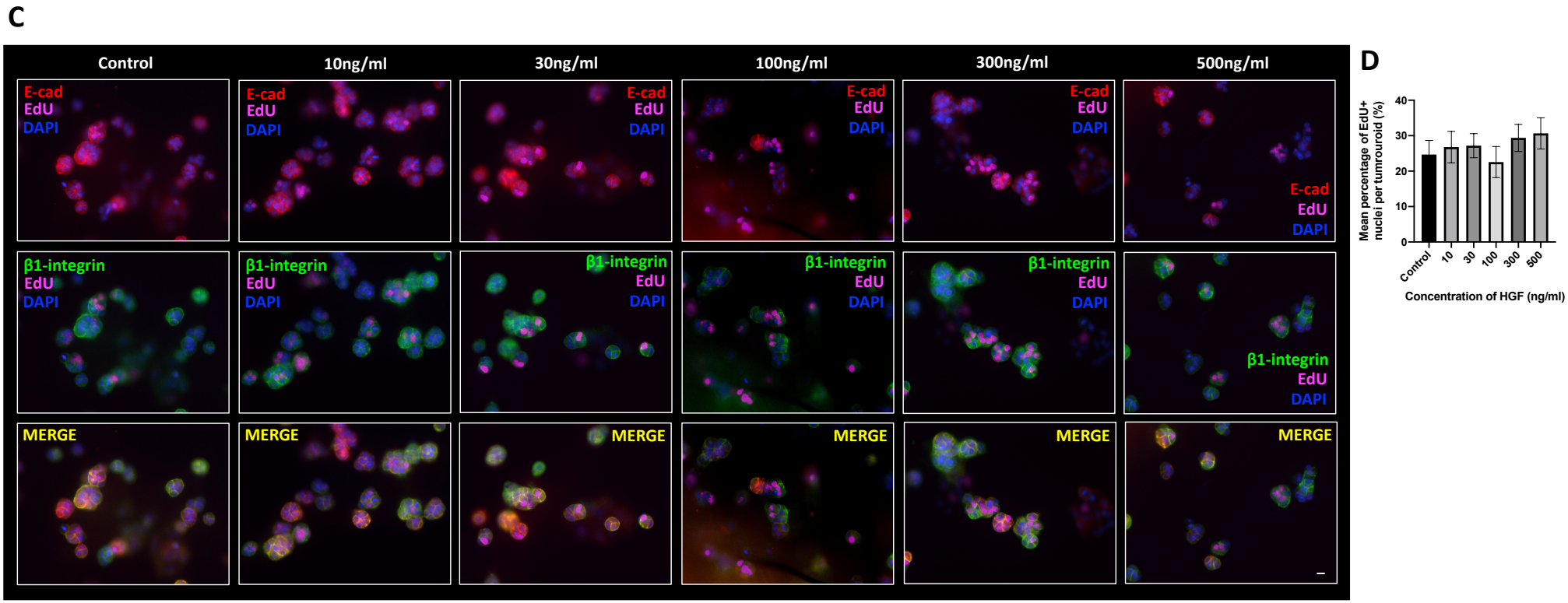
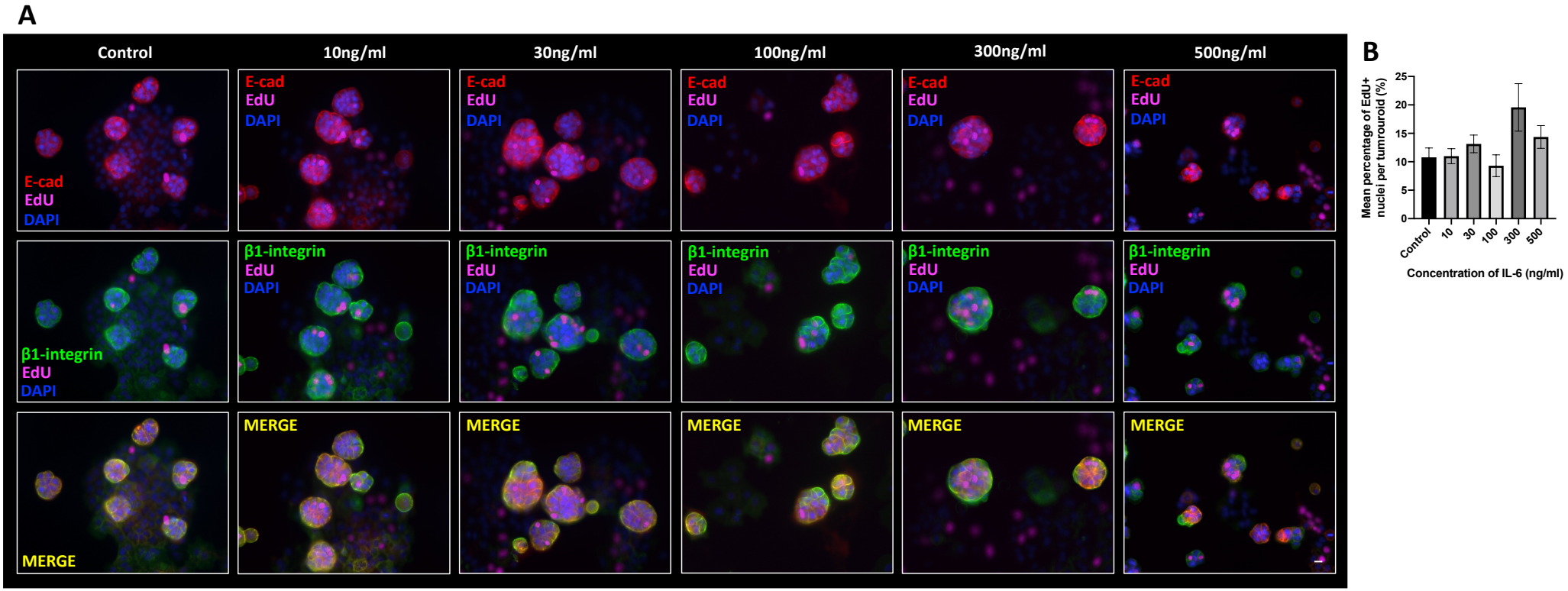


Figure 8.2: IL-6 and HGF has no effect on A549 tumouroid development. A: Representative epifluorescence images show E-cadherin (red), β1-integrin (green), EdU incorporated nuclei (pink) and DAPI (blue) stained nuclei of A549 tumouroids treated with IL-6 (0-500ng/ml) on day 0 for 3 days. B: The histogram shows no difference between the mean percentage of EdU incorporated nuclei between control tumouroids and the concentrations of IL-6 treated A549 tumouroids C: Representative epifluorescence images show E-cadherin (red), β1-integrin (green), EdU incorporated nuclei (pink) and DAPI (blue) stained nuclei of A549 tumouroids treated with HGF (0-500ng/ml) for 3 days. D: The histogram shows no difference between the mean percentage of EdU incorporated nuclei between control tumouroids and the concentrations of HGF treated A549 tumouroids. Values are expressed as mean ± SEM, n=1, N ≥37. Scale bar 10µm,

8.2.3 72-hour HGF and IL-6 treatment at day 3 had no effect on EdU incorporation of A549 tumouroids

To determine the effect of HGF and IL-6 on A549 tumouroid growth, A549 tumouroids were treated with IL-6 (0-500ng/ml) and HGF (0-500ng/ml) in 10% FBS supplemented DMEM media on day 3 and left to grow for 72 hours in culture. EdU (pink) incorporation and immunofluorescence labelling of cell surface markers E-cadherin (red) and β1-integrin (green) was undertaken for the A549 tumouroids (Fig8.3A&C). In control, IL-6-(10-500ng/ml) and HGF-treated (10-500ng/ml) cells, there was no change in E-cadherin (red) and β1-integrin (green) localisation, both E-cadherin (red) and β1-integrin (green) remained localised at the cell membrane of the bordering A549 cells within the tumouroids across all conditions (Fig8.3A&C). Moreover, In the presence of HGF (10ng/ml-500ng/ml), the A549 cells did not scatter in the Matrigel and the tumouroids remained intact throughout the 72-hour culture period (Fig8.3C). There was no increase in EdU incorporated nuclei of A549 tumouroids across the treated concentrations of IL-6 compared to control (Fig8.3B). There was also no increase in EdU incorporated nuclei of A549 tumouroids across the treated concentrations of HGF compared to control (Fig8.3D).


A
Control
10ng/ml
30ng/ml
100ng/ml
300ng/ml
500ng/ml
E-cad
EdU
DAPI
β1-integrin
MERGE
B
Mean percentage of EdU+ nuclei per tumrouroid (%)
25
20
15
10
5
0
Control
10
30
100
300
500
Concentration of IL-6 (ng/ml)

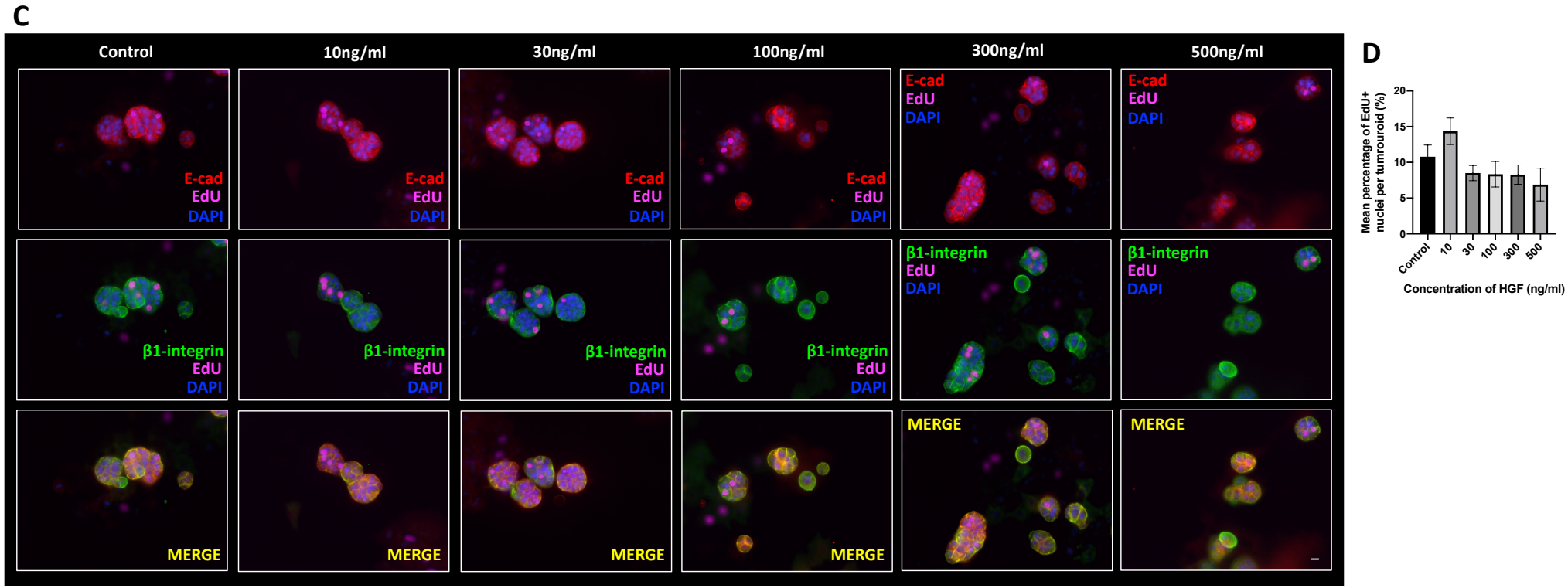


Figure 8.3: IL-6 and HGF has no effect on A549 tumouroid growth. A: Representative epifluorescence images show E-cadherin (red), β1-integrin (green), EdU incorporated nuclei (pink) and DAPI (blue) stained nuclei of A549 tumouroids treated with IL-6 (0-500ng/ml) on day 3 for 2 days. B: The histogram shows no difference between the mean percentage of EdU incorporated nuclei between control tumouroids and the concentrations of IL-6 treated A549 tumouroids C: Representative epifluorescence images show E-cadherin (red), β1-integrin (green), EdU incorporated nuclei (pink) and DAPI (blue) stained nuclei of A549 tumouroids treated with HGF (0-500ng/ml) on day 3 for 2 days. D: The histogram shows no difference between the mean percentage of EdU incorporated nuclei between control tumouroids and the concentrations of HGF treated A549 tumouroids. Values are expressed as mean ± SEM, n=1, N ≥17. Scale bar

After establishing HGF and IL-6 had no effect on A549 tumouroid growth, we next investigated the role of eosinophils, an understudied immune cell in NSCLC, and its effect on mediating A549 tumouroid growth. To address this, we developed a novel eosinophil and A549 tumouroid co-culture model.

8.2.4 Development of a HL-60/eos and A549 tumouroid co-culture model

To set up the eosinophil and A549 tumouroid co-culture model, the differentiation of the HL-60 cell line towards an eosinophil-like phenotype as per Fischkoff et al was first conducted (Fischkoff, Brown, and Pollak 1986), which involved culturing the HL-60 cells for 5 days with 0.5mM of butyric. Diff-Quick staining (Fig8.4A) was then undertaken to confirm the presence of characteristic eosinophil bi-lobed nucleus (blue arrow) and cytoplasmic acidic granule content (pink arrow). This was further quantified to obtain the mean percentage of bi-lobed nucleus and the mean percentage of HL-60 with granules on day 5 (Fig5.4B&C). Due to the low percentage of the bi-lobed nucleus, immunofluorescence labelling of the eosinophil-specific marker CCR3 was undertaken to confirm the presence of an eosinophil-like phenotype present (Fig5.4D). The HL-60/eos positively expressed CCR3 thus confirming the differentiation of HL-60 cells to an eosinophil-like phenotype. Trypan blue viability test was also conducted daily to ensure the HL-60/eos on day 5 (93.9%) were viable for use in co-culture (Table 8.1).

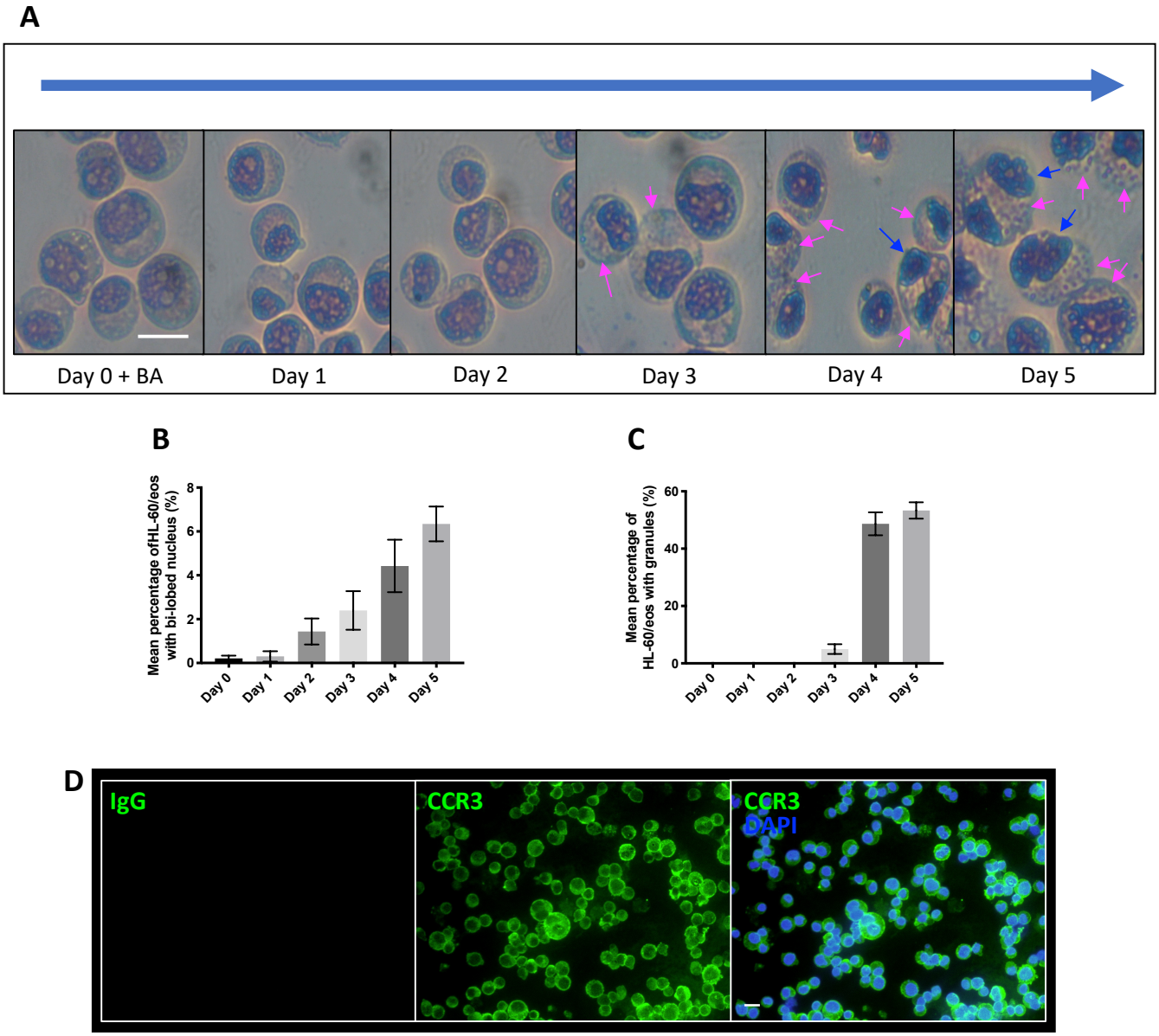


Figure 8.4: HL-60 cells differentiate towards an eosinophil-likel phenotype. A: Daily H&E staining of the HL-60 cells with butyric acid (0.5mM) was undertaken to visualise the characteristic bi-lobed nucleus and presence of acidic granules by day 5. B: The histogram shows the mean percentage of HL-60 cells with a bi-lobed nucleus over 5 days of differentiation with butyric acid. C: The histogram shows the mean percentage of HL-60 cells with the presence of acidic granules over 5 days of differentiation with butyric acid. Values are expressed as mean ± SEM, n=2. D: Representative epifluorescent images of IgG and CCR3 (green) labelled HL-60/eos. Immunofluorescence labelling of day 5 HL-60/eos showed positive expression of the characteristic eosinophil marker CCR3 (green). Representative images were obtained from 3 individual experiments. Scale bar 10µm.

Day 0+Butyric acid	Day 1	Day 2	Day 3	Day 4	Day 5
100%	95.7%	95.7%	95.3%	95%	93.9%

Table 8.1: HL-60/eos trypan blue viability test. Daily trypan blue viability test was undertaken for the HL-60 cells treated with 0.5mM of butyric acid over the 5 days of differentiation towards an eosinophil phenotype.

8.2.5 HL-60/eos had no effect on caspase-3 positive A549 cells and EdU-incorporated A549 nuclei

After confirming the differentiation of HL-60 cells into an eosinophil-like phenotype, the HL-60/eos were co-cultured with A549 tumouroids either *via* the 'IN' or 'ON' method. For the 'IN' method, the HL-60/eos and A549 cells were resuspended together at the time of seeding into Matrigel and allowing 3 days for the tumouroid to develop. For the 'ON' method, the A549 tumouroids were first established in Matrigel for 3 days before the HL-60/eos were added in the media to cover the Matrigel for a further 3 days. The 'IN' and 'ON' method was used to determine whether the effect on A549 cell proliferation/death was either contact-mediated or due to secreted factors respectively. Immunofluorescence labelling with E-cadherin and caspase-3 was then undertaken for both the 'IN' (Fig8.5A) and 'ON' (Fig8.5B) co-culture of HL-60/eos and A549 tumouroids. Multiple HL-60/eos (white arrows) localised around the A549 tumouroid when co-cultured with the 'IN' method (Fig8.5A). The HL-60/eos (white arrows) mainly localised to the edge of the Matrigel when co-cultured with the 'ON' method, however, there were a few HL-60/eos (white arrow) which have migrated into the Matrigel and are attached to the A549 tumouroid (Fig8.5B). There was a lack of caspase-3 positive A549 cells when co-cultured with HL-60/eos for both methods (Fig8.5A&B). As a high density of the HL-60/eos was added in co-culture with the A549 tumouroids, quantification of the caspase-3 positive A549 cells was difficult to distinguish between the HL-60/eos cells which were also caspase-3 positive when co-cultured with the 'IN' method (Fig8.5A). Moreover, for the 'ON' method, the accumulated HL-60/eos around the Matrigel edge were caspase-3 positive (Fig8.5B).

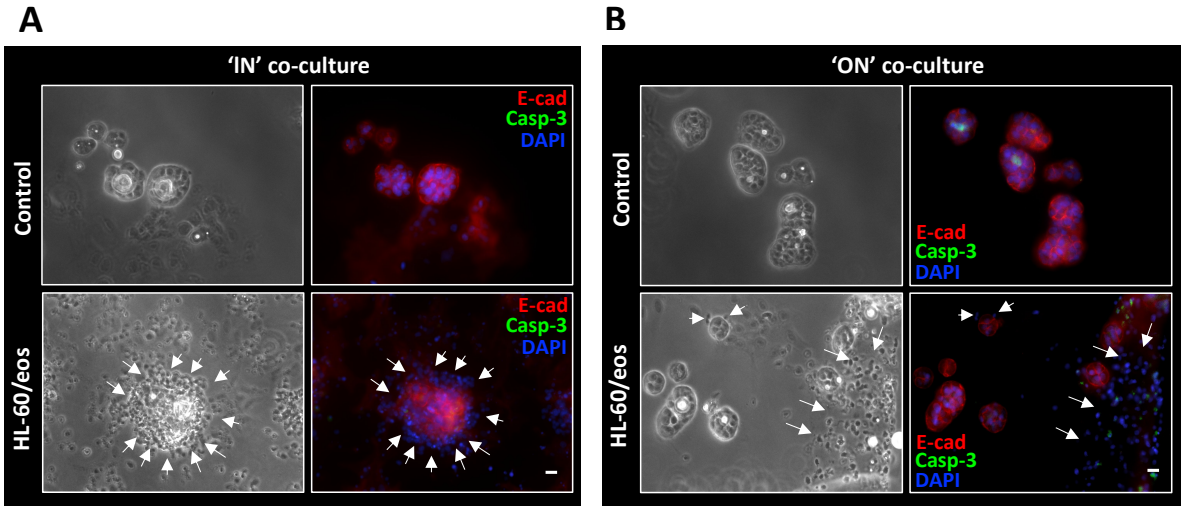


Figure 8.5: The 'IN' and 'ON' co-cultures of A549 tumouroids with HL-60/eos. A: Representative white light and epifluorescennt images show the HL-60/eos co-cultured with A549 tumouroids via the 'IN' method. HL-60/eos were observed in contact with the A549 tumouroid (white arrows) when co-cultured *via* the 'IN' method. B: Representative white light and epifluorescennt images show the HL-60/eos co-cultured with A549 tumouroids via the 'ON' method. Multiple HL-60/eos (white arrows) localised along the periphery of the Matrigel when co-cultured *via* the 'ON' method. There were also HL-60/eos (white arrows) observed in contact with an A549 tumouroid when co-cultured via the 'ON' method. Caspase-3 positive A549 cells were difficult to distinguish in both co-cultures. Representative images were obtained from 1 individual experiment. Scale bar 10μm.

To ensure the survival of the HL-60/eos was not due to being cultured in DMEM media rather than RPMI media, The HL-60/eos on day 5 were seeded at a range of seeding densities (1x10^5 cells/well, 2x10^5 cells/well, 3x10^5 cells/well) in either DMEM or RPMI media for 48 hours. Diff-Quick staining was then undertaken to quantify the percentage of apoptotic nuclei of the HL-60/eos. Apoptotic nuclei was identified through distinct nuclear condensation and DNA fragmentation (black arrow)(Fig8.6A). The quantification showed an increase in mean percentage of apoptotic nuclei for both DMEM and RPMI media when there was an increase in seeding density (Fig8.6B). Therefore, for future experiments, the A549 tumouroids were co-cultured in DMEM media at a density of 1x10^5 cells/coverslip, as this was the lowest mean percentage of apoptosis of HL-60/eos observed.

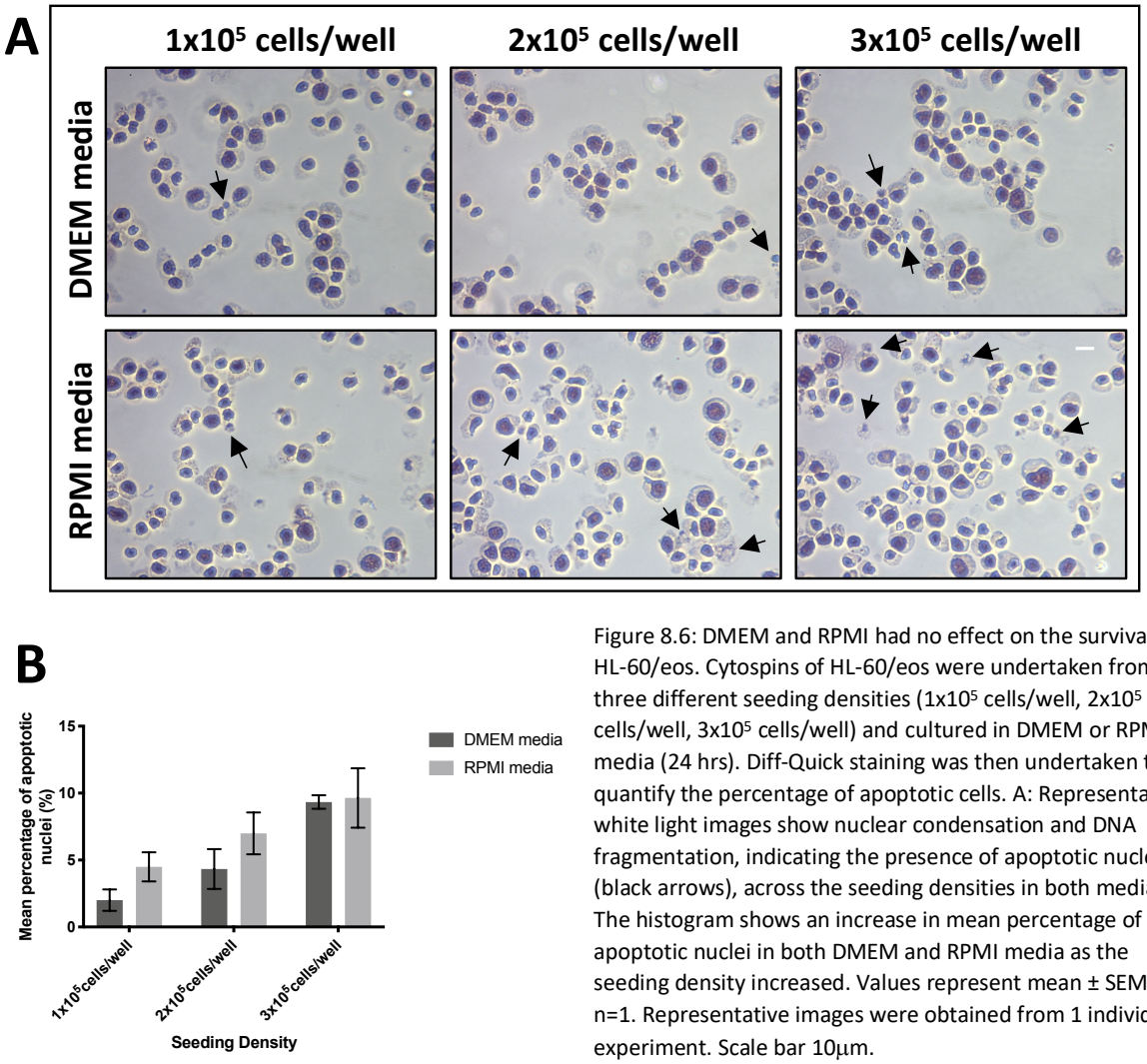


Figure 8.6: DMEM and RPMI had no effect on the survival of HL-60/eos. Cytospins of HL-60/eos were undertaken from three different seeding densities (1x10^5 cells/well, 2x10^5 cells/well, 3x10^5 cells/well) and cultured in DMEM or RPMI media (24 hrs). Diff-Quick staining was then undertaken to quantify the percentage of apoptotic cells. A: Representative white light images show nuclear condensation and DNA fragmentation, indicating the presence of apoptotic nuclei (black arrows), across the seeding densities in both media. B: The histogram shows an increase in mean percentage of apoptotic nuclei in both DMEM and RPMI media as the seeding density increased. Values represent mean ± SEM, n=1. Representative images were obtained from 1 individual experiment. Scale bar 10μm.

When the A549 tumouroids were co-cultured with HL-6/eos (1x10^5 cells/well) *via* the 'IN' method. Although there were HL-60/eos in contact with the A549 tumouroid (as previously shown in Fig8.5A), due to the extensive washing and processing required after fixation, this resulted in the loss of HL-60/eos and therefore, no HL-60/eos were found present in the immunofluorescent

labelled images (Fig8.7A). There was also no difference in mean percentage of EdU incorporated A549 nuclei between control and the HL-60/eos co-cultured A549 tumouroids (Fig8.7B). There was also no difference in mean percentage of caspase-3 positive A549 cells between control and HL-60/eos co-cultured A549 tumouroids (Fig8.7C).

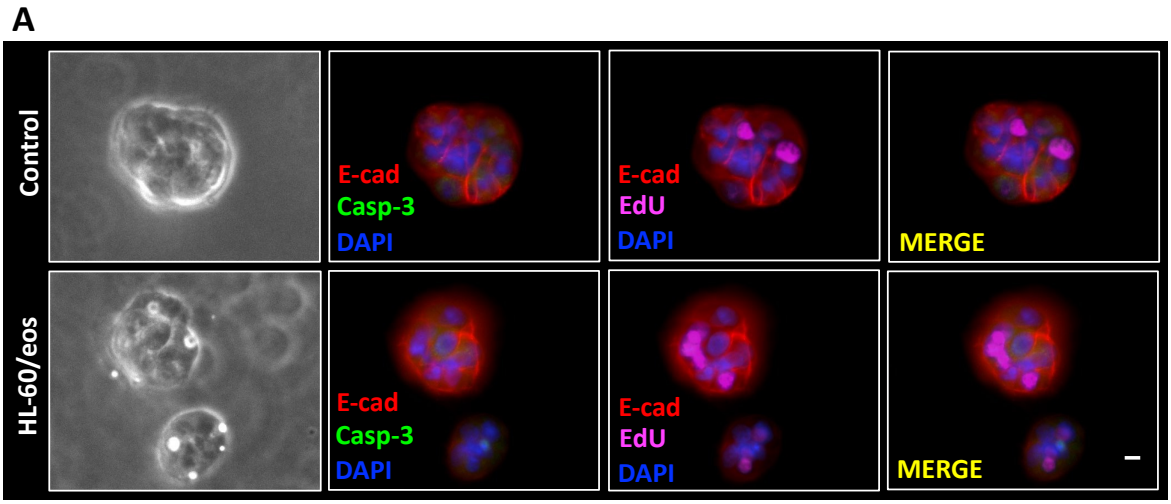


Figure 8.7: The 'IN' co-culture of A549 tumouroids with HL-60/eos. A: Representative white light phase contrast epifluorescence images show A549 tumouroids with EdU incorporated nuclei and E-cadherin and caspase-3 immunofluorescent labelling. B: The histogram shows there was no difference between the mean percentage of EdU positive A549 nuclei in control and HL-60/eos co-cultured A549 tumouroids. C: The histogram shows there was no difference between the mean percentage of caspase-3 positive A549 nuclei in control and HL-60/eos co-cultured A549 tumouroids. Values represent mean ± SEM, n=1. Representative images were obtained from 1 individual experiment. Scale bar 10μm.

When the A549 tumouroids were co-cultured with HL-6/eos (1x10^5 cells/well) *via* the 'ON' method (Fig8.8A), there was also no difference in mean percentage of EdU incorporated A549 nuclei between control and the HL-60/eos co-cultured A549 tumouroids (Fig8.8B). There was no difference in mean percentage of caspase-3 positive A549 cells between control and HL-60/eos co-cultured A549 tumouroids (Fig8.8C). Likewise with the 'ON' method, the extensive washing and processing required after fixation resulted in the loss of HL-60/eos and therefore, no HL-60/eos were found present in the immunofluorescent labelled images (Fig8.8A).

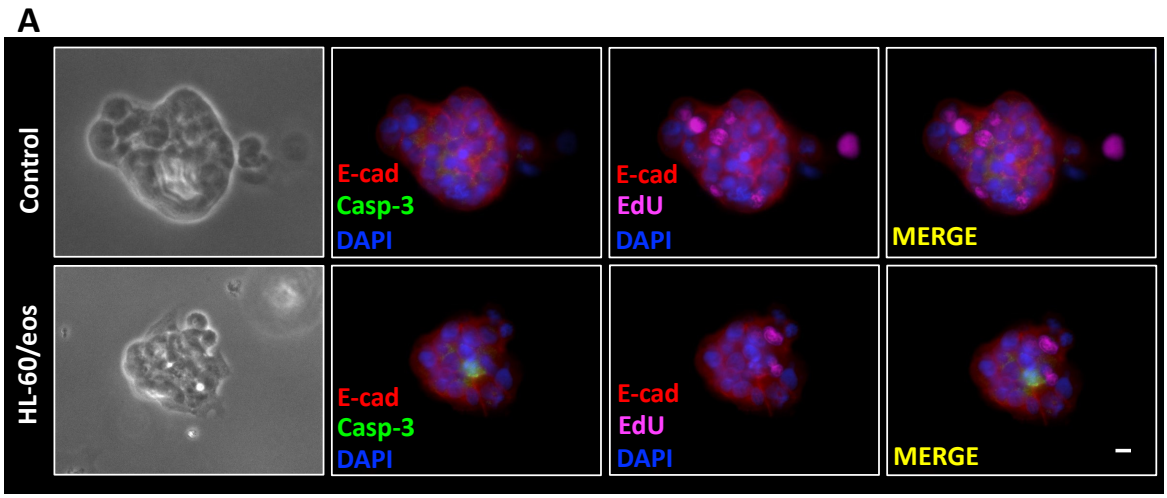


Figure 8.8: The 'ON' co-culture of A549 tumouroids with HL-60/eos. A: Representative white light phase contrast and epifluorescence images show A549 tumouroids with EdU incorporated nuclei and E-cadherin and caspase-3 immunofluorescent labelling. B: The histogram show no difference between the mean percentage of EdU -positive A549 nuclei in control and HL-60/eos co-cultured A549 tumouroids. C: The histogram show no difference between the mean percentage of caspase-3 positive A549 nuclei in control and HL-60/eos co-cultured A549 tumouroids. Values represent mean ± SEM, n=1. Representative images were obtained from 1 individual experiment. Scale bar 10μm.

Although the 3D A549 tumouroid system showed HL-60/eos, HGF and IL-6 had no effect on A549 tumouroid growth, we next utilised the A549 tumouroid model to determine the effect of a chemotherapeutic agent, namely triptolide, currently under investigation by the O'Connell lab, on TNT formation.

8.2.6 Triptolide induced the formation of TNT-like structures between A549 tumouroids

As HGF and IL-6 had no effect on A549 tumouroid development and growth, we next used the 3D A549 tumouroid culture to visualise TNT formation. A549 tumouroids were grown for 4 days and treated with triptolide (0.1μM) for 48 hours before undertaking white light imaging. A TNT-like structure (black arrow) was observed forming between two tumoroids after Triptolide treatment (48 hours) whereas no TNTs were observed in control (Fig8.9).

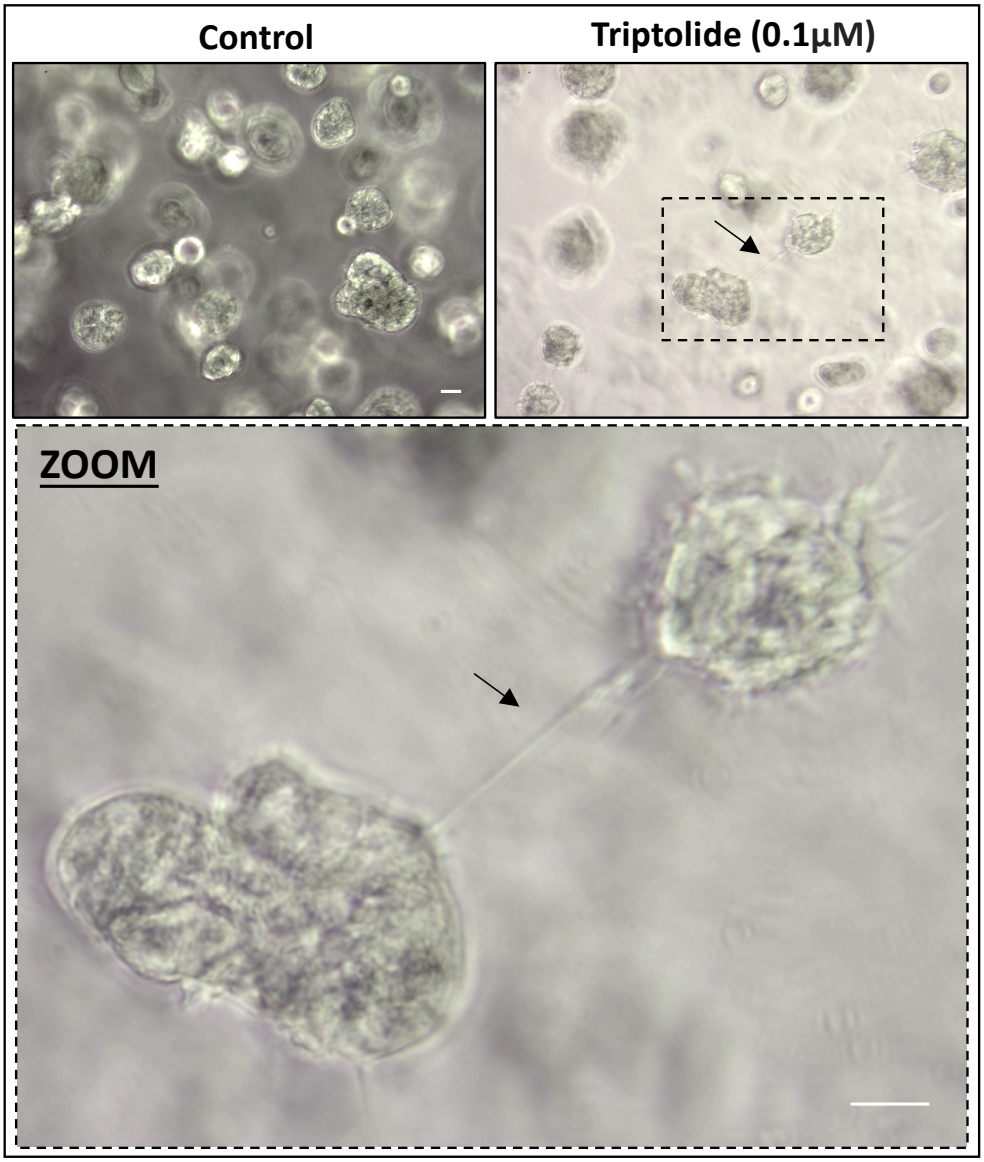


Figure 8.9: Triptolide induced the formation of TNT-like structures between A549 tumouroids. A549 tumouroids were grown for 4 days before being treated with triptolide (0.1μM) for 48 hours. Representative white light images show control and triptolide-treated tumouroids. A TNT-like structure (black arrow) was observed between two tumouroids when treated with triptolide. The black arrow denotes a TNT structure. The dotted region denotes a zoomed area. Scale bar 10μm. Representative images were obtained from 2 individual experiments.

8.3 Discussion

In this chapter, we demonstrate HGF and IL-6 have no effect on A549 tumouroid development and growth. Furthermore, to investigate the understudied role of eosinophils in the TME of NSCLC, a novel co-culture system with HL-60/eos with A549 tumouroids was developed. However, the co-cultures of A549 tumouroids with HL-60/eos revealed no effect on A549 cell death *via* caspase-3 activation or growth *via* EdU incorporation. Triptolide treatment of A549 tumouroid resulted in a novel observation of TNT-like structures forming between tumouroids. This highlights the potential role for TNTs mediating the survival of drug-treated cells *in vivo*.

8.3.1 HGF and IL-6 has no effect on A549 tumouroid development and growth

A549 cells cultured in Matrigel formed 3D spherical tumouroids on day 3 and increased in size up until day 9. This morphology has also been observed in other studies culturing A549 cells in Matrigel (Fessart, Begueret, and Delom 2013). 3D tumouroid cultures serve as an intermediary between 2D monolayer cultures and *in vivo* tumours as they more closely mimic *in vivo* proliferation, differences in metabolic environment (i.e. tumourigenic hypoxic and normoxic states) and cell-cell/cell-matrix contacts (Souter et al. 2010; Chitcholtan et al. 2013; Santini, Rainaldi, and Indovina 2000; Fessart, Begueret, and Delom 2013). However, this study showed HGF and IL-6 did not induce an effect on A549 tumouroid growth or development. Further repeats are required to confirm the statistical significance of the effect of HGF and IL-6. Moreover, there are several factors in the experimental conditions which may be affecting the HGF and IL-6-induced A549 tumouroid growth. The A549 tumouroids were cultured and treated in 10% FBS-supplemented media which may mask the proliferative capacity of HGF and IL-6. Additional experiments would be required, either using 2% FBS-supplemented media with HGF and IL-6 treatment or serum starving the cells before HGF and IL-6 treatment, to determine whether the growth factors present in serum were affecting the HGF and IL-6-induced A549 tumouroid growth. The exact composition of the growth factors and ECM components in Matrigel is not specifically known as it is derived from an animal which leads to inconsistencies between the batches and their contents (Serban and Prestwich 2008). The concentration of growth factors and ECM components can impact the proliferation of the A549 tumouroids, whereby cooperative signalling between the growth factors/ECM with HGF or IL-6 can lead to receptor internalisation and deregulation (Hammond et al. 2001; Wolf, Rose-John, and Garbers 2014). Moreover, in chapter 3, we also demonstrate the proliferative role of laminin in A549 cells, as laminin is the main component of Matrigel (Serban and Prestwich 2008), this can also mask the HGF and IL-6-induced proliferation in A549 tumouroids.

However, previous studies have alluded to a reduction in proliferation rates in 3D tumouroid cultures. One study demonstrated that A549 cells grown in Matrigel behave similarly to drug-resistant dormant cancer cells whereby a decrease in proliferation, migration, invasion was observed (Keeratichamroen, Lirdprapamongkol, and Svasti 2018). The same study showed a decrease in p-ERK, p-Akt and p-STAT3 expression in 3D cultures compared to 2D cultures (Keeratichamroen, Lirdprapamongkol, and Svasti 2018). Another study using endometrial cells cultured in reconstituted basement membrane showed no significant activation of p-Akt when treated exogenously with EGF (Chitcholtan et al. 2013). Furthermore, reduced levels of p-ERK are associated with tumour dormancy *in vivo*. Furthermore, a reduction in p-ERK and p-STAT3 inhibits cell cycle progression to the S phase by decreasing cyclin D1 thus increasing p21 levels (Modi et al. 2012). High levels of p21 can also negatively downregulate Akt levels thus promoting cell cycle arrest (Rössig et al. 2001). It would be of interest to identify whether HGF and IL-6 treatment also resulted in no significant changes in p-ERK, p-Akt and p-STAT3 *via* western blots. This would confirm the presence of a non-proliferative dormant phenotype of A549 cells in 3D culture. A lack of effect could also potentially be due to the high concentration range used in this study. Nanomolar concentrations of EGF was shown to induce growth in A431 cells in 3D culture (Mansbridge et al. 1992). The mixed findings in the EGF-mediated growth of tumouroids highlight the cell-specific nature of proliferation responses. The same study also showed the A431 tumouroid displayed lower expression of EGFR compared to 2D monolayer cultures (Mansbridge et al. 1994). This suggests a potential EGF autocrine loop in 3D culture. Therefore, future studies using lower concentrations of HGF and IL-6 can determine whether a proliferation response is observed in A549 tumouroids. The expression of c-Met and gp130 receptors using western blot can also be conducted to identify whether a lower expression is also observed. A longer culture time may be required to observe the increase in proliferation as one study exogenously treated pancreatic cancer tumouroids for 8 days with EGF and TGF-β (Sempere, Gunn, and Korc 2011). Daily white light images of HGF and IL-6-treated tumouroids can be obtained for image analysis of tumouroid area to assess the appropriate timepoint at which the tumouroid growth is observed. Furthermore, the same study also showed EGF and TGF-β induced an additive effect on pancreatic cancer tumouroid growth when cultured in Matrigel, although TGF-β treatment alone did not induce significant growth (Sempere, Gunn, and Korc 2011). Therefore, HGF and IL-6 co-treatment may be required to induce a proliferative effect in A549 tumouroids.

Our study also demonstrated β1-integrin and E-cadherin were expressed along the cell membrane of the A549 tumouroids in our study. β1-integrin and E-cadherin (Liu et al. 2011) cell membrane localisation was also similarly observed in other A549 tumouroid studies (Lu et al. 2014; Liu et al. 2011). Interestingly, HGF and IL-6 did not induce a change in E-cadherin localisation and epithelial

cell morphology in the tumouroids, as both pleiotropic cytokines are implicated in EMT (Liu, Song, et al. 2017; Zheng et al. 2019). HGF also did not induce a change in β1-integrin localisation despite previous studies highlighting the co-internalisation between c-Met and β1-integrin (Barrow-McGee, Kishi, Joffre, Ménard, Hervieu, Bakhouche, Noval, Mai, Guzmán, and Robert-Masson 2016). However, these studies were conducted in 2D monolayer cultures, therefore other signalling mechanisms may be contributing towards difference cellular effects. It is possible that HGF and IL-6 treatment induces an increase in A549 tumouroid adhesion to the ECM instead of an increase in migration and invasion. A study in myeloma cells demonstrated an increase in β1-integrin adhesion led to an increase in IL-6-induced STAT3 signalling (Shain et al. 2009). Moreover, the CD133+ stem cells may be responsible for inducing growth with HGF and IL-6 treatment (Lee et al. 2016). Future studies could involve using FACS sorted CD133+ A549 cells before seeding in Matrigel and undertaking EdU incorporation of the HGF and IL-6 treated tumouroids. The localisation of E-cadherin and β1-integrin can also be assessed to determine whether the stem cells are contributing towards enhanced migration of the tumouroids. Interestingly, several studies have also identified concurrent proliferation and invasion in 3D cultures are regulated by β1-integrin (Wang et al. 1998; Shibue and Weinberg 2009). The highly metastatic mouse mammary carcinoma D1A2 cells were able to proliferate in 3D culture *via* β1-integrin/FAK signalling whereas the less metastatic D2.0R and D2.1 cells did not proliferate in 3D cultures (Shibue and Weinberg 2009). Moreover, crosstalk between β1-integrin and EGFR mediated growth in 3D breast cancer cultures *via* the MAPK pathway (Wang et al. 1998). Overall, with the potential for A549 cells to behave like dormant cancer cells in 3D Matrigel culture, it would be of future interest to investigate the drug responses of A549 tumouroids and its impact on growth and resistance.

8.3.2 HL-60/eos has no effect on A549 tumouroid growth or death

Our *in vitro* co-culture studies show a physical interaction between the HL-60/eos and the A549 tumouroid. Eosinophils have been shown to recruit to the lung during inflammatory conditions via cytokines (IL-4, IL-5, IL-13 and IL33)(Moser, Fehr, and Bruijnzeel 1992; Horie et al. 1997; Sher et al. 1990; Milovanovic et al. 2012), β1-integrin (Bochner and Schleimer 1994) and eotaxins-1,-2 and -3 (Rosenwasser et al. 2003). As the HL-60/eos have been found to express CCR3 in our study, furthermore, A549 cells have been shown to express eotaxin (protein and mRNA) when stimulated with IL-1β and TNFα (Jedrzkiewicz et al. 2000; Lilly et al. 1997). Therefore, the HL-60/eos expressing CCR3 may be responding to the expression of Eotaxin-1 on the A549 tumouroid.

However, despite the physical interaction observed in our co-culture system, HL-60/eos showed no effect in A549 tumouroid growth or death. A more comprehensive dose-response experiment would need to be conducted to determine whether HL-60/eos influences A549 tumouroid death or growth.

Furthermore, at the lower concentration of HL-60/eos co-cultured, the HL-60/eos were not observed to be in direct physical contact with any A549 tumouroid. This may be due to the insufficient concentration of cells and therefore there would be a decrease likelihood of encountering HL-60/eos in contact with an A549 tumouroid. Moreover, the extensive washes conducted for immunofluorescent labelling processing tends to wash away most of the cells contained within the Matrigel. Future studies using blood eosinophils would be required to also determine the effect of eosinophils in NSCLC. Although limited studies have observed the effect of eosinophils in NSCLC, the dual-faceted role of eosinophils in cancer may indicate their functional plasticity. Currently, there are conflicting studies which show both the anti- and pro-tumourigenic effect of eosinophils in cancer. Upregulation of eosinophil-related cytokines including IL-4, IL-33, Eotaxin-1 and IL-5 caused a decrease in growth in correlation with enhanced eosinophil infiltration (Lucarini et al. 2017; Simson et al. 2007; Tepper, Coffman, and Leder 1992). Eosinophils have been shown to exert its tumouricidal effect through degranulation (Lucarini et al. 2017; Legrand et al. 2010). Eosinophils which contained higher amount of granules were able to inhibit prostate cancer cell growth more effectively than the eosinophils which contained less granules (Furbert-Harris et al. 2003). In Hodgkin's lymphoma cell lines (Glimelius et al. 2011), colorectal cell lines (Gatault et al. 2012) and human oral squamous cell carcinoma cell lines (De Lima et al. 2015), ECP was known to exert a cytotoxic effect on the respiratory epithelium. ECP exerts its cytotoxic effect by binding to the cell membrane of oral squamous cells which causes pores to form and osmotic lysis to occur (Dorta et al. 2002a). Eosinophil-derived MBP was also found in the tissue of lung metastases (Mattes et al. 2003). Conversely, studies have also reported a pro-tumourigenic role for eosinophils. Tumour-associated blood eosinophilia (TABE) is known to be associated with the metastatic stages of cancer thus correlating with poor survival rates. This has been reported in the carcinomas of kidney, thyroid, liver, gallbladder, pancreas, breast, cervical and in Hodgkin's lymphoma (as reviewed in (Sakkal et al. 2016)). In particular, 80% of eosinophilia has been reported in malignant cases of Hodgkin's lymphoma (Davis and Rothenberg 2014). Furthermore, the cytotoxic effect of ECP varied in Hodgkin's lymphoma (HL) cancer cell lines with some HL cells surviving (Glimelius et al. 2011). Eosinophils may adapt to different roles in the TME of many cancers with IL-5 favouring a pro-tumourigenic role whilst IFNγ and IL-33 favour an anti-tumourigenic response in lung cancer (Lucarini et al. 2017; Kataoka et al. 2004; Zaynagetdinov et al. 2015). Therefore, the HL-60/eos and blood eosinophils may need to be activated towards a pro-tumourigenic phenotype *via* treatment with IL-5 to investigate the effect their degranulation has on A549 tumouroid growth/death.

Eosinophils can also crosstalk with other immune cells to mediate a cytotoxic effect on cancer cells. Activated eosinophils can facilitate tumour rejection by recruiting and activating Natural Killer (NK)

cells, cytotoxic $CD8^+$ T cells and dendritic cells (Legrand et al. 2010; Carretero et al. 2015; O'Flaherty et al. 2017; Lotfi and Lotze 2008). Eosinophils also possess the ability to polarise macrophages to an antitumour M1 phenotype (Simson et al. 2007). Therefore, future co-culture experiments with activated eosinophils and other immune cells may be required to observe the potential cytotoxic effect on A549 tumouroids.

8.3.3 Triptolide induces TNT formation between A549 tumouroids

3D cultures are also an effective tool in assessing drug responses and assessing the mechanisms of resistance (as reviewed in (Lv et al. 2017). Our early observation showed TNT-like structure forming between A549 tumouroids treated with triptolide. This is a novel observation as previous studies have only identified TNTs early in the development of tumouroids or within the periphery of individual tumouroids in 3D *in vitro* cultures (Whitehead et al. 2020; Zhang et al. 2018; Sáenz-de-Santa-María et al. 2017; Pulze et al. 2020). However, the dense cellular environment of mature tumouroids may mask the visibility of TNTs within the tumouroids and TNTs may be present within the hypoxic core. Moreover, future studies would be needed to determine whether the structures contain characteristic and novel components: F-actin, α-tubulin, M-sec, c-Met, β1-integrin and paxillin. This can be achieved through high resolution confocal imaging and z-stack acquisition of the TNT-like structures to visualise the localisation of the characteristic and novel components of TNTs. Time-lapse imaging of the triptolide-treated tumouroids can be undertaken to observe the formation of the TNT-like structures. It would be of interest to visualise whether the TNTs are formed through a similar cell-to-cell dislodgement mechanism whereby a single A549 tumouroids either splits apart whilst being connected *via* a TNT or two migrating A549 tumouroids form contact and establish a TNT whilst migrating apart. Interestingly, the latter would demonstrate that numerous cells within the A549 tumouroids are able to respond and behave like individual cells. If the TNT is formed from a single tumouroid breaking apart this could implicate triptolide in inducing metastasis similarly *in vivo*. It would also be of interest to investigate the potential pathways involved in the triptolide-mediated formation of TNTs.

Triptolide is known to induce apoptosis through inhibition of NF-κB in lung cancer cells by upregulating pro-apoptotic TRAIL (Lee et al. 2002) and *via* a p53-independent pathway in human anaplastic thyroid carcinoma cells (Zhu et al. 2009). Triptolide can also upregulate ROS levels whilst upregulating cytochrome c levels and decreasing levels of mitochondrial membrane potential (Wu et al. 2011). TNTs are also known to form as part of a stress response in cancer (Wang and Gerdes 2015; Caicedo et al. 2015; Lin et al. 2019) and has been linked to drug-induced ROS production (Rustom 2016; Liang 2018). Therefore, it can be hypothesised that the triptolide-mediated ROS production may enhance mitochondria transport *via* TNTs to provide metabolic rescue. Moreover,

A549 cells have been shown to transfer healthy mitochondria to other A549 cells suffering from drug-induced mitochondrial loss (Spees et al. 2006). Rustom also proposed mitochondrial transfer may also be mechanism to clear excess ROS in cancer cells (Rustom 2016). TNTs are also known to mediate chemoresistance through the transport of mitochondria, vesicles, p-glycoprotein, and miRNA (as discussed in chapter 4) (Pasquier et al. 2013; Kolba et al. 2019; Kretschmer et al. 2019). Therefore, the triptolide-induced TNT structures may also form to propagate chemoresistance through the A549 tumouroid population. Future live-cell imaging experiments can be conducted to determine the cellular cargo being transported along the TNTs. and the path of the cellular cargo, whether it remains in the recipient cell or gets exchanged to other neighbouring cells. Also, A549 tumouroids in Matrigel have been shown to behave like dormant cells and acquire cancer stem cell (CSC)-like properties (Keeratichamroen, Lirdprapamongkol, and Svasti 2018). CSCs are activated during inflicted stress/injury, such as triptolide drug treatment, and obtain the necessary mutations to metastasise and develop resistance to chemotherapies (Trumpp, Essers, and Wilson 2010). FACS sorting could be used in future studies to identify whether the CD133+ A549 cells grown in Matrigel are more likely to form TNTs and survive drug treatment compared to the non-CSC population.

8.3.4 Future work

3D *in vitro* tumour models help to bridge the gap between basic cellular research and translational pre-clinical studies. However, there are a few limitations in culturing tumouroids in Matrigel. The technique requires centrifugal force to form the cell pellet before resuspension in Matrigel which can inflict damage to the cells (Habanjar et al. 2021). There is also a lack of uniformity in tumouroid size which can impact proliferation responses and affect comparisons of tumouroid area. The complex TME is difficult to remodel given the heterogeneity of tumours in patients however there have been current advances to better model the biological parameters required for tumour growth, metastasis, angiogenesis, ECM remodeling and tumour dormancy *in vitro*. Currently, organ-on-chip technology and microfluidic devices show promising progress in achieving this (Komen et al. 2021; Duval et al. 2017). The biochemical and biophysical properties can be further manipulated in these systems, altering nutrient gradients, oxygen levels, drug concentrations, angiogenesis, mechanical cues and cell interactions within the TME (Khalid et al. 2020). The lung-on-a-chip in particular has seen considerable advances whereby the breathing mechanism is replicated, and the second-generation lung-on-a-chip (Huh et al. 2010) includes an elastic alveolar basal membrane (Zamprogno et al. 2021). HGF, IL-6 and triptolide can be treated accordingly with the appropriate biochemical and biophysical properties altered to mimic the TME of NSCLC. Furthermore, to visualise TNT formation and mitochondria transport, the triptolide-treated cells within the organ-on-a-chip system can be loaded with Mitotracker and SiR-actin before being brought for live confocal imaging. This

would also help to determine whether cell survival is correlated with TNT-mediated mitochondria transport during triptolide treatment. These surviving cells may potentially be CSCs, therefore the surviving cells can be further isolated and characterised *via* FACS sorting with CSC markers to determine this. The surviving cells may also harbour mutational upregulation of genes (including MET), therefore quantitative real-time PCR can be used to unravel the mutational amplification of genes. Moreover, organotypic microfluidic chip system consisting of co-cultures of CAFs and breast cancer had been previously conducted (Truong et al. 2019). Therefore, a similar concept can be used whereby patient-derived NSCLC cells and primary or tumour-derived eosinophils can be co-cultured on the 3D tumour and stroma microfluidic system before quantifying positive EdU expression to measure growth.

9. Chapter 9. General discussion and future work

The major findings described in the previous chapters show the importance of HGF and its signalling relationship with β1-integrin in driving NSCLC growth (Chapter 3) and TNT formation (chapter 3&4). Crosstalk between HGF and other pleiotropic cytokines with IL-6 (Chapter 3) and EGF (Chapter 6) also demonstrates the need for multi-drug targeting to fully inhibit growth and TNT formation in NSCLC. Moreover, the discovery of a subpopulation of A549 cells capable of simultaneous migration, TNT formation and cell division highlights the insidious implications of the development of early metastasis in NSCLC. A physical interaction was also observed between eosinophils and A549 tumouroids thus highlighting the potential role of eosinophil in the pathogenesis of NSCLC. This chapter will emphasise on implementing the integrated findings with other experimental models whilst addressing the future challenges with multi-drug targeting of HGF and its varied signalling partners.

9.5 Key findings and concepts

As the TME in NSCLC evolves throughout disease progression, there is extensive heterogeneity in the composition of stromal and cancer cells, shaping the differing localised cytokine milieu and their interactions with the ECM (Lambrechts et al. 2018; Graves, Maity, and Le 2010). Our findings have shown the diverse role of HGF and its relationship with other pleiotropic cytokines and the ECM/integrin signalling pathways in NSCLC. Our results in Chapter 3 unravelled a novel signalling cooperation between HGF, IL-6 and β1-integrin in A549 cell growth which may be implicated in the initial tumour development. Moreover, in Chapters 4 and 5 we describe a novel role for HGF/c-Met/β1-integrin in TNT formation via paxillin recruitment and downstream activation of the Arp2/3 complex, MAPK and PI3K pathways. The crosstalk between HGF and EGF signalling also regulated TNT formation *via* the MAPK and PI3K pathways, as described in Chapter 6. The molecular mechanism underlying TNT formation has remained poorly defined since its discovery by Rustom and his colleagues in 2004 (Rustom et al. 2004)., moreover, there are no known strategies to target and inhibit TNT formation in cancer. Therefore, establishing upregulated growth factors and their signalling partners in TNT formation highlights the potential drug targeting of HGF, β1-integrin and EGF to inhibit TNTs. The formation of TNTs has not been linked to the disease stage however upregulated MET transcription has been shown to be induced by hypoxia, angiogenic factors and cytokines associated with inflammation (Pennacchietti et al. 2003; Bhowmick, Neilson, and Moses 2004). This suggests that c-Met activation is most prominent at a later stage of the disease, thus potentially aggravating the pro-invasive and chemoresistance cell phenotype via TNT-mediated transport of mitochondria or miRNA either at the hypoxic core or metastatic tumour edge (Pasquier et al. 2013; Lu et al. 2017; Thayanithy et al. 2014)(Fig9.1). As lower concentrations of HGF are used

in this study to induce proliferation (as detailed in Chapter 3) whilst a higher concentration is required to achieve maximal HGF-induced TNT formation. This may reflect the different stages of cancer progression whereby lower levels of HGF/c-Met activation is required for the initial proliferative phenotype of tumour cells whilst the later development of the hypoxic and pro-inflammatory microenvironment may trigger overexpression of HGF and c-Met leading to TNT formation. Our TNT studies have also led to the discovery of a subset of cells undergoing a novel phenomenon which we termed 'go and grow' TNTs, as described in Chapter 7. This subpopulation of cells possesses the unique ability to undergo simultaneous migration, TNT formation and proliferation, and may potentially be involved in the metastatic dissemination of NSCLC at the early or late stage of the disease. Moreover, these cells may reflect the behaviour of unique phenotypes within the TME, such as CSCs or CTCs which can remain dormant at the site of metastasis (Dasgupta, Lim, and Ghajar 2017; Patel and Chen 2012).

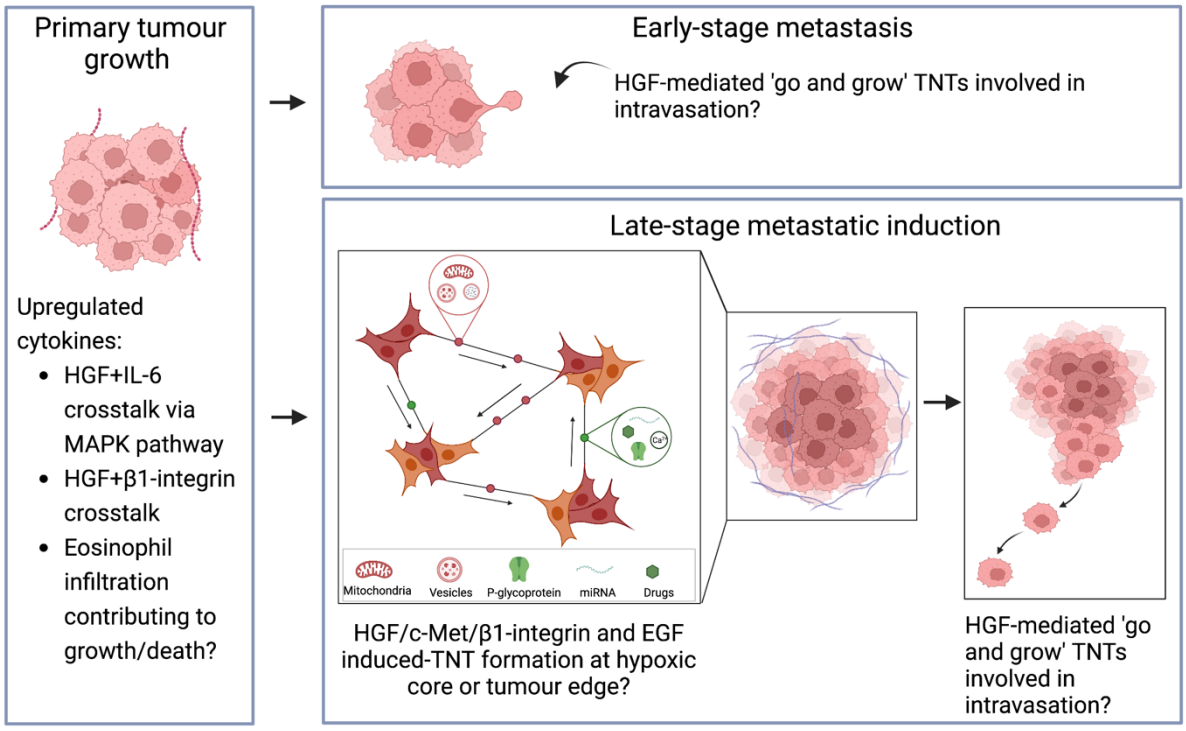


Figure 9.1. The implications of the HGF-mediated growth and TNT outcomes in NSCLC. The schematic shows the role of HGF/IL-6/MAPK pathway and HGF/β1-integrin crosstalk involved in the potential primary growth of the tumour. HGF may potentially induce early dissemination of tumour cells *via* upregulating the proliferative and migratory phenotype of 'go and grow' cells. Furthermore, TNT formation at the hypoxic core or the tumour edge may be induced by HGF/c-Met/β1-integrin co-activation or HGF/EGF crosstalk during the later stages of the disease. The TNT-mediated transfer of mitochondria and miRNA can alter the recipient phenotype of the cancer cells towards a more aggressive phenotype. HGF may also induce 'go and grow' TNT-forming cells to metastasise at this later stage of the disease.

However, other microenvironmental factors ranging from levels of oxygenation, nutrients, pH and interstitial pressure can vary widely within the tumour and contribute to the pathogenesis of cancer (Graves, Maity, and Le 2010). An A549 tumouroid culture was established in Chapter 8 to investigate HGF and IL-6 growth regulation, TNT formation and eosinophil interactions within the replicated 3D *in vivo*-like structure; whilst polyacrylamide hydrogels were used to visualise HGF-induced TNT formation at the appropriate tumour stiffness in Chapter 7. However, to better recapitulate the different microenvironmental factors *in vivo*, an organ-on-a-chip model can be used to functionally investigate whether the HGF/c-Met/β1-integrin signalling axis and EGF crosstalk-induced TNT formation would lead to enhanced proliferation or resistance propagation. Moreover, patient-derived blood eosinophils can also be used to observe its effects within these models as their role within the TME of NSCLC is still not known.

9.6 Elucidating the integrated biology of HGF using an organ-on-a-chip model

There have been recent developments to create novel 3D culture systems to better mimic complex tumour interactions. Microscale organotypic models have recently emerged to produce organ structures on a chip providing accurate control of cell-cell, cell-matrix and cell-soluble cytokine interactions (Sung and Beebe 2014). Therefore, these organotypic microfluidic-based models are ideal to study the potential combined growth, TNT and overall metastatic effects induced by HGF and its crosstalk with IL-6, EGF, ECM/β1-integrin and eosinophils. A three-layered micro-engineered microfluidic designed by Nagaraju et al can be used to measure the HGF-induced outcomes (Nagaraju et al. 2018). The device consists of an inner chamber which hosts the tumour region, a second chamber which hosts the stroma region and the third outermost vascular region (Fig9.2). Experimentally, a co-culture of A549 cells with patient-derived blood eosinophils or tumour-derived eosinophils can be encapsulated with collagen IV (i.e. the most highly expressed ECM protein in NSCL (Hodkinson et al. 2006)) or Matrigel to produce a dense 3D cluster of cells whilst HGF± EGF±IL-6 can be supplemented to the media, allowing for diffusion and creating a concentration gradient of the cytokines (Fig9.1). Tumour-derived eosinophils can be taken from either the hypoxic core of the tumour or at the periphery of the tumour and compared with the blood eosinophils, to further distinguish the pro-tumourigenic or anti-tumourigenic effect of eosinophils located in the different regions of the TME. The stroma region would consist of collagen IV for the cancer cells to initially invade whilst the vascular region consists of HUVEC cells embedded in a fibrin hydrogel to produce in vivo-like capillaries (Nagaraju et al. 2018)(Fig9.2). Real-time phase-contrast imaging can then be used visualised within these models to confirm the presence of TNTs or ‘go and grow’ TNTs and to count the number of invading cells within the stroma. F-actin and Ki67 labelling can also be

undertaken to undertake image analysis for TNT formation and growth respectively (Nagaraju et al. 2018; Truong et al. 2016).

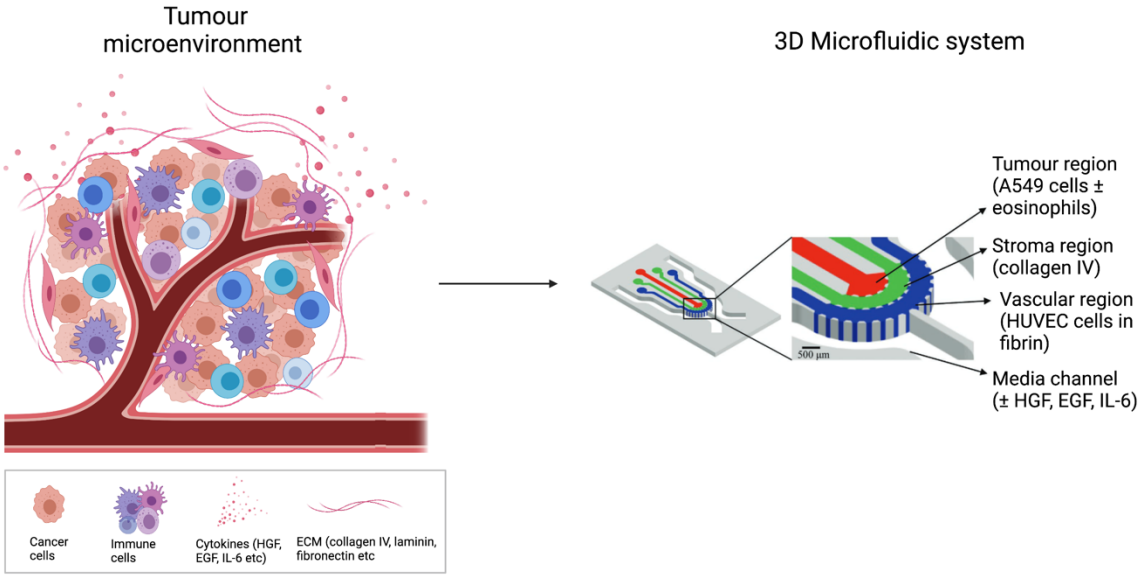


Figure 9.2. A schematic showing of the tumour microenvironment of NSCLC in comparison to the microfluidic system (adapted from (Nagaraju et al. 2018). The TME of NSCLC is highly vascularised and consists of a range of cells (e.g. cancer cells, immune cells) surrounded by the remodeled ECM (collagen IV, laminin, fibronectin etc). Pleiotropic cytokines including HGF, EGF and IL-6 are mutationally upregulated and drive the development of cancer. The 3D microfluidic system shows three spatially separate compartments: the tumour region (formed by a solid 3D tumour A549 ± eosinophil cells in collagen IV/Matrigel), the stroma region (consisting of collagen IV) and the vascular region (HUVEC cells embedded on a fibrin hydrogel) which models the TME. The media channel also allows for diffusion of a variety of growth factor-supplemented media (e.g. HGF, EGF and IL-6).

9.7 Therapeutic strategies to target the crosstalk HGF signalling in NSCLC

The results presented in this thesis highlight the importance of multi-drug targeting and precision medicine in NSCLC. There have been recent advances in identifying molecular targets and their approved treatment in NSCLC (see Table 9.1). However, despite the recent progress in the development of NSCLC-targeted therapies, the progression-free survival (PFS) and overall survival (OS) of patients administered targeted therapies remain low: PFS of patients on erlotinib was 13 months whilst OS of patients on erlotinib was 45 months (Aguilar et al. 2022) and OS of patietns on crizotinib was 6.8 years (Pacheco et al. 2019).

Targeted mutations	Targeted therapy
EGFR tyrosine kinase	Gefitinib, Erlotinib, Afatinib
EGFR	Cetuximab
EGFR Thr790Met point mutation (T790M)	Osimertinib
VEGF	Bevacizumab
ROS1 fusion	Cizotinib, Ceritinib
ALK	Cizotinib
Programmed cell death protein 1 (PD-1)	Nibolumab, Pembrolizumab
Programmed death-ligand 1 (PD-L1)	Atezolizumab, Avelumab, Durvalumab
BRAF	Dabrafenib, trametinib
MET exon 14 skipping mutation	Capmatinib
RET fusion	Praselsetinib, selpercatinib

Table 9.1: Summary of the targeted therapies approved for NSCLC treatment (Robbins and Kummet 2018)

Moreover, patients harbour multiple mutations and therefore require a personalised multi-drug targeted to fully inhibit the progression of NSCLC. A personalised approach is required to identify potential MET, IL-6, EGFR mutations for appropriate patient stratification for the targeted therapies. Clinical trials using genomic testing and targeting for KRAS has been proven to improve patient survival in NSCLC (Riely, Marks, and Pao 2009), therefore this approach needs to be expanded for other potential mutations commonly harboured in NSCLC patients. MET gene amplification has been reported in 4% of all lung adenocarcinomas (Sattler et al. 2011). Moreover, MET-amplified mutations are implicated in both primary intrinsic (Turke et al. 2010) and acquired resistance (Engelman, Zejnullahu, Gale, et al. 2007). As TNT-mediated mitochondria transport has been shown to propagate chemoresistance (Pasquier et al. 2013; Wang and Gerdes 2015), the findings of our study suggest HGF/c-Met/β1-integrin-induced formation of TNTs may transport mitochondria to facilitate chemoresistance. Furthermore, inhibition of both EGF and HGF signalling is required to ameliorate TNT formation, as the HGF/c-Met-mediated MAPK and PI3K pathway activation can bypass the sole inhibition of EGF/EGFR signalling. However, therapeutic inhibition of the relevant molecular targets with minimum toxicity and side effects proves to be a challenge within the clinical landscape (Xie and Bourne 2015). To overcome these issues, the development of photodynamic nanoparticle therapy has emerged as a mode of localised drug delivery. Photodynamic therapy uses light to irradiate a photosensitiser which generates cytotoxic reactive oxygen species to the localised tumour (Buchner et al. 2019; Conte et al. 2016; Del Valle, Hirsch, and Marin 2022). Photodynamic therapy has been used in several phase I and phase II clinical trials of NSCLC, demonstrating promising patient outcomes and minimal phototoxic side effects (Shafirstein et al. 2016; Usuda et al. 2006). Ligand-mediated targeting using monoclonal antibodies to EGFR, c-Met and β1-integrin can be conjugated to an upconverting nanoparticle functionalised with a photosensitiser (Fig9.3). This leads

to the uptake of the nanoparticle in the tumour cells *via* endocytosis where localised reactive oxygen species are generated upon light exposure (Fig9.3). Furthermore, to test the effectiveness of the drug conjugated nanoparticles, the nanoparticles can be added to the media within the microfluidic system (Fig9.2) and activated with a light source to confirm the inhibition of NSCLC growth, TNT formation and invasion.

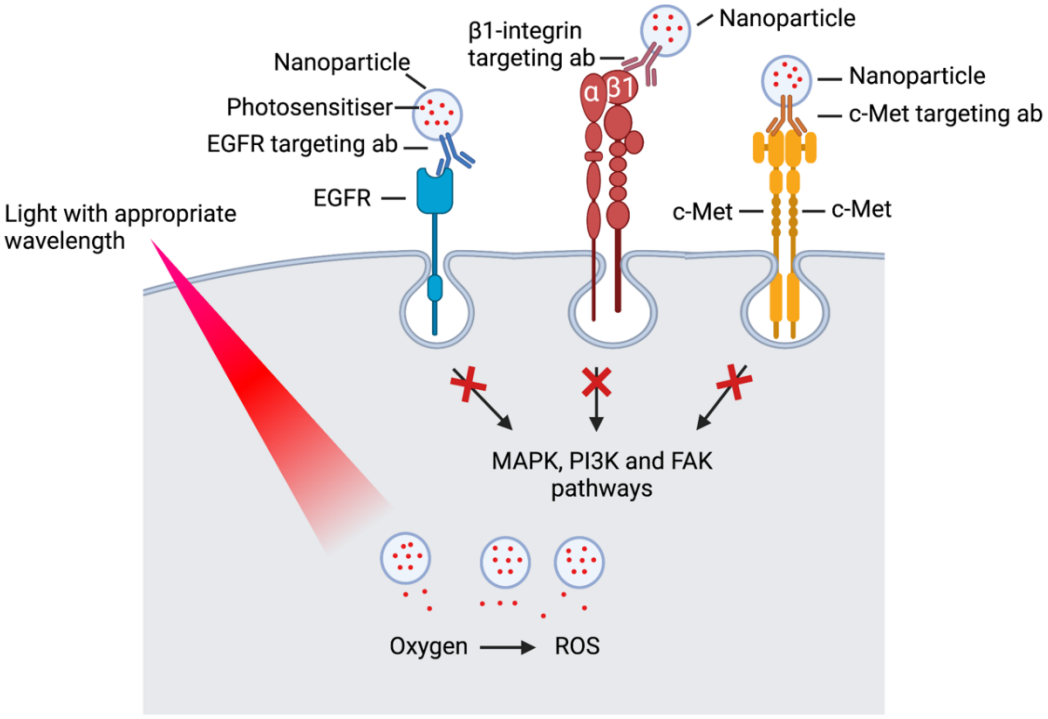


Figure 9.3: Schematic representing photodynamic therapy with nanoparticles conjugated with EGFR, c-Met and β1-integrin targeting antibodies. Nanoparticles functionalised with photosensitisers and conjugated with antibodies target the EGFR, c-Met and β1-integrin. Binding of the respective antibodies conjugated on the nanoparticle blocks EGF, HGF ligand binding and subsequent β1-integrin cross-activation thus inhibiting the downstream PI3K, MAPK and FAK pathways involved in cell proliferation, migration, TNT formation and invasion. Furthermore, the nanoparticles undergo endocytosis after binding with the receptors resulting in the release of the photosensitisers within the cytosol. The photosensitisers, upon activation *via* a light source with the appropriate wavelength, convert oxygen into ROS thus triggering cellular apoptosis.

9.8 Concluding remarks

HGF is a critical factor in driving the progression of NSCLC through its crosstalk with other pleiotropic cytokines and the ECM. In summary, the results show HGF and IL-6-induced proliferation *via* convergent signalling on the MAPK pathway. HGF also induced A549 cell proliferation through crosstalk with β1-integrin. Furthermore, a novel role for the co-activation of HGF/c-Met, β1-integrin, paxillin and downstream MAPK, PI3K and Arp2/3 complex pathways was identified in regulating TNT formation in A549 cells. HGF/c-Met was also shown to crosstalk with EGF/EGFR to induce TNT formation. A novel subpopulation of A549 cells was identified with the unique ability to undergo simultaneous migration, TNT formation and proliferation. 3D A549 tumouroid models also revealed

novel triptolide-induced TNT formation and the potential interaction occurring with eosinophils. An integrated organ-on-a-chip model was proposed for future studies to elicit the different HGF-mediated outcomes implicated in NSCLC growth, TNT formation, metastasis and chemoresistance. Moreover, photodynamic therapy with nanoparticles was also proposed to deliver localised cytotoxic ROS and tumour inhibition of HGF/c-Met, EGFR and β1-integrin signalling. Overall, these findings highlight the multi-faceted role of HGF within the TME and the importance of developing a personalised approach in NSCLC therapy.

10. References

Abdel-Haleem, Alyaa M, Nathan E Lewis, Neema Jamshidi, Katsuhiko Mineta, Xin Gao, and Takashi Gojobori. 2017. 'The emerging facets of non-cancerous warburg effect', *Frontiers in endocrinology*, 8: 279.

Abounit, Saïda, and Chiara Zurzolo. 2012. 'Wiring through tunneling nanotubes–from electrical signals to organelle transfer', *Journal of cell science*, 125: 1089-98.

Accornero, Paolo, Silvia Miretti, Laura Starvaggi Cucuzza, Eugenio Martignani, and Mario Baratta. 2010. 'Epidermal growth factor and hepatocyte growth factor cooperate to enhance cell proliferation, scatter, and invasion in murine mammary epithelial cells', *Journal of molecular endocrinology*, 44: 115-25.

Aggarwal, Charu, Mary Weber Redman, Primo Lara, Hossein Borghaei, Philip C Hoffman, Jeffrey D Bradley, Katie Griffin, Jieling Miao, Philip C Mack, and Vassiliki Papadimitrakopoulou. 2017. "Phase II study of the FGFR inhibitor AZD4547 in previously treated patients with FGF pathway-activated stage IV squamous cell lung cancer (SqNSCLC): LUNG-MAP sub-study SWOG S1400D." In.: American Society of Clinical Oncology.

Ahmad, Tanveer, Shravani Mukherjee, Bijay Pattnaik, Manish Kumar, Suchita Singh, Manish Kumar, Rakhshinda Rehman, Brijendra K Tiwari, Kumar A Jha, and Amruta P Barhanpurkar. 2014. 'Miro1 regulates intercellular mitochondrial transport & enhances mesenchymal stem cell rescue efficacy', *The EMBO journal*, 33: 994-1010.

Aksorn, Nithikoon, and Pithi Chanvorachote. 2019. 'Integrin as a molecular target for anti-cancer approaches in lung cancer', *Anticancer research*, 39: 541-48.

Al Heialy, Saba, Melissa Zeroual, Soroor Farahnak, Toby McGovern, Paul-André Risse, Mauro Novali, Anne-Marie Lauzon, Horia N Roman, and James G Martin. 2015. 'Nanotubes connect CD4+ T cells to airway smooth muscle cells: novel mechanism of T cell survival', *The Journal of Immunology*, 194: 5626-34.

Alberg, Anthony J, Malcolm V Brock, Jean G Ford, Jonathan M Samet, and Simon D Spivack. 2013. 'Epidemiology of lung cancer: Diagnosis and management of lung cancer: American College of Chest Physicians evidence-based clinical practice guidelines', *Chest*, 143: e1S-e29S.

Almatroodi, Saleh Abdulrahman, Christine F McDonald, Ian A Darby, and Dodie S Pouniotis. 2016. 'Characterization of M1/M2 tumour-associated macrophages (TAMs) and Th1/Th2 cytokine profiles in patients with NSCLC', *Cancer Microenvironment*, 9: 1-11.

Alpha, Kyle M, Weiyi Xu, and Christopher E Turner. 2020. 'Paxillin family of focal adhesion adaptor proteins and regulation of cancer cell invasion.' in, *International review of cell and molecular biology* (Elsevier).

Altorki, Nasser K, Geoffrey J Markowitz, Dingcheng Gao, Jeffrey L Port, Ashish Saxena, Brendon Stiles, Timothy McGraw, and Vivek Mittal. 2019. 'The lung microenvironment: an important regulator of tumour growth and metastasis', *Nature Reviews Cancer*, 19: 9-31.

Ananthakrishnan, Revathi, and Allen Ehrlicher. 2007. 'The forces behind cell movement', *International journal of biological sciences*, 3: 303.

Ariazi, Jennifer, Andrew Benowitz, Vern De Biasi, Monique L Den Boer, Stephanie Cherqui, Haifeng Cui, Nathalie Douillet, Eliseo A Eugenin, David Favre, and Spencer Goodman. 2017. 'Tunneling nanotubes and gap junctions–their role in long-range intercellular communication during development, health, and disease conditions', *Frontiers in molecular neuroscience*, 10: 333.

Arkwright, Peter D, Francesca Luchetti, Julien Tour, Charlotte Roberts, Rahna Ayub, Ana P Morales, José J Rodríguez, Andrew Gilmore, Barbara Canonico, and Stefano Papa. 2010. 'Fas stimulation of T lymphocytes promotes rapid intercellular exchange of death signals via membrane nanotubes', *Cell research*, 20: 72-88.

Arriola, E, I Canadas, M Arumi-Uria, M Dómine, JA Lopez-Vilarino, O Arpí, M Salido, S Menéndez, E Grande, and FR Hirsch. 2011. 'MET phosphorylation predicts poor outcome in small cell lung

carcinoma and its inhibition blocks HGF-induced effects in MET mutant cell lines', *British journal of cancer*, 105: 814-23.
Arteaga, Carlos. 2003. "Targeting HER1/EGFR: a molecular approach to cancer therapy." In *Seminars in oncology*, 3-14. Elsevier.
Asano, Shuichi, Satoru Ito, Kota Takahashi, Kishio Furuya, Masashi Kondo, Masahiro Sokabe, and Yoshinori Hasegawa. 2017. 'Matrix stiffness regulates migration of human lung fibroblasts', *Physiological reports*, 5: e13281.
Assoian, Richard K, and Xiaoyun Zhu. 1997. 'Cell anchorage and the cytoskeleton as partners in growth factor dependent cell cycle progression', *Current opinion in cell biology*, 9: 93-98.
Aumailley, Monique, and Barbara Gayraud. 1998. 'Structure and biological activity of the extracellular matrix', *Journal of Molecular Medicine*, 76: 253-65.
Austefjord, Magnus Wiger, Hans-Hermann Gerdes, and Xiang Wang. 2014. 'Tunneling nanotubes: Diversity in morphology and structure', *Communicative & integrative biology*, 7: e27934.
Awad, Mark Magdi, Geoffrey Raymond Oxnard, David M Jackman, Daniel O Savukoski, Dimity Hall, Priyanka Shivdasani, Jennifer C Heng, Suzanne Eleanor Dahlberg, Pasi Antero Janne, and Suman Verma. 2016. "MET exon 14 mutations in non–small-cell lung cancer are associated with advanced age and stage-dependent MET genomic amplification and c-Met overexpression." In.: American Society of Clinical Oncology (ASCO).
Ayoub, Nehad M, Kamal M Al-Shami, Mohammad A Alqudah, and Nizar M Mhaidat. 2017. 'Crizotinib, a MET inhibitor, inhibits growth, migration, and invasion of breast cancer cells in vitro and synergizes with chemotherapeutic agents', *OncoTargets and therapy*, 10: 4869.
Baghban, Roghayyeh, Leila Roshangar, Rana Jahanban-Esfahlan, Khaled Seidi, Abbas Ebrahimi-Kalan, Mehdi Jaymand, Saeed Kolahian, Tahereh Javaheri, and Peyman Zare. 2020. 'Tumor microenvironment complexity and therapeutic implications at a glance', *Cell Communication and Signaling*, 18: 1-19.
Bagrodia, Shubha, and Richard A Cerione. 1999. 'Pak to the future', *Trends in Cell Biology*, 9: 350-55.
Bahcall, Magda, Taebo Sim, Cloud P Paweletz, Jyoti D Patel, Ryan S Alden, Yanan Kuang, Adrian G Sacher, Nam Doo Kim, Christine A Lydon, and Mark M Awad. 2016. 'Acquired METD1228V mutation and resistance to MET inhibition in lung cancer', *Cancer discovery*, 6: 1334-41.
Ballard, Peter, James WT Yates, Zhenfan Yang, Dong-Wan Kim, James Chih-Hsin Yang, Mireille Cantarini, Kathryn Pickup, Angela Jordan, Mike Hickey, and Matthew Grist. 2016. 'Preclinical Comparison of Osimertinib with Other EGFR-TKIs in EGFR-Mutant NSCLC Brain Metastases Models, and Early Evidence of Clinical Brain Metastases ActivityOsimertinib in Models of EGFR-Mutant NSCLC Brain Metastases', *Clinical cancer research*, 22: 5130-40.
Bareschino, Maria A, Clorinda Schettino, Teresa Troiani, Erika Martinelli, Floriana Morgillo, and Fortunato Ciardiello. 2007. 'Erlotinib in cancer treatment', *Annals of oncology*, 18: vi35-vi41.
Barkan, Dalit, Hynda Kleinman, Justin L Simmons, Holly Asmussen, Anil K Kamaraju, Mark J Hoenorhoff, Zi-yao Liu, Sylvain V Costes, Edward H Cho, and Stephen Lockett. 2008. 'Inhibition of metastatic outgrowth from single dormant tumor cells by targeting the cytoskeleton', *Cancer research*, 68: 6241-50.
Barrow-McGee, Rachel, Naoki Kishi, Carine Joffre, Ludovic Ménard, Alexia Hervieu, Bakhouche A Bakhouche, Alejandro J Noval, Anja Mai, Camilo Guzmán, and Luisa Robbez-Masson. 2016a. 'Beta 1-integrin–c-Met cooperation reveals an inside-in survival signalling on autophagy-related endomembranes', *Nature communications*, 7: 11942.
Barzilai, Sagi, Ronnie Blecher-Gonen, Zohar Barnett-Itzhaki, Ayelet Zauberman, Yaeli Lebel-Haviv, Ido Amit, and Ronen Alon. 2016. 'M-sec regulates polarized secretion of inflammatory endothelial chemokines and facilitates CCL2-mediated lymphocyte transendothelial migration', *Journal of leukocyte biology*, 99: 1045-55.
Bayliss, Trevor J, Jeff T Smith, Michael Schuster, Konstantin H Dragnev, and James R Rigas. 2011. 'A humanized anti-IL-6 antibody (ALD518) in non-small cell lung cancer', *Expert opinion on biological therapy*, 11: 1663-68.

Bean, James, Cameron Brennan, Jin-Yuan Shih, Gregory Riely, Agnes Viale, Lu Wang, Dhananjay Chitale, Noriko Motoi, Janos Szoke, and Stephen Broderick. 2007. 'MET amplification occurs with or without T790M mutations in EGFR mutant lung tumors with acquired resistance to gefitinib or erlotinib', *Proceedings of the National Academy of Sciences*, 104: 20932-37.

Beli, Petra, Debora Mascheroni, Dalu Xu, and Metello Innocenti. 2008. 'WAVE and Arp2/3 jointly inhibit filopodium formation by entering into a complex with mDia2', *Nature cell biology*, 10: 849-57.

Benard, Magalie, Damien Schapman, Alexis Lebon, Baptiste Monterroso, Marine Bellenger, Frank Le Foll, Jennifer Pasquier, Hubert Vaudry, David Vaudry, and Ludovic Galas. 2015. 'Structural and functional analysis of tunneling nanotubes (TnTs) using gCW STED and gconfocal approaches', *Biology of the Cell*, 107: 419-25.

Bergers, Gabriele, Rolf Brekken, Gerald McMahon, Thiennu H Vu, Takeshi Itoh, Kazuhiko Tamaki, Kazuhiko Tanzawa, Philip Thorpe, Shigeyoshi Itohara, and Zena Werb. 2000. 'Matrix metalloproteinase-9 triggers the angiogenic switch during carcinogenesis', *Nature cell biology*, 2: 737-44.

Bergström, J Daniel, Bengt Westermark, and Nils-Erik Heldin. 2000. 'Epidermal growth factor receptor signaling activates met in human anaplastic thyroid carcinoma cells', *Experimental cell research*, 259: 293-99.

Best, Sarah A, Sheryl Ding, Ariena Kersbergen, Xueyi Dong, Ji-Ying Song, Yi Xie, Boris Reljic, Kaiming Li, James E Vince, and Vivek Rathi. 2019. 'Distinct initiating events underpin the immune and metabolic heterogeneity of KRAS-mutant lung adenocarcinoma', *Nature communications*, 10: 1-14.

Bethune, Gillian, Drew Bethune, Neale Ridgway, and Zhaolin Xu. 2010. 'Epidermal growth factor receptor (EGFR) in lung cancer: an overview and update', *Journal of thoracic disease*, 2: 48.

Bhowmick, Neil A, Eric G Neilson, and Harold L Moses. 2004. 'Stromal fibroblasts in cancer initiation and progression', *Nature*, 432: 332-37.

Bianconi, Daniela, Matthias Unseld, and Gerald Prager. 2016. 'Integrins in the Spotlight of Cancer', *International journal of molecular sciences*, 17: 2037.

Bihl, Michel, Michael Tamm, Markus Nauck, Heinrich Wieland, André P Perruchoud, and Michael Roth. 1998. 'Proliferation of Human Non–Small-Cell Lung Cancer Cell Lines: Role of Interleukin-6', *American journal of respiratory cell and molecular biology*, 19: 606-12.

Birchmeier, Carmen, and Ermanno Gherardi. 1998. 'Developmental roles of HGF/SF and its receptor, the c-Met tyrosine kinase', *Trends in cell biology*, 8: 404-10.

Blanchard, Carine, and Marc E Rothenberg. 2009. 'Biology of the eosinophil', *Advances in immunology*, 101: 81-121.

Boccaccio, Carla, Margherita Ando, Luca Tamagnone, Alberto Bardelli, Paolo Michieli, Carlo Battistini, and Paolo M Comoglio. 1998. 'Induction of epithelial tubules by growth factor HGF depends on the STAT pathway', *Nature*, 391: 285.

Boccaccio, Carla, Giovanni Gaudino, Giovanna Gambarotta, Francesco Galimi, and Paolo M Comoglio. 1994. 'Hepatocyte growth factor (HGF) receptor expression is inducible and is part of the delayed-early response to HGF', *Journal of Biological Chemistry*, 269: 12846-51.

Bochner, Bruce S, and Robert P Schleimer. 1994. 'The role of adhesion molecules in human eosinophil and basophil recruitment', *Journal of allergy and clinical immunology*, 94: 427-38.

Bonine-Summers, Alyssa R, Mary E Aakre, Kimberly A Brown, Carlos L Arteaga, Jennifer A Pietenpol, Harold L Moses, and Nikki Cheng. 2007. 'Epidermal growth factor receptor plays a significant role in hepatocyte growth factor mediated biological responses in mammary epithelial cells', *Cancer biology & therapy*, 6: 561-70.

Booth, Adam J, Ryan Hadley, Ashley M Cornett, Alyssa A Dreffs, Stephanie A Matthes, Jessica L Tsui, Kevin Weiss, Jeffrey C Horowitz, Vincent F Fiore, and Thomas H Barker. 2012. 'Acellular normal and fibrotic human lung matrices as a culture system for in vitro investigation', *American journal of respiratory and critical care medicine*, 186: 866-76.

Bowles, DW, WW Ma, N Senzer, JR Brahmer, AA Adjei, M Davies, AJ Lazar, A Vo, S Peterson, and L Walker. 2013. 'A multicenter phase 1 study of PX-866 in combination with docetaxel in patients with advanced solid tumours', *British journal of cancer*, 109: 1085-92.

Bremnes, Roy M, Carlos Camps, and Rafael Sirera. 2006. 'Angiogenesis in non-small cell lung cancer: the prognostic impact of neoangiogenesis and the cytokines VEGF and bFGF in tumours and blood', *Lung Cancer*, 51: 143-58.

Bretschneider, Franklin, and Jan R De Weille. 2018. *Introduction to electrophysiological methods and instrumentation* (Academic Press).

Brown, Michael C, Joseph A Perrotta, and Christopher E Turner. 1996. 'Identification of LIM3 as the principal determinant of paxillin focal adhesion localization and characterization of a novel motif on paxillin directing vinculin and focal adhesion kinase binding', *The Journal of cell biology*, 135: 1109-23.

Brown, Michael C, and Christopher E Turner. 2004. 'Paxillin: adapting to change', *Physiological reviews*, 84: 1315-39.

Buchner, Markus, Paula García Calavia, Verena Muhr, Anna Kröninger, Antje J Baeumner, Thomas Hirsch, David A Russell, and Maria J Marin. 2019. 'Photosensitiser functionalised luminescent upconverting nanoparticles for efficient photodynamic therapy of breast cancer cells', *Photochemical & Photobiological Sciences*, 18: 98-109.

Caccavari, Francesca, Donatella Valdembri, Chiara Sandri, Federico Bussolino, and Guido Serini. 2010. 'Integrin signaling and lung cancer', *Cell adhesion & migration*, 4: 124-29.

Caicedo, Andrés, Vanessa Fritz, Jean-Marc Brondello, Mickaël Ayala, Indira Dennemont, Naoill Abdellaoui, Florence de Fraipont, Anaïck Moisan, Claire Angebault Prouteau, and Hassan Boukhaddaoui. 2015. 'MitoCeption as a new tool to assess the effects of mesenchymal stem/stromal cell mitochondria on cancer cell metabolism and function', *Scientific reports*, 5: 1-10.

Caliari, Steven R, and Jason A Burdick. 2016. 'A practical guide to hydrogels for cell culture', *Nature methods*, 13: 405-14.

Carpenter, Graham, and Stanley Cohen. 1979. 'Epidermal growth factor', *Annual review of biochemistry*, 48: 193-216.

Carretero, Rafael, Ibrahim M Sektioglu, Natalio Garbi, Oscar C Salgado, Philipp Beckhove, and Günter J Hämmerling. 2015. 'Eosinophils orchestrate cancer rejection by normalizing tumor vessels and enhancing infiltration of CD8+ T cells', *Nature immunology*, 16: 609-17.

Carter, Kiersten P, Samer Hanna, Alessandro Genna, Daniel Lewis, Jeffrey E Segall, and Dianne Cox. 2019. 'Macrophages enhance 3D invasion in a breast cancer cell line by induction of tumor cell tunneling nanotubes', *Cancer Reports*, 2: e1213.

Case, Lindsay B, and Clare M Waterman. 2015. 'Integration of actin dynamics and cell adhesion by a three-dimensional, mechanosensitive molecular clutch', *Nature cell biology*, 17: 955-63.

Cheadle, Eleanor J, Kallingal Riyad, Daren Subar, Dominic G Rothwell, Garry Ashton, Hayley Batha, David J Sherlock, Robert E Hawkins, and David E Gilham. 2007. 'Eotaxin-2 and colorectal cancer: a potential target for immune therapy', *Clinical cancer research*, 13: 5719-28.

Chemi, Francesca, Sumitra Mohan, Tatiana Guevara, Alexandra Clipson, Dominic G Rothwell, and Caroline Dive. 2021. 'Early dissemination of circulating tumor cells: biological and clinical insights', *Frontiers in Oncology*, 11: 672195.

Chen, Elizabeth H, Eric Grote, William Mohler, and Agnès Vignery. 2007. 'Cell–cell fusion', *FEBS letters*, 581: 2181-93.

Chen, Wei, Qiang Gao, Siqi Han, Fei Pan, and Wei Fan. 2015. 'The CCL2/CCR2 axis enhances IL-6-induced epithelial-mesenchymal transition by cooperatively activating STAT3-Twist signaling', *Tumor Biology*, 36: 973-81.

Chen, Xiaoji, Ching-Wei Chang, Jill M Spoerke, Kathryn E Yoh, Vidushi Kapoor, Charles Baudo, Junko Aimi, Mamie Yu, May MY Liang-Chu, and Rebecca Suttmann. 2019. 'Low-pass whole-genome

sequencing of circulating cell-free DNA demonstrates dynamic changes in genomic copy number in a squamous lung cancer clinical cohort', *Clinical cancer research*, 25: 2254-63.
Cheng, Ying, and Hongqi Tian. 2017. 'Current development status of MEK inhibitors', *Molecules*, 22: 1551.
Chinnery, Holly R, Eric Pearlman, and Paul G McMenamin. 2008. 'Cutting edge: Membrane nanotubes in vivo: a feature of MHC class II+ cells in the mouse cornea', *The Journal of Immunology*, 180: 5779-83.
Chitcholtan, Kenny, Eric Asselin, Sophie Parent, Peter H Sykes, and John J Evans. 2013. 'Differences in growth properties of endometrial cancer in three dimensional (3D) culture and 2D cell monolayer', *Experimental cell research*, 319: 75-87.
Chung, Jun, Sang-Oh Yoon, Elizabeth A Lipscomb, and Arthur M Mercurio. 2004. 'The Met receptor and α6β4 integrin can function independently to promote carcinoma invasion', *Journal of Biological Chemistry*, 279: 32287-93.
Ciardiello, Fortunato, Roberto Bianco, Roberta Caputo, Rosa Caputo, Vincenzo Damiano, Teresa Troiani, Davide Melisi, Ferdinando De Vita, Sabino De Placido, and A Raffaele Bianco. 2004. 'Antitumor activity of ZD6474, a vascular endothelial growth factor receptor tyrosine kinase inhibitor, in human cancer cells with acquired resistance to antiepidermal growth factor receptor therapy', *Clinical cancer research*, 10: 784-93.
Cole, Jennifer M, Richard Dahl, and Karen D Cowden Dahl. 2021. 'MAPK Signaling Is Required for Generation of Tunneling Nanotube-Like Structures in Ovarian Cancer Cells', *Cancers*, 13: 274.
Comoglio, Paolo M, Silvia Giordano, and Livio Trusolino. 2008. 'Drug development of MET inhibitors: targeting oncogene addiction and expedience', *Nature reviews Drug discovery*, 7: 504-16.
Comoglio, Paolo M, Livio Trusolino, and Carla Boccaccio. 2018. 'Known and novel roles of the MET oncogene in cancer: a coherent approach to targeted therapy', *Nature Reviews Cancer*: 1.
Conte, Claudia, Sara Maiolino, Diogo Silva Pellosi, Agnese Miro, Francesca Ungaro, and Fabiana Quaglia. 2016. 'Polymeric nanoparticles for cancer photodynamic therapy', *Light-responsive nanostructured systems for applications in nanomedicine*: 61-112.
Conway, Kevin, Patricia Price, Keith G Harding, and Wen G Jiang. 2006. 'The molecular and clinical impact of hepatocyte growth factor, its receptor, activators, and inhibitors in wound healing', *Wound Repair and Regeneration*, 14: 2-10.
Cook, Danielle R, Kent L Rossman, and Channing J Der. 2014. 'Rho guanine nucleotide exchange factors: regulators of Rho GTPase activity in development and disease', *Oncogene*, 33: 4021-35.
Corcoran, Amy, and Rolando F Del Maestro. 2003. 'Testing the “go or grow” hypothesis in human medulloblastoma cell lines in two and three dimensions', *Neurosurgery*, 53: 174-85.
Cordero Cervantes, Diego, and Chiara Zurzolo. 2021. 'Peering into tunneling nanotubes—The path forward', *The EMBO journal*, 40: e105789.
Côté, Jean-François, Christopher E Turner, and Michel L Tremblay. 1999. 'Intact LIM 3 and LIM 4 domains of paxillin are required for the association to a novel polyproline region (Pro 2) of protein-tyrosine phosphatase-PEST', *Journal of Biological Chemistry*, 274: 20550-60.
Crestani, Bruno, Sylvain Marchand-Adam, Christophe Quesnel, Laurent Plantier, Keren Borensztajn, Joelle Marchal, Arnaud Mailleux, Paul Soler, and Monique Dehoux. 2012. 'Hepatocyte growth factor and lung fibrosis', *Proceedings of the American Thoracic Society*, 9: 158-63.
Crouch, Sonya, Celee S Spidel, and J Suzanne %J Experimental cell research Lindsey. 2004. 'HGF and ligation of αvβ5 integrin induce a novel, cancer cell-specific gene expression required for cell scattering', 292: 274-87.
Crowe, David L, and Arthur Ohannessian. 2004. 'Recruitment of focal adhesion kinase and paxillin to β1 integrin promotes cancer cell migration via mitogen activated protein kinase activation', *BMC cancer*, 4: 1-8.
Cruz, Charles S Dela, Lynn T Tanoue, and Richard A Matthay. 2011. 'Lung cancer: epidemiology, etiology, and prevention', *Clinics in chest medicine*, 32: 605-44.

Cui, Tailin, Masahiko Kusunose, Atsuhide Hamada, Masahide Ono, Mitsuhiko Miyamura, Saburo Yoshioka, Shojiro Kyotani, and Yutaka Nishioka. 2003. 'Relationship between the eosinophilia of bronchoalveolar lavage fluid (BALF) and the severity of pulmonary fibrosis induced by bleomycin in rats', *Biological and Pharmaceutical Bulletin*, 26: 959-63.

Czirók, András, Katalin Schlett, Emília Madarász, and Tamás Vicsek. 1998. 'Exponential distribution of locomotion activity in cell cultures', *Physical Review Letters*, 81: 3038.

Dao, Vi Thuy, Aurélien Guy Dupuy, Olivier Gavet, Emmanuelle Caron, and Jean de Gunzburg. 2009. 'Dynamic changes in Rap1 activity are required for cell retraction and spreading during mitosis', *Journal of cell science*, 122: 2996-3004.

Dasgupta, Arko, Andrea R Lim, and Cyrus M Ghajar. 2017. 'Circulating and disseminated tumor cells: harbingers or initiators of metastasis?', *Molecular oncology*, 11: 40-61.

Davis, Benjamin P, and Marc E Rothenberg. 2014. 'Eosinophils and cancer', *Cancer immunology research*, 2: 1-8.

De Donatis, Alina, Giusy Comito, Francesca Buricchi, Maria C Vinci, Astrid Parenti, Anna Caselli, Guido Camici, Giampaolo Manao, Giampietro Ramponi, and Paolo Cirri. 2008. 'Proliferation versus migration in platelet-derived growth factor signaling: the key role of endocytosis', *Journal of Biological Chemistry*, 283: 19948-56.

De Donatis, Alina, Francesco Ranaldi, and Paolo Cirri. 2010. 'Reciprocal control of cell proliferation and migration', *Cell Communication and Signaling*, 8: 1-4.

De Jong, KP, MM Van Gameren, J Bijzet, PC Limburg, WJ Sluiter, MJH Slooff, and EGE De Vries. 2001. 'Recombinant human interleukin-6 induces hepatocyte growth factor production in cancer patients', *Scandinavian journal of gastroenterology*, 36: 636-40.

De Lima, Priscila Oliveira, Fabio Vieira Dos Santos, Denise Tostes Oliveira, Roberta Carvalho de Figueiredo, and Michele Conceição Pereira. 2015. 'Effect of eosinophil cationic protein on human oral squamous carcinoma cell viability', *Molecular and clinical oncology*, 3: 353-56.

Deakin, Nicholas O, and Christopher E Turner. 2008. 'Paxillin comes of age', *Journal of cell science*, 121: 2435-44.

Del Valle, Carla Arnau, Thomas Hirsch, and Maria Marin. 2022. 'Recent advances in near infrared upconverting nanomaterials for targeted photodynamic therapy of cancer', *Methods and Applications in Fluorescence*.

Delage, Elise, Diégo Cordero Cervantes, Esthel Pénard, Christine Schmitt, Sylvie Syan, Andrea Disanza, Giorgio Scita, and Chiara Zurzolo. 2016. 'Differential identity of Filopodia and Tunneling Nanotubes revealed by the opposite functions of actin regulatory complexes', *Scientific reports*, 6: 1-12.

Desai, Tushar J, and Wellington V Cardoso. 2001. 'Growth factors in lung development and disease: friends or foe?', *Respiratory research*, 3: 1-4.

Desgrosellier, Jay S, and David A Cheresh. 2010. 'Integrins in cancer: biological implications and therapeutic opportunities', *Nature Reviews Cancer*, 10: 9.

Desir, Snider, Elizabeth L Dickson, Rachel I Vogel, Venugopal Thayanithy, Phillip Wong, Deanna Teoh, Melissa A Geller, Clifford J Steer, Subbaya Subramanian, and Emil Lou. 2016. 'Tunneling nanotube formation is stimulated by hypoxia in ovarian cancer cells', *Oncotarget*, 7: 43150.

Desir, Snider, Patrick O'Hare, Rachel Isaksson Vogel, William Sperduto, Akshat Sarkari, Elizabeth L Dickson, Phillip Wong, Andrew C Nelson, Yuman Fong, and Clifford J Steer. 2018. 'Chemotherapy-induced tunneling nanotubes mediate intercellular drug efflux in pancreatic cancer', *Scientific reports*, 8: 1-13.

Desir, Snider, Phillip Wong, Thomas Turbyville, De Chen, Mihir Shetty, Christopher Clark, Edward Zhai, Yevgeniy Romin, Katia Manova-Todorova, and Timothy K Starr. 2019. 'Intercellular transfer of oncogenic KRAS via tunneling nanotubes introduces intracellular mutational heterogeneity in colon cancer cells', *Cancers*, 11: 892.

Ding, Li, Gad Getz, David A Wheeler, Elaine R Mardis, Michael D McLellan, Kristian Cibulskis, Carrie Sougnez, Heidi Greulich, Donna M Muzny, and Margaret B Morgan. 2008. 'Somatic mutations affect key pathways in lung adenocarcinoma', *Nature*, 455: 1069-75.

Dix, Christina L, Helen K Matthews, Marina Uroz, Susannah McLaren, Lucie Wolf, Nicholas Heatley, Zaw Win, Pedro Almada, Ricardo Henriques, and Michael Boutros. 2018. 'The role of mitotic cell-substrate adhesion re-modeling in animal cell division', *Developmental cell*, 45: 132-45. e3.

Donnem, Tom, Christopher G Fenton, Kenneth Lonvik, Thomas Berg, Katrine Eklo, Sigve Andersen, Helge Stenvold, Khalid Al-Shibli, Samer Al-Saad, and Roy M Bremnes. 2012. 'MicroRNA signatures in tumor tissue related to angiogenesis in non-small cell lung cancer', *PLoS One*, 7: e29671.

Dorta, RG, G Landman, LP Kowalski, JRP Lauris, MRDO Latorre, and DT Oliveira. 2002a. 'Tumour-associated tissue eosinophilia as a prognostic factor in oral squamous cell carcinomas', *Histopathology*, 41: 152-57.

Dorta, RG, Gilles Landman, Luiz Paulo Kowalski, José Roberto Pereira Lauris, MRDO Latorre, and Denise Tostes Oliveira. 2002b. 'Tumour-associated tissue eosinophilia as a prognostic factor in oral squamous cell carcinomas', *Histopathology*, 41: 152-57.

Dotto, Gian Paolo, Robert A Weinberg, and Aurelio Ariza. 1988. 'Malignant transformation of mouse primary keratinocytes by Harvey sarcoma virus and its modulation by surrounding normal cells', *Proceedings of the National Academy of Sciences*, 85: 6389-93.

Duan, Shanzhou, Ying Tsai, Peter Keng, Yongbing Chen, Soo Ok Lee, and Yuhchyau Chen. 2015. 'IL-6 signaling contributes to cisplatin resistance in non-small cell lung cancer via the up-regulation of anti-apoptotic and DNA repair associated molecules', *Oncotarget*, 6: 27651.

Dubois, Fatéméh, Magalie Bénard, Bastien Jean-Jacques, Damien Schapman, Hélène Roberge, Alexis Lebon, Didier Goux, Baptiste Monterroso, Nicolas Elie, and Hitoshi Komuro. 2020. 'Investigating tunneling nanotubes in cancer cells: guidelines for structural and functional studies through cell imaging', *BioMed research international*, 2020.

Dubois, Fatéméh, Bastien Jean-Jacques, Hélène Roberge, Magalie Bénard, Ludovic Galas, Damien Schapman, Nicolas Elie, Didier Goux, Maureen Keller, and Elodie Maille. 2018. 'A role for RASSF1A in tunneling nanotube formation between cells through GEFH1/Rab11 pathway control', *Cell Communication and Signaling*, 16: 1-20.

Dulbecco, R, and MGP Stoker. 1970. 'Conditions determining initiation of DNA synthesis in 3T3 cells', *Proceedings of the National Academy of Sciences*, 66: 204-10.

Dupont, Maeva, Shanti Souriant, Luciana Balboa, Thien-Phong Vu Manh, Karine Pingris, Stella Rousset, Céline Cougoule, Yoann Rombouts, Renaud Poincloux, and Myriam Ben Neji. 2020. 'Tuberculosis-associated IFN-I induces Siglec-1 on tunneling nanotubes and favors HIV-1 spread in macrophages', *Elife*, 9: e52535.

Duval, Kayla, Hannah Grover, Li-Hsin Han, Yongchao Mou, Adrian F Pegoraro, Jeffery Fredberg, and Zi Chen. 2017. 'Modeling physiological events in 2D vs. 3D cell culture', *Physiology*, 32: 266-77.

Dvorak, AM, P Estrella, and T Ishizaka. 1994. 'Vesicular transport of peroxidase in human eosinophilic myelocytes', *Clinical & Experimental Allergy*, 24: 10-18.

Elenbaas, Brian, and Robert A Weinberg. 2001. 'Heterotypic signaling between epithelial tumor cells and fibroblasts in carcinoma formation', *Experimental cell research*, 264: 169-84.

Engblom, Camilla, Christina Pfirschke, Rapolas Zilionis, Janaina Da Silva Martins, Stijn A Bos, Gabriel Courties, Steffen Rickelt, Nicolas Severe, Ninib Baryawno, and Julien Faget. 2017. 'Osteoblasts remotely supply lung tumors with cancer-promoting SiglecFhigh neutrophils', *Science*, 358: eaal5081.

Engelman, Jeffrey A, Kreshnik Zejnullahu, Christopher-Michael Gale, Eugene Lifshits, Andrea J Gonzales, Takeshi Shimamura, Feng Zhao, Patrick W Vincent, George N Naumov, and James E Bradner. 2007. 'PF00299804, an irreversible pan-ERBB inhibitor, is effective in lung cancer

models with EGFR and ERBB2 mutations that are resistant to gefitinib', *Cancer research*, 67: 11924-32.

Engelman, Jeffrey A, Kreshnik Zejnullahu, Tetsuya Mitsudomi, Youngchul Song, Courtney Hyland, Joon Oh Park, Neal Lindeman, Christopher-Michael Gale, Xiaojun Zhao, and James Christensen. 2007. 'MET amplification leads to gefitinib resistance in lung cancer by activating ERBB3 signaling', *Science*, 316: 1039-43.

Eramo, A, F Lotti, G Sette, E Pilozzi, M Biffoni, Aet Di Virgilio, C Conticello, L Ruco, C Peschle, and R De Maria. 2008. 'Identification and expansion of the tumorigenic lung cancer stem cell population', *Cell Death & Differentiation*, 15: 504-14.

Etienne-Manneville, S. 2008. 'Polarity proteins in migration and invasion', *Oncogene*, 27: 6970-80.

Ettinger, David S, Wallace Akerley, Gerold Bepler, Matthew G Blum, Andrew Chang, Richard T Cheney, Lucian R Chirieac, Thomas A D'Amico, Todd L Demmy, and Apar Kishor P Ganti. 2010. 'Non–small cell lung cancer', *Journal of the national comprehensive cancer network*, 8: 740-801.

Ettinger, David S, Wallace Akerley, Hossein Borghaei, Andrew C Chang, Richard T Cheney, Lucian R Chirieac, Thomas A D'amico, Todd L Demmy, Ramaswamy Govindan, and Frederic W Grannis. 2013. 'Non–small cell lung cancer, version 2.2013', *Journal of the National Comprehensive Cancer Network*, 11: 645-53.

Faix, Jan, and Klemens Rottner. 2006. 'The making of filopodia', *Current opinion in cell biology*, 18: 18-25.

Fan, Saijun, Min Gao, Qinghui Meng, John J Laterra, Marc H Symons, Sal Coniglio, Richard G Pestell, Itzhak D Goldberg, and Eliot M Rosen. 2005. 'Role of NF-κB signaling in hepatocyte growth factor/scatter factor-mediated cell protection', *Oncogene*, 24: 1749.

Fattet, Laurent, Hae-Yun Jung, Mike W Matsumoto, Brandon E Aubol, Aditya Kumar, Joseph A Adams, Albert C Chen, Robert L Sah, Adam J Engler, and Elena B Pasquale. 2020. 'Matrix rigidity controls epithelial-mesenchymal plasticity and tumor metastasis via a mechanoresponsive EPHA2/LYN complex', *Developmental cell*, 54: 302-16. e7.

Ferrara, Napoleone, and Robert S Kerbel. 2005. 'Angiogenesis as a therapeutic target', *Nature*, 438: 967-74.

Fessart, Delphine, Hugues Begueret, and Frederic Delom. 2013. 'Three-dimensional culture model to distinguish normal from malignant human bronchial epithelial cells', *European Respiratory Journal*, 42: 1345-56.

Finocchiaro, Giovanna, Luca Toschi, Letizia Gianoncelli, Marina Baretti, and Armando Santoro. 2015. 'Prognostic and predictive value of MET deregulation in non-small cell lung cancer', *Annals of translational medicine*, 3.

Fischer, Oliver M, Silvia Giordano, Paolo M Comoglio, and Axel Ullrich. 2004. 'Reactive oxygen species mediate Met receptor transactivation by G protein-coupled receptors and the epidermal growth factor receptor in human carcinoma cells', *Journal of Biological Chemistry*, 279: 28970-78.

Fischkoff, Steven A, Glenn E Brown, and Avrom Pollak. 1986. 'Synthesis of eosinophil-associated enzymes in HL-60 promyelocytic leukemia cells'.

Fixman, Elizabeth D, Tanya M Fournier, Darren M Kamikura, Monica A Naujokas, and Morag Park. 1996. 'Pathways downstream of Shc and Grb2 are required for cell transformation by the tpr-Met oncoprotein', *Journal of Biological Chemistry*, 271: 13116-22.

Flynn, John F, Christina Wong, and Joseph M Wu. 2009. 'Anti-EGFR therapy: mechanism and advances in clinical efficacy in breast cancer', *Journal of oncology*, 2009.

Frampton, Garrett M, Siraj M Ali, Mark Rosenzweig, Juliann Chmielecki, Xinyuan Lu, Todd M Bauer, Mikhail Akimov, Jose A Bufill, Carrie Lee, and David Jentz. 2015. 'Activation of MET via diverse exon 14 splicing alterations occurs in multiple tumor types and confers clinical sensitivity to MET inhibitors', *Cancer discovery*, 5: 850-59.

Franchi, Marco, Zoi Piperigkou, Eirini Riti, Valentina Masola, Maurizio Onisto, and Nikos K Karamanos. 2020. 'Long filopodia and tunneling nanotubes define new phenotypes of breast cancer cells in 3D cultures', *Matrix Biology Plus*: 100026.

Frémont, Stéphane, Guillaume Romet-Lemonne, Anne Houdusse, and Arnaud Echard. 2017. 'Emerging roles of MICAL family proteins–from actin oxidation to membrane trafficking during cytokinesis', *Journal of cell science*, 130: 1509-17.

Fukuoka, Masahiro, Seiji Yano, Giuseppe Giaccone, Tomohide Tamura, Kazuhiko Nakagawa, Jean-Yves Douillard, Yutaka Nishiwaki, Johan Vansteenkiste, Shinzoh Kudoh, and Danny Rischin. 2003. 'Multi-institutional randomized phase II trial of gefitinib for previously treated patients with advanced non–small-cell lung cancer', *Journal of clinical oncology*, 21: 2237-46.

Funk, Sarah E, and E Helene Sage. 1991. 'The Ca2 (+)-binding glycoprotein SPARC modulates cell cycle progression in bovine aortic endothelial cells', *Proceedings of the National Academy of Sciences*, 88: 2648-52.

Furbert-Harris, Paulette, Debra Parish-Gause, Ibrahim Laniyan, Keith A Hunter, Josephine Okomo-Awich, Theresa R Vaughn, Kesha C Forrest, Christina Howland, Abier Abdelnaby, and Oladipo A Oredipe. 2003. 'Inhibition of prostate cancer cell growth by activated eosinophils', *The Prostate*, 57: 165-75.

Gajewski, Thomas F, Hans Schreiber, and Yang-Xin Fu. 2013. 'Innate and adaptive immune cells in the tumor microenvironment', *Nature immunology*, 14: 1014-22.

Ganser, GAIL L, GEORGE P Stricklin, and LYNN M Matrisian. 2004. 'EGF and TGF alpha influence in vitro lung development by the induction of matrix-degrading metalloproteinases', *International Journal of Developmental Biology*, 35: 453-61.

Gao, Sizhi Paul, Kevin G Mark, Kenneth Leslie, William Pao, Noriko Motoi, William L Gerald, William D Travis, William Bornmann, Darren Veach, and Bayard Clarkson. 2007. 'Mutations in the EGFR kinase domain mediate STAT3 activation via IL-6 production in human lung adenocarcinomas', *The Journal of clinical investigation*, 117: 3846.

Garay, Tamás, Éva Juhász, Eszter Molnár, Maria Eisenbauer, András Czirók, Barbara Dekan, Viktória László, Mir Alireza Hoda, Balázs Döme, and József Tímár. 2013. 'Cell migration or cytokinesis and proliferation?–revisiting the “go or grow” hypothesis in cancer cells in vitro', *Experimental cell research*, 319: 3094-103.

Garbers, Christoph, Sylvia Heink, Thomas Korn, and Stefan Rose-John. 2018. 'Interleukin-6: designing specific therapeutics for a complex cytokine', *Nature Reviews Drug Discovery*, 17: 395.

Gatault, Solène, Fanny Legrand, Marie Delbeke, Sylvie Loiseau, and Monique Capron. 2012. 'Involvement of eosinophils in the anti-tumor response', *Cancer Immunology, Immunotherapy*, 61: 1527-34.

Gately, Kathy, Lydia Forde, Sinead Cuffe, Robert Cummins, Elaine W Kay, Friedrich Feuerhake, and Kenneth J O'Byrne. 2014. 'High coexpression of both EGFR and IGF1R correlates with poor patient prognosis in resected non–small-cell lung cancer', *Clinical lung cancer*, 15: 58-66.

Gatenby, Robert A, and Robert J Gillies. 2004. 'Why do cancers have high aerobic glycolysis?', *Nature Reviews Cancer*, 4: 891-99.

Gerdes, Hans-Hermann, and Raquel Negrão Carvalho. 2008. 'Intercellular transfer mediated by tunneling nanotubes', *Current opinion in cell biology*, 20: 470-75.

Gerdes, Hans-Hermann, Amin Rustom, and Xiang Wang. 2013. 'Tunneling nanotubes, an emerging intercellular communication route in development', *Mechanisms of development*, 130: 381-87.

Giacinti, C, and Antonion Giordano. 2006. 'RB and cell cycle progression', *Oncogene*, 25: 5220-27.

Giese, A, R Bjerkvig, ME Berens, and M Westphal. 2003. 'Cost of migration: invasion of malignant gliomas and implications for treatment', *Journal of clinical oncology*, 21: 1624-36.

Giese, Alf, Melinda A Loo, Nhan Tran, Dorothy Haskett, Stephen W Coons, and Michael E Berens. 1996. 'Dichotomy of astrocytoma migration and proliferation', *International Journal of Cancer*, 67: 275-82.

Glenney Jr, John R, and Liza Zokas. 1989. 'Novel tyrosine kinase substrates from Rous sarcoma virus-transformed cells are present in the membrane skeleton', *The Journal of cell biology*, 108: 2401-08.

Glimelius, Ingrid, Jenny Rubin, Marie Fischer, Daniel Molin, Rose-Marie Amini, Per Venge, and Gunilla Enblad. 2011. 'Effect of eosinophil cationic protein (ECP) on Hodgkin lymphoma cell lines', *Experimental hematology*, 39: 850-58.

Goss, BC, Kiaran P McGee, EC Ehman, A Manduca, and RL Ehman. 2006. 'Magnetic resonance elastography of the lung: technical feasibility', *Magnetic Resonance in Medicine: An Official Journal of the International Society for Magnetic Resonance in Medicine*, 56: 1060-66.

Graves, Edward E, Amit Maity, and Quynh-Thu Le. 2010. "The tumor microenvironment in non–small-cell lung cancer." In *Seminars in radiation oncology*, 156-63. Elsevier.

Gross, Lan, Diane W Dynia, Seamus A Rooney, Douglas A Smart, Joseph B Warshaw, Janice F Sissom, and Steven B Hoath. 1986. 'Influence of epidermal growth factor on fetal rat lung development in vitro', *Pediatric research*, 20: 473-77.

Guaragnella, Nicoletta, Sergio Giannattasio, and Loredana Moro. 2014. 'Mitochondrial dysfunction in cancer chemoresistance', *Biochemical pharmacology*, 92: 62-72.

Guo, Yuqi, Feng Xu, TianJian Lu, Zhenfeng Duan, and Zhan Zhang. 2012. 'Interleukin-6 signaling pathway in targeted therapy for cancer', *Cancer treatment reviews*, 38: 904-10.

Gupta, Ruta, Aditi M Dastane, Farahnaz Forozan, Amin Riley-Portuguez, Fai Chung, Jean Lopategui, and Alberto M Marchevsky. 2009. 'Evaluation of EGFR abnormalities in patients with pulmonary adenocarcinoma: the need to test neoplasms with more than one method', *Modern Pathology*, 22: 128-33.

Gurunathan, Sangiliyandi, Min-Hee Kang, Muhammad Qasim, and Jin-Hoi Kim. 2018. 'Nanoparticle-mediated combination therapy: Two-in-one approach for cancer', *International journal of molecular sciences*, 19: 3264.

Habanjar, Ola, Mona Diab-Assaf, Florence Caldefie-Chezet, and Laetitia Delort. 2021. '3D cell culture systems: tumor application, advantages, and disadvantages', *International journal of molecular sciences*, 22: 12200.

Haglund, Kaisa, Ioannis P Nezis, and Harald Stenmark. 2011. 'Structure and functions of stable intercellular bridges formed by incomplete cytokinesis during development', *Communicative & integrative biology*, 4: 1-9.

Hamid, Qutayba, Julia Barkans, Qiu Meng, Sun Ying, John S Abrams, A Barry Kay, and Redwan Moqbel. 1992. 'Human eosinophils synthesize and secrete interleukin-6, in vitro'.

Hammond, Dean E, Sylvie Urbé, George F Vande Woude, and Michael J Clague. 2001. 'Down-regulation of MET, the receptor for hepatocyte growth factor', *Oncogene*, 20: 2761-70.

Han, Ji-Youn, Hong Sug Kim, Sug Hyung Lee, Won Sang Park, Jung Young Lee, and Nam Jin Yoo. 2003. 'Immunohistochemical expression of integrins and extracellular matrix proteins in non-small cell lung cancer: correlation with lymph node metastasis', *Lung Cancer*, 41: 65-70.

Han, Jing, Nobuko Ohno, Sylvie Pasco, Jean-Claude Monboisse, Jacques P Borel, and Nicholas A Kefalides. 1997. 'A cell binding domain from the α3 chain of type IV collagen inhibits proliferation of melanoma cells', *Journal of Biological Chemistry*, 272: 20395-401.

Han, ShouWei, Fadlo R Khuri, and Jesse Roman. 2006. 'Fibronectin stimulates non–small cell lung carcinoma cell growth through activation of Akt/mammalian target of rapamycin/S6 kinase and inactivation of LKB1/AMP-activated protein kinase signal pathways', *Cancer research*, 66: 315-23.

Han, Shouwei, Neil Sidell, and Jesse Roman. 2005. 'Fibronectin stimulates human lung carcinoma cell proliferation by suppressing p21 gene expression via signals involving Erk and Rho kinase', *Cancer letters*, 219: 71-81.

Han, Shouwei, Neil Sidell, Susanne Roser-Page, and Jesse Roman. 2004. 'Fibronectin stimulates human lung carcinoma cell growth by inducing cyclooxygenase-2 (COX-2) expression', *International Journal of Cancer*, 111: 322-31.

Hanahan, Douglas, and Robert A Weinberg. 2011. 'Hallmarks of cancer: the next generation', *cell*, 144: 646-74.

Hanna, Nasser, David Johnson, Sarah Temin, Sherman Baker Jr, Julie Brahmer, Peter M Ellis, Giuseppe Giaccone, Paul J Hesketh, Ishmael Jaiyesimi, and Natasha B Leighl. 2017. 'Systemic therapy for stage IV non–small-cell lung cancer: American Society of Clinical Oncology clinical practice guideline update', *Journal of clinical oncology*.

Hanna, Samer J, Kessler McCoy-Simandle, Edison Leung, Alessandro Genna, John Condeelis, and Dianne Cox. 2019. 'Tunneling nanotubes, a novel mode of tumor cell–macrophage communication in tumor cell invasion', *Journal of Cell Science*, 132: jcs223321.

Hanna, Samer J, Kessler McCoy-Simandle, Veronika Miskolci, Peng Guo, Michael Cammer, Louis Hodgson, and Dianne Cox. 2017. 'The role of Rho-GTPases and actin polymerization during macrophage tunneling nanotube biogenesis', *Scientific reports*, 7: 1-16.

Harrison, Susan MW, Teresa Knifley, Min Chen, and Kathleen L O'Connor. 2013. 'LPA, HGF, and EGF utilize distinct combinations of signaling pathways to promote migration and invasion of MDA-MB-231 breast carcinoma cells', *BMC cancer*, 13: 1-8.

Harvey, P, A Warn, P Newman, LJ Perry, RY Ball, and RM Warn. 1996. 'Immunoreactivity for hepatocyte growth factor/scatter factor and its receptor, met, in human lung carcinomas and malignant mesotheliomas', *The Journal of pathology*, 180: 389-94.

Hase, Koji, Shunsuke Kimura, Hiroyuki Takatsu, Masumi Ohmae, Sayaka Kawano, Hiroshi Kitamura, Masatoshi Ito, Hiroshi Watarai, C Clayton Hazelett, and Charles Yeaman. 2009. 'M-Sec promotes membrane nanotube formation by interacting with Ral and the exocyst complex', *Nature cell biology*, 11: 1427-32.

Hastings, Jordan F, Joanna N Skhinas, Dirk Fey, David R Croucher, and Thomas R Cox. 2019. 'The extracellular matrix as a key regulator of intracellular signalling networks', *British journal of pharmacology*, 176: 82-92.

Haura, Eric B, Sandy Livingston, and Domenico Coppola. 2006. 'Autocrine Interleukin-6/Interleukin-6 Receptor Stimulation in Non–Small-Cell Lung Cancer', *Clinical lung cancer*, 7: 273-75.

Heink, Sylvia, Nir Yogev, Christoph Garbers, Marina Herwerth, Lilian Aly, Christiane Gasperi, Veronika Husterer, Andrew L Croxford, Katja Möller-Hackbarth, and Harald S Bartsch. 2017. 'Trans-presentation of IL-6 by dendritic cells is required for the priming of pathogenic T H 17 cells', *Nature immunology*, 18: 74.

Heinrich, Peter C, Iris Behrmann, Haan Serge, Heike M Hermanns, Gerhard Müller-Newen, and Fred Schaper. 2003. 'Principles of interleukin (IL)-6-type cytokine signalling and its regulation', *Biochemical journal*, 374: 1-20.

Heng, Boon Chin, Paula Porto Bezerra, Peter Rainer Preiser, SK Alex Law, Yun Xia, Freddy Boey, and Subbu S Venkatraman. 2011. 'Effect of cell-seeding density on the proliferation and gene expression profile of human umbilical vein endothelial cells within ex vivo culture', *Cytotherapy*, 13: 606-17.

Herreros, Lourdes, José Luis Rodrıguez-Fernández, Michael C Brown, José L Alonso-Lebrero, Carlos Cabañas, Francisco Sánchez-Madrid, Natividad Longo, Christopher E Turner, and Paloma Sánchez-Mateos. 2000. 'Paxillin localizes to the lymphocyte microtubule organizing center and associates with the microtubule cytoskeleton', *Journal of Biological Chemistry*, 275: 26436-40.

Hodkinson, PS, T Elliott, WS Wong, RC Rintoul, AC Mackinnon, C Haslett, and T Sethi. 2006. 'ECM overrides DNA damage-induced cell cycle arrest and apoptosis in small-cell lung cancer cells through β1 integrin-dependent activation of PI3-kinase', *Cell Death & Differentiation*, 13: 1776-88.

Horie, Shiro, Yoshio Okubo, Mahboob Hossain, Etsuro SATO, Hiroshi NOMURA, Sekiya KOYAMA, Jun-ichi SUZUKI, Mitsuaki ISOBE, and Mode SEKIGUCHI. 1997. 'Interleukin-13 but not interleukin-4 prolongs eosinophil survival and induces eosinophil chemotaxis', *Internal Medicine*, 36: 179-85.

Hov, Håkon, Erming Tian, Toril Holien, Randi Utne Holt, Thea K Våtsveen, Unn-Merete Fagerli, Anders Waage, Magne Børset, and Anders Sundan. 2009. 'c-Met signaling promotes IL-6-induced myeloma cell proliferation', *European journal of haematology*, 82: 277-87.

Hov, Håkon, Erming Tian, Anders Waage, Magne Børset, and Anders Sundan. 2007. 'IL-6 and IGF-1 Act in Synergy with HGF in Myeloma Cells by Modulating the Ras-MAPK Pathway', *Blood*, 110: 4793.

Hsiung, Frank, Felipe-Andrès Ramirez-Weber, D David Iwaki, and Thomas B Kornberg. 2005. 'Dependence of Drosophila wing imaginal disc cytonemes on Decapentaplegic', *Nature*, 437: 560-63.

Huang, Caiqun, and Jun Chen. 2021. 'Laminin-332 mediates proliferation, apoptosis, invasion, migration and epithelial-to-mesenchymal transition in pancreatic ductal adenocarcinoma', *Molecular Medicine Reports*, 23: 1-1.

Huh, Dongeun, Benjamin D Matthews, Akiko Mammoto, Martín Montoya-Zavala, Hong Yuan Hsin, and Donald E Ingber. 2010. 'Reconstituting organ-level lung functions on a chip', *Science*, 328: 1662-68.

Humphries, Jonathan D, Pengbo Wang, Charles Streuli, Benny Geiger, Martin J Humphries, and Christoph Ballestrem. 2007. 'Vinculin controls focal adhesion formation by direct interactions with talin and actin', *The Journal of cell biology*, 179: 1043-57.

Hynds, Robert E, Kristopher K Frese, David R Pearce, Eva Grönroos, Caroline Dive, and Charles Swanton. 2021. 'Progress towards non-small-cell lung cancer models that represent clinical evolutionary trajectories', *Open biology*, 11: 200247.

Hynes, Richard O. 1992. 'Integrins: versatility, modulation, and signaling in cell adhesion', *Cell*, 69: 11-25.

Hynes, Richard O. 2002. 'Integrins: bidirectional, allosteric signaling machines', *Cell*, 110: 673-87.

Hynes, Richard O. 2004. 'The emergence of integrins: a personal and historical perspective', *Matrix biology: journal of the International Society for Matrix Biology*, 23: 333.

Ichimura, Eiji, Arafumi Maeshima, Takashi Nakajima, and Toshikazu Nakamura. 1996. 'Expression of c-met/HGF receptor in human non-small cell lung carcinomas in vitro and in vivo and its prognostic significance', *Japanese journal of cancer research*, 87: 1063-69.

Inaba, Junichi, Elizabeth McConnell, and Keith Davis. 2014. 'Lunasin sensitivity in non-small cell lung cancer cells is linked to suppression of integrin signaling and changes in histone acetylation', *International journal of molecular sciences*, 15: 23705-24.

Inaba, Mayu, Michael Buszczak, and Yukiko M Yamashita. 2015. 'Nanotubes mediate niche–stem-cell signalling in the Drosophila testis', *Nature*, 523: 329-32.

Innocenti, Metello. 2018. 'New insights into the formation and the function of lamellipodia and ruffles in mesenchymal cell migration', *Cell adhesion & migration*, 12: 401-16.

Ishibe, Shuta, Dominique Joly, Zhen-Xiang Liu, and Lloyd G Cantley. 2004. 'Paxillin serves as an ERK-regulated scaffold for coordinating FAK and Rac activation in epithelial morphogenesis', *Molecular cell*, 16: 257-67.

Ishibe, Shuta, Dominique Joly, Xiaolei Zhu, and Lloyd G Cantley. 2003. 'Phosphorylation-dependent paxillin-ERK association mediates hepatocyte growth factor-stimulated epithelial morphogenesis', *Molecular cell*, 12: 1275-85.

Ishihara, Seiichiro, and Hisashi Haga. 2022. 'Matrix Stiffness Contributes to Cancer Progression by Regulating Transcription Factors', *Cancers*, 14: 1049.

Ishizawa, Kota, Hiroshi Kubo, Mitsuhiro Yamada, Seiichi Kobayashi, Takashi Suzuki, Shinya Mizuno, Toshikazu Nakamura, and Hidetada Sasaki. 2004. 'Hepatocyte growth factor induces angiogenesis in injured lungs through mobilizing endothelial progenitor cells', *Biochemical and biophysical research communications*, 324: 276-80.

Islam, Mohammad Naimul, Shonit R Das, Memet T Emin, Michelle Wei, Li Sun, Kristin Westphalen, David J Rowlands, Sadiqa K Quadri, Sunita Bhattacharya, and Jahar Bhattacharya. 2012.

'Mitochondrial transfer from bone-marrow–derived stromal cells to pulmonary alveoli protects against acute lung injury', *Nature medicine*, 18: 759.

Ito, W, T Chiba, A Kanehiro, H Kato, K Yamaguchi, S Ueki, H Kayaba, and J Chihara. 2007. 'Hepatocyte growth factor attenuates eotaxin and PGD2-induced chemotaxis of human eosinophils', *Allergy*, 62: 415-22.

Ito, Yoko, Kelly Correll, John A Schiel, Jay H Finigan, Rytis Prekeris, and Robert J Mason. 2014. 'Lung fibroblasts accelerate wound closure in human alveolar epithelial cells through hepatocyte growth factor/c-Met signaling', *American Journal of Physiology-Lung Cellular and Molecular Physiology*, 307: L94-L105.

Jagadeeswaran, Ramasamy, Sujatha Jagadeeswaran, Vytas P Bindokas, and Ravi Salgia. 2007. 'Activation of HGF/c-Met pathway contributes to the reactive oxygen species generation and motility of small cell lung cancer cells', *American Journal of Physiology-Lung Cellular and Molecular Physiology*, 292: L1488-L94.

Jagadeeswaran, Ramasamy, Hanna Surawska, Soundararajan Krishnaswamy, Varalakshmi Janamanchi, A Craig Mackinnon, Tanguy Y Seiwert, Sivakumar Loganathan, Rajani Kanteti, Trevor Reichman, and Vidya Nallasura. 2008. 'Paxillin is a target for somatic mutations in lung cancer: implications for cell growth and invasion', *Cancer research*, 68: 132-42.

Jahangiri, Arman, Alan Nguyen, Ankush Chandra, Maxim K Sidorov, Garima Yagnik, Jonathan Rick, Sung Won Han, William Chen, Patrick M Flanigan, and Dina Schneidman-Duhovny. 2017. 'Cross-activating c-Met/β1 integrin complex drives metastasis and invasive resistance in cancer', *Proceedings of the National Academy of Sciences*, 114: E8685-E94.

Jain, Anisha S, Ashwini Prasad, Sushma Pradeep, Chandan Dharmashekar, Raghu Ram Achar, Ekaterina Silina, Victor Stupin, Raghavendra G Amachawadi, Shashanka K Prasad, and R Pruthvish. 2021. 'Everything old is new again: drug repurposing approach for non-small cell lung cancer targeting MAPK signaling pathway', *Frontiers in Oncology*, 11: 741326.

Jana, Aniket, Katherine Ladner, Emil Lou, and Amrinder S Nain. 2022. 'Tunneling Nanotubes between Cells Migrating in ECM Mimicking Fibrous Environments', *Cancers*, 14: 1989.

Jansens, Robert JJ, Wim Van den Broeck, Steffi De Pelsmaeker, Jochen AS Lamote, Cliff Van Waesberghe, Liesbeth Couck, and Herman W Favoreel. 2017. 'Pseudorabies virus US3-induced tunneling nanotubes contain stabilized microtubules, interact with neighboring cells via cadherins, and allow intercellular molecular communication', *Journal of virology*, 91: e00749-17.

Jedrzkiewicz, Sean, Hidetoshi Nakamura, Eric S Silverman, Andrew D Luster, Naresh Mansharamani, Kwang Ho In, Gen Tamura, and Craig M Lilly. 2000. 'IL-1β induces eotaxin gene transcription in A549 airway epithelial cells through NF-κB', *American Journal of Physiology-Lung Cellular and Molecular Physiology*, 279: L1058-L65.

Jemal, Ahmedin, Freddie Bray, Melissa M Center, Jacques Ferlay, Elizabeth Ward, and David Forman. 2011. 'Global cancer statistics', *CA: a cancer journal for clinicians*, 61: 69-90.

Jena, Bhanu P. 2011. 'Role of SNAREs in membrane fusion.' in, *Cell Fusion in Health and Disease* (Springer).

Jetten, ANTON M. 1991. 'Growth and differentiation factors in tracheobronchial epithelium', *American Journal of Physiology-Lung Cellular and Molecular Physiology*, 260: L361-L73.

Jiao, Demin, Jian Wang, Wei Lu, Xiali Tang, Jun Chen, Hao Mou, and Qing-yong Chen. 2016. 'Curcumin inhibited HGF-induced EMT and angiogenesis through regulating c-Met dependent PI3K/Akt/mTOR signaling pathways in lung cancer', *Molecular Therapy-Oncolytics*, 3: 16018.

Jin, H, and J Varner. 2004. 'Integrins: roles in cancer development and as treatment targets', *British journal of cancer*, 90: 561.

Jo, Minji, Donna Beer Stolz, James E Esplen, Kenneth Dorko, George K Michalopoulos, and Stephen C Strom. 2000. 'Cross-talk between epidermal growth factor receptor and c-Met signal pathways in transformed cells', *Journal of Biological Chemistry*, 275: 8806-11.

Jones, Simon A %J The Journal of Immunology. 2005. 'Directing transition from innate to acquired immunity: defining a role for IL-6', 175: 3463-68.

Jorissen, Robert N, Francesca Walker, Normand Pouliot, Thomas PJ Garrett, Colin W Ward, and Antony W Burgess. 2003. 'Epidermal growth factor receptor: mechanisms of activation and signalling', *The EGF receptor family*: 33-55.

Ju, Lixia, and Caicun Zhou. 2013. 'Association of integrin beta1 and c-MET in mediating EGFR TKI gefitinib resistance in non-small cell lung cancer', *Cancer cell international*, 13: 1-8.

Junttila, Melissa R, and Frederic J De Sauvage. 2013. 'Influence of tumour micro-environment heterogeneity on therapeutic response', *Nature*, 501: 346-54.

Kalluri, Raghu. 2003. 'Basement membranes: structure, assembly and role in tumour angiogenesis', *Nature Reviews Cancer*, 3: 422-33.

Kamer, Iris, Yael Steuerman, Inbal Daniel-Meshulam, Gili Perry, Shai Izraeli, Marina Perelman, Nir Golan, David Simansky, Iris Barshack, and Alon Ben Nun. 2020. 'Predicting brain metastasis in early stage non-small cell lung cancer patients by gene expression profiling', *Translational Lung Cancer Research*, 9: 682.

Kang, Xiao-Hong, Zhen-Ye Xu, Ya-Bin Gong, Li-fang Wang, Zhong-Qi Wang, Ling Xu, Fei Cao, and Ming-juan Liao. 2013. 'Bufalin reverses HGF-induced resistance to EGFR-TKIs in EGFR mutant lung cancer cells via blockage of Met/PI3k/Akt pathway and induction of apoptosis', *Evidence-Based Complementary and Alternative Medicine*, 2013.

Karlsen, Emma-Anne, Sam Kahler, Joan Tefay, Shannon R Joseph, and Fiona Simpson. 2021. 'Epidermal growth factor receptor expression and resistance patterns to targeted therapy in non-small cell lung cancer: A review', *Cells*, 10: 1206.

Kastenmüller, Wolfgang, Kathrin Kastenmüller, Christian Kurts, and Robert A Seder. 2014. 'Dendritic cell-targeted vaccines—hope or hype?', *Nature Reviews Immunology*, 14: 705-11.

Kataoka, Sayo, Yuko Konishi, Youhei Nishio, Kiyomi Fujikawa-Adachi, and Akira Tominaga. 2004. 'Antitumor activity of eosinophils activated by IL-5 and eotaxin against hepatocellular carcinoma', *DNA and cell biology*, 23: 549-60.

Katayama, Ryohei, Alice T Shaw, Tahsin M Khan, Mari Mino-Kenudson, Benjamin J Solomon, Balazs Halmos, Nicholas A Jessop, John C Wain, Alan Tien Yeo, and Cyril Benes. 2012. 'Mechanisms of acquired crizotinib resistance in ALK-rearranged lung cancers', *Science translational medicine*, 4: 120ra17-20ra17.

Keeratichamroen, Siriporn, Kriengsak Lirdprapamongkol, and Jisnuson Svasti. 2018. 'Mechanism of ECM-induced dormancy and chemoresistance in A549 human lung carcinoma cells', *Oncology reports*, 39: 1765-74.

Keller, Kate E. 2020. 'Tunneling nanotubes and actin cytoskeleton dynamics in glaucoma', *Neural Regeneration Research*, 15: 2031.

Keller, Kate E, John M Bradley, Ying Ying Sun, Yong-Feng Yang, and Ted S Acott. 2017. 'Tunneling nanotubes are novel cellular structures that communicate signals between trabecular meshwork cells', *Investigative ophthalmology & visual science*, 58: 5298-307.

Kelly, Karen, John Crowley, Paul A Bunn Jr, Cary A Presant, Patra K Grevstad, Carol M Moinpour, Scott D Ramsey, Antoinette J Wozniak, Geoffrey R Weiss, and Dennis F Moore. 2001. 'Randomized phase III trial of paclitaxel plus carboplatin versus vinorelbine plus cisplatin in the treatment of patients with advanced non–small-cell lung cancer: a Southwest Oncology Group trial', *Journal of clinical oncology*, 19: 3210-18.

Kermorgant, SPPJ, and PJ Parker. 2005. 'c-Met signalling: spatio-temporal decisions', *Cell cycle*, 4: 352-55.

Khalid, Muhammad Asad Ullah, Young Soo Kim, Muhsin Ali, Byung Gul Lee, Young-Jae Cho, and Kyung Hyun Choi. 2020. 'A lung cancer-on-chip platform with integrated biosensors for physiological monitoring and toxicity assessment', *Biochemical Engineering Journal*, 155: 107469.

Khoshyomn, Sami, Sean Lew, Joseph DeMattia, Elan B Singer, and Paul L Penar. 1999. 'Brain tumor invasion rate measured in vitro does not correlate with Ki-67 expression', *Journal of neuro-oncology*, 45: 111-16.

Kim, Janice P, John D Chen, Mark S Wilke, Thomas J Schall, and David T Woodley. 1994. 'Human keratinocyte migration on type IV collagen. Roles of heparin-binding site and alpha 2 beta 1 integrin', *Laboratory investigation; a journal of technical methods and pathology*, 71: 401-08.

Kim, Na-Hyun, Seong-Kwan Kim, Dong-Soon Kim, Dan Zhang, Jin-A Park, Hee Yi, Jin-Suk Kim, and Ho-Chul Shin. 2015. 'Anti-proliferative action of IL-6R-targeted antibody tocilizumab for non-small cell lung cancer cells', *Oncology letters*, 9: 2283-88.

Kimura, Shunsuke, Koji Hase, and Hiroshi Ohno. 2012. 'Tunneling nanotubes: emerging view of their molecular components and formation mechanisms', *Experimental cell research*, 318: 1699-706.

Kimura, Shunsuke, Koji Hase, and Hiroshi Ohno. 2013. 'The molecular basis of induction and formation of tunneling nanotubes', *Cell and tissue research*, 352: 67-76.

Kimura, Shunsuke, Masami Yamashita, Megumi Yamakami-Kimura, Yusuke Sato, Atsushi Yamagata, Yoshihiro Kobashigawa, Fuyuhiko Inagaki, Takako Amada, Koji Hase, and Toshihiko Iwanaga. 2016. 'Distinct roles for the N-and C-terminal regions of M-Sec in plasma membrane deformation during tunneling nanotube formation', *Scientific reports*, 6: 1-12.

Kirfel, Gregor, Alexander Rigort, Bodo Borm, and Volker Herzog. 2004. 'Cell migration: mechanisms of rear detachment and the formation of migration tracks', *European journal of cell biology*, 83: 717-24.

Kobayashi, Susumu, Titus J Boggon, Tajhal Dayaram, Pasi A Jänne, Olivier Kocher, Matthew Meyerson, Bruce E Johnson, Michael J Eck, Daniel G Tenen, and Balázs Halmos. 2005. 'EGFR mutation and resistance of non–small-cell lung cancer to gefitinib', *New England journal of medicine*, 352: 786-92.

Kolba, Marta D, Wioleta Dudka, Monika Zaręba-Kozioł, Agata Kominek, Paolo Ronchi, Laura Turos, Piotr Chroscicki, Jakub Wlodarczyk, Yannick Schwab, and Agata Klejman. 2019. 'Tunneling nanotube-mediated intercellular vesicle and protein transfer in the stroma-provided imatinib resistance in chronic myeloid leukemia cells', *Cell death & disease*, 10: 1-16.

Komen, Job, Sanne M van Neerven, Albert van den Berg, Louis Vermeulen, and Andries D van der Meer. 2021. 'Mimicking and surpassing the xenograft model with cancer-on-chip technology', *EBioMedicine*, 66: 103303.

Koochekpour, S, A Merzak, and GJ Pilkington. 1995. 'Extracellular matrix proteins inhibit proliferation, upregulate migration and induce morphological changes in human glioma cell lines', *European Journal of Cancer*, 31: 375-80.

Korenkova, Olga, Anna Pepe, and Chiara Zurzolo. 2020. 'Fine intercellular connections in development: TNTs, cytonemes, or intercellular bridges?', *Cell Stress*.

Kreidberg, Jordan A, Michael J Donovan, Stuart L Goldstein, Helmut Rennke, Kenneth Shepherd, Rosemary C Jones, and Rudolf Jaenisch. 1996. 'Alpha 3 beta 1 integrin has a crucial role in kidney and lung organogenesis', *Development*, 122: 3537-47.

Kretschmer, Alexander, Fan Zhang, Syam Prakash Somasekharan, Charan Tse, Lauren Leachman, Anna Gleave, Brian Li, Ivan Asmaro, Teresa Huang, and Leszek Kotula. 2019. 'Stress-induced tunneling nanotubes support treatment adaptation in prostate cancer', *Scientific reports*, 9: 1-13.

Kumar, Ajay, Catherine Corey, Iain Scott, Sruti Shiva, and Jonathan D'Cunha. 2016. 'Minnelide/Triptolide impairs mitochondrial function by regulating SIRT3 in P53-dependent manner in non-small cell lung cancer', *PLoS One*, 11: e0160783.

Kumar, Amit, Edward T Petri, Balazs Halmos, and Titus J Boggon. 2008. 'Structure and clinical relevance of the epidermal growth factor receptor in human cancer', *Journal of clinical oncology*, 26: 1742-51.

Kumar, Amrita, Jin Hyang Kim, Priya Ranjan, Maureen G Metcalfe, Weiping Cao, Margarita Mishina, Shivaprakash Gangappa, Zhu Guo, Edward S Boyden, and Sherif Zaki. 2017. 'Influenza virus exploits tunneling nanotubes for cell-to-cell spread', *Scientific reports*, 7: 1-14.

Kumar, D, K Tiwari, and MS Rajala. 2017. 'Analysis of A549 cell proteome alteration in response to recombinant influenza A virus nucleoprotein and its interaction with cellular proteins, a preliminary study', *Acta virologica*, 61: 56-65.

Kupchan, SM, DAILEY RG JR, GILMORE CJ, and BRYAN RF. 1972. 'Triptolide and tripdiolide. Novel antileukemic diterpenoid triepoxides from Tripterygium wilfordii'.

Lachambre, Simon, Christophe Chopard, and Bruno Beaumelle. 2014. 'Preliminary characterisation of nanotubes connecting T-cells and their use by HIV-1', *Biology of the Cell*, 106: 394-404.

Ladanyi, Marc, and William Pao. 2008. 'Lung adenocarcinoma: guiding EGFR-targeted therapy and beyond', *Modern Pathology*, 21: S16-S22.

Lai, Andrea Z, Jasmine V Abella, and Morag Park. 2009. 'Crosstalk in Met receptor oncogenesis', *Trends in cell biology*, 19: 542-51.

Lai, Jui-Fen, Shu-Chen Kao, Si-Tse Jiang, Ming-Jer Tang, Po-Chao Chan, and Hong-Chen Chen. 2000. 'Involvement of focal adhesion kinase in hepatocyte growth factor-induced scatter of Madin-Darby canine kidney cells', *Journal of Biological Chemistry*, 275: 7474-80.

Lamarche, Nathalie, and Alan Hall. 1994. 'GAPs for rho-related GTPases', *Trends in Genetics*, 10: 436-40.

Lambrechts, Diether, Els Wauters, Bram Boeckx, Sara Aibar, David Nittner, Oliver Burton, Ayse Bassez, Herbert Decaluwé, Andreas Pircher, and Kathleen Van den Eynde. 2018. 'Phenotype molding of stromal cells in the lung tumor microenvironment', *Nature medicine*, 24: 1277-89.

Laukaitis, Christina M, Donna J Webb, Karen Donais, and Alan F Horwitz. 2001. 'Differential dynamics of α5 integrin, paxillin, and α-actinin during formation and disassembly of adhesions in migrating cells', *The Journal of cell biology*, 153: 1427-40.

Lee, Chong-Chou, and Kenneth M Yamada. 1995. 'Alternatively Spliced Juxtamembrane Domain of a Tyrosine Kinase Receptor Is a Multifunctional Regulatory Site: DELETION ALTERS CELLULAR TYROSINE PHOSPHORYLATION PATTERN AND FACILITATES BINDING OF PHOSPHATIDYLINOSITOL-3-OH KINASE TO THE HEPATOCYTE GROWTH FACTOR RECEPTOR (∗)', *Journal of Biological Chemistry*, 270: 507-10.

Lee, Jonathan M, Shoukat Dedhar, Raghu Kalluri, and Erik W Thompson. 2006. 'The epithelial–mesenchymal transition: new insights in signaling, development, and disease', *The Journal of cell biology*, 172: 973-81.

Lee, Kye Young, Jae Seuk Park, Young Koo Jee, and Glenn D Rosen. 2002. 'Triptolide sensitizes lung cancer cells to TNF-related apoptosis-inducing ligand (TRAIL)-induced apoptosis by inhibition of NF-κB activation', *Experimental & molecular medicine*, 34: 462-68.

Lee, Soo Ok, Xiaodong Yang, Shanzhou Duan, Ying Tsai, Laura R Strojny, Peter Keng, and Yuhchyau Chen. 2016. 'IL-6 promotes growth and epithelial-mesenchymal transition of CD133+ cells of non-small cell lung cancer', *Oncotarget*, 7: 6626.

Legrand, Fanny, Virginie Driss, Marie Delbeke, Sylvie Loiseau, Emmanuel Hermann, David Dombrowicz, and Monique Capron. 2010. 'Human eosinophils exert TNF-α and granzyme A-mediated tumoricidal activity toward colon carcinoma cells', *The Journal of Immunology*, 185: 7443-51.

Lemjabbar-Alaoui, Hassan, Omer UI Hassan, Yi-Wei Yang, and Petra Buchanan. 2015. 'Lung cancer: Biology and treatment options', *Biochimica et Biophysica Acta (BBA)-Reviews on Cancer*, 1856: 189-210.

Lemmon, Mark A, and Joseph Schlessinger. 2010. 'Cell signaling by receptor tyrosine kinases', *Cell*, 141: 1117-34.

Lennon, Donald P, Stephen E Haynesworth, Scott P Bruder, Neelam Jaiswal, and Arnold I Caplan. 1996. 'Human and animal mesenchymal progenitor cells from bone marrow: identification of

serum for optimal selection and proliferation', *In Vitro Cellular & Developmental Biology-Animal*, 32: 602-11.

Lennon, Donald P, Stephen E Haynesworth, Randell G Young, James E Dennis, and Arnold I Caplan. 1995. 'A chemically defined medium supports in vitro proliferation and maintains the osteochondral potential of rat marrow-derived mesenchymal stem cells', *Experimental cell research*, 219: 211-22.

Li, Fang, Tengjiao Zhu, Yao Yue, Xiang Zhu, Jiadong Wang, and Li Liang. 2018. 'Preliminary mechanisms of regulating PD-L1 expression in non-small cell lung cancer during the EMT process', *Oncology reports*, 40: 775-82.

Li, Juan, Tian Lan, Cuixiang Zhang, Cheng Zeng, Jincai Hou, Zhicheng Yang, Min Zhang, Jianxun Liu, and Bing Liu. 2015. 'Reciprocal activation between IL-6/STAT3 and NOX4/Akt signalings promotes proliferation and survival of non-small cell lung cancer cells', *Oncotarget*, 6: 1031.

Li, Xiang, Yuelin Zhang, Sze C Yeung, Yingmin Liang, Xiaoting Liang, Yue Ding, Mary SM Ip, Hung-Fat Tse, Judith CW Mak, and Qizhou Lian. 2014. 'Mitochondrial transfer of induced pluripotent stem cell–derived mesenchymal stem cells to airway epithelial cells attenuates cigarette smoke–induced damage', *American journal of respiratory cell and molecular biology*, 51: 455-65.

Li, Ying, Yang Lv, Yu Zhu, Xiaodong Yang, Boya Lin, Mengqing Li, Yaqi Zhou, Zhibo Tan, Eun Ha Choi, and Junjie Wang. 2022. 'Low-Temperature Plasma-Activated Medium Inhibited Proliferation and Progression of Lung Cancer by Targeting the PI3K/Akt and MAPK Pathways', *Oxidative medicine and cellular longevity*, 2022.

Liang, Dacheng. 2018. 'A salutary role of reactive oxygen species in intercellular tunnel-mediated communication', *Frontiers in cell and developmental biology*, 6: 2.

Liang, Hongge, and Mengzhao Wang. 2020. 'MET oncogene in non-small cell lung cancer: mechanism of MET dysregulation and agents targeting the HGF/c-Met axis', *OncoTargets and therapy*, 13: 2491.

Liao, ZJ, YH Guo, Z Zhao, JT Yao, R Xu, and KJ Nan. 2014. 'Gemcitabine inhibits the micrometastasis of non-small cell lung cancer by targeting the EpCAM-positive circulating tumor cells via the HGF/cMET pathway', *International journal of oncology*, 45: 651-58.

Lilly, Craig M, Hidetoshi Nakamura, Howard Kesselman, Cathryn Nagler-Anderson, Koichiro Asano, Eduardo A Garcia-Zepeda, Marc E Rothenberg, Jeffery M Drazen, and Andrew D Luster. 1997. 'Expression of eotaxin by human lung epithelial cells: induction by cytokines and inhibition by glucocorticoids', *The Journal of clinical investigation*, 99: 1767-73.

Lin, Tsu-Kung, Shang-Der Chen, Yao-Chung Chuang, Min-Yu Lan, Jiin-Haur Chuang, Pei-Wen Wang, Te-Yao Hsu, Feng-Sheng Wang, Meng-Han Tsai, and Sheng-Teng Huang. 2019. 'Mitochondrial transfer of wharton's jelly mesenchymal stem cells eliminates mutation burden and rescues mitochondrial bioenergetics in rotenone-stressed MELAS fibroblasts', *Oxidative medicine and cellular longevity*, 2019.

Liska, David, Chin-Tung Chen, Thomas Bachleitner-Hofmann, James G Christensen, and Martin R Weiser. 2011. 'HGF Rescues Colorectal Cancer Cells from EGFR Inhibition via MET ActivationHGF-MET Mediated Resistance to EGFR Inhibition', *Clinical cancer research*, 17: 472-82.

Liu, Chen-Chi, Jiun-Han Lin, Tien-Wei Hsu, Jyuan-Wei Hsu, Jer-Wei Chang, Kelly Su, Han-Shui Hsu, and Shih-Chieh Hung. 2018. 'Collagen XVII/laminin-5 activates epithelial-to-mesenchymal transition and is associated with poor prognosis in lung cancer', *Oncotarget*, 9: 1656.

Liu, Chen-Chi, Jiun-Han Lin, Tien-Wei Hsu, Kelly Su, Anna Fen-Yau Li, Han-Shui Hsu, and Shih-Chieh Hung. 2015. 'IL-6 enriched lung cancer stem-like cell population by inhibition of cell cycle regulators via DNMT1 upregulation', *International Journal of Cancer*, 136: 547-59.

Liu, Fang, Shasha Song, Zhi Yi, Min Zhang, Jiali Li, Fang Yang, Hongtao Yin, Xiufeng Yu, Chao Guan, and Ying Liu. 2017. 'HGF induces EMT in non-small-cell lung cancer through the hBVR pathway', *European journal of pharmacology*, 811: 180-90.

Liu, Jian, Wondwossen Abate, Jinsheng Xu, David Corry, Baksho Kaul, and Simon K Jackson. 2011. 'Three-dimensional spheroid cultures of A549 and HepG2 cells exhibit different lipopolysaccharide (LPS) receptor expression and LPS-induced cytokine response compared with monolayer cultures', *Innate immunity*, 17: 245-55.

Liu, Jianglan, Yuting Zhao, Yujie Sun, Bing He, Changsong Yang, Tatyana Svitkina, Yale E Goldman, and Wei Guo. 2012. 'Exo70 stimulates the Arp2/3 complex for lamellipodia formation and directional cell migration', *Current biology*, 22: 1510-15.

Liu, Qiuyan. 2011. 'Triptolide and its expanding multiple pharmacological functions', *International immunopharmacology*, 11: 377-83.

Liu, Tie-Cheng, Xin Jin, Yan Wang, and Ke Wang. 2017. 'Role of epidermal growth factor receptor in lung cancer and targeted therapies', *American journal of cancer research*, 7: 187.

Liu, Zhen-Xiang, Cheng Fang Yu, Christian Nickel, Sheila Thomas, and Lloyd G Cantley. 2002. 'Hepatocyte growth factor induces ERK-dependent paxillin phosphorylation and regulates paxillin-focal adhesion kinase association', *Journal of Biological Chemistry*, 277: 10452-58.

Ljubojevic, Nina, J Michael Henderson, and Chiara Zurzolo. 2021. 'The ways of actin: why tunneling nanotubes are unique cell protrusions', *Trends in Cell Biology*, 31: 130-42.

Lo, Chun-Min, Hong-Bei Wang, Micah Dembo, and Yu-li Wang. 2000. 'Cell movement is guided by the rigidity of the substrate', *Biophysical journal*, 79: 144-52.

Lock, Jeffrey T, Ian Parker, and Ian F Smith. 2016. 'Communication of Ca2+ signals via tunneling membrane nanotubes is mediated by transmission of inositol trisphosphate through gap junctions', *Cell Calcium*, 60: 266-72.

López-Colomé, Ana María, Irene Lee-Rivera, Regina Benavides-Hidalgo, and Edith López. 2017. 'Paxillin: a crossroad in pathological cell migration', *Journal of hematology & oncology*, 10: 1-15.

Lotfi, Ramin, and Michael Thomas Lotze. 2008. 'Eosinophils induce DC maturation, regulating immunity', *Journal of leukocyte biology*, 83: 456-60.

Lou, Emil, Sho Fujisawa, Afsar Barlas, Yevgeniy Romin, Katia Manova-Todorova, Malcolm AS Moore, and Subbaya Subramanian. 2012. 'Tunneling Nanotubes: A new paradigm for studying intercellular communication and therapeutics in cancer', *Communicative & integrative biology*, 5: 399-403.

Lou, Emil, Sho Fujisawa, Alexei Morozov, Afsar Barlas, Yevgeniy Romin, Yildirim Dogan, Sepideh Gholami, André L Moreira, Katia Manova-Todorova, and Malcolm AS Moore. 2012. 'Tunneling nanotubes provide a unique conduit for intercellular transfer of cellular contents in human malignant pleural mesothelioma', *PloS one*, 7: e33093.

Lou, Emil, Edward Zhai, Akshat Sarkari, Snider Desir, Phillip Wong, Yoshie Iizuka, Jianbo Yang, Subbaya Subramanian, James McCarthy, and Martina Bazzaro. 2018. 'Cellular and molecular networking within the ecosystem of cancer cell communication via tunneling nanotubes', *Frontiers in cell and developmental biology*, 6: 95.

Lu, He-Shu, Ji-Jie Chai, Ming Li, Bing-Ren Huang, Cun-Heng He, and Ru-Chang Bi. 2001. 'Crystal structure of human epidermal growth factor and its dimerization', *Journal of Biological Chemistry*, 276: 34913-17.

Lu, Jin Jin, Wei Min Yang, Fan Li, Wei Zhu, and Zhong Chen. 2019. 'Tunneling nanotubes mediated microRNA-155 intercellular transportation promotes bladder cancer cells' invasive and proliferative capacity', *International journal of nanomedicine*, 14: 9731.

Lu, Jinjin, Xiufen Zheng, Fan Li, Yang Yu, Zhong Chen, Zheng Liu, Zhihua Wang, Hua Xu, and Weimin Yang. 2017. 'Tunneling nanotubes promote intercellular mitochondria transfer followed by increased invasiveness in bladder cancer cells', *Oncotarget*, 8: 15539.

Lu, Ning, Tine V Karlsen, Rolf K Reed, Marion Kusche-Gullberg, and Donald Gullberg. 2014. 'Fibroblast α11β1 integrin regulates tensional homeostasis in fibroblast/A549 carcinoma heterospheroids', *PLoS One*, 9: e103173.

Lucarini, Valeria, Giovanna Ziccheddu, Iole Macchia, Valentina La Sorsa, Francesca Peschiaroli, Carla Buccione, Antonella Sistigu, Massimo Sanchez, Sara Andreone, and Maria Teresa D'Urso. 2017. 'IL-33 restricts tumor growth and inhibits pulmonary metastasis in melanoma-bearing mice through eosinophils', *Oncoimmunology*, 6: e1317420.

Lund-Johansen, Morten, Rolf Bjerkvig, Peter A Humphrey, Sandra H Bigner, Darell D Bigner, and Ole-Didrik Laerum. 1990. 'Effect of epidermal growth factor on glioma cell growth, migration, and invasion in vitro', *Cancer research*, 50: 6039-44.

Lutterbach, Bart, Qinwen Zeng, Lenora J Davis, Harold Hatch, Gaozhen Hang, Nancy E Kohl, Jackson B Gibbs, and Bo-Sheng Pan. 2007. 'Lung cancer cell lines harboring MET gene amplification are dependent on Met for growth and survival', *Cancer research*, 67: 2081-88.

Lv, Donglai, Zongtao Hu, Lin Lu, Husheng Lu, and Xiuli Xu. 2017. 'Three-dimensional cell culture: A powerful tool in tumor research and drug discovery', *Oncology letters*, 14: 6999-7010.

Lyon, Malcolm, Jon A Deakin, Kensaku Mizuno, Toshikazu Nakamura, and John T Gallagher. 1994. 'Interaction of hepatocyte growth factor with heparan sulfate. Elucidation of the major heparan sulfate structural determinants', *Journal of Biological Chemistry*, 269: 11216-23.

Ma, Patrick C, Simha Jagadeesh, Ramasamy Jagadeeswaran, Edward A Fox, James Christensen, Gautam Maulik, Katsuhiko Naoki, Erik Schaefer, Alan Lader, and William Richards. 2004. 'c-MET expression/activation, functions, and mutations in non-small cell lung cancer', *Cancer research*, 64: 430-31.

Ma, Patrick C, Ramasamy Jagadeeswaran, Simha Jagadeesh, Maria S Tretiakova, Vidya Nallasura, Edward A Fox, Mark Hansen, Erik Schaefer, Katsuhiko Naoki, and Alan Lader. 2005. 'Functional expression and mutations of c-Met and its therapeutic inhibition with SU11274 and small interfering RNA in non–small cell lung cancer', *Cancer research*, 65: 1479-88.

Ma, Patrick C, Takashi Kijima, Gautam Maulik, Edward A Fox, Martin Sattler, James D Griffin, Bruce E Johnson, and Ravi Salgia. 2003. 'c-MET mutational analysis in small cell lung cancer', *Cancer research*, 63: 6272-81.

Ma, Patrick C, Gautam Maulik, James Christensen, and Ravi Salgia. 2003. 'c-Met: structure, functions and potential for therapeutic inhibition', *Cancer and Metastasis Reviews*, 22: 309-25.

Ma, PC, MS Tretiakova, V Nallasura, R Jagadeeswaran, AN Husain, and R Salgia. 2007. 'Downstream signalling and specific inhibition of c-MET/HGF pathway in small cell lung cancer: implications for tumour invasion', *British journal of cancer*, 97: 368-77.

Malik, Gunjan, Lynn M Knowles, Rajiv Dhir, Shuping Xu, Shuting Yang, Erkki Ruoslahti, and Jan Pilch. 2010. 'Plasma fibronectin promotes lung metastasis by contributions to fibrin clots and tumor cell invasion', *Cancer research*, 70: 4327-34.

Mansbridge, JN, WA Ausserer, MA Knapp, and RM Sutherland. 1994. 'Adaptation of EGF receptor signal transduction to three-dimensional culture conditions: Changes in surface receptor expression and protein tyrosine phosphorylation', *Journal of cellular physiology*, 161: 374-82.

Mansbridge, JN, R Knüchel, MA Knapp, and RM Sutherland. 1992. 'Modulation of EGF signal transduction by cell-cell contact and microenvironments: involvement of tyrosine phosphatases', *J Cell Physiol*, 151: 433-42.

Maroun, Christiane R, Monica A Naujokas, Marina Holgado-Madruga, Albert J Wong, and Morag Park. 2000. 'The tyrosine phosphatase SHP-2 is required for sustained activation of extracellular signal-regulated kinase and epithelial morphogenesis downstream from the met receptor tyrosine kinase', *Molecular and cellular biology*, 20: 8513-25.

Martin-Urdiroz, Magdalena, Michael J Deeks, Connor G Horton, Helen R Dawe, and Isabelle Jourdain. 2016. 'The exocyst complex in health and disease', *Frontiers in cell and developmental biology*, 4: 24.

Martin, Katherine J, Denis R Patrick, Mina J Bissell, and Marcia V Fournier. 2008. 'Prognostic breast cancer signature identified from 3D culture model accurately predicts clinical outcome across independent datasets', *PLoS One*, 3: e2994.

Mason, Robert J. 2002. 'Hepatocyte growth factor: the key to alveolar septation?', *American journal of respiratory cell and molecular biology*, 26: 517-20.
Masters, Gregory A, Sarah Temin, Christopher G Azzoli, Giuseppe Giaccone, Sherman Baker Jr, Julie R Brahmer, Peter M Ellis, Ajeet Gajra, Nancy Rackear, and Joan H Schiller. 2015. 'Systemic therapy for stage IV non–small-cell lung cancer: American Society of Clinical Oncology clinical practice guideline update', *Journal of clinical oncology*, 33: 3488.
Masuya, D, C Huang, D Liu, T Nakashima, K Kameyama, R Haba, M Ueno, and H Yokomise. 2004. 'The tumour–stromal interaction between intratumoral c-Met and stromal hepatocyte growth factor associated with tumour growth and prognosis in non-small-cell lung cancer patients', *British journal of cancer*, 90: 1555-62.
Matejka, Nicole, and Judith Reindl. 2019. 'Perspectives of cellular communication through tunneling nanotubes in cancer cells and the connection to radiation effects', *Radiation Oncology*, 14: 1-11.
Matsumoto, Kentaro, Barry L Ziober, Chung-Chen Yao, and Randall H Kramer. 1995. 'Growth factor regulation of integrin-mediated cell motility', *Cancer and Metastasis Reviews*, 14: 205-17.
Matsumoto, Kunio, and Toshikazu Nakamura. 1997. "HGF: its organotrophic role and therapeutic potential." In *Ciba Symp*, 198-211.
Matsumoto, Kunio, Masataka Umitsu, Dinuka M De Silva, Arpita Roy, and Donald P Bottaro. 2017. 'Hepatocyte growth factor/MET in cancer progression and biomarker discovery', *Cancer science*, 108: 296-307.
Mattes, Joerg, Mark Hulett, Wei Xie, Simon Hogan, Marc E Rothenberg, Paul Foster, and Christopher Parish. 2003. 'Immunotherapy of cytotoxic T cell–resistant tumors by T helper 2 cells: an eotaxin and STAT6-dependent process', *The Journal of experimental medicine*, 197: 387-93.
Matthews, Helen K, Cosetta Bertoli, and Robertus AM de Bruin. 2022. 'Cell cycle control in cancer', *Nature reviews Molecular cell biology*, 23: 74-88.
Matthews, Vance B, TL Allen, S Risis, MHS Chan, Darren C Henstridge, N Watson, LA Zaffino, Jenny R Babb, J Boon, and Peter J Meikle. 2010. 'Interleukin-6-deficient mice develop hepatic inflammation and systemic insulin resistance', *Diabetologia*, 53: 2431-41.
Maulik, G, P Madhiwala, S Brooks, PC Ma, T Kijima, EV Tibaldi, E Schaefer, K Parmar, and Ravi Salgia. 2002. 'Activated c-Met signals through PI3K with dramatic effects on cytoskeletal functions in small cell lung cancer', *Journal of cellular and molecular medicine*, 6: 539-53.
Maulik, Gautam, Amol Shrikhande, Takashi Kijima, Patrick C Ma, Paul T Morrison, and Ravi Salgia. 2002. 'Role of the hepatocyte growth factor receptor, c-Met, in oncogenesis and potential for therapeutic inhibition', *Cytokine & growth factor reviews*, 13: 41-59.
McNamee, Helen P, Donald E Ingber, and Martin Alexander Schwartz. 1993. 'Adhesion to fibronectin stimulates inositol lipid synthesis and enhances PDGF-induced inositol lipid breakdown', *The Journal of cell biology*, 121: 673-78.
Meert, Anne-Pascale, Marianne Paesmans, Benoît Martin, Philippe Delmotte, Thierry Berghmans, Jean-Marc Verdebout, Jean-Jacques Lafitte, Céline Mascaux, and Jean-Paul Sculier. 2002. 'The role of microvessel density on the survival of patients with lung cancer: a systematic review of the literature with meta-analysis', *British journal of cancer*, 87: 694-701.
Mehrabi, Masomeh, Kamran Mansouri, Bijan Soleymani, Zohreh Hoseinkhani, Mohsen Shahlaie, and Reza Khodarahmi. 2017. 'Development of a human epidermal growth factor derivative with EGFR-blocking and depleted biological activities: A comparative in vitro study using EGFR-positive breast cancer cells', *International journal of biological macromolecules*, 103: 275-85.
Mendoza, Michelle C, E Emrah Er, Wenjuan Zhang, Bryan A Ballif, Hunter L Elliott, Gaudenz Danuser, and John Blenis. 2011. 'ERK-MAPK drives lamellipodia protrusion by activating the WAVE2 regulatory complex', *Molecular cell*, 41: 661-71.
Miller, Jeffrey, Scott E Fraser, and David McClay. 1995. 'Dynamics of thin filopodia during sea urchin gastrulation', *Development*, 121: 2501-11.

Milovanovic, Marija, Vladislav Volarevic, Gordana Radosavljevic, Ivan Jovanovic, Nada Pejnovic, Nebojsa Arsenijevic, and Miodrag L Lukic. 2012. 'IL-33/ST2 axis in inflammation and immunopathology', *Immunologic research*, 52: 89-99.

Minaisah, Rose-Marie, Susan Cox, and Derek T Warren. 2016. 'The use of polyacrylamide hydrogels to study the effects of matrix stiffness on nuclear envelope properties.' in, *The Nuclear Envelope* (Springer).

Mitra, AK, K Sawada, P Tiwari, K Mui, K Gwin, and E Lengyel. 2011. 'Ligand-independent activation of c-Met by fibronectin and α5β1-integrin regulates ovarian cancer invasion and metastasis', *Oncogene*, 30: 1566-76.

Mitra, Satyajit K, and David D Schlaepfer. 2006. 'Integrin-regulated FAK–Src signaling in normal and cancer cells', *Current opinion in cell biology*, 18: 516-23.

Miyamoto, Shingo, Steven K Akiyama, and Kenneth M Yamada. 1995. 'Synergistic roles for receptor occupancy and aggregation in integrin transmembrane function', *Science*, 267: 883-85.

Miyazawa, Ayako, Satoru Ito, Shuichi Asano, Ichidai Tanaka, Mitsuo Sato, Masashi Kondo, and Yoshinori Hasegawa. 2018. 'Regulation of PD-L1 expression by matrix stiffness in lung cancer cells', *Biochemical and biophysical research communications*, 495: 2344-49.

Modi, Prashant Kumar, Narayana Komaravelli, Neha Singh, and Pushkar Sharma. 2012. 'Interplay between MEK-ERK signaling, cyclin D1, and cyclin-dependent kinase 5 regulates cell cycle reentry and apoptosis of neurons', *Molecular biology of the cell*, 23: 3722-30.

Moghul, Alan, Lin Lin, Ari Beedle, AMAL Kanbour-Shakir, Marie C DeFrances, Youhua Liu, and Reza Zarnegar. 1994. 'Modulation of c-MET proto-oncogene (HGF receptor) mRNA abundance by cytokines and hormones: evidence for rapid decay of the 8 kb c-MET transcript', *Oncogene*, 9: 2045-52.

Molin, Daniel. 2004. 'Bystander cells and prognosis in Hodgkin lymphoma', *Upsala journal of medical sciences*, 109: 179-228.

Moon, YW, G Rao, JJ Kim, HS Shim, KS Park, SS An, B Kim, PS Steeg, S Sarfaraz, and L Changwoo Lee. 2015. 'LAMC2 enhances the metastatic potential of lung adenocarcinoma', *Cell Death & Differentiation*, 22: 1341-52.

Moser, R, J Fehr, and PL Bruijnzeel. 1992. 'IL-4 controls the selective endothelium-driven transmigration of eosinophils from allergic individuals', *The Journal of Immunology*, 149: 1432-38.

Moskalenko, Serge, Dale O Henry, Carine Rosse, Gladys Mirey, Jacques H Camonis, and Michael A White. 2002. 'The exocyst is a Ral effector complex', *Nature cell biology*, 4: 66-72.

Mukhopadhyay, Nishit K, David Gilchrist, Gavin J Gordon, Chang-Jie Chen, Raphael Bueno, Michael L Lu, Ravi Salgia, David J Sugarbaker, and Michael T Jaklitsch. 2004. 'Integrin dependent protein tyrosine phosphorylation is a key regulatory event in collagen IV mediated adhesion and proliferation of human lung tumor cell line, Calu-1', *The Annals of thoracic surgery*, 78: 450-57.

Müller-Tidow, Carsten, Sven Diederichs, Etmar Bulk, Thorsten Pohle, Björn Steffen, Joachim Schwäble, Sylvia Plewka, Michael Thomas, Ralf Metzger, and Paul M Schneider. 2005. 'Identification of metastasis-associated receptor tyrosine kinases in non–small cell lung cancer', *Cancer research*, 65: 1778-82.

Müller, Markus, Alessandro Morotti, and Carola Ponzetto. 2002. 'Activation of NF-κB is essential for hepatocyte growth factor-mediated proliferation and tubulogenesis', *Molecular and cellular biology*, 22: 1060-72.

Nagaraju, Supriya, Danh Truong, Ghassan Mouneimne, and Mehdi Nikkhah. 2018. 'Microfluidic tumor–vascular model to study breast cancer cell invasion and intravasation', *Advanced healthcare materials*, 7: 1701257.

Nakamura, T. 1994. "Hepatocyte growth factor as mitogen, motogen and morphogen, and its roles in organ regeneration." In *Princess Takamatsu Symposia*, 195-213.

Naldini, L, E Vigna, RP Narsimhan, G Gaudino, R Zarnegar, GK Michalopoulos, and PM Comoglio. 1991. 'Hepatocyte growth factor (HGF) stimulates the tyrosine kinase activity of the receptor encoded by the proto-oncogene c-MET', *Oncogene*, 6: 501-04.

Naldini, Luigi, Elisa Vigna, Alberto Bardelli, Antonia Follenzi, Francesco Galimi, and Paolo M Comoglio. 1995. 'Biological activation of pro-HGF (hepatocyte growth factor) by urokinase is controlled by a stoichiometric reaction', *Journal of Biological Chemistry*, 270: 603-11.

Naugler, Willscott E, and Michael Karin. 2008. 'The wolf in sheep's clothing: the role of interleukin-6 in immunity, inflammation and cancer', *Trends in molecular medicine*, 14: 109-19.

Navab, R, D Strumpf, C To, E Pasko, KS Kim, CJ Park, J Hai, J Liu, J Jonkman, and M Barczyk. 2016. 'Integrin α11β1 regulates cancer stromal stiffness and promotes tumorigenicity and metastasis in non-small cell lung cancer', *Oncogene*, 35: 1899-908.

Network, Cancer Genome Atlas Research. 2014. 'Comprehensive molecular profiling of lung adenocarcinoma', *Nature*, 511: 543.

Nielsen, Maja, Lise Christensen, and Reidar Albrechtsen. 1983. 'The basement membrane component laminin in breast carcinomas and axillary lymph node metastases', *Acta Pathologica Microbiologica Scandinavica Series A: Pathology*, 91: 257-64.

Nikolic, Damjan S, Martin Lehmann, Richard Felts, Eduardo Garcia, Fabien P Blanchet, Sriram Subramaniam, and Vincent Piguet. 2011. 'HIV-1 activates Cdc42 and induces membrane extensions in immature dendritic cells to facilitate cell-to-cell virus propagation', *Blood, The Journal of the American Society of Hematology*, 118: 4841-52.

Nishimoto, Norihiro, Yuzuru Kanakura, Katsuyuki Aozasa, Takeshi Johkoh, Minoru Nakamura, Shuji Nakano, Nobuaki Nakano, Yasuo Ikeda, Takeshi Sasaki, and Kiyoshi Nishioka. 2005. 'Humanized anti–interleukin-6 receptor antibody treatment of multicentric Castleman disease', *Blood*, 106: 2627-32.

Noriega-Guerra, Heydi, and Vanessa Freitas. 2018. 'Extracellular Matrix Influencing HGF/c-MET Signaling Pathway: Impact on Cancer Progression', *International journal of molecular sciences*, 19: 3300.

Normanno, Nicola, Antonella De Luca, Caterina Bianco, Luigi Strizzi, Mario Mancino, Monica R Maiello, Adele Carotenuto, Gianfranco De Feo, Francesco Caponigro, and David S Salomon. 2006. 'Epidermal growth factor receptor (EGFR) signaling in cancer', *Gene*, 366: 2-16.

O'Flaherty, SM, K Sutummaporn, WL Häggtoft, AP Worrall, M Rizzo, V Braniste, P Höglund, N Kadri, and BJ Chambers. 2017. 'TLR-Stimulated Eosinophils Mediate Recruitment and Activation of NK Cells In Vivo', *Scandinavian Journal of Immunology*, 85: 417-24.

Obara, Masanobu, Mohinder S Kang, and Kenneth M Yamada. 1988. 'Site-directed mutagenesis of the cell-binding domain of human fibronectin: separable, synergistic sites mediate adhesive function', *Cell*, 53: 649-57.

Oda, Kanae, Yukiko Matsuoka, Akira Funahashi, and Hiroaki Kitano. 2005. 'A comprehensive pathway map of epidermal growth factor receptor signaling', *Molecular systems biology*, 1: 2005.0010.

Ogata, Riko. 1998. 'Type IV collagen and laminin enhance the motility, adhesion, and proliferation of hepatoma cells', *The Kurume medical journal*, 45: 11-20.

Ohmichi, Hidenori, Uichi Koshimizu, Kunio Matsumoto, and Toshikazu Nakamura. 1998. 'Hepatocyte growth factor (HGF) acts as a mesenchyme-derived morphogenic factor during fetal lung development', *Development*, 125: 1315-24.

Ohta, Yasutaka, Nobuchika Suzuki, Shun Nakamura, John H Hartwig, and Thomas P Stossel. 1999. 'The small GTPase RalA targets filamin to induce filopodia', *Proceedings of the National Academy of Sciences*, 96: 2122-28.

Ohtsubo, Motoaki, Anne M Theodoras, Jill Schumacher, James M Roberts, and Michele Pagano. 1995. 'Human cyclin E, a nuclear protein essential for the G1-to-S phase transition', *Molecular and cellular biology*, 15: 2612-24.

Omsland, Maria, Vibeke Andresen, Stein-Erik Gullaksen, Pilar Ayuda-Durán, Mihaela Popa, Randi Hovland, Atle Brendehaug, Jorrit Enserink, Emmet McCormack, and Bjørn Tore Gjertsen. 2020. 'Tyrosine kinase inhibitors and interferon-α increase tunneling nanotube (TNT) formation and cell adhesion in chronic myeloid leukemia (CML) cell lines', *The FASEB Journal*, 34: 3773-91.

Omsland, Maria, Øystein Bruserud, Bjørn T Gjertsen, and Vibeke Andresen. 2017. 'Tunneling nanotube (TNT) formation is downregulated by cytarabine and NF-κB inhibition in acute myeloid leukemia (AML)', *Oncotarget*, 8: 7946.

Önfelt, Björn, Shlomo Nedvetzki, Richard KP Benninger, Marco A Purbhoo, Stefanie Sowinski, Alistair N Hume, Miguel C Seabra, Mark AA Neil, Paul MW French, and Daniel M Davis. 2006. 'Structurally distinct membrane nanotubes between human macrophages support long-distance vesicular traffic or surfing of bacteria', *The Journal of Immunology*, 177: 8476-83.

Onitsuka, Takamitsu, Hidetaka Uramoto, Kenji Ono, Mitsuhiro Takenoyama, Takeshi Hanagiri, Tsunehiro Oyama, Hiroto Izumi, Kimitoshi Kohno, and Kosei Yasumoto. 2010. 'Comprehensive molecular analyses of lung adenocarcinoma with regard to the epidermal growth factor receptor, K-ras, MET, and hepatocyte growth factor status', *Journal of Thoracic Oncology*, 5: 591-96.

Onozato, Ryoichi, Takayuki Kosaka, Hiroyuki Kuwano, Yoshitaka Sekido, Yasushi Yatabe, and Tetsuya Mitsudomi. 2009. 'Activation of MET by gene amplification or by splice mutations deleting the juxtamembrane domain in primary resected lung cancers', *Journal of Thoracic Oncology*, 4: 5-11.

Organ, Shawna Leslie, Ming-Sound Tsao, and Johann S de Bono. 2011. 'An overview of the c-MET signaling pathway', *Therapeutic advances in medical oncology*, 3: S7-S19.

Oridate, Nobuhiko, Reuben Lotan, and Dafna Lotan. 1996. 'Reconstituted basement membrane (matrigel®): a useful semisolid medium for growth of tumor cell colonies', *In Vitro Cellular & Developmental Biology-Animal*, 32: 192-93.

Ornitz, David M, and Nobuyuki Itoh. 2015. 'The fibroblast growth factor signaling pathway', *Wiley Interdisciplinary Reviews: Developmental Biology*, 4: 215-66.

Osswald, Matthias, Erik Jung, Felix Sahm, Gergely Solecki, Varun Venkataramani, Jonas Blaes, Sophie Weil, Heinz Horstmann, Benedikt Wiestler, and Mustafa Syed. 2015. 'Brain tumour cells interconnect to a functional and resistant network', *Nature*, 528: 93.

Osteikoetxea-Molnár, Anikó, Edina Szabó-Meleg, Eszter Angéla Tóth, Ádám Oszvald, Emese Izsépi, Mariann Kremlitzka, Beáta Biri, László Nyitray, Tamás Bozó, and Péter Németh. 2016. 'The growth determinants and transport properties of tunneling nanotube networks between B lymphocytes', *Cellular and Molecular Life Sciences*, 73: 4531-45.

Padavano, Julianna, Rebecca S Henkhaus, Hwudaurw Chen, Bethany A Skovan, Haiyan Cui, and Natalia A Ignatenko. 2015. 'Mutant K-RAS promotes invasion and metastasis in pancreatic cancer through GTPase signaling pathways', *Cancer Growth and Metastasis*, 8: CGM. S29407.

Pai, Rama, Toshikazu Nakamura, Woo S Moon, and Andrzej S Tarnawski. 2003. 'Prostaglandins promote colon cancer cell invasion; signaling by cross-talk between two distinct growth factor receptors', *The FASEB Journal*, 17: 1640-47.

Paik, Paul K, Alexander Drilon, Pang-Dian Fan, Helena Yu, Natasha Rekhtman, Michelle S Ginsberg, Laetitia Borsu, Nikolaus Schultz, Michael F Berger, and Charles M Rudin. 2015. 'Response to MET inhibitors in patients with stage IV lung adenocarcinomas harboring MET mutations causing exon 14 skipping', *Cancer discovery*, 5: 842-49.

Paluch, Ewa, Matthieu Piel, Jacques Prost, Michel Bornens, and Cécile Sykes. 2005. 'Cortical actomyosin breakage triggers shape oscillations in cells and cell fragments', *Biophysical journal*, 89: 724-33.

Panasiuk, Mirosława, Michał Rychłowski, Natalia Derewońko, and Krystyna Bieńkowska-Szewczyk. 2018. 'Tunneling nanotubes as a novel route of cell-to-cell spread of herpesviruses', *Journal of virology*, 92: e00090-18.

Pandit, Renu, Aaron Scholnik, Louis Wulfekuhler, and Nikolay Dimitrov. 2007. 'Non-small-cell lung cancer associated with excessive eosinophilia and secretion of interleukin-5 as a paraneoplastic syndrome', *American journal of hematology*, 82: 234-37.

Panganiban, Ronald Allan M, and Regina M Day. 2011. 'Hepatocyte growth factor in lung repair and pulmonary fibrosis', *Acta Pharmacologica Sinica*, 32: 12.

Pankova, Daniela, Yulong Chen, Masahiko Terajima, Mark J Schliekelman, Brandi N Baird, Monica Fahrenholtz, Li Sun, Bartley J Gill, Tegy J Vadakkan, and Min P Kim. 2016. 'Cancer-associated fibroblasts induce a collagen cross-link switch in tumor stroma', *Molecular Cancer Research*, 14: 287-95.

Pantazaka, Evangelia, Vasileios Vardas, Argyro Roumeliotou, Stavros Kakavogiannis, and Galatea Kallergi. 2021. 'Clinical relevance of mesenchymal-and stem-associated phenotypes in circulating tumor cells isolated from lung cancer patients', *Cancers*, 13: 2158.

Pao, William, and Juliann Chmielecki. 2010. 'Rational, biologically based treatment of EGFR-mutant non-small-cell lung cancer', *Nature Reviews Cancer*, 10: 760-74.

Papaccio, Federica, Carminia Della Corte, Giuseppe Viscardi, Raimondo Di Liello, Giovanna Esposito, Francesca Sparano, Fortunato Ciardiello, and Floriana Morgillo. 2018. 'HGF/MET and the Immune System: Relevance for Cancer Immunotherapy', *International journal of molecular sciences*, 19: 3595.

Park, Morag, Michael Dean, Colin S Cooper, Martin Schmidt, Stephen J O'Brien, Donald G Blair, and George F Vande Woude. 1986. 'Mechanism of met oncogene activation', *cell*, 45: 895-904.

Park, Morag, Michael Dean, Karen Kaul, Michael J Braun, Matthew A Gonda, and G Vande Woude. 1987. 'Sequence of MET protooncogene cDNA has features characteristic of the tyrosine kinase family of growth-factor receptors', *Proceedings of the National Academy of Sciences*, 84: 6379-83.

Parr, Christian, G Davies, T Nakamura, Kei Matsumoto, Malcolm David Mason, and Wen Guo Jiang. 2001. 'The HGF/SF-induced phosphorylation of paxillin, matrix adhesion, and invasion of prostate cancer cells were suppressed by NK4, an HGF/SF variant', *Biochemical and biophysical research communications*, 285: 1330-37.

Pasquier, Jennifer, Ludovic Galas, Céline Boulangé-Lecomte, Damien Rioult, Florence Bultelle, Pierre Magal, Glenn Webb, and Frank Le Foll. 2012. 'Different modalities of intercellular membrane exchanges mediate cell-to-cell p-glycoprotein transfers in MCF-7 breast cancer cells', *Journal of Biological Chemistry*, 287: 7374-87.

Pasquier, Jennifer, Bella S Guerrouahen, Hamda Al Thawadi, Pegah Ghiabi, Mahtab Maleki, Nadine Abu-Kaoud, Arthur Jacob, Massoud Mirshahi, Ludovic Galas, and Shahin Rafii. 2013. 'Preferential transfer of mitochondria from endothelial to cancer cells through tunneling nanotubes modulates chemoresistance', *Journal of translational medicine*, 11: 94.

Patel, Purvi, and Emily I Chen. 2012. 'Cancer stem cells, tumor dormancy, and metastasis', *Frontiers in endocrinology*, 3: 125.

Paulsson, M. 1992. 'Basement membrane proteins: structure, assembly, and cellular interactions', *Critical reviews in biochemistry and molecular biology*, 27: 93-127.

Pelicano, Hélène, Rui-hua Xu, Min Du, Li Feng, Ryohei Sasaki, Jennifer S Carew, Yumin Hu, Latha Ramdas, Limei Hu, and Michael J Keating. 2006. 'Mitochondrial respiration defects in cancer cells cause activation of Akt survival pathway through a redox-mediated mechanism', *The Journal of cell biology*, 175: 913-23.

Pennacchietti, Selma, Paolo Michieli, Maria Galluzzo, Massimiliano Mazzone, Silvia Giordano, and Paolo M Comoglio. 2003. 'Hypoxia promotes invasive growth by transcriptional activation of the met protooncogene', *Cancer cell*, 3: 347-61.

Pérez-Alvarado, Gabriela C, Colleen Miles, James W Michelsen, Heather A Louis, Dennis R Winge, Mary C Beckerle, and Michael F Summers. 1994. 'Structure of the carboxy-terminal LIM domain from the cysteine rich protein CRP', *Nature structural biology*, 1: 388-98.

Petrek, Hannah, and Ai-Ming Yu. 2019. 'MicroRNAs in non-small cell lung cancer: Gene regulation, impact on cancer cellular processes, and therapeutic potential', *Pharmacology research & perspectives*, 7: e00528.

Pine, Sharon R, Leah E Mechanic, Lindsey Enewold, Anil K Chaturvedi, Hormuzd A Katki, Yun-Ling Zheng, Elise D Bowman, Eric A Engels, Neil E Caporaso, and Curtis C Harris. 2011. 'Increased levels of circulating interleukin 6, interleukin 8, C-reactive protein, and risk of lung cancer', *Journal of the National Cancer Institute*, 103: 1112-22.

Pinto, Giulia, Christel Brou, and Chiara Zurzolo. 2020. 'Tunneling nanotubes: the fuel of tumor progression?', *Trends in cancer*, 6: 874-88.

Polanska, Urszula M, and Akira Orimo. 2013. 'Carcinoma-associated fibroblasts: non-neoplastic tumour-promoting mesenchymal cells', *Journal of cellular physiology*, 228: 1651-57.

Pollack, Vincent A, Douglas M Savage, Deborah A Baker, Konstantinos E Tsaparikos, Donald E Sloan, James D Moyer, Elsa G Barbacci, Leslie R Pustilnik, Teresa A Smolarek, and John A Davis. 1999. 'Inhibition of epidermal growth factor receptor-associated tyrosine phosphorylation in human carcinomas with CP-358,774: dynamics of receptor inhibition in situ and antitumor effects in athymic mice', *Journal of Pharmacology and Experimental Therapeutics*, 291: 739-48.

Pollard, Thomas D, and Gary G Borisy. 2003. 'Cellular motility driven by assembly and disassembly of actin filaments', *Cell*, 112: 453-65.

Ponzetto, Carola, Alberto Bardelli, Zhu Zhen, Flavio Maina, Paolo dalla Zonca, Silvia Giordano, Andrea Graziani, George Panayotou, and Paolo M Comoglio. 1994. 'A multifunctional docking site mediates signaling and transformation by the hepatocyte growth factor/scatter factor receptor family', *cell*, 77: 261-71.

Popper, Helmut H. 2016. 'Progression and metastasis of lung cancer', *Cancer and Metastasis Reviews*, 35: 75-91.

Porter, Lauren, Rose-Marie Minaisah, Sultan Ahmed, Seema Ali, Rosemary Norton, Qiuping Zhang, Elisa Ferraro, Chris Molenaar, Mark Holt, and Susan Cox. 2020. 'SUN1/2 are essential for RhoA/ROCK-regulated actomyosin activity in isolated vascular smooth muscle cells', *Cells*, 9: 132.

Pulze, Laura, Terenzio Congiu, Tiziana AL Brevini, Annalisa Grimaldi, Gianluca Tettamanti, Paola D'Antona, Nicolò Baranzini, Francesco Acquati, Federico Ferraro, and Magda de Eguileor. 2020. 'MCF7 spheroid development: New insight about spatio/temporal arrangements of TNTs, amyloid fibrils, cell connections, and cellular bridges', *International journal of molecular sciences*, 21: 5400.

Puri, Neelu, and Ravi Salgia. 2008. 'Synergism of EGFR and c-Met pathways, cross-talk and inhibition, in non-small cell lung cancer', *Journal of carcinogenesis*, 7.

Quesnelle, Kelly M, Amanda L Boehm, and Jennifer R Grandis. 2007. 'STAT-mediated EGFR signaling in cancer', *Journal of cellular biochemistry*, 102: 311-19.

Raftopoulou, Myrto, and Alan Hall. 2004. 'Cell migration: Rho GTPases lead the way', *Developmental biology*, 265: 23-32.

Rahman, Salman, Yatin Patel, Jacqueline Murray, Kirti V Patel, Rushika Sumathipala, Michael Sobel, and Errol S Wijelath. 2005. 'Novel hepatocyte growth factor (HGF) binding domains on fibronectin and vitronectin coordinate a distinct and amplified Met-integrin induced signalling pathway in endothelial cells', *BMC cell biology*, 6: 8.

Ramírez-Weber, Felipe-Andrés, and Thomas B Kornberg. 1999. 'Cytonemes: cellular processes that project to the principal signaling center in Drosophila imaginal discs', *Cell*, 97: 599-607.

Resnik, Nataša, Tim Prezelj, Giulia Maria Rita De Luca, Erik Manders, Roman Polishchuk, Peter Veranič, and Mateja Erdani Kreft. 2018. 'Helical organization of microtubules occurs in a minority of tunneling membrane nanotubes in normal and cancer urothelial cells', *Scientific reports*, 8: 1-8.

Reznik, Thomas E, Yingying Sang, Yongxian Ma, Roger Abounader, Eliot M Rosen, Shuli Xia, and John Laterra. 2008. 'Transcription-dependent epidermal growth factor receptor activation by hepatocyte growth factor', *Molecular Cancer Research*, 6: 139-50.

Ricart, Alejandro D, Anthony W Tolcher, Glenn Liu, Kyle Holen, Garry Schwartz, Mark Albertini, Geoffrey Weiss, Salim Yazji, Chee Ng, and George Wilding. 2008. 'Volociximab, a chimeric monoclonal antibody that specifically binds α5β1 integrin: a phase I, pharmacokinetic, and biological correlative study', *Clinical cancer research*, 14: 7924-29.

Riely, Gregory J, Jenifer Marks, and William Pao. 2009. 'KRAS mutations in non–small cell lung cancer', *Proceedings of the American Thoracic Society*, 6: 201-05.

Rosenberg, Helene F, Kimberly D Dyer, and Paul S Foster. 2013. 'Eosinophils: changing perspectives in health and disease', *Nature Reviews Immunology*, 13: 9-22.

Rosenwasser, Lanny J, Nives Zimmermann, Gurjit Khurana Hershey, Paul S Foster, and Marc E Rothenberg. 2003. 'Chemokines in asthma: cooperative interaction between chemokines and IL-13', *Journal of allergy and clinical immunology*, 111: 227-42.

Rössig, Lothar, Amir S Jadidi, Carmen Urbich, Cornel Badorff, Andreas M Zeiher, and Stefanie Dimmeler. 2001. 'Akt-dependent phosphorylation of p21Cip1 regulates PCNA binding and proliferation of endothelial cells', *Molecular and cellular biology*, 21: 5644-57.

Roth, Wilfried, Christine Wild-Bode, Michael Platten, Cornelia Grimmel, Hovsep S Melkonyan, Johannes Dichgans, and Michael Weller. 2000. 'Secreted Frizzled-related proteins inhibit motility and promote growth of human malignant glioma cells', *Oncogene*, 19: 4210-20.

Rotow, Julia, and Trever G Bivona. 2017. 'Understanding and targeting resistance mechanisms in NSCLC', *Nature Reviews Cancer*, 17: 637-58.

Rousalova, Ilona, Sulagna Banerjee, Veena Sangwan, Kristen Evenson, Joel A McCauley, Robert Kratzke, Selwyn M Vickers, Ashok Saluja, and Jonathan D'Cunha. 2013. 'Minnelide: a novel therapeutic that promotes apoptosis in non-small cell lung carcinoma in vivo', *PLoS One*, 8: e77411.

Ruocco, Sandrine, Aude Lallemand, Jean Marie Tournier, and Dominique Gaillard. 1996. 'Expression and localization of epidermal growth factor, transforming growth factor-α, and localization of their common receptor in fetal human lung development', *Pediatric research*, 39: 448-55.

Rustom, Amin. 2016. 'The missing link: does tunnelling nanotube-based supercellularity provide a new understanding of chronic and lifestyle diseases?', *Open biology*, 6: 160057.

Rustom, Amin, Rainer Saffrich, Ivanka Markovic, Paul Walther, and Hans-Hermann Gerdes. 2004. 'Nanotubular highways for intercellular organelle transport', *Science*, 303: 1007-10.

Sáenz-de-Santa-María, Inés, Cristóbal Bernardo-Castiñeira, Eduardo Enciso, Inmaculada García-Moreno, Jose Luis Chiara, Carlos Suarez, and María-Dolores Chiara. 2017. 'Control of long-distance cell-to-cell communication and autophagosome transfer in squamous cell carcinoma via tunneling nanotubes', *Oncotarget*, 8: 20939.

Sainz de Aja, J, AFM Dost, and CF Kim. 2021. 'Alveolar progenitor cells and the origin of lung cancer', *Journal of internal medicine*, 289: 629-35.

Sakamaki, Yasushi, Kunio Matsumoto, Shinya Mizuno, Shinichiro Miyoshi, Hikaru Matsuda, and Toshikazu Nakamura. 2002. 'Hepatocyte growth factor stimulates proliferation of respiratory epithelial cells during postpneumonectomy compensatory lung growth in mice', *American journal of respiratory cell and molecular biology*, 26: 525-33.

Sakaue-Sawano, Asako, Hiroshi Kurokawa, Toshifumi Morimura, Aki Hanyu, Hiroshi Hama, Hatsuki Osawa, Saori Kashiwagi, Kiyoko Fukami, Takaki Miyata, and Hiroyuki Miyoshi. 2008. 'Visualizing spatiotemporal dynamics of multicellular cell-cycle progression', *Cell*, 132: 487-98.

Sakkal, Samy, Sarah Miller, Vasso Apostolopoulos, and Kulmira Nurgali. 2016. 'Eosinophils in cancer: favourable or unfavourable?', *Current medicinal chemistry*, 23: 650-66.

Samoszuk, Michael. 1997. 'Eosinophils and human cancer', *Histology and histopathology*.

Sanchez-Salcedo, Pablo, Juan Berto, Juan P de-Torres, Arantzazu Campo, Ana B Alcaide, Gorka Bastarrika, Jesús C Pueyo, Alberto Villanueva, José I Echeveste, and Maria D Lozano. 2015. 'Lung cancer screening: fourteen year experience of the Pamplona early detection program (P-IELCAP)', *Archivos de Bronconeumología (English Edition)*, 51: 169-76.

Santini, Maria Teresa, Gabriella Rainaldi, and Pietro Luigi Indovina. 2000. 'Apoptosis, cell adhesion and the extracellular matrix in the three-dimensional growth of multicellular tumor spheroids', *Critical reviews in oncology/hematology*, 36: 75-87.

Sarma, Vidya, FW Wolf, RM Marks, TB Shows, and VM Dixit. 1992. 'Cloning of a novel tumor necrosis factor-alpha-inducible primary response gene that is differentially expressed in development and capillary tube-like formation in vitro', *The Journal of Immunology*, 148: 3302-12.

Sartori-Rupp, Anna, Diégo Cordero Cervantes, Anna Pepe, Karine Gousset, Elise Delage, Simon Corroyer-Dulmont, Christine Schmitt, Jacomina Krijnse-Locker, and Chiara Zurzolo. 2019. 'Correlative cryo-electron microscopy reveals the structure of TNTs in neuronal cells', *Nature communications*, 10: 1-16.

Sastry, Sarita K, Margot Lakonishok, Stanley Wu, Tho Q Truong, Anna Huttenlocher, Christopher E Turner, and Alan F Horwitz. 1999. 'Quantitative changes in integrin and focal adhesion signaling regulate myoblast cell cycle withdrawal', *The Journal of cell biology*, 144: 1295-309.

Sattler, Martin, Rifat Hasina, Mamatha M Reddy, Tara Gangadhar, and Ravi Salgia. 2011. 'The role of the c-Met pathway in lung cancer and the potential for targeted therapy', *Therapeutic advances in medical oncology*, 3: 171-84.

Scagliotti, Giorgio Vittorio, Joachim Von Pawel, Silvia Novello, Rodryg Ramlau, Adolfo Favaretto, Fabrice Barlesi, Wallace Akerley, Sergey Orlov, Armando Santoro, and David Spigel. 2015. 'Phase III multinational, randomized, double-blind, placebo-controlled study of tivantinib (ARQ 197) plus erlotinib versus erlotinib alone in previously treated patients with locally advanced or metastatic nonsquamous non-small-cell lung cancer'.

Schaller, Michael D, Carol A Otey, Jeffrey D Hildebrand, and J Thomas Parsons. 1995. 'Focal adhesion kinase and paxillin bind to peptides mimicking beta integrin cytoplasmic domains', *The Journal of cell biology*, 130: 1181-87.

Scheiblich, Hannah, Cira Dansokho, Dilek Mercan, Susanne V Schmidt, Luc Bousset, Lena Wischhof, Frederik Eikens, Alexandru Odainic, Jasper Spitzer, and Angelika Griep. 2021. 'Microglia jointly degrade fibrillar alpha-synuclein cargo by distribution through tunneling nanotubes', *Cell*, 184: 5089-106. e21.

Scheller, Jürgen, Athena Chalaris, Dirk Schmidt-Arras, and Stefan Rose-John. 2011. 'The pro-and anti-inflammatory properties of the cytokine interleukin-6', *Biochimica et Biophysica Acta (BBA)-Molecular Cell Research*, 1813: 878-88.

Schiller, Christian, Kalliope N Diakopoulos, Ina Rohwedder, Elisabeth Kremmer, Christine von Toerne, Marius Ueffing, Ulrich H Weidle, Hiroshi Ohno, and Elisabeth H Weiss. 2013. 'LST1 promotes the assembly of a molecular machinery responsible for tunneling nanotube formation', *Journal of cell science*, 126: 767-77.

Schiller, Joan H, David Harrington, Chandra P Belani, Corey Langer, Alan Sandler, James Krook, Junming Zhu, and David H Johnson. 2002. 'Comparison of four chemotherapy regimens for advanced non–small-cell lung cancer', *New England journal of medicine*, 346: 92-98.

Schliekelman, Mark J, Ayumu Taguchi, Jun Zhu, Xudong Dai, Jaime Rodriguez, Muge Celiktas, Qing Zhang, Alice Chin, Chee-Hong Wong, and Hong Wang. 2015. 'Molecular portraits of epithelial, mesenchymal, and hybrid States in lung adenocarcinoma and their relevance to survival', *Cancer research*, 75: 1789-800.

Schliwa, M, U Euteneuer, R Gräf, and M Ueda. 1999. "Centrosomes, microtubules and cell migration." In *Biochemical Society symposium*, 223-31.

Schmeichel, Karen L, and Mary C Beckerle. 1994. 'The LIM domain is a modular protein-binding interface', *Cell*, 79: 211-19.

Schultz, Chad, Nancy Lemke, Shugang Ge, William A Golembieski, and Sandra A Rempel. 2002. 'Secreted protein acidic and rich in cysteine promotes glioma invasion and delays tumor growth in vivo', *Cancer research*, 62: 6270-77.

Seigel, R, D Naishadham, and A Jemal. 2012. 'Cancer statistics', *Ca Cancer J Clin*, 62: 10-29.

Sempere, Lorenzo F, Jason R Gunn, and Murray Korc. 2011. 'A novel 3-dimensional culture system uncovers growth stimulatory actions by TGFβ in pancreatic cancer cells', *Cancer biology & therapy*, 12: 198-207.

Serban, Monica A, and Glenn D Prestwich. 2008. 'Modular extracellular matrices: solutions for the puzzle', *Methods*, 45: 93-98.

Shafirstein, Gal, Athar Battoo, Kassem Harris, Heinz Baumann, Sandra O Gollnick, Joerg Lindenmann, and Chukwumere E Nwogu. 2016. 'Photodynamic therapy of non–small cell lung cancer. Narrative review and future directions', *Annals of the American Thoracic Society*, 13: 265-75.

Shain, Kenneth H, Danielle N Yarde, Mark B Meads, Mei Huang, Richard Jove, Lori A Hazlehurst, and William S Dalton. 2009. 'β1 integrin adhesion enhances IL-6–mediated STAT3 signaling in myeloma cells: implications for microenvironment influence on tumor survival and proliferation', *Cancer research*, 69: 1009-15.

Shepherd, Frances A, José Rodrigues Pereira, Tudor Ciuleanu, Eng Huat Tan, Vera Hirsh, Sumitra Thongprasert, Daniel Campos, Savitree Maoleekoonpiroj, Michael Smylie, and Renato Martins. 2005. 'Erlotinib in previously treated non–small-cell lung cancer', *New England journal of medicine*, 353: 123-32.

Sher, ALAN, ROBERT L Coffman, SARA Hieny, and ALLEN W Cheever. 1990. 'Ablation of eosinophil and IgE responses with anti-IL-5 or anti-IL-4 antibodies fails to affect immunity against Schistosoma mansoni in the mouse', *The Journal of Immunology*, 145: 3911-16.

Sherr, Charles J. 1994. 'G1 phase progression: cycling on cue', *Cell*, 79: 551-55.

Shestov, Alexander A, Seung-Cheol Lee, Kavindra Nath, Lili Guo, David S Nelson, Jeffrey C Roman, Dennis B Leeper, Mariusz A Wasik, Ian A Blair, and Jerry D Glickson. 2016. '13C MRS and LC–MS flux analysis of tumor intermediary metabolism', *Frontiers in Oncology*, 6: 135.

Shibue, Tsukasa, and Robert A Weinberg. 2009. 'Integrin β1-focal adhesion kinase signaling directs the proliferation of metastatic cancer cells disseminated in the lungs', *Proceedings of the National Academy of Sciences*, 106: 10290-95.

Shigematsu, Hisayuki, and Adi F Gazdar. 2006. 'Somatic mutations of epidermal growth factor receptor signaling pathway in lung cancers', *International Journal of Cancer*, 118: 257-62.

Shintani, Yasushi, Masato Maeda, Nina Chaika, Keith R Johnson, and Margaret J Wheelock. 2008. 'Collagen I promotes epithelial-to-mesenchymal transition in lung cancer cells via transforming growth factor–β signaling', *American journal of respiratory cell and molecular biology*, 38: 95-104.

Shukla, VC, N Higuita-Castro, P Nana-Sinkam, and SN Ghadiali. 2016. 'Substrate stiffness modulates lung cancer cell migration but not epithelial to mesenchymal transition', *Journal of Biomedical Materials Research Part A*, 104: 1182-93.

Silva, Estela Maria, Vânia Sammartino Mariano, Paula Roberta Aguiar Pastrez, Miguel Cordoba Pinto, Antonio Gil Castro, Kari Juhani Syrjanen, and Adhemar Longatto-Filho. 2017. 'High systemic IL-6 is associated with worse prognosis in patients with non-small cell lung cancer', *PloS one*, 12: e0181125.

Simson, Ljubov, Julia I Ellyard, Lindsay A Dent, Klaus I Matthaei, Marc E Rothenberg, Paul S Foster, Mark J Smyth, and Christopher R Parish. 2007. 'Regulation of carcinogenesis by IL-5 and CCL11: a potential role for eosinophils in tumor immune surveillance', *The Journal of Immunology*, 178: 4222-29.

Sionov, Ronit Vogt, Zvi G Fridlender, and Zvi Granot. 2015. 'The multifaceted roles neutrophils play in the tumor microenvironment', *Cancer Microenvironment*, 8: 125-58.

Skardal, Aleksander, David Mack, Anthony Atala, and Shay Soker. 2013. 'Substrate elasticity controls cell proliferation, surface marker expression and motile phenotype in amniotic fluid-derived stem cells', *Journal of the mechanical behavior of biomedical materials*, 17: 307-16.

Skurk, Thomas, Catherine Alberti-Huber, Christian Herder, and Hans Hauner. 2007. 'Relationship between adipocyte size and adipokine expression and secretion', *The Journal of Clinical Endocrinology & Metabolism*, 92: 1023-33.

Small, J Victor, Klemens Rottner, Irina Kaverina, and Kurt I Anderson. 1998. 'Assembling an actin cytoskeleton for cell attachment and movement', *Biochimica Et Biophysica Acta (BBA)-Molecular Cell Research*, 1404: 271-81.

Smith, Ian F, Jianwei Shuai, and Ian Parker. 2011. 'Active generation and propagation of Ca2+ signals within tunneling membrane nanotubes', *Biophysical journal*, 100: L37-L39.

Snead, ML, W Luo, P Oliver, M Nakamura, G Don-Wheeler, C Bessem, GI Bell, LB Rall, and HC Slavkin. 1989. 'Localization of epidermal growth factor precursor in tooth and lung during embryonic mouse development', *Developmental biology*, 134: 420-29.

Song, Lanxi, Bhupendra Rawal, Jeffrey A Nemeth, and Eric B Haura. 2011. 'JAK1 activates STAT3 activity in non-small–cell lung cancer cells and IL-6 neutralizing antibodies can suppress JAK1-STAT3 signaling', *Molecular cancer therapeutics*, 10: 481-94.

Song, Lanxi, James Turkson, James G Karras, Richard Jove, and Eric B Haura. 2003. 'Activation of Stat3 by receptor tyrosine kinases and cytokines regulates survival in human non-small cell carcinoma cells', *Oncogene*, 22: 4150-65.

Sonnenberg, Eva, Dirk Meyer, K Michael Weidner, and Carmen Birchmeier. 1993. 'Scatter factor/hepatocyte growth factor and its receptor, the c-met tyrosine kinase, can mediate a signal exchange between mesenchyme and epithelia during mouse development', *The Journal of cell biology*, 123: 223-35.

Sorkin, Alexander, and Mark Von Zastrow. 2009. 'Endocytosis and signalling: intertwining molecular networks', *Nature reviews Molecular cell biology*, 10: 609-22.

Souter, Lesley H, Joseph D Andrews, Guihua Zhang, Amy C Cook, Carl O Postenka, Waleed Al-Katib, Hon S Leong, David I Rodenhiser, Ann F Chambers, and Alan B Tuck. 2010. 'Human 21T breast epithelial cell lines mimic breast cancer progression in vivo and in vitro and show stage-specific gene expression patterns', *Laboratory investigation*, 90: 1247-58.

Sowinski, Stefanie, Clare Jolly, Otto Berninghausen, Marco A Purbhoo, Anne Chauveau, Karsten Köhler, Stephane Oddos, Philipp Eissmann, Frances M Brodsky, and Colin Hopkins. 2008. 'Membrane nanotubes physically connect T cells over long distances presenting a novel route for HIV-1 transmission', *Nature cell biology*, 10: 211-19.

Spees, Jeffrey L, Scott D Olson, Mandolin J Whitney, and Darwin J Prockop. 2006. 'Mitochondrial transfer between cells can rescue aerobic respiration', *Proceedings of the National Academy of Sciences*, 103: 1283-88.

Spigel, David R, Martin J Edelman, Kenneth J O'Byrne, Luis Paz-Ares, Simonetta Mocci, David S Shames, Dustin Smith, Wei Yu, Viginia E Paton, and Tony Mok. 2017. 'Results from the phase III randomized trial of onartuzumab plus erlotinib versus erlotinib in previously treated stage IIIB or IV non–small-cell lung cancer: METLung', *Journal of Clinical Oncology*, 35: 412-20.

Spigel, David R, Martin J Edelman, Kenneth O'Byrne, Luis Gonzaga Paz Ares, Simonetta Mocci, David S Shames, Dustin Smith, Wei Yu, Virginia E Paton, and Tony Mok. 2017. 'Results from the phase III randomized trial of onartuzumab plus erlotinib versus erlotinib in previously treated stage IIIB or IV non-small-cell lung cancer: METLung'.

Sridhar, Srikala S, Lesley Seymour, and Frances A Shepherd. 2003. 'Inhibitors of epidermal-growth-factor receptors: a review of clinical research with a focus on non-small-cell lung cancer', *The lancet oncology*, 4: 397-406.

Stewart, Martin P, Jonne Helenius, Yusuke Toyoda, Subramanian P Ramanathan, Daniel J Muller, and Anthony A Hyman. 2011. 'Hydrostatic pressure and the actomyosin cortex drive mitotic cell rounding', *Nature*, 469: 226-30.

Stoker, MGP, and H Rubin. 1967. 'Density dependent inhibition of cell growth in culture', *Nature*, 215: 171-72.
Stoker, Michael, Ermanno Gherardi, Marion Perryman, and Julia Gray. 1987. 'Scatter factor is a fibroblast-derived modulator of epithelial cell mobility', *Nature*, 327: 239-42.
Sun, X, Y Wang, J Zhang, J Tu, XJ Wang, XD Su, L Wang, and Y Zhang. 2012. 'Tunneling-nanotube direction determination in neurons and astrocytes', *Cell death & disease*, 3: e438-e38.
Sundell, Hakan W, Mary E Gray, Fredrik S Serenius, Marilyn B Escobedo, and MT Stahlman. 1980. 'Effects of epidermal growth factor on lung maturation in fetal lambs', *The American Journal of Pathology*, 100: 707.
Sung, Kyung Eun, and David J Beebe. 2014. 'Microfluidic 3D models of cancer', *Advanced drug delivery reviews*, 79: 68-78.
Taipale, Jussi, and Jorma Keski-Oja. 1996. 'Hepatocyte growth factor releases epithelial and endothelial cells from growth arrest induced by transforming growth factor-1', *Journal of Biological Chemistry*, 271: 4342-48.
Takenawa, Tadaomi, and Shiro Suetsugu. 2007. 'The WASP–WAVE protein network: connecting the membrane to the cytoskeleton', *Nature reviews Molecular cell biology*, 8: 37-48.
Takizawa, Hajime, Takayuki Ohtoshi, Ken Ohta, Naomi Yamashita, Shunsei Hirohata, Koichi Hirai, Keiichi Hiramatsu, and Koji Ito. 1993. 'Growth inhibition of human lung cancer cell lines by interleukin 6 in vitro: a possible role in tumor growth via an autocrine mechanism', *Cancer research*, 53: 4175-81.
Tamaki, Masashi, Warren McDonald, Verena R Amberger, Emi Moore, and Rolando F Del Maestro. 1997. 'Implantation of C6 astrocytoma spheroid into collagen type I gels: invasive, proliferative, and enzymatic characterizations', *Journal of neurosurgery*, 87: 602-09.
Tan, Aaron C. 2020. 'Targeting the PI3K/Akt/mTOR pathway in non-small cell lung cancer (NSCLC)', *Thoracic cancer*, 11: 511-18.
Tapon, Nicolas, and Alan Hall. 1997. 'Rho, Rac and Cdc42 GTPases regulate the organization of the actin cytoskeleton', *Current opinion in cell biology*, 9: 86-92.
Tepper, Robert I, Robert L Coffman, and Philip Leder. 1992. 'An eosinophil-dependent mechanism for the antitumor effect of interleukin-4', *Science*, 257: 548-51.
Testa, Ugo, Germana Castelli, and Elvira Pelosi. 2018. 'Lung cancers: molecular characterization, clonal heterogeneity and evolution, and cancer stem cells', *Cancers*, 10: 248.
Thayanithy, Venugopal, Elizabeth L Dickson, Clifford Steer, Subbaya Subramanian, and Emil Lou. 2014. 'Tumor-stromal cross talk: direct cell-to-cell transfer of oncogenic microRNAs via tunneling nanotubes', *Translational Research*, 164: 359-65.
Tilghman, Robert W, Catharine R Cowan, Justin D Mih, Yulia Koryakina, Daniel Gioeli, Jill K Slack-Davis, Brett R Blackman, Daniel J Tschumperlin, and J Thomas Parsons. 2010. 'Matrix rigidity regulates cancer cell growth and cellular phenotype', *PLoS One*, 5: e12905.
To, Yasuo, Makoto Dohi, Kunio Matsumoto, Ryoichi Tanaka, Atsushi Sato, Kazuyuki Nakagome, Toshikazu Nakamura, and Kazuhiko Yamamoto. 2002. 'A two-way interaction between hepatocyte growth factor and interleukin-6 in tissue invasion of lung cancer cell line', *American journal of respiratory cell and molecular biology*, 27: 220-26.
Todaro, George J, Gerald K Lazar, and Howard Green. 1965. 'The initiation of cell division in a contact-inhibited mammalian cell line', *Journal of Cellular and Comparative Physiology*, 66: 325-33.
Travis, William D, Elisabeth Brambilla, and Gregory J Riely. 2013. 'New pathologic classification of lung cancer: relevance for clinical practice and clinical trials', *J Clin Oncol*, 31: 992-1001.
Trédan, Olivier, Carlos M Galmarini, Krupa Patel, and Ian F Tannock. 2007. 'Drug resistance and the solid tumor microenvironment', *Journal of the National Cancer Institute*, 99: 1441-54.
Trumpp, Andreas, Marieke Essers, and Anne Wilson. 2010. 'Awakening dormant haematopoietic stem cells', *Nature Reviews Immunology*, 10: 201-09.

Truong, Danh D, Alexander Kratz, Jin G Park, Eric S Barrientos, Harpinder Saini, Toan Nguyen, Barbara Pockaj, Ghassan Mouneimne, Joshua LaBaer, and Mehdi Nikkhah. 2019. 'A Human Organotypic Microfluidic Tumor Model Permits Investigation of the Interplay between Patient-Derived Fibroblasts and Breast Cancer CellsPatient-Derived Fibroblasts Promote Cancer Invasion Behavior', *Cancer research*, 79: 3139-51.

Truong, Danh, Julieann Puleo, Alison Llave, Ghassan Mouneimne, Roger D Kamm, and Mehdi Nikkhah. 2016. 'Breast cancer cell invasion into a three dimensional tumor-stroma microenvironment', *Scientific reports*, 6: 1-18.

Trusolino, Livio, Andrea Bertotti, and Paolo M Comoglio. 2010. 'MET signalling: principles and functions in development, organ regeneration and cancer', *Nature reviews Molecular cell biology*, 11: 834.

Trusolino, Livio, Andrea Bertotti, and Paolo M %J Cell Comoglio. 2001. 'A signaling adapter function for α6β4 integrin in the control of HGF-dependent invasive growth', 107: 643-54.

Trusolino, Livio, Silvia Cavassa, Paola Angelini, Margherita AndÒ, Andrea Bertotti, Paolo M Comoglio, and Carla Boccaccio. 2000. 'HGF/scatter factor selectively promotes cell invasion by increasing integrin avidity', *The FASEB Journal*, 14: 1629-40.

Tsao, Ming-Sound, Ni Liu, Jim-Ray Chen, J Pappas, James Ho, Christine To, Jean Viallet, Morag Park, and Hong Zhu. 1998. 'Differential expression of Met/hepatocyte growth factor receptor in subtypes of non-small cell lung cancers', *Lung cancer*, 20: 1-16.

Tsuta, Koji, Yoshiki Kozu, Takahiro Mimae, Akihiko Yoshida, Takashi Kohno, Ikuo Sekine, Tomohide Tamura, Hisao Asamura, Koh Furuta, and Hitoshi Tsuda. 2012. 'c-MET/phospho-MET protein expression and MET gene copy number in non-small cell lung carcinomas', *Journal of Thoracic Oncology*, 7: 331-39.

Tumbarello, David A, Michael C Brown, and Christopher E Turner. 2002. 'The paxillin LD motifs', *FEBS letters*, 513: 114-18.

Turke, Alexa B, Kreshnik Zejnullahu, Yi-Long Wu, Youngchul Song, Dora Dias-Santagata, Eugene Lifshits, Luca Toschi, Andrew Rogers, Tony Mok, and Lecia Sequist. 2010. 'Preexistence and clonal selection of MET amplification in EGFR mutant NSCLC', *Cancer cell*, 17: 77-88.

Turner, Christopher E, John R Glenney Jr, and Keith Burridge. 1990. 'Paxillin: a new vinculin-binding protein present in focal adhesions', *The Journal of cell biology*, 111: 1059-68.

Usuda, Jitsuo, Harubumi Kato, Tetsuya Okunaka, Kinya Furukawa, Hidemitsu Tsutsui, Kimito Yamada, Yasuhiro Suga, Hidetoshi Honda, Yoshitaka Nagatsuka, and Tatsuo Ohira. 2006. 'Photodynamic therapy (PDT) for lung cancers', *Journal of Thoracic Oncology*, 1: 489-93.

van Dam, Ellen M, and Phillip J Robinson. 2006. 'Ral: mediator of membrane trafficking', *The international journal of biochemistry & cell biology*, 38: 1841-47.

Veranič, Peter, Maruša Lokar, Gerhard J Schütz, Julian Weghuber, Stefan Wieser, Henry Hägerstrand, Veronika Kralj-Iglič, and Aleš Iglič. 2008. 'Different types of cell-to-cell connections mediated by nanotubular structures', *Biophysical journal*, 95: 4416-25.

Vermeulen, Katrien, Dirk R Van Bockstaele, and Zwi N Berneman. 2003. 'The cell cycle: a review of regulation, deregulation and therapeutic targets in cancer', *Cell proliferation*, 36: 131-49.

Verstraeten, AS, A De Weerdt, G van Den Eynden, E Van Marck, A Snoeckx, and PG Jorens. 2011. 'Excessive eosinophilia as paraneoplastic syndrome in a patient with non-small-cell lung carcinoma: a case report and review of the literature', *Acta Clinica Belgica*, 66: 293-97.

Votteler, Miriam, Petra J Kluger, Heike Walles, and Katja Schenke-Layland. 2010. 'Stem Cell Microenvironments-Unveiling the Secret of How Stem Cell Fate is Defined', *Macromolecular bioscience*, 10: 1302-15.

Wang, Fei, Xiaoping Chen, Haipeng Cheng, Lu Song, Jianghong Liu, Steve Caplan, Li Zhu, and Jane Y Wu. 2021. 'MICAL2PV suppresses the formation of tunneling nanotubes and modulates mitochondrial trafficking', *EMBO reports*, 22: e52006.

Wang, Fei, Valerie M Weaver, Ole W Petersen, Carolyn A Larabell, Shoukat Dedhar, Per Briand, Ruth Lupu, and Mina J Bissell. 1998. 'Reciprocal interactions between β1-integrin and epidermal

growth factor receptor in three-dimensional basement membrane breast cultures: a different perspective in epithelial biology', *Proceedings of the National Academy of Sciences*, 95: 14821-26.
Wang, Xiang, and Hans-Hermann Gerdes. 2012. 'Long-distance electrical coupling via tunneling nanotubes', *Biochimica et Biophysica Acta (BBA)-Biomembranes*, 1818: 2082-86.
Wang, Xiang, and Hans-Hermann Gerde. 2015. 'Transfer of mitochondria via tunneling nanotubes rescues apoptotic PC12 cells', *Cell Death & Differentiation*, 22: 1181-91.
Wang, Xiang, Margaret Lin Veruki, Nickolay V Bukoreshtliev, Espen Hartveit, and Hans-Hermann Gerdes. 2010. 'Animal cells connected by nanotubes can be electrically coupled through interposed gap-junction channels', *Proceedings of the National Academy of Sciences*, 107: 17194-99.
Wang, Y, J Cui, X Sun, and Y Zhang. 2011. 'Tunneling-nanotube development in astrocytes depends on p53 activation', *Cell Death & Differentiation*, 18: 732-42.
Wang, Zhi-Gang, Shu-Lin Liu, Zhi-Quan Tian, Zhi-Ling Zhang, Hong-Wu Tang, and Dai-Wen Pang. 2012. 'Myosin-driven intercellular transportation of wheat germ agglutinin mediated by membrane nanotubes between human lung cancer cells', *ACS nano*, 6: 10033-41.
Wang, Zhixiang. 2017. 'ErbB receptors and cancer', *ErbB Receptor Signaling*: 3-35.
Wang, Zhufeng, Bigui Chen, Yu Fu, Changxing Ou, Qiuping Rong, Xuetao Kong, Wei Xu, Yangqing Deng, Mei Jiang, and Jiaxing Xie. 2022. 'Eosinophilia and Lung Cancer: Analysis From Real-World Data and Mendelian Randomization Study', *Frontiers in medicine*: 484.
Warburg, Otto. 1956. 'On the origin of cancer cells', *Science*, 123: 309-14.
Warburton, David, Margaret Schwarz, Denise Tefft, Guillermo Flores-Delgado, Kathryn D Anderson, and Wellington V Cardoso. 2000. 'The molecular basis of lung morphogenesis', *Mechanisms of development*, 92: 55-81.
Warburton, David, Rajeev Seth, Lillian Shum, Philip G Horcher, Frederick L Hall, Zena Werb, and Harold C Slavkin. 1992. 'Epigenetic role of epidermal growth factor expression and signalling in embryonic mouse lung morphogenesis', *Developmental biology*, 149: 123-33.
Ware, Matthew J, Sophia Tinger, Kevin L Colbert, Stuart J Corr, Paul Rees, Nadezhda Koshkina, Steven Curley, HD Summers, and Biana Godin. 2015. 'Radiofrequency treatment alters cancer cell phenotype', *Scientific reports*, 5: 1-14.
Wee, Ping, and Zhixiang Wang. 2017. 'Epidermal growth factor receptor cell proliferation signaling pathways', *Cancers*, 9: 52.
Wei, Spencer C, Laurent Fattet, Jeff H Tsai, Yurong Guo, Vincent H Pai, Hannah E Majeski, Albert C Chen, Robert L Sah, Susan S Taylor, and Adam J Engler. 2015. 'Matrix stiffness drives epithelial–mesenchymal transition and tumour metastasis through a TWIST1–G3BP2 mechanotransduction pathway', *Nature cell biology*, 17: 678-88.
Weller, PF, AM Dvorak, W Busse, and ST Holgate. 1994. 'Asthma and rhinitis'.
Weng, Zhigang, JA Taylor, CE Turner, JS Brugge, and C Seidel-Dugan. 1993. 'Detection of Src homology 3-binding proteins, including paxillin, in normal and v-Src-transformed Balb/c 3T3 cells', *Journal of Biological Chemistry*, 268: 14956-63.
Whitehead, Jacklyn, Jiali Zhang, Jenna N Harvestine, Alefia Kothambawala, Gang-yu Liu, and J Kent Leach. 2020. 'Tunneling nanotubes mediate the expression of senescence markers in mesenchymal stem/stromal cell spheroids', *Stem Cells*, 38: 80-89.
Whitman, Malcolm, and DA Melton. 1989. 'Growth factors in early embryogenesis', *Annual review of cell biology*, 5: 93-117.
Whitsett, Jeffrey A, Timothy E Weaver, Michael A Lieberman, Jean C Clark, and Cynthia Daugherty. 1987. 'Differential effects of epidermal growth factor and transforming growth factor-beta on synthesis of Mr= 35,000 surfactant-associated protein in fetal lung', *Journal of Biological Chemistry*, 262: 7908-13.

Winkler, Juliane, Abisola Abisoye-Ogunniyan, Kevin J Metcalf, and Zena Werb. 2020. 'Concepts of extracellular matrix remodelling in tumour progression and metastasis', *Nature communications*, 11: 1-19.

Wolf, Janina, Stefan Rose-John, and Christoph Garbers. 2014. 'Interleukin-6 and its receptors: a highly regulated and dynamic system', *Cytokine*, 70: 11-20.

Wu, Ping-Ping, Kuo-Ching Liu, Wen-Wen Huang, Chia-Yu Ma, Hung Lin, Jai-Sing Yang, and Jing-Gung Chung. 2011. 'Triptolide induces apoptosis in human adrenal cancer NCI-H295 cells through a mitochondrial-dependent pathway', *Oncology reports*, 25: 551-57.

Xiao, Guang-Hui, Michael Jeffers, Alfonso Bellacosa, Yasuhiro Mitsuuchi, George F Vande Woude, and Joseph R Testa. 2001. 'Anti-apoptotic signaling by hepatocyte growth factor/Met via the phosphatidylinositol 3-kinase/Akt and mitogen-activated protein kinase pathways', *Proceedings of the National Academy of Sciences*, 98: 247-52.

Xie, Lei, and Philip E Bourne. 2015. "Developing multi-target therapeutics to fine-tune the evolutionary dynamics of the cancer ecosystem." In, 209. Frontiers Media SA.

Yamada, Tadaaki, Kunio Matsumoto, Wei Wang, Qi Li, Yasuhiko Nishioka, Yoshitaka Sekido, Saburo Sone, and Seiji Yano. 2010. 'Hepatocyte growth factor reduces susceptibility to an irreversible epidermal growth factor receptor inhibitor in EGFR-T790M mutant lung cancer', *Clinical cancer research*, 16: 174-83.

Yamada, Tadaaki, Shinji Takeuchi, Kenji Kita, Hideaki Bando, Takahiro Nakamura, Kunio Matsumoto, and Seiji Yano. 2012. 'Hepatocyte growth factor induces resistance to anti-epidermal growth factor receptor antibody in lung cancer', *Journal of Thoracic Oncology*, 7: 272-80.

Yamaji, Haruko, Toshihiko Iizasa, Eitetsu Koh, Makoto Suzuki, Mizuto Otsuji, Hao Chang, Shinichiro Motohashi, Sana Yokoi, Kenzo Hiroshima, and Masatoshi Tagawa. 2004. 'Correlation between interleukin 6 production and tumor proliferation in non-small cell lung cancer', *Cancer Immunology, Immunotherapy*, 53: 786-92.

Yamamoto, Hiroaki, Eun Jun Yun, Hans-Peter Gerber, Napoleone Ferrara, Jeffrey A Whitsett, and Thiennu H Vu. 2007. 'Epithelial–vascular cross talk mediated by VEGF-A and HGF signaling directs primary septae formation during distal lung morphogenesis', *Developmental biology*, 308: 44-53.

Yamashita, Yukiko M, Mayu Inaba, and Michael Buszczak. 2018. 'Specialized intercellular communications via cytonemes and nanotubes', *Annual review of cell and developmental biology*, 34: 59-84.

Yan, XU, ZHAO Yinmin, SU Bo, CHEN Ying, and ZHOU Caicun. 2006. 'Expression of collagen IV, fibronectin, laminin in non-small cell lung cancer and its correlation with chemosensitivities and apoptosis', *The Chinese-German Journal of Clinical Oncology*, 5: 58-62.

Yanagawa, H, S Sone, Y Takahashi, T Haku, S Yano, T Shinohara, and T Ogura. 1995. 'Serum levels of interleukin 6 in patients with lung cancer', *British journal of cancer*, 71: 1095-98.

Yanagita, Kimihiko, Kunio Matsumoto, K Sekiguchi, H Ishibashi, Y Niho, and T Nakamura. 1993. 'Hepatocyte growth factor may act as a pulmotrophic factor on lung regeneration after acute lung injury', *Journal of Biological Chemistry*, 268: 21212-17.

Yanagita, Kimihiko, Mika Nagaike, Hiromi Ishibashi, Yoshiyuki Niho, Kunio Matsumoto, and Toshikazu Nakamura. 1992. 'Lung may have an endocrine function producing hepatocyte growth factor in response to injury of distal organs', *Biochemical and biophysical research communications*, 182: 802-09.

Yang, Chang, Bai-Rong Xia, Wei-Lin Jin, and Ge Lou. 2019. 'Circulating tumor cells in precision oncology: Clinical applications in liquid biopsy and 3D organoid model', *Cancer cell international*, 19: 1-13.

Yano, Seiji, Wei Wang, QI Li, Kunio Matsumoto, Haruko Sakurama, Takahiro Nakamura, Hirokazu Ogino, Soji Kakiuchi, Masaki Hanibuchi, and Yasuhiko Nishioka. 2008. 'Hepatocyte growth factor induces gefitinib resistance of lung adenocarcinoma with epidermal growth factor receptor–activating mutations', *Cancer research*, 68: 9479-87.

Yao, Xin, Jiaqi Huang, Haihong Zhong, Nan Shen, Raffaella Faggioni, Michael Fung, and Yihong Yao. 2014. 'Targeting interleukin-6 in inflammatory autoimmune diseases and cancers', *Pharmacology & therapeutics*, 141: 125-39.

Yarden, Yosef. 2001. 'The EGFR family and its ligands in human cancer: signalling mechanisms and therapeutic opportunities', *European journal of cancer*, 37: 3-8.

Yarden, Yosef, and Mark X Sliwkowski. 2001. 'Untangling the ErbB signalling network', *Nature reviews Molecular cell biology*, 2: 127-37.

Yi, S, JR Chen, J Viallet, RH Schwall, T Nakamura, and MS Tsao. 1998. 'Paracrine effects of hepatocyte growth factor/scatter factor on non-small-cell lung carcinoma cell lines', *British journal of cancer*, 77: 2162-70.

Yi, Seung, and Ming-Sound Tsao. 2000. 'Activation of hepatocyte growth factor-met autocrine loop enhances tumorigenicity in a human lung adenocarcinoma cell line', *Neoplasia*, 2: 226-34.

Yokomuro, Shigeki, Hirokazu Tsuji, John G Lunz, Toshiki Sakamoto, Tsukasa Ezure, Noriko Murase, and Anthony J Demetris. 2000. 'Growth control of human biliary epithelial cells by interleukin 6, hepatocyte growth factor, transforming growth factor β1, and activin a: Comparison of a cholangiocarcinoma cell line with primary cultures of non-neoplastic biliary epithelial cells', *Hepatology*, 32: 26-35.

Yuan, Yonggang, Weiliang Zhong, Ge Ma, Baoxiang Zhang, and Hui Tian. 2015. 'Yes-associated protein regulates the growth of human non-small cell lung cancer in response to matrix stiffness', *Molecular Medicine Reports*, 11: 4267-72.

Yue, Beatrice %J Journal of glaucoma. 2014. 'Biology of the extracellular matrix: an overview': S20.

Zamprogno, Pauline, Simon Wüthrich, Sven Achenbach, Giuditta Thoma, Janick D Stucki, Nina Hobi, Nicole Schneider-Daum, Claus-Michael Lehr, Hanno Huwer, and Thomas Geiser. 2021. 'Second-generation lung-on-a-chip with an array of stretchable alveoli made with a biological membrane', *Communications biology*, 4: 1-10.

Zappa, Cecilia, and Shaker A Mousa. 2016. 'Non-small cell lung cancer: current treatment and future advances', *Translational Lung Cancer Research*, 5: 288.

Zaynagetdinov, Rinat, Taylor P Sherrill, Linda A Gleaves, Allyson G McLoed, Jamie A Saxon, Arun C Habermann, Linda Connelly, Daniel Dulek, R Stokes Peebles, and Barbara Fingleton. 2015. 'Interleukin-5 Facilitates Lung Metastasis by Modulating the Immune MicroenvironmentIL5 Facilitates Lung Metastasis', *Cancer research*, 75: 1624-34.

Zhang, Jiali, Jacklyn Whitehead, Yang Liu, Qingbo Yang, J Kent Leach, and Gang-yu Liu. 2018. 'Direct observation of tunneling nanotubes within human mesenchymal stem cell spheroids', *The Journal of Physical Chemistry B*, 122: 9920-26.

Zhang, Jianjun, Junya Fujimoto, Jianhua Zhang, David C Wedge, Xingzhi Song, Jiexin Zhang, Sahil Seth, Chi-Wan Chow, Yu Cao, and Curtis Gumbs. 2014. 'Intratumor heterogeneity in localized lung adenocarcinomas delineated by multiregion sequencing', *Science*, 346: 256-59.

Zhang, Suli, Marcelo G Kazanietz, and Mariana Cooke. 2020. 'Rho GTPases and the emerging role of tunneling nanotubes in physiology and disease', *American Journal of Physiology-Cell Physiology*, 319: C877-C84.

Zhang, Xian, Guoying Jiang, Yunfei Cai, Susan J Monkley, David R Critchley, and Michael P Sheetz. 2008. 'Talin depletion reveals independence of initial cell spreading from integrin activation and traction', *Nature cell biology*, 10: 1062-68.

Zhang, Yu-Wen, and George F Vande Woude. 2003. 'HGF/SF-met signaling in the control of branching morphogenesis and invasion', *Journal of cellular biochemistry*, 88: 408-17.

Zhang, Zhe, Sen Yang, and Qiming Wang. 2019. 'Impact of MET alterations on targeted therapy with EGFR-tyrosine kinase inhibitors for EGFR-mutant lung cancer', *Biomarker Research*, 7: 1-7.

Zhao, Zhongquan, Xiaoming Cheng, Yubo Wang, Rui Han, Li Li, Tong Xiang, Luhang He, Haixia Long, Bo Zhu, and Yong He. 2014. 'Metformin inhibits the IL-6-induced epithelial-mesenchymal transition and lung adenocarcinoma growth and metastasis', *PLoS One*, 9: e95884.

Zheng, Xianan, Guohua Lu, Yinan Yao, and Wei Gu. 2019. 'An Autocrine IL-6/IGF-1R Loop Mediates EMT and Promotes Tumor Growth in Non-small Cell Lung Cancer', *International journal of biological sciences*, 15: 1882.

Zhou, Caicun, Yi-Long Wu, Gongyan Chen, Jifeng Feng, Xiao-Qing Liu, Changli Wang, Shucai Zhang, Jie Wang, Songwen Zhou, and Shengxiang Ren. 2011. 'Erlotinib versus chemotherapy as first-line treatment for patients with advanced EGFR mutation-positive non-small-cell lung cancer (OPTIMAL, CTONG-0802): a multicentre, open-label, randomised, phase 3 study', *The lancet oncology*, 12: 735-42.

Zhou, Hong Y, Yuen L Pon, and Alice ST Wong. 2007. 'Synergistic effects of epidermal growth factor and hepatocyte growth factor on human ovarian cancer cell invasion and migration: role of extracellular signal-regulated kinase 1/2 and p38 mitogen-activated protein kinase', *Endocrinology*, 148: 5195-208.

Zhu, Donghui, Kevin S Tan, Xiaolin Zhang, Albert Y Sun, Grace Y Sun, and James C-M Lee. 2005. 'Hydrogen peroxide alters membrane and cytoskeleton properties and increases intercellular connections in astrocytes', *Journal of Cell Science*, 118: 3695-703.

Zhu, Tianhao, Xunxia Bao, Mingyu Chen, Rui Lin, Jianan Zhuyan, Timing Zhen, Kaichen Xing, Wei Zhou, and Sibo Zhu. 2020. 'Mechanisms and future of non-small cell lung cancer metastasis', *Frontiers in Oncology*, 10: 585284.

Zhu, Viola W, Alexa B Schrock, Siraj M Ali, and Sai-Hong Ignatius Ou. 2019. 'Differential response to a combination of full-dose osimertinib and crizotinib in a patient with EGFR-mutant non-small cell lung cancer and emergent MET amplification', *Lung Cancer: Targets and Therapy*, 10: 21.

Zhu, Wenbo, Haiyan Hu, Pengxin Qiu, and Guangmei Yan. 2009. 'Triptolide induces apoptosis in human anaplastic thyroid carcinoma cells by a p53-independent but NF-κB-related mechanism', *Oncology reports*, 22: 1397-401.